International Linear Collider Technical Review Committee

Second Report

2003

This report was produced on behalf of the International Linear Collider Technical Review Committee by the Stanford Linear Accelerator Center under contract DE-AC03-76SF00515 with the U.S. Department of Energy. Copies may be obtained by requesting SLAC-R-606 from the following address:

Stanford Linear Accelerator Center
Technical Publications Department
2575 Sand Hill Road, MS-68
Menlo Park, CA 94025
E-mail address: epubs-l@slac.stanford.edu

CONTENTS

LIST of FIGURES

LIST of TABLES

Executive Summary

INTRODUCTION

As this report is being published, the international high energy physics (HEP) community finds itself confronting a set of fascinating discoveries and new questions regarding the nature of matter and its fundamental particles and forces. The observation of neutrino oscillations that indicates that neutrinos have mass, measurements of the accelerating expansion of the universe that may be due to dark energy, and evidence for a period of rapid inflation at the beginning of the Big Bang are stimulating the entire field. Looming on the horizon are the potential discoveries of a Higgs particle that may reveal the origin of mass and of a whole family of supersymmetric particles that may be part of the cosmic dark matter. For the HEP community to elucidate these mysteries, new accelerators are indispensable.

At this time, after careful deliberations, all three regional organizations of the HEP community (ACFA in Asia, HEPAP in North America, and ECFA in Europe) have reached the common conclusion that the next accelerator should be an electron-positron linear collider with an initial center-of-mass energy of 500 Giga-electronvolts (GeV), later upgradable to higher energies, and that it should be built and operated in parallel with the Large Hadron Collider under construction at CERN. Hence, this second report of the International Linear Collider Technical Review Committee (ILC-TRC) comes at a very timely moment. The report was requested by the International Committee on Future Accelerators (ICFA) in February 2001 to assess the current technical status of electron-positron linear collider designs in the various regions. Note that the ILC-TRC was not asked to concern itself with either cost studies or the ultimate selection process of a machine.

This Executive Summary gives a short outline of the genesis of the report, the charge given to the committee, and its organization. It then presents a brief description of four electron-positron linear collider designs at hand. The methodology used to assess these designs is described in some detail. The assessments are followed by a list of R&D tasks recommended by the committee for the next few years. The tasks are ranked according to certain specific criteria. The summary concludes with a few remarks outlining upcoming developments that may guide ICFA and the HEP community in their future plans to promote and execute an international project.

The Executive Summary stands alone in the sense that it allows a busy reader, who may not have the time to read the entire report, to become familiar with its essential contents.

GENESIS, CHARGE, AND ORGANIZATION

The ILC-TRC was originally created by the Interlaboratory Collaboration for R&D toward TeV-Scale Electron-Positron Linear Colliders at a meeting in London, England, in June 1994. By the end of 1995, the ILC-TRC produced its first report which for the first time gathered in one document the current status of eight major e^+e^- linear collider designs in the world. As each design progressed, large tables that listed all the major parameters of the machines in the report were updated regularly until the beginning of 2000. By that time, while three of the original eight designs had been abandoned, the five remaining ones had greatly matured.

In 2001, as a result of deliberations at the ICFA meeting of February 8 and 9 at DESY, Professor H. Sugawara as Chair of ICFA requested that the ILC-TRC reconvene its activities to produce a second report. G. Loew, the original Chair of the ILC-TRC, agreed to conduct this second study. ICFA also recommended that a Steering Committee of four members be formed within the ILC-TRC to represent the major e^+e^- linear collider designs in the world to be covered in the second report: TESLA, JLC-C, JLC-X, NLC, and CLIC. Accordingly, R. Brinkmann from DESY was chosen for TESLA, K. Yokoya from KEK for JLC-C and JLC-X, T. Raubenheimer from SLAC for NLC, and G. Guignard from CERN for CLIC. In practice, the designs of JLC-X and NLC became essentially identical, and hence only four basic designs remained to be examined.

The Chair and the full Steering Committee met for the first time at Snowmass, Colorado, on July 5, 2001. During this meeting, the committee reviewed the charge that had been broadly sketched by ICFA and converged on the approximate contents of the report to be produced. The charge was streamlined during subsequent months, and the final version is summarized as follows:

SECOND ILC-TRC CHARGE:

- To assess the present technical status of the four LC designs at hand, and their potential for meeting the advertised parameters at 500 GeV c.m. Use common criteria, definitions, computer codes, *etc.*, for the assessments
- To assess the potential of each design for reaching higher energies above 500 GeV c.m.
- To establish, for each design, the R&D work that remains to be done in the next few years
- To suggest future areas of collaboration

The Steering Committee decided to accomplish its mission by dividing it into two major parts:

- Descriptions of the four machines, their upgrade paths and respective test facilities, setting the foundations for the assessments
- Assessments of the four machines as outlined by the charge

The Steering Committee took full responsibility for the first activity and decided that the assessments should be carried out by two separate Working Groups: one for **Technology, RF Power, and Energy Performance** chaired by D. Boussard, recently retired from CERN, the other for **Luminosity Performance** chaired by G. Dugan from Cornell. The Chair submitted this proposed plan to the ICFA meeting in Rome, Italy, on July 27, 2001, and ICFA accepted the proposal.

From then on, all the work of the ILC-TRC was done via e-mail, teleconferences, and four pivotal meetings. The two Working Groups each consisted of their Chairs and thirteen scientists selected from the Linear Collider world community. During the course of their assessments, the Working Groups realized that a third task, common to both of them, would be of key importance to the ultimate commissioning and successful operation of any of the linear colliders. This task was labelled **Reliability, Availability, and Operability**, and several members of both Working Groups formed a third Working Group to handle this task. All pertinent details can be found in Chapter 1. The overall organization of the second ILC-TRC is summarized in Table 1.

TABLE 1
Second ILC-TRC Overall Organization

Chair	Gregory Loew
Steering Committee	Reinhard Brinkmann Kaoru Yokoya Tor Raubenheimer Gilbert Guignard
Working Groups	
Technology, RF Power, and Energy Performance Assessments	Daniel Boussard
Luminosity Performance Assessments	Gerry Dugan
Reliability, Availability and Operability	Nan Phinney Ralph Pasquinelli

The Table of Contents for this report is fairly self-explanatory. This Executive Summary was written by the Chair, who incorporated numerous comments from the entire committee. Chapter 1, also written by the Chair, summarizes the ILC-TRC's procedures,

organization, and milestones. T. Raubenheimer volunteered to be the central "keeper" responsible for putting together the six megatables given in Chapter 2. Chapter 3 on descriptions of the four machines at 500 GeV c.m., Chapter 4 on the upgrade paths to higher energies, and Chapter 5 on the test facilities and other project R&D programs, were written by the members of the Steering Committee for their respective projects. Chapters 6, 7, and 8, presenting the respective assessments of the three Working Groups, were assembled by their Chairs from text prepared by the Subgroup Chairs, with the help of their respective members. Finally, Chapter 9, which summarizes the lists and ranks of all the R&D studies still deemed necessary, was put together by D. Boussard and G. Dugan. It should be noted here that the Working Group members did not always agree with all the statements made by the machine proponents in Chapters 3, 4, and 5, and these disagreements are reflected in their assessments.

BRIEF DESCRIPTIONS OF THE FOUR LINEAR COLLIDER DESIGNS

Even though the final technology choice for an international electron-positron collider has not yet been made, the HEP community agrees that the machine should start with an energy of 500 GeV c.m. and be expandable later to higher energies. While all linear collider designs have undergone remarkable progress in the past 15 years, the machines reviewed here are not all in the same state of readiness. TESLA is most advanced in terms of the rf system feasibility tests mainly conducted at TTF (DESY). JLC-C consists only of a 400 GeV c.m. rf design based on technology being developed for a linac-based FEL at SPring-8 in Japan. JLC-X/NLC have an rf design based on ongoing tests at NLCTA and ASSET (SLAC). Both TESLA and JLC-X/NLC have fairly mature conceptual designs. CLIC follows a more novel approach based on a two-beam system studied at CTF (CERN), but it needs more time to be developed. If successful, CLIC could eventually reach 3 TeV c.m. within a footprint similar to the other schemes. Aside from the rf systems, all of the machines have benefited from advanced tests at FFTB (SLAC) and at ATF (KEK), and from experience with the first linear collider, the SLC, which operated at SLAC from 1988 through 1998. The SLC experience has been essential in understanding the luminosity potential of these four designs.

Note that throughout the report, the committee concentrated its studies on e^+e^- colliders. In most cases, it was assumed that e^-e^- collisions would not require major design changes, although the luminosities would be lower, and that $\gamma\gamma$ collisions would be considered in detail later.

TESLA

TESLA's main characteristics and parameters are shown in Table 2 and illustrated in Figure 1, Figure 2, and Figure 3. The DESY site length is currently fixed at 33 km. The main linacs are based on 1.3 GHz superconducting technology operating at 2 K. The cryoplant, of a size comparable to that of the LHC, consists of seven subsystems strung along the machines every 5 km. RF accelerator structures consist of close to 21,000 9-cell niobium cavities operating at gradients of 23.8 MV/m (unloaded as well as beam loaded)

TABLE 2: Summary of Machine Parameters

	TESLA		**JLC-C**		**JLC-X/NLC**[a]		**CLIC**	
Center of mass energy [GeV]	500	800	500	1000	500	1000	500	3000
RF frequency of main linac [GHz]	1.3		5.7	5.7/11.4[b]	11.4		30	
Design luminosity [10^{33} cm^{-2}s^{-1}]	34.0	58.0	14.1	25.0	25.0 (20.0)	25.0 (30.0)	21.0	80.0
Linac repetition rate [Hz]	5	4	100		150 (120)	100 (120)	200	100
Number of particles/bunch at IP [10^{10}]	2	1.4	0.75		0.75		0.4	
$\gamma\varepsilon_x^*$ / $\gamma\varepsilon_y^*$ emit. at IP [m·rad $\times$ 10^{-6}]	10 / 0.03	8 / 0.015	3.6 / 0.04		3.6 / 0.04		2.0 / 0.01	0.68 / 0.01
$\beta_x^\star$ / β_y^* at IP [mm]	15 / 0.40	15 / 0.40	8 / 0.20	13 / 0.11	8 / 0.11	13 / 0.11	10 / 0.05	16 / 0.07
$\sigma_x^\star$ / σ_y^* at IP before pinch[c] [nm]	554 / 5.0	392 / 2.8	243 / 4.0	219 / 2.1	243 / 3.0	219 / 2.1	202 / 1.2	60 / 0.7
$\sigma_z^\star$ at IP [μm]	300		200	110	110		35	
Number of bunches/pulse	2820	4886	192		192		154	
Bunch separation [nsec]	337	176	1.4		1.4		0.67	
Bunch train length [μsec]	950	860	0.267		0.267		0.102	
Beam power/beam [MW]	11.3	17.5	5.8	11.5	8.7 (6.9)	11.5 (13.8)	4.9	14.8
Unloaded/loaded gradient[d] [MV/m]	23.8 / 23.8[e]	35 / 35	41.8/31.5	41.8/31.5 / 70/55	65 / 50		172 / 150	
Total number of klystrons	572	1212	4276	3392/4640	4064	8256	448	
Number of sections	20592	21816	8552	6784/13920	12192	24768	7272	44000
Total two-linac length [km]	30	30	17.1	29.2	13.8	27.6	5.0	28.0
Total beam delivery length [km]	3		3.7		3.7		5.2	
Proposed site length [km]	33		33		32		10.2	33.2
Total site AC power[f] [MW]	140	200	233	300	243 (195)	292 (350)	175	410
Tunnel configuration[g]	Single		Double		Double		Single	

[a]Numbers in ( ) for the JLC-X/NLC correspond to the NLC design with 120 Hz repetition rate.

[b]The 1 TeV JLC-C collider uses a C-band rf system for the first 200 GeV of each linac followed by an X-band rf system for the remaining 300 GeV of acceleration—the X-band rf system would be identical to that described for the JLC-X band collider.

[c]For all designs except CLIC, the IP spot sizes are calculated as usual from the emittances and beta functions. With the design emittances in CLIC, nonlinear aberrations in the final focus system increase the final spot size by 20 to 40%.

[d]The main linac loaded gradient includes the effect of single-bunch (all modes) and multibunch beam loading, assuming that the bunches ride on crest. Beam loading is based on bunch charges in the linacs, which are slightly higher than at the IP.

[e]With the present site layout for TESLA, 23.4 MV/m was the required energy gain per meter of accelerator structure. A detailed analysis by the ILC-TRC revealed that the gradient has to be increased to 23.8 MV/m when rf phasing, especially for BNS damping, is taken into account.

[f]Total site power includes AC for linac rf and cooling systems as well as power for all other beam lines and site facilities.

[g]The single tunnel layout has both the klystrons and accelerator structures in the main linac tunnel while the double tunnel layout places the klystrons and modulators in a separate enclosure. In the CLIC scheme, the main linac uses a single tunnel since there are no klystrons or modulators associated with it. The 300 m-long CLIC drive beam accelerator is located in a tunnel with a separate klystron gallery on the surface.

for 500 GeV c.m. operation. These cavities are supplied with rf power in groups of 36 by 572 10 MW klystrons and modulators. The rf pulse length is 1370 μs and the repetition rate is 5 Hz. At a later stage, the machine energy may be upgraded to 800 GeV c.m. by raising the gradient to 35 MV/m. So far, TTF at DESY has had fairly extensive operation of two cryomodules at 15–18 MV/m for FEL runs, and one module was tested up to 21.4 MV/m with beam, which is close to the design value of 23.8 MV/m. A few 9-cell electropolished cavities have reached 35 MV/m in test cryostats. The upgrade will be achieved by raising the number of klystrons to 1212 and reducing the repetition rate to 4 Hz. The capacity of the original cryoplant will be doubled.

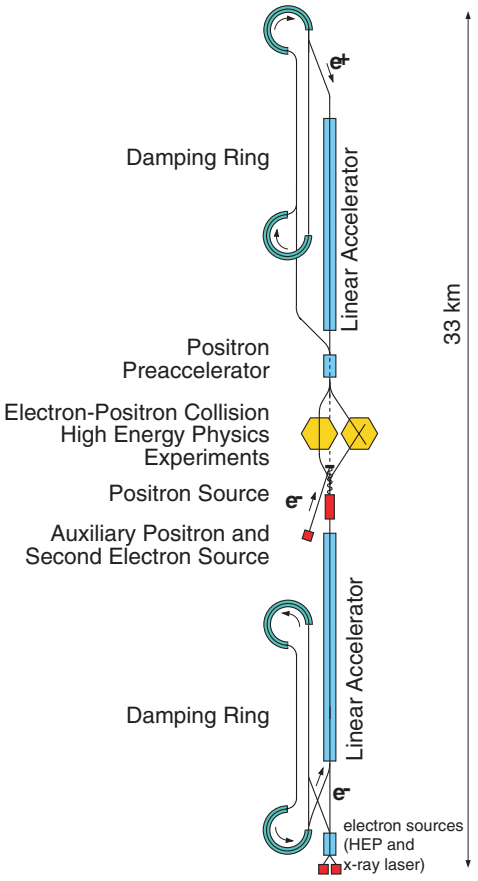

FIGURE 1. TESLA layout

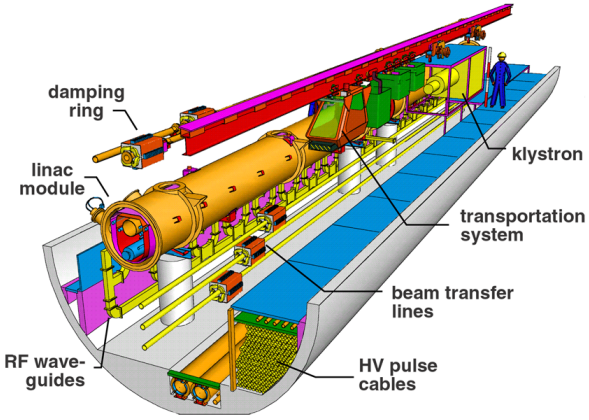

FIGURE 2. Sketch of the 5 m diameter TESLA linac tunnel

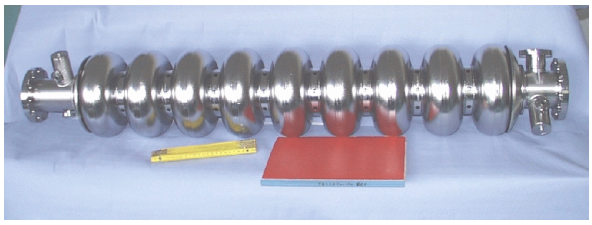

FIGURE 3. The 9-cell niobium cavity for TESLA

All the major TESLA beam parameters are listed in Table 2. Because of the long rf pulses, the bunch trains and bunch spacing can also afford to be long: 950 μs (860 μs) and 337 ns (176 ns) at 500 GeV c.m. (800 GeV c.m.). These parameters have two major consequences: (1) a fast bunch-to-bunch feedback can be used to correct orbits within one beam pulse, and a fast safety system can turn off the beam within a fraction of a pulse; (2) the bunch trains from the electron and positron sources have to be compressed by a factor of about 17 to fit into long 5 GeV damping rings, 17 km in perimeter. These damping rings are

"dog-bone" shaped so that their long straight sections can be located in the same tunnels as the linacs, the klystrons, the high-voltage cables, and other beam transfer lines. A 5 GeV electron source is located at one end.

The positron bunch train is produced by a "bootstrap" operation, which uses gamma rays radiated by the primary electron beam passing through an undulator at the end of the linac. The gamma rays impinge on a thin titanium target and the extracted positron bunches are sent to a positron pre-accelerator on the other side of the IR, after which they are stored in the positron damping ring. The proposed design for the primary IR assumes head-on collisions. The design luminosity is 34 (58)$\times 10^{33}$ cm^{-2}s^{-1} for 500 (800) GeV c.m. Even if the 500 GeV c.m. machine is not upgraded but the cavities are built to sustain 35 MV/m from the beginning, the energy can be increased to 700 GeV c.m. at a reduced luminosity of 12×10^{33} cm^{-2}s^{-1} by turning down the beam current.

JLC-C

The JLC-C is limited to an rf design using main linacs running at 5.7 GHz up to 400–500 GeV c.m. The idea is that it could be built with layouts, injectors and beam specifications very similar to JLC-X/NLC, described in the next section, and that it might be extended later using X-band technology up to 1 TeV. The rf system is shown in Figure 4 and consists of 1696 units, each with pairs of 50 MW klystrons, pairs of SLED-I type compact rf pulse compressors, and four so-called "choke mode" accelerator structures for higher-order mode suppression. The unloaded gradient is about 42 MV/m and the beam-loaded gradient is about 32 MV/m, resulting in a two-linac length at 5.7 GHz of 17 km for a 400 GeV c.m. energy.

JLC-X/NLC

The JLC-X and NLC are now essentially unified into a single design with common parameters given in Table 2 and shown in Figure 5 and Figure 6. The main linacs are based on 11.4 GHz, room temperature copper technology. The full site is approximately 32 km long. The electron and positron injectors are independent and located at opposite ends. The electron source produces polarized electrons that are accelerated to 2 GeV in an S-band linac, stored in a damping ring, and then again accelerated in a 6 GeV S-band pre-linac. The positrons are generated by an electromagnetic shower from 6 GeV electrons accelerated by an S-band linac, which collide with three parallel tungsten-rhenium targets. These positrons are collected and accelerated to 2 GeV in a large acceptance L-band linac and sequentially damped in a pre-damping and a main damping ring. Then, after two stages of longitudinal compression, electrons and positrons are ready for acceleration in their respective X-band linacs. Three bypass lines are provided along the way to extract particles respectively at 50, 175, and 250 GeV for collisions at two possible interaction points, one for a low-energy detector, the other for a high-energy detector. Crossing angles at the high energy and low energy IRs are 20 and 30 mrad respectively in the NLC design. In the JLC-X, the high energy IR has a crossing angle of 7 mrad.

The main linacs operate at an unloaded gradient of 65 MV/m, beam-loaded to 50 MV/m. These gradients have been achieved in test accelerator structures; structures with the

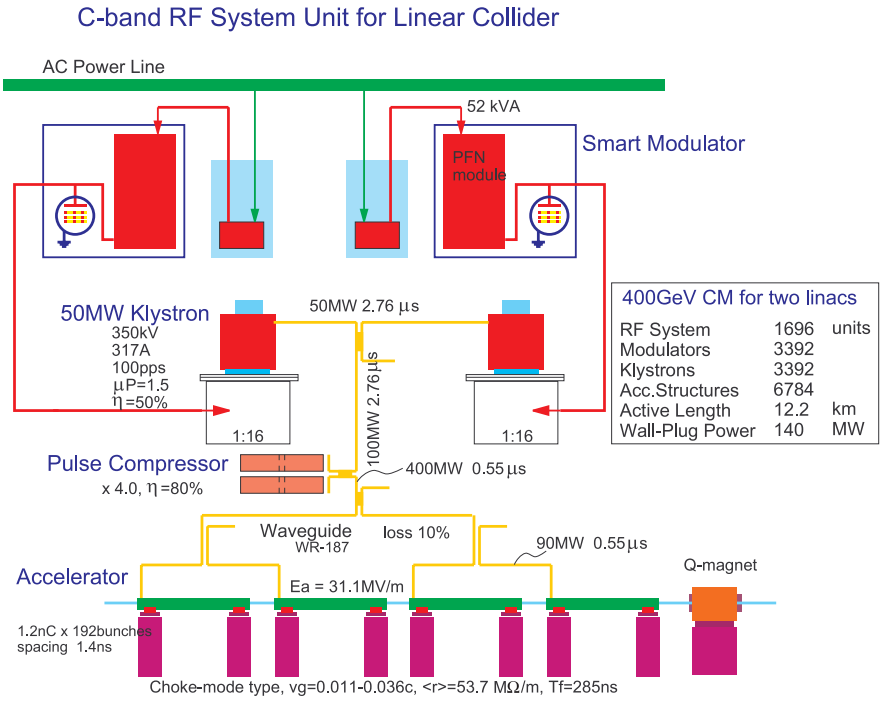

FIGURE 4. Schematic of a JLC-C linac rf unit (one of 848 per linac)

required damping characteristics are under development. The rf systems and accelerator structures are located in two parallel tunnels for each linac. For 500 GeV c.m. energy, these rf systems and accelerator structures are only installed in the first 7 km of each linac. The upgrade to 1 TeV is obtained by filling the rest of each linac, for a total two-linac length of 28 km. The rf systems for 500 GeV c.m. consist of 4064 75 MW Periodic Permanent Magnet (PPM) klystrons arranged in groups of 8, followed by 2032 SLED-II rf pulse compression systems similar to those originally tested at the NLC Test Accelerator at SLAC in 1996. The 12,192 accelerator structures are of a damped-detuned design engineered to suppress deleterious higher-order modes. The structures are mounted on rigid but remotely movable girders. The bunch trains have 192 bunches, with a separation of 1.4 ns at a repetition rate of either 120 or 150 pulses per second. Design luminosity ranges between 20 and 30×10^{33} cm^{-2}s^{-1}, depending on repetition rate and final energy. If one decreases the beam currents by a factor of about 7, then an energy of 1.3 TeV c.m. may be obtained with a gradient of roughly 65 MV/m at a luminosity of about 5×10^{33} cm^{-2}s^{-1}.

CLIC

An overall schematic layout of the CLIC complex is shown in Figure 7. The main linac rf power is produced by decelerating a high-current (150 A) low-energy (2.1 GeV) drive beam (DB), shown in Figure 8. In the short (300 m), low-frequency DB accelerator, a long beam pulse is efficiently accelerated in fully loaded structures. With a delay loop and two combiner rings, this pulse is cut into short segments which are interleaved, simultaneously

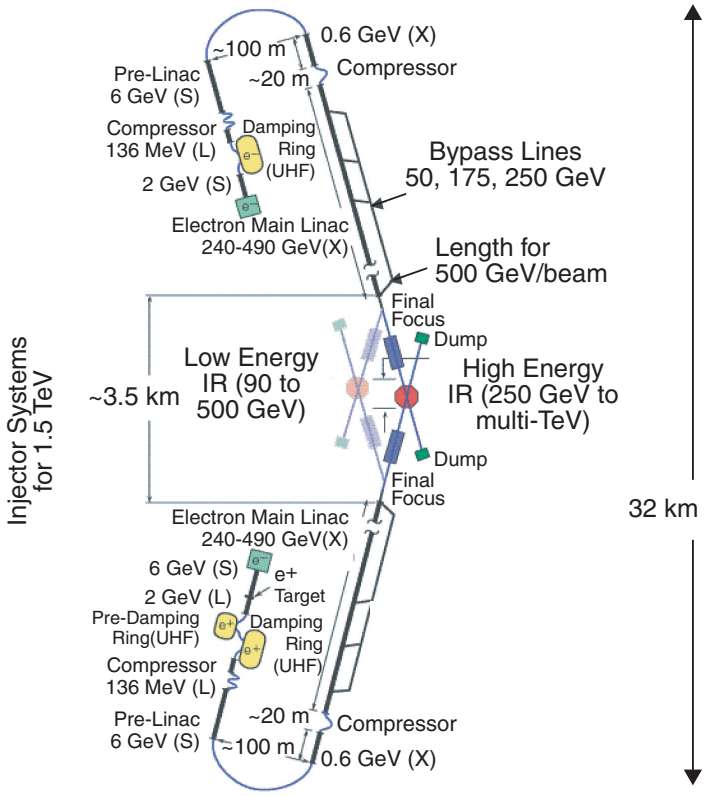

FIGURE 5. JLC-X/NLC layout

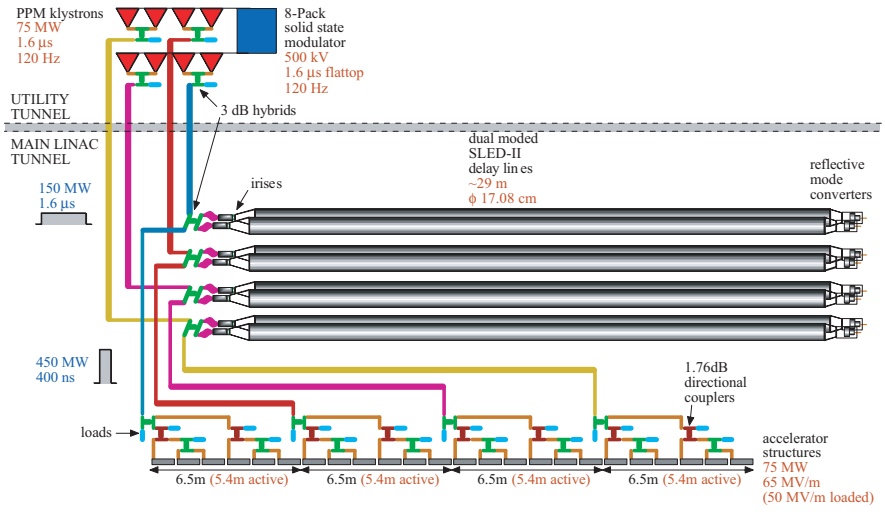

FIGURE 6. Schematic of a JLC-X/NLC linac rf unit (one of 254 per linac)

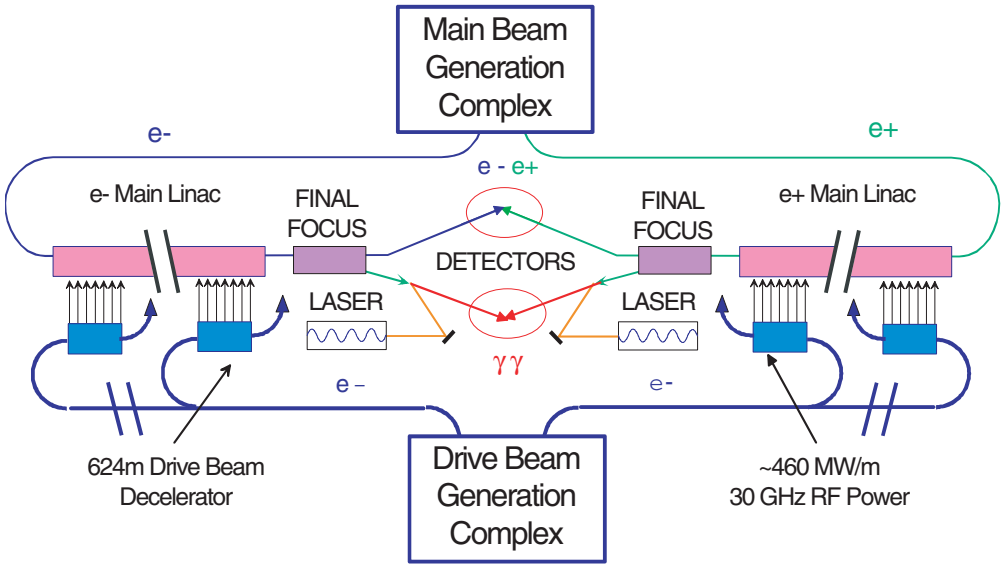

FIGURE 7. CLIC layout (two-linac length at 500 GeV c.m. is 5 km)

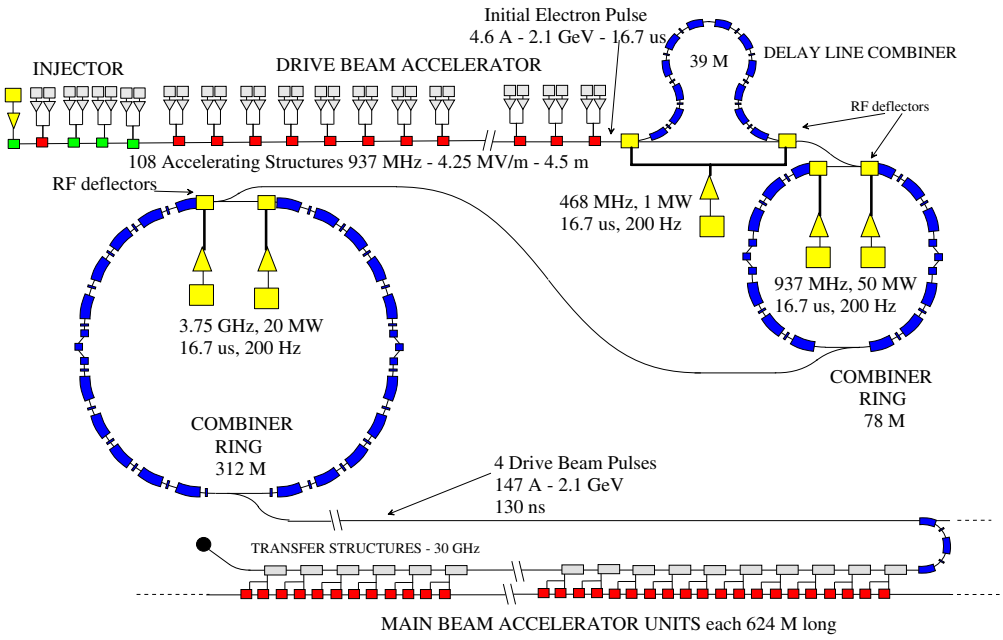

FIGURE 8. Drive-beam generation complex

increasing the pulse frequency and peak current. The resulting four beam pulses of 130 ns each are sent upstream where they are bent around to feed the four DB decelerators, which are parallel to the main linac in a common tunnel. Each of the 450 power-transfer structures of one decelerator produces the rf power feeding two main linac accelerator structures, each with 230 MW. The nominal accelerating gradient of 150 MV/m (corresponding to 172 MV/m unloaded gradient) has been achieved in short test structures without damping and with a pulse shorter by a factor of about 8 compared to the nominal pulse. The two-linac length (∼3600 structures per linac) is 5 km.

The main-beam and drive-beam generation is centralized in the middle of the collider. This layout allows the concentration of all the klystrons and modulators, making the maintenance easier and sharing the hardware for electron and positron production. The system is similar to that of JLC-X/NLC; it provides polarized or unpolarized electrons and unpolarized positrons. Different schemes to create polarized positrons are under study.

Upgrades up to 3 TeV c.m. can be obtained by adding more DB decelerators upstream on each side and by increasing the length of the pulse in the DB accelerator to obtain more DB trains after the combiner rings. The total length of the machine is 33 km at 3 TeV c.m. The main-beam injection complex and the DB generation remain the same except for the length of the 937 MHz klystron pulse.

The beam characteristics are found in Table 2. The repetition rate is 200 Hz at 500 GeV c.m. and 100 Hz at 3 TeV c.m. The bunch trains are 100 ns long with a bunch separation of 0.67 ns. Design luminosity goes from 21×10^{33} cm^{-2}s^{-1} at 500 GeV c.m. to 80×10^{33} cm^{-2}s^{-1} at 3 TeV c.m. Two detectors can be accommodated in CLIC. One of them may be used for $\gamma\gamma$ collisions (Figure 7). The beam delivery system is 2 × 2.6 km long. It is designed for 3 TeV c.m. but has a layout which can be kept unchanged at lower energies.

METHODOLOGY

As mentioned earlier, the assessments of the four linear colliders were carried out by three separate working groups, which in turn subdivided their tasks as follows:

1. Technology, RF Power and Energy Performance:
    - Injectors, Damping Rings and Beam Delivery
    - Power Sources (Klystrons, Power Supplies, Modulators and Low Level RF)
    - Power Distribution (RF Pulse Compression, Waveguides, Two-beam)
    - Accelerator Structures
2. Luminosity Performance
    - Electron and Positron Sources (up to Damping Rings)
    - Damping Rings
    - Low Emittance Transport (from Damping Rings to IP)
    - Machine Detector Interface

3. Reliability, Availability and Operability
    - Compilation of data from existing machines
    - Component reliability issues
    - Machine Protection Systems
    - Commissioning, tuning, and maintenance

The groups assessed their respective systems and topics for all machines, examining schedules and milestones for all the systems, large and small. They summarized their positive reactions as well as their concerns about all relevant design details, then translated their concerns into R&D topics and milestones required to mitigate these concerns. About 120 R&D issues were addressed. The ILC-TRC as a whole then ranked the R&D issues according to the following four criteria:

Ranking 1: R&D needed for feasibility demonstration of the machine

The objective of these R&D items is to show that the key machine parameters are not unrealistic. In particular, a proof of existence of the basic critical constituents of the machines should be available upon completion of the Ranking 1 R&D items.

Ranking 2: R&D needed to finalize design choices and ensure reliability of the machine

These R&D items should validate the design of the machine, in a broad sense. They address the anticipated difficulties in areas such as the architecture of the subsystems, beam physics and instabilities, and tolerances. A very important objective is also to examine the reliability and operability of the machine, given the very large number of components and their complexity.

Ranking 3: R&D needed before starting production of systems and components

These R&D items describe detailed studies needed to specify machine components before construction and to verify their adequacy with respect to beam parameters and operating procedures.

Ranking 4: R&D desirable for technical or cost optimization

In parallel to the main stream of R&D needed to build a linear collider, there should be other studies aimed at exploring alternative solutions or improving our understanding of the problems encountered. The results of the Ranking 4 R&D items are likely to be exploited for improved technical performance, energy upgrades, or cost reduction.

OVERALL ASSESSMENTS

- Upon studying all the machines, the ILC-TRC did not find any insurmountable obstacles to building TESLA, JLC-X/NLC, or JLC-C in the next few years and CLIC in a more distant future. This means that the ILC-TRC could not prove that any of these machines could not be built, given enough time, effort, and resources. The ILC-TRC also noted that the TESLA linac rf technology for 500 GeV c.m. is the most

mature. Having said this, the ILC-TRC found through the methodology described above that many R&D topics should still be addressed between now and the time any one of the machines reaches the final construction stage. Of the 120 R&D issues that were identified, about 40 issues were common to all machines (which could generate collaborations between various labs) and the remaining issues were distributed among individual machines.

- The ILC-TRC felt that insufficient funding is currently available to adequately advance the state of all the machines in parallel, a comment that should encourage international collaboration.

- The ILC-TRC also felt that several of the existing Test Facilities are not exploited as effectively as needed to accomplish the necessary R&D, either because of lack of resources or because they are shared with other users.

- Finally, the ILC-TRC felt that linear colliders of the proposed size and complexity require much greater attention to reliability, availability, and operability than has been given before, and that substantial R&D items, in particular those under R1 and R2 listed here, need to be urgently addressed to ensure that the design specifications can be reached and commissioning does not take too long.

RANKING OF RECOMMENDED R&D ISSUES

Specific concerns and assessments (which are described in great detail in Chapter 6, Chapter 7, and Chapter 8) resulted in targeted R&D tasks ranked in categories R1, R2, R3, and R4 listed in Chapter 9. Only R1 and R2 tasks are included here in the Executive Summary, both because of space and because they lead to important conclusions for the immediate future.

Ranking 1

TESLA Upgrade to 800 GeV c.m.

Energy

The Energy Working Group considers that a feasibility demonstration of the machine requires the proof of existence of the basic building blocks of the linacs. In the case of TESLA at 500 GeV, such demonstration requires in particular that s.c. cavities installed in a cryomodule be running at the design gradient of 23.8 MV/m. This has been practically demonstrated at TTF1 with cavities treated by chemical processing[1]. The other critical elements of a linac unit (multibeam klystron, modulator and power distribution) already exist.

- The feasibility demonstration of the TESLA energy upgrade to about 800 GeV requires that a cryomodule be assembled and tested at the design gradient of

[1]Knowing that electropolished cavities sustain significantly higher gradients than chemically polished cavities, there is little doubt that cryomodules running at about 24 MV/m can be built.

35 MV/m. The test should prove that quench rates and breakdowns, including couplers, are commensurate with the operational expectations. It should also show that dark currents at the design gradient are manageable, which means that several cavities should be assembled together in the cryomodule. Tests with electropolished cavities assembled in a cryomodule are foreseen in 2003.

JLC-C

Energy

- The proposed choke-mode structures have not been tested at high power yet. High power testing of structures and pulse compressors at the design parameters are needed for JLC-C. Tests are foreseen at KEK and at the SPring-8 facility in the next years.

JLC-X/NLC

Energy

- For JLC-X/NLC, the validation of the presently achieved performance (gradient and trip rates) of low group velocity structures—but with an acceptable average iris radius, dipole mode detuning and manifolds for damping—constitutes the most critical Ranking 1 R&D issue. Tests of structures with these features are foreseen in 2003.
- The other critical element of the rf system is the dual-moded SLED-II pulse compression system. Tests of its rf power and energy handling capability at JLC-X/NLC design levels are planned in 2003. As far as the 75 MW X-band PPM klystron is concerned, the Working Group considers the JLC-X PPM-2 klystron a proof of existence (although tested only at half the repetition rate). A similar comment can be made regarding the solid-state modulator tested at SLAC.

CLIC

Energy

- The presently tested CLIC structures have only been exposed to very short pulses (30 ns maximum) and were not equipped with wakefield damping. The first Ranking 1 R&D issue is to test the complete CLIC structures at the design gradient and with the design pulse length (130 ns). Tests with design pulse length and with undamped structures are foreseen when CTF3 is available (April 2004).
- The validation of the drive beam generation with a fully loaded linac is foreseen in CTF3. Beam dynamics issues and achieving the overall efficiency look challenging.

Reliability

- In the present CLIC design, an entire drive beam section must be turned off on any fault (in particular on any cavity fault). CLIC needs to develop a mechanism to turn off only a few structures in the event of a fault. At the time of writing this report, there is no specific R&D program aimed at that objective but possible schemes are being studied.

Ranking 2

TESLA

Energy

- To finalize the design choices and evaluate reliability issues it is important to fully test the basic building block of the linac. For TESLA, this means several cryomodules installed in their future machine environment, with all auxiliaries running, like pumps, controls, *etc.* The test should as much as possible simulate realistic machine operating conditions, with the proposed klystron, power distribution system and with beam. The cavities must be equipped with their final HOM couplers, and their relative alignment must be shown to be within requirements. The cryomodules must be run at or above their nominal field for long enough periods to realistically evaluate their quench and breakdown rates. This Ranking 2 R&D requirement also applies to the upgrade. Here, the objectives and time scale are obviously much more difficult.
- The development of a damping ring kicker with very fast rise and fall times is needed.

Luminosity

Damping Rings

- For the TESLA damping ring particle loss simulations, systematic and random multipole errors, and random wiggler errors must be included. Further dynamic aperture optimization of the rings is also needed.
- The energy and luminosity upgrade to 800 GeV will put tighter requirements on damping ring alignment tolerances, and on suppression of electron and ion instabilities in the rings. Further studies of these effects are required.

Machine-Detector Interface

- In the present TESLA design, the beams collide head-on in one of the IRs. The trade-offs between head-on and crossing-angle collisions must be reviewed, especially the implications of the present extraction-line design. Pending the outcome of this review, the possibility of eventually adopting a crossing-angle layout should be retained.

Reliability

- The TESLA single tunnel configuration appears to pose a significant reliability and operability risk because of the possible frequency of required linac accesses and the impact of these accesses on other systems, particularly the damping rings. TESLA needs a detailed analysis of the impact on operability resulting from a single tunnel.

JLC-C

Energy

- The klystrons and modulators should be tested successfully at the nominal 100 Hz repetition rate.
- This should lead to the full test of the linac subunit, with beam. This will include klystrons, modulator, pulse compression system, LLRF control and several structures in their future environment.

JLC-X/NLC

Energy

- There must be a full test of the JLC-X PPM klystron at the specified repetition rate of 120 or 150 Hz.
- These klystrons should be tested with the NLC modulator (at full specs and including arcing tests) and form part of a linac subunit test. The latter should also comprise the dual-moded SLED-II complete system, several damped and detuned structures, installed in the accelerator environment (with temperature control, for instance), and LLRF and controls systems. The test should be made with beam. The present plan is to perform this sort of test with a full girder of structures (some of them being detuned and damped) in 2004.

CLIC

Energy

- Present tests have demonstrated the advantages of tungsten and molybdenum irises in reaching the highest gradients in accelerator structures. These tests should be pursued, possibly also with other materials, for application to CLIC and possibly other machines.
- The very high power of the drive beam and its stability are serious concerns for CLIC. The drive beam stability should be validated, and the drive beam Machine Protection System, which is likely to be a complex system, should be designed to protect the decelerator structures.
- The test of a relevant linac subunit with beam is required. This is one of the purposes of CTF3, which should start operation in 2004.

- The validation of the proposed multibeam klystron performance is needed to finalize the design choices for the CLIC drive beam generation. This applies particularly to the 3 TeV energy upgrade (long pulse).

Luminosity

Low Emittance Transport

- Calculations of the effects of coherent synchrotron radiation on the CLIC bunch compressors must be performed.

Machine-Detector Interface

- An extraction line design for 3 TeV c.m. must be developed.

Items Common to All Machines

Luminosity

Damping Rings

- For all the damping ring designs, further simulation studies are needed to understand the magnitude of the electron cloud effects and to explore possible means of suppressing these effects. Experiments in existing rings are needed to test the electron cloud simulations. Possible cures for the electron cloud (including chamber coatings, superimposed magnetic fields, and gaps in the bunch pattern) need to be experimentally investigated.
- Further simulations of the fast ion instability are also necessary. Experiments in the ATF and other suitable rings are needed to test the predictions of these simulations.
- Damping ring extraction kicker stability, required at the level of $<10^{-3}$, is an important issue. Continued studies including experiments with the ATF double kicker system are needed.
- Finally, additional simulations of emittance correction in the damping rings are needed, including the effects listed in Section 7.2.3.2. Additional experiments in the ATF and other operating rings are needed to test the emittance correction algorithms.

Low Emittance Transport

- For all low emittance transport designs, the static tuning studies, including dynamic effects during correction, must be completed.
- The most critical beam instrumentation, including the intra-train luminosity monitor, must be developed, and an acceptable laser-wire profile monitor must be provided where needed in each design. A vigorous R&D program is mandatory for beam instrumentation in general; it would be appropriate for a collaborative effort between laboratories.
- A sufficiently detailed prototype of the main linac module (girder or cryomodule with quadrupole) must be developed to provide information about on-girder sources of vibration.

Reliability

- A detailed evaluation of critical subsystem reliability is needed to demonstrate that adequate redundancy is provided and that the assumed failure rate of individual components has been achieved.
- The performance of beam based tuning procedures to align magnets and structures must be demonstrated by complete simulations, in the presence of a wide variety of errors, both in the beam and in the components.

OVERALL IMPACT OF RELIABILITY ON PEAK AND INTEGRATED LUMINOSITY

As one looks at high energy particle colliders around the world, it is becoming increasingly clear that designing them for high peak luminosity is only part of the game. Designing for high integrated luminosity is just as essential. Both are crucial to keep up with the decrease of physical cross-sections with increasing c.m. energy.

The ILC-TRC spent considerable time and effort discussing the problem of reliability, availability, and operability, and the results of these discussions are summarized in Chapter 8. Much work has been done but much more is needed, regardless of which machine is selected. Unlike for storage rings, every pulse for a linear collider is a complete cycle from beginning to end. Experience with the SLC at SLAC from 1988 to 1998 showed that such a machine cannot reach its peak luminosity unless the hardware is reliable and machine tuning algorithms are highly automated. Without these conditions, the process of improving the luminosity does not converge. Furthermore, the major obstacles in running the SLC efficiently turned out to arise not from the linac rf system (which can be tested with prototypes), but from the damping rings, the positron source, the arcs, and the final focus. The future LC will not contain arcs but it will have long beam delivery systems with many collimators. None of these systems will be testable ahead of time in their entirety. Extrapolations to a linear collider that will be ten times as long and complex make these considerations even more stringent.

Even so, experience with existing accelerators (outlined in Section 8.3), can guide us by focusing on certain factors which are helpful in realistically estimating integrated luminosity. Four quantities, ST, HA, BE, and NL, are defined here.

ST is the total scheduled calendar time for the machine in a year.

HA is the fraction of time the machine hardware is available to produce beam. Hardware downtime includes both unscheduled repairs (when something critical breaks), scheduled repairs (either at regular intervals or when enough problems have accumulated), and all associated cooldown, warmup, and recovery times. For an accelerator, one must consider not only how long it takes to repair a failed component, but also the total time the beam is off because of the fault, including time lost due to access and the time taken to retune the beam.

BE is the effective fraction of beam time actually delivering luminosity. Beam inefficiencies include Machine Development (time spent studying and improving the accelerator),

the impact of tuning procedures, injection, and the luminosity decay during a store (for storage rings), Machine Protection trips and recovery (for linacs), and last but not least, the simple fact that accelerators do not manage to deliver the same luminosity on every pulse or for every store.

NL is the nominal luminosity during a particular run. It may be greater or less than the design luminosity, but it usually increases steadily as the accelerator becomes better understood. For a storage ring, it is the typical luminosity at the beginning of a store. For a linear collider, it is the luminosity when the beams are colliding well.

Multiplying these four quantities together yields the integrated luminosity. The reader may perform such a calculation by making his or her own guesses based on other machines such as those tabulated in Chapter 8 of the report. If, for example, one takes an ST of 6500 hours, an HA of 80% (perhaps somewhat optimistic), a BE of 80% (which includes 10% for Machine Development and 10% for all other inefficiencies), and a hypothetical NL of, say 10×10^{33} $\mathrm{cm}^{-2}\mathrm{s}^{-1}$, then one gets an integrated luminosity of 150 inverse femtobarns for that year.

The reader is cautioned not to take the above numbers as predictions, but rather to see this example as a reminder to the designers and builders of a linear collider of the importance of reliability, operability, and tunability. If the machine is to deliver its desired performance, the design must be robust, the hardware must be very reliable, the commissioning must proceed rapidly, and the luminosity must approach its design value as rapidly as possible.

ADDED VALUE OF THE ILC-TRC

The ILC-TRC in this report described all the machine designs, assessed them, and ranked the R&D tasks remaining to be done. In addition, the work of the ILC-TRC accomplished the following:

- By its studies, the ILC-TRC directly or indirectly caused significant changes in the various designs. Examples for TESLA and JLC-X/NLC can be found in Chapter 1.
- Perhaps the greatest collaborative contribution of the ILC-TRC was the advancement of beam dynamics simulations for the damping rings and especially for the so-called low emittance transport from the damping rings to the IP. The latter started with perfect machines, introduced static errors likely to exist upon installation, made corrections using Beam Based Alignment (BBA), then introduced dynamic errors from hypothetical ground motions and mechanical vibrations, and finally attempted to estimate luminosity in the presence of these effects. This effort is still a "work in progress" and a future task will be to verify that tuning algorithms still converge in the presence of all dynamic errors.
- Finally, as already seen, the ILC-TRC as a group came up with a significant number of R&D tasks which are common to all machines. These tasks will inevitably foment further collaborations as needs develop, and people and resources become available. How and which of these new collaborations will be formed beyond those which

already exist is a dynamic process that the ILC-TRC did not have time to prescribe. It is likely that these collaborations will develop naturally as needs arise in the coming years.

CONCLUDING REMARKS

Two years have gone by since ICFA requested this second ILC-TRC study. Producing the report has been an exciting and demanding task. The document is obviously not perfect, it is longer than originally planned, there are probably errors, and some of the conclusions may remain controversial and/or incomplete. Much technical work remains to be done, and the international HEP community also needs some time to set the stage for the next steps. These include the selection of a single technology for an international machine and the creation of world institutions that will be able to promote and execute such a large project.

As was mentioned in the Introduction, the charge to the ILC-TRC was to assess the current technical status of the machine designs at hand. It did not include the examination of costs nor the difficult step of technology selection. In spite of this, during the course of the study, many outsiders frequently asked the Chair how he thought the committee's work would help ICFA and the HEP community in the selection process. On this, the Chair cannot speak for the whole committee but he can make a few observations on the developments and choices that lie ahead:

- The timeline to accomplish the R1 tasks listed in this summary depends on a number of factors and varies from machine to machine. As mentioned earlier, TESLA and JLC-X/NLC at present have fairly mature conceptual designs and their main linac rf systems are undergoing intensive tests. The progress of JLC-C will depend on the developments at SPring-8 in Japan and that of CLIC on the developments at the test facilities at CERN.
  - TESLA has essentially demonstrated its main linac rf performance specifications for 500 GeV c.m. By the end of 2003, one will hopefully know if TESLA can reach 800 GeV c.m. by testing of the cryomodules at 35 MV/m.
  - By the end of 2003, one will also hopefully know if JLC-X/NLC can meet its main linac rf systems specifications (equally applicable to 500 GeV and 1 TeV c.m.).
  - JLC-C will conduct a partial test in 2003, comprising a modulator, klystron, and rf pulse compressor feeding one accelerator structure with gradients above the design value. A full rf unit is likely to be tested in 2004 or 2005.
  - By 2007, the results of the CLIC tests in CTF3 will become available, hopefully confirming the concept of drive beam generation and the nominal gradient in accelerator structures with the nominal rf pulse length.
- Assuming the above demonstrations of the TESLA and JLC-X/NLC subsystems are successful within the above schedule, by the beginning of 2004 the two machines will be on an equal footing from the point of view of their rf systems for the main linacs. If at that time the HEP community wanted to make a choice between these two

technologies, it could do so by weighing all the technical differences between the two machines and the challenges presented by the remaining R2 tasks. Besides their main linacs, this comparison should also include their injectors, positron sources, damping rings, beam delivery systems and interaction regions, as well as their energy reach, luminosity reach, reliability, and probably cost.

Whatever the international HEP community decides to do, the Chair wants to point out that the ILC-TRC brought together a sizeable group of the best linear collider experts in the world. The process taught them how to work as a team, let them be critical of each other's work in a constructive way, and helped them improve each other's designs by pooling their expertise. It is fair to say that there is no group in the world today that has a comparable global grasp of the respective strengths and weaknesses of the four machine designs. As the procedure to select a machine is put into place, the HEP community would be wise to continue to take advantage of this collective expertise. In particular, a mechanism should be found to vigorously pursue the beam dynamics simulations which the ILC-TRC started so successfully but was not able to complete within the time available. And independently of how the future unfolds, the ILC-TRC should have no doubt that through its hard and incisive work, it substantially advanced the cause of the linear collider and hopefully opened the door to its eventual realization somewhere in the world.

ACKNOWLEDGEMENTS

The Chair is most grateful for having had the opportunity of working with such a smart, argumentative, and congenial group of dedicated and hard-working physicists. The Chair also wishes to thank his assistant, Linda DuShane White, for her great help and support during this entire enterprise, Rebecca Reitmeyer for her outstanding job as Production Editor, and Terry Anderson for his contribution to the cover design.

Gregory A. Loew
February 7, 2003

CHAPTER 1

Steering Committee, Charge, Working Groups, Milestones, and Methodology

1.1 INTRODUCTION

The International Linear Collider Technical Review Committee (ILC-TRC) was originally created by the Interlaboratory Collaboration for R&D toward TeV-Scale Electron-Positron Linear Colliders at a meeting in London, England in June 1994. By the end of 1995, the ILC-TRC produced its first report[1] which attempted to gather in one document the current status of eight major electron-positron linear collider designs in the world. As each design progressed, large tables ("megatables") that listed all the major parameters of the machines in the report were updated regularly until the beginning of 2000. By that time, however, three of the original eight designs had been abandoned.

As a result of deliberations at the ICFA meeting of February 8 and 9, 2001 at DESY, Professor H. Sugawara as Chair of ICFA requested that the ILC-TRC reconvene its activities to produce a second report. G. Loew, the original chair of the ILC-TRC, agreed to conduct this second study.

1.2 STEERING COMMITTEE AND CHARGE

ICFA requested that a steering committee be formed with representation from the four major labs. The following members were chosen:

- Reinhard Brinkmann, from DESY
- Gilbert Guignard, from CERN
- Tor O. Raubenheimer, from SLAC
- Kaoru Yokoya, from KEK

[1] SLAC-R-95-471, available from Stanford Linear Accelerator Center, Technical Publications Department, 2575 Sand Hill Road, MS 68, Menlo Park, CA 94025.

The Chair and the full Steering Committee met for the first time at Snowmass, Colorado, on July 5, 2001. During this meeting, the committee reviewed the charge that had been broadly sketched by ICFA and converged on the approximate contents of the report to be produced. The charge was streamlined during the subsequent months, and the final version is summarized as follows:

SECOND ILC-TRC CHARGE:

- To assess the present technical status of the four LC designs at hand, and their potential for meeting the advertised parameters at 500 GeV c.m. Use common criteria, definitions, computer codes, *etc.*, for the assessments
- To assess the potential of each design for reaching higher energies above 500 GeV c.m.
- To establish, for each design, the R&D work that remains to be done in the next few years
- To suggest future areas of collaboration

The four machines to be assessed were:

- TESLA
- JLC-C
- JLC-X/NLC
- CLIC

The Steering Committee discussed in some detail how it would accomplish its tasks and decided that they should be divided into two major parts:

- Descriptions of these machines, their upgrade paths and respective test facilities, setting the foundations for the assessments
- Assessments of the machines as outlined by the charge

The Steering Committee took full responsibility for the first activity and decided that the assessments should be carried out by two separate Working Groups: one for Technology, RF Power, and Energy Performance, the other for Luminosity Performance.

The Chair submitted this proposed plan to ICFA in Rome, Italy on July 27, 2001, and Professor H. Sugawara soon thereafter indicated that ICFA had accepted the proposal.

1.3 WORKING GROUPS AND MILESTONES

From August through October 2001, the Chair and the Steering Committee discussed in great detail how they thought the two Working Groups should operate. This division of labor had the purpose of forming two separate teams of experts with different lines of specialization and complementary ways of assessing machine performance. As it turned out, this process worked out very successfully. Furthermore, during the course of their assessments, the Working Groups came to realize that a third task, common to both of them, would be crucial to the ultimate commissioning and successful operation of any of the linear colliders. This task was labelled "Reliability, Availability, and Operability," and several members of both Working Groups formed a third Working Group to handle this task.

The final overall organization of the Second ILC-TRC is shown in Table 1.1. Memberships of the three Working Groups are shown in Table 1.2, Table 1.3, and Table 1.4, together with the respective subgroups into which they broke up to assess the designs.

TABLE 1.1
Second ILC-TRC overall organization

Chair	Gregory Loew
Steering Committee	Reinhard Brinkmann Kaoru Yokoya Tor Raubenheimer Gilbert Guignard
Working Groups	
Technology, RF Power, and Energy Performance Assessments	Daniel Boussard
Luminosity Performance Assessments	Gerry Dugan
Reliability, Availability and Operability	Nan Phinney Ralph Pasquinelli

TABLE 1.2
Technology, RF Power, and Energy Working Group

Member Name	Institution
Chair: Daniel Boussard	Retired from CERN
Chris Adolphsen	SLAC
Hans H. Braun	CERN
YongHo Chin	KEK
Helen Edwards	FNAL
Kurt Hübner	CERN
Lutz Lilje	DESY
Pavel Logatchov	BINP
Ralph Pasquinelli	FNAL
Marc Ross	SLAC
Tsumoru Shintake	KEK
Nobu Toge	KEK
Hans Weise	DESY
Perry Wilson	SLAC

Subgroup	Group Name	Chair
1	Injectors, Damping Rings and Beam Delivery	Hans Weise
2	Power Sources (Klystrons, Power Supplies, Modulators and Low Level RF)	YongHo Chin
3	Power Distribution (RF Pulse Compression, Waveguides, Two-beam)	Kurt Hübner
4	Accelerator Structures	Perry Wilson

TABLE 1.3
Luminosity Performance Working Group

Member Name	Institution
Chair: Gerry Dugan	Cornell
Ralph Assmann	CERN
Winfried Decking	DESY
Jacques Gareyte	CERN
Witold Kozanecki	CEA Saclay
Kiyoshi Kubo	KEK
Nan Phinney	SLAC
Joe Rogers	Cornell
Daniel Schulte	CERN
Andrei Seryi	SLAC
Ronald Settles	MPI
Peter Tenenbaum	SLAC
Nick Walker	DESY
Andy Wolski	LBNL

Subgroup	Group Name	Chair
1	Electron and Positron Sources (up to Damping Rings)	Winfried Decking
2	Damping Rings	Joe Rogers
3	Low Emittance Transport (from Damping Rings to IP)	Daniel Schulte and Peter Tenenbaum
4	Machine Detector Interface	Witold Kozanecki

TABLE 1.4
Reliability, Availability, and Operability Working Group

Member Name	Institution
Co-chair: Nan Phinney	SLAC
Co-chair: Ralph Pasquinelli	FNAL
Chris Adolphsen	SLAC
Ralph Assmann	CERN
YongHo Chin	KEK
Helen Edwards	FNAL
Kurt Hübner	CERN
Witold Kozanecki	CEA Saclay
Marc Ross	SLAC
Tsumoru Shintake	KEK
Daniel Schulte	CERN
Peter Tenenbaum	SLAC
Nobu Toge	KEK
Nick Walker	DESY
Hans Weise	DESY

Table 1.5 is a record of the principal milestones and meetings of the ILC-TRC. A very large number of discussions and transactions were also conducted by e-mails and conference calls. The entire process resulted in the creation of strong bonds within the entire committee, congenial interactions, a good team spirit and a genuine desire to work toward a common goal.

TABLE 1.5
Major milestones and meetings

February 8–9, 2001	ICFA at its DESY meeting requests second ILC-TRC study and report
July 27, 2001	ILC-TRC Steering Committee is formed, and new proposal is submitted to ICFA in Rome. ICFA accepts proposal.
August–October 2001	Formation of the Working Groups
February 4–8, 2002	First review and discussion of Working Group tasks at LC 2002 (SLAC)
April 10–12, 2002	Second review (CERN)
June 7–9, 2002	Third review following EPAC (Paris)
July 30, 2002	Interim report to ICFA in Amsterdam
September 9–12, 2002	Fourth review (DESY)
October 9, 2002	Report to ICFA at CERN
February 2003	Completion of Report

1.4 CONTENTS AND METHODOLOGY

The Table of Contents for this report is fairly self-explanatory. The Executive Summary was written by the Chair, who incorporated numerous comments from the entire committee. Chapter 1, also written by the Chair, summarizes the ILC-TRC's procedures, organization, and milestones. T. Raubenheimer volunteered to be the central "keeper" responsible for putting together the six megatables given in Chapter 2. Chapter 3 on descriptions of the four machines at 500 GeV c.m., Chapter 4 on the upgrade paths to higher energies, and Chapter 5 on the test facilities and other project R&D programs, were written by the members of the Steering Committee for their respective projects. Chapter 6, 7, and 8, presenting the respective assessments of the three Working Groups, were assembled by their Chairs from text prepared by the Subgroup Chairs, with the help of their respective members. Finally, Chapter 9, which summarizes the lists and ranks of all the R&D studies still deemed necessary, was put together by D. Boussard and G. Dugan. It should be noted here that the Working Group members did not always agree with all the statements made by the machine proponents in Chapters 3, 4, and 5, and these disagreements are reflected in their assessments.

In discussing their assessments in Chapter 6, Chapter 7, and Chapter 8, the Working Groups expressed their positive reactions as well as their concerns regarding the status of a large number of issues and systems. Many of these concerns, in turn, were translated into

R&D topics which they felt are needed to allay these concerns. Toward the end of the ILC-TRC process, a critical effort went into ranking these R&D issues according to the following hierarchy of criteria:

Ranking 1: R&D needed for feasibility demonstration of the machine

Ranking 2: R&D needed to finalize design choices and ensure reliability of the machine

Ranking 3: R&D needed before starting production of systems and components

Ranking 4: R&D desirable for technical or cost optimization

A more complete description of these criteria as well as all the final R&D rankings are given in Chapter 9.

1.5 ADDED VALUE OF THE ILC-TRC

The ILC-TRC in this report described all the machine designs, assessed them, and ranked the R&D tasks remaining to be done. In addition, the work of the ILC-TRC accomplished the following:

1. It brought together a sizeable group of the best linear collider experts in the world and taught them how to work as a team, let them be critical of each other's work but in a constructive way, and helped them improve each other's designs by pooling their expertise. It is fair to say that there is no group in the world today that has a comparable global grasp of the respective strengths and weaknesses of the four machine designs.

2. By its studies, the ILC-TRC directly or indirectly caused significant changes in the various designs. Here are a few examples for TESLA and JLC-X/NLC:

   TESLA

   - The design pressure in the TESLA damping ring straight sections was reduced from 10^{-9} to 10^{-10} Torr to combat the fast ion instability.
   - The wiggler design for the damping ring was modified to reduce magnetic nonlinearities.
   - The spin rotator optics was redesigned.
   - Difficulties were flagged in the detector extraction line system for head-on collisions, prompting a possible redesign.

   JLC-X/NLC

   - Assessment of the complexity and probable delays caused by the necessary testing of the DLDS rf pulse compression system prompted SLAC and KEK to revert to a more modular dual-moded SLED-II system for the base line design.
   - The injection/extraction transport for the linac bypass line was redesigned to reduce synchrotron radiation and high-order dispersive emittance growth.

3. Perhaps the greatest collaborative contribution of the ILC-TRC was the advancement of beam dynamics simulations for the damping rings and especially for the so-called low emittance transport from the damping rings to the IP. The latter started with perfect machines, introduced static errors likely to exist upon installation, made corrections using Beam Based Alignment (BBA), then introduced dynamic errors from hypothetical ground motions and mechanical vibrations, and finally attempted to estimate luminosity in the presence of these effects. This effort is still a "work in progress" and a future task will be to verify that tuning algorithms still converge in the presence of all dynamic errors.

4. Finally, the ILC-TRC by working together came up with a large number of R&D tasks which are common to all machines. These tasks will inevitably foment further collaborations as needs develop, and people and resources become available. How and which of these new collaborations will be formed beyond those which already exist is a dynamic process that the ILC-TRC did not have time to prescribe. It is likely that these collaborations will develop naturally as needs arise in the coming years.

1.6 ACKNOWLEDGEMENTS

The ILC-TRC wishes to thank a large number of colleagues who were not official members of the committee but who provided considerable help:

From CEA Saclay: O. Napoly

From CERN: E. D'Amico, R. Corsini, E. Jensen, P. Pearce, L. Rinolfi, I. Syratchev, I. Wilson, W. Wuensch, F. Zimmermann

From DESY: D. Barber, S. Choroba, M. Ebert, J. Eckholt, K. Flöttmann, P. Schmüser

From FNAL: A. Drozhdin, N. Mokhov

From LBNL: M. Pivi

From SLAC: J. Cornuelle, P. Emma, L. Hendrickson, S. Hertzbach, L. Keller, R. Larsen, T. Lavine, T. Markiewicz, T. Maruyama, Y. Nosochkov, R. Pitthan, J. Sheppard, S. Tantawi, M. Woodley

From University of London: G. Blair

CHAPTER 2

The Megatables

Table 2.1, Table 2.2, Table 2.3, Table 2.4, Table 2.5, and Table 2.6 contain summary information for all the machines.

TABLE 2.1: Overall parameters

	TESLA		**JLC-C**		**JLC-X/NLC**[a]		**CLIC**	
Center of mass energy [GeV]	500	800	500	1000	500	1000	500	3000
RF frequency of main linac [GHz]	1.3		5.7	5.7/11.4[b]	11.4		30	
Design luminosity [10^{33} cm^{-2}s^{-1}]	34.0	58.0	14.1	25.0	25.0 (20.0)	25.0 (30.0)	21.0	80.0
Linac repetition rate [Hz]	5	4	100		150 (120)	100 (120)	200	100
Number of particles/bunch at IP [10^{10}]	2	1.4	0.75		0.75		0.4	
Number of bunches/pulse	2820	4886	192		192		154	
Bunch separation [nsec]	337	176	1.4		1.4		0.67	
Bunch train length [μsec]	950	860	0.267		0.267		0.102	
Beam power/beam [MW]	11.3	17.5	5.8	11.5	8.7 (6.9)	11.5 (13.8)	4.9	14.8
Unloaded/loaded gradient[c] [MV/m]	23.8 / 23.8[d]	35 / 35	41.8/31.5	41.8/31.5 / 70/55	65 / 50		172 / 150	
Total two-linac length [km]	30	30	17.1	29.2	13.8	27.6	5.0	28.0
Total beam delivery length [km]	3		3.7		3.7		5.2	
Proposed site length [km]	33		33		32		10.2	33.2
Total site AC power[e] [MW]	140	200	233	300	243 (195)	292 (350)	175	410
Tunnel configuration[f]	Single		Double		Double		Single	

[a]Numbers in ( ) for the JLC-X/NLC correspond to the NLC design with 120 Hz repetition rate.

[b]The 1 TeV JLC-C collider uses a C-band rf system for the first 200 GeV of each linac followed by an X-band rf system for the remaining 300 GeV of acceleration—the X-band rf system would be identical to that described for the JLC-X band collider.

[c]The main linac loaded gradient includes the effect of single-bunch (all modes) and multibunch beam loading, assuming that the bunches ride on crest. Beam loading is based on bunch charges in the linacs, which are slightly higher than at the IP.

[d]With the present site layout for TESLA, 23.4 MV/m was the required energy gain per meter of accelerator structure. A detailed analysis by the ILC-TRC revealed that the gradient has to be increased to 23.8 MV/m when rf phasing, especially for BNS damping, is taken into account.

[e]Total site power includes AC for linac rf and cooling systems as well as power for all other beam lines and site facilities.

[f]The single tunnel layout has both the klystrons and accelerator structures in the main linac tunnel while the double tunnel layout places the klystrons and modulators in a separate enclosure. In the CLIC scheme, the main linac uses a single tunnel since there are no klystrons or modulators associated with it. However, the 300 m-long CLIC drive beam accelerator has a double tunnel layout.

TABLE 2.2: Linear colliders: electron and positron sources

	TESLA		**JLC-C**		**JLC-X/NLC**[a]		**CLIC**	
	500 GeV	800 GeV	500 GeV	1000 GeV	500 GeV	1000 GeV	500 GeV	3000 GeV
Repetition Rate [Hz]	5	4	Same as JLC-X/NLC		150 (120)	100 (120)	200	100
Number of bunches/train	2820	4886			192		154	
Bunch spacing [ns]	337	176			1.4		0.67	
Electron Source								
Style	Subharm. buncher				Subharm. buncher		Subharm. buncher	
e^- beam energy[b] [GeV]	0.5				0.08		0.2	
Number particles/bunch [10^{10}]	2.3				0.8		0.625	
Polarization [%]	80				80		75	
Emittance [rms] $\gamma\varepsilon_x$ / $\gamma\varepsilon_y$ [μm·rad]	40 / 40				100 / 100		7	
Bunch length Δz_{FWHM} [mm]	8				10		7	
Bunch energy spread $\Delta E/E_{FWHM}$ (%)	1				2		2	
Positron Source								
Style	Undulator				Conv. target		Conv. target	
e^+ beam energy[b] [GeV]	0.29				0.250		0.2	
Number particles/bunch [10^{10}]	2.0	1.4			0.9		0.84	
Polarization [%]	0				0		0	
Emittance [edge] $\gamma\varepsilon_x$ / $\gamma\varepsilon_y$[c] [μm·rad]	14,000				30,000 / 30,000		90,000 / 90,000	
Bunch length Δz_{FWHM} [mm]	5				15		7	
Bunch energy spread $\Delta E/E_{FWHM}$ [%]	7				15		10	
Incident beam energy [GeV]	250–150				6.2		2	
Target material / thickness [r.l.]	Ti / 0.4				WRe / 4		WRe / 4	
Number of targets	1				3		1	
Incident beam spot size [mm]	0.7				1.6		2	
Yield at damping ring[d] [e^+ / e^-]	2 at 500 GeV / 1 at 300 GeV				>1		0.7	

[a]Numbers in ( ) correspond to US site with 120 Hz repetition rate.

[b]Beam energy is given at the end of the injector system.

[c]Positron emittance is listed as the 'edge' emittance although the TESLA design specifies an rms value—the edge emittance listed is 1.4 times the specified rms value for TESLA.

[d]Yield is evaluated as number of captured e^+ at the system exit or in the damping ring versus number of incident e^-.

TABLE 2.3: Damping rings

	TESLA		**JLC-C**		**JLC-X/NLC**[a]		**CLIC**	
	500 GeV	800 GeV	500 GeV	1000 GeV	500 GeV	1000 GeV	500 GeV	3000 GeV
Damping Ring Systems								
Damping ring complex energy [GeV]	5		Same as JLC-X/NLC		1.98		2.424	
Number of rings in complex	2				3		3	
Number of bunches/train	2820	4886			192		154	
Number of particles/bunch [10^{10}]	2	1.4			0.8		0.42	
Bunch spacing [ns]	20	11.5			1.4		0.66	
Injected beam emit.[b] $\gamma\epsilon_{e+}$ / $\gamma\epsilon_{e-}$ [μm·rad]	14,000 / 40				45,000 / 150		10	
Extr. beam emit.[b] $\gamma\varepsilon_x$ / $\gamma\varepsilon_y$ [μm·rad]	8.0 / 0.020	6.0 / 0.010			3.0 / 0.020		1.6 / 0.005	0.45 / 0.003
Positron (Pre-)Damping Rings[c]								
Ring circumference [m]	17,000				231		No design	
Number of trains stored	1				2			
RF frequency & voltage [MHz/MV]	500 / 54				714 / 1.5			
Wiggler length [m]	432				50			
Damping times ($\tau_x/\tau_y/\tau_z$) [ms]	28 / 28 / 14				5.8 / 5.8 / 2.9			
Tunes ($\nu_x/\nu_y/\nu_z$)	72.28 / 44.18 / 0.100				11.45 / 5.45 / 0.011			
Bunch len. σ_z & energy spr. $\frac{\sigma_E}{E}$ [mm / %]	6.0 / 0.13				5.1 / 0.08			
Equil. beam emit. $\gamma\varepsilon_x$ / $\gamma\varepsilon_y$ [μm·rad]	8.0 / 0.014	6.0 / 0.010			30 / 30			
Electron Damping Ring[d]								
Ring circumference [m]	17,000				300		375	
Number of trains stored	1				3		9	
RF frequency & voltage [MHz/MV]	500 / 34				714 / 1.1		1500	
Wiggler length [m]	284				46		158	
Damping times ($\tau_x/\tau_y/\tau_z$) [ms]	44 / 44 / 22				4.8 / 5.0 / 2.6		2.7 / 2.7 / 1.4	
Tunes ($\nu_x/\nu_y/\nu_z$)	72.28 / 44.18 / 0.10				27.26 / 11.13 / 0.004		69.21 / 29.63 / 0.004	
Bunch len. σ_z & energy spr. $\frac{\sigma_E}{E}$ [mm / %]	6.0 / 0.10				3.6 / 0.09		1.3 / 0.14	
Equil. beam emit. $\gamma\varepsilon_x$ / $\gamma\varepsilon_y$ [μm·rad]	8.0 / 0.014	6.0 / 0.010			2.2 / 0.013		0.62 / 0.007	

[a]Numbers in table correspond to NLC damping ring designs with 120 Hz repetition rate.

[b]Injected emittances are assumed round but different for e^+ and e^- while extracted emittances are equal for e^+ and e^- but asymmetric. All emittances are rms values except the injected positron emittance which is the 'edge' emittance although the TESLA design specifies an rms value—the edge emittance listed is 1.4 times the specified rms value for TESLA.

[c]Positron Ring table describes TESLA e^+ ring and JLC-X/NLC/CLIC positron pre-damping rings.

[d]Electron Ring table describes TESLA e^- ring and JLC-X/NLC/CLIC electron and positron main damping rings.

TABLE 2.4: Pre-linacs and bunch compressors

	TESLA		**JLC-C**		**JLC-X/NLC**[a]		**CLIC**	
	500 GeV	800 GeV	500 GeV	1000 GeV	500 GeV	1000 GeV	500 GeV	3000 GeV
Electron booster linac (e^- source → damping rings)								
Initial and final energy [GeV]	0.5 / 5.0		Same as JLC-X/NLC		0.08 / 1.98		0.2 / 2.424	
RF frequency [GHz]	1.3				2.8		1.5	
Unloaded and loaded gradient[b] [MV/m]	20.0 / 20.0				19.3 / 16.2		21.0 / 17.0	
Total length [m]	305				164		150	
Positron booster linac (e^+ source → damping rings)								
Initial and final energy [GeV]	0.29 / 5.0				0.25 / 1.98		0.2 / 2.424	
RF frequency [GHz]	1.3				1.4		1.5	
Unloaded and loaded gradient[b] [MV/m]	20.0 / 20.0				14.1 / 12.5		21.0 / 17.0	
Total length [m]	400				164		150	
First stage bunch compressor								
Initial and final bunch length [mm]	6.0 / 0.3				4.0 / 0.5		1.3 / 0.33	
Initial and final energy spread [%]	0.13 / 2.7				0.09 / 1.0		0.13 / 0.54	
RF frequency [GHz]	1.3				1.4		3	
RF voltage [MV]	890				139		154	
Total length [m]	400				51		80	
Pre-linac (damping rings → 2nd bunch compressor)								
Initial and final energy [GeV]	Not needed				1.98 / 8.0		2.424 / 9.0	
RF frequency [GHz]					2.8		3	
Unloaded and loaded gradient[b] [MV/m]					19.3 / 16.8		26.0 / 21.0	
Total length [m]					485		360	
Second stage bunch compressor								
Initial and final bunch length [mm]	Not needed				0.5 / 0.11		0.33 / 0.035	
Initial and final energy spread [%]					0.25 / 1.5		0.14 / 1.36	
RF frequency [GHz]					11.4		30	
RF voltage [MV]					583		592	
Total length [m]					212		90	

[a]Numbers in table correspond to NLC design with a 120 Hz repetition rate.

[b]The linac loaded gradient includes the effect of single-bunch (all modes) and multibunch beam loading, assuming that the bunches ride on crest. Beam loading is based on bunch charges in the linacs, which might be slightly higher than at the IP.

TABLE 2.5: Main linac parameters

	TESLA		**JLC-C**		**JLC-X/NLC**[a]		**CLIC**	
	500 GeV	800 GeV	500 GeV	1000 GeV[b]	500 GeV	1000 GeV	500 GeV	3000 GeV
Initial Energy [GeV]	5.0		8.0		8.0		9.0	
RF frequency [GHz]	1.3		5.7	5.7/11.4	11.4		30	
Unloaded/loaded[c] gradient [MV/m]	23.8 / 23.8[d]	35 / 35	41.8 / 31.5		65 / 50		172 / 150	
Overhead for fdbk & repair [%]	2		0		5		6	6
Overhead for off-crest operation [%]	0.4		0		5		7	5
Active two-linac length [km]	21.6	23	15.4	12.2/12.5	11.1	22.4	3.6	22.0
Total two-linac length [km]	30	30	17.1	29.2	13.8	27.6	5.0	28.0
Total number of klystrons	572	1212	4276	3392/4640	4064	8256	448	
Total number of modulators	572	1212	4276	3392/580	508	1032	448	
Klystron peak power [MW]	9.7		50	50/75	75		50	
Klystron repetition rate [Hz]	5	4	100	100	150 (120)	100 (120)	200	100
Klystron pulse length [μsec]	1370		2.8	2.8/1.6	1.6		16.7	92
Pulse compression ratio	1		5	5/4	4		32×4	32×22
Pulse compression gain	1		3.6	3.6/3.4	3.0		32×4	32×22
RF pulse length at linac [μsec]	1370		0.55	0.55/0.40	0.40		0.13	0.13
Number of sections	20592	21816	8552	6784/13920	12192	24768	7272	44000
Section length [m]	1.04		1.8		0.9		0.5	
a/λ (range if applicable)	0.15		0.171–0.126		0.210–0.148		0.225–0.175	
v_g/c [%]	—		3.6–1.1		5.1–1.1		10.4–5.2	
Filling time [ns]	4.2×10^5	5.1×10^5	285		120		30	
Q Unloaded	10^{10}		9772		9055–8093		3628–3621	
Shunt impedance [MΩ/m]	10^7		54.1		81.2		20.2–27.1	
Total AC power for linacs[e] [MW]	95	160	175	280	188 (150)	254 (305)	105	319
Wall plug $\rightarrow$ Rf efficiency [%]	37.3		24.1	26	28.0		40.3	
RF $\rightarrow$ beam efficiency [%]	62.4	56.5	25.9	28.7	31.5		23.1	

[a]Numbers in ( ) for the JLC-X/NLC correspond to the NLC design with 120 Hz repetition rate.

[b]The 1 TeV JLC-C collider uses a C-band rf system for the first 200 GeV of each linac followed by an X-band rf system for the remaining 300 GeV of acceleration—the X-band rf system would be identical to that described for the JLC-X band collider. Numbers in the table that are missing are simply found from values in the JLC-C (500) and the JLC-X (500) columns.

[c]The main linac loaded gradient includes the effect of single-bunch (all modes) and multibunch beam loading, assuming that the bunches ride on crest. Beam loading is based on bunch charges in the linacs, which are slightly higher than at the IP.

[d]With the present site layout for TESLA, 23.4 MV/m was the required energy gain per meter of accelerator structure. A detailed analysis by the ILC-TRC revealed that the gradient has to be increased to 23.8 MV/m when rf phasing, especially for BNS damping, is taken into account.

[e]Total AC power includes power for the cryo-plant in a superconducting facility and it includes power for cooling water in a normal conducting facility. It does not include power for distribution and it does not include power for magnets, movers, instrumentation or lighting.

TABLE 2.6: Linear colliders: beam delivery system and interaction point parameters

	TESLA		**JLC-C**		**JLC-X/NLC**[a]		**CLIC**	
	500 GeV	800 GeV	500 GeV	1000 GeV	500 GeV	1000 GeV	500 GeV	3000 GeV
Beam delivery system length[b] [km]	3.2		3.8		3.8		5.2	
Collimation system length[b] [km]	1.4		1.4		1.4		4.1	
Final Focus system length[b] [km]	1.2		1.6		1.6		1.1	
$\gamma\varepsilon_x^*$ / $\gamma\varepsilon_y^*$ [m·rad $\times 10^{-6}$]	10 / 0.03	8 / 0.015	3.6 / 0.04		3.6 / 0.04		2.0 / 0.01	0.68 / 0.01
$\beta_x^\star$ / β_y^* [mm]	15 / 0.40	15 / 0.40	8 / 0.20	13 / 0.11	8 / 0.11	13 / 0.11	10 / 0.05	16 / 0.07
$\sigma_x^\star$ / σ_y^* before pinch[c] [nm]	554 / 5.0	392 / 2.8	243 / 4.0	219 / 2.1	243 / 3.0	219 / 2.1	202 / 1.2	60 / 0.7
$\sigma_z^\star$ [μm]	300		200	110	110		35	
$\sigma^\star_{\Delta E/E}$[d] [%]	0.14 / 0.04		0.25		0.25		0.25	0.35
Distance between IP and last quad	3.0		4	3.5	3.5		4.3	
Crossing Angle at IP [mrad]	0		7		7 (20)		20	
Disruptions D_x / D_y	0.23 / 25.3	0.20 / 28.0	0.29 / 17.5	0.10 / 10.3	0.16 / 13.1	0.10 / 10.3	0.04 / 6.4	0.07 / 6.3
Υ_0	0.05	0.09	0.07	0.28	0.13	0.28	0.25	5.0
δ_B [%]	3.2	4.3	3.4	7.5	4.6	7.5	4.4	21.1
n_γ [number of γs per e]	1.56	1.51	1.36	1.30	1.26	1.30	0.75	1.53
$N_{\rm pairs}(p_T^{\rm min} = 20$ MeV/c, $\Theta_{\rm min} = 0.2)$	39.4	37.3	10.7	15.0	11.9	15.0	7.2	43
$N_{\rm hadron\ events}$/crossing	0.248	0.399	0.075	0.270	0.103	0.270	0.066	2.26
$N_{\rm jets} \times 10^{-2}$ [$p_T^{\rm min} = 3.2$ GeV/c]	0.74	1.90	0.23	2.27	0.36	2.72	0.29	150.5
Geometric Luminosity[e] [10^{33} cm^{-2}s^{-1}]	16.4	28.1	8.76	18.5	17.7 (14.2)	18.5 (22.2)	16.0	47.0
H_D	2.11	1.90	1.61	1.42	1.49	1.42	1.42	1.70
Luminosity dilution for tuning [%]	0		5		5		10	0
Peak Luminosity[e] [10^{33} cm^{-2}s^{-1}]	34.5	53.4	13.6	24.9	25.1 (20.1)	25.0 (30.0)	21.0	80.0
$L_{99\%}$ [%]	66	62	67	58	64	58	71	41
$L_{95\%}$ [%]	91	86	90	86	85	77	87	53
$L_{90\%}$ [%]	98	95	97	87	94	87	93	62

[a]Numbers in ( ) correspond to US site with 120 Hz repetition rate.

[b]System length includes both incoming beamlines.

[c]For all designs except CLIC, the IP spot sizes are calculated as usual from the emittances and beta functions. With the design emittances in CLIC, nonlinear aberrations in the final focus system increase the final spot size by 20 to 40%.

[d]Energy spread is for electrons / positrons if different.

[e]For the sake of uniformity, the geometric luminosity is simply defined as $N^2/4\pi\,\sigma_x^*\sigma_y^*$ times the number of crossings per second, and in all cases assumes head-on collisions, no hour-glass effect and no pinch. The peak luminosity is calculated using the Guinea Pig program and incorporates all the effects, including the pinch enhancement, hour-glass, and crossing angle where applicable, plus any additional IP dilutions that may be expected.

CHAPTER 3

Descriptions of the Four Machines at 500 GeV c.m.

3.1 TESLA

3.1.1 Overview

3.1.1.1 Introduction

The design work and technical R&D for a next generation linear collider based on superconducting technology began in 1992 and is performed by a broad international collaboration, with DESY in Hamburg being the coordinating laboratory. At present, the TESLA collaboration has more than 40 member institutes from 10 countries. The complete layout of the TESLA facility is described in a technical report published in 2001 [1], which includes an update of the earlier design study [2], an estimate of the cost and construction schedule, and a description of the proposed TESLA site next to the DESY laboratory.

TESLA uses 9-cell niobium cavities (Figure 3.1) cooled by superfluid Helium to $T = 2$ K and operating at L-band frequency (1.3 GHz). The design gradient at $E_{cm} = 500$ GeV is $E_{acc} = 23.8$ MV/m and the quality factor $Q_0 = 10^{10}$. Because the power dissipation in the cavity walls is extremely small, the accelerating field can be produced with long, low peak power rf pulses; this results in a high rf to beam power transfer efficiency, allowing a high average beam power while keeping the electrical power consumption within acceptable limits ($\sim$100 MW).

The relatively low frequency of the TESLA linac is beneficial for accelerating and *conserving* ultra-small emittance beams. As a result, the emittance dilution can be reduced to acceptable levels in TESLA using relatively relaxed alignment tolerances for the linac components (see Section 3.1.3).

The choice of superconducting rf also permits to use a long rf pulse (1 ms) and a relatively large bunch spacing (337 ns at E_{cm}=500 GeV). Three benefits result directly from this long bunch train:

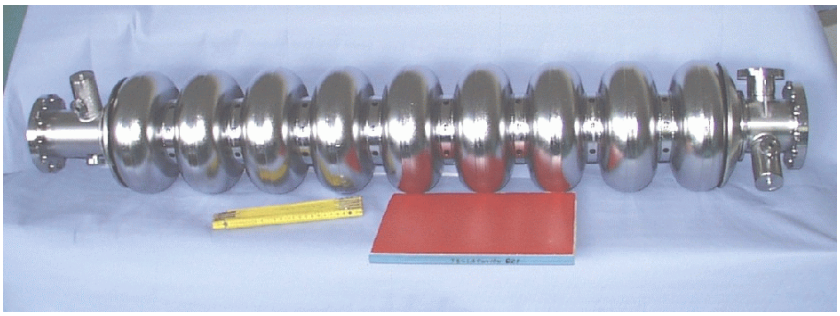

FIGURE 3.1. The 9-cell niobium cavity for TESLA.

- A fast (MHz) bunch-to-bunch feedback can be used to correct the orbit within one beam pulse. Such a feedback system will maintain the beams in collision at the IP, making TESLA relatively insensitive to mechanical vibrations which could otherwise lead to serious luminosity reduction.
- A head-on (zero crossing-angle) collision scheme can be used, with large-aperture superconducting quadrupoles in the interaction region.
- In the event of an emergency, a fast safety system can "turn off" the beam within a fraction of a pulse.

The potential benefits of superconducting rf summarized previously have been acknowledged since the beginning of linear collider R&D. However, in the early 1990s when the R&D program was launched at the TESLA Test Facility (TTF), the projected costs based on existing superconducting rf installations were considered too high. The main challenge for TESLA, therefore, was a reduction in the cost per unit accelerating voltage by a large factor. The approach adopted to reduce the cost was to:

- Increase the achievable gradients available at that time (5–8 MV/m) by about a factor of 4
- Reduce the cost per unit length of the superconducting structures by a similar factor

The achievements during the first phase of the TTF program are summarized in Section 3.1.2. To date, more than seventy 9-cell cavities have been processed and tested. The results show that a gradient of about 25 MV/m is feasible with a reliability sufficient for large scale industrial production. Furthermore, the integrated system test performed in the TTF linac demonstrated beam acceleration with parameters close to the TESLA-500 design goal.

Further progress on the cavity performance has recently been obtained by applying electropolishing to the niobium surface. Test results with single-cell resonators repeatedly show gradients above 30 MV/m. The best single-cell performance obtained to date is E_{acc}=42 MV/m. First results for 9-cell electropolished cavities also show gradients well

above 30 MV/m. We are therefore confident that the cavities in the TESLA linac will be able to operate at a gradient above 30 MV/m, allowing a significant increase in the achievable center-of-mass energy.

On the basis of industrial studies, a cost estimate for the superconducting linac and all other main subsystems of the collider has been worked out and published in March 2001 as part of the Technical Design Report. The total investment cost amounts to 3,136 million Euro, out of which 1,131 million Euro are for the superconducting accelerator modules. This latter figure is well in accord with the original cost goal of US$2,000 per MV of accelerating voltage.

3.1.1.2 General Layout and Parameters

A sketch of the overall layout of the TESLA linear collider is shown in Figure 3.2. The figure also indicates schematically the X-ray Free Electron Laser Facility, which is an integral part of the proposed TESLA facility. Since the impact of the FEL integration on the collider design and performance is, if any, very small and the FEL itself is not of concern for this report, it will not be considered further in the following.

The baseline design for the TESLA linear collider has a single interaction region with head-on collisions (Section 3.1.5). As indicated in Figure 3.2 an optional second IR with crossing angle is foreseen. The crossing angle permits using this IR for photon-photon collisions, as described in Appendix 1, part-VI of the TDR. The beam switchyard for the second IR is included in the baseline layout for the delivery system.

The positron source makes use of an elegant scheme originally proposed at Novosibirsk. Positrons are produced from γ-conversion in a thin target (Section 3.1.4), after which they are preaccelerated in a conventional 200 MeV L-band linac, followed by a 5 GeV superconducting accelerator. The photons are generated by passing the high-energy electron beam through an undulator placed after the main linac, before transporting the beam to the IP.

The electron beam is generated in a polarized laser-driven gun (Section 3.1.4). After a short section of conventional linac, the beam is accelerated to 5 GeV in superconducting structures identical to the ones used for the main linac. The baseline design assumes that the electrons are stored in a damping ring very similar to the one required for the positron beam. The possibility of replacing the electron ring by a flat-beam low emittance electron gun is presently under study.

The positron beam is injected into the damping ring at an energy of 5 GeV. The bunch train is stored in the ring in a compressed mode, with the bunch spacing reduced by about a factor of 16; even with this compression, a large ring circumference of about 17 km is still required. To avoid building an additional large ring tunnel, a so-called “dog-bone” design is used (Section 3.1.4). The layout has two 8 km straight sections placed entirely in the main linac tunnel; additional tunnels are only required for the 1 km circumference loops at either end.

The two main linear accelerators (Section 3.1.3) are each constructed from roughly ten-thousand one-meter long superconducting cavities. Groups of twelve cavities are installed in a common cryostat (cryomodule); the current design is based on that used in the TTF, modified to be slightly more compact. The cryomodules also contain

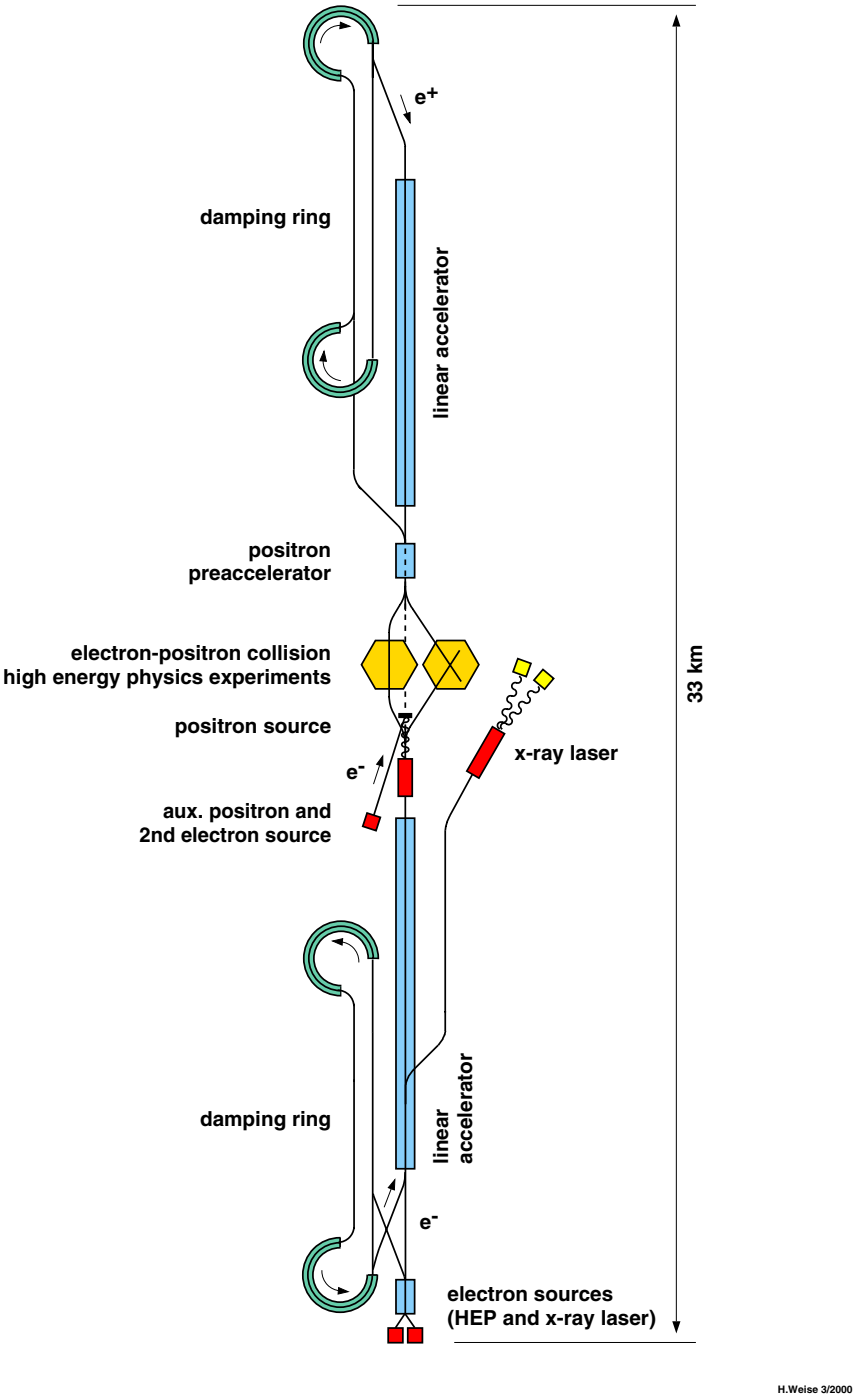

FIGURE 3.2. Sketch of the overall layout of TESLA.

superconducting magnets for beam focusing and steering, beam position monitors, and higher-order mode absorbers.

The rf power is generated by some 300 klystrons per linac, each feeding 36 9-cell cavities. The required ∼10 MW peak power per klystron includes a 10% overhead for correcting phase errors during the beam pulse which arise from Lorentz force detuning and microphonics. The high-voltage pulses for the klystrons are provided by conventional modulators.

The cryogenic system for the TESLA linac is comparable in size and complexity to the one currently under construction for the LHC at CERN. Seven cryogenic plants are foreseen, each one serving a ∼5 km long linac subsection. The cooling capacity of the first section of the electron linac is increased to accommodate the higher load from the additional FEL beam pulses.

The beam delivery system between the linac and the IP (Section 3.1.5) consists of collimation, beam diagnostics and correction, and final focus sections. The design of the final focus system is essentially the same as the Final Focus Test Beam (FFTB) system successfully tested at SLAC. Beam size demagnification and chromatic corrections for the TESLA design parameters are no more ambitious than at the FFTB. The beams can be kept in collision at the IP to a high precision by using a fast bunch-to-bunch feedback, which measures and corrects the beam-beam offset and crossing angle on a time scale small compared to the beam pulse length. The design of the beam delivery system is optimized for a single head-on interaction point. The complete system of ∼3.3 km will fit into a straight tunnel between the linacs. All the magnet systems and beamline geometry are designed to allow an upgrade to a beam energy of 400 GeV. As previously mentioned, a second IR with a 34 mrad crossing angle is also foreseen, which could be used for $\gamma\gamma$ or $e^-\gamma$ collisions. On the electron linac side, care has been taken to place the positron source (undulator) upstream of the beam switchyard, so as not to exclude the possibility of e^+e^- collisions at the second IR.

The two linear accelerators as well as the beam delivery system will be installed in an underground tunnel of 5 m diameter (see Figure 3.3). A 2000 m^2 experimental hall is foreseen to house the detector; the hall can be extended to house a second detector should the second IR be constructed. Seven additional surface halls are required for the cryogenic plants, spaced at intervals of about 5 km along the linacs, and are connected to the underground tunnel by access shafts. The halls will also contain the modulators which generate the HV pulses for the klystrons. The pulse transformers are placed in the tunnel close to the klystrons; the long cables required to connect the modulators to the transformers contribute a few percent to the total power losses, but it is an advantage to allow access to the modulators for maintenance during machine operation. Exchange of klystrons, however, will require an interruption of the machine operation: with an energy overhead of 2% foreseen in the design, and assuming an average klystron lifetime of 40,000 hr, maintenance breaks of one day every few weeks will be necessary.

Within the TESLA collaboration there is broad agreement that the facility should be constructed at an existing High Energy Physics laboratory to reduce project costs and construction time. Both DESY and FNAL have been considered as possible sites. DESY as the coordinating laboratory in the collaboration has taken over the task of working out a detailed plan for the TESLA site North-West of the DESY laboratory. In this scenario, the

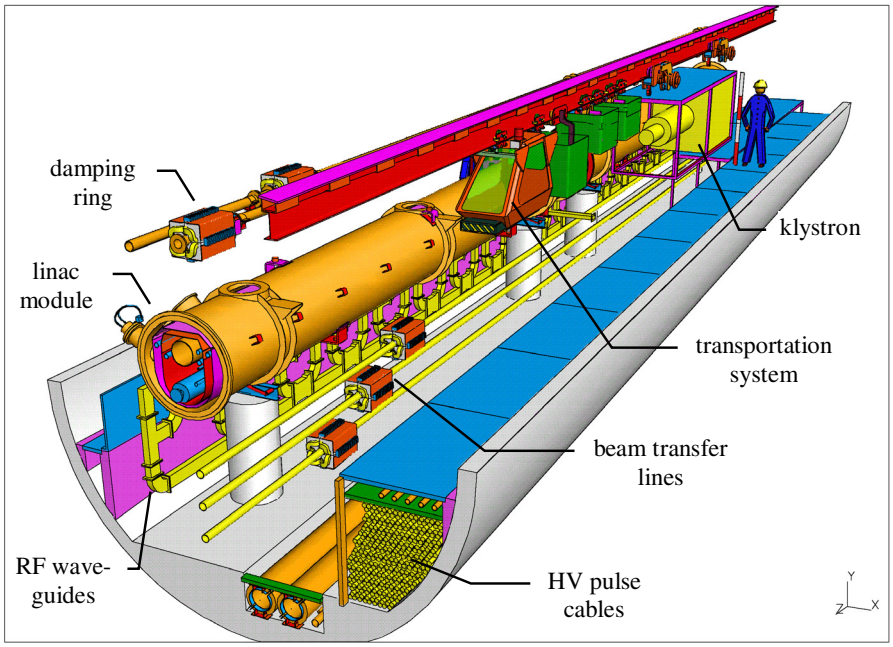

FIGURE 3.3. Sketch of the 5 m diameter TESLA linac tunnel.

linac tunnel starts at the DESY site in a direction tangential to the west straight section of HERA, so as not to exclude an electron-proton linac-ring collider option. The central area is situated about 16 km from the DESY site in a rural part of the North German state (Bundesland) of Schleswig-Holstein, and accommodates both the collider detector hall for Particle Physics and the FEL radiation user facility.

3.1.1.3 Parameters for 500 GeV

Besides the center-of-mass energy of the colliding beams, the second key parameter for a linear collider is the luminosity L, given by

$$L = \frac{n_b N_e^2 f_{rep}}{4\pi\sigma_x^*\sigma_y^*} \times H_D$$

where

	n_b	number of bunches per pulse
	N_e	number of electrons (positrons) per bunch
	f_{rep}	pulse repetition frequency
	$\sigma^*_{x,y}$	horizontal (vertical) beam size at interaction point
	H_D	disruption enhancement factor (typically $H_D \sim 2$)

An important constraint on the choice of IP parameters is the effect of beamstrahlung: the particles emit hard synchrotron radiation in the strong electromagnetic space-charge field of

the opposing bunch. Beamstrahlung causes a reduction and a spread of the collision energy and can lead to background in the detector. The energy loss δ_E is therefore typically limited to a few percent. By choosing a large aspect ratio $R = \sigma_x^*/\sigma_y^* >> 1$, δ_E becomes independent of the vertical beam size and the luminosity can be increased by making σ_y^* as small as possible. The TESLA parameter set (Table 3.1) reflects these considerations: it demonstrates the potential for high luminosity, while maintaining a low level of beamstrahlung.

TABLE 3.1
TESLA parameters for the E_{cm}=500 GeV baseline design. The machine length includes a 2% overhead for energy management.

		TESLA-500
Accelerating gradient	E_{acc} [MV/m]	23.8[a]
RF frequency	f_{rf} [GHz]	1.3
Total site length	L_{tot} [km]	33
Active length	[km]	21.8
Repetition rate	f_{rep} [Hz]	5
Beam pulse length	T_P [μs]	950
Number of bunches per pulse	n_b	2820
Bunch spacing	Δt_b [ns]	337
Charge per bunch	N_e [10^{10}]	2
Emittance at IP	$\gamma\varepsilon_{x,y}$ [10^{-6} m·rad]	10, 0.03
Beta at IP	$\beta^*_{x,y}$ [mm]	15, 0.4
Beam size at IP	$\sigma^*_{x,y}$ [nm]	553, 5
Bunch length at IP	σ_z [mm]	0.3
Beamstrahlung	δ_E [%]	3.2
Luminosity	L_{e+e-} [10^{34} cm^{-2}s^{-1}]	3.4
Power per beam	$P_b/2$ [MW]	11.3
Two-linac primary electric power	P_{AC} [MW]	97
(main linac rf and cryogenic systems)		
e^-e^- collision mode:		
Beamstrahlung	$\delta_{E,e-e-}$ [%]	2.0
Luminosity	L_{e-e-} [10^{34} cm^{-2}s^{-1}]	0.47

[a] With the present site layout for TESLA, 23.4 MV/m was the required energy gain per meter of accelerator structure. A detailed analysis by the ILC-TRC revealed that the gradient has to be increased to 23.8 MV/m when rf phasing, especially for BNS damping, is taken into account.

3.1.1.4 Operation at Lower Energies

Operating the linac at reduced accelerating gradient for lower center-of-mass energy is an obvious possibility. In principle, an optimum match of the rf system to the beam impedance can be done by changing the external load, thus allowing for an increase in beam current and pulse length. On the other hand, at lower gradient the emittance growth in the linac increases. In order to obtain an approximate scaling of the luminosity at reduced energy, we disregard both the possibility of higher beam intensity and enhanced emittance dilution. In this case, the luminosity scales simply as $L \propto E_{cm}$ as a result of reduced adiabatic damping of the emittances. Simultaneously, the beamstrahlung goes down approximately as $\delta_B \propto E_{cm}^2$. It has been checked that the acceptance of the beam delivery system is sufficient to accommodate the larger absolute beam emittance down to an energy of about 50 GeV (Z-pole).

A serious complication for low energy operation arises from the positron source. The source is laid out for an overhead factor of 2 (number of positrons within the damping ring acceptance per electron in the high energy drive beam) at an electron energy of 250 GeV. This overhead reduces to 20% at 175 GeV beam energy. Since a certain amount of overhead in the source intensity is likely to be necessary to achieve full positron intensity in routine operation, we consider 175 GeV beam energy (E_{cm}=350 GeV) as the lowest energy for which the positron linac can operate at full design beam current. For beam energies of 175–100 GeV, the positron intensity drops approximately linearly with energy and the luminosity goes down as $\propto E_{cm}^2$. There is a possibility, though, to retain full intensity even for operation at the Z-pole. This can be accomplished by splitting up the electron linac into a section which accelerates the colliding beam and a section which produces the drive beam for the positron source. This would require an additional electron source and a bypass line for the colliding (50 GeV) beam. The details of such a layout have not yet been worked out.

The luminosity as a function of energy resulting from these assumptions is shown in Table 3.2.

TABLE 3.2
Estimated luminosity at lower energies (see text).

c.m. Energy [GeV]	Luminosity [10^{34} cm^{-2}s^{-1}]
350	2.38
200	0.78
100	0.6 (with bypass)

3.1.1.5 Electron-Electron and $\gamma\gamma$ Collisions

The head-on e^+e^- interaction region can also be operated in e^-e^- mode. The disadvantage here is that the luminosity enhancement arising from self-focusing for oppositely charged bunches turns into a de-focusing effect for like charges, with $H_D < 1$. Assuming identical beam parameters, we find a luminosity seven times smaller than for the e^+e^- mode (see Table 3.1).

The photon collider option, where the electrons are converted into high energy photons by interaction with a laser beam just upstream of the IP, requires construction of the second interaction region with the large crossing angle. Unlike the e^+e^- case, the beamstrahlung constraint is not present for $\gamma\gamma$ collisions, and the horizontal beam size at the IP can be reduced still further. Table 3.3 lists a possible $\gamma\gamma$ parameter set which reflects the lack of the beamstrahlung constraint: the horizontal emittance is at the limit achievable with the present damping ring design, while the IP beta-functions are compatible with a final focus system design similar to the e^+e^- collider version (except, of course, for the crossing angle). Additional improvements are conceivable, but require further design studies of these subsystems. Crab-crossing is assumed to avoid a luminosity reduction caused by the crossing angle. The actual usable $\gamma\gamma$ luminosity is smaller than the geometric value by an order of magnitude, since not all the electrons are converted by Compton scattering, and only part of the luminosity spectrum is within a few percent of the peak collision energy.

TABLE 3.3
Beam parameters for the $\gamma\gamma$ option. The effective luminosity takes into account only the high energy peak of the luminosity spectrum ($E_{cm,\gamma\gamma}$ ~400 GeV).

		TESLA-500,$\gamma\gamma$
Repetition rate	f_{rep} [Hz]	5
Beam pulse length	T_P [μs]	950
Number of bunches per pulse	n_b	2820
Bunch spacing	Δt_b [ns]	337
Charge per bunch	N_e [10^{10}]	2
Emittance at IP	$\gamma\varepsilon_{x,y}$ [10^{-6} m·rad]	3, 0.03
Beta at IP	$\beta^*_{x,y}$ [mm]	4, 0.4
Beam size at IP	$\sigma^*_{x,y}$ [nm]	157, 5
Bunch length at IP	σ_z [mm]	0.3
Geometric luminosity	L_{geom} [10^{34} cm^{-2}s^{-1}]	5.8
Effective $\gamma\gamma$ luminosity	$L_{\gamma\gamma}$ [10^{34} cm^{-2}s^{-1}]	0.6

3.1.2 Results of Superconducting Accelerator Development

3.1.2.1 Superconducting Cavities

The TESLA cavity is a 9-cell standing wave structure of about 1 m length whose fundamental TM mode has a frequency of 1300 MHz. The cavity is made from solid niobium and is bath-cooled by superfluid helium at 2 K. Each cavity is equipped with: a helium tank; a tuning system driven by a stepping motor; a coaxial rf power coupler; a pickup probe; and two higher-order mode (HOM) couplers. A side view of the TTF cavity with the beam tube sections and the coupler ports is shown in Figure 3.4. The important cavity parameters are listed in Table 3.4.

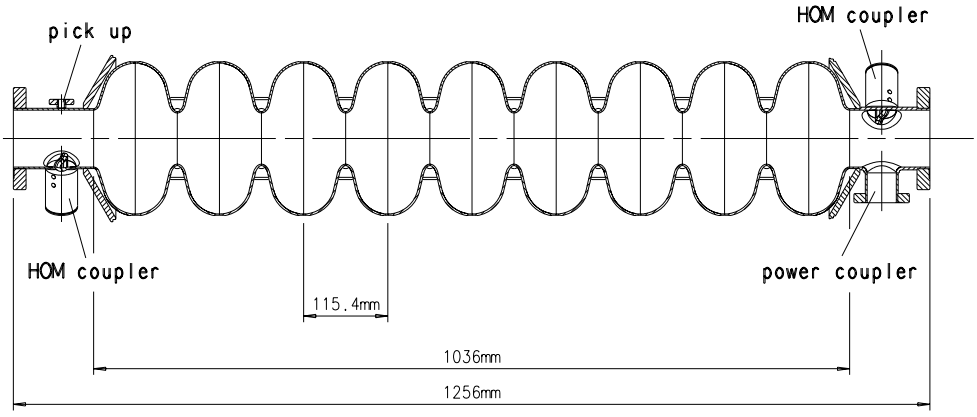

FIGURE 3.4. Side view of the 9-cell cavity with the main power coupler port and two higher-order mode couplers.

TABLE 3.4
Parameters of the 9-cell cavity (note that we adopt here the definition of shunt impedance by the relation $R = V^2/P$, where P is the dissipated power and V the peak voltage in the equivalent parallel LCR circuit).

Type of accelerator structure	standing wave
Accelerating mode	TM_{010} , π-mode
Fundamental frequency	1300 MHz
Nominal gradient E_{acc} for TESLA-500	23.8 MV/m
Quality factor Q_0	$> 10^{10}$
Active length L	1.038 m
Cell-to-cell coupling k_{cc}	1.87%
Iris diameter	70 mm
R/Q	1036 Ω
E_{peak}/E_{acc}	2.0
B_{peak}/E_{acc}	4.26 mT/(MV/m)
Tuning range	$\pm$ 300 kHz
$\Delta f/\Delta L$	315 kHz/mm
Lorentz force detuning constant K_{Lor}	$\sim$1 Hz/(MV/m)^2
Q_{ext} of input coupler	2.5×10^6
Cavity bandwidth at Q_{ext}=2.5×10^6	520 Hz
Fill time	420 μs
Number of HOM couplers	2

The superconducting resonators are fabricated from bulk niobium by electron-beam (EB) welding of deep-drawn half cells. The tubes for the beam pipes and the coupler ports are made by back extrusion and are joined to the cavity by EB welds. Stiffening rings are welded between cells to reduce the Lorentz force detuning by a factor of 2 to about 400 Hz at 23.8 MV/m. A tuning mechanism is used to adjust the cavity resonance frequency. By inserting a piezo element into the tuning system, the dynamic Lorentz force detuning during the rf pulse can be completely compensated, as was successfully demonstrated with tests at the TTF. This would reduce the 10% overhead in rf power for gradient stabilization, which is presently still included in the rf system design parameters.

The TESLA cavities are similar in layout to the 5-cell 1.5 GHz cavities of the electron accelerator CEBAF, which were developed at Cornell University and fabricated by industry. At that time the cavities considerably exceeded the design gradient of 5 MV/m: hence they were considered to have a significant potential for further improvement, and the CEBAF cavity manufacturing methods were adopted for TESLA. Improved quality control of the superconducting material and of the fabrication methods were made, and important new steps were introduced into the cavity preparation:

- Chemical removal of a thicker layer from the inner cavity surface
- Eddy current scanning to identify bulk inclusions of macroscopic impurities (*e.g.*, Tantalum) in the Niobium sheets prior to cavity fabrication
- A 1400°C annealing with a titanium getter to improve the niobium heat conductivity and to homogenize the material
- Rinsing with ultra-pure water at high pressure (100 bar) to remove surface contaminants
- Destruction of field emitters using High Power Processing

Application of these techniques—combined with an extremely careful handling of the cavities in a clean-room environment—has led to accelerating fields which exceed the TESLA-500 design goal of 23.8 MV/m. Figure 3.5 shows the excitation curves (quality factor Q_0 versus gradient E_{acc}) for nine cavities from the third industrial production series. These measurements are done in a vertical cryostat with CW rf excitation. About half of the more than 70 cavities tested so far were also measured in pulsed operation (at full design pulse length and repetition rate), fully equipped with rf input and HOM couplers and mounted in a horizontal cryostat. No degradation in performance with respect to the vertical tests was observed: the average gradient of 31 cavities was 24.5 MV/m in the vertical test and 25.5 MV/m in pulsed operation.

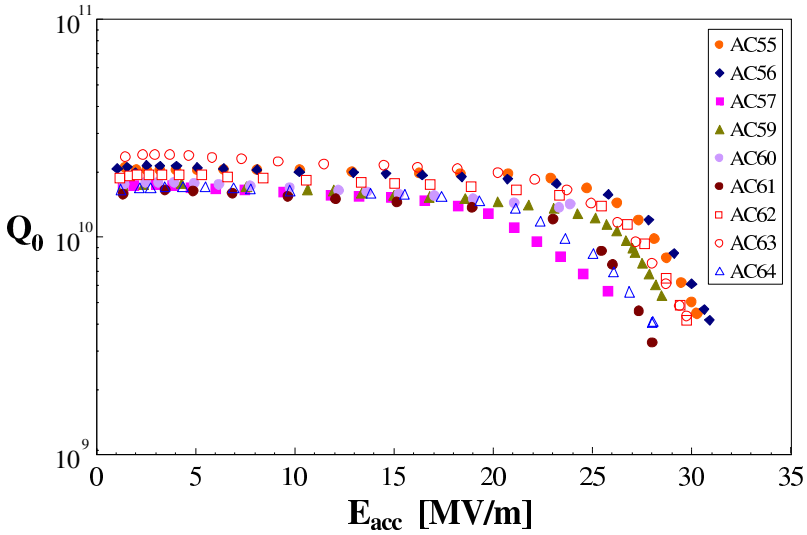

FIGURE 3.5. Excitation curves of cavities of the third production series.

3.1.2.2 Developments Toward Higher Gradients

At present, three main obstacles might prevent us from approaching the superconductor limit of ∼50 MV/m in multicell niobium cavities:

- Foreign material contamination in the niobium
- Insufficient quality and cleanliness of the inner rf surface
- Quality of the welds

Niobium for microwave resonators has to be of extreme purity for two reasons: dissolved gases like hydrogen, oxygen and nitrogen impair the heat conductivity at liquid helium temperature; and contamination by normal-conducting or weakly superconducting clusters close to the rf surface may cause a premature breakdown of the superconducting state. The niobium for the TTF cavities was processed in industry with plants which are in addition used for other metals. For the large series production of cavities needed for the TESLA collider, it would be economical to install dedicated facilities for the niobium refinery and the forging and sheet rolling operations. A substantial improvement in material quality can be expected from specialized installations which are designed for the highest cleanliness, and which are free of contamination by other metals. The same applies for the electron-beam welding machines which must conform to Ultra High Vacuum standards: such a high-quality EB welding machine will be used at DESY in the cavity R&D program.

The recent TTF cavities have been made from eddy-current-checked niobium with gas contents in the few ppm range and an RRR of 300. Ten 9-cell cavities have been tested before and after the 1400°C heat treatment which raises the RRR to more than 500. The average gain in gradient was 4 MV/m. The result implies that, with the present surface preparation by chemical etching, the heat treatment is an indispensable step in achieving

the TESLA-500 goal. From tests at KEK there is some evidence that the tedious and costly 1400°C heat treatment may not be needed in cavities prepared by electropolishing.

The Buffered Chemical Polishing (BCP) used at TTF to remove a 100–200 μm thick damage layer produces a rough niobium surface with strong grain boundary etching. An alternative method is "electropolishing" (EP) in which the material is removed in an acid mixture under current flow. Sharp edges and burrs are smoothed out and a very glossy surface can be obtained.

Since 1995, gradients above 35 MV/m have been routinely obtained at KEK in several electropolished L-band single-cell niobium cavities. Most of these cavities were made from *RRR* 200 material and not subjected to a high temperature heat treatment for post-purification. A KEK-Saclay collaboration demonstrated that EP raised the accelerating field of a 1-cell cavity by more than 7 MV/m with respect to BCP. When the electropolished surface was subjected to a subsequent BCP, the cavity suffered a clear degradation in rf performance which could be recovered by a new EP. Thus there is strong evidence that EP is the superior surface treatment method.

CERN, DESY, KEK and Saclay started a joint R&D program with EP of half cells and 1-cell cavities in August 1998. Gradients between 35 and 42 MV/m are now routinely being achieved (see Figure 3.6). The current program focuses on cavities made from niobium with *RRR*=300. An important goal is to determine whether or not the high gradients so far achieved can be obtained without the time-consuming 1400°C heat treatment.

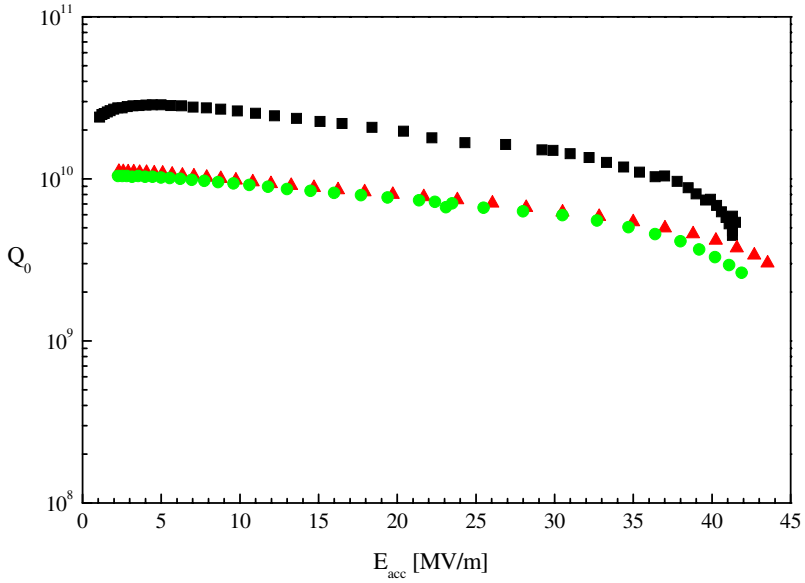

FIGURE 3.6. Excitation curves of three electropolished single-cell cavities without heat treatment at 1400°C. The tests have been performed in different cryostats and under slightly different conditions (magnetic shielding, helium temperature).

Recently it has been found that an *in-situ* baking of the evacuated cavity at 100–150°C (following the EP and clean water rinsing) is an essential step in reaching higher gradients

without a strong degradation in quality factor. The underlying mechanism is not yet understood. The baking was applied to all single-cell cavities.

The transfer of the EP technique to multicell cavities requires considerable investment. In a first test a 9-cell TESLA resonator has been electropolished by a Japanese company, improving its performance from 22 to 32 MV/m (Figure 3.7). An EP facility for 9-cell cavities is under construction at DESY. Given the results obtained so far, it is likely that EP will form an essential part of producing cavities capable of achieving the 35 MV/m operating gradient needed for TESLA-800.

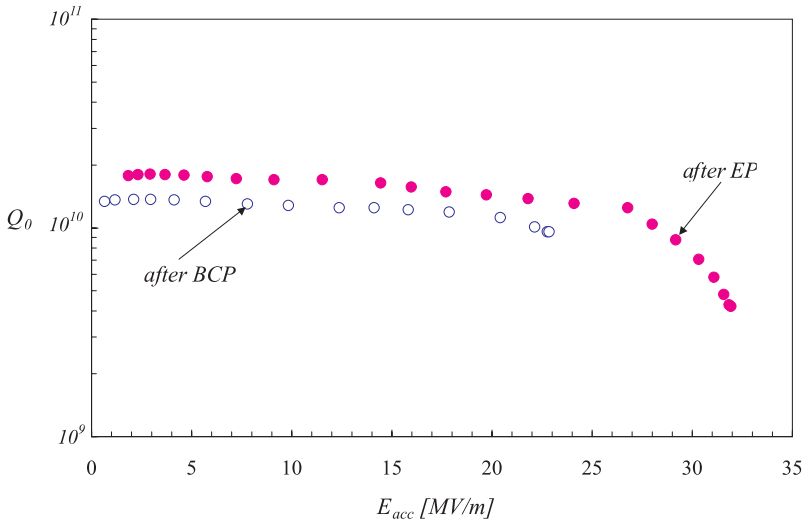

FIGURE 3.7. Excitation curve of a TESLA 9-cell cavity after buffered chemical polishing (BCP) and electropolishing (EP), but before application of the baking procedure.

3.1.2.3 The Superstructure Concept

A fundamental design goal for a linear collider is to maximize the active acceleration length in the machine and to reduce the cost of the radio frequency system. Hence it is desirable to use accelerator structures with as many cells as possible both to increase the filling factor and to reduce the number of power couplers and waveguide components. However, the number of cells per cavity (N) is limited by the conditions of field homogeneity and the presence of trapped modes. The sensitivity of the field pattern to small perturbations grows quadratically with the number of cells. The probability of trapping higher-order modes within a structure also increases with N; such modes with a small field amplitude in the end cells are difficult to extract by the HOM couplers.

The limitations on the number of cells per cavity can be circumvented by joining several multicell cavities to form a so-called superstructure. Short tubes of sufficient diameter (114 mm) enable power flow from one cavity to the next. Two types of superstructures have been investigated in detail: Superstructure I consisting of four 7-cell resonators; and, more

recently, Superstructure II consisting of two 9-cell resonators. The chain of cavities is powered by a single input coupler mounted at one end. HOM couplers are located at the interconnections and at the ends. All cavities are equipped with their own tuners. The cell-to-cell coupling is k_{cc}=1.9%, while the coupling between two adjacent cavities in a superstructure is two orders of magnitude smaller at $k_{ss} \sim 3 \times 10^{-4}$: due to this comparatively weak inter-cavity coupling the issues of field homogeneity and HOM damping are much less of a problem than in a single long cavity with $N = 28$ or 18 cells. The shape of the center cells is identical to those in the 9-cell TTF structures while the end cells have been redesigned to accommodate the larger aperture of the beam tube. The gain in filling factor with the (preferred) version II is 6% and the number of power couplers is reduced by a factor of 2 compared to the baseline design of the TESLA linac. With an accelerating gradient of 35 MV/m the energy reach of TESLA is 800 GeV when built with these superstructures. Whether to go from the baseline design to the superstructure concept will be decided after the tests with beam in the TTF linac, which are scheduled for 2002.

3.1.2.4 Integrated System Test

In order to demonstrate the feasibility of the TESLA technology in a fully integrated system test with beam, a test linac was set up at the TTF. In this linac, accelerator modules containing eight 9-cell cavities each, together with focusing and steering magnets and beam instrumentation are installed. The beam is generated in a low-emittance photocathode rf gun. Additional sections in the beam line are a bunch compressor, collimation section, undulator section for the Free Electron Laser and high energy electron and photon beam analysis area.

So far three accelerator modules have been tested, two of which have been continuously in operation over the past two years, accumulating about 10,000 hr of beam time. A substantial fraction of the beam time was allocated to the FEL studies, which yielded first lasing at 100 nm wavelength in February 2000 and saturation of the FEL radiation in September 2001. The FEL studies were done at reduced beam energy with accelerating gradients between about 12 and 17 MV/m.

The studies performed with the accelerator modules include measurements of maximum beam acceleration, determination of the static and dynamic cryogenic load, active stabilization of the energy gain over the length of the bunch train and excitation of Higher Order Modes.

The static load is in accord with the design values at 4.5 K and 70 K and slightly exceeds the design value at 2 K due to additional diagnostic equipment which will not be present in the TESLA linac.

The average accelerating gradients measured with beam for modules 1, 2, and 3 are 14, 19, and 22 MV/m, respectively. The measured cryogenic load was in accord with the design value for the unloaded quality factor of $Q_0 = 10^{10}$. This confirmed that no significant degradation in cavity performance had happened from the vertical test stand to operation in the module.

Acceleration of a bunch train with the full TTF design specifications (0.8 ms pulse length, 8 mA pulse current) was demonstrated and the rms bunch-to-bunch energy spread was measured to be below 10^{-3} (see Figure 3.8).

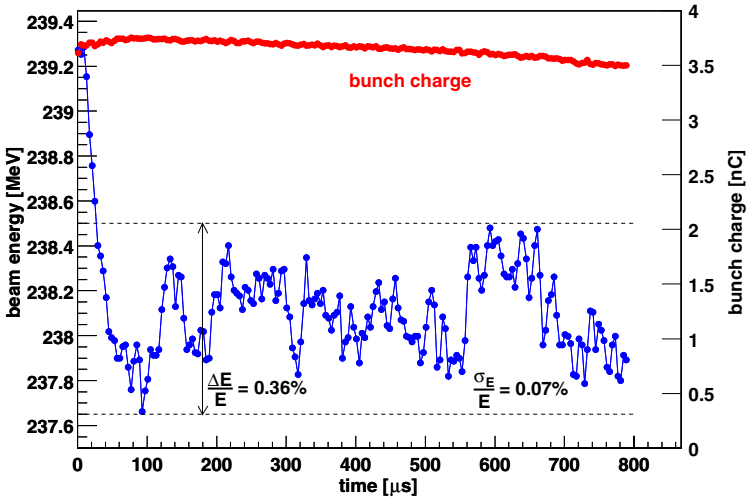

FIGURE 3.8. Acceleration of long macro pulses. The beam energy and the bunch charge within one single macro pulse are shown. The rf control system was operated with the feedback loop active for beam loading compensation. The bunch spacing was 444 ns.

3.1.3 Main Linac

3.1.3.1 Layout and Parameters

The main linac is built with accelerator modules which are conceptually very similar to the ones at TTF. The main difference is a slight improvement in filling factor, by reducing the inter-cavity spacing from 0.34 m to 0.28 m and by accommodating twelve instead of eight 9-cell cavities in a length of about 17 m instead of 12 m, thus saving on the number of module inter-connections. In the first half of the linac every second and in the second half every third module includes a quadrupole, steering coils and BPMs. This step in the otherwise constant-beta lattice is merely introduced to save space and components, the impact on the beam dynamics is small. An overview of the main linac components and parameters is given in Table 3.5.

The rf power is provided by 10 MW multibeam klystrons, each driving three accelerator modules (36 cavities total). The power requirement takes into account a 10% regulation reserve for accelerating field stabilization and 6% losses in the waveguide system. An overview of power consumption and efficiencies is given in Table 3.6. The klystrons are powered by 12 kV modulators with solid state IGBT switches, followed by a 1:12 step up pulse transformer. The modulators are installed in external halls (accessible for maintenance and repair during machine operation) and are connected to the pulse transformers installed next to the klystrons in the tunnel by 12 kV pulse cables.

TABLE 3.5
Overview of components in each of the two main linacs. A 2% overhead for energy management is included.

Injection energy [GeV]	5
Energy gain at E_{acc}=23.8 MV/m [GeV]	245
Total length [km]	14.4
Active length [km]	10.7
Number of cavities per module	12
Number of modules	858
Module length (with quad) [m]	15.9 (16.8)
Number of quadrupoles	350
Number of klystrons	286
Number of cavities per klystron	36
Peak power per klystron [MW]	9.7
RF power to beam per cavity [kW]	231
RF pulse/beam pulse length [ms]	1.37/0.95

TABLE 3.6
Overview of power consumption and efficiencies for the main linac.

Klystron efficiency [%]	65
Modulator efficiency [%]	85
AC power per modulator/klystron [kW]	120
AC power for auxiliaries per rf station [kW]	14
Total AC power for rf per linac [MW]	37.5
AC to beam efficiency for rf [%]	30.1
AC power cryogenics at 2 K per linac [MW]	4.8
AC power cryogenics at 5–8 K per linac [MW]	2.4
AC power cryogenics at 40–80 K per linac [MW]	2.7
Total AC power per linac [MW]	47.4
Overall AC to beam efficiency [%]	23.3

The cooling power at the different temperature levels required for the modules is provided by three cryogenic plants for each linac, which are installed in external halls spaced by about 5 km along the site[1]. The power requirements for the cryogenics are listed in Table 3.6.

[1]The asymmetry of the cryogenic plant distribution as described in the TDR is due to the cryogenic load from operating part of the electron linac with additional pulses for the FEL facility. This particular detail of the TESLA design is ignored here.

3.1.3.2 Beam Dynamics

The focusing lattice is characterized by a 60°-FODO cell length of 65 m and 97 m with maximum β-functions of 127 m and 167 m in the first and second half of the linac, respectively. Vertical steering coils and BPMs are foreseen at every quadrupole, horizontal steering coils at every second (horizontal focusing) quadrupole. The vertical steerers are set to provide an average bending radius of $6{\times}10^6$ m to follow the curvature of the earth.

The assumed alignment errors and resulting single bunch emittance dilutions are listed in Table 3.7. Alignment of the accelerator modules is done with respect to reference points in the tunnel which are defined by a hydrostatic levelling system with an accuracy of 20 μm over a correlation length of 600 m.

Single bunch dynamics have been studied without and with BNS damping. The latter can be easily implemented for the (almost) constant beta lattice with a correlated energy spread in the first part (5 to 25 GeV) of the linac by operating $-27°$ off-crest. In the rest of the linac the longitudinal wakefield is compensated by a $+5°$ off-crest phasing. The beneficial effect of the BNS damping on correlated emittance growth (having a $y-z$ or $y'-z$ correlation in phase space) due to orbit jitter is shown in Figure 3.9. The emittance growth due to the transverse wakefield from cavity and module misalignments is well within the available 50% dilution budget from the damping ring extraction to the IP. However, in view of the sensitivity of the luminosity to correlated bunch deformations (see Section 3.1.5) a further reduction of this effect is desirable. It can be provided by empirical optimization with non-dispersive orbit bumps, as shown in Figure 3.10. Since filamentation in the linac is small, intermediate emittance diagnostic stations are not required and the optimization can be done by observing the luminosity signal directly.

For initial linac commissioning a simple one-to-one steering procedure (through the BPM centers) is sufficient, but to reduce dispersive emittance growth the orbit must be smoothed (*i.e.*, the rms orbit kick minimized) by beam based methods, *e.g.*, the shunt method or dispersion free (DF) steering. In effect, after applying beam based alignment, the absolute offsets of the BPMs are replaced by their resolution. It is found that an iterative DF algorithm using sections of 20 FODO cells per step works well and leads to a dispersive emittance growth of about 2% of the design emittance at the IP, more than half of which is related to the initial uncorrelated energy spread. An alternative procedure in which individual quads are switched off and the BPM-to-quad alignment is determined by minimizing the difference orbit downstream (so-called shunt or ballistic method) yields similar results.

The rf kicks, which result from tilted cavities, have originally not been included in the DF steering simulations. They are found to have a significant effect in the first few hundred meters of the linac where the beam energy is relatively low and the uncorrelated energy spread large. For an rms tilt angle of 0.3 mrad the DF steering procedure is perturbed by the presence of the kicks, resulting in a dispersive emittance growth of 50%. This problem can be cured by switching off rf stations in those sections in which the DF steering or ballistic method is applied. After switching the rf back on, the orbit is re-steered to the one obtained by the previous procedure. The residual effect of the structure tilts amounts to about 3.5% emittance growth.

TABLE 3.7
Parameters related to single bunch emittance dilution. Note that the relative emittance dilution is quoted with respect to the design emittance at the IP.

Normalized design emittance ϵ_x, ϵ_y [10^{-6} m·rad]	10, 0.03 (at IP)
Normalized emittance at injection ϵ_x, ϵ_y [10^{-6} m·rad]	8, 0.02
Beam size at injection $\sigma_{x,i}$, $\sigma_{y,i}$ [μm]	320, 16
Beam size at linac exit $\sigma_{x,f}$, $\sigma_{y,f}$ [μm]	60, 3
Initial uncorr. energy spread $\sigma_{E,i}/E$ [%]	2.5
Off-crest rf phase Φ_{rf} (5 to 25 / 25 to 250 GeV) [°]	-27 / 5
Energy spread $\sigma_{E,f}/E$ at linac exit [10^{-4}]	7
Cavity to module axis alignment [mm rms]	0.3
Quad to module axis alignment [mm rms]	0.2
Module alignment [mm rms]	0.2
BPM resolution [μm rms]	10
Orbit jitter (injection and quad vibration) [σ_y]	0.7–1
Static dilution $\Delta\epsilon_y/\epsilon_y$ from transverse wake [%]	14
Static dilution $\Delta\epsilon_y/\epsilon_y$ from dispersion with DF steering [%]	2
Correlated dilution $\Delta\epsilon_y/\epsilon_y$ from orbit jitter without/w BNS [%]	2–4 / <0.5
Uncorrelated dilution $\Delta\epsilon_y/\epsilon_y$ from orbit jitter [%]	3–6

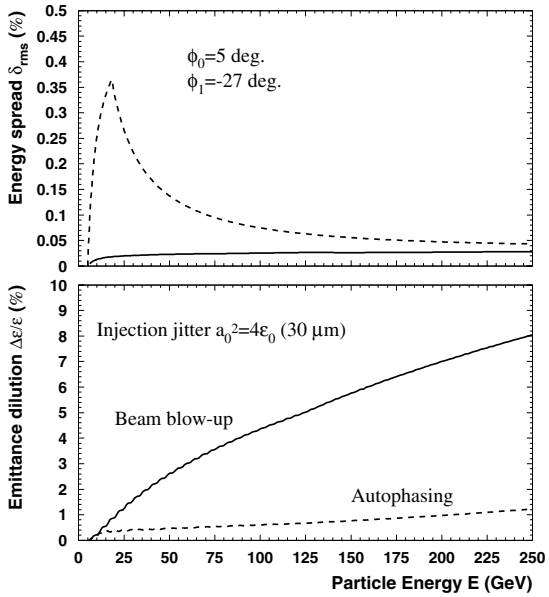

FIGURE 3.9. Illustration of BNS damping in TESLA. The correlated energy spread (dashed curve in upper figure, full curve without BNS) is generated in the 5 to 25 GeV section of the linac and the beneficial effect is shown in the dashed autophasing curve.

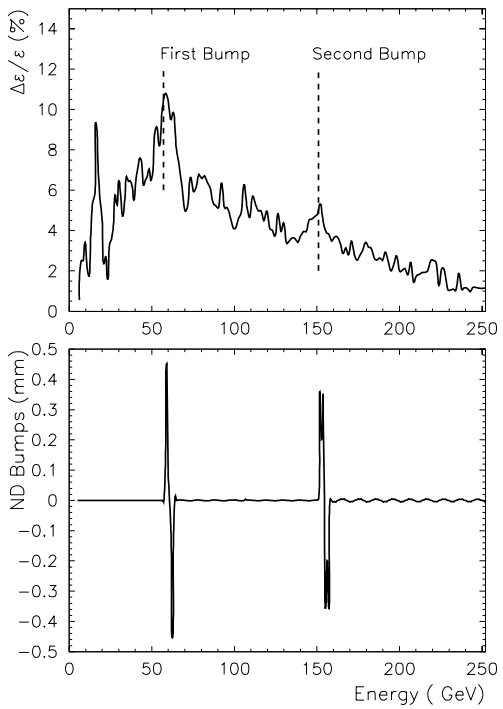

FIGURE 3.10. Example of (non-dispersive) wakefield correction bumps for one particular random seed of misalignments. With two bumps, the emittance growth is reduced by one order of magnitude.

Another detrimental effect of kicks from tilted rf structures occurs in the bunch compressor. Here, the effect is an emittance growth due to the spread of the kick over the length of the bunch. This emittance growth can be tuned out with a dispersion bump applied downstream from the compressor rf section, making use of the almost perfect correlation of the energy deviation with longitudinal position in the bunch. This minimization of emittance dilution is essentially limited by the resolution of the emittance diagnostic section between the compressor and the main linac.

The long range wakefields excited by the beam in the cavities are potentially dangerous, because they can lead to growing bunch oscillation amplitudes over the length of the beam pulse. The higher order modes in the 9-cell cavities have been carefully investigated by numerical calculations, measurements with a network analyzer and resonant excitation with beam in the TTF linac. The HOM couplers are specified such that the quality factors of those modes which couple strongly to the beam are around or below 10^5. The measurements confirmed that the specifications are met, except for one mode at 2.58 GHz in the third dipole passband. The reason for the insufficient damping can be explained by simultaneous weak coupling of one polarization of the mode to both couplers on either end of the cavity. A slight re-arrangement of the couplers is expected to cure this problem.

The beam dynamics calculations with the specified mode properties, including a random mode frequency spread of 10^{-3} from cavity to cavity, show that multibunch beam breakup is not a serious problem. The multibunch emittance growth, averaged over 10 random seeds of cavity misalignments, amounts to 4%. Due to the large bunch spacing, a steady state of HOM excitation is reached after about 100 μs, 10% of the pulse length. A significant bunch-to-bunch orbit variation is only present at the beginning of the train. Even this can be very efficiently corrected: the multibunch orbit pattern is essentially static, *i.e.*, independent of small changes in the beam orbit or the individual bunch charges (see Figure 3.11). By using a fast intra-train orbit correction system, this static part of the bunch-to-bunch orbit variation can be removed. The rms variation of the individual bunch orbits with respect to the average orbit remains below $0.01\sigma_y$ for injection orbit jitter of $1\sigma_y$ or random bunch charge fluctuation of 1%.

The orbit stability in the linac has been investigated using the ground and orbit motion measurements performed at HERA. On a long time scale the motion is expected to be diffusion-like, *i.e.*, following the ATL rule with a constant A=4×10^{-6} $\mu\mathrm{m}^2\mathrm{m}^{-1}\mathrm{s}^{-1}$ derived from the HERA data. The resulting drift at the end of the linac amounts to $1\sigma_y$ after 30 s (150 beam pulses). These long term drifts can be corrected with a slow orbit feedback using the steering coils. Concerning jitter on a time scale of a few beam pulses, the ground vibration studies at HERA predict an rms amplitude of 0.5–1 σ_y at the linac exit. This causes an uncorrelated emittance growth (from the energy spread at injection) of a few percent and a correlated emittance growth (with BNS damping) of a few tenth of a percent. The resulting jitter in offset and angle of the colliding beams is corrected by the feedback system in the BDS (Section 3.1.5).

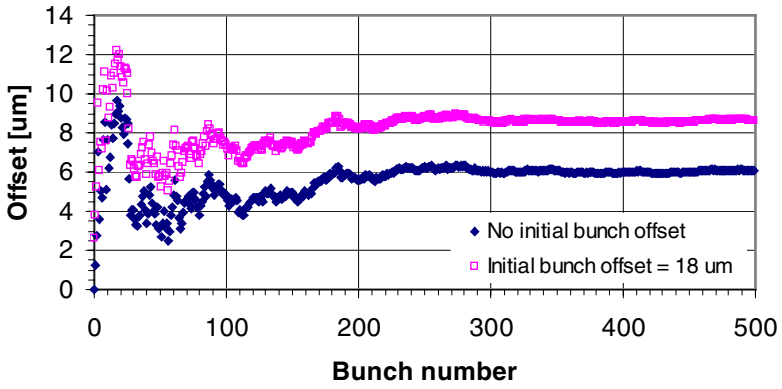

FIGURE 3.11. Orbit offsets in μm of the first 500 bunches at the end of the linac. The lower curve shows the effects of cavity misalignments only ($\Delta y_c = 0.5$ mm rms, one seed). The upper curve shows the effects of the same misalignments, but with an additional one σ_y injection error of the beam (coherent betatron oscillation).

3.1.4 Injection System and Damping Rings

3.1.4.1 Electron Source

The layout of the polarized electron gun is based on the experience with the polarized source at the SLC and the design for the NLC. The gun uses a GaAs cathode illuminated with 840 nm wavelength light from a Ti:Sapphire laser. It is operated with 1 ms long pulses of 120 kV. The large bunch spacing (337 ns) avoids the potential charge limit problem of the cathode, since it is well above the expected cathode recovery time of 10–100 ns. The initial bunch length of 2 ns (full length) is compressed in a three stage buncher system operating at 108 MHz, 433 MHz and 1.3 GHz, respectively. The final bunch length is σ_z=3.4 mm at a beam energy of 12 MeV. The normalized beam emittance obtained from computer simulations is 42 μm·rad for a bunch charge of 3.7 nC, 15% higher than the design bunch charge in the main linac. The buncher section is followed by a normal conducting 1.3 GHz accelerator section (two 5-cell cavities powered by one 10 MW klystron) and two standard main linac superconducting accelerator modules, which together increase the beam energy to 500 MeV.

In addition to the polarized source, an unpolarized source is foreseen, the layout of which is very similar to the existing setup at the TTF. This source is thought to be used for commissioning, machine study and unpolarized luminosity operation purposes. The beam lines of the two sources are merged by means of a switching magnet prior to injection into the 0.5 to 5 GeV electron pre-accelerator. This 4.5 GeV linac consists of 18 standard main linac cryomodules operating at a gradient of 21 MV/m and powered by six 10 MW klystrons.

3.1.4.2 Positron Source

The positron injection system has to provide a total charge of about 5×10^{13} e^+ per beam pulse, which is not realistically feasible with a conventional (electron on thick target) source. Instead, a scheme, originally proposed at Novosibirsk, is used where photons are generated by the high energy electron beam in an undulator and converted into e^+e^- pairs in a thin target (Figure 3.12). This leads to a comparatively low heat load on the target and better capture efficiency behind the target due to the smaller transverse momentum spread of the particles emerging from the target. The particles are captured in a strong, tapered solenoidal field (adiabatic matching device) and pre-accelerated to 250 MeV in a normal conducting 1.3 GHz linac. The linac requires seven 10 MW rf stations of the TESLA main linac type. The beam is transferred in a 2 km long beam line to the positron linac tunnel on the opposite side of the interaction region. Part of this beam line (500 m) is installed in a separate tunnel to bypass the experimental hall. Acceleration to 5 GeV takes place in a superconducting linac of the standard TESLA type, except for an enhanced focusing (reduced quadrupole spacing) in the first accelerator modules.

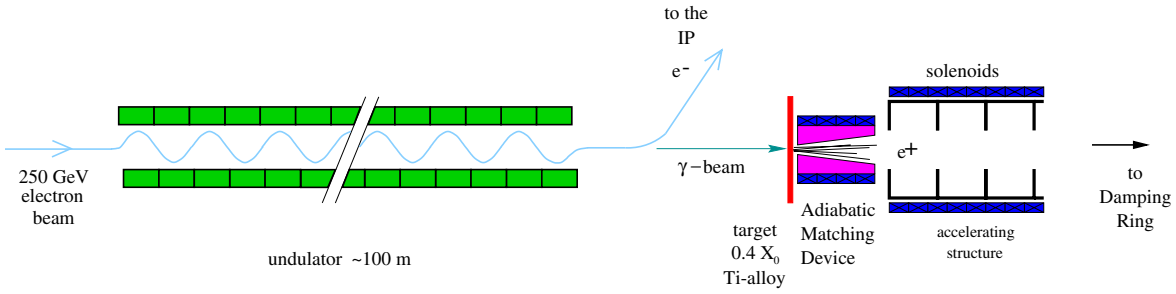

FIGURE 3.12. Sketch of the positron source layout.

The main parameters of the positron source are shown in Table 3.8.

Passage through the undulator, placed between the end of the 250 GeV linac and the beam delivery system, causes the energy spread in the electron beam to increase from 0.5×10^{-3} to 1.5×10^{-3}, with an average energy loss of 1.2%, both of which appear tolerable. The emittance growth is small in both planes (0.1%) with field strength and alignment tolerances of 1% and 1 mrad, respectively, per period of the planar undulator. The undulator-based positron source requires an electron beam energy greater than 150 GeV for full design positron beam intensity. At center-of-mass energies below 300 GeV the luminosity is reduced due to a lower positron beam current. If lower energy running at maximum luminosity becomes important, then additional electron beam pulses and bypass-beamlines are foreseen to drive the positron source independently from the (lower-energy) beam used for physics.

When the planar undulator is replaced by a superconducting helical undulator, polarized positrons can be produced. The polarized positron option is technically more ambitious and is considered a potential upgrade at a later stage of operation. The achievable polarization ranges from 45% to 60%.

TABLE 3.8
Overview of the positron source main parameters.

Undulator	
Peak field	0.75 T
Length	100 m
Period length	14.2 mm
Gap height	5 mm
γ-spot size on target	0.7 mm
Photon beam power	135 kW
Target	
Material	Ti-alloy
Thickness	1.42 cm ($0.4X_0$)
Pulse temperature rise	420 K
Average power deposition	5 kW
Adiabatic Matching Device	
Initial field	6 T
Taper parameter	30 m^{-1}
End field	0.16 T
Capture cavity iris radius	23 mm
General	
Capture efficiency	16%
Number of positrons per electron	2
Normalized e^+-beam rms emittance	0.01 m
Beam energy at pre acc. exit	250 MeV
Total energy width	$\pm$30 MeV
Total phase spread at 1.3 GHz	$\pm7.5^\circ$
Required D.R. normalized acceptance	0.048 m

In addition to the main undulator-based source, a low-intensity auxiliary e^+ source will be installed for commissioning and machine study purposes. The auxiliary source should be capable of generating a bunch train of a few percent of the design intensity.

3.1.4.3 Damping Rings

The positron (electron) beam is injected into the damping ring at an energy of 5 GeV. The bunch train is stored in the ring in a compressed mode, with the bunch spacing reduced by a factor of about 17; even with this compression, a large ring circumference of about 17 km is still required. To avoid building an additional large ring tunnel, a so-called "dog-bone" design is used (Figure 3.13). The layout has two 7.5 km straight sections placed entirely in the main linac tunnel; additional tunnels are only required for the 1 km circumference loops at either end. About 400 m of wiggler sections are needed to achieve sufficient damping. Fast kickers with <20 ns rise and fall time are required for compression and decompression of the bunch train at injection and extraction respectively.

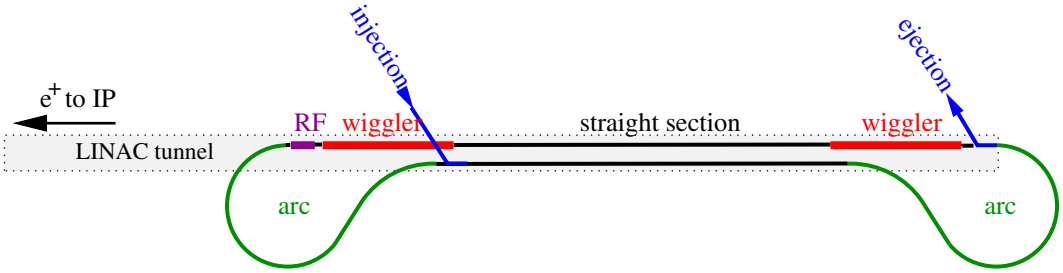

FIGURE 3.13. Conceptual layout of the positron damping ring. The electron ring is similar with the exception that the injection point is located close to the indicated ejection position at the beginning of the linac.

An overview of the damping ring parameters is given in Table 3.9.

Despite its unconventional shape, the damping ring does not exhibit any unusual beam dynamics. The only exception, related to the large ratio of circumference to beam energy, is a large incoherent space charge tune shift. The effect can be significantly reduced, however, by artificially increasing the beam cross-section in the long straight sections.

The ring arcs use a TME-type lattice with 15.2 m cell length (50 cells per arc). The field strength of the dipole magnets is relatively weak (0.2 T) and consequently the arcs contribute only about 5% to the damping. The emittance contribution from the arcs amounts to $\epsilon_{x,arc}$=2×10^{-6} m. The cells are tunable for smaller emittance, at the expense of reduced dynamic aperture, a feature which can be made use of for the photon collider option of TESLA. The lattice in the long straight sections is a simple FODO structure with 100 m cell length and 45° phase advance.

The permanent magnet wigglers have a peak field of 1.67 T with 25 mm gap height and 40 cm period length. There are in total 90 wiggler modules of 4.8 m length each, installed in a FODO lattice with 12 m cell length. The emittance contribution from the wigglers can be adjusted in a range $\epsilon_{x,wiggler}$=2.5 to 8×10^{-6} m·rad by varying the horizontal beta function.

TABLE 3.9
Parameters for the TESLA positron damping ring. Where different, values for the electron damping ring are given in parentheses.

Energy E	5 GeV
Circumference C	17 km
Horizontal extracted emittance $\gamma\varepsilon_x$	8×10^{-6} m·rad
Vertical extracted emittance $\gamma\varepsilon_y$	2×10^{-8} m·rad
Injected emittance $\gamma\varepsilon_{x(y)}$	0.01 m·rad (10^{-5} m·rad)
Number of damping times n_τ	7.2 (4.0)
Cycle time T_c	0.2 s
Damping time τ_d	28 ms (44 ms)
Number of bunches n_b	2820
Bunch spacing $\Delta\tau_b$	20 ns
Number of particles per bunch N_e	2.0×10^{10}
Current	160 mA
Energy loss/turn	21 MeV (14 MeV)
Total radiated power	3.2 MW (2.1 MW)
Tunes Q_x, Q_y	72.28, 44.18
Chromaticities ξ_x, ξ_y	-125, -68
Momentum compaction α_c	1.2×10^{-4}
Equilibrium bunch length σ_z	6 mm
Equilibrium momentum spread σ_p/P_0	0.13%
Transverse normalized acceptance $A_{x\|y}$	0.05 m
Momentum spread acceptance A_p	$\pm1\%$

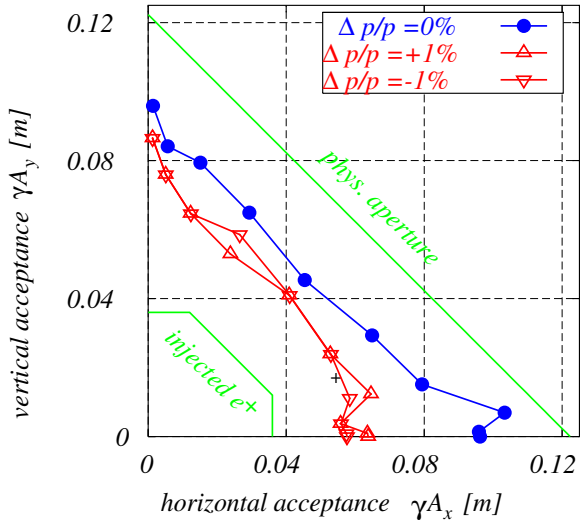

FIGURE 3.14. Dynamic acceptance of the damping ring. The simulations include quadrupole and sextupole alignment errors which result in an average emittance coupling of 1%, and the real physical aperture as the maximum amplitude limit. The phase space volume of the incoming beam as defined by acceptance of the positron pre-accelerator is also shown.

The single particle beam dynamics have been investigated assuming 0.1 mm rms position errors and 0.2 m·rad rms roll angles for the magnets and 10 μm resolution for the beam position monitors. The dynamic acceptance obtained from tracking simulations is larger than the required 0.05 m (normalized) over the $\pm 1\%$ range of momentum deviation (Figure 3.14). The small emittance ratio ϵ_y/ϵ_x=0.2% requires minimization of betatron coupling and spurious vertical dispersion in addition to the usual standard orbit correction. Correction of the coupling can be done with a set of skew quadrupoles, whereas the dispersion correction can be done systematically by measuring difference orbits with shifted rf frequency or empirically by tuning dispersion bumps. Once a "golden orbit" is established, it must be maintained at a level of 10 μm BPM resolution. From the expected diffusive ground motion, this requires orbit correction to be applied once every few minutes, which is not problematic. A possibly harmful effect on the orbit and emittance stability could also arise from magnetic stray fields in the tunnel varying with time. At present such effects are not quantitatively sufficiently well known. Possible counter-measures would be magnetic shielding of the vacuum pipe and/or a faster orbit correction feedback.

The unusually large circumference to energy ratio together with the small beam emittance causes the incoherent space charge tune shift to reach a value (ΔQ_y=0.23) uncommon for high energy electron storage rings. In a collider ring like LEP the total beam-beam tune shift has a similar value and the ring has operated routinely with an emittance ratio of 0.5%. The situation in the damping ring is different in two respects: first, the space charge effect is spread over the entire length of the ring instead of localized in a few positions (collision points). This practically eliminates the resonances which are present in the collider case. Second, in the damping ring the tune shift is modulated at twice the synchrotron frequency, because the charge density and thus the tune shift depends on the

longitudinal position of a particle in the bunch. Depending on the choice of tunes, this can lead to a crossing of low order resonances (in particular $Q_x = Q_y$) and to an increase of the vertical betatron amplitude. This effect has been observed in simulations in which the space charge effect was included. In order to reduce the tune shift, a closed betatron coupling bump is inserted over the length of the two long straight sections, which transforms the flat beam into a round one. Inside this insertion, the particle motion is characterized by a rotating mode in 4D phase space. The closure of the bump is insensitive to phase errors such as arising from the lattice chromaticity, as long as they are equal in x and y. The space charge tune shift is reduced by almost one order of magnitude and simulations including the coupling transformation show that there is no vertical blow-up, for the nominal design parameters and even for a case with the horizontal emittance reduced by factor of 4.

The rf system has to provide a circumferential voltage of 54 MV and deliver an average power of 3.2 MW to the beam. A system of 12 single cell 500 MHz superconducting cavities very similar to the ones in operation at CESR is used. The strong higher order mode damping in this approach avoids problems with HOM driven multibunch instabilities. Therefore only a low bandwidth feedback system which cures the unstable mode driven by the resistive wall impedance is required. Regarding single bunch instabilities, the design bunch charge is safely below the limits for turbulent bunch lengthening or transverse mode coupling.

The fast beam-ion instability has been investigated with simulations. With a N_2 equivalent vacuum pressure of 10^{-9} mbar, the electron bunch train is found to remain stable.[2] A detailed investigation of the electron cloud instability for the positron beam has not yet been done.

3.1.4.4 Bunch Compressor

The bunch compressor provides a reduction of the bunch length by a factor of 20 (from 6 to 0.3 mm) prior to injection of the beam into the main linac. It consists of three standard accelerator modules operating at a gradient of 23.8 MV/m and with a phase of 113° relative to the bunch center, and a 90 m long wiggler-type lattice with a momentum compaction of R_{56}=0.215 m. Incoherent and coherent synchrotron radiation effects have been investigated, the resulting growth of the horizontal emittance is less than 1%. The final energy spread at the exit of the compressor is 2.7% rms. The compressor section is followed by a beam diagnostics and coupling correction section. It is thought that this section together with the compressor lattice can be used for pre-linac beam collimation. A detailed study of this collimation system has not yet been performed.

Between the damping ring extraction and the compressor a spin rotator section is inserted. It uses a pair of solenoids interleaved with an 8° bending magnet and is capable of adjusting the spin polarization vector in any direction of solid angle[3]. The betatron coupling effect of the solenoids is cancelled by means of a $-I$ transformation between the solenoids. The residual emittance growth due to chromaticity is 1% at maximum solenoid strength.

[2]The simulations were performed for a beam at equilibrium emittances and without the coupling bump in the straight sections. A refined analysis done during the ILC-TRC process showed that a vacuum pressure of 10^{-10} mbar is necessary in the straight sections.

[3]Note that for longitudinal polarization at the IP the spin at injection into the linac must have a vertical component, because, due to the curvature of the earth, it is rotated in the main linac.

3.1.5 Beam Delivery System

3.1.5.1 Basic Layout and Optics

The TESLA BDS for the primary e^+e^- IR is about 3.3 km in length (linac to linac). The IR itself sits slightly off-center, with the e^- and e^+ delivery systems being 1759 m and 1677 m in length respectively. The slight asymmetry is due to the undulator-based e^+ source at the exit of the e^- linac. From the first bend magnet in the switchyard both lattices are identical. The system is laid out for a maximum beam energy of 400 GeV.

Figure 3.15 plots $\sqrt{\beta_{x,y}}$ and the dispersion function (D_x) for the BDS (e^-). Figure 3.16 shows the geometry of the electron BDS, including the Fast Emergency Extraction Line (FEXL), and an indication of the location of the positron source system. The IP has a transverse offset with respect to the linac of 1.82 m, and the net bending angle is zero. The various modules which separate out the functionality of the BDS are:

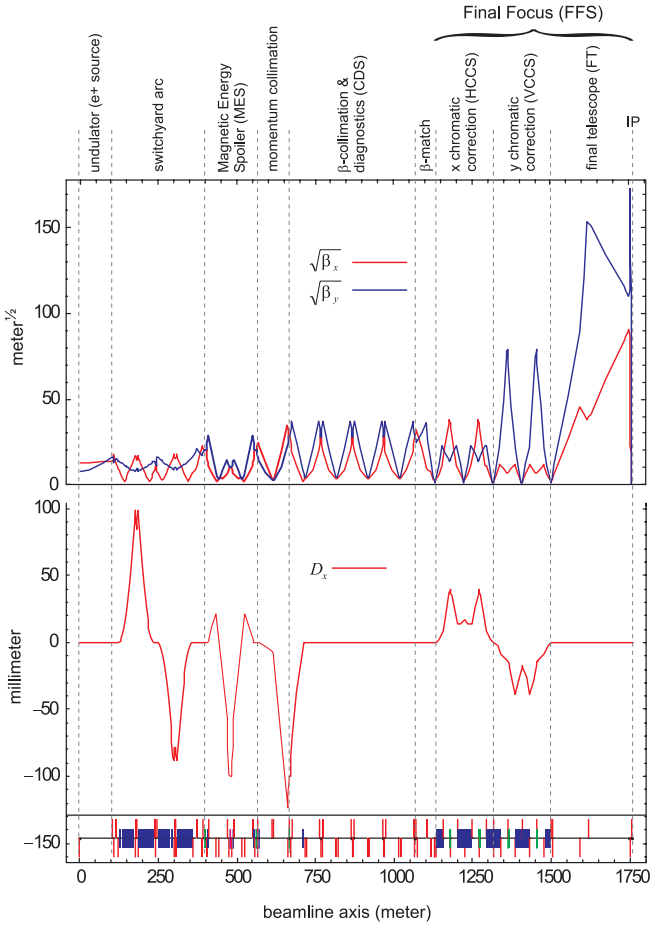

FIGURE 3.15. Optics functions for the TESLA BDS (e^-).

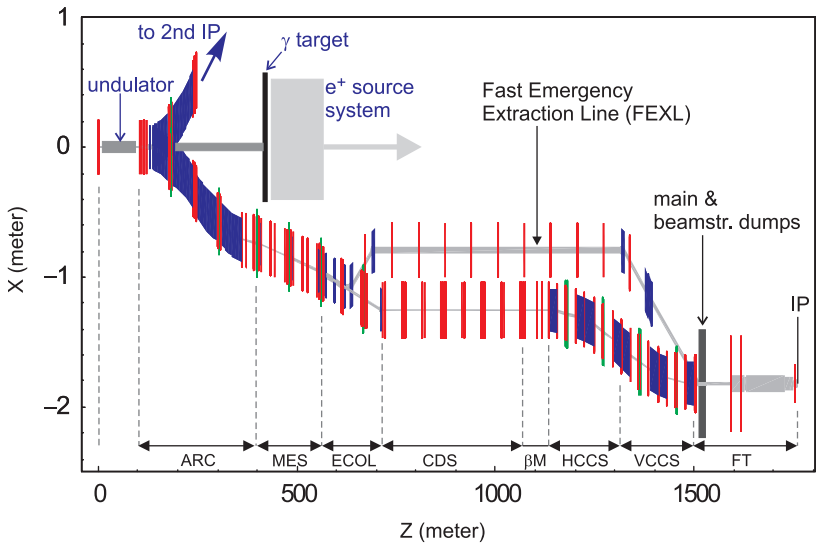

FIGURE 3.16. Geometry of the primary e^- BDS from linac to IP.

e^+ Source Undulator: Contains space for the e^+ source undulator (Section 3.1.4).

Switchyard Arc: A double bend achromat arc which acts as a switch to a second IR and allows enough clearance for the e^+ source photon target (Section 3.1.4). The emittance growth due to synchrotron radiation is negligible at 250 GeV beam energy, but it adds $\Delta\epsilon_x$=1.1×10^{-6} m to the normalized horizontal emittance at 400 GeV.

Magnetic Energy Spoiler (MES): A dispersive section containing non-linear elements which "blow up" the beam at the downstream energy collimator in the event of a large energy error. It works in the following way: an octupole positioned at a high linear dispersion point generates a 3^{rd} order dispersion which causes the off-energy beam to pass off-axis through a downstream skew sextupole. The sextupole then generates horizontal to vertical coupling which increases the vertical beam size on the collimator. The beam size magnification is a factor of 6 for an energy deviation of −2%, which protects the collimator from damage when hit by several bunches in the train—this gives sufficient time to trigger the fast emergency dump kickers which send the rest of the beam onto the beam dump through the extraction line (see below).

Momentum Collimation: A point of high dispersion where the primary energy collimator will be placed.

Collimation and Diagnostics Section (CDS): A repetitive lattice where a series of spoilers and absorbers are used to collimate the beam halo. This section provides relatively high beta (∼1000 m) points 45° apart in phase advance and also supports the emittance measurement station. The required transverse collimation depth is defined by the apertures in the interaction region and amounts to $12\sigma_x$ and $74\sigma_y$, energy collimation is set at ±1.5%.

β-Match: Matching from the CDS to the entrance (image point) of the Final Focus System.

Final Focus System (FFS): A second-order achromatic telescope system which focuses the beam at the IP. The optics uses two pairs of non-interleaved sextupoles, very similar to the design of the FFTB successfully tested at SLAC. The final transformer, which provides the necessary beam size demagnification at the IP, has been increased in length in order to allow a clear extraction path for the beamstrahlung to the main beam dump hall, about 250 m from the IP. The momentum bandwidth of the system is $\pm 0.4\%$, sufficient for the incoming beam energy spread (1.6×10^{-3} rms for electrons and 0.6×10^{-3} rms for positrons, respectively).

Fast Emergency Extraction Line (FEXL): This beam line is primarily intended to extract the remainder of the bunch train safely to the beam dump in the event of a machine protection trip. The latter can be triggered by, for example, large orbit offsets at high dispersion or large beta points, enhanced loss rates at collimators or failure of components (especially power supplies) during the beam pulse. Emergency extraction of the beam is provided by a 200 μrad fast kicker followed by a 6 mrad septum magnet, with a delay of no more than a few bunches. In the initial machine commissioning phase and possibly later for dedicated machine studies a DC magnet can be used in order to permanently direct the beam to the dump instead of passing it through the final focus and interaction region.

3.1.5.2 Interaction Region

The layout of the IR is shown in Figure 3.17. The most important components are:

- The cryostat housing the final superconducting quadrupole doublet
- One stripline and two cavity beam position monitors (BPM), which are primarily used by the inter-bunch fast feedback system
- A laser interferometer for single beam profile measurement at 0.8 m from the IP
- The instrumented mask constructed from high Z material to absorb most of the e^+e^- pairs and their secondaries
- One luminosity monitor (pair counter) on each side of the IP located at the lowest aperture radius of 1.2 cm on the inner mask

In the beam direction, the aperture limitations are set by the forward cylindrical mask of 24 mm diameter housing the pair luminosity monitor, and by the superconducting quadrupole doublet itself, consisting of a 1.7 m and a 1.0 m long quadrupole (dB_y/dx=250 T/m), with an inner diameter of 48 mm.

The beam-beam interaction can be characterized by the disruption parameter D_y and the beamstrahlung parameter Υ. The former is defined as the ratio of bunch length to focal length of the beam-beam space charge force, which tends to decrease the beam size during bunch collision and therefore enhances the luminosity by a factor H_D with respect to the nominal geometric luminosity. For TESLA the disruption effect is strong ($D_y \sim$25), which

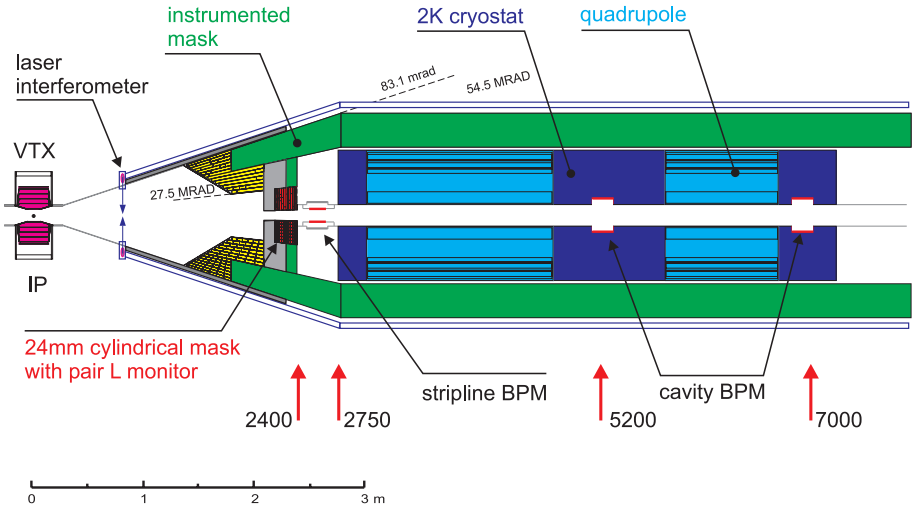

FIGURE 3.17. Interaction region layout.

has consequences for luminosity stabilization, as discussed in Section 3.1.5.4. The enhancement factor can be optimized by shifting the waist position to $0.8\sigma_z$ before the position of the IP: in this case H_D=2.1.

The beamstrahlung parameter relates the beamstrahlung photon energy to the beam energy, the small value Υ=0.06 (0.09) at 500 (800) GeV indicates that beamstrahlung is essentially in the classical regime. The average number of photons radiated per electron (positron) is 1.6 and the typical photon energy a few GeV. The associated luminosity spectrum $d\mathcal{L}/d\sqrt{s}$ is characterized by a peak close to the nominal center of mass energy and a low-energy tail (see Figure 3.18). The fractional luminosity in the 99.5–100% E_{cm} energy bin amounts to 58%.

A small fraction of the beamstrahlung photons creates e^+e^- pairs (about 10^5 particles per bunch crossing with typical energy of a few GeV). The Tungsten mask shown in Figure 3.17 shields the detector from background radiation generated by the pairs. The inner part of the cylindrical mask is equipped with a counter which can be used as a fast luminosity detector. With this monitor a complete scan of relative luminosity with a resolution of about 1% can be performed within a single beam pulse. The parameters scanned can be, for example, relative beam position and angle at the IP, waist position or spurious dispersion.

3.1.5.3 Beam Extraction and Dump

The head-on colliding beams are separated outside the IR by a 20 m long electrostatic deflector. A magnetic field is superimposed on the electric field such as to zero the deflection for the incoming beam. The total deflection angle for the outgoing beam is 0.8 mrad in the vertical plane (downward). The angle is further increased to a total of 15 mrad by subsequent septum and dipole magnets. At the position of the main beam dump (250 m from the IP) the outgoing beam has reached a vertical separation of about 2 m from the incoming beam. Furthermore, the downward deflection reduces the muon

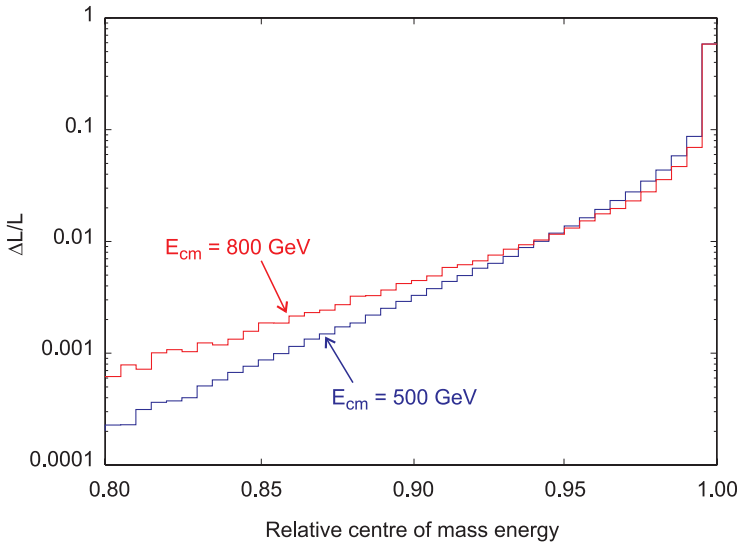

FIGURE 3.18. Luminosity spectra for 500 GeV and 800 GeV center of mass energy.

radiation at the surface to a safely acceptable level. The beam extraction line is equipped with protective collimators in front of some of the magnets to shield them from losses of particles in the low energy tail of the spent beam. The total losses between the IP and the dump amount to 0.1% of the beam power. The optics of the extraction line is designed to provide a minimum beam cross section of 0.4 mm^2 in the worst case of a non-colliding beam. This together with a slow beam sweeping system guarantees to keep the temperature rise in the water dump below 40°C and the particle density on the dump entrance window an order of magnitude below the long-term failure limit. The beam dump system requires a sophisticated water preparation plant in order to handle the chemical and radiological effects in the water in the absorber vessel. In addition, the dump hall is shielded by 4 m of heavy concrete to avoid neutron activation of the surrounding soil and ground water.

The beamstrahlung is transported to the main dump hall essentially without losses (less than 50 W out of 360 kW total power). About 90% of the power is absorbed in the beamstrahlung dump at 250 m, roughly 40 kW of power escape through the hole in the absorber required for passage of the incoming beam. This remaining power is absorbed after the beamstrahlung photons are separated from the incoming beam by the dipole magnets of the FFS.

3.1.5.4 Luminosity Stabilization

Maintaining the luminosity stable at the design value has essentially two aspects regarding the BDS: first, the beams must be kept in collision at the IP and second, spot size dilution must be avoided. Both issues are much more severe in the vertical plane than in the horizontal plane, and the latter will be ignored in the following.

The tolerances for relative offset and angle at the IP are tight as a result of the high disruption parameter, which gives rise to the so-called single bunch kink instability, a

special version of the two-stream type of collective instabilities. The effect of this instability is that initial relative displacements of the bunches or deformations (such as the "banana" shape resulting from wakefields in the linac) are amplified during collision. In linear approximation the growth in oscillation amplitude can be shown to be exponential with a rate proportional to $\sqrt{D_y}$. The sensitivity of the luminosity to offsets and angles has been studied with beam-beam simulations. It turns out that in order to limit the luminosity reduction to less than 10% the orbit at the IP must be stabilized within one tenth of a sigma in both offset and angle (without the instability one would naively expect this tolerance to be about half a sigma).

The expected orbit jitter amplitude, generated by quadrupole vibration in the BDS, has been derived from a ground motion model based on measurements at HERA. The HERA ring is built about 15 m underground in the North-West region of the city of Hamburg. Several main roads with usually heavy traffic pass nearby or even over the ring tunnel. One may therefore consider the HERA data as a worst case (upper limit) scenario for the orbit stability predictions in TESLA.

The rms amplitude of ground motion measured in the HERA tunnel amounts to about 70 nm at frequencies above 1 Hz (*i.e.*, integrated over the spectrum) and to about 20 nm above 5 Hz. In order to accurately determine the effect on the orbit, the spatial correlations of the ground motion must also be known. Measurements of the coherence of the ground motion as a function of distance have been performed with a pair of seismometers. From these the relative motion of two points at distance s can be derived. The result of the analysis for the case of frequencies at and above 5 Hz are shown in Figure 3.19 as an example. From these data a relative (π-mode) vibration amplitude of the two final doublets (with a separation of $\sim$8 m) of about 10 nm can be concluded, which alone yields a pulse-to-pulse relative orbit jitter of $2\sigma_y$ at the IP. Taking into account the other quadrupoles in the BDS it is estimated that the orbit jitter which must be handled by the fast orbit feedback amounts to about 10–30σ in offset and 2σ in angle at the IP. The fast angle feedback uses a BPM installed at a high beta point in the FFS and a kicker magnet at appropriate phase upstream from the FFS. The specified BPM resolution is 1 μm for the required 0.1σ stabilization in angle at the IP. The angle jitter produced by quadrupoles downstream from the BPM is negligible. The offset feedback makes use of the strong beam-beam deflection which bunches colliding with an offset receive (about 5 μrad for $0.1\sigma_y$ offset). This orbit kick is measured by BPM's on either side of the IP. The specified BPM resolution is 5 μm and the time resolution must be <15 ns to separate incoming from outgoing bunches.

Orbit variations due to quadrupole vibrations are also a source of beam size dilution, caused by dispersive and xy coupling effects. It is found that with an uncorrelated quadrupole motion of 70 nm rms the reduction in luminosity amounts to 12% of the design value. This effect can be reduced by an order of magnitude by actively stabilizing the few most sensitive quadrupoles. An actively stabilized magnet support was tested and reduced the rms vibration amplitude to 20 nm at frequencies above about 1 Hz. On a longer time scale, diffusion-like ground motion becomes important. The so-called ATL-rule states that the mean square relative motion of two points is proportional to time and the distance between the points. From long-term orbit drift measurements in HERA a constant A=4×10^{-6} $\mu\mathrm{m}^2\mathrm{m}^{-1}\mathrm{s}^{-1}$ has been derived. Using this model, simulations for the BDS show that with a BPM resolution of 1 μm a simple one-to-one orbit correction applied once

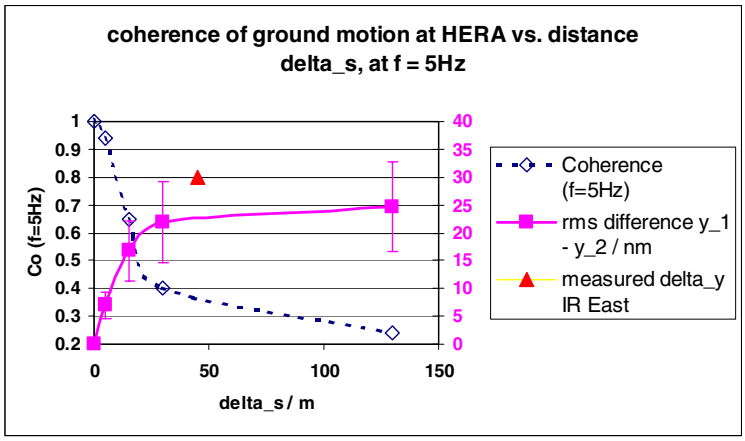

FIGURE 3.19. Relative rms vibration amplitude ($f \geq 5$ Hz) in the HERA tunnel as a function of distance between the points where the seismometers were placed (squares, right hand scale) and the measured coherence (diamonds, left hand scale). These data were taken in 1995. A more recent (2000) result for the difference amplitude across the interaction region East is also shown (triangle).

every 5 s (25 linac pulses) limits the luminosity reduction to about 2%. On a time scale of days an additional dispersion tuning must be applied.

As mentioned previously, correlated emittance growth, *i.e.*, $z-y$ and $z-y'$ correlations in the bunches have a stronger effect on the luminosity than uncorrelated growth because of the kink instability. This effect and its detailed dependence on various parameters is being studied in great detail in collaboration with the CLIC and NLC groups. Some of the beam-beam simulation results obtained for TESLA are discussed in what follows.

Calculations of the luminosity were performed assuming uncorrelated vertical emittances of 2.4×10^{-8} m·rad and 2.2×10^{-8} m·rad at the IP for electrons and positrons, respectively (electrons have a larger energy spread after passing through the e^+ source wiggler and will therefore experience more dispersive dilution in the BDS). To the uncorrelated phase space distribution $z-y$ and $z-y'$ correlations are added which reflect the functional form of the transverse and longitudinal wakefields in the linac. The two contributions are assumed to have equal amplitude, but independent random phase in y, y' space for both of the colliding bunches. The beam-beam simulation is repeated for many random seeds of the phases. The resulting average luminosity as a function of correlated emittance growth is shown in Figure 3.20. One notices that the luminosity reduction for 1% correlated emittance dilution is as large as 15%, in contrast to a 0.5% reduction expected for an uncorrelated dilution of equal magnitude. For larger relative dilution, this difference becomes smaller but remains significant.

The simulations reveal that even though the initial charge distributions of the two colliding bunches have zero average offset, there is often (depending on the phases of the correlated distortions) a net deflection angle for the bunches present after collision. This will in practice be interpreted by the IP feedback as a "real" offset, and appropriate re-steering of the orbit will be generated. Taking this into account the simulation yields a systematically

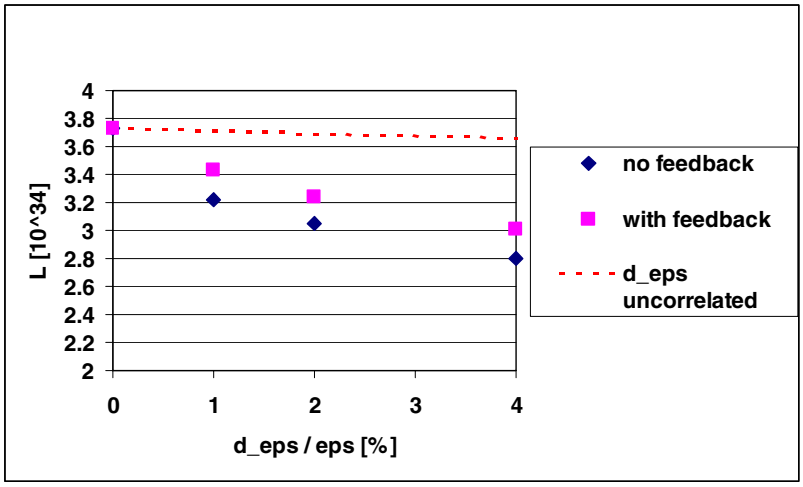

FIGURE 3.20. Luminosity as a function of correlated emittance growth obtained from beam-beam simulations (see text). The diamonds are the results without feedback, the squares with IP steering feedback "on." The dashed line denotes the expected luminosity if the emittance growth was uncorrelated.

higher luminosity, but only a fraction of the luminosity loss is recovered (see Figure 3.20). When empirically re-steering the bunches in both offset and angle, most of the luminosity can be recovered.

In order to achieve the design luminosity, the correlated emittance growth has to be kept at the level of 1%. Since the static part of emittance dilution in the linac can be tuned out, using the luminosity as the sensitive parameter to optimize, this tight requirement applies only to the bunch-to-bunch and pulse-to-pulse variations of the wakefield effects. According to the main linac studies, a 1% limit for the dynamic part of correlated emittance dilution is achievable, although marginally.

One possibility to reduce the sensitivity of the luminosity to correlated emittance growth is a reduction of the disruption parameter by shortening the bunches. An alternative parameter set with σ_z reduced by a factor of 2 to 0.15 mm, β_x increased from 15 to 20 mm and β_y decreased from 0.4 to 0.3 mm has been investigated. The beam-beam simulations show clearly (Figure 3.21) a more stable luminosity than for the reference parameters. This also applies to the required accuracy for IP steering, where the tolerance could be relaxed from 0.1σ to 0.3σ in offset and angle. The price to pay for such a modification is a higher beamstrahlung (δ_B increases from 3.2% to 3.9%) and a second stage bunch compressor. In view of the relatively limited uncertainty in the achievable luminosity due to the kink instability effect, which is not more than about 10 to 15% for the reference parameters, the need for such a design modification may be considered questionable.

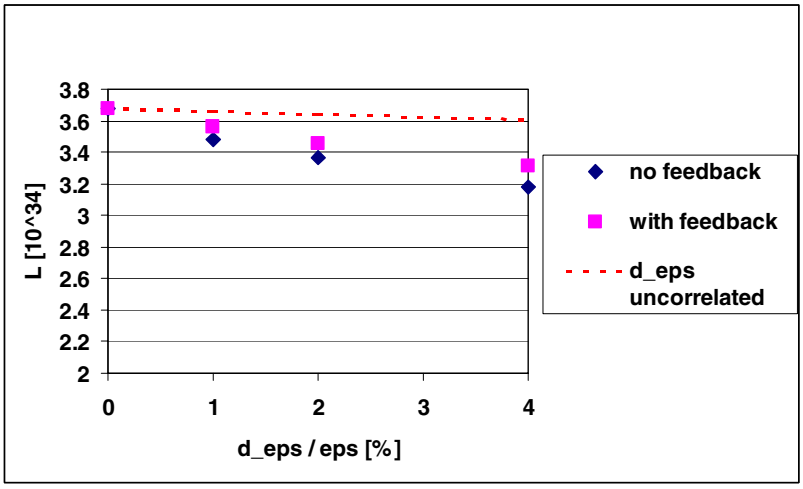

FIGURE 3.21. Same as Figure 3.20, but for a modified parameter set with reduced disruption parameter (see text).

3.2 JLC-C

3.2.1 Introduction

JLC-C is a version of an electron-positron linear collider based on normal-conducting, C-band rf technology at 5.712 GHz. The development of the JLC started in 1986 for a TeV-range collider project with X-band (11.424 GHz) as the most probable Main Linac frequency. Since around 1991, C-band has also been studied as an alternative main linac frequency, putting more emphasis on the lower end of the energy range desired for the linear collider, E_{CM} $\leq$500 GeV, and on the possibility of earlier construction [3].

Obviously, higher frequencies are more advantageous for attaining higher accelerating gradients and hence higher beam energies within a given site length. However, there is no intrinsic advantage, with respect to the luminosity, of going to higher frequencies at a given maximum wall-plug power. On the other hand the technical issues, such as the high current density in the klystrons and the tolerances related to the accelerator structure, become more serious as the frequency goes higher. The choice of C-band is a trade-off between the gradient requirement and the technical problems. Thus the motivation for the C-band collider is technical conservativeness. In the design process we did not pursue extremely high luminosity but instead tried to keep every parameter within a safe region. For instance the beam voltage of the klystron has been chosen to be as low as 350 kV, giving relatively low power efficiency ($\sim$50%), which is one of the reasons why the luminosity per unit wall-plug power is lower than in the X-band design. We expect, however, that the actual integrated luminosity, taking into account the possible machine tuning and down time, will not be lower.

We have so far studied the rf system of the C-band collider. Studies of other parts such as injectors and the beam delivery specific to the C-band linacs have not yet been done mainly due to manpower but also because we do not foresee major difficulties in these parts compared with X-band. Therefore, we only describe the C-band rf system here.

3.2.2 Parameters

The overall C-band designs so far published have emphasized the lower end of the energy range desired for the linear collider, 500 GeV c.m., and have not described the upgrade path to higher energies in detail. It has been assumed that a double-power klystron can be developed and that the site can be lengthened by factor $\sqrt{2}$ to reach 1 TeV. However, the feasibility of the double-power klystron is not obvious. In addition, the progress of the X-band technology has shown that an X-band collider will be possible within a few years.

Thus, our strategy for C-band is that a C-band collider should be built as early as possible and later, when the X-band technology has matured, an X-band extension should be added to reach 1 TeV. In keeping with this scenario we have chosen a parameter set compatible with the later addition of an X-band extension. In fact the beam parameters are basically identical to those in the X-band design. The adaptation to the X-band beam parameters does not actually reduce the luminosity of the C-band collider. In this respect the key parameter is the beam train length. Normally, the optimum train length is longer in lower frequency linacs. However, it is even shorter in the old designs of the C-band than in the X-band collider, basically because a short train length is preferred for the C-band rf pulse compressor. Thus, we do not lose luminosity by adopting the X-band beam parameters.

The important parameters of the C-band collider are summarized in Table 3.10 and Table 3.11. Although the center-of-mass energy in the megatable is 500 GeV, here we present the parameter set for 400 GeV c.m. because that energy seems to be enough for the first stage experiments on Higgs and top quark physics, and because the shorter length of the C-band linacs is preferred when they are to be extended later with X-band for higher energy within a limited site length. This choice is obviously tentative. It may change if the physics situation changes.

In this table the DLDS pulse compression system is assumed for the X-band section in the energy upgrade stage. We can replace it with the SLED-II system but at least several years are expected from the first to the second stage so that the DLDS technology is expected to be mature.

Since the study of compatibility with an X-band extension has started only recently, the parameters that appear in the following sections are not completely consistent with those in Table 3.10 and Table 3.11. In particular, the rf pulse length and the beam train length in Table 3.10 are longer by up to 4/3 compared to (for example) the klystron pulse length in the following sections. We believe the differences will not cause serious changes to the hardware already developed.

TABLE 3.10
C-band and C-X hybrid parameters.

	C Alone	Hybrid C	Hybrid X	Units
Center-of-mass energy (E_{CM})	400	1000		GeV
Beam Property				
Initial beam energy (E_i)	8	8	200	GeV
Final beam energy (E_f)	200	200	500	GeV
Number of particles per bunch (N)	0.75	0.75		$\times 10^{10}$
Number of bunches per pulse (n_b)	192	192		
Number of particles per pulse ($n_b N$)	144	144		$\times 10^{10}$
Bunch spacing (t_b)	1.4	1.4		ns
Beam pulse length ($n_b t_b$)	268.8	268.8		ns
Repetition frequency (f_{rep})	100	100		Hz
Normalized emittance (DR exit) ($\gamma\epsilon_x$)	3×10^{-6}	3×10^{-6}		m·rad
($\gamma\epsilon_y$)	2×10^{-8}	2×10^{-8}		m·rad
R.m.s. bunch length (σ_z)	200	110		μm
Main Linac				
Unloaded gradient (G_0)	41.8	41.8	70	MV/m
Loaded gradient[a] (G)	31.1	31.1	53.8	MV/m
Active length (each linac) (L_{act})	6.11		6.16	km
Wall plug power (P_{AC})	140	140	122	MW
AC to rf efficiency ($\eta_{AC\to RF}$)	24.12	24.12	37.4	%
RF to beam efficiency ($\eta_{RF\to B}$)	25.9	25.9	26.7	%
Modulator				
Efficiency (η_{mod})	67		80	%
Number of modulators (/beam)	1696		285	
Klystron				
Peak power	50.12		75	MW
Pulse length	2.762		1.60	μs
Efficiency (η_{kly})	50		60	%
Number of klystrons (/beam)	1696		2280	
Pulse Compressor				
Type	Diskloaded		SLED-II	
Time compression factor	1/5			
Efficiency (η_{cmpr})	80			%
Waveguide loss	10			%

Continued in Table 3.11.

[a] Includes single/multibunch loading and $\cos\phi_{RF}$.

TABLE 3.11
C-band and C-X hybrid parameters (continued).

	C Alone	Hybrid C	Hybrid X	Units
Center-of-mass energy (E_{CM})	400		1000	GeV

Continued from Table 3.10.

Accelerator Structure				
Structure type		CG choke-mode $3\pi/4$	RDDS $5\pi/6$	
Structure length		1.8	0.9	m
Iris radius (a/λ)		0.171–0.126	0.210–0.148	
(average) ($\langle a/\lambda \rangle$)		0.148	0.18	
Group velocity (v_g/c)		3.60–1.14	5.1–1.1	%
(average) ($\langle v_g \rangle /c$)		2.12	2.5	%
Filling time (T_f)		285	120	ns
Attenuation parameter (τ)		0.524	0.511	
Average Q-factor (Q)		9772	8574	
Shunt impedance (r_s)		53.7	81.2	MΩ/m
Number of structures (/beam)		3392	6840	
Peak power into a structure		90.2	85	MW
Interaction Point				
Number of particles per bunch (N^*)	0.75	0.75		$\times 10^{10}$
Normalized emittance ($\gamma\epsilon_x$)	3.6×10^{-6}	3.6×10^{-6}		m·rad
($\gamma\epsilon_y$)	4.0×10^{-8}	4.0×10^{-8}		m·rad
Crossing angle (ϕ_{cross})	7	7		mrad
Beta function (β_x)	8	13		mm
(β_y)	0.2	0.11		mm
RMS beam size (σ_x)	271	219		nm
(σ_y)	4.52	2.3		nm
Disruption parameter (D_x/D_y)	0.289/17.3	0.08/10.0		
Number of beamstr. photons (n_γ)	1.30	1.3		
Energy loss by bremsstrahlung (δ_{BS})	2.72	8.9		%
Average Upsilon parameter ($\langle \Upsilon \rangle$)	0.057	0.29		
Nominal luminosity	7.01	15.7		10^{33} cm^{-2}s^{-1}
Luminosity[b] ($\mathcal{L}$)	10.1	25		10^{33} cm^{-2}s^{-1}
Luminosity / 100 MW AC ($\mathcal{L}/P_{AC}$)	7.24	9.54		10^{33}

[b] Includes pinch effect but does not include the crossing angle.

3.2.3 Main Linacs

The C-band rf unit is shown schematically in Figure 3.22. Two 50-MW klystrons, each driven by a separate modulator, are combined in a 3-dB hybrid and compressed to 350 MW by a pulse compressor with disk-loaded coupled cavities to feed four 1.8-m-long accelerator structures.

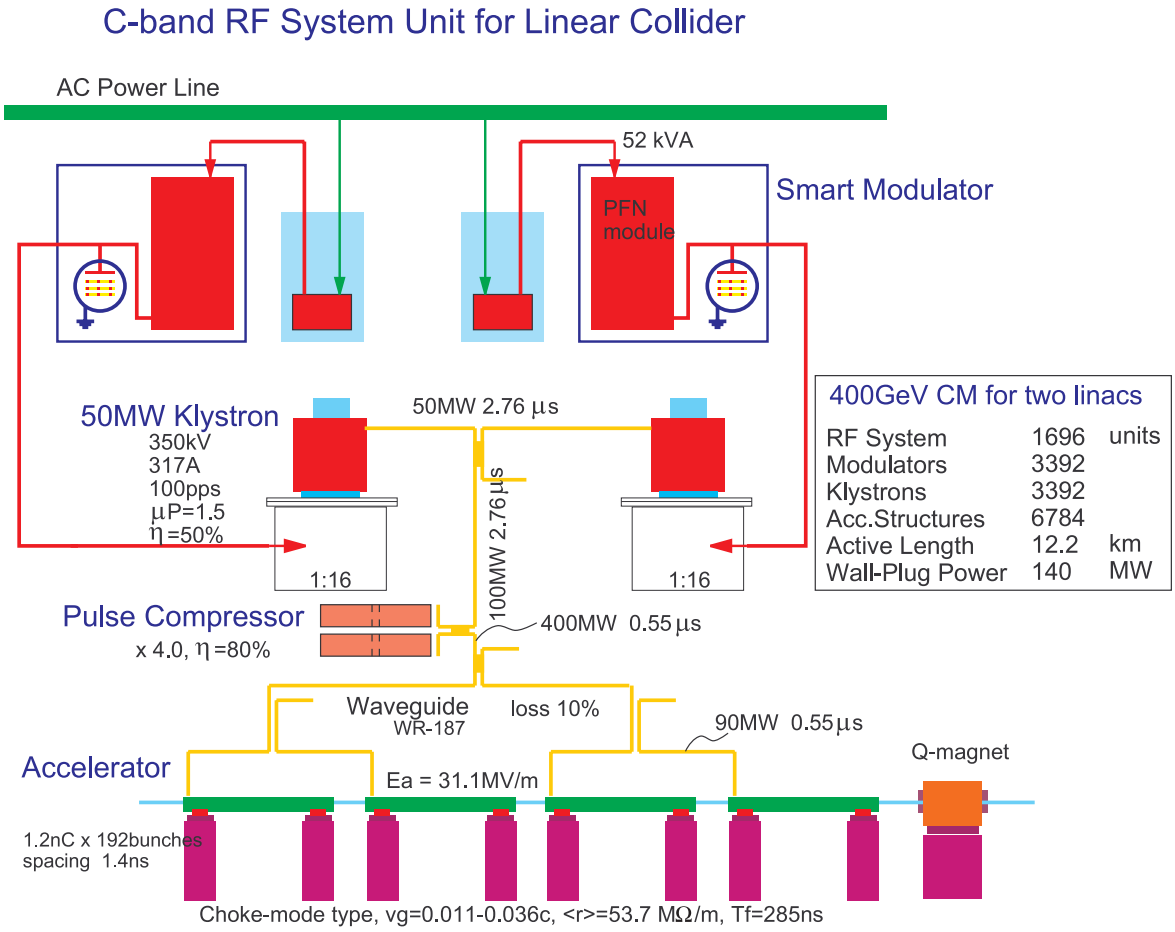

FIGURE 3.22. Schematic diagram of the C-band rf unit.

3.2.3.1 Modulators

In conventional modulator systems the thyratron switch is one of the most troublesome components. Its lifetime is short ($\sim 3 \times 10^9$ shots) and varies from tube to tube. The protection circuits, consisting of a number of diodes, snubber capacitors, and resistors, occupy a lot of space. Conventional modulator tanks are massive, expensive, and require oil for insulation.

Our modulator for the C-band system is different from conventional ones. The charging power supply is a constant current source using an inverter power supply. The short-circuit

current is limited below a few amperes by the inverter power supply. The PFN charging starts after a long delay controlled by a master trigger generator, which will provide fault-free operation of the thyratron.

Figure 3.23 is a simplified circuit diagram. The PFN is an 18-stage Guillemin E-type LC network. We do not need a de-Q'ing system to regulate the PFN voltage. There is no bulky thyrite to present the low inverse voltage required for thyratron deionization in the EOLC circuit, owing to the command-charging scheme of the inverter power supply.

Figure 3.24 shows the waveform with the klystron load. The leading edge of the pulse is clean due to the low noise. The peak voltage at the flat top is 350 kV, which is measured with a capacitive voltage divider mounted inside the pulse tank. The pulse width at 75% of the peak voltage is 4.35 μs. The rise time (10% to 90%) is 0.96 μs. The ripple at the flat top is less than $\pm$0.5% and the pulse-to-pulse voltage stability is as low as 0.35% owing to the regulation precision of the inverter power supply. The inverse voltage is less than 35 kV which is small enough to guarantee reliable operation of the active components such as the inverter power supply, the thyratron, and the klystron tube. The measured time jitter of the klystron beam pulses at the 350-kV pulse voltage is 1.2 ns.

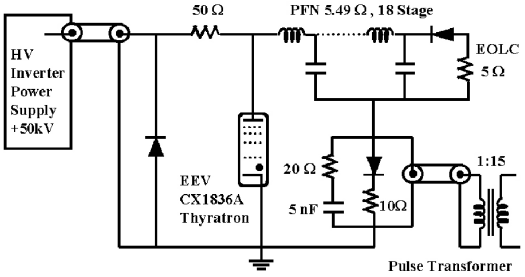

FIGURE 3.23. Schematic diagram of the C-band modulator circuit.

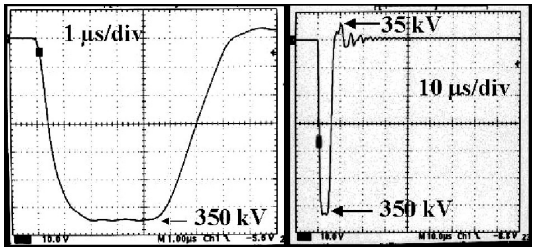

FIGURE 3.24. Output waveform of the modulator.

The efficiency of the present modulator system is 47.9% (85% charging efficiency and 56.4% pulsing efficiency). A relaxation of the ripple requirement, which can be achieved by using a pulse compressor and phase-amplitude modulation, will allow a larger ripple up to 2–3%. We expect to obtain efficiency as high as 67%.

3.2.3.2 Klystrons

We have developed and tested 50-MW C-band klystrons (the E3746 series). Figure 3.25 shows a cross-sectional view of the klystron. We constructed two tubes with different output cavities: one with a single gap and the other with a three-cell traveling-wave cavity. The second tube was designed to reduce the electric field gradient at the output cavity and to raise the power efficiency by smoother deceleration of the electron beam.

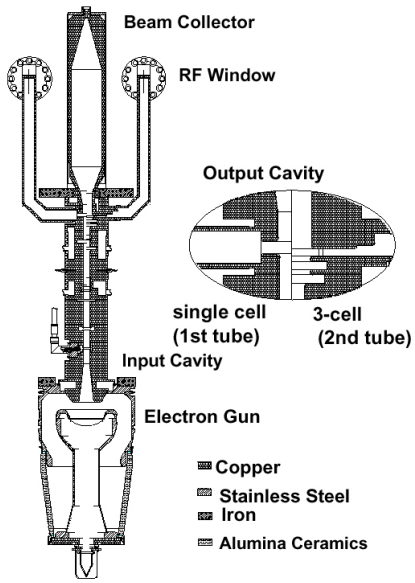

FIGURE 3.25. Cross-sectional view of the E3746 C-band klystron.

The second klystron achieved 54 MW of output power at the 369-kV beam voltage, 2.5-μs pulse width and 50-Hz repetition rate in the test performed in 1998. The test results and design parameters are summarized in Table 3.12. Figure 3.26 shows the output waveform from the second tube. Figure 3.27 compares the measured output power and efficiency with the computer simulation using the FCI code. The agreement is extremely good—within 1%.

TABLE 3.12
Design parameters and test results for the E3746 klystron.

	Design	Test
Output power [MW]	49	53.9
Beam voltage [kV]	350	368.7
Beam current [A]	317	333.0
Drive power [W]	300	323
Power efficiency [%]	44	43.9
RF pulse width [μs]	2.5	2.5
Beam perveance [μA/V$^{3/2}$]	1.53	1.49
Repetition rate [Hz]	50	50
Solenoid coil power [kW]		4.55

The power consumption of the C-band klystron's solenoid magnet ($\sim$5 kW) is not large compared to the total power consumption. However, by replacing the solenoid magnet with a permanent magnet one can eliminate the DC power supply, the water cooling system and its interlock. This will make the klystron system much simpler.

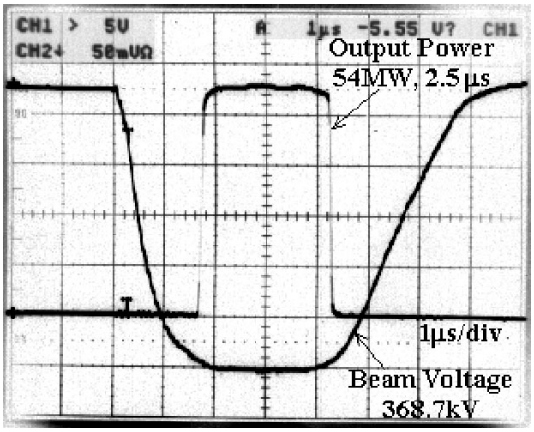

FIGURE 3.26. Output waveform of the klystron.

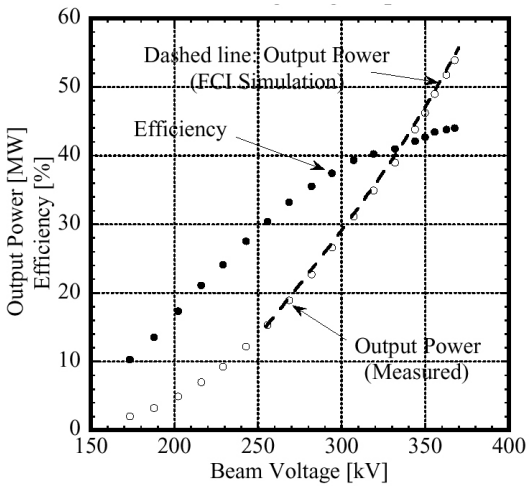

FIGURE 3.27. Output power and efficiency of E3746 klystron. The dashed line is a result of computer simulation using FCI and the circles represent the measured results.

In order to minimize the required R&D for the first C-band PPM klystron, we adopted the same design as the third solenoid-focused E3746 tube, except for the drift tube region. The cutaway view is shown in Figure 3.28 and the specification is summarized in Table 3.13. We chose magnetic stainless steel (Mag-SUS) for the pole-piece material instead of pure iron and neodymium ($Nd_2Fe_{14}B$) as the magnet material. Simply stacking disks alternately of Mag-SUS and OFC, and processing in an HIP vessel filled with pressurized Ar gas at 1200 kgf/cm^2 and temperature 800°C for 2 hours, we bonded them in one block by diffusion bonding. No brazing-alloys were used in this process. After machining the rf cavities and beam drift tube on the bonded PPM stack, they were assembled together by conventional brazing.

TABLE 3.13
Target parameters of C-band PPM klystron.

Output power [MW]	50	Permanent magnet	Neodymium N40A
RF pulse width [μs]	2.5	Residual induction, B_r [Tesla]	1.2
Beam voltage [kV]	350	Coercive force, H_c [kOe]	11
Beam current [A]	317	Peak field (on axis, upstream) [kG]	2.0
Power efficiency [%]	48	PPM pitch [mm]	30
Perveance (10^{-6}) [A/V$^{3/2}$]	1.53	Pole-piece	Mag-SUS
Drift tube radius (upstream) [mm]	7.5		Fe+14%Cr+C(20ppm)
(downstream) [mm]	9.0		
Beam radius (upstream) [mm]	5.0		

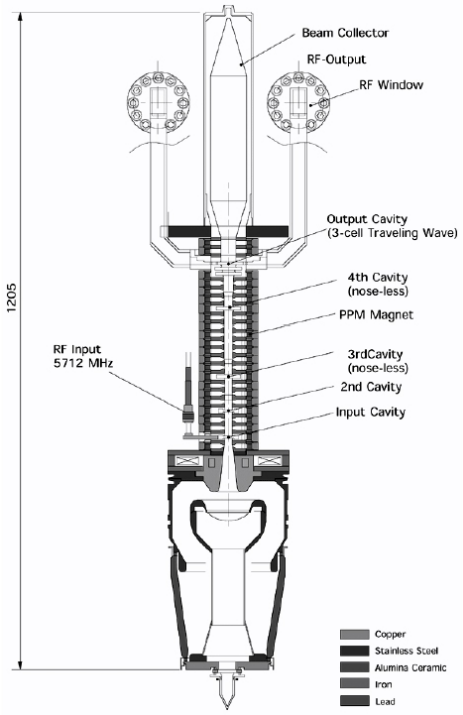

FIGURE 3.28. Cut-away view of the first C-band PPM klystron, TOSHIBA-E3747.

Figure 3.29 shows the waveform of the output power together with the beam voltage and the input drive power. The first C-band PPM klystron generated 37 MW at the 350-kV beam voltage, 2.5-μs pulse width, and 50-Hz repetition rate. The measured beam loss was less than 1%. Figure 3.30 shows the measured output power as a function of the beam voltage.

A parasitic oscillation was found when the gun voltage exceeded 320 kV. Its frequency was around 5726 MHz, which is in the gain-bandwidth. We believe the oscillation is due to back-streaming electrons from the beam collector, which causes a positive feedback of an rf signal from the output cavity to the input cavity. The second PPM klystron is being designed to avoid this problem.

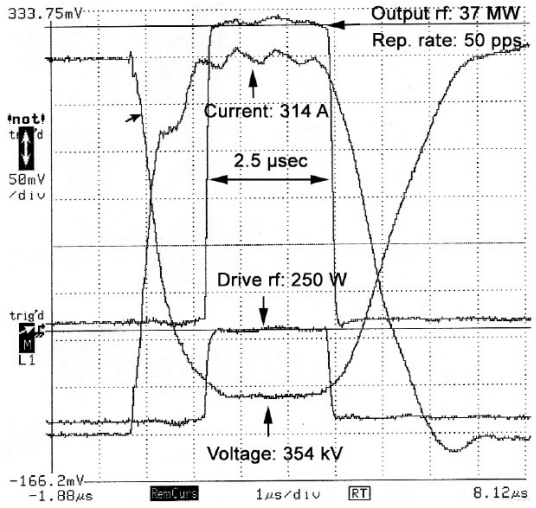

FIGURE 3.29. Output waveform of C-band PPM klystron.

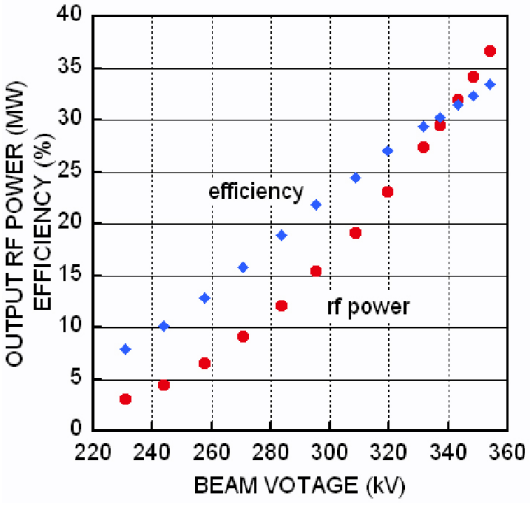

FIGURE 3.30. Output power and efficiency of C-band PPM klystron.

3.2.3.3 Pulse Compressor

We use a three-cell coupled-cavity pulse compressor instead of a delay-line type compressor like SLED-II. The cavity is very compact, having a length of 800 mm and a diameter of 160 mm. It is very easy to fabricate at low cost. To compensate for the ringing response associated with the multicell structure, the amplitude modulation is applied to the input power. A cold-test model of this type of pulse compression succeeded in generating a flat pulse in 1997.

In order to obtain higher efficiency we introduced a new scheme of phase modulation. It makes use of the power that otherwise would be wasted during the rise time of the modulator pulse. The system is depicted schematically in Figure 3.31. It consists of a fast phase modulator, a vector rf voltage detector, a solid-state driver amplifier, and a feedback control computer. In this system the voltage detector monitors the power flow at several points: the klystron output, the pulse compressor output, and the output coupler of the accelerator structure. Software computes the deviations from the target values and stores the phase modulation pattern in the memory of the fast phase modulator. The feedback loop is applied to successive pulses to maintain a constant energy gain. The feedback is automatically controlled to compensate for various situations: system failure, temperature change, timing drift, *etc.* In the two-klystron system shown in Figure 3.31 the phase-to-amplitude conversion is performed to flip the input voltage of the rf pulse compressor.

A cold test was performed with the pulse compressor, the modulator (flat-top pulse length 2.0 μs) and the E3746 klystron. The resulting power gain is plotted in Figure 3.32. We observed an enhancement of 1.25 due to the phase modulation and obtained a power gain of 3.5. It should be noted that a 2.5-μs flat pulse would have been needed to reach this power gain if the phase modulation were not applied.

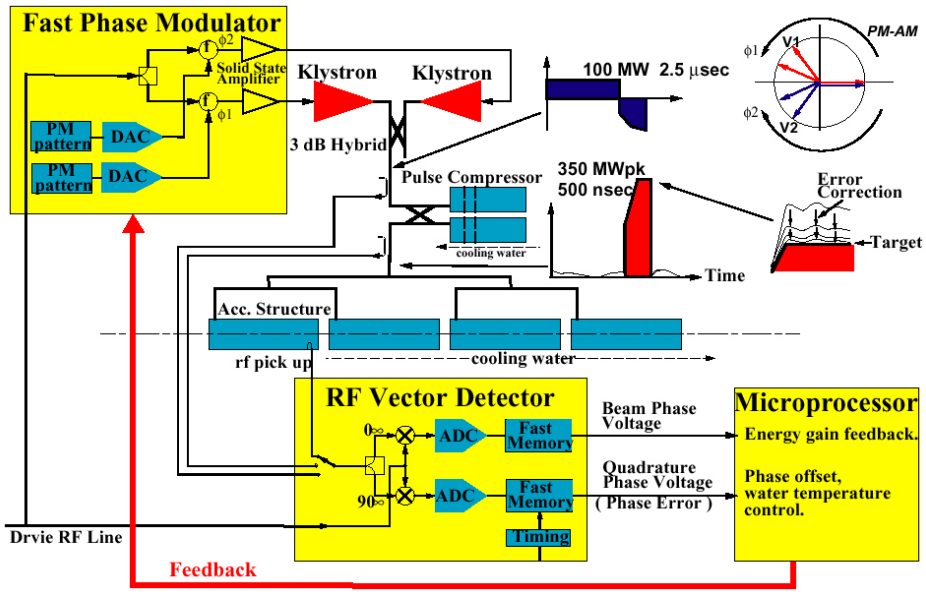

FIGURE 3.31. Schematic diagram of the phase modulation system.

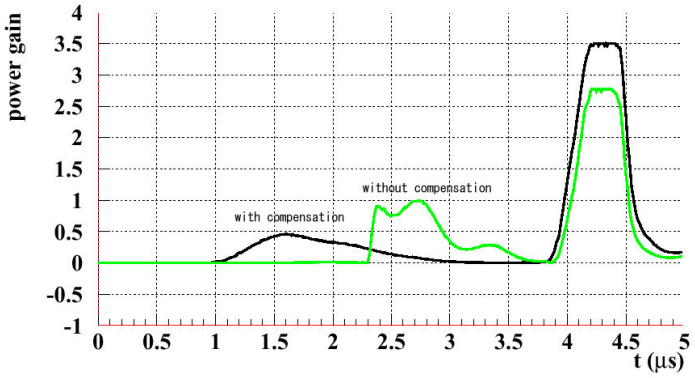

FIGURE 3.32. The power gain of the rf pulse compressor with and without phase compensation.

The pulse compressor requires the highest Q value of all the normal-conducting cavities used in linear colliders. In the three-cell design the first and third cavities resonate in $TE_{01,15}$ and the second cavity resonates in $TE_{01,5}$. The theoretical Q values for OFC are 185,400 and 82,600. The power gain is sensitive to the properties of the third cavity since the microwave energy is stored mainly in that cavity. In particular the shift of the resonance frequency is 10.8 kHz and 6.6 kHz under 1-μm changes of the length and diameter, respectively. In order to limit the decrease of the power gain within 1%, the change of the frequency must be less than 25 kHz, corresponding to a length change of 2.3 μm. If copper is used, then the temperature must be controlled within 0.3°C.

In order to relax the temperature stability requirement we are developing a compressor made of copper-plated super-invar, whose thermal expansion coefficient is smaller than copper by 1/40. A single cell in the $TE_{01,15}$ mode was constructed using super-invar material made by casting for lower cost. It was low-power tested in 2001. The change of the resonance frequency with temperature was measured. The result was better than that for the copper cavity by a factor of 1/4 but was not fully satisfactory. This is possibly due to the thermal expansion of the copper endplate which was electron-beam welded to the super-invar body. (Copper was chosen because of a thermal conductivity problem.) High power tests will be done soon.

3.2.3.4 Accelerator Structure

In the linacs for linear colliders it is an essential requirement to damp the long-range transverse deflecting wave generated by the beam. In 1992, the so-called choke-mode cavity was proposed which is an axisymmetric open cavity. The beam-induced wave is strongly damped by the electromagnetic radiation through a radial line into open space (and is absorbed by an absorbing material) while the accelerating rf wave is trapped inside the cavity by a choke filter. The concept was confirmed in the experimental test performed at ATF-KEK in 1994, where a bunched electron beam was successfully accelerated in a prototype choke-mode cavity designed for S-band up to a gradient of ∼50 MV/m.

Figure 3.33 shows the C-band model. The whole structure is constructed by stacking axially symmetric cells. The cell body, the annulus of the choke, and the space for the HOM absorber are machined on a copper disk by turning on a lathe. The vacuum seal and mechanical structure are maintained by stacking the cells and plating a copper layer from outside. The SiC ceramic ring is the HOM absorber, and it is mounted in the disk with a metal spring insert (MC Multilum-contact). Since all parts are axially symmetric and can be turned on a lathe, the choke-mode approach has a big advantage for manufacturing compared to other ideas for wakefield damping.

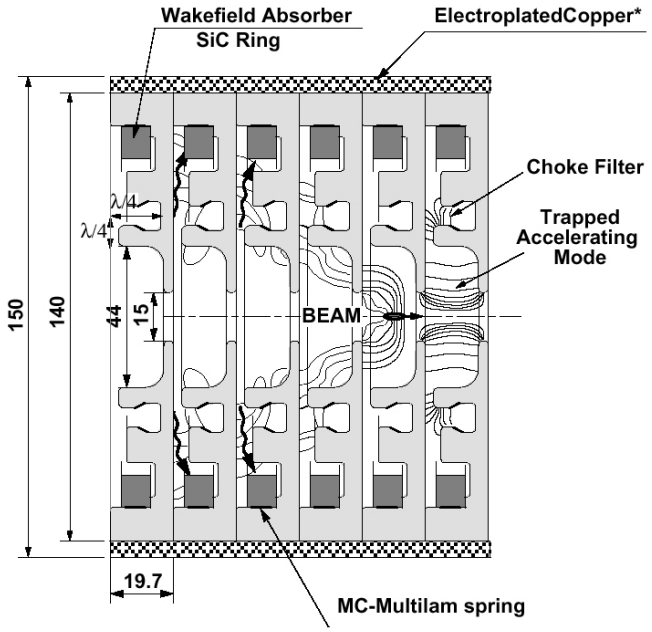

FIGURE 3.33. Cut-away view of the C-band choke-mode structure.

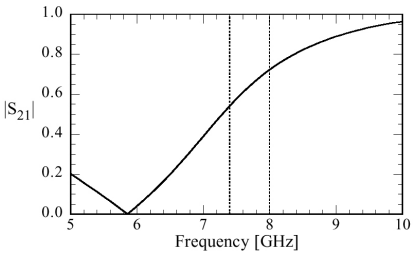

FIGURE 3.34. Dipole transmission of the choke.

The choke-mode concept has solved the multibunch problem but there is still the short-range wakefield problem, which causes tight fabrication and alignment tolerances for high-frequency cavities. The choice of C-band will be reasonable, considering the technical difficulties of tolerances at higher frequencies. The straightness tolerance is ± 50 μm (maximum bow) for a 1.8-m structure and the cavity-to-cavity random misalignment tolerance is ~ 30 μm for an emittance increase of 25%. (These numbers are based on old studies.) However, the effect of the decrease of the charge per bunch from old designs (1.1×10^{10} to 0.75×10^{10}) more than compensates the effect of the decrease of the target vertical emittance (3×10^{-8}m·rad to 2×10^{-8}) so that the tolerance will be even looser.

The frequency of the HOMs is not constant along the structure since we adopt a semi-constant gradient structure. The dimensions of cells, the choke filters, and the absorbers are designed in the following manner.

First, let us describe the optimization of individual cells. A part of the wakefield is reflected at the choke even though the radial line effectively extracts the wakefield. This can be a serious problem if the frequency of the main wakefield component is near the dipole stop-band frequency of the choke. In our case the main contribution to the transverse wakefield comes from TM_{110} whose frequency ranges from 7.4 to 8 GHz depending on the iris aperture ($2a$). Figure 3.34 shows the transmission coefficient of the choke. The dominant TM_{110} mode is in the region between the two dashed lines. One finds that only 1/3 to 1/2 of the TM_{110} power is transmitted to the absorber. Because of this effect a simple matched (no reflection) absorber at the outer end of the radial line does not provide sufficient damping. This problem can be solved by deliberately introducing some reflection to the absorber.

As shown in Figure 3.33, the absorber is a ring of SiC ceramics of rectangular cross section. This simple shape was adopted for three reasons: (a) it is easy to fabricate, (b) the reflection coefficient of the TM_{110} mode can be controlled by the width, and (c) the reflection coefficient above TM_{110} is relatively low. The width of the SiC ring is chosen to optimize the amplitude of the optimum reflection coefficient at the TM_{110} frequency. Although the reflection coefficient is optimized at the dominant TM_{110} frequency, absorption of all the field energy is sufficient for smaller peaks at higher frequencies. By the optimization of the absorber one can get faster damping by a factor of 2–3.

Next, consider the whole structure. The iris diameter $2a$ changes linearly with the cell number from 17.4 mm to 12.54 mm. This variation of the cell dimension introduces detuning of the HOMs and additional damping by spectral broadening. All the choke dimensions including the radial position are the same for the whole structure. The absorber dimension optimized by the procedure changes slightly from entrance to exit. The radial position changes from 46.5 mm to 44.5 mm but the width is fixed to 10 mm since the optimized reflection coefficient is almost the same over the whole structure.

A test structure was fabricated at KEK and installed in ASSET at SLAC in 1998 for wakefield tests. It was confirmed that the wakefield is damped as expected (the solid line in Figure 3.35) up to 1.6 ns (0.5 m) from about 15 to 1 V/pC/m/mm. This means that the basic concept of the choke-mode structure is confirmed. However, after this point, the measured wakefield showed a high frequency oscillation with amplitude of 0.8–1.0 V/pC/m/mm. This would cause a marginal emittance dilution of about 25%. This oscillation has spectral components at 20 and 23 GHz. It was realized with computer simulations that under certain conditions a mode can be trapped at a very high frequency whose field pattern has a node at the slot location, thus causing no power to leak out to the absorber. It turned out that a shift of the z-location of the damping slot by 2 mm can eliminate the trapped modes.

In the context of the wake function one constraint comes from the requirement of compatibility with the future X-band extension to the C-band linac. We adopted the bunch spacing of 1.4 ns for C-band collider as well as for the future X-band extension. It is possible to adopt 2.8 ns for the C-band collider but 1.4 ns is absolutely needed for the second stage. In Figure 3.35, the wake at 1.4 ns is still sizeable even when the trapped modes are eliminated. The value of the wake is marginal (possibly fatal) for the acceptable emittance increase. However, one can fine-adjust the cavity dimension without changing the major properties so that a node of the wake is located at 1.4 ns. If the wake has to be smaller for example by a factor of 5 (actually this is more than enough), then the phase of the wake must be less than 0.2 radian after about ten oscillations. This only requires the fabrication accuracy of 1/300, which is actually not a constraint.

In the test cavity a set of three rf-BPMs was installed in some cells (upstream, center, and downstream) as shown in Figure 3.36. The design of the rf BPM is depicted in Figure 3.37. The rf signal from the two rf BPM's, the wakefield monitor and the reference cavity are processed with the band-pass filters (7854 MHz, 3% bandwidth), down-converted to 310 MHz, and finally sampled with a four-channel digital scope. The reference signal is used to find the beam timing and the beam phase. The wakefield signal from the two pickup

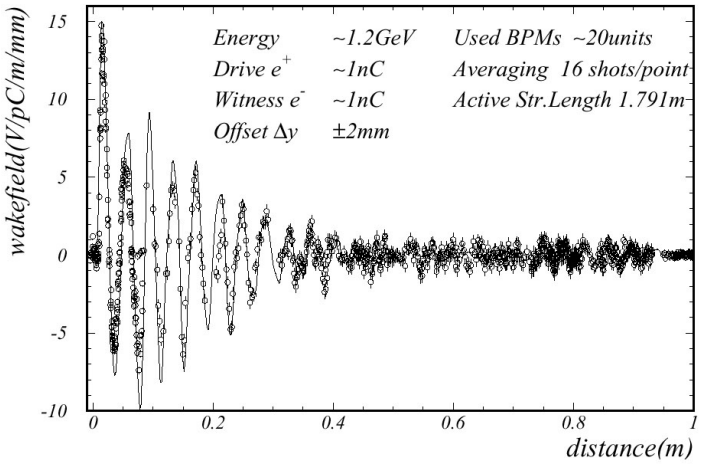

FIGURE 3.35. Measured (circles) and expected (solid line) wakefield.

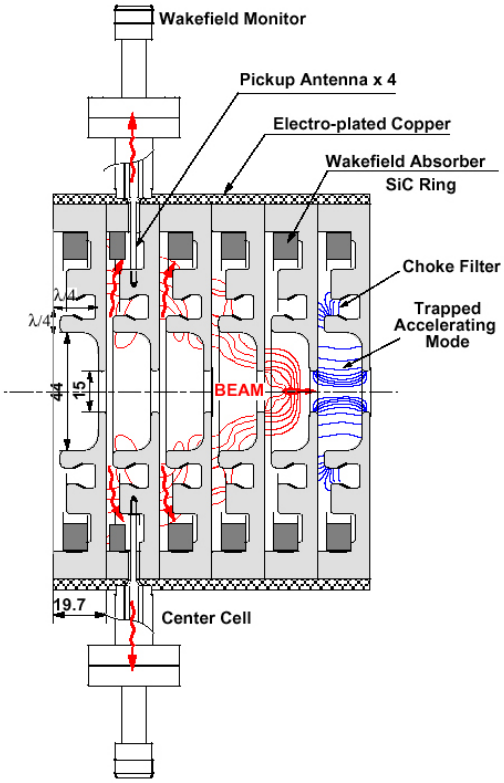

FIGURE 3.36. Choke-mode structure with rf-BPM.

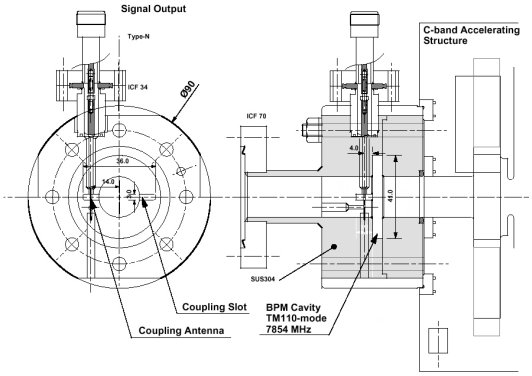

FIGURE 3.37. RF BPM with common-mode-less design.

antennas at the center BPM are combined in a 180-degree hybrid to eliminate the common-mode power. The data analysis showed that the center BPM had an offset of 63 μm with respect to the mean center of the upstream and downstream BPMs. By taking into account the calibration data, the straightness of the structure was found to be 49 μm, which is just at the border of the design tolerance. The observed spatial resolution was about 8 μm (limited by high digital noise in the sampling scope).

High power tests of the C-band choke-mode cavities have not yet been done. However, the same model is adopted in the SCCS (SPring-8 Compact SASE Source) project which will be constructed shortly. We do not foresee the breakdown problem found in X-band structures since the surface field is lower and the group velocity is low (in the range 3.6% to 1.1% of c).

3.3 JLC-X/NLC

3.3.1 Introduction

The JLC-X/NLC is a linear collider designed to provide luminosity at center-of-mass (c.m.) energies between 90 GeV and 1.3 TeV. It is based on normal conducting X-band rf technology. This technology was chosen for four reasons. First, at the higher rf frequency, the X-band technology is a reasonable extrapolation from the well understood S-band technology and it permits much higher accelerator gradients. Although the gradients achieved so far have not proved to be as high as initially thought, they are still much higher than possible at lower rf frequencies. Second, although the higher rf frequency demands tighter tolerances than S-band or lower frequencies, these tolerances have either been achieved in test facilities or are a small extrapolation (a factor of 2–3) from what has been attained. Third, the normal conducting design allows the linear collider subsystem designs to be based on other operating accelerators or accelerator subsystems. This is very important because, while the rf systems can be demonstrated in relatively inexpensive test facilities, it would be difficult and expensive to verify the other subsystems which are essential for the luminosity performance of the collider. Finally, all technologies which have presently been considered for reaching the multi-TeV region will have challenges similar to those that have been addressed in the X-band design but more difficult. Thus, the normal-conducting design provides an essential link to still higher collision energies.

The JLC and NLC have been presented in detail in the *1997 JLC Design Study* (JDS) [3] and the *1996 Zeroth-Order Design Report* (ZDR) [4]. During the last five years, the two designs have converged on a common parameter set while the linear collider R&D programs have led to substantial improvements over the original proposals. In addition, over the last five years, the physics program for a linear collider has evolved significantly, and as a consequence, the JLC-X/NLC has been modified to provide greater flexibility and higher luminosity. Further details on the design can be found in the *2000 International Study Group Report* [5] and the *2001 Report on the Next Linear Collider* [6].

The X-band linear collider is based on extensive experience from the first linear collider, the Stanford Linear Collider (SLC), as well as other modern accelerators and numerous test facilities including ASSET, the Final Focus Test Beam (FFTB) and the NLC Test Accelerator (NLCTA) at SLAC, and the Accelerator Test Facility (ATF) at KEK. In particular, the polarized electron source and the positron production system are modest

extensions of the SLC sources. The damping rings are similar to third-generation synchrotron light sources and are required to produce an equilibrium emittance that is only a factor of 2 below what has been achieved at the Advanced Light Source (ALS) in Berkeley or the ATF at KEK. The bunch compressor is based on experience from the SLC bunch compressor and is similar to, although not as difficult, as the bunch compressors for the new SASE-based short wavelength FEL drivers. Finally, a prototype X-band rf system has been operated successfully at the NLCTA since 1997. In principle, this system could be used today to build a 500-GeV c.m. collider, but there is active R&D on a next generation of components that are more efficient and less expensive to build and operate.

To preserve the small beam emittance during acceleration, the X-band structures must be designed to minimize wakefields, and both the structures and the focusing quadrupoles must be aligned to very tight tolerances. Structures fabricated in Japan and the United States already meet construction tolerances tighter than those required for JLC-X/NLC. The wakefield properties of these prototype structures have been measured precisely in the ASSET test facility and agree well with the calculations. The required alignment accuracy has also been demonstrated in ASSET. Beam-based alignment techniques developed for the SLC and FFTB quadrupoles have achieved close to the necessary accuracy, and extensive simulations indicate that these techniques are capable of preserving the emittance through a 14-km linac using diagnostics and correction hardware which needs to be only a factor of 2–3 better than that used at the FFTB. The FFTB also demonstrated the validity of the final-focus optics and achieved a demagnification of the beam size greater than required for JLC-X/NLC. All of these results have led to improvements in the design and increased confidence in its capabilities.

The JLC-X/NLC will be described in the following sections. It should be noted that although the JLC and NLC have the same rf system designs and the same beam parameters, small differences still exist between the two designs. The JLC would likely operate at a repetition rate that is a multiple of the 50 Hz line frequency while the NLC would operate at 120 Hz—this leads to different luminosities for the same beam parameters and requires slightly different damping rings. Finally, many of the detailed optical designs differ, partly because the NLC designs have continued to be refined while many of the JLC designs have not been revisited since the 1997 JDS. To address this problem, this chapter will present only the optics of the current NLC design but will note the differences where they exist. Finally, the optical decks contain detailed information on the placement of the diagnostic and control equipment which is essential for operating the collider, but these systems will not be discussed because of space limitations.

3.3.2 Parameters and Layout

The JLC-X/NLC collider parameters and layout have evolved over the last five years. These changes have been motivated by a desire to provide additional physics opportunities and to reduce the capital costs of the facility. The facility is designed for optimal performance at a c.m. energy of 1 TeV, but with flexibility to begin operation at 500 GeV and be upgraded to match the needs of physics as they evolve. Key areas and systems are designed for energies above 1 TeV. In particular, by reducing the beam current, the presently envisioned linac that would deliver beam for 1 TeV collisions, would still be able to deliver substantial luminosity at a c.m. energy of 1.3 TeV.

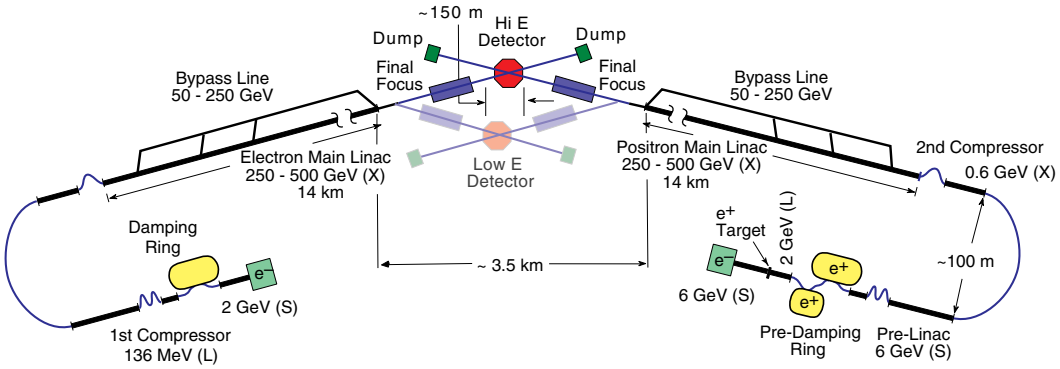

FIGURE 3.38. Schematic of the JLC-X/NLC.

The collider configuration is shown schematically in Figure 3.38. The 1 TeV collider is roughly 30 km in length. The main linac rf systems are capable of generating 250 GeV beams (500 GeV c.m. collisions) in one half of the two 14-km long linac tunnels that are part of the initial configuration. The upgrade to 1 TeV c.m. energy can be achieved by completing the main linacs with replicas of the rf components used in the initial construction, or, more likely, with improved versions of those components. Bypass lines along the main linac allow beams of various energies to be transported to the experiments, fully covering the energy range from 90 GeV to 1.3 TeV. The beam sources and damping rings that make up the injectors for the main linacs are designed to meet specifications for 1.5 TeV collisions.

To accommodate the physics demands for energy flexibility, the design includes two interaction regions. One is optimized for high energy, 250 GeV to 1.5 TeV, and is configured so that it is ultimately upgradable to multi-TeV. The other is designed for precision measurements at lower energy, 90 to 500 GeV, although it could be upgraded to operate at ∼1 TeV as well. The final focus can actually accommodate beams of up to 2.5 TeV in a length of about 800 meters. To capitalize on the multi-TeV potential of the new design, it was also necessary to eliminate other bending between the linac and the high energy IP. In the NLC design, a 20 mrad crossing angle at the IP is used to avoid parasitic interactions of one bunch with the later bunches in the opposing train and to ease the extraction line design. The linacs are not collinear but are oriented with a shallow 20 mrad angle between them to produce the desired crossing angle at the high-energy IR without additional bending. The beams to the second IR are bent by about 25 mrad, which is acceptable for energies up to ∼1 TeV. The low-energy IR has a larger 30 mrad crossing angle for compatibility with a possible γ/γ option. Finally, in the JLC design, the primary IP has a crossing angle of 7 or 8 mrad and the non-collinear linac layout has not been planned. However, the crossing angle of the second IP is 30 mrad as in the NLC design.

The primary e^+/e^- parameters for the JLC-X/NLC are listed in Table 3.14. The beams consist of bunch trains with 192 bunches separated by 1.4 ns. The repetition rate would be 150 Hz for Stage I and 100 Hz at Stage II in Japan while, in the US, the repetition rate would remain 120 Hz at both stages. Although not listed, the collider is also designed to operate with 96 bunches of 1.5×10^{10} particles and a 2.8 ns bunch spacing—this later

TABLE 3.14
Parameters for Stage I and Stage II of the JLC-X/NLC.

	Stage I		Stage II	
Center-of-mass energy [GeV]	500		1000	
Site	Japan	US	Japan	US
Luminosity [10^{33}] incl. dilutions	25	20	25	30
Repetition rate [Hz]	150	120	100	120
Luminosity within 1% of $E_{c.m.}$ [%]	64		58	
Bunch charge [10^{10}]	0.75		0.75	
Bunches/rf pulse	192		192	
Bunch separation [ns]	1.4		1.4	
Lum. dilution for tuning and jitter [%]	5		5	
Injected $\gamma\epsilon_x$ / $\gamma\epsilon_y$ [10^{-8} m·rad]	300 / 2		300 / 2	
$\gamma\epsilon_x$ / $\gamma\epsilon_y$ at IP [10^{-8} m·rad]	360 / 4		360 / 4	
β_x / β_y at IP [mm]	8 / 0.11		13 / 0.11	
σ_x / σ_y at IP [nm]	243 / 3.0		219 / 2.1	
σ_z at IP [μm]	110		110	
Upsilon average	0.13		0.28	
Pinch enhancement	1.49		1.42	
Beamstrahlung δ_B [%]	4.6		7.5	
Photons per e^+/e^-	1.3		1.3	
Loaded gradient [MV/m]	50		50	
Linac length [km]	6.9		13.8	

option might be preferred for γ-γ collisions but also provides higher e^+/e^- luminosity while increasing the beamstrahlung and emittance dilution. During the initial stage, the center-of-mass energy is assumed to be 500 GeV with a luminosity of 2.5×10^{34} cm^{-2}s^{-1} (2.0×10^{34} cm^{-2}s^{-1}) at the repetition rate of 150 Hz (120 Hz), although the collider might be started with a lower initial energy depending on the physics interest. The second stage assumes the installation of the full rf system to reach a center-of-mass energy of 1 TeV with a luminosity of 2.5×10^{34} cm^{-2}s^{-1} (3.0×10^{34} cm^{-2}s^{-1}) at a repetition rate of 100 Hz (120 Hz). In addition, sets of nominal parameters for operation of the low-energy IR are listed in Table 3.15.

TABLE 3.15
Low energy operation parameters for the NLC.

Center-of-mass energy [GeV]	92	250	350
Luminosity [10^{33}]	3.5	9.4	13.2
Luminosity within 1% of $E_{c.m.}$ [%]	92	75	65
Repetition rate [Hz]	120	120	120
Bunch charge [10^{10}]	0.75	0.75	0.75
σ_x / σ_y at IP [nm]	630 / 6.2	380 / 3.8	320 / 3.2
Beamstrahlung δ_B [%]	0.18	1.1	2
Photons per e^+/e^-	0.49	0.79	0.92
Polarization loss [%]	0.08	0.21	0.34

It should be noted that the JLC-X/NLC traveling wave accelerator structures are tested to the full unloaded gradient of 65 MV/m; this differs from the testing of the standing-wave superconducting structures which are only tested to the maximum *loaded* gradient of 23 to 35 MV/m. Because the cavities are tested to the full unloaded gradient, the JLC-X/NLC collider could operate at an energy roughly 25% higher than nominal with 30% of the nominal luminosity by reducing the average beam current. Thus, without modification to the rf system, the Stage II JLC (NLC) could deliver a luminosity of 7×10^{33} cm^{-2}s^{-1} (9×10^{33} cm^{-2}s^{-1}) at a c.m. energy of 1.25 TeV. A plot of the luminosity versus energy for the Stage II NLC is plotted in Figure 3.39; using the bypass lines and the two interaction regions, the collider is designed to fully cover the energy region between 90 GeV and 1.3 TeV.

The beam parameters listed in Table 3.14 and Table 3.15 have been chosen to balance total luminosity against the fraction of luminosity close to the center-of-mass energy and the bremsstrahlung-related backgrounds. The luminosity spectrum can be described by two parameters, the number of beamstrahlung photons radiated per incident electron n_γ and the average energy lost to the beamstrahlung δ_B. These parameters can be traded against each other to optimize the total luminosity and the luminosity spectrum for any given experiment. The parameters presented in Table 3.14 and Table 3.15 are only an illustrative set.

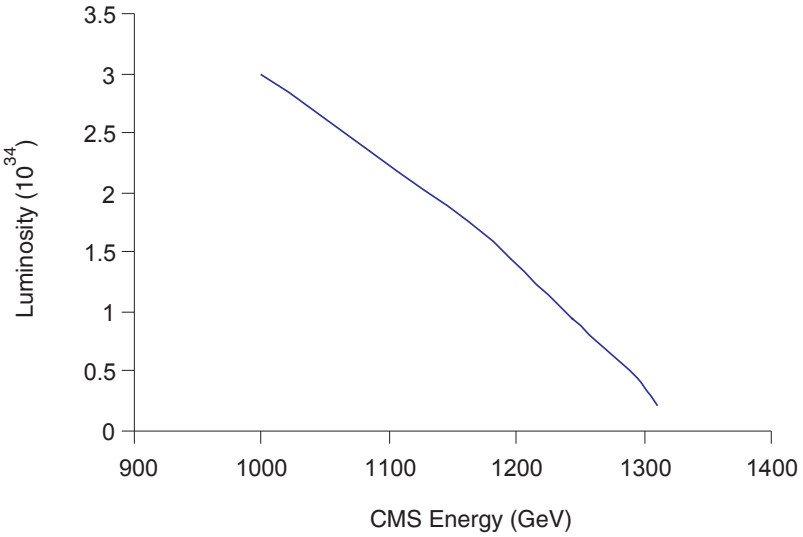

FIGURE 3.39. Energy versus luminosity for Stage II NLC rf system.

Detailed emittance and beam-jitter budgets are shown in Table 3.16; these are discussed in Section 3.3.6 along with the beam-based alignment and jitter-stabilization techniques. The design luminosities, listed in Table 3.14, include 5% luminosity degradation beyond the explicit emittance dilutions to account for beam jitter and beam tuning. It is important to emphasize that the JLC-X/NLC has been designed with generous margins throughout to facilitate attaining the design luminosity rapidly.

It should also be noted that the ultimate luminosity of the collider is roughly a factor of 2 higher than the design. This higher luminosity might be attained if the beam-based alignment techniques can be pushed to even higher precision and the beam-beam limitations due to the high disruption parameter that impact the TESLA design can be overcome; the disruption parameter for these high luminosity parameters is roughly 20 which is still less than the TESLA values of 25–28. The ultimate luminosity, referred to as the "intrinsic luminosity," is determined by physical limitations such as the finite damping time of the damping rings and synchrotron-radiation emission in the bunch compressors and final focus. These intrinsic beam emittances and luminosity are listed in Table 3.17 for comparison with the design values.

Next, possible parameters for operation as a γ/γ collider are listed in Table 3.18. These parameters are based on the JLC-X/NLC beam with a 2.8 ns spacing and 96 bunches as noted earlier. The γ/γ interaction region would be located in the "Low Energy IR" (LEIR) which has a large crossing angle of 30 mrad to facilitate extracting the disrupted e^- beams. To take full advantage of the photon interaction, the horizontal and vertical beta functions have been reduced at the IP which has been verified with tracking simulations.

Finally, as described, the JLC-X/NLC is designed to operate with center-of-mass energies up to ∼1.5 TeV. The next logical step for electron-positron facilities would then be a linear collider that operates in the 3-TeV to 5-TeV center-of-mass range with a luminosity of 10^{35} or more, using a design such as CLIC. The history of accelerator laboratories makes one

TABLE 3.16
NLC Design Emittance and Jitter budgets for 500 GeV c.m. parameters.

Region	$\gamma\epsilon_x$ [μm·rad]	$\gamma\epsilon_y$ [μm·rad]	X jitter [σ_x]	Y jitter [σ_y]
Damping ring	3.0	0.020	0.1	0.1
Injector (8 GeV)	0.2	0.002	0.1	0.1
Main linac	0.1	0.010	0.1	0.3
Beam delivery	0.3	0.008	0.1	0.3
Final doublet			0.1	0.25
Total at IP	3.6	0.04	0.22	0.51

TABLE 3.17
Intrinsic versus design emittances and luminosity for JLC-X/NLC at 1 TeV.

	Intrinsic	Design
Damping rings $\gamma\epsilon_x$ / $\gamma\epsilon_y$ [10^{-8} m·rad]	300 / 1	300 / 2
Main linac $\gamma\epsilon_x$ / $\gamma\epsilon_y$ [10^{-8} m·rad]	315 / 1	330 / 3
Beam delivery $\gamma\epsilon_x$ / $\gamma\epsilon_y$ [10^{-8} m·rad]	330 / 1	360 / 4
Luminosity [10^{33}]	63	30

TABLE 3.18
Parameters for γ/γ collisions at the JLC-X/NLC.

Beam energy	250 GeV
Luminosity including dilutions	3.2×10^{33}
Repetition rate	120 Hz
Bunches/rf pulse × bunch separation	96 × 2.8 ns
Bunch charge	1.5×10^{10}
$\gamma\epsilon_x$ / $\gamma\epsilon_y$ at IP	360 / 7.1 $\times 10^{-8}$ m·rad
β_x / β_y at IP	4 / 0.065 mm
σ_x / σ_y at IP	172 / 3.1 nm
σ_z at IP	156 μm
Conversion point → IP	2 mm

point clear: the investment in the infrastructure of the accelerators, including the beamline housings, is significant and therefore the infrastructure should be used and reused for as long as possible. This has led to the use of existing synchrotrons as injectors for new synchrotrons, and in some cases to the decommissioning of existing accelerators so that the tunnels or components can be recycled for use in new accelerators. It is this history that has shaped the decision to make the design as compatible as possible with future energy upgrades.

While it is too early to determine the technologies that will be used at a multi-TeV linear collider, a general review of the issues discussed previously reveals many of the requirements of such a facility. The JLC-X/NLC configuration has been developed with these requirements in mind. For example, the multi-TeV linear collider will require a site with low levels of ground motion, a crossing angle of at least 20 mrad, beam delivery systems with weak bend magnets, and in all probability a main-linac tunnel that can accommodate a second beamline for the "drive beam." All of these features are included in the design. In many cases, the requirements are identical to those of a future facility. In other cases, configuring the design to accommodate a future linear collider did not cause additional financial or technical penalties. This permits the injectors, beam delivery systems, and main-linac housings to be used in a multi-TeV collider, although the main-linac accelerator structures and rf power sources would need to be replaced and some upgrades of the damping rings, bunch compressors, and final-focus beamlines would be required.

3.3.3 Main Linacs and RF Systems

The main JLC-X/NLC linac tunnels are each 13.8 km long and contain the necessary rf system as well as three diagnostic regions and three extraction sections that feed the bypass line (see Figure 3.40). The tunnels are designed to be long enough to hold the full complement of accelerator structures to reach 1 TeV in the center-of-mass at the design luminosity, although, in the first stage of the project, only the first half of the tunnels would be filled with structures. The installation would start from the low-energy end of the tunnel to allow maximum flexibility in choosing the appropriate energy upgrade steps to match physics interests and funding profiles.

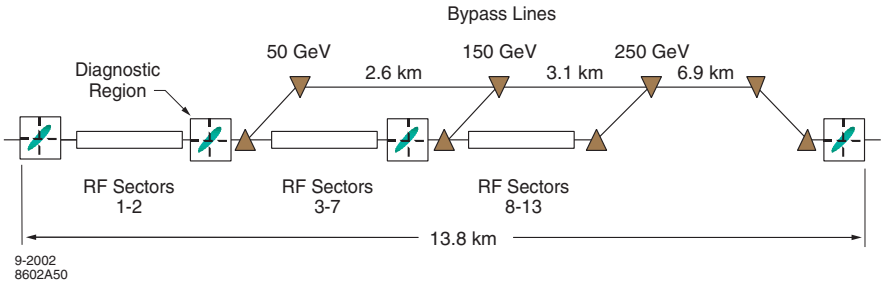

FIGURE 3.40. Schematic of the JLC-X/NLC linac layout; each sector contains 20 rf units in a length of 520 meters.

The JLC-X/NLC linac would contain 254 rf units at Stage I (500 GeV c.m.). Each rf unit contains one solid-state induction modulator driving eight 75-MW 1.6-μs klystrons arranged in pairs. Each of the four klystron pairs powers a dual-mode SLED-II pulse compression system which feeds an rf girder with six 0.9-m accelerator structures. The linac beam-line enclosure would contain the accelerator structures while the modulators and klystrons will be installed in a separate utility enclosure. This simplifies access and maintenance which is essential to ensure the desired reliability and collider availability. The SLED-II lines could be placed in either the main linac tunnel or in the utility tunnel—both options have advantages: the main linac tunnel has better temperature control however the utility tunnel allows easy access for upgrades and maintenance of the SLED-II systems.

Because of the transverse wakefields of the accelerator structures, it is undesirable to transport the beam through a large number of unpowered structures. In order to maximize luminosity at lower energy, a non-accelerating "bypass" line is provided to bring the low-energy beams to the end of the linac. The bypass line will share the main-linac tunnel, and will be installed at the same elevation as the main beamline. The design includes three transfer points where the beam can be diverted into the bypass line at 50, 150 and 250 GeV, and a return at the end of the linac to bring the beam back into the collimation section. These are sufficient to support a continuous variation of beam energy over the whole range.

The linac transport optics were chosen to minimize the dispersive and wakefield-related beam emittance growth. In the NLC design, quadrupole magnets, in a FODO configuration, are located after every (one, two, or three) rf girders at the (beginning, middle, or end) of each linac. The quadrupoles in the rf regions will have 12.7-mm-diameter apertures and vary in length from 0.32 m to 0.96 m. The rf girders and quadrupoles will be supported on movers that will be remotely adjusted during beam operation based on signals from the structure manifolds and beam position monitors (BPMs) in the quadrupole magnets.

As will be discussed in Section 3.3.6, extensive effort has been made to ensure that the beam emittance can be preserved along the linac. The signals from the structure manifolds will be used to directly align the accelerator structures to the beam; as discussed in Section 3.3.3.5 measurements using the manifolds in prototype structures have already shown the required precision. The BPMs located at the quadrupole magnets will be used to align the quadrupoles. Although the required quadrupole alignment is roughly 25 times smaller than that achieved in the SLC and about 3 times smaller than in FFTB, the BPMs are specified to have resolutions of 0.3 μm which has been demonstrated in prototype rf BPMs and is 50 times smaller than that in the SLC linac and 3 times smaller than that in the FFTB. Because the expected alignment precision scales with the diagnostic resolution, using the quad-shunting beam-based alignment technique utilized at the FFTB with the improved BPM resolution should attain the desired alignment.

Simulations indicate that the desired alignment precision will be attained. However, to provide additional safety margin, provision has been made to utilize two other beam-based alignment techniques pioneered at the SLC: dispersion-free steering and emittance correction bumps. These techniques are relatively sensitive to details of the energy profile along the linac and the beam optics. To monitor the beam energy, energy spread, and emittance, there will be four diagnostic regions along the length of the linac where these parameters can be measured parasitically. In addition to being needed for the beam-based alignment and emittance correction techniques, continuous, non-invasive monitoring was

found to be essential during the SLC operation because it facilitates rapid diagnosis of faults and makes it possible to correlate disparate effects.

In the following sections, the rf system will be described in greater detail and then, in Section 3.3.6, the emittance preservation and luminosity performance issues will be discussed.

3.3.3.1 RF Systems

Outstanding progress has been made in applying and extending the science and engineering of microwave power and acceleration systems from S-band, the enabling technology for the SLAC linac, to X-band, which can provide the significant performance improvements and cost reductions needed for a high-energy linear collider. New modulators, klystrons, microwave power distribution systems, and accelerator structures that can meet the challenging demands of a linear collider are in the final stages of development. The R&D on these components has been pursued as a joint effort between SLAC and KEK as part of the International Study Group (ISG) developing designs for an X-band linear collider.

The 11.424-GHz rf systems are similar in character to those in the SLAC linac. Electrical energy is transformed in several stages: the induction modulators convert AC power to high-voltage pulsed DC; the klystrons transform the pulsed DC to high-power rf; the SLED-II pulse compression system combines the power from two klystrons with pulse lengths of 1.6 μs and, by storing the power, compresses it into pulse lengths of 400 ns and sends it to sets of six accelerator structures; and finally, the six structures on each rf girder accelerate the beam. The baseline JLC-X/NLC rf system is illustrated in Figure 3.41.

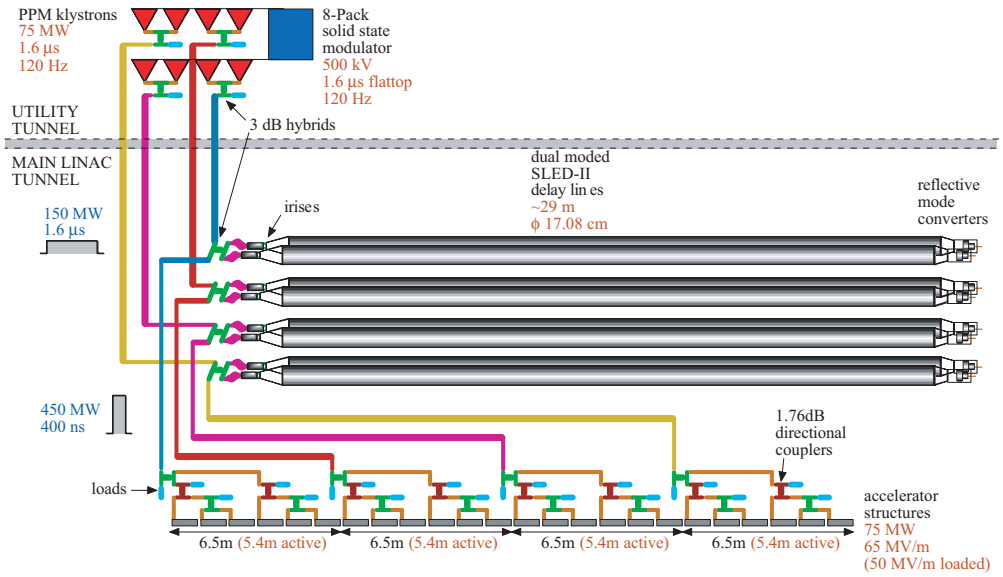

FIGURE 3.41. Schematic of a JLC-X/NLC linac rf unit (one of 254 per linac); the SLED-II delay lines could be located in either the linac or utility tunnels.

Because the AC power required to drive the accelerator is high, especially at a c.m. energy of 1 TeV, much effort has been focused on maximizing the efficiency of the conversion and transfer of energy at every stage of the rf system. Both the JLC and NLC design teams have been investigating alternate pulse compression systems with higher efficiency than the SLED-II rf system. In particular, the Delay Line Distribution System (DLDS) will be pursued as a possible high efficiency option to the SLED-II pulse compression system. However, because of the simpler topology of the SLED-II system, it will be faster to demonstrate a SLED-II pulse compression system at the full JLC-X/NLC power specifications than it will be to test a full DLDS system. In addition, the JLC-X/NLC SLED-II pulse compression system is based on the SLED-II systems that have operated at the NLCTA for over five years, providing confidence in the design. We believe that, by first pursuing the SLED-II-based baseline rf design and then moving toward a higher efficiency system, we will be able to demonstrate the feasibility of the X-band rf system while still working to improve the system efficiency.

The parameters of the JLC-X/NLC major rf subsystems (klystrons, modulators, rf distribution, and accelerator structures) are listed in Table 3.19. The unloaded gradient (G_U) of 65 MV/m is close to optimal in the tradeoff between energy-related costs (*e.g.*, modulators and klystrons), which scale roughly as G_U, and length-related costs (*e.g.*, structures and beam-line tunnel), which scale roughly as $1/G_U$. However, the overall linac cost has a fairly weak dependence on unloaded gradient in the range of interest for the JLC-X/NLC (50 to 100 MV/m). The beam parameters were chosen as a tradeoff between increasing rf-to-beam efficiency and easing tolerances related to both short-range and long-range transverse wakefields effects.

A brief description, including design choices and R&D progress, of each major rf subsystem follows.

3.3.3.2 Modulators

The 75-MW PPM klystrons require pulses of roughly 500 kV and 260 A. Initially, conventional line-type modulators like those used in the SLAC linac were considered for this purpose. These modulators contain pulse-forming networks that are slowly charged and then rapidly discharged, via a thyratron, through a step-up transformer to generate the high-voltage pulse. These modulators have several drawbacks including low efficiency and the use of thyratrons, which have relatively short lifetimes (10,000–20,000 hr) and require periodic adjustments. As an alternative, the idea of a solid-state induction-type modulator was explored, based on recent advances in high-power, solid-state switches (Insulated Gate Bipolar Transistors or IGBTs). The concept is to sum many low-voltage sources (2–4 kV) inductively to yield the desired klystron voltage. This has been implemented by having each source drive a toroidal-shaped transformer made with Metglass or Finemet cores. The cores are stacked so secondary windings, which sum the output voltages, can be threaded through them. Each source is essentially a capacitor that is slowly charged and then partially discharged through an IGBT switch to generate the pulse.

The solid state NLC modulator is designed to power eight klystrons. It is constructed from 42 Metglass cores, each driven by two 6.5 kV IGBTs operating at 4 kV and 3 kA. These drive a 3-turn secondary winding for an output pulse of 500 kV, 2160 Amps that is 1.6 μs long. The modulator is roughly 2 meters high and consists of two stacks of 21 cores.

TABLE 3.19
JLC-X and NLC rf system parameters.

	JLC-X	NLC
RF units per linac (500 GeV c.m.)	254	
AC power for modulators per linac	65.9 MW	
AC power for other rf + cooling rf system per linac	9.6 MW	
Total AC power related to rf per linac	75.5 MW	
Beam power per linac	6.9 MW	
AC-to-beam power efficiency	8.8%	
Modulator type	1:1 linear induction	1:3 induction
Modulator efficiency	80%	80%
Number of rf modulators per rf unit	1	1
Klystron type	PPM	
Beam voltage/current	490 MV / 260 A	
Output power	75 MW	
Klystron pulse length	1590 ns	
Klystron efficiency	55%	
Number of klystrons per rf unit	8	
Type	SLED-II	
Modes	TE_{01} & TE_{02}	
Power gain = number of feeds per rf unit	4	
Switching time	8 ns	
RF pulse length per feed	396 ns	
Compression efficiency	75%	
RF phase advance per cell	150 degrees	
Structure input group velocity	5.1% c	
Structure length	0.90 m	
Field attenuation factor (τ)	0.510	
Number of structures per rf feed	6	
Fill time	120 ns	
Average acceleration shunt impedance	81.2 Mohm/m	
Loading shunt impedance	82.4 Mohm/m	
Peak rf power into structure	75.0 MW	
Unloaded accelerator gradient (G_u)	64.8 MV/m	
Beam loading	23%	
Multibunch loading	14.7 MV/m	
Single bunch loading	0.30 MV/m	
Loaded accelerating gradient	49.8 MV/m	
Average rf phase	11.0 degrees	
RF overhead (3% BNS + 3% failed + 2% FB)	8%	
Length of powered linac	6.6 km	
Length of unpowered linac (for upgrade to 1 TeV c.m.)	6.6 km	
Total length of diagnostic and bypass regions	0.6 km	
Total length of each linac tunnel	13.8 km	

FIGURE 3.42. Photograph of the NLC induction modulator with three of the SLAC 5045 klystrons that are used as a load.

A full-scale prototype based on 4.5 kV IGBTs is shown in Figure 3.42. The JLC modulator, referred to as the Linear Induction Modulator, is similar except that it uses a single-turn secondary to produce 500 kV and 2 kAmps to eliminate the production and installation of the secondary windings. The design has three times the number of cores although, on average, cores are smaller.

For fast pulse performance, the IGBT drivers must be operated in a regime where they are not well modelled. The drivers are designed for locomotive traction, requiring continuous high power operation at a few kV and 600–800 A. The pulsed-power requirements of the modulator are very high dI/dt, peak currents that nearly saturate the bipolar switch, high voltage lasting only for a few microseconds, and inductive connections through the drivers to capacitive loads (klystrons). After each pulse, the core has to be reset, and stored energy recovered. This must be done without producing transients on the gate of the IGBT sufficient to exceed its ratings and destroy the transistor. Several key technical challenges encountered in bringing the designs from concept to working prototype include:

- IGBTs have a known susceptibility to neutron radiation induced from cosmic rays, or accelerators, which can cause a Single Event Upset (SEU) that latches and destroys the bipolar transistor. Shielding solves this problem in the JLC-X/NLC applications.
- Many studies have been conducted to develop circuits that will protect the IGBTs under conditions of a short circuit to the load and of core saturation. Some wiring layout changes have been made in the transistor itself to minimize unwanted transients.
- To protect the stack if one IGBT fails, a circuit was developed that assures that, on failure, the device is shorted and disconnects its drive voltage from the cell primary single turn. Therefore, the stack suffers an incremental drop in voltage due to the loss of the one cell, which could be compensated by either slightly raising the supply

voltage on each cell or by turning on spare "hot" IGBT cards which will be installed in each modulator. This fail-soft feature will enable longer periods of continuous operation without interruptions for maintenance.

- Two approaches are being adopted to limit the energy delivered if one of the klystrons arcs. Passive inductance from the stack to each tube, and between tubes, is used to slow the transfer of charge to the faulting tube. In addition, the entire stack is designed to sense the fault and shut off in about 400 ns, drawing most of the load's stored charge and shunting it to ground. Klystron faults have been studied on pairs of X-Band klystrons in NLCTA at SLAC, so far with no apparent degradation.

- Recently, current and voltage distribution in the two commercial IGBT hybrid packages currently being used have been modelled on a 3D simulator. The commercial hybrid circuits consist of between 9 and 16 bonded dies, each with multiple IGBTs, on a single substrate mounted on a heat sink. The cause of observed failures in one of the layouts has been traced to the highly non-uniform distribution of high dI/dT current densities as a function of chip location on the die, due to unsymmetrical placement with respect to buses, and uneven wire bonding. During the fast rise time transient currents in different bond wires and single chips vary by more than 10:1. A new symmetrical geometry has been modelled which eliminates this effect entirely. Also some simple bond wire changes with the present layout will improve distribution by a factor of 2–3. While the IGBTs now in hand are totally sufficient to support the present program, development of a more robust device for fast pulse applications is being pursued with manufacturers.

At SLAC, a full-scale prototype induction modulator has been built using 3.3 kV IGBTs and a stack of 76 ferrite cores. Testing began in October 2001 (Figure 3.42) and proceeded to full voltage at low power using a water load. The modulator was then tested to near full power, but less than full voltage, using three 5045 S-band klystrons operating as diodes. These klystrons are the only loads available that permit testing close to the full power. To study the modulator in extreme conditions, the voltage was further raised to deliberately arc the 5045 klystrons. During the arc testing, damage occurred to the IGBTs. This problem was solved by adding "snubber" circuits to damp the high frequency reflections and upgrading the IGBTs to 4.5 kV models. This prototype modulator has now been moved to the NLCTA to power the SLED-II pulse compression system and demonstrate the JLC-X/NLC baseline X-band rf system. Another 8-pack modulator using 6.5 kV IGBTs is under construction at the Lawrence Livermore Laboratory and should be completed in 2003. At KEK, the design for the Linear Induction Modulator, shown in Figure 3.43, is nearing completion and a full prototype should be operating in 2003.

3.3.3.3 Klystrons

The X-band power required for the JLC-X/NLC has driven the development of klystrons much further than those available commercially. The designs first considered were similar in concept to the solenoid-focused S-band klystrons used in the SLAC linac. The general design goal was to achieve the highest peak power and the longest pulses possible while minimizing the overall klystron cost. As a first step, the XL4 klystron was designed in the early 1990s and achieved its target power of 50 MW. Thirteen of these XL4s have been

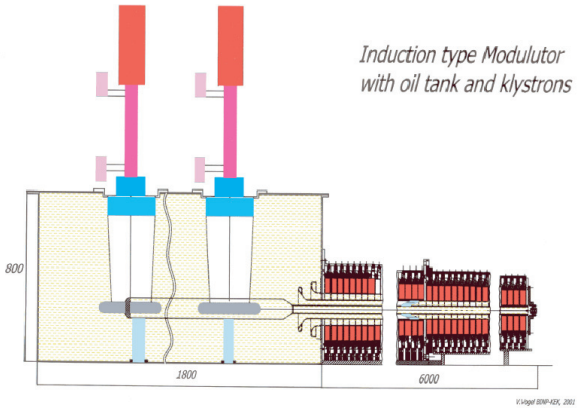

FIGURE 3.43. Schematic of the JLC Linear Induction Modulator design.

built. They are used as X-band rf sources for R&D at the SLAC Klystron Test Laboratory and the Next Linear Collider Test Accelerator (NLCTA). They reliably generate 1.5-μs, 50-MW pulses with a 43% beam-to-rf efficiency. In a test, one XL4 klystron was run at 120 Hz with 75-MW, 1.5-μs pulses which were produced with 48% efficiency. An XL4 has also been operated at 2.4 μs and 50 MW without difficulty. At KEK, two similar klystrons (XB72K-9 and XB72K-10) also operate with 1.5-μs pulses at 50 MW. The integrated running time of the XL4/XB72K klystrons is around 40,000 hours, during which there have been no major failures (the JLC-X/NLC lifetime goal is 20,000 hours).

With the success of these solenoid focused klystrons, attention turned to developing a permanent magnet focusing system which would consume no power. In the Periodic Permanent Magnet (PPM) design, many magnet rings with alternating polarities are interleaved with iron pole pieces to generate a periodic axial field between the gun anode and beam collector. The resulting focusing strength is about 2 kG, which is smaller than the 5-kG field in the solenoid-focused klystrons. The weaker PPM field has led to a klystron design with a higher voltage-to-current ratio, which reduces the space charge defocusing and increases the klystron efficiency; the microperveance of the 75 MW PPM klystrons is between 0.70 and 0.80 and the klystrons operate at roughly 500 kV and 250 A.

The first PPM klystron was built at SLAC in 1996 to generate 50-MW pulses, like the XL4s. It worked well, producing 1.5-μs, 50-MW pulses with an efficiency of 55%, close to the predicted performance. The next klystron, referred to as the XP1, then was designed for 75 MW. After modification, the klystron delivered over 90 MW in a 0.7-μs pulse length and 79 MW at 2.8 μs with 60% efficiency. The repetition rate was limited to 1-Hz due to heating of the uncooled magnet stack. The most recent klystron at SLAC, the XP3, has been designed to operate at a 60 Hz repetition rate at 75 MW and a 3.2 μs pulse length; the 3.2 μs pulse length, which is twice the rf system requirement, was chosen to increase the energy output from each klystron and thereby reduce the required number of klystrons by a factor of 2. Two of these klystrons have been built however neither reached the desired output power due to fabrication errors; a third is being constructed.

At KEK, three PPM klystrons have been designed and built by industry. The first, PPM-1, was completed in 2000 and produced 56 MW with pulse lengths of 1.5 μs and roughly 50%

efficiency. The second, PPM-2, was completed in 2001 and produced 70 MW in a pulse length of 1.5 μs with a 55% efficiency before a modulator problem halted testing. This klystron was operated at 25 Hz. The most recent klystron, PPM-3, is being tested. It has operated at 68 MW with a 1.5-μs pulse length and 53% efficiency. The repetition rate is limited by the modulator to 50 Hz, however, thermal measurements show that the tube could safely operate at 100 Hz without additional cooling. With further testing it is expected that the klystron will produce the desired 75-MW power with an efficiency of about 55%.

Finally, next-generation klystrons are being designed at SLAC and KEK. At KEK, the PPM-4 is a version of the PPM-3 optimized for mass production and should be delivered in February 2003. At SLAC, the XP4 is being designed for completion in 2003. The goal of both programs is to produce a number of klystrons to be lifetime tested.

3.3.3.4 RF Pulse Compression

Using the klystron output power to drive the accelerator structures is complicated by the different pulse-length and peak power requirements. While long, relatively low power klystron pulses are optimal from a klystron cost perspective, shorter pulses are needed to power the structures to minimize overall cost. An rf pulse compression system is used to match these conditions.

The goal in compressing the pulse (and increasing the peak power) is to make the transition efficiently with as little waveguide as possible. The Delay Line Distribution System (DLDS), proposed at KEK, is a very efficient system. Other options include the Binary Pulse Compression system, which has comparable efficiency, and the SLED-II system, which is less efficient but requires less waveguide. All of these rf distribution systems are characterized by the ratio of the klystron to structure pulse length or the compression ratio. In the JLC-X/NLC design, a compression ratio of four is needed. The rf system is based on a dual-moded SLED-II compression system which was chosen for two reasons. First, while other pulse compression systems are more efficient, they are more complicated and, unfortunately, this will delay the demonstration of the system. Second, the NLC Test Accelerator group has a lot of operational experience with SLED-II pulse compression whose technology has been established for years. The only challenge is that the full power JLC-X/NLC version must produce 400 ns pulses of 450 MW—the SLED-II systems at the NLC Test Accelerator and the Klystron Test Laboratory have generated 240 ns pulses of 270 MW and 150 ns pulses of 480 MW. The new over-moded components that have been developed are expected to have no trouble operating at the higher field levels. Finally, the routing of the rf power is controlled with the klystron phases. An 8-ns period is allotted for each phase shift, making the total klystron pulse length needed to accelerate the JLC-X/NLC bunch train equal to 1.59-μs.

To fully demonstrate the SLED-II system, the prototype NLC solid state modulator has been moved to the NLC Test Accelerator. Four 50-MW klystrons will be used to power a dual-moded SLED-II system as illustrated in Figure 3.44. With four times pulse compression, the SLED-II system will be able to produce 600-MW in a 400 ns pulse; this is 33% higher power than required in the JLC-X/NLC, giving confidence in the SLED-II design. The system could also be operated with a 2.4-μs input pulse and six times compression to deliver over 800 MW. The high power tests will be complete by mid-2003 at

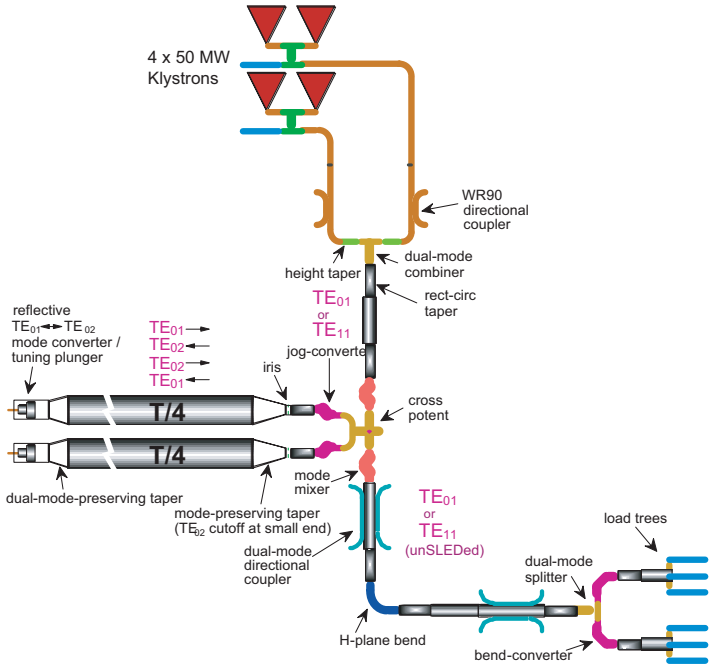

FIGURE 3.44. Schematic of the dual-moded SLED-II demonstration at the NLCTA.

which point the rf power will be directed into the NLCTA enclosure to power one rf girder of accelerator structures.

To prevent significant attenuation while transmitting the power through the long waveguides, the rf power is transported in low-loss circular modes. A low-power transmission test of the three circular modes in a 55-m delay line was performed at KEK to verify the expected power attenuation per unit length of the modes. The results of the test confirm the viability of any of the TE_{01}, TE_{02}, or TE_{12} modes for a pulse compression system. At the present time, the JLC-X/NLC SLED-II delay lines use two circular modes, the TE_{01} and TE_{02}.

Finally, two tunnel configurations have been considered: a Cut and Cover construction, where the klystron galleries can be much shorter than the linac tunnel, and a dual tunnel construction, where the klystrons and modulators are placed in the parallel tunnel. These layouts have an impact on the pulse compression scheme. In the SLED-II pulse compression scheme, the rf units can be configured in either a distributed or localized manner, although, if the rf units are localized, additional waveguide is needed to direct the power to the respective rf girders which will reduce the efficiency of the system.

3.3.3.5 Structures

The JLC-X/NLC linacs will each contain about 5 km of X-band accelerator structures to increase the beam energy from the 8 GeV at injection to 250 GeV for collisions at the IP. There are three basic requirements on the structure design: it must transfer the rf energy to the beam efficiently to keep the machine cost low; it must be optimized to reduce the

short-range wakefields which depend on the average iris radius; and it must suppress the long-range transverse wakefields to prevent multibunch beam breakup.

As part of the JLC-X/NLC development, many X-band accelerator structures have been constructed ranging in length from 20 cm to 1.8 meters. Originally, the focus of the structure R&D was on controlling the long-range wakefields. The acceleration gradient was not a major concern—short structures had quickly reached gradients much higher than needed in the JLC-X/NLC design and the longer structures were not tested because there was insufficient rf power available.

The long-range wakefield suppression was challenging because the wakefields must be reduced by two orders-of-magnitude within an inter-bunch spacing of 1.4 ns. The solution is to use a combination of detuning and damping. The detuning is generated by choosing the frequencies of the lowest (and strongest) band of dipole modes so that the modes excited by an off-axis bunch do not add constructively. This detuning produces an approximately Gaussian falloff in the net wakefield generated by each bunch. Detuning works well to suppress the wakefield for about the first 30 ns, after which the amplitude increases due to a partial recoherence of the mode excitations. To offset this rise, weak mode damping was introduced. The damping is achieved by coupling each cell through a longitudinal slot to four TE_{11} circular waveguides that run parallel to the structure. Two of the circular waveguide manifolds are in the horizontal plane and couple to the vertically deflecting dipole modes while two are in the vertical plane and couple to the horizontally deflecting modes. At the ends of the structures, the circular manifold waveguide makes a transition to rectangular waveguide, which transports the power out of the structure to processing electronics so the signals can be used for beam position monitoring.

Until recently, the JLC-X/NLC design choice was a traveling-wave 1.8-m Rounded Damped Detuned Structure (RDDS) with 206-cells. The rf group velocity varies from 12% c at the upstream end to 3% c at the downstream end to achieve a nearly constant gradient along the structure. The basic parameters were defined primarily by the choice of average cell iris size, which determines the strength of the short-range (intra-bunch) transverse wakefield. The phase advance was chosen to be 120 degrees per cell, the same as in the SLAC S-band structure. This value gives a high shunt impedance per unit length for good efficiency. An average iris radius equal to 18% of the rf wavelength was chosen to limit the wakefield-related bunch emittance growth in the JLC-X/NLC linacs.

To build a structure, disks and cells are first rough-machined using regular lathes and milling machines. At this stage, more than 40 μm of extra copper are left on all surfaces except the coupling slots and manifolds. Final machining is done to micron accuracy and 50 nm surface finish using single crystal diamond turning. The cells are carefully cleaned and rinsed with ozonized water, and then stacked in the V-block of a special fixture. The whole stack is pre-diffusion bonded at 180°C and final-diffusion bonded at 890°C. The final assembly including flanges, vacuum ports, WR90 waveguides for the fundamental mode, and WR62 waveguides for the dipole modes are brazed in a hydrogen furnace at 1020°C. The brazed section is then installed on a strongback for final mechanical measurement and straightening in a CMM (Coordinate Measuring Machine). Straightness at the ± 20 μm level has been achieved over the length for some of the 1.8-m structures; this exceeds the JLC-X/NLC requirements.

During the assembly process, microwave quality control is used to evaluate the cell and structure properties at several steps. This is particularly important since the cells are not designed to be tuned. As the cells are fabricated, the fundamental and dipole modes are measured to look for significant cell-to-cell deviations. Stacks of cells are also measured to verify that the phase advance is correct at 11.424 GHz. If the net phase error deviates by more than several degrees, then the dimensions of subsequent cells are modified to compensate the phase shift. After the structure is assembled, a semi-automated bead pull system is used to measure the field phase and amplitude along the structure.

To determine if the long-range wakefield of the structure is as predicted, the wakefield is measured in the Accelerator Structure SETup (ASSET) facility in the SLAC Linac. The positron beam passes first through the structure and induces a wakefield the effects of which are then observed with a trailing electron bunch. A comparison of the measurements and prediction is shown in Figure 3.45 for the RDDS1 structure. Although the agreement is excellent, the wakefield is larger than originally designed and is not acceptable for JLC-X/NLC. This is due to a defect in the final assembly procedure. Several cells of the structure were distorted by a support ring during the final braze of the vacuum manifolds onto the outside of the structure. This changed their frequency by about 30 MHz. To estimate the effect of this error, the phase advance of the fundamental mode was measured after assembly. A corresponding change in the dipole frequencies was then included in the wakefield prediction. Despite this localized defect, the random dipole frequency error of the rest of the cells is less than 1 MHz, which is demonstrated by the fact the wakefield dips to the 0.1 V/pC/m/mm level at about 25 ns. In earlier structures (DDS1 and DDS3), smaller wakefields were achieved.

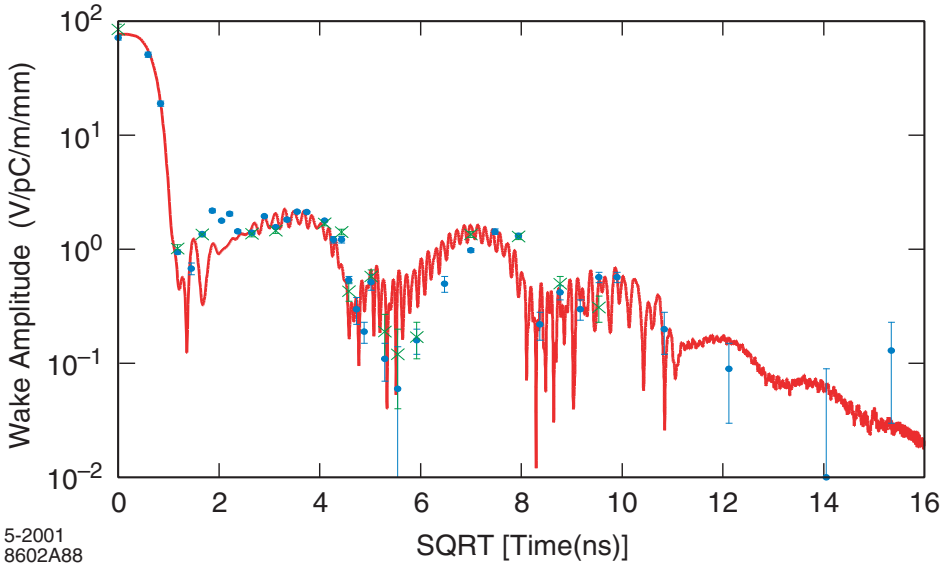

FIGURE 3.45. Comparison of measured and predicted wakefield for the RDDS1 structure.

Centering tests were also performed in ASSET using the dipole signals from the manifolds. The measured positions along the structure from the manifolds were compared with the results of mechanical measurements of the relative cell misalignments. The agreement was excellent at the 1–2 μm level. In another test, two dipole readings were used as a guide to position the positron beam; this models the beam-based alignment technique proposed for the JLC-X/NLC. Measurements of the resulting short-range wakefield (< 300 ps) indicated that the beam had been centered to less than 12 μm rms in the structure. This measurement incorporates both the precision of the dipole mode measurement (estimated to be 1–2 μm rms) and the internal structure misalignments. The resulting precision is close to the requirement for JLC-X/NLC operation.

The original design for the NLC Test Accelerator only delivered ∼100 MW to each 1.8-m accelerator structure to produce a gradient of roughly 50 MV/m—this was essentially the design described in the 1996 NLC ZDR. Four of the 1.8-m long structures that had been developed for the wakefield suppression studies were installed in the NLCTA and processed up to the desired 50-MV/m gradients.

The gradient limitations in the JLC-X/NLC prototype structures were only seen in 1999 when higher-power X-band sources were installed with the goal of generating gradients in excess of 70 MV/m. During this period, a 1.3-m JLC structure was also tested at the Klystron Test Laboratory at SLAC and it achieved gradients up to 85 MV/m with 150-ns pulses. However, the phase profiles from before and after processing of the JLC structure showed that the net phase shift through the structure had changed by 25 degrees, indicating significant changes to the cell dimensions. This shift occurred only in the upstream two-thirds of the structure with most of it at the upstream end. A visual inspection showed pitting along the irises of these upstream cells.

A similar pattern of damage was also observed when processing one of the 1.8 m damped, detuned structures to 70 MV/m with 240-ns pulses in the NLCTA. During about 1,000 hours of operation at high gradient, the net phase shift increased by 90 degrees. Once this degradation was seen, bead-pull measurements were made on the remaining three 1.8-m structures. All of these had about 500 hours of operation at gradients less than 55 MV/m. Although the phase shifts were much smaller, the same pattern of damage was observed.

Based on these results, it was hypothesized that the damage causing the phase shifts was related to the higher group velocity at the upstream end of the structures. To study the factors contributing to the damage, a series of six structures were built (called the T-Series) with different lengths (20, 53 and 105 cm) and lower group velocities (5% c and 3% c at the upstream ends). In addition, various improvements were made to the structure cleaning, handling and processing procedures to determine their impact on high-gradient performance.

The rf processing of the T-Series structures started at higher gradients (55–65 MV/m) than that (35–45 MV/m) for the 1.8 m structures. In addition, much less damage was observed in these structures at gradients above 70 MV/m than in the 1.8 m structures at gradients of 50–65 MV/m. After processing to 80–85 MV/m, the breakdown rate at 70 MV/m was dominated by events in the input and output couplers. The breakdown rates in the body of the structures (*i.e.*, excluding the couplers) at 70 MV/m were close to acceptable for the JLC-X/NLC at the design pulse width of 400 ns. For the three 53 cm, 3% c initial group

velocity structures that were tested, the breakdown rates were < 0.1, 0.2 and 0.3 per hour, respectively, while the goal is < 0.1 per hour.

An autopsy of the input coupler on one of the structures revealed melting along the edges of the waveguide openings to the cell, and extensive pitting near these edges and on the coupler iris. The waveguide edges see large rf currents that are a strong function of their sharpness, and the associated pulse heating can be significant. By design, the edges in the T-Series structures were sharper (76-μm radius) than those in the 1.8-m structures (500-μm radius). Recent calculations have shown that the pulse heating for the T-Series structures is in the 130–270°C range, well below the copper melting point, but high enough to produce stress-induced cracking, which might enhance the heating.

Based on these observations, a 53 cm, 3% c structure was built with couplers designed to have much lower pulse heating. This structure is currently being tested and has performed very well, with no obvious enhancement of the coupler breakdown rates relative to the other cells. For the full structure, breakdown rates of about 1 per 25 hours at 73 MV/m and 1 per hour at 92 MV/m have been measured with 400 ns pulses. All future structures will be made with couplers similar those used in this test.

Although the results from the T-Series structures are very encouraging, their average cell iris radii are too small to meet JLC-X/NLC short-range wakefield requirements. To increase the iris size while maintaining a low group velocity, a structure design with thicker irises and a higher phase advance per cell (150° instead of 120°) design has been adopted. Two such structures (H-Series) have been built, one 60 cm long with an initial group velocity of 3% c, and the other 90 cm long with an initial group velocity of 5% c. Both are detuned for wakefield suppression, but do include manifolds for wakefield damping.

Unfortunately, these structures have the earlier, T-Series type couplers since they were built before the coupler pulse heating problem was discovered. Making the problem worse, the H-Series structures have lower shunt impedance than the T-Series structures, so the pulse heating is relatively high. During their processing at NLCTA, the coupler breakdowns have indeed limited the gradient to values lower than that achieved with the T-Series structures. In addition, at short pulse lengths where the coupler events did not dominate, the processing rate was much slower than that for the T-Series structures. The larger iris thicknesses of the H-Series structures are certainly a contributing factor, but they do not explain the full difference.

The best results to date in an H-series structure have been achieved with the 60 cm, 3% c structure, which has been processed to 72 MV/m with 400 ns pulses. At 65 MV/m, the current JLC-X/NLC design gradient, the breakdown rate in the body of this structure meets the goal of < 1 per 10 hours. The program until Summer 2003 is to test several H-Series structures with improved couplers, culminating in one that is fully damped and detuned for wakefield suppression. Later, 5.4 m of such structures will be powered with the SLED-II rf source to demonstrate full system integration and to improve performance statistics.

3.3.4 Injectors

The NLC Injector System is designed to produce low emittance, 8 GeV electron and positron beams at 120 Hz for injection into the main linacs. Each beam consists of a train of 192 bunches of 0.75×10^{10} particles spaced by 1.4 ns. The horizontal and vertical

emittances are specified to be $\gamma\epsilon_x$=3.2 μm·rad and $\gamma\epsilon_y = 0.022$ μm·rad at injection into the main linacs, and the bunch length is in the range of 90 to 150 μm. Electron polarization of greater than 80% is required. Electron and positron beams are generated in separate accelerator complexes, each of which contains the source, damping ring systems, L-band, S-band, and X-band linacs, bunch length compressors, and collimation regions.

The need for low technical risk, reliable injector subsystems has been a major consideration in the design effort. Technologies chosen for the design of the injector systems are solidly based on experience with previously built and operated high energy colliders and with third-generation synchrotron light sources. Polarized electrons are produced using a dc photocathode gun which is very similar to the successful SLC polarized source. Unpolarized positrons are generated using multiplexed target systems which will be run in parallel; the peak energy deposition in each target assembly is designed to be identical to that of the SLC positron system, which ran for more than 5 years without incident. The parameters of the two main damping rings are similar to the present generation of synchrotron light sources and the B-Factory colliders in that they must store high-current beams ($\sim$1 A) while attaining small normalized emittances. The acceleration gradient in the injector S-band linacs is only modestly higher than the gradient in the SLC linac and the S-band klystrons are based on the 65 MW SLAC 5045 klystrons. Injector L-band linacs have been designed with low gradients to avoid problems associated with high fields in the structures or ancillary rf distribution systems. The X-band rf for the bunch length compressors is adapted from the main linac rf development.

There are two separate injector complexes to produce the low-emittance trains of electron and positron bunches for injection into the main linac. The electron injector includes a polarized photocathode gun, a bunching system and an S-band booster linac to deliver a 1.98 GeV beam to the damping ring. For the positron injector, an unpolarized electron gun and bunching system followed by a 6 GeV (10 GeV) drive linac provides the electron beam needed to produce positrons in the NLC (JLC) design. Multiple positron targets are required to keep the energy deposited in each target below the threshold for material damage. The electrons are split by an rf separator and directed onto 3 out of 4 multiplexed targets and positron capture sections. The bunches are then recombined into the desired bunch train format and accelerated in a 1.98 GeV L-band (S-band) linac to the positron pre-damping ring in the NLC (JLC) design. Because of the large emittance of the captured positrons, large-aperture L-band rf is used for acceleration and a pre-damping ring is required to reduce the emittance of the positrons before injection into the main damping ring. Two identical rings are used to damp the positron and electron bunch trains from the injectors to a normalized emittance of 3 μm·rad in the horizontal and 0.02 μm·rad in the vertical for the nominal 1.4 ns bunch spacing.

After extraction from the damping rings, the beam passes through a spin rotator system that can be used to orient the electron spin in an arbitrary direction to ensure longitudinal polarization of the beams at the IP. In the baseline design, the spin rotating solenoids are only installed in the electron beamline. However, the positron beamline is identical so that additional solenoids can easily be installed later for operation with either polarized positrons or with polarized electrons.

After the spin rotators, the bunch length must be compressed from 4 mm to 110 μm before injection into the main X-band linacs. This is accomplished in a 2-stage bunch compressor that is identical for the two beams. The first stage uses an L-band rf section followed by a

wiggler to compress the bunch to a length of about 0.5 mm. This is followed by a 6 GeV S-band pre-linac and the second-stage bunch compressor with a 180° arc, an X-band rf section and a chicane. The second stage can produce a bunch length between 90 and 150 μm. In the present layout, the electron booster and pre-linac are housed in the same tunnel to minimize infrastructure costs. The positron drive linac, booster and pre-linacs also share a common tunnel and support buildings.

Descriptions of the choice of injector layouts, the polarized electron source, the positron system, damping ring systems, and bunch length compression systems follow.

3.3.4.1 Polarized Electron Source

The electron injector source system creates polarized electron beams of the required energy and emittance for injection into the electron damping ring system. The polarized electron beams are produced with a DC photocathode electron gun, bunched in a 714 MHz subharmonic rf system and accelerated in an S-band linac to 1.98 GeV, the energy of the damping ring. Each beam consists of a bunch train of 192 bunches with 0.8×10^{10} particles per bunch that are spaced by 1.4 ns. The electrons at the end of the source booster linac are predicted to have an rms emittance of 50 μm·rad from PARMELA simulations. To ensure reliable operation, the system is required to produce beams with rms emittances that are less than twice the simulated value, *i.e.*, 100 μm·rad. In addition, the transverse jitter is specified to be less than the rms beam size and the energy jitter less than 1%. Finally, the spin polarization is specified to be 80%. All of these requirements are similar to those attained during operation of the SLC. A summary of the design parameters is given in Table 3.20.

The polarized electron source consists of a polarized high-power laser and a high-voltage dc gun with a semiconductor photocathode. Many of the performance requirements for the injector are similar to those in the SLC and the design of the injector is based on the successful SLC injector. The SLC polarized source generated 80% beam polarization. As long as ultra high vacuum conditions were maintained, the cathode lifetimes exceeded thousands of hours, and system availability approached 99%. The most notable differences between the present and the SLC design are the increase in gun high voltage from the SLC value of 120 kV to 175–200 kV and the use of 714 MHz rf for subharmonic bunching. For comparison, a 200 kV polarized electron gun is being developed at Nagoya University.

Improvement of the SLC photocathodes is required for the JLC-X/NLC operation because of the higher pulse charge requirements; the SLC source operated with a single polarized bunch of $\sim 5 \times 10^{10}$. Efforts by SLAC and the University of Wisconsin, and at Nagoya University are concentrating on developing cathodes with a highly doped surface layer to permit rapid dissipation of surface charge that builds up as beam is extracted. Recent tests using a strained layer cathode with a 75 Angstrom surface layer are extremely promising. Operating at 120 kV, up to 8×10^{11} electrons have been extracted by illuminating a 1 cm radius spot on the cathode. The polarization of the electrons was measured to be about 78% and no evidence of surface charge limit was observed. The maximum charge extracted was limited by available laser energy in the test laboratory. After being moved to the CID gun in the SLAC linac, the cathode has produced roughly 10^{13} e^- in 300 ns, many times the JLC-X/NLC requirement of $2{\times}10^{12}$ e^- in 267 ns from the gun. This cathode has been

TABLE 3.20
Beam parameters as delivered by the electron source system to the electron main damping ring system for the 1.4 ns bunch spacing option.

Bunch spacing	1.4 ns
Number of bunches	192
Particles/bunch	0.8×10^{10}
Energy	1.98 GeV
Energy adjustability	$\pm 5\%$
Bunch energy variation	1% Full Width
Single bunch energy spread	1% Full Width
Emittance $\gamma\epsilon_{x,y}$ [rms]	100 μm·rad
Bunch length σ_z	<10 mm
Train population uniformity	1% Full Width
Bunch-to-bunch population uniformity	2% rms
Repetition rate	120 Hz
Horizontal beam jitter $\Delta\gamma J_x$	50 μm·rad
Vertical beam jitter $\Delta\gamma J_y$	50 μm·rad
Polarization	80%
Beam power	58 kW

routinely operating for 6 months during the E-158 physics run. The polarization measured during the E-158 run was about 85%.

An S-band linac is used to accelerate the captured electrons up to the damping ring energy of 1.98 GeV. The loaded gradient of the linac is 17 MeV/m. This linac will use KEK-style SLED systems for rf pulse compression which have been designed and operated at higher field levels than the original SLAC-style SLED systems. Beam emittance growth through the booster linac is not a problem because of the low charge per bunch (in comparison to SLC operation) and because of the relatively large damping ring design acceptance. Standard quadrupole focusing elements are employed together with discrete steering dipoles along the length of the booster linac. Multibunch beam loading in the linac is compensated using the ΔT method in which the beam is injected into the accelerator before the rf has fully filled the structures. Fine tuning of the amplitude of the rf in a prescribed fashion after the beam has been injected provides additional control over the energy spread. An energy compression system has been included in the transport line that leads from the end of the linac to the main damping ring to further stabilize the energy and reduce the energy spread of injected bunches by a factor of roughly 2.

To measure the beam emittance, 4-wire parasitic emittance diagnostics are located after the e^- source (at 80 MeV) and before injection into the main damping ring. In addition, energy, energy spread, and bunch length diagnostics are located in a chicane at the 80 MeV point and in the 60° arc before injection into the main damping ring. To preserve electron helicity, the spin must be rotated into the vertical direction prior to injection into the

damping ring. The 60° arc also rotates the polarization vector from the longitudinal direction into the $x-y$ plane and a subsequent superconducting solenoid then orients the polarization vertically. To stabilize the trajectory and preserve the emittance, all the quadrupoles have BPMs with 10 μm resolution and horizontal or vertical steering correctors depending on the focusing plane.

3.3.4.2 Positron Source

The positron injector source system creates positron beams of the required energy and emittance for injection into the positron damping rings. In the NLC design, positrons are produced by colliding 6.2 GeV electrons into three separate high Z material targets, capturing the resulting positrons, and accelerating them to the 1.98 GeV energy of the pre-damping ring system. Each beam consists of a bunch train of 192 bunches with 0.9×10^{10} particles that are spaced by 1.4 ns (or 96 bunches with twice the charge that are spaced by 2.8 ns). As required by the pre-damping ring acceptance, the positrons have an edge emittance of 0.03 m·rad and a transverse jitter that is less than 0.015 m·rad; this jitter corresponds to about a 7 mm oscillation at the damping ring entrance. Table 3.21 lists the positron beam parameters required for injection into the pre-damping ring system.

TABLE 3.21
Beam parameters delivered by the positron source system to the positron pre-damping ring system for the 1.4 bunch spacing option.

Bunch spacing	1.4 ns
Number of bunches	192
Particles/bunch	0.9×10^{10}
Energy	1.98 GeV
Energy adjustability	±5%
Bunch energy variation	1% Full Width
Single bunch energy spread	2% Full Width
Emittance $\gamma\epsilon_{x,y}$ (edge)	30,000 μm·rad
Bunch length σ_z	<10 mm
Train population uniformity	1% Full Width
Bunch-to-bunch population uniformity	2% rms
Repetition rate	120 Hz
Horizontal beam jitter $\Delta\gamma J_x$	15,000 μm·rad
Vertical beam jitter $\Delta\gamma J_x$	15,000 μm·rad
Beam power	65 kW

The design of the positron system is based on the system used for the SLC, which demonstrated excellent reliability over many years of operation. The total number of positrons required for the JLC-X/NLC bunch train is almost two orders of magnitude greater than the number of positrons in the single SLC bunch. The design goal is to build a

target system which is expected to survive a 9 month run (120 Hz, 24 hours per day, 7 days per week, with no scheduled outages for maintenance). Targets can be replaced/repaired annually in a scheduled 3 month maintenance period.

Positrons are produced by targeting a 6.2 GeV electron beam onto a WRe target to create an electro-magnetic shower. The positrons produced in the shower are collected using a 5.8 Tesla magnetic flux concentrator, accelerated to 250 MeV in L-band structures encased in a 0.5 Tesla solenoidal magnetic field, and then injected into an L-band linac and accelerated to 1.98 GeV. The average deposited power is handled by rotating the target and removing the excess heat through water cooling. Of critical concern for target damage is the instantaneous energy deposition per unit volume.

After approximately 1000 days of operation (∼5 calendar years), the SLC positron system failed. Upon examination it was found that a water-to-vacuum leak had occurred in one of the target cooling tubes. In addition, cracking and material ejection were found on the exit face of the target.

The peak energy deposition in the SLC target was about 50 J/g under the conditions at which the target failed. This level produces an instantaneous mechanical shock in the WRe target material which is about a factor of 2 below the expected ultimate tensile strength of pristine material. However, material hardening of a factor of about 2 from target entrance to target exit was measured along the beam path. The calculated radiation damage to the material is in excess of 3 dislocations per atom (dpa) and the target embrittlement and subsequent loss of material integrity are consistent with the calculated exposure level.

Because of the consistency of the observed damage with expectations from the simulations, it has been decided to limit the shock in the targets to that of the SLC system. In particular, the peak energy deposition and irradiation fluences will be kept by design to less than 50 J/g and 1 dpa. Investigations into the connection between radiation damage due to electrons with that from neutron/proton exposure are continuing. It is useful to tap into the data on material property degradation due to neutron/proton damage since the database of electron induced damage is comparatively limited. Beam tests at SLAC are underway to determine the threshold for material damage and a model of the expected damage is being developed. To date, samples of Ti, Cu, GlidCop, Ni, Ta, W, and WRe have been irradiated in the FFTB area at SLAC. Additional studies will be aimed at developing an optimized target material. Induced damage to candidate target materials will be studied using the E158 beam at SLAC (5×10^{11} e^-/pulse at 45 GeV, 200–300 ns pulse width, and focusable to small spots).

In order to keep the peak shock stress in the target below the threshold for damage, three e^+ targets operating in parallel are planned to produce the JLC-X/NLC beam. To assure overall system availability, a layout has been adopted where there are 4 target/capture modules, 3 of which are operating at any one time as illustrated in Figure 3.46. The bunches are separated using an rf separator and then directed to the desired targets using dc bending magnets. Access is possible to the fourth target/capture module for maintenance and repair while the other 3 modules are in operation.

The 6.2 GeV electron drive beam, which is used to create the positrons, is based on S-band technology. Because of the need to use three quasi-independent target/capture sections for positron production, the electrons will be generated using a photocathode based source. Fine tuning of the individual electron bunch populations within the drive train is possible

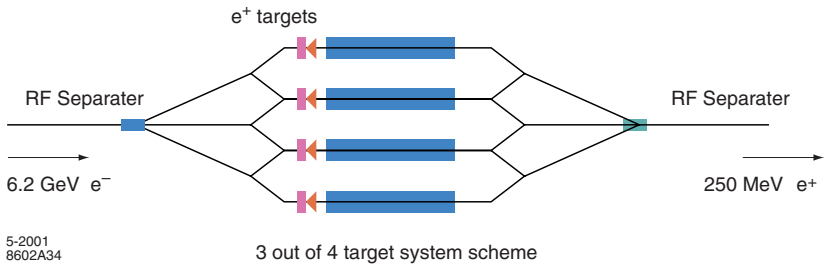

FIGURE 3.46. Schematic of the conventional e^+ production system.

through bunch-to-bunch intensity adjustments at the source laser. The unpolarized electron source system is essentially identical to the polarized electron source with the exception that shorter laser wavelengths and photocathodes with higher quantum yields will be used.

Positron yield is defined as the number of positrons captured in the pre-damping ring divided by the number of electrons incident on the target. The NLC has adopted the use of L-band (1.4 GHz) for both the initial 250 MeV capture and 1.73 GeV booster linacs. The larger aperture and longer wavelength of the L-band affords a factor of about 30 increase in acceptance over an S-band system. Yield into the pre-damping ring acceptance is calculated based on the initial e^+ distribution, generated using EGS4. The calculated yield is about 1.5, but experience with the SLC shows that this yield can be rapidly degraded by alignment and optical errors in the transport between the e^+ source and the damping rings. It is believed that a 50% margin in the yield should be sufficient. If necessary, the population of the drive e^- beam can be increased somewhat to produce the desired number of e^+.

To measure the beam emittance, 4-wire parasitic emittance diagnostics will be located after the 250 MeV point in the e^+ beam line and before injection into the pre-damping ring. In addition, energy, energy spread, and bunch length diagnostics are located in a chicane at the 250 MeV point and in the 60° arc before injection into the pre-damping ring. To stabilize the trajectory and preserve the emittance all of the quadrupoles have BPMs with 10 μm resolution and horizontal or vertical steering correctors depending on the focusing plane.

3.3.4.3 Damping Rings

The JLC-X/NLC damping rings are designed to damp the incoming electron and positron beams to the small emittances needed for collisions. The rings have three purposes: (1) damping the incoming emittances in all three planes, (2) damping incoming transients and providing a stable platform for the downstream portion of the accelerator, and (3) delaying the bunches so that feedforward systems can be used to compensate for charge fluctuations. To meet these goals, three damping rings have been designed: two identical main damping rings, one for the electrons and one for the positrons, and a pre-damping ring for the positrons. The pre-damping ring is needed because the emittance of the incoming positrons is much larger than that of the electrons. Each damping ring will store multiple trains of bunches at once. At every machine cycle, a single fully damped bunch train is extracted from the ring while a new bunch train is injected. In this manner, each bunch train can be damped for many machine cycles.

At the SLC, the damping rings were one of the most problematic subsystems. This was because the downstream systems are extremely sensitive to small changes in the injected beams, and because the beams are stored in the rings for a relatively long time, which makes them more sensitive to subtle accelerator physics effects. The parameters of the JLC-X/NLC main damping rings are similar to the present generation of synchrotron light sources and the B-Factory colliders in that they must store high-current beams (∼1 A) while attaining small normalized emittances. Table 3.22 compares the damping ring parameters with those of the SLAC B-Factory Low-Energy Ring (PEP-II LER), the Advanced Light Source (ALS) at Lawrence Berkeley National Laboratory, and the Accelerator Test Facility (ATF) damping ring at KEK in Japan. In particular, the stored beam currents are less than half of what the PEP-II LER has achieved, while the emittance, energy, and size of the rings are similar to those of the ALS and the ATF. These other rings have been largely successful in meeting their design parameters, and have been able to test and verify many of the accelerator physics and technology issues that will arise in the damping rings. We believe that this provides confidence that the JLC-X/NLC rings will operate as required.

TABLE 3.22
Comparison of NLC main damping rings with design parameters of other rings.

	NLC MDR	PEP-II LER	LBNL ALS	KEK ATF
Energy [GeV]	1.98	3.1	1.5	1.54
Circumference [m]	300	2200	197	139
Current [A]	0.8	2.16	0.4	0.6
Equilib. $\gamma\epsilon_x$ [μm·rad]	2.17	400	12	2.8
Equilib. $\gamma\epsilon_y$ [μm·rad]	0.014	12	0.12	0.028

Issues associated with the very small beam emittances, such as intrabeam scattering and ion trapping, continue to be studied in the ALS and ATF. The ATF has achieved emittances of $\gamma\epsilon_x$=2.8 μm·rad and $\gamma\epsilon_y$=0.028 μm·rad, close to those desired in the main damping rings; work continues to improve the performance, which is primarily limited by the diagnostics in that machine. Experiments have also been performed at low energy (1 GeV) in the ALS, where the measured emittances of 10^9 particles are $\gamma\epsilon_x$=4 μm·rad and $\gamma\epsilon_y$=0.07 μm·rad. These measurements, combined with theoretical modelling, are designed to improve the understanding of the process of intrabeam scattering in electron storage rings, and to increase confidence in the predictions for the damping rings.

In addition, the PEP-II LER at SLAC, the KEK-B LER at KEK, and the Advanced Photon Source (APS) at Argonne have been used to study the electron-cloud instability and have shown success in controlling and understanding the phenomenon. Simulations based on a simple circular vacuum chamber predict that the growth times of transverse instabilities driven by the electron cloud are greater than 100 μs and can be controlled with a broadband feedback system. The NLC vacuum system design includes an antechamber in which synchrotron radiation is absorbed, significantly reducing the number of photoelectrons in the beam duct and the chamber will likely use a TiN or similar coating to reduce the number of secondary electrons.

The similarities with other rings have also simplified the design process, and experience at these other accelerators will continue to be applied to benefit the damping rings designs. For example: the damping ring rf system is based on the higher-order-mode damped cavity designs successfully operating at the SLAC B-Factory and the ATF damping ring, the multibunch feedback systems are based upon the feedback systems successfully verified at the SLAC B-Factory and the ALS, and the vacuum system is similar to that used by the ALS. Furthermore, the design uses "C" quadrupole and sextupole magnets similar to those used at the ALS and the APS, a high-field permanent magnet wiggler similar to those in use at third generation light sources, and a double kicker system for extraction similar to one operational in the ATF. The successful demonstration of these and other systems and components allows a high degree of confidence in achieving the damping ring parameters.

The NLC damping ring complex is designed to operate with the parameters listed in Table 3.23 and the positron damping ring complex is illustrated schematically in Figure 3.47; the JLC design is similar although the repetition rate is slightly different. These design parameters satisfy the requirements of all presently considered NLC upgrades. The rings produce extracted electron and positron beams with emittances $\gamma\epsilon_x$=3 μm·rad and $\gamma\epsilon_y$=0.02 μm·rad, at a repetition rate of 120 Hz. Designs have also been developed which allow repetition rates as high as 180 Hz; in this case, the use of two main damping rings is proposed. The beams in the damping rings consist of multiple trains of 192 bunches with an injected single bunch charge of 0.8×10^{10}. To provide operational flexibility, the rings have been designed to also accommodate trains of 96 bunches spaced by 2.8 ns with maximum single bunch charge of 1.6×10^{10} in the main rings (1.8×10^{10} in the pre-damping ring), and to operate with a peak current roughly 15% higher than the nominal peak current. In addition, the electron source has been designed to provide additional charge to allow for at least 10% losses during injection into the electron damping ring. Similarly, the positron source has been designed to produce at least 20% additional charge to provide for losses during injection into the pre-damping ring. Finally, the rings have been designed to operate at 1.98 GeV, with an energy range of 5%—1.98 GeV corresponds to a spin tune of 4.5 where depolarizing spin resonances are expected to be small. The energy adjustability will allow the damping rate and/or spin tunes to be shifted, if necessary.

TABLE 3.23
Requirements for NLC main damping rings.

Repetition rate [Hz]	120
Bunches per train	192
Bunch spacing [ns]	1.4
Bunch population	0.8×10^{10}
$\gamma\epsilon_x$ equilib. / $\gamma\epsilon_x$ extract. [10^{-6} m·rad]	3.0 / 3.0
$\gamma\epsilon_y$ equilib. / $\gamma\epsilon_y$ extract. [10^{-8} m·rad]	1.4 / 2.0

3.3.4.3.1 Main Damping Rings The NLC main damping rings are roughly 300 m in circumference and they measure roughly 60 m by 100 m with a nominal energy of 1.98 GeV. The rings are designed in a racetrack form with two arcs separated by straight

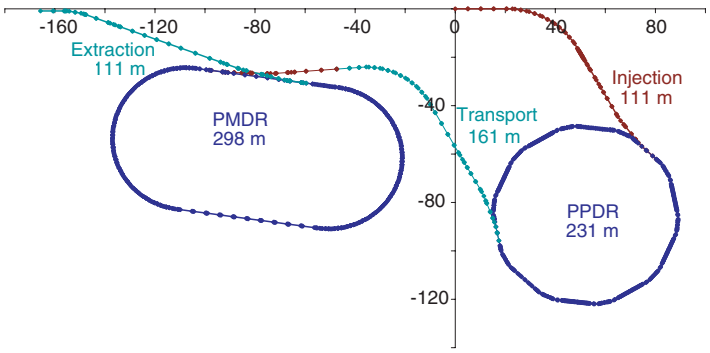

FIGURE 3.47. Schematic of NLC positron damping ring complex.

sections. The main damping rings are designed to damp beams with injected emittances $\gamma\epsilon_{x,y}$=1.5×10^{-4} m·rad to give extracted beam emittances of $\gamma\epsilon_x$=3×10^{-6} m·rad and $\gamma\epsilon_y$=2×10^{-8} m·rad. The rings will operate at 120 Hz. They provide sufficient damping to decrease the injected emittance by four orders of magnitude. The parameters are summarized in Table 3.24 for the main damping rings (MDR), and the positron pre-damping ring (PPDR). The main damping ring lattice is based on detuned Theoretical Minimum Emittance (TME) cells, which were chosen because of efficiency in generating low emittance and eased requirements on the combined-function bending magnets. The chromaticity is corrected with two families of sextupoles and the dynamic aperture is more than sufficient to ensure lossless injection. The damping is performed using both high-field bending magnets and ten 4.6 m sections of damping wiggler.

The dynamic aperture, including effects of errors, is predicted to be in excess of 15 times the injected beam size. Potential limitations due to the contribution from the 46 m of wiggler magnet have been studied. Analytical expressions of arbitrary three-dimensional wiggler fields have been developed, and tracking including the non-linear components of the wiggler field will be used to determine the minimum pole width requirement for the 2.15 T hybrid wiggler magnet. Preliminary analysis indicates that the wiggler with a magnet pole width of 11 cm does not seriously impact the dynamic aperture.

The rings operate with three trains of 192 bunches spaced by 1.4 ns or 96 bunches spaced by 2.8 ns. The bunch trains are injected onto and extracted from the closed orbit using pulsed kickers and DC septa. The bunch trains are separated by 65 ns to allow for the rise and fall times of the injection and extraction kickers. To avoid coupled-bunch instabilities the rf cavities use higher-order-mode damping, based on the PEP-II design, and a transverse bunch-by-bunch feedback system. As stated, the rings are designed to operate with maximum bunch charges of 1.6×10^{10} particles; this is roughly 10% more than the maximum needed at the IP with a 2.8 ns bunch spacing.

Finally, because the rings must generate extremely small beam emittances, there are tight jitter and alignment tolerances. Extensive effort has been made to include cancellations and tuning procedures in the design that will ease the tolerances to reasonable levels. Skew quadrupole windings will be incorporated in sextupole magnets to facilitate coupling correction. Quadrupoles and sextupoles will have independent trim control, and magnet movers will be used to facilitate beam-based alignment. BPMs, having a 1 μm resolution

TABLE 3.24
Parameters for main damping rings and the pre-damping ring.

	MDR	PPDR
Circumference [m]	299.792	230.933
Energy [GeV]	1.98	1.98
Maximum current [A]	0.8	0.75
Maximum repetition rate [Hz]	120	120
Bunch trains × bunches per train	3 × 192	2 × 192
Train / bunch separation [ns]	65 / 1.4	100 / 1.4
ν_x, ν_y, ν_s	27.26, 11.13, 0.0035	11.45, 5.45, 0.0114
$\gamma\epsilon_x$ equilib. [μm·rad]	2.17	60
$\gamma\epsilon_x$ extract., $\gamma\epsilon_y$ extract. [μm·rad]	3.0, 0.02	127, 70
$\sigma_{\Delta E/E}$, σ_z	0.09%, 3.6 mm	0.08%, 5.1 mm
ξ_x uncorr., ξ_y uncorr.	−37.12, −28.24	−10.39, −12.23
τ_x, τ_y, τ_ϵ [ms]	4.76, 5.00, 2.60	5.85, 5.81, 2.90
U_{sr} [kV/turn]	777	525
α_p	2.95×10^{-4}	2.00×10^{-3}
V_{RF}	1.1 MV, 714 MHz	1.5 MV, 714 MHz
Lattice	36 TME cells	10 DBA cells

for single turn measurements and < 0.3 μm resolution for the stored orbit, will be located at every quadrupole. In addition, a synchrotron radiation port will be used for bunch length and initial beam size measurements and, a laser wire, like the system commissioned at the ATF at KEK, will likely be used to measure the damped beam. There will be a 4-wire parasitic emittance measurement as well as energy and energy spread diagnostics located in the extraction line before the spin rotator and first stage bunch compressor. Additional emittance, energy spread and bunch length diagnostics will be located in and after the first stage bunch compressor.

3.3.4.3.2 Positron Pre-Damping Ring The pre-damping ring is roughly 230 m in circumference and has 10 dispersion-free straight sections for injection, extraction, rf, circumference correction chicanes, and damping wigglers; the latter have a total length of roughly 50 m. The ring has a radius of roughly 40 meters. It stores two bunch trains which are separated by more than 100 ns to allow for the rise and fall times of the injection and extraction kickers—these kickers must provide larger deflections than those in the main damping rings. To minimize rf transients during injection and extraction, a new bunch train will be injected one half turn after a train is extracted. In addition, the rf cavities are placed downstream of the injection kicker and upstream of the extraction kicker so that the injection/extraction process will not interrupt the beam current seen by the cavities.

The positron pre-damping ring is designed to damp the large emittance beam from the positron source to an emittance of less than $\gamma\epsilon_{x,y}$=1.5×10^{-4} m·rad; the parameters are

summarized in Table 3.24. The extracted positrons are then injected into the main damping ring where they are damped to the desired final emittances. The pre-damping ring allows the large aperture requirements for the incoming positron beams to be decoupled from the final emittance requirements of the linear collider.

The magnets and vacuum systems are designed to provide sufficient aperture to accept a 2-GeV beam with an edge emittance of $\gamma\epsilon_{x,y}$=0.03 m·rad and momentum spread of $|dp/p|$=1.5% plus betatron-action jitter of $\Delta\gamma J_{x,y}$=0.015 m·rad for misalignments and missteering; this provides a substantial margin for injection and internal mismatches. In addition, the injector specifications allow significant overhead for injection losses into the pre-damping ring. The pre-damping ring is designed to operate with a maximum bunch charge that is roughly 20% greater than the maximum required at the IP.

Like the main damping rings, quadrupoles and sextupoles will have independent trim control, and magnet movers will be used to facilitate beam-based alignment as well as matching of the lattice functions, which is especially important in the pre-damping ring because of the limited aperture. BPMs will be located at every quadrupole and will have a resolution better than 15 μm for a single turn and 5 μm after averaging the stored orbit. In addition, a synchrotron radiation port will be used for bunch length and beam size measurements. There will be a beam size as well as energy and energy spread diagnostics located in the transfer line to the main damping ring.

3.3.4.4 Bunch Length Compressors

The bunch compressors must reduce the $\sim$ 4 mm rms length of the bunches extracted from the damping rings to the 90 to 150 μm bunch length required for the main linacs and final focus systems. A two-stage compressor system has been designed in which the first stage follows the damping ring and the second stage is at the exit of the S-band pre-linac at a beam energy of 8 GeV. Electron and positron bunch compression systems are identical. The bunch compressor system has been designed to meet the following additional goals: (1) Multibunch phase variations in the damping ring of up to $\pm$5 mm should not produce relative energy variations that are larger than $\pm$0.1% in the final focus systems. (2) The system should include a 180° turn-around arc to permit future main linac extensions and to allow beam abort and feedforward systems. (3) The transverse emittances must be preserved to within a reasonable budget with diagnostics and correction elements included in the design. (4) The compression systems should not depolarize the beams.

The two-stage system has a number of advantages over a single-stage compressor. In particular, it keeps the rms energy spread less than about 2% and the bunch length is more naturally matched to the acceleration rf frequency so that energy spread due to the longitudinal wakefields can be cancelled locally. The disadvantage of the two-stage design is that it is more complex and lengthy than a single-stage compressor. The first stage rotates the longitudinal phase by $\frac{\pi}{2}$ while the second stage performs a 2π rotation. In this manner, phase errors due to the beam loading in the damping rings and energy errors due to imperfect multibunch energy compensation in the 6 GeV S-band pre-linacs do not affect the beam phase at injection into the main linac.

Assuming an incoming rms energy spread of $\sigma_\delta = 1 \times 10^{-3}$ and rms bunch length of σ_z=5 mm, the first stage compresses the damping ring beam to a bunch length of about

0.6 mm. This stage consists of a 140 MV L-band (1.4 GHz) rf section followed by a long period wiggler which generates the momentum compaction needed for the bunch compression. The second bunch compression stage follows the 6 GeV pre-linac. The nominal configuration compresses the beam to a bunch length of 110 μm. This compressor is a telescope in longitudinal phase space which rotates the phase space by 2π. It consists of a 180° arc which is followed by a 600 MeV X-band (11.4 GHz) rf section and a chicane. Adjustments to either the low-energy or the high-energy compressors permit control of the final bunch length over the specified range of 150 to 90 μm.

One of the rationales behind the compressor design has been to utilize naturally achromatic magnetic lattices wherever the beam energy spread is large. In particular, the optics is chosen so that quadrupoles are not placed in regions of large dispersion and strong sextupoles are not needed. This choice arises from experience with the second-order achromats in the SLC bunch compressors in which quadrupoles are located in dispersive regions and strong sextupoles are used to cancel the chromatic aberrations. Unfortunately, the SLC design was difficult to operate and tune because of large nonlinearities and sensitivity to multipole errors in the quadrupoles; over the years additional nonlinear elements were added (skew sextupoles and octupoles) to help cancel the residual aberrations but tuning remained problematic. To facilitate tuning, orthogonal tuning controls and diagnostics have been explicitly designed into the NLC system, which should make it relatively straightforward to operate. Details of the diagnostic equipment can be found in the optics decks.

Finally, although the tolerances on components in the bunch compressor systems are not nearly as tight as in the main linacs or the final focus systems, the same methods of beam-based alignment and tuning have been adopted. In particular, to ease the alignment procedures, all of the quadrupoles will be mounted on magnet movers and each quadrupole will contain a BPM with a resolution of < 2 μm. Similarly, all of the accelerator structures will be instrumented with rf BPMs to measure the induced dipole modes and each rf girder will be remotely movable for minimization of wakefields. There will be 4-wire parasitic emittance measurement sections and subsequent tune-up dumps after the first-stage bunch compressors, the 6 GeV pre-linacs, and the second-stage bunch compressors before injection into the main linac. There will also be synchrotron radiation-based bunch length and energy spread diagnostics in the first-stage wigglers, the second-stage arcs, and the second stage chicanes and there will be rf deflector-based bunch length monitors before injection into the main linac.

3.3.5 Beam Delivery

The beam delivery system (BDS) must both reduce the beams to the sizes required to produce luminosity and remove any particles that are far enough from the beam core to produce unacceptable detector backgrounds. In addition, the BDS must provide protection for the detector and beamline components against missteered beams emerging from the main linacs, and must safely transport the collided beams to water-cooled dumps which can absorb the high beam power density without damage. Finally, the BDS must provide instrumentation that can monitor the parameters of the collided beams, such as the energy spread and polarization after collision, which are required by the particle physics experiments.

Although the parameters of the JLC-X/NLC BDS are far beyond anything that has been achieved in a storage ring, the SLC demonstrated the viability of a fully integrated linear collider beam delivery system with millimeter-sized betatron functions and routine collision of beams with rms sizes of under 1 μm. The FFTB at SLAC was a single-beam demonstration of a linear collider beam delivery system with IP betatron functions comparable to those in the JLC-X/NLC. The BDS design is based upon experience from these two facilities. In addition, a vigorous R&D program on passive and active magnet position stabilization, ground motion, materials damage thresholds, and instabilities driven by collimators close to the beam have all yielded insights which have been incorporated into the design of the system.

The layout of the BDS components is shown in Figure 3.48. The six main subsystems of the beam delivery, from upstream to downstream, are: the emittance diagnostic and skew correction region, which provides parasitic measurement of the beam emittance and an orthogonal set of four skew quadrupoles to correct all sources of betatron coupling in the beam; the IR transport, which separates the beamlines to the low and high-energy IRs; the collimation system, which provides protection from errant beams and removes particles which might cause backgrounds; the final focus (FF), which focuses the beams down to the small spots; the IRs, which provides detector masking and specialized supports for the final doublet quadrupoles of the final focus; and the extraction line, which transports the spent beams to their respective dumps and provides the post-collision beam measurements. In addition, a high-power pulsed beam dump, which is not shown, is located in the energy collimation region to allow the full-power linac beam to be tuned before sending the beam through the final focus.

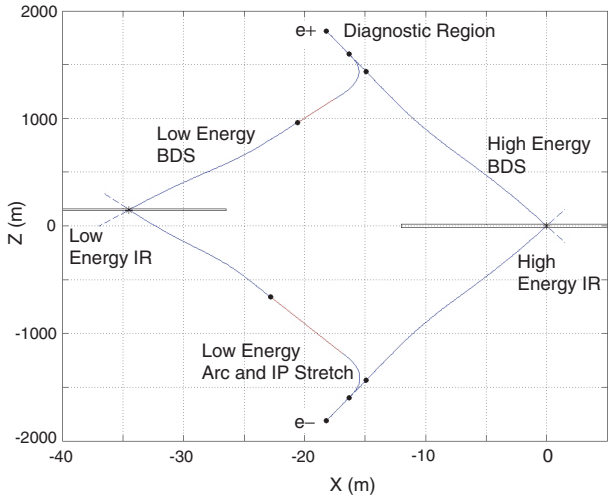

FIGURE 3.48. Beam delivery system layout with two interaction regions separated by 150 m longitudinally.

The beamline for the high energy IR is 1.8 km long. This distance includes a 1.4 km long collimation and final focus region, a 150 meter region where the beamlines for the low-energy IR diverge, and a 200 meter emittance diagnostic and skew correction section. The low-energy IR beamline splits off at the end of diagnostic region and includes arcs that bend the beam by about 25 mrad and a shorter 800 meter collimation region and final focus. The two IRs are separated by about 35 m transversely and 150 m longitudinally to provide vibration isolation and shielding so either IR hall may be accessed while the other is in operation.

3.3.5.1 Final Focus

The role of the final focus is to reduce the size of the beam at the IP sufficiently to provide the required luminosity. The small beam sizes are achieved using strong quadrupole magnets close to the IP to focus the low emittance beams and reducing $\beta^{\star}_{x,y}$ to 8×0.11 mm. Unfortunately, the final quadrupoles also generate a huge chromaticity which, if uncorrected, would increase the spot sizes by one to two orders of magnitude.

Correcting the chromaticity of the final quadrupole doublet is the issue that drives much of the design. In the final focus systems used at the SLC and the FFTB, which were also the basis of the 1996 NLC ZDR final focus design, the chromaticity correction was accomplished in dedicated "chromaticity correction sections." In these sections, a combination of bend magnets and sextupoles generated a chromaticity equal-and-opposite to that of the final doublet. Once the chromaticity of the final focus was corrected, the principal aberration to be cancelled was generated by the sextupoles that were required for chromaticity correction. This was accomplished by placing additional sextupoles in the beamline, with optical transformations between sextupoles which caused the geometric aberrations of the sextupoles to cancel while the chromatic aberrations remained.

In the SLC and FFTB, each of the sextupoles in a matched pair contributed 50% of the chromaticity correction. The combined effect of the chromaticities of the sextupoles, the quads between the sextupoles, the quads between the last sextupole and the final doublet, and the doublet chromaticity caused these designs to provide correct focusing to only a narrow range of particle energies. The 1997 JLC design by Oide ameliorated this limitation by generating as much of the chromaticity correction as possible in the sextupoles closest to the IP, rather than splitting it equally among the pairs of sextupoles in a given family.

The present NLC final focus design uses an extreme form of Oide's asymmetric solution which places the chromaticity correction sextupoles in the final doublet itself. This configuration requires a horizontal dispersion through the final doublet, which is tuned to be exactly zero at the IP. The optics of the combined NLC final focus and the upstream collimations system are shown in Figure 3.49.

There are three clear advantages of the new final focus optics: first, the system requires many fewer magnets and is conceptually simpler. Second, it addresses a limitation of the earlier designs where the energy loss from synchrotron radiation between the last sextupole and the IP had to be minimized to avoid causing a breakdown of the chromaticity correction. Because of this requirement the bending magnets in the conventional final foci were weak, and the systems were correspondingly long. The present NLC configuration is much shorter than previous final-focus systems: less than 0.4 km is required for 750-GeV

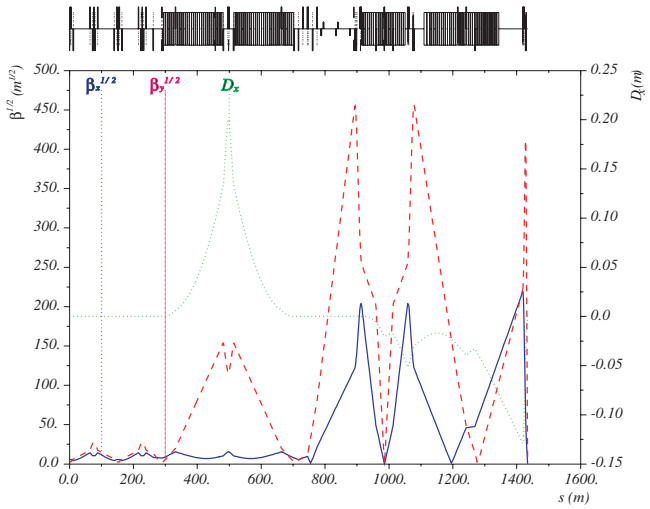

FIGURE 3.49. Optics of the NLC collimation and final focus systems.

beams as compared to 1.8 km in the NLC ZDR design and the present length of 0.7 km will handle 2500-GeV beams; the energy reach of the final focus is shown in Figure 3.50. Third, in the new design, off-energy particles tend to have small amplitudes in the final doublet magnet, whereas nonlinearities in the traditional final-focus systems tended to drive off-energy particles to very large amplitudes in the final doublet. The effect of the nonlinear amplitudes has not been considered in the past but the new design will simplify the beam collimation requirements significantly.

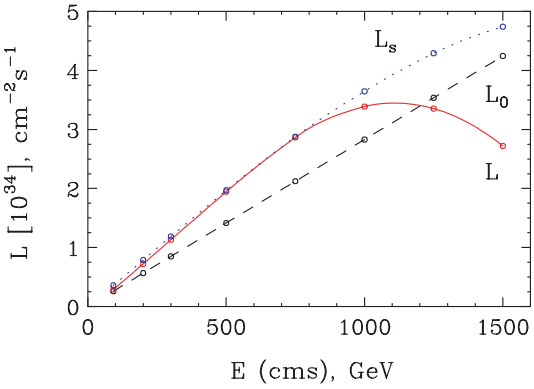

FIGURE 3.50. Energy reach of the NLC final focus where L_0 is the luminosity without the pinch enhancement, L is the nominal luminosity, and L_s is the luminosity after scaling the bending magnets. By scaling the bending magnets in a manner to maintain the IP position the present system can accommodate beam energies well above 1500 GeV.

3.3.5.2 Collimation System

The collimation system must remove particles in the beam tails that can generate backgrounds in the detector and it must protect the final focus and detector from errant beams. As is well known, the population and distribution of the beam tails can be very hard to calculate and, because the backgrounds can severely limit the luminosity recorded by the detector, the collimation system must be designed quite conservatively. Beam collimation was one of the limiting factors in the SLC operation.

The collimation system must remove all primary beam particles which could be lost near the detector. However, tighter constraints arise due to the synchrotron radiation produced by the large amplitude particles in the final doublet focusing magnets. Because of the high beam energy, the photons emitted as the beam is focused in the final doublet have energies that are too high to be able to shield the detector with masking in the IR. Ray tracing shows that to prevent any synchrotron radiation photons from hitting in the IR, the angular divergence of the beam at the IP cannot exceed a rectangular aperture of 570 μrad horizontally by 1400 μrad vertically. This restriction on the beam tails is significantly tighter than that to prevent primary particles from hitting the vacuum apertures.

Another important consideration is the muons produced by the collimators when the high energy tails are removed. Simulation studies have shown that as many as 10^9 primary electrons or positrons per train can be removed by a collimation system located well upstream of the final focus without producing an unacceptable muon flux in the detector, although this number depends somewhat upon the exact configuration of the beamline. The number of primary particles that can be stopped within the final focus without unacceptable muon production is only 10^4.

The most easily estimated source of beam tails in the linac is elastic scattering off the residual gas in the vacuum system; this process generates less than 10^5 large amplitude particles per bunch train. Transverse wakefields have little effect on a beam with a gaussian longitudinal profile unless the trajectory has huge oscillations that will also lead to unacceptably large ($\sim 2000\%$) emittance dilutions. Unfortunately, the beam will not likely have a gaussian longitudinal distribution on exit from the damping rings and the bunch compressors, but it is difficult to estimate the exact form of the distribution until better estimates of the ring impedance and sources of nonlinearity in the bunch compressors are obtained. Generous estimates of these effects would still limit the number of particles in the beam tails to be less than 10^6 per train. Other possible sources of tails are parasitic rf buckets that are populated in the bunch compressors or the damping rings. Parasitic bunches with charges as high as a few percent of the primary beam were seen in the SLC damping rings. Because of the uncertainties and the importance of limiting the backgrounds, the NLC has been designed to remove 10^9 primary particles per bunch train which is a tail population that is 0.1% of the beam—this is the halo population that was observed during the last run of the SLC, which is thought to be a generous over-estimate of the possible load.

Because of the muon generation, the NLC collimation system is designed in four stages. First, there will be a transverse collimation section immediately after the damping rings at 1.98 GeV. This is desired because beam-gas and intrabeam scattering will generate beam tails that fill the damping ring vacuum aperture and it is pointless to accelerate all of these particles to high energy. This system has not yet been designed but is thought to be

straightforward. Second, after the pre-linacs at 8 GeV, the longitudinal phase space is collimated. This system removes many of the particles in the longitudinal tails, preventing them from being deflected into the transverse phase space by wakefields during the subsequent acceleration. Next, the primary collimation system is located at the end of the main linac. This system collimates both the transverse and longitudinal phase spaces with an efficiency of $\sim 10^5$—thus for 10^9 incident tail particles, only 10^4 will pass through the system. Finally, both the longitudinal and transverse phase spaces are collimated in the final focus itself. This is necessary to remove particles that escape the primary collimation system as well as additional particles scattered by the residual gas downstream of the collimation section; the latter is estimated to be less than 10^3 particles per bunch train.

All of these systems have dual purposes: they must collimate the beam tails and they form an integral part of the machine protection system (MPS). Because the particle beams have such high charge densities, a single bunch at the end of the linac or a few bunches at the linac entrance will damage almost any material unless the beam size is increased to very large values. Unfortunately, this requires an optics which is itself chromatic and can generate more halo particles. In practice, to limit the betatron functions in the collimation region, the collimation systems rely on thin spoilers (0.25–0.5 radiation length) which scrape the halo and which, if accidentally struck by the full power beam, will enlarge the spot size via multiple coulomb scattering. The scattered halo and enlarged beam are then stopped on thick (20 radiation length) absorbers. Although the damage threshold of the spoilers is considerably higher than that of the absorbers, the design outlined still requires an enlarged beam size at the spoiler location if the spoiler itself is to survive damage from an errant bunch train.

The betatron collimation system scrapes the beam halo and provides machine protection against infrequent orbit disruption of on-energy beams. Based on the SLC experience, very few of these events are expected to occur in each run. A lattice with relaxed tolerances has been designed that uses the concept of "consumable spoilers." These are cylindrical spoilers or scrapers that can be rotated to present a clean surface to the beam if damaged by an errant pulse. Their circumference is such that approximately 1000 damaging pulses can be permitted before replacement is necessary. Tracking studies indicate that this system gives the 5 orders of magnitude of halo reduction required.

In contrast, the energy collimators are designed to be capable of surviving hits from a full bunch train because klystron trips causing off-energy beams may be relatively frequent events and can occur with only microseconds of warning. As seen in Figure 3.49, the system combines a large horizontal dispersion and a large vertical betatron function to ensure that the transverse size of beam pulses at the 0.5 radiation length spoilers is large enough that the charge density is below the damage threshold. Multiple coulomb scattering in the spoiler further increases the beam size before the spoiled bunch train is stopped in an absorber downstream.

Because of these difficulties, the collimation spoiler has been the subject of a substantial research program. There are three elements in the R&D program. The first is the fabrication of a prototype consumable spoiler from beryllium and copper to investigate the engineering challenge of providing accurately aligned surfaces in a piece of moving machinery that must operate under vacuum. A configuration in which each collimator jaw is a rotating wheel has been selected and a prototype has been constructed. This prototype

has pointed the way to minor design modifications and demonstrated that collimation devices of this type can be incorporated reliably into any final system design.

The second element of the collimator R&D effort is a series of beam damage experiments. Samples of various materials have been exposed to single shots of 30-GeV beam of 3 and 20×10^9 electrons with rms transverse areas of 50–200 μm^2 at the FFTB. The samples were then inspected to help understand the resulting damage. To date, thin samples of copper, nickel, titanium, and tungsten-rhenium alloy have been tested. The tests have indicated that, for targets which are less than 1 radiation length in thickness, the damage threshold which is naively calculated is a considerable underestimate of the instantaneous heating which the materials can tolerate. This is believed to be due to the fact that in thin targets the heated material is not fully constrained. Further tests of samples that more completely approximate an NLC spoiler are planned.

The third element of the collimation system R&D effort is a series of experiments to measure the collimator wakefields. The collimator gaps are on the order of 500 μm. Wakefield effects due to the collimator shape, resistivity or smoothness may produce enough jitter amplification to adversely impact luminosity. A movable vacuum enclosure holding four collimator samples plus a standard large-diameter round beam pipe has been installed at the SLAC linac. Two sets of measurements have been performed: a set of tapered copper collimator jaws to study the geometric wakefields of such objects and a set of graphite collimates designed and built by the TESLA collaboration. Future tests will focus on additional resistive and geometric wakefields and on the surface roughness.

Finally, a recent development in the collimation system is the use of octupole doublets which permit the beam halo in one betatron phase to be reduced in amplitude, while leaving the beam core nearly unaffected. A pair of these doublets, located in the beta match section at the beginning of the final focus, has been shown to reduce the halo in the critical final doublet betatron phase by a factor of 4, which in turn would permit equivalently larger collimator apertures in that phase. This would also dramatically decrease the impact of collimator wakefields, as the wakefields are believed to scale with the inverse square of the gap size. There are plans to verify this concept in the FFTB or the LINX test facility at the SLC final focus.

3.3.6 Beam Dynamics and Luminosity Performance Studies

As described in Table 3.16 in Section 3.3.2, the JLC-X/NLC injectors are designed to produce 8 GeV bunch trains with normalized emittances of 3.2 μm·rad in the horizontal and 0.022 μm·rad in the vertical. The main linac and beam delivery regions must preserve these small emittances, and must collide beams with very small transverse sizes in order to achieve the luminosity goals. The main-linac and beam-delivery system designs must ensure that the dual goals of emittance preservation and colliding of ultra-small bunches are achievable. The emittance and jitter budgets for these subsystems are listed in Table 3.16.

Because of the relatively strong wakefields and tight tolerances, the topics of emittance preservation and jitter control have been studied extensively in the X-band designs. To ensure the collider will attain the performance goals, generous emittance and jitter budgets have been applied and multiple redundant emittance control solutions have been incorporated into the design. Furthermore, the diagnostic and controls required to preserve

the beam emittance have been explicitly designed into the facility and the required diagnostic performance has either been demonstrated or is a reasonable extrapolation from demonstrations in operating accelerators or test facilities. The performance of the systems has been studied extensively using simulation tools that were benchmarked with the SLC.

When discussing the luminosity performance, it is also important to separate the timescales. There are three regimes which are determined by the ability to feedback on the trajectory motion: beam jitter, which occurs at high frequencies $f \gtrsim$ few Hz where the feedback systems have little impact and thus the beam overlap at the IP is degraded; emittance control, which occurs at low frequencies $f \lesssim 0.01$ Hz where the trajectory errors increase the beam emittance and thereby the spot size at the IP; and the intermediate regime. Fortunately, the intermediate regime is not important in the JLC-X/NLC because the motion tends to be well correlated and beam-based feedbacks can easily damp any residual. The tolerances in these two regimes typically differ by two to three orders of magnitude. Furthermore, while the horizontal and vertical beam sizes at the IP are both quite small, the large IP aspect and emittance ratios (both approximately 100:1) imply that the challenges in the vertical plane will be 1–2 orders of magnitude more difficult than those in the horizontal.

An example of the vertical tolerances in the final focus can be seen in Figure 3.51 where the emittance control tolerances correspond to the "drift" tolerances. Without emittance correction and beam-based alignment techniques, the typical beam-to-quad *random* alignment tolerance throughout the JLC-X/NLC is between 1 μm and 10 μm, and the typical quadrupole *random* jitter tolerance is between 1 nm and 10 nm. These tolerances are very tight by the standards of today's accelerators, however, when discussing tolerances, it is also important to consider the correlation of the motion and the response of the optics. In general, the beam is very insensitive to misalignments with wavelengths long compared to the betatron wavelength—this is ∼100 meters in the main linacs and beam delivery system. As an example, the luminosity impact of aligning the linear collider to follow the earth's curvature is minimal although this implies a "misalignment" of roughly 10 meters at the IP. Fortunately, the micro-seismic ground motion tends to be highly correlated at low frequencies where its amplitude is large and tends to have small amplitudes at high frequencies where the correlation length is short. Similarly, both beam and mechanical alignment techniques tend to have good resolution over relatively short distances and much poorer accuracy over longer baselines.

In the following, we will first discuss the diagnostics and controls that are essential to the emittance preservation. Then, we will discuss the sources of beam jitter and, finally, we will cover the beam emittance control that is necessary for the luminosity.

3.3.6.1 Diagnostics and Controls

The JLC-X/NLC alignment tolerances can only be achieved through the use of beam-based diagnostics and corrections. For this reason, all subsystems in the accelerator have been designed to permit the use of beam-based techniques to measure the misalignments, and precision remotely controlled translation stages to position misaligned magnets. Use of beam-based techniques allows a tremendous improvement in the alignment precision over conventional survey methods. In the FFTB, for example, magnet alignment of 50 μm was achieved by mechanical survey, but beam-based alignment achieved resolutions as small as

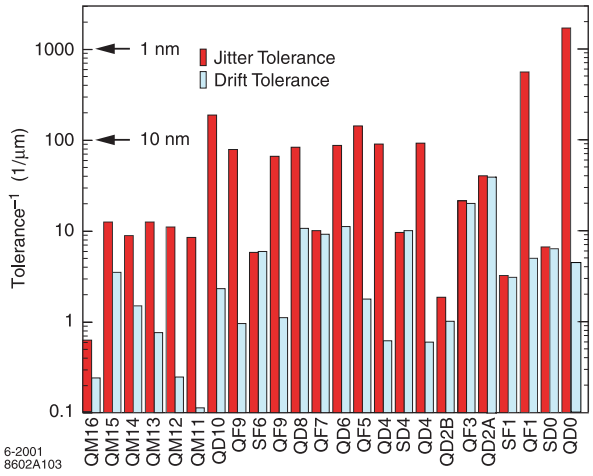

FIGURE 3.51. Magnet position jitter and drift (or alignment) tolerance of the NLC FFS calculated using the FFADA program. "Jitter" tolerance relates to the magnet's capacity to steer beams out of collision at the IP, while "drift" refers to the magnet's capacity to cause the beams at the IP to be too large. Reciprocal tolerances are shown, so in this case bigger is more difficult. Note the large jitter sensitivity of the final doublet magnets QF1 and QD0.

1 μm; independent techniques have been used to set an upper bound on the quadrupole misalignments of 7 μm. These beam-based techniques are only possible with adequate diagnostic and control equipment. The diagnostic and correction devices needed to meet these tolerances are shown in Table 3.25. In general, the required capabilities are at most an incremental improvement upon existing hardware.

In addition to the devices listed in Table 3.25, the JLC-X/NLC will require a set of tuning algorithms that will convert the measurements of the diagnostics into new settings of the correction elements. Here again, the design will rely upon widely used and well-understood techniques in accelerator physics: quadrupole shunting, which has achieved beam-to-quad resolutions as small as 1 μm in the FFTB; dispersion-free steering (DFS), which enabled both SLC and LEP to achieve record luminosities; and closed orbit bumps for global emittance tuning, which have been used routinely in the SLAC linac for many years. Because the JLC-X/NLC builds on the demonstrated success of existing colliders and test facilities, it is expected that modest advances in a few areas of the technology are all that will be required to achieve the performance goals.

3.3.6.2 Beam Jitter and Vibration

Beam jitter will arise from the motion of the quadrupole magnets along the beamline. This relatively high frequency motion of the beam has two effects: first, it causes the beams to be offset at the IP, directly reducing the luminosity, and, second, it degrades the performance of the beam position and beam size diagnostics. The direct impact of the beam jitter on the luminosity is straightforward to evaluate and is not the largest concern. Instead, the beam jitter will reduce the effectiveness of the beam-based alignment and tuning techniques without which it will not be possible to attain reasonable luminosity.

TABLE 3.25: Requirements for JLC-X/NLC diagnostic and correction devices, compared with achieved capabilities of existing equipment.

Item	Specification	Achieved	Improvement Needed
Quadrupole BPMs	0.3 μm resolution	1 μm resolution (FFTB striplines)	3×
		0.025 μm resolution (FFTB cavities)	None
		0.23 μm resolution (NLC prototype cavity)	None
RF structure BPMs	5.0 μm resolution	2 μm resolution (DDS3 and RDDS1 structure prototypes)	None
Magnet movers	0.05 μm step size	0.3 μm step size (FFTB magnet movers)	6×
RF girder movers	1 μm step size	0.3 μm step size (FFTB magnet movers)	None
Laser profile monitor	1 μm rms beam size	1 μm rms beam size (SLC laser wire)	None
		0.06 μm rms beam size (FFTB laser interferometer profile monitor)	None
Magnet/girder supports	$<$ 3 nm vibration w.r.t. tunnel floor	$\sim$ 2 nm vibration w.r.t. tunnel floor (FFTB quadrupole supports)	None

The motion of the magnets will be driven by natural ground motion, vibrations caused by accelerator equipment such as pumps and cooling water, and other human-made "cultural noise." Other phenomena, such as the tendency of mechanical supports to amplify vibrations in some frequency band, can also make the problem significantly more difficult. The natural characteristics of the micro-seismic ground motion are that low-frequency motion, which typically accounts for hundreds of nanometers of rms motion, is highly coherent, while high-frequency motion, which is nearly incoherent, accounts for only a few nanometers of motion. Figure 3.52 shows a series of measurements of the power spectrum of micro-seismic motion, which have been taken at various sites around the world. Included are measurements taken in the SLAC tunnel at 2 AM during a period when the beam and rf structures were off but cooling water was flowing normally, data taken in the LEP, HERA and UNK tunnels, and data taken in the Hiidenvesi cave in Finland. All of the measurements indicate that the power density of natural micro-seismic motion is a strong function of frequency, with a characteristic $1/\omega^4$ dependence. Although high frequencies are potentially the most deleterious from the point of view of beam-beam jitter, Figure 3.52 shows that natural ground motion contains very little power in frequencies above 1 Hz while the large amplitude peak at 0.15 Hz has a wavelength of ∼10 km. The JLC-X/NLC beam-beam jitter sensitivity favors a deep tunnel in relatively strong material at a location with minimal cultural noise, but these characteristics can be traded off against each other. A shallow tunnel site at a relatively deserted location can have noise characteristics comparable to a deep tunnel in a populated area. The most important lesson to be learned from the power spectral density measurements is that not all sites are equally viable for the JLC-X/NLC.

In order to minimize the "cultural noise" from the accelerator equipment vibrations and the impact of magnet supports, it will be necessary to subject every piece of hardware in the accelerator complex to carefully developed engineering criteria, in essence to establish a "vibration budget" for the equipment similar to the "impedance budget" of modern-day storage ring vacuum system. While achieving the vibration goals will require appropriate planning and design, as a proof-of-principle, magnets on the FFTB magnet supports were measured to have motions that were only 2 nm larger than that of the underlying ground. Comparable measurements have been made on NLC prototype quadrupoles which were also attached to rf structures. Other sources of cultural noise, for example the use of motor vehicles on site, will be addressed through appropriate selection of a site and of a tunnel depth. The LEP tunnel measurements in Figure 3.52 show that even a tunnel in a suburban area can be made relatively free of cultural noise sources. Thus, while many sources of accelerator component misalignment can be minimized or eliminated through engineering, the natural ground motion of the site is a potential source of misalignments that is not itself amenable to direct engineering.

When the influences of beam-based steering feedback, lattice response, and correlated motion are considered, it can be shown that quadrupole motion at frequencies below approximately 1 Hz will generally not contribute significantly to beam-beam jitter at the IP. For most of the quadrupoles in the JLC-X/NLC, considered as an ensemble, uncorrelated rms motion of 10 nm in the frequency range above 1 Hz will be acceptable. For example, Figure 3.51 shows that, with the exception of the final doublet, typical jitter tolerances in the final focus are on the order of 10 nm for incoherent motion of the magnets while the sensitivity of the luminosity to correlated motion is much smaller. If the SLAC

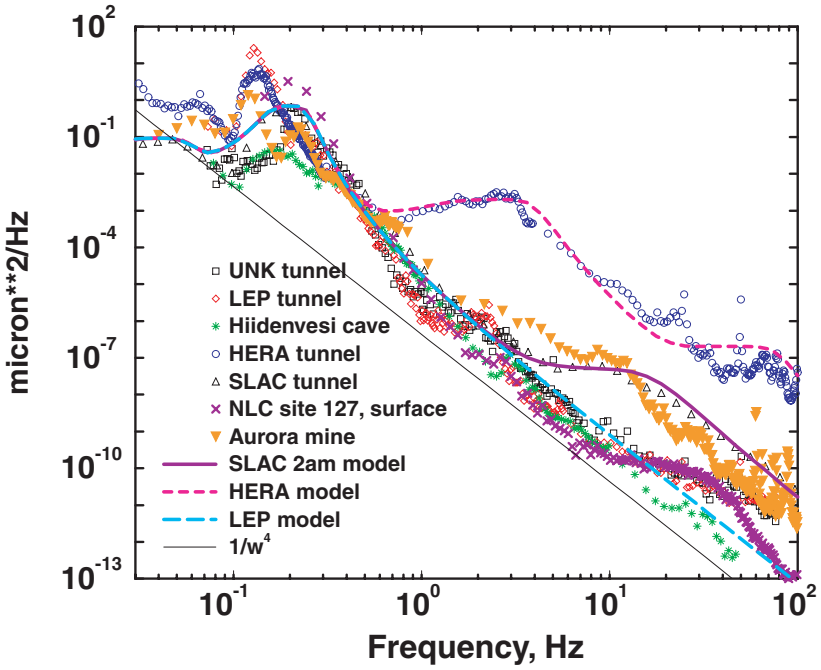

FIGURE 3.52. Power spectrum of ground motion, in units of $\mu m^2/Hz$, from several accelerator tunnels and a cave. The strong peak at 0.15 Hz in all spectra is from ocean waves. The shoulder at 4 Hz in the HERA data is most likely due to "cultural noise," vibration sources within the accelerator complex and from the surrounding urban area.

integrated ground motion and the FFTB quadrupole supports are used as a basis, then the rms quadrupole motion will be less than 4 nm in this frequency range. Thus, for a reasonable choice of site and magnet support technology, it will be possible to provide stability for most of the quadrupole magnets in an entirely passive manner.

In contrast, the jitter tolerances of the final doublet quadrupoles, QD0 and QF1, are roughly an order of magnitude tighter than those in the rest of the final focus. The final doublet quads are the only ones in the JLC-X/NLC that cannot meet their tolerances through passive stabilization alone. However, because the final doublets contain a small number of elements in a reasonably compact space, it is possible to contemplate solutions to the doublet motion problem that are too complex to be applied to a larger number of elements. Thus, jitter suppression for these magnets must include a combination of passive and active methods. Passive methods include locating the IR hall sufficiently far from cultural sources of vibration, minimizing potential vibration sources that can be controlled through proper engineering, and engineering to ensure that the detector, magnet technology, and doublet support girders are stable and do not amplify motion. Active vibration suppression techniques are based on feedback systems to control piezoelectric movers or other fast translation-stage technology which would allow constant position adjustment of the magnets at frequencies far above the beam repetition rate. Two different technologies for measuring the motion of the magnets with high resolution over a wide frequency band are under consideration: an optical anchor, which measures the positions of the final doublet magnets with respect to a fixed point on the detector floor; and inertial sensors which can measure the accelerations of the magnets directly. Both technologies would allow the additional vibrations of the detector to be suppressed, and would allow one doublet to be held fixed in position with respect to the other.

The measures described are expected to limit luminosity loss from beam-beam jitter to a few percent, which is acceptable. An additional measure, which can potentially provide further reduction, is a feedback at the interaction point that operates within a single bunch train. An intra-train collision feedback would use the beam-beam deflection to estimate the relative offset of the two bunch trains from the measured deflections of the first few bunches and would then be used to steer subsequent bunches back into collision. Such a feedback has been studied for the TESLA bunch train. The JLC-X/NLC implementation for such a feedback is made more complicated by the fact that both the bunch train and the intra-bunch spacing are much shorter than in TESLA. Nonetheless, a design of the system using available components has been developed and the system will be tested in the NLCTA.

3.3.6.3 Beam Emittance Control

The beam emittance dilutions primarily arise from misalignments of the beamline components. The BNS damping mechanism, a technique proven at the SLC, suppresses the Beam BreakUp instability (BBU) and eliminates emittance dilution from coherent (betatron) oscillations of the beam but requires a large energy spread of 0.7–1% which will make the beam more sensitive to incoherent misalignments of the quadrupole magnets. Similarly, incoherent rf-structure misalignments will lead to emittance dilution from short-range dipole wakefields, and construction errors in the structures can introduce substantial multibunch emittance dilution. The most serious sources of emittance dilution

are single-bunch effects due to misaligned magnets and rf structures. As discussed, the relevant scale in this case is about 1000 times larger than that for beam jitter and is microns. These misalignments are due to slow motion 0.01 Hz $\gtrsim f \gtrsim$ d.c. and are referred to as static misalignments.

The alignment requirements are beyond what can be achieved by conventional survey techniques. Fortunately, it is possible to use beam-based alignment algorithms to achieve the most challenging tolerances in the main linac. Figure 3.53 shows the beamline hardware associated with beam-based alignment: remotely controlled translation stages for quadrupoles and rf girders, and high resolution BPMs in the quads and the rf structures. The equipment and instrumentation builds on the successful prototypes demonstrated at the FFTB and in ASSET as discussed in Section 3.3.6.1.

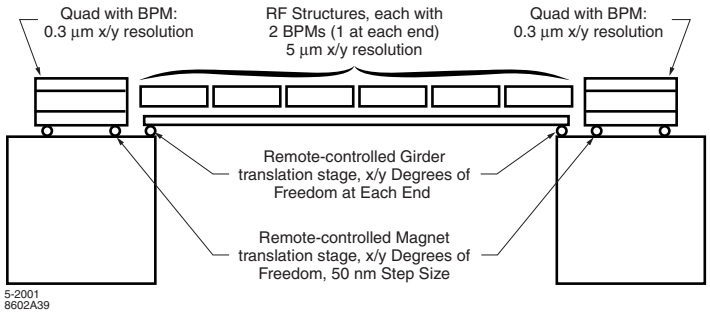

FIGURE 3.53. Beam-based alignment hardware in the NLC main linac.

There are several sources of multibunch emittance dilution in the main linac which cause the various bunches in a given bunch train to follow different trajectories down the beamline. Provided the BBU due to the long-range wakefield is kept small by the combination of detuning and damping, the jitter amplification will be negligible. In this case, the rf structure defects will generate a set of bunch-by-bunch deflections. The tolerances on the structure alignment to limit the multibunch dilutions are loose compared to those imposed by the single bunch effects; tolerances for 10% emittance dilution are shown in Figure 3.54. In addition, the multibunch dilutions will be nearly constant in time, and, as a result, they will be amenable to a feedback that corrects bunch positions within a train. Such a feedback is simultaneously fast (*i.e.*, its BPMs and correctors have a bandwidth of several-hundred MHz) and slow (*i.e.*, the system applies nearly the same set of corrections to each train). The linac design includes several subtrain feedback systems that utilize high-bandwidth BPMs and stripline kickers similar in many ways to the high-bandwidth transverse feedbacks of modern storage rings. Analytic estimates indicate that such systems can reduce the emittance dilution from multibunch sources by roughly a factor of 10, limited by the system bandwidth and the signal-to-noise performance of the BPMs.

Given that the emittance dilution is dominated by the single bunch effects, the primary issue is to attain and maintain the alignment of the quadrupoles and the rf girders. The following procedure is used to do this:

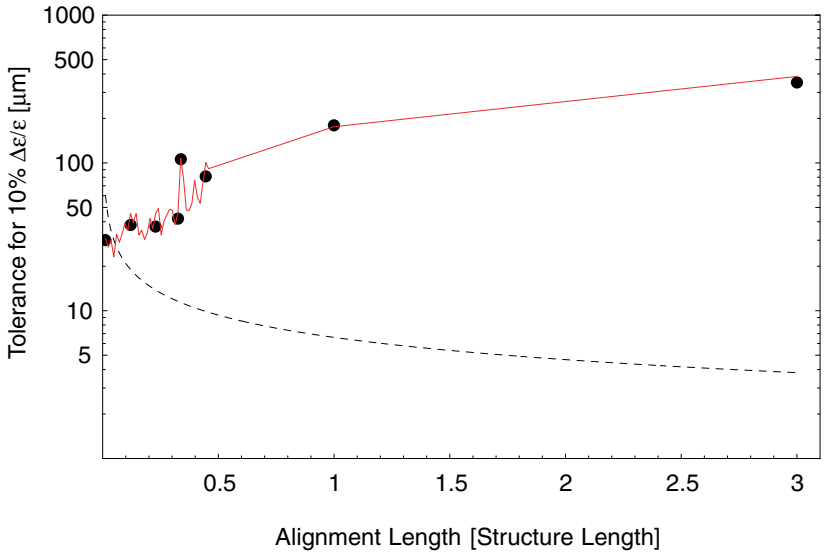

FIGURE 3.54. Misalignment amplitude leading to 10% $\Delta\varepsilon/\varepsilon$ as a function of the accelerator structure length (90 cm) for the long-range (solid) and short-range transverse wakefields. An alignment length of one structure corresponds to random rigid misalignments of individual structures while lengths of less than one structure correspond to random piecewise misalignments of the structures. With the S-BPM and structure mover system, the JLC-X/NLC essentially eliminates the short-range wakefield tolerances.

1. Determine the "gold orbit" of the linac. This is the set of quadrupole BPM readings that corresponds to high luminosity. In the absence of BPM-to-quad offsets, the gold orbit would simply be zero on all BPMs.

2. Move the quadrupole magnets using the magnet movers until the gold orbit is achieved and then move the rf girders using the rf structure BPMs to align these to the beam trajectory.

3. Use a set of discrete steering feedback loops in the main linac to minimize the orbit drift due to component motion as a function of time. The steering feedback can operate quickly (at the level of 1 Hz or faster), and is entirely compatible with colliding for luminosity.

4. As diffusive ground motion moves the accelerator components, the luminosity will gradually decline. This is because the misalignments between the feedback correctors will become sufficiently large that the feedback can no longer maintain a reasonable approximation of the gold orbit. At this time, recover the gold orbit by returning to Step 2. This procedure should be compatible with colliding for luminosity if the magnet mover step sizes are small and the steering feedback loops are operating.

5. Over even longer time scales, the gold orbit will gradually cease to provide good luminosity. This is because the electrical centers of the Q-BPMs, the magnetic centers of the quadrupoles, and other parameters are subject to change over time. Once this has happened, return to step 1 and determine a new gold orbit using invasive procedures.

Determining the gold orbit is a crucial step in the algorithm as the quality of the gold orbit will determine the maximum luminosity performance of the collider. Ideally, the BPM-to-quad offsets can all be measured by the beam with sufficient accuracy by varying the focusing strength of each quadrupole and measuring the resulting deflection of the beam on downstream BPMs. This allows determination of the beam-to-quad offset, and the quad-to-BPM offset of the nearest BPM can then be deduced by subtraction. This procedure was demonstrated at the FFTB. For the main linac, a resolution of 1 μm would be straightforward to achieve for each quad, if the technique were not limited by systematic errors. The primary systematic error arises if the quadrupole center moves as the quadrupole strength is varied. Measurements of the quadrupole center motion, implies that electromagnetic quadrupoles could be aligned at the tolerance level of 2 μm while the alignment would be roughly 10 times worse with permanent magnets; permanent magnets have been considered for the main linac due to reliability and cost considerations.

Because the accurate determination of the BPM offsets will still provide the most local (hence most stable) correction of the emittance, the quad-varying technique remains the method of choice for determining the gold orbit. However, because of the sensitivity to quad-center variation, this technique may not be adequate by itself. An alternative technique for generating a gold orbit is Dispersion Free Steering (DFS), in which the dispersion is measured by varying the energy of the beam or beamline and measuring the change in the trajectory. This technique is less local than varying a single quadrupole at a time and measuring the resulting deflection, but it directly measures the dispersion. Furthermore, DFS relies only upon the BPM resolution to achieve an acceptable trajectory, and the BPMs will have a resolution that is much better than the knowledge of the BPM-to-quad offset under almost any imaginable circumstances. The emittance dilution after convergence is 20% with a 0.3 μm BPM resolution.

Additional improvement to the emittance can be achieved by applying closed-orbit bumps over a small region of the linac. These bumps generate dispersion or wakefields at a particular phase and in a particular location, which can cancel any existing dispersion at that phase and location. A simulation has been performed in which a set of dispersion bumps was applied to the main linac after DF steering. In the case where 0.3 μm BPM resolution was assumed for DFS, the final DFS + bumps emittance dilution is 5%.

As suggested in Step 5, the emittance obtained by repeatedly steering to the gold orbit in Step 2 will increase, as the BPM-to-quad offsets change with the passage of time. Once this has happened, it is necessary to repeat the procedure that was used to determine the gold orbit in the first place. The length of time between determinations of the gold orbit is difficult to estimate. Unfortunately, determining the gold orbit can be invasive and incompatible with colliding for luminosity. Measurements of the BPM centers in the FFTB stripline BPMs suggest that the gold orbit will not have to be re-measured more often than once a month and aggressive use of emittance bumps can further extend the life of a gold orbit.

As discussed in Step 3, another important technique for maintaining the luminosity is the use of steering feedback loops which stabilize the beam trajectory at frequencies up to $\sim$1 Hz. The main linac will use several discrete sets of fast, weak dipole correctors to provide steering feedback at 5 to 10 locations within the beamline. The main linac feedback provides partial reduction of the emittance dilution arising from diffusive ground motion. Figure 3.55 shows the emittance as a function of time at the end of the main linac due to

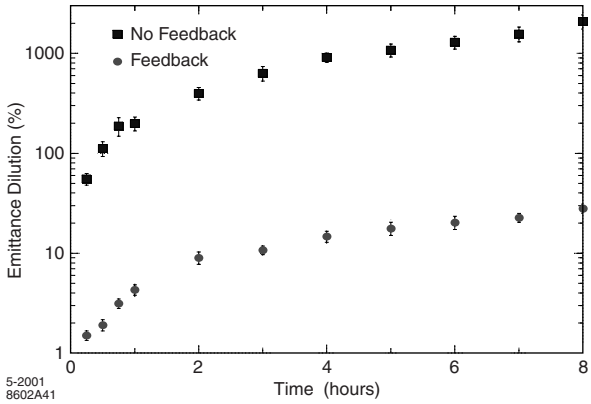

FIGURE 3.55. Emittance dilution (%) in the NLC main linacs due to diffusive ground motion, assuming an ATL coefficient comparable to that measured at SLAC. A case with no linac feedbacks (squares) and a case with the proposed NLC steering feedback architecture (circles) are both considered.

ATL motion, assuming a coefficient A of 5×10^{-7} μm^2/m/s, both with and without steering feedback in the main linac. Without feedback, the emittance dilution in the main linac would become unacceptable within minutes, while the addition of steering feedback preserves the emittance for hours. After this time period, it is necessary to recover the gold orbit throughout the linac by moving all of the quadrupoles on their magnet movers. The steering feedbacks also reduce the luminosity dilution that happens while the quadrupoles are being moved. Figure 3.55 suggests that the time-averaged luminosity loss from the slow completion of mover steering will be on the order of 2%.

Finally, Table 3.26 shows a tentative distribution of the main linac emittance budget amongst the various sources of dilution. Since the studies were performed with the 1 TeV c.m. configuration of the JLC-X/NLC, the lower-energy configurations, which have fewer rf structures and thus less challenging beam dynamics, should be substantially more tolerant. In addition, Table 3.26 assumes that DFS + bumps must be used for generation of a gold orbit, and that only a 1.0 μm effective BPM resolution is achieved which is 3 times worse than the design specification.

The procedure described works well for the main linac. However, the beam dynamics in the final focus can be different from that in the main linac. The number of quadrupoles and the rms beam energy spread are both quite small, so phase mixing in the final focus is not a serious problem. This in turn implies that global knobs of various kinds will be more effective than in the linac. The final focus also contains horizontal bend magnets, so it is possible to adjust the dispersion with normal or skew quads at high-dispersion points rather than by varying the beam trajectory, as is done in the linac. On the other hand, the final focus contains many strong aberrations, such as chromaticity, sextupoles, and skew quadrupole effects, which typically are delicately balanced against one another. Therefore, the BDS has looser tolerances on the conditions that must be met before global corrections are applied than the main linac has, but the tolerances on stability over time are much tighter than in the main linac.

TABLE 3.26
Distribution of the main linac emittance budget and resulting engineering tolerances. Dilutions are applied to the vertical plane except where indicated. Beam-to-quad misalignment is an "effective misalignment" assuming DFS + bumps with 1.0 μm effective BPM resolution. Multibunch sources assume factor of 10 suppression via subtrain feedback. Note that the tolerance on structure dipole frequencies is for the worst-case error mode (random cell-by-cell frequency errors which are reproduced in every structure), and all other distributions of frequency errors have considerably looser tolerances.

Effect	Tolerance	Resulting Emittance Dilution
Beam-to-quad misalignments	2.0 μm (effective)	25%
Quad strength errors	0.1%	0.7% (x) / 0.5% (y)
Structure-to-girder misalignments	30 μm	8%
Structure-to-girder tilts	30 mrad	4%
Quadrupole rotations	200 mrad	4%
Structure BPM resolution	5 μm	3%
Mover steering interval	30 minutes	2%
Structure straightness (bow)	50 μm	1% (incl. feedback)
Cell-to-cell misalignments	3.5 μm	1% (incl. feedback)
Structure dipole frequencies	1 MHz	1%
Synchrotron radiation		3% (x)
Total		3.7% (x) / 50% (y)

Of course, the final focus of the JLC-X/NLC, like the main linacs, is designed with powerful diagnostic capabilities and robust correction devices. Every quadrupole and sextupole is on a remotely controlled magnet mover, similar to those in the main linac. Each quadrupole is paired with a BPM with submicron resolution, and in some critical locations ultra-high resolution cavity BPMs with resolutions better than 100 nm are also used. Laser-based beam-size monitors are installed at critical locations. All sextupoles, bends, and quads except for the final doublet are iron-dominated electromagnets, with high-precision power supplies. In addition, the final focus has two powerful diagnostics not available at other locations, the luminosity and the beam-beam deflection, each of which will be measured on every pulse in order to provide signals for feedback systems.

The tolerances for the final focus components are shown in Figure 3.51. Although these are small, it is important to note that these are so-called "bare" tolerances—tolerances in the absence of feedback systems or other non-invasive correction algorithms which can stabilize accelerator performance. Understanding the real performance of the final focus requires simulation studies that include the planned diagnostic and correction systems, and their algorithms. As an example, one of the most serious potential sources of emittance dilution is beamline magnet misalignments driven by diffusive ground motion. Figure 3.56 is the result of a simulation that misaligns the elements of the 1-TeV BDS configuration according to the ATL law with $A = 5 \times 10^{-7}$ μm^2/m/s. The curves show that luminosity would degrade under ATL motion in approximately 2 minutes if only the beam-beam deflection collision stabilization feedback was present. If, in addition, orbit control feedback is allowed to steer the beam through the centers of critical quadrupole and sextupole magnets, then

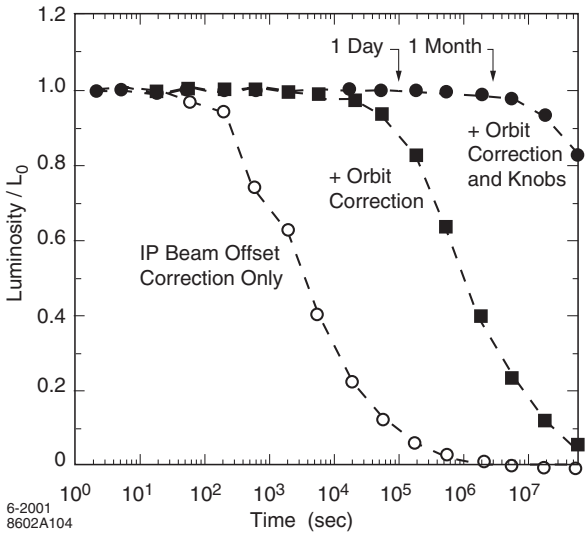

FIGURE 3.56. Degradation of alignment under ATL ground motion with IP beam-beam deflection based feedback only, with orbit feedback added, and with direct luminosity optimization added.

the time for luminosity degradation increases to approximately 1 day. Finally, if direct optimization of the main aberrations via global knobs is added to the system, then the luminosity lifetime increases to several months, after which a disruptive realignment procedure would be required.

3.4 CLIC

3.4.1 Introduction

3.4.1.1 Overview of the Complex

The CLIC (Compact Linear Collider) study aims at a multi-TeV, high luminosity e^+e^- linear collider design. Beam acceleration uses high frequency (30 GHz), normal conducting structures operating at high accelerating gradients (150 MV/m), in order to reduce the length and, as a consequence, the cost of the linac. The cost-effective rf power production scheme, based on the so-called Two-beam Acceleration method, enables electrons and positrons to be collided at energies ranging from about 0.1 TeV up to 5 TeV, in stages. Though the study has been optimized for a nominal center-of-mass (c.m.) energy of 3 TeV with a luminosity of 10^{35} cm^{-2}s^{-1} [7], the CLIC design is however such that its construction could be staged without major modifications (right side of Figure 3.57). The implementation of the lower energy phases for physics will depend on the existence or not of other accelerator facilities, but in a first stage it could cover, if required, the c.m. energies between ∼0.1 and 0.5 TeV with $\mathcal{L}$=10^{33}–10^{34} cm^{-2}s^{-1}, where interesting physics and overlap with LHC (Large Hadron Collider) are expected. This stage could be extended to 1 TeV with $\mathcal{L}$ above 10^{34} cm^{-2}s^{-1}. Next would come the desirable $e^{\pm}$ collisions at 3 TeV which should break new physics ground, while the final stage might be 5 TeV.

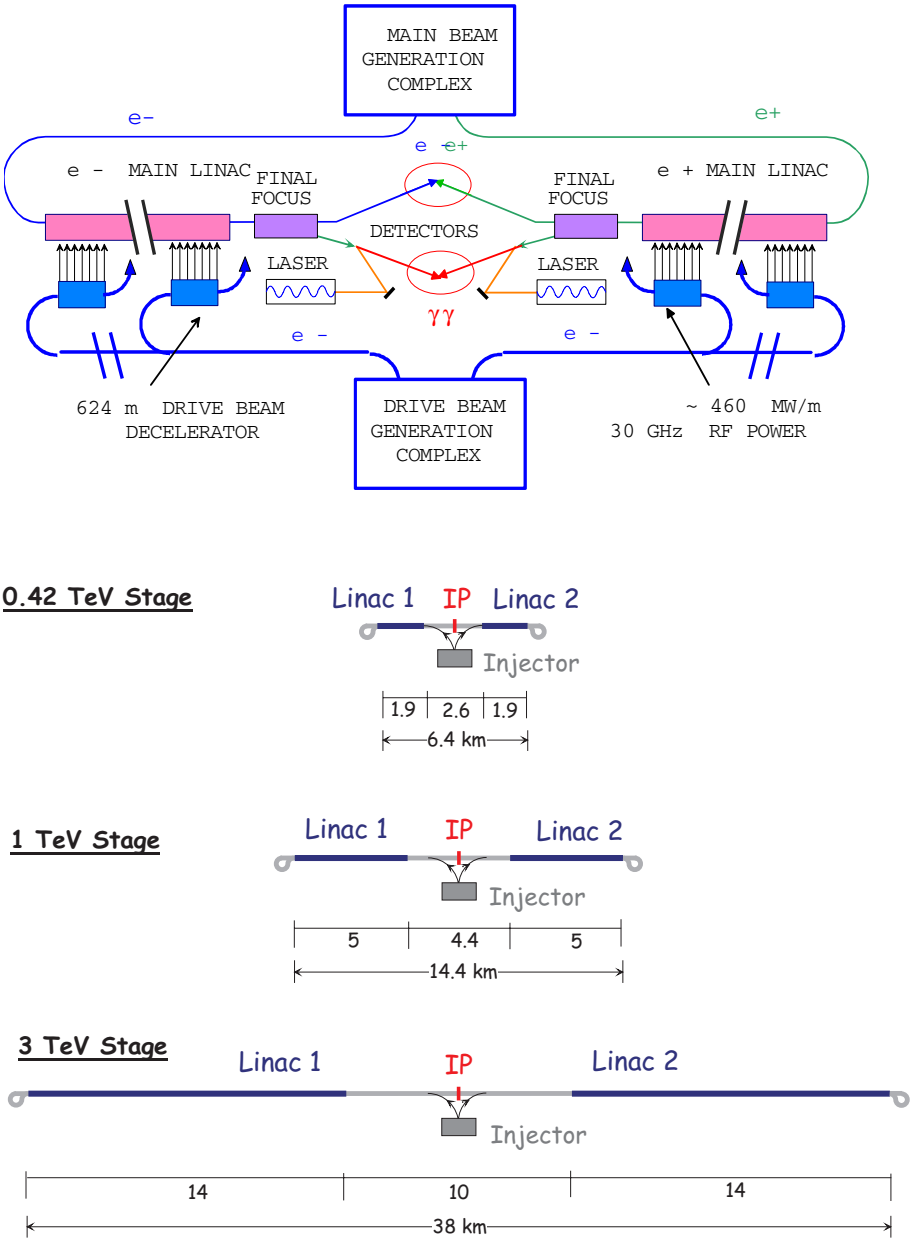

FIGURE 3.57. The top shows the overall layout of the CLIC complex and the bottom shows the tunnel lengths (km) for the linacs and the BDS (base-line design) on each side of the IP, at various cm energies.

The left side of Figure 3.57 gives an overall layout of the complex which shows the linear decelerator units running parallel to the main beam [8]. Each unit is 625 m long and decelerates a low-energy high-intensity e^- beam (so-called drive-beam) which provides the rf power for each corresponding unit of the main linac through energy-extracting rf structures. Hence, there are no active elements in the main tunnel. With a gradient of 150 MV/m, the main beam is accelerated by ∼70 GeV in each unit. Consequently, the natural lowest-value and step-size of the colliding beam energy in the center-of-mass (c.m.) is ∼140 GeV, though both can be tuned by some adjustment of the drive-beam and decelerator. The minimum energy corresponds to 1 unit and the energy step to the addition of one unit, on either side of the interaction point (IP). The nominal energy of 3 TeV requires 2 × 22 units (a total two-linac length of ∼28 km), each unit containing 500 power-extraction transfer structures (PETS) feeding 1000 accelerator structures. The 500 GeV c.m. energy needs 2 × 4 units (a two-linac length of ∼5 km) and reaching exactly this energy implies to rearrange the decelerator and the linac so that a unit includes 455 PETS and 909 accelerator structures (gain of 62.5 GeV per unit instead of ∼70 GeV). It must be noted that this arbitrary choice of c.m. energy has no specific physics justification and that in practice an energy more natural for the CLIC scheme (∼560 GeV with 2 × 4 units) would be selected.

This modularity is facilitated by the fact that the complexes for the generation of all the beams and the Interaction Point (IP) are both in a central position, where all the power sources are concentrated. The main straight tunnel houses both linacs, the various beam transfer lines and, in its middle part, the two Beam Delivery Systems (BDS). The fact that there is such a single tunnel results in a simple and easily extendable arrangement. The right side of Figure 3.57 gives examples of estimated tunnel lengths for various energies in the center-of-mass.

The general description of the CLIC two-beam technology, of the main-beam complex and of the rf power source at 30 GHz is given in [7]. It also summarizes the main-beam (main-linac) and drive-beam (decelerator and accelerator) parameters at the nominal energy of 3 TeV as well as some possible main-beam parameters at various other energies. For the purpose of the present review however, the possible design of CLIC at 500 GeV has been studied more specifically than in the past and optimized to some extent. This work is still going on and the following description gives the status of this 500 GeV study with the corresponding parameters (see Megatables) and subsystem characteristics. Many of these systems are subjects of a continuing research and development program, in particular the high-gradient structures, the damping rings, the dynamic time-dependent effects, the vibration stabilization and the beam delivery system. In its present stage, the description of the 500 GeV design is therefore not totally self-consistent. In addition, the model of the main-linac accelerator structures and some consequent parameters used for beam-dynamics analysis do not exactly correspond to the structure design and to the rf power source associated with this design, as described in this report. Updating the simulations was however not considered urgent since the numerical model used gives pessimistic results. The CLIC nominal 3 TeV case will be described in the separate chapter on energy upgrade.

3.4.1.1.1 Layout and Civil Engineering Preliminary investigations on the engineering feasibility and impact of the large CLIC facility have been carried out using a possible site near CERN. For the civil-engineering arrangement, the guidelines retained are the following: to find out the right underground level for the main tunnel to be within favorable geological

conditions, to locate the IP on the CERN site, to minimize the environmental impact of the surface buildings of the injector-areas and shaft-areas, and to provide the lowest cost for the most suitable layout. A molasse of similar quality to that which was found for the SPS and LEP/LHC tunnels would give the most advantageous and cheapest conditions for CLIC. In these conditions, the maximum straight length available is about 40 km and this makes it possible to have a tunnel housing both the main linacs and the most conservative beam delivery systems (∼10 km long base-line BDS, total) for a c.m. energy of 3 TeV. However, prospects also indicate that a straight length of approximately 52 km can be envisaged between two major faults. In addition, it is considered after further optimization that a total BDS length of ∼5.2 km is sufficient at both 500 GeV and 3 TeV c.m. A shaft for engineering work and maintenance should be planned at about every 3.2 km or 5 drive-beam units. Two return loops for the main linac beam with an average radius of 115 m are foreseen at each extremity of the tunnels. The injector complexes for both the main-beams and the drive-beams would require additional tunnel lengths of about 7 km and 5 km respectively (linacs and transfer lines). They remain the same at all cm energies and should be located in a central area, near the IP detector hall. In this way, the service buildings and the power sources (klystrons-modulators) could be concentrated in this central area.

The available data about the top of the molasse, the faults, the Piemont of the Jura and the water tables indicate that the 40 km long tunnel mentioned previously can be entirely positioned in the molasse if it lies at an average level of ∼140 m below ground level. The main tunnel could then be done by a tunnelling-boring machine. The excavation of the beam dump caverns, of the beam turn-around loops and of the IP experimental hall cavern would be carried out by a road-header (maybe by using explosives in the cavern). The minimum and maximum depths of the shafts would be about 80 m and 165 m respectively. The diameter of the main tunnel could be 3.8 m and that of the shafts 7 m (a total of 13 of them are required at 3 TeV and between 3 and 5 at 500 GeV). In the central area, it is possible to place the injectors (all the linacs of the injection complexes) close to the surface so as to make most of the injector tunnels by cut and cover method, hence reducing the cost and making the installation of the klystrons and modulators easier.

3.4.1.1.2 Cooling and Ventilation System The three main parts of the cooling system are related to the main tunnel, the injector complexes and the main beam dump area. In the main tunnel, the total power dissipated at 3 TeV by the quadrupoles and other systems (∼32 MW), by the drive beam dumps located at the end of each 625 m long unit (∼29 MW total) and by the accelerating and power-transfer structures (∼114 MW) amounts to 175 MW, and approximately to 3 times less at 500 GeV. The cooling system there consists of primary water circuits which serve as a cold source for primary/secondary heat exchangers placed in the surface buildings. The primary circuit will probably consist of closed circuits with cooling water towers built around a limited number of tunnel access pits (*e.g.*, 2, 5, 9, and 11 at 3 TeV), in order to limit the environmental impact. The secondary circuit goes down the shafts to cool the tunnel equipment. The air quality is controlled by a main chilled water-cooled HVAC unit. For minimizing variations of temperature on the rf structures, air temperature gradient is reduced by using 32 intermediate HVAC units which cool the air through chilled water supplied from the surface.

The main-beam injector dissipates ∼7 MW (2 times more at 500 GeV because of a higher repetition rate) while the drive-beam generation system dissipates ∼145 MW at 3 TeV

(about 3 times less at 500 GeV). The cooling and ventilation of these subsystems located in the central area follows the same principle as for the main tunnel, with a closed primary circuit and a cooling water. The two main-beam dumps dissipate 14.7 MW each at 3 TeV (∼5 MW at 500 GeV). In order to minimize shock-waves at each pulse, it is foreseen to cool these dumps with water at the set point of 4° C and to use a small temperature difference between inlet and outlet of 0.4°. Cooling towers provide cooling water to the chillers placed in an underground cooling plant. The chillers supply water to a pool used for the dumps in a closed circuit to reduce the water contamination.

3.4.1.1.3 Power Distribution A first study of a possible powering strategy has been carried out, assuming that CLIC and LHC would work simultaneously and that the central area is near the North-area of CERN. The power requirements cover, in decreasing order of importance, the rf system of the drive-beam generation, the main-beam injectors, the detectors, the magnets, the cooling and ventilation, and the general services. Considering the required power, the connection to the grid must be at 400 kV. The important power needs of the drive-beam rf require a separate primary system at 36 kV and a secondary system at 7.2 kV to adapt to the power converters of the klystrons. The main distribution voltage proposed for the central area would be 24 kV. For the long tunnel, major surface supply points are foreseen at each shaft, with an underground supply point and an additional underground supply point at 1280 m from the latter; a voltage of 24 kV is proposed for the system distribution. A major 24 kV substation would be needed in the central area. This major station might however be broken into smaller units, given the size of the central area. The main tunnel requires less power (about 1.5 MVA per km). Because of the distances, the distribution voltage level would be 24 kV, with underground supply points and 630 kVA transformers.

3.4.2 Main-Beam Subsystems

3.4.2.1 Injection System

3.4.2.1.1 Basic Parameters The bunch spacing in the main-beam train imposes an rf acceleration frequency of 1.5 GHz. The rf gun and the injector linacs run at L-band except the Booster Linac which runs at S-band. The particle production rate is 0.9×10^{14} $e^{\pm}$/s. A total incoherent energy spread of $\Delta E/E=\pm$ 1% corresponds to a maximum rms bunch length of σ_z=3 mm. The same bunch length is assumed from the rf gun, producing an e^- beam for e^+ production, up to the first bunch compressor downstream to the e^+ damping ring. For e^-, the bunch length of 3 mm is obtained after bunch compression upstream the e^- pre-injector linac. Two stages of bunch compression are foreseen. The first, at the damping ring exit, operates at 3 GHz while the second, at the entrance of the main linac, uses 30 GHz. The normalized transverse beam emittances at the I.P. are imposed by the required luminosity. The damping rings are designed in order to produce the necessary emittances taking into account the expected emittance growth in the main linac with the input emittances provided by the sources of the leptons. The maximum single bunch charge is 5 % higher than the charge at the IP to allow for beam losses in the injector complex and collimation at the entrance of the main linac. Table 3.27 summarizes the CLIC injector basic parameters.

TABLE 3.27
Basic target parameters at different stages of the injection.

General Parameters	Unit	Value
At main linac injection		
Energy	GeV	9
Nb particles per bunch	10^{10} $e^{\pm}$	0.42
Bunch length	μm	35
Energy spread	%	1.4
Transverse emittance ($\gamma\epsilon_x$)	10^{-9} m·rad	1800
Transverse emittance ($\gamma\epsilon_y$)	10^{-9} m·rad	5
At damping ring exit		
Energy	GeV	2.424
N_b particles per bunch	10^{10} $e^{\pm}$	0.42
Bunch length	μm	1300
Energy spread	%	0.135
Transverse emittance ($\gamma\epsilon_x$)	10^{-9} m·rad	1600
Transverse emittance ($\gamma\epsilon_y$)	10^{-9} m·rad	3

3.4.2.1.2 Injection Complex of the Main Beam The general layout of the main-beam injection complex is given in Figure 3.58. This complex is composed of the two following systems:

i. The system for the electron beam: The laser system and the photo-cathode DC electron gun, followed by an rf accelerating cavity, generate a 10 MeV, low charge beam. The pre-injector linac provides an energy gain of 190 MeV and an e^- beam energy at the exit of 200 MeV. The injector linac accelerates the beam by 2.224 GeV, giving a final energy of 2.424 GeV. This linac accelerates alternately the train of electrons and the train of positrons. A DC dipole magnet separates the e^- beam from the e^+ beam. It also makes it possible to send the beam toward a dump where some beam instrumentation will be implemented. Then, there are successively, the damping ring for e^-, the first stage of the bunch compressor working at 3 GHz and 2.424 GeV, the booster linac accelerating alternately e^- and e^+ beams up to 9 GeV, the transfer line and finally the second stage of the bunch compressor working at 30 GHz and 9 GeV at the entrance of the e^- main linac.

ii. The system for the positron beam: The laser system and the photo-cathode rf electron gun generate a 10 MeV, high charge beam. The e^- Primary Beam Linac sends a 2 GeV beam onto the e^+ target. Following the conventional positron source, which receives the high-intensity primary e^- beam, the e^+ Pre-injector Linac accelerates e^+ (and secondaries e^-) up to 200 MeV. The injector linac (common to e^- and e^+) provides a 2.224 GeV energy gain. Then the pre-damping ring and

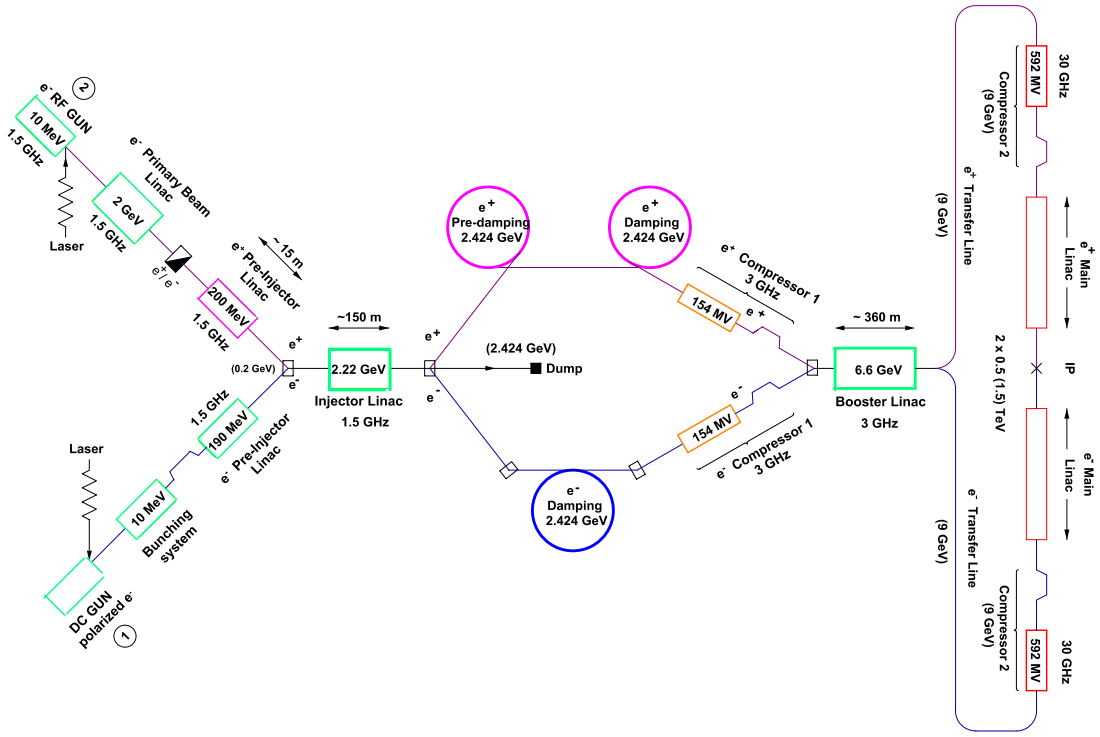

CLIC INJECTOR COMPLEX FOR THE e⁺ and e⁻ MAIN BEAMS

FIGURE 3.58. CLIC injector complex for the e^+ and e^- main beams.

the damping ring for e^+ follow. The rest of the system consists of the same kind of compressors and transfer lines as for the e^- and includes the common booster linac.

Electron Source for the Main Linac The DC gun should produce 1 nC/bunch. The charge of 0.62×10^{10} e^- per bunch takes into account the transfer efficiency between the DC gun and the damping ring exit, at 2.424 GeV. A total charge of 150 nC is not an issue for the DC gun assuming that the bunch length and bunch spacing are adequate for the surface charge limit. The expected normalized edge emittances are 10×10^{-6} m·rad in both planes. It is required that the train-to-train charge jitter be below 0.5% (rms) and the bunch-to-bunch charge jitter (inside the train) be below 1% (rms). The transverse laser spot size on the photo-cathode should have a diameter variation smaller than 1%.

Positron Source for the Main Linac The rf gun works at 1.5 GHz with an electric field of 50 MV/m (on axis) and should deliver 2×10^{10} e^- per bunch. The expected normalized emittances are 13×10^{-6} m·rad (both planes) for the 2.2 nC per bunch needed to create the train for positrons production. The positron source for CLIC is a conventional one based on an electromagnetic shower created by electrons impinging on a high-Z material target. The source and its associated 2 GeV linac meet the specifications for the 500 GeV option. The

normalized yield is 0.31 e^+/e^- per GeV at the exit of the e^+ pre-injector linac. The charge per bunch for the primary electron beam is 1.35×10^{10} e^-. The incoming e^+ emittance (edges) into the pre-damping ring is 0.09 m·rad for both planes. The longitudinal characteristics are 20 MeV energy spread (full width) and 50 ps bunch length (edge).

The Linacs Taking into account the necessary beam loading compensation, the e^+ Pre-injector linac accelerates the particles up to 200 MeV with a loaded gradient of 24 MV/m. Therefore the final energy of the e^- beam at the end of the Pre-injector linac is the same as for the e^+ beam. The energy gain in the e^- Primary Beam linac is a free parameter that will be adjusted for a good trade-off between cost and efficiency. The Injector linac (1.5 GHz) is based on a loaded gradient of 17 MV/m and is ∼150 m long in order to accelerate both beams to 2.424 GeV. The Booster linac (3 GHz) has a loaded gradient of 21 MV/m and is ∼360 m long in order to accelerate both beams up to 9 GeV. The rf pulse is 10 μs long and accommodates two consecutive SLED pulses. The first is for e^+ and the second for e^- acceleration respectively.

3.4.2.1.3 Klystrons and Modulators

The main beams injector complex is required to deliver e^+ and e^- beams at 9 GeV via the transfer lines to the CLIC main beam accelerator. The present injector design layout uses a series of linacs to accelerate the electron and positron beams. These L-band linacs (Figure 3.58), operating at a frequency of 1.5 GHz enable the energy of each beam to be increased to 2.424 GeV before injection into the damping rings. The klystron-modulators used in these linacs produce a 5 μs rf pulse at peak powers up to 80 MW. Standard line-type modulators could be used for these pulsed rf sources except for the Injector Linac modulators where a configuration similar to the drive-beam modulators would be more appropriate because of the high average power per klystron. The S-band 3 GHz Booster Linac that follows the damping rings and the 3 GHz bunch compressors, will accelerate both electron and positron beams up to 9 GeV before injection into the 30 GHz compressors and the CLIC main linacs. The klystron-modulators in this linac are required to produce a long 10 μs pulse with a peak rf power up to 80 MW. A high-duty cycle line-type modulator with the same configuration as for the drive-beam linac could also be used for this task as well again because of the high average power in each klystron. Table 3.28 gives a summary of the klystron and modulator requirements for the main-beam injector complex in the present 500 GeV CLIC scheme.

3.4.2.2 Damping Rings

The damping ring design (identical for e^+ and e^-) is based on the most demanding requirements at 3 TeV and some parameters are then adapted for the 500 GeV collision energy keeping the ring layout unchanged [9]. The need for very low emittances in the CLIC main linac implies a lattice with a small I_5 synchrotron integral, which is obtained by using a TME (Theoretical Minimum Emittance) lattice, with compact arcs. The wiggler magnets needed in addition, as well as the injection and extraction insertions are located in dispersion-free regions. Making use in these regions of FODO-cells with zero dispersion, the average beta function $\langle\beta_x\rangle$ through the wigglers can be kept reasonably small. In the limit of many wiggler poles and a short wiggler period λ, the damping and the quantum

TABLE 3.28: Main-beam klystron-modulator requirements. MDK= Modulator-Klystron system, SBK= Single-Beam Klystron, MBK= Multibeam Klystron.

MDK RF System	Number MDKs	Klystron Type	Repetition Rate [Hz]	Pulse Width [μs]	Frequency [MHz]	Peak Power [MW]	Average Power [kW]
e^-/e^+ pre-inj. linacs	4	SBK/MBK	200	5	1500	80	100
e^- primary beam linac	24	SBK/MBK	200	5	1500	80	100
Injector linac	52	SBK/MBK	400	5	1500	40	100
Booster linac	52	SBK/MBK	200	10	3000	40	100

excitation only occur in the wiggler magnets and the final emittance without IBS (Intra Beam Scattering) does not depend on the unperturbed beam emittance in the arcs.

The ring circumference C is determined by the harmonic number h, the rf frequency, the number of bunch trains to be accommodated and the kicker rise-time or fall-time for injection and extraction. The ring energy is constrained by the IBS and by the spin tune selected to avoid integer spin resonances. In addition, avoiding instabilities implies keeping the momentum compaction α_p relatively large. With these constraints, the optimum strengths of the arc dipoles and of the wigglers were then inferred from the minimum transverse emittance computed at extraction in the presence of IBS, for which the magnet fields were still considered reasonable.

Table 3.29 summarizes the main parameters required for the CLIC damping ring.

TABLE 3.29
Target beam parameters for the damping ring at 500 GeV (3 TeV).

Parameter	Symbol	Value
Bunch population	N_b	4.2×10^9
Number of bunches per train	k_{bt}	154
Repetition frequency	f_r	200 (100) Hz
Bunch spacing	τ_b	0.2 m
Maximum kicker rise time	τ_k	25 ns
Final transverse emittances	$\gamma\epsilon_{x,y}$	1600 (450), 3 nm·rad
Longitudinal emittance	$\gamma mc^2\epsilon_t$	$\leq$ 5000 eV·m

The optics design proceeded by first solving the three differential equations describing the emittance time evolution in a smooth approximation, taking into account radiation damping and IBS parameterized by the Piwinski formalism, and by then constructing a MAD optics for the optimum parameters so determined. The energy for the damping ring is chosen as 2.424 GeV. The emittance is minimum if the horizontal phase advance μ_x per TEM arc cell is 284°. This phase advance is far from ideal with regard to chromatic correction, and the horizontal and vertical phase advances per TME arc cell were adjusted to 212°/72°. These values are close enough to the ones minimizing the emittance and allow good positioning of the sextupoles distributed in order to reduce both the non-linear chromaticity and the resonance driving terms. The damping ring accommodates two long straight wiggler-sections, in which the dispersion is almost negligible and the chromaticity is compensated by the arc sextupoles. The sextupole strengths are not as high as in previous designs while achieving a good correction of the nonlinear chromaticity, given the lattice characteristics summarized below. Preliminary results seem to indicate, however, that the resulting dynamic aperture is not yet sufficient and that a further optimization of the lattice and sextupole location is needed. Work on the damping ring optics is therefore actively pursued.

Starting from a generic TME layout, the CLIC arc lattice evolved toward a sequence of cells which comprise four quadrupoles and a combined function bending magnet. The cell optics

is shown in Figure 3.59 (Left). Compared with a three-quadrupole cell, the four-quadrupole cell provides larger dispersion amplitudes at these quadrupoles (∼1.25 cm and ∼0.9 cm at the QF and QD, respectively) where the sextupoles are located. The emittance detuning factor for this cell is $\varepsilon_r = 1.71$. The defocusing gradient in the bending magnet decreases the emittance by about 10–15% via the associated change of the damping partition J_x. The combined function magnet also facilitates the matching. The defocusing gradient retained is close to 150 kG/m.

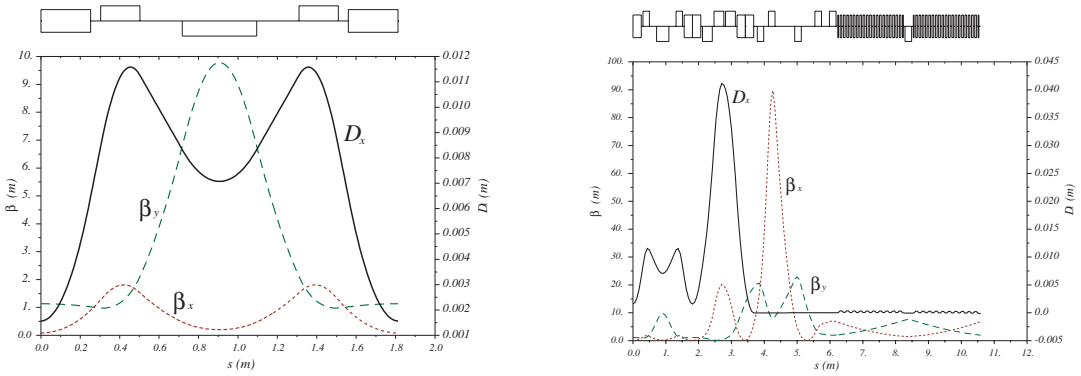

FIGURE 3.59. Left: Optical functions over the arc cell. Right: Optical functions from the end of the arc to the first wiggler FODO cell.

At the two edges of each of the two arcs, a dispersion suppressor is located which connects them to the dispersion-free straight sections that include rf cavities, FODO cells with wigglers, and injection/extraction sections, as is illustrated in Figure 3.59 (Right). In the straight sections, the phase advances of the FODO cells are 90°/70° for the horizontal and vertical motion, respectively. The damping ring parameters for the design lattice are listed in Table 3.30. The rms bunch-length σ_z and energy-spread σ_δ at extraction are compatible with the requirements for the subsequent bunch compressors. However, the obtained transverse emittances do not completely meet the target (nominal) values required (Table 3.29), in particular in the vertical plane. First an improvement of the damping ring design and then a revision of the overall emittance budget might resolve this inconsistency at 3 TeV. At 500 GeV, the conditions are relaxed and a larger horizontal emittance will likely allow the nominal vertical value to be reached. If it is not reached, then the luminosity would approximately go down with the square root of the ratio of the nominal to the actual emittances at the linac end, ratio which does not increase much when assuming that identical blow-ups add to the damping ring values (*e.g.*, $\gamma\varepsilon_y$ at the DR extraction going from 3 to 5 nm implies an increase from 10 to 12 nm at the linac exit and a ∼10% luminosity loss). In any case, a reduction of β^* makes it possible to obtain a luminosity larger than 10^{34} cm^{-2}s^{-1} as aimed at, and thus to compensate for emittances somewhat larger than nominal. For the 200 Hz operation mode considered at 500 GeV, the store time of 45 ms is about equal to 20 transverse damping times, which assures that the beam at extraction is always in a steady state.

TABLE 3.30
CLIC damping ring parameters (3 TeV present design).

Parameter	Symbol	Value
Nominal e^+ ring energy	γmc^2	2.424 GeV
Number of bunch trains stored	N_{train}	9
Ring circumference	C	374.3 m
Number of cells	N_{cell}	100
Betatron coupling	$\varepsilon_y/\varepsilon_x$	2.1%
Extracted horizontal emittance	$\gamma\varepsilon_x$	619 nm·rad
Extracted vertical emittance	$\gamma\varepsilon_y$	7.5 nm·rad
Extracted longitudinal emittance	$\gamma mc^2\varepsilon_t$	4297 eV·m
Extracted energy spread	σ_δ	1.35×10^{-3}
Extracted bunch length	σ_z	1.31 mm
Damping time	τ_x	2.676 msec
Damping time	τ_y	2.735 msec
Damping time	τ_t	1.383 msec
Horizontal tune	Q_x	69.21
Vertical tune	Q_y	29.63
Horizontal emittance wihtout IBS	$\gamma\varepsilon_{x0}$	343 nm·rad
Field of bending magnet	B_a	10 kG
Field of wiggler	B_w	17.64 kG
Wiggler period	λ_w	20 cm
Length of bending magnet	L	0.506 m
Total length of wigglers	L_w	158 m
Energy loss per turn	U_0	2.213 MeV
RF voltage	V_0	3.0 MV
RF frequency	f_{rf}	1500 MHz
Harmonic number	h	1871
Momentum compaction	α_p	0.662×10^{-4}

The strength of IBS increases with decreasing bunch dimensions. To achieve the low equilibrium emittances required at the highest energies, the damping times have to be considerably decreased using wigglers. The wiggler sections include a total of 76 units, each 2.1 m long and consisting of 21 pairs of magnetic poles.

3.4.2.3 Bunch Compressors and Transfer Lines

The damping ring is designed to deliver a beam at the energy of 2.424 GeV, bunched at the rf frequency of 3 GHz, of relative rms energy spread 0.135% and of rms length of 1.31 mm. The required bunch length in the main linac of 35 μm results from a compromise between the reduction of the dilution effect of transverse wakefields on the vertical emittance and of the optimization of the energy-spread with a minimal phase-shift with respect to the rf voltage crest. The corresponding compression ratio is about 37.4 which cannot be obtained by a single compression stage because of the resulting energy spread which is too large for the following isochronous turn-around loop located at the entrance of each main linac. Thus two stages of compression are proposed one at 2.424 GeV and one at 9 GeV to benefit from a higher gradient and a larger rf frequency. A compromise has to be found between an acceptable rms energy spread at the exit of the first stage and the R_{56} required by the second stage. The compression factor of 4 of the first stage has been chosen because the rms energy spread at the exit is an acceptable value of 0.54% and the resulting R_{56} of the second stage is sufficiently small (-0.024 m) to prevent large CSR (Coherent Synchrotron Radiation) effects after optimization of the chicane design. In these conditions the compression ratio of the second stage is equal to 9.35 (rms bunch length shortened form 327.5 μm to 35 μm) and the uncorrelated rms energy spread at the entrance of the main linacs is 1.36%. The rf voltages are 154 MV at 3 GHz and 592 MV at 30 GHz and the corresponding R_{56} amount to 0.235 m and 0.024 m, for the first and second compressor respectively. The second pseudo rotation in the longitudinal phase space is achieved by a magnetic chicane consisting of two parts one being the mirror image of the other. Each part is composed of two rectangular dipoles, of length L_m and bending angle θ, separated by a drift space of length L. The chicanes have been optimized to reduce the maximum values of the β Twiss function. Their optical functions are shown in Figure 3.60 and their lengths (including the triplets making the matching to any FODO lattice possible) are equal to 68 and 79 m respectively.

Simulations indicate that the high-order magnetic effects of the chicane and of the wakefields are small, only slightly lengthening the bunch by one micron. The effect of the coherent radiation has not been investigated but a rough estimate suggests that it should be negligible. The 360° turn-round consists of 72 isochronous modules, each one made of three identical dipoles (1 m long) and of four quadrupoles. Symmetric triplets match the modules between them. The overall diameter of the turn-round is 231 m approximately, in order to limit to 45 nm·rad the horizontal emittance growth due to the incoherent synchrotron radiation.

3.4.2.4 Main Linac

3.4.2.4.1 Lattice Description The main linac of CLIC at a center-of-mass energy of 500 GeV is based on the one for 3 TeV cut at the point where the beam reaches

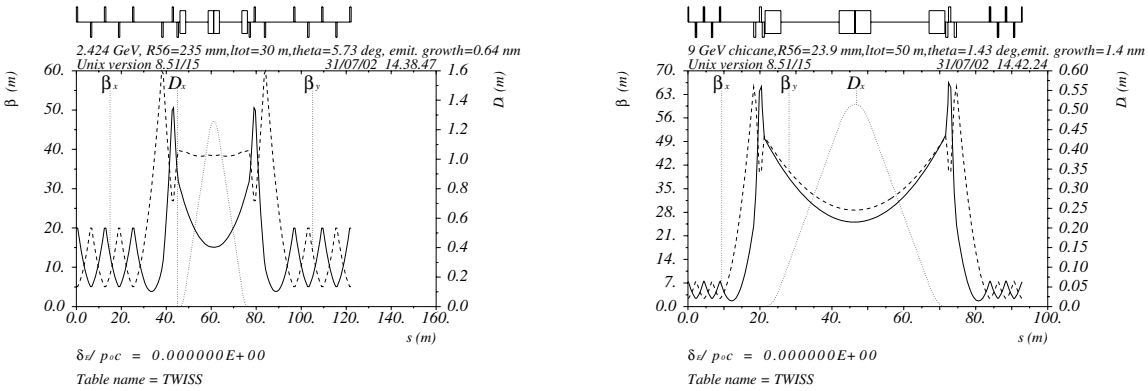

FIGURE 3.60. Left: Optical functions in the first chicane. Right: in the second chicane.

E=250 GeV. The rf phases have been readjusted but no further optimization has been performed. Note that the cavity parameters used in the quoted simulations correspond to those estimated for an accelerator structure of $\pi/2$ phase-advance, introduced for solving the surface-field problem. Since this structure still suffers from pulse surface heating, another design addressing both problems is being studied, but it is not yet completed and therefore not presented here. Consequently, though not strictly consistent with the accelerator structure described in the next section, tracking results obtained with the $\pi/2$ cavity have been kept since they are slightly pessimistic with respect to the ones corresponding to the description given.

In order to facilitate the geometrical matching of the drive beam decelerators and of the main linac, both are built of 2.23 m long modules. Each main linac module contains four 0.5 m long accelerator structures. Between one and four of these structures may be replaced by a quadrupole to provide the necessary focusing. A beam-position monitor (BPM) is placed at the head of each girder. The beam line of the whole linac consists of five sectors, each containing FODO cells of equal length and equal phase advance. In order to keep the cavity filling-factor and the BNS stability margin roughly constant along the linac, the target values of the focal length f and the quadrupole spacing L are scaled from the initial values f_0=1.5 m and L_0=2.5 m with the energy E as $L(E) = L_0(E/E0)^{1/2}$ and $f(E) = f_0(E/E0)^{1/2}$. The actual values in each sector are adjusted to the hardware geometry. Figure 3.61 shows the vertical beta-function along the linac. The phase advance is about 70° per cell but varies slightly from sector to sector. This small value allows a better compromise between time-dependent and static misalignments. The optics matching between two sectors is achieved by adjusting the strengths of the last three quadrupoles of the previous sector and the first two of the following one. The cavity filling-factor is 73.5%.

The beam consists of a train of 154 bunches spaced by 20 cm with a charge of 4×10^9 particles per bunch. The bunch length is σ_z=30 μm, and the initial, normalized, vertical and horizontal emittances are is $\gamma\epsilon_x$=1800 nm·rad and $\gamma\epsilon_y$=5 nm·rad, respectively. The target for the increase of $\gamma\epsilon_y$ is less than 5 nm·rad.

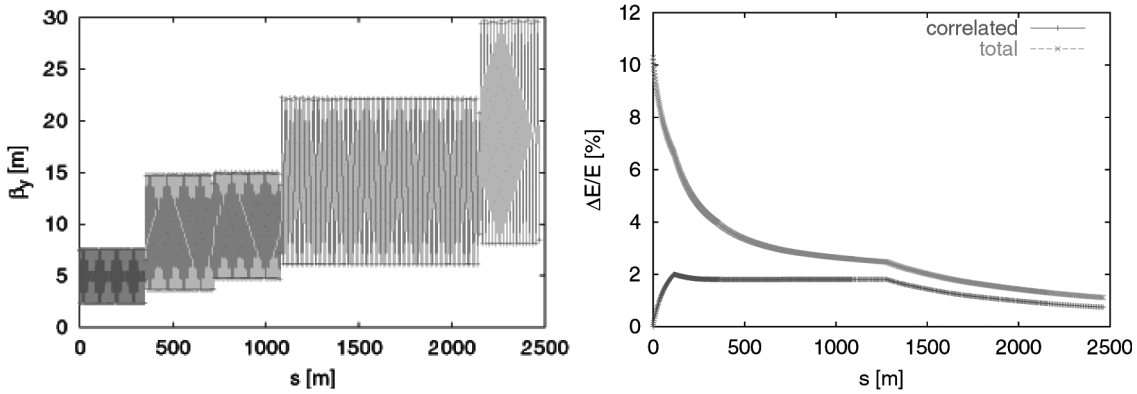

FIGURE 3.61. Left: The beta-function in the main linac lattice. Right: The full width energy spread along the linac. To estimate the total energy spread the uncorrelated incoming energy spread is cut at $\pm 2.5\sigma_E$.

In order to stabilize the beam, BNS damping is used. For energies between 9 and 20 GeV, the rf phase is set so as to create a relative energy spread in the bunch, which is then maintained in the main part of the linac by using another phase. In the last part, the rf phase is set in order to decrease the correlated energy spread to a full width of 0.75% so that the beam can pass the final focus system. The optimum phases will have to be determined experimentally in practice. In the presence of ground motion, a larger energy spread leads to better results if a few feedbacks are used to re-steer the beam, while a smaller energy spread is advantageous if a one-to-one correction is used for the same purpose. For the present simulations $\Phi_{RF} = 4^\circ$ is retained in the main part of the linac, leading to the energy spread shown in Figure 3.61.

The control of the bunch-to-bunch energy spread requires the compensation of the beam loading in the main linac. It is proposed to achieve this compensation by generating a ramp in the rf power output of the Power Extraction and Transfer Structures (PETS). Simulations show that a full bunch-to-bunch energy spread of less than 5×10^{-4} can be obtained in the main beam with the rf voltage resulting from a delayed phase-switching technique.

3.4.2.4.2 Static Correction Before beam-based correction, the beam-line elements will be pre-aligned by means of a sophisticated system of wires. This system, which will also be used in the LHC, has been modelled to simulate 100 different cases of initial misalignments of the straight lines defined by the wires (resulting from the survey pre-alignment). The beamline components are randomly scattered around these straight lines. The r.m.s. amplitudes of their consequent misalignments are expected to be less than 10 μm. While this accuracy is relevant for the beam-position monitors (BPMs) and for the accelerator structures pre-aligned on every girder with respect to the BPMs, it is not really critical for the quadrupoles which are re-aligned with the beam as explained here; for instance, an initial 50 μm r.m.s. scattering is acceptable for quadrupoles. The relative misalignments of the girders are defined by those assumed for the BPMs.

This precision of 10 μm is not sufficient to keep the growth of the vertical emittance smaller than 5 nm·rad in the main linac (corresponding to a relative growth of 100%). Therefore, beam-based alignment of the beam-line elements is necessary. In the so-called ballistic alignment method, first the BPMs and then the quadrupoles will be aligned. In the next step the accelerator structures need to be aligned on the beam trajectory. Finally emittance tuning bumps are used to minimize the remaining emittance growth.

In the ballistic alignment method the beam line is divided into a number of bins, containing 12 quadrupoles each, and the correction is applied successively in each bin. In the first step of the correction all the quadrupoles in the bin are switched off, except the first one. The beam is then steered into the last BPM of the bin. The other BPMs are moved onto the trajectory of the beam. It has been verified that the beam divergence does not generate a transverse beam-size larger than $\sim$75 μm r.m.s. over the length of a bin. The possible perturbing effect of weak remnant or earth magnetic fields can be reduced by either shielding, correcting or measuring and modelling them. In the second step of the correction, the quadrupoles are switched on again and a simple few-to-few correction is performed. This method allows all the BPMs in a bin to be aligned on a relatively straight line and thus to reduce the dispersion to a very small value. The remaining emittance growth is almost entirely due to the wakefields of the structures that are scattered around the beam trajectory. It therefore depends very little on the rf phases chosen.

In the simulations, all elements are assumed to be scattered around a common axis following a normal distribution with an r.m.s. of 10 μm for BPMs and structures and 50 μm for quadrupoles for the reasons explained previously. The BPM resolution is 100 nm.

Beam jitter during correction, remanent fields of the quadrupoles when switched off and the shift of the quadrupole center with field strength (from remanent to nominal field) are also possible error sources. In the simulation, a position jitter of the incoming beam of 0.1 σ is included. If the jitter is larger, then one can average over a number of pulses. The size of the remanent field is sampled from a constant distribution between 0% and 2% of the nominal quadrupole strength. The shift of the quadrupole center is assumed to follow a Gaussian distribution with an r.m.s. of 10 μm. The effect of these imperfections can be very large at the first correction step, but iterating the correction in a bin solves the problem almost completely. The emittance growth simulated with PLACET is about $\Delta\epsilon_y/\epsilon_y$=110%, which is still larger than the goal set. This method of correction is robust and will be the basic static correction applied when starting the linac. Another method that is based on varying the strengths of the quadrupoles by a small amount ($\sim$5%) and therefore avoiding switching them off could complement the ballistic alignment. This method, termed multistep lining-up correction, is based on the estimates of the quadrupole displacements from the measured trajectory difference. A fit through the BPM's readouts of one trajectory gives the steering angle required to recenter the beam in one bin. The quadrupoles and the BPMs can then be re-aligned.

A further reduction of the emittance growth after ballistic correction is necessary. A possible way to achieve this additional reduction consists of applying a number of local emittance-tuning bumps distributed along the linac. In the simulation case, these bumps are based on two groups of accelerator structures around two quadrupoles followed by a feedback system. The feedback system consists of two quadrupoles that are about $\pi/2$ apart and serve to steer the beam onto the initial trajectory. Also a measurement station is necessary to measure the emittance. One could have one station after each bump inside the

linac or a single station at the end of the linac used for all the bumps. Having one station per bump is simpler in operation, but its integration inside the linac has to be studied. Having a single station at the end of the linac leads to slightly better performance and the design of the system could be simpler. However, the tuning procedure is less straightforward and an abnormal emittance growth localized in one part of the linac is more difficult to track down. To perform the tuning the two groups of accelerator structures are displaced and the feedback system is used in order to minimize the emittance at the measurement station. By inserting 2 bumps in the linac, the vertical emittance growth can be reduced to about 22% for $\Phi_{RF} = 4^\circ$ (left side of Figure 3.62). Here, the results significantly depend on the rf phases because the emittance growth due to the dispersion is almost completely cancelled by the ballistic correction while the bumps prevent the emittance growth due to wakefields. The remaining blow-up corresponds to the cross talk between the dispersion and the wakefield effects. Using five bumps results in about 7% emittance growth after all the static corrections. For the machine with E_{cm}=3 TeV, it has been shown that the multibunch results are very close to those for single bunches.

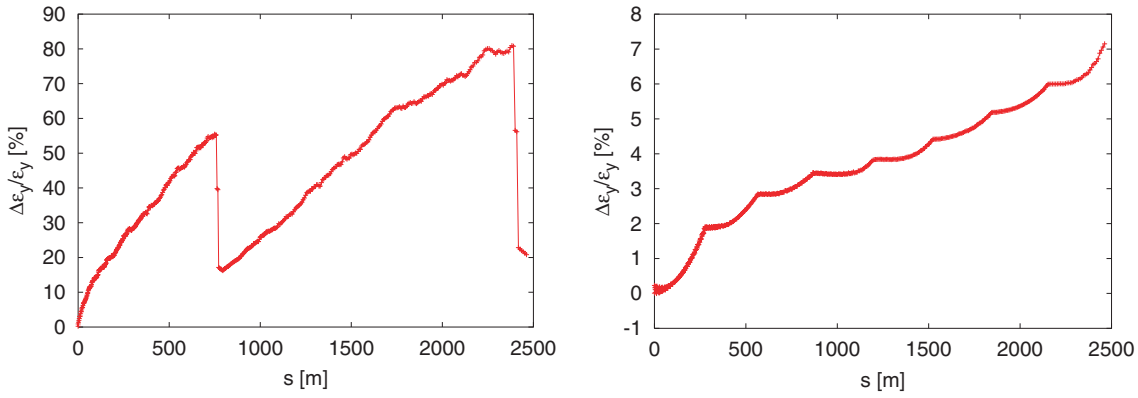

FIGURE 3.62. Left: The emittance growth in the linac after the ballistic alignment and optimization of the emittance tuning bumps. Right: The emittance growth after 1000 s of ground motion if seven feedbacks are used.

3.4.2.4.3 Time Dependent Effects Transverse position jitter of accelerator structures and quadrupoles can lead to an emittance growth. Here we define the emittance with respect to the average beam trajectory, *i.e.*, we integrate over a number of consecutive pulses. A 6% growth of the vertical emittance results from a position jitter of the quadrupoles with a r.m.s. of 3 nm or a pitch angle jitter of 0.45 μrad, as well as from a structure position jitter of 1.75 μm or a pitch angle jitter of 0.75 μrad. It must be noted that the emittance growth due to an initial beam jitter is not significantly increased by the effects of the wakefields along the main linac.

Long-term, diffusive ground motion can also lead to emittance growth. We assume a simplified model following the ATL-law with A=0.5×10^{-6} μm^2/(m·s). Using seven feedbacks in the linac one finds $\Delta\epsilon_y/\epsilon_y \approx 7\%$ after 1000 s (right side of Figure 3.62). Even

if one assumes that no information is transferred from one feedback to the next and that the beam has a transverse position jitter at injection of 0.3 σ_y one can still choose a gain of 0.1. This ensures that the effects of ground motion during the response time of the feedbacks are kept to a small fraction of a percent.

3.4.2.5 Main Linac Accelerator Structures

The CLIC main linac accelerator structure, the TDS (Tapered Damped Structure) consists of 150 cells and is 500 mm long. It operates in the $2\pi/3$ traveling wave mode. The design of the structure is driven by extreme performance requirements: accelerating gradients well in excess of 150 MV/m, power flows in excess of 200 MW, a 10 μm structure straightness and alignment tolerance (to preserve single bunch emittance), long-range transverse wakefield suppression of over two orders of magnitude (to preserve train emittance) and ultimately a low mass production cost. The issues of gradient, power and tolerances are each in part addressed by ultra-high precision diamond turning the copper disks that make up the sections. This technique gives a 1–2 μm dimensional tolerances and an optical quality surface finish. The 10 μm tolerance of assembled sections is guaranteed by a specially developed hybrid brazing/diffusion bonding technique. Measured Q factors correspond to 98% of the theoretical value in (undamped) constant impedance structures. Constant impedance structures were tested in CTF1 to 125 MV/m (albeit with pulses that reached these peak levels for only a few nanoseconds). Long-range transverse wakefields are suppressed through a combination of strong damping and detuning. The damping is accomplished by coupling four individually terminated waveguides to each cell of the structure. The damping waveguides have a rectangular cross-section of 4.5 mm by 1.9 mm, thus a cutoff frequency of 33.3 GHz, which is above the fundamental but below all higher order modes. In this way higher-order mode energy propagates out of the cells via the damping waveguides but the fundamental mode energy does not. This results in a Q of approximately 16 for the lowest, and most dangerous, dipole passband. A taper in the iris diameter from 4.5 mm at the head of the structure to 3.5 mm at the tail provides a detuning frequency spread of 2 GHz (5.4%). The layout of the structure cells can be seen in Figure 3.63.

Cell dimensions and some of the fundamental mode characteristics of the beginning, middle and end cells are given in Table 3.31. Using these calculated fundamental mode characteristics, the power flow, the accelerating gradient (left side of Figure 3.64) and other quantities along the structure have been obtained. The nominal average gradient of 150 MV/m is obtained with 250 MW input power.

A number of methods have been developed to calculate the transverse wakefield of the TDS (right side of Figure 3.64). These include an uncoupled circuit model, a semi-coupled time domain model, a complex wave number model and a double band circuit model. The validity of the long-range wakefield analysis and of the TDS design has been directly demonstrated by the measurement of a 15 GHz structure at the ASSET facility at SLAC (left side of Figure 3.65).

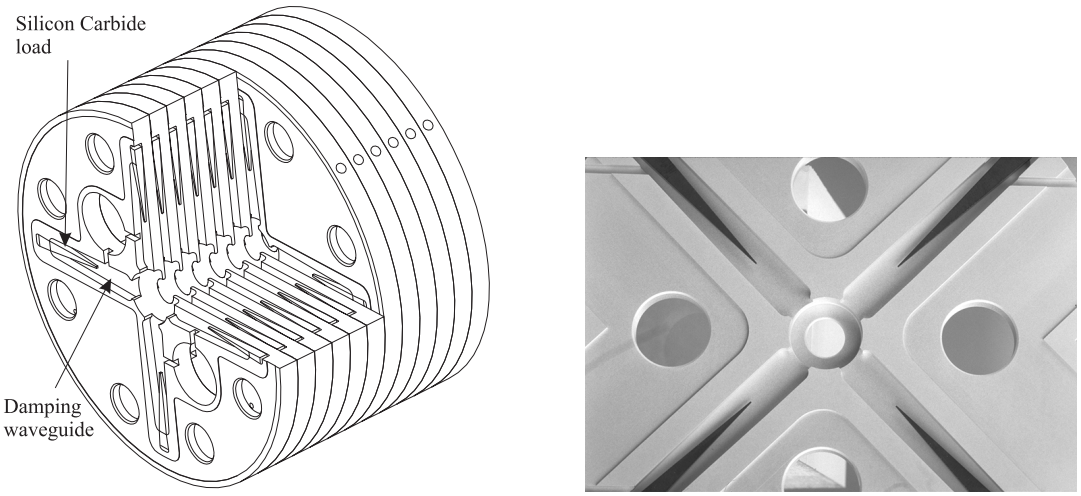

FIGURE 3.63. Left: Cross-sectional view of the TDS geometry. Right: Photograph of a TDS cell with damping waveguides and SiC loads.

TABLE 3.31
Fundamental mode parameters of the TDS as calculated using HFSS.

Cell Radius [mm]	Iris Radius [mm]	Q	R'/Q [k Ω /m]	v_g/c
4.255	2.250	3628	20.2	10.4
4.111	2.000	3615	23.0	7.5
3.984	1.750	3621	27.1	5.2

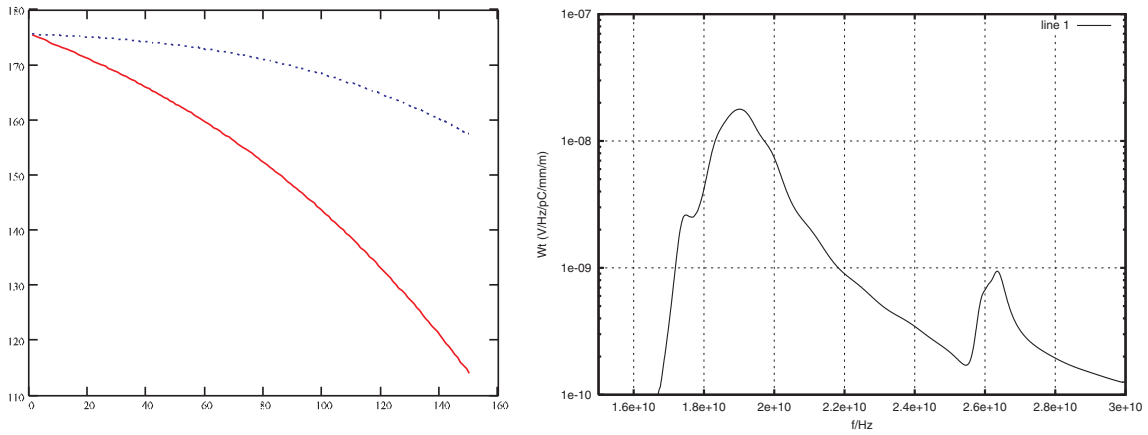

FIGURE 3.64. Left: Accelerating gradient in MV/m as a function of cell number. The solid line is with beam and the dotted one without. Right: Transverse wake spectrum in V/Hz/pC/mm/m between 16 and 30 GHz.

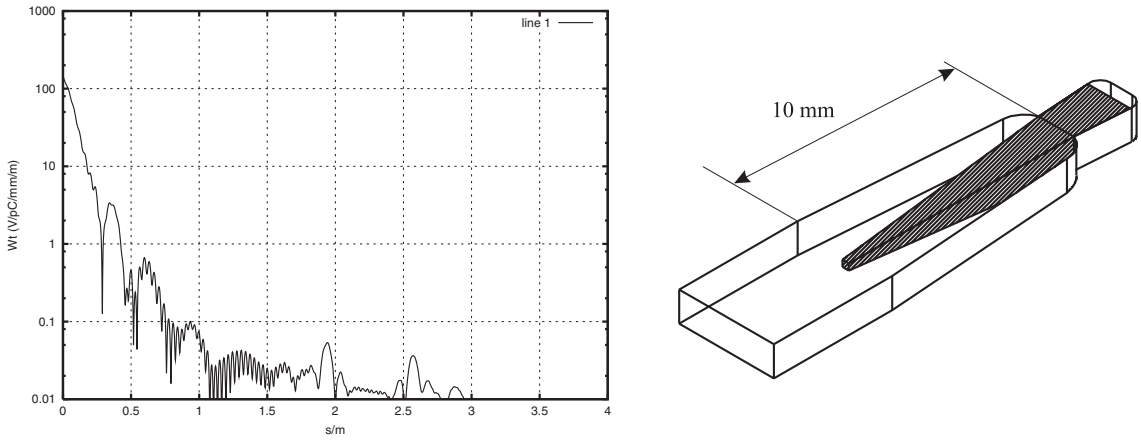

FIGURE 3.65. Left: Transverse wake of the TDS with the 10 mm load, as computed by the double-band circuit model (n.b. the computation has been made for a 15 GHz structure). Right: Detail of the TDS load. The load is 2 mm wide at its base and 0.2 mm^2 at the tip.

The damping waveguide load must simultaneously be well matched down to near the waveguide cut-off frequency, compact, vacuum compatible, and compatible with assembly by brazing of the accelerator structure. A low reflection coefficient is obtained by using a taper of Silicon Carbide (right side of Figure 3.65). The performance of the load near the cut-off is improved by tapering *inward* the damping waveguide at the point at which the load begins. In this way the impedance change caused by the SiC is partially compensated by the impedance change of the narrowing waveguide. The current load design has been optimized using HFSS and has an overall length of 10 mm.

Operation of this structure with the nominal average accelerating gradient of 150 MV/m has not yet been demonstrated. The feasibility of such a gradient has been established with a small-aperture (6 mm) copper X-band structure which has been conditioned to an accelerating gradient of 154 MV/m with 150 ns pulses without any damage. Damage has however been observed in the copper input couplers of 30 GHz accelerator structures tested in CTF2. The surface field where the damage occurred was about 260 MV/m limiting the accelerating gradient to 60 MV/m. Two main approaches are being pursued to raise the achievable accelerating gradient and to avoid damage: changes to the rf design and new materials. In a recent test, a 30 cell structure with a reduced surface field geometry and irises made from molybdenum reached a peak accelerating gradient of 193 MV/m with a pulse length of 15 ns. No damage was observed.

It has to be noted that, during the process of modifying the structure design in view of solving the problems due to surface fields, an accelerator structure of $\pi/2$ phase advance was considered. This explains why simulations of the main beam dynamics have been done with such a designed structure, although this solution will likely not be retained for reasons mentioned elsewhere. Further developments presently focus on $2\pi/3$ structures of aperture smaller than the one described in this section with optimized geometry and rf-coupler.

3.4.2.6 Beam Delivery System

The beam delivery system (BDS) comprises energy and betatron collimation, a beta-matching section, and the final focus. The system described here was designed for 3 TeV and then scaled back for 500 GeV keeping the same overall length of 2.6 km, significantly smaller than the one of the base-line design [7]. The most recent BDS design [10] is indeed based on a short collimation system made of one module instead of two for the energy collimation and a compact final focus as proposed at SLAC, which features a nonzero dispersion across the final doublet and chromaticity sextupoles located next to the final quadrupoles. In front of these quadrupoles is a 200 m long bending section, which produces the dispersion. Upstream sextupoles correct the geometric aberrations. The free length between the final quadrupole and the IP is as large as $l^* = 4.3$ m. This might be a major advantage of the compact final focus for the final quadrupole remains outside of the detector solenoid and its fringe. The length of the compact Final Focus system is 550 m.

The 3 TeV collimation optics upstream of the compact final focus is based on the collimation lattice developed for the NLC. Starting from this lattice, the length of the energy collimation was scaled by a factor of 5 and the bending angles by a factor of 1/12. The I_5 radiation integral at this high energy amounts to 1.9×10^{-19} m, which corresponds to an emittance growth of $\Delta(\gamma\epsilon_x) \approx 0.09$ μm, near the tolerable limit. At 500 GeV, the bending angles as well as the dispersion are increased, but only by 20%, and the emittance growth from synchrotron radiation is of course much smaller. Accepting the quoted emittance blow-up at 3 TeV and a possible reduction of the collimation efficiency still to be estimated, the total length of the collimation system now proposed amounts to slightly more than 2 km.

Both energy-collimations and betatron-collimations are included in this system. The transverse beam halo must indeed be collimated in order to ensure acceptable background in the detector. The transverse collimation depth is set by the requirement that the synchrotron-radiation fan generated in the final quadrupoles does not hit any aperture upstream of the collision point. Leaving a margin of $2\sigma_x$ and $3\sigma_y$, respectively, the betatron collimation should be set at 3 TeV to $\pm12\sigma_x$ and $\pm80\sigma_y$. The same collimation depths are assumed for 500 GeV, where the aperture of the final quadrupoles can be largely increased. The situation is different for the energy collimation. Here, the requirements are imposed by failure modes in the linac. According to a detailed study energy collimation at about $\pm1.5\%$ will protect the downstream parts of the beam delivery system against all the linac failures considered, including the associated betatron oscillations. Main-beam energy errors, due to failures in the drive-beam sector, are not always accompanied by large emittance growth, and thus call for a reliable energy collimation (by contrast, pure betatron oscillations in the linac rapidly filament and give rise to largely increased emittances). The tight energy collimation planned will however ensure that a beam perturbed in energy is intercepted at the energy spoiler without hitting downstream betatron collimators. Hence the energy collimation depth is determined by the effect of failure modes and, collimator survival is not required for the betatron spoilers at the nominal emittances.

In the final focus, a high field in the last quadrupole doublet reduces the chromaticity generated by this doublet and consequently reduces the high-order aberrations of the final-focus. Given the limited space and the tight requirements on the mechanical stability, a permanent magnet is the most adequate solution. It uses Sm_2Co_{17} material for its

thermal stability and radiation hardness. The beam-pipe radius in the last quadrupole is 3.8 mm in order to produce a gradient of 388 T/m as required by the optics at 3 TeV, while the corresponding values for the preceding quadrupole of the doublet are ∼10 mm and ∼135 T/m respectively. Much weaker magnets are needed at 500 GeV. It is assumed that the permanent-magnet field cannot be varied and that fine tuning of the IP beta functions is done using upstream quadrupoles, as it has been done at the SLC. The bending angles and the dispersion function in the final focus are 4.25 times larger at 500 GeV than at 3 TeV and the sextupole fields are correspondingly reduced (decreasing the high-order aberrations). Since the Oide effect is much weaker at 500 GeV, the β functions at the IP can be squeezed down to values as small as β_x^*=3 mm, and β_y^*=50 μm. Note that the IP distribution then becomes distinctly non-Gaussian and the rms beam size is no longer a good indication of the luminosity. Tracking shows that, for constant emittances at the entrance of the final focus, the geometric luminosity without pinch increases from L=1.02×10^{34} cm^{-2}s^{-1} for β_y^*=150 μm, β_x^*=10 mm, to L=1.85×10^{34} cm^{-2}s^{-1} for β_y^*=50 μm, β_x^*=3 mm (at 200 Hz with $\gamma\epsilon_y$=10 nm, $\gamma\epsilon_x$=2 μm). This is almost twice the desired L target value. The luminosity with pinch is inferred from integrated simulations, which show that reducing only β_y^* and leaving β_x^* at 10 mm preserves the quality of the luminosity spectrum. With the assumed emittances, the effective rms spot sizes $\sigma_{x,y}$ are 178 nm and 4.07 nm respectively. The optical functions at 500 GeV are displayed in Figure 3.66. The bandwidth of this optics in the presence of synchrotron radiation exceeds a relative momentum full width of 1%. At 500 GeV the inner radius of the final quadrupole must be increased, by about a factor of 2, in order to provide a beam stay clear of 6–10 σ_x. A study covering optics layout, muon background, collimator survival, and wakefield effects is being carried out, but all these aspects will be relaxed at 500 GeV compared to 3 TeV.

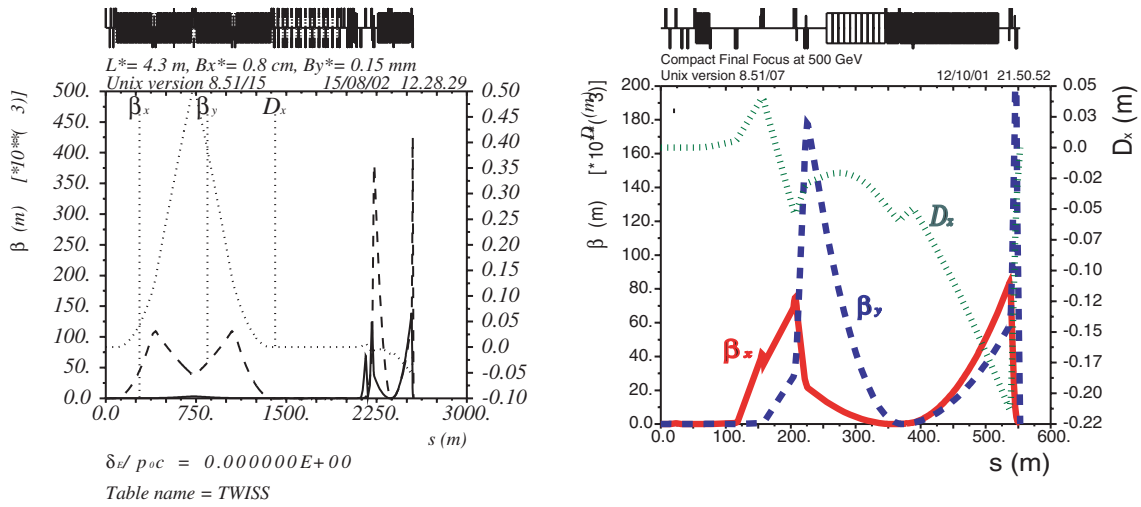

FIGURE 3.66. 500-GeV optics for the compact beam delivery (left) and final focus (right) systems.

Extraction of the disrupted beam from the interaction point necessitates collisions with a crossing angle. The crossing angle is set to 20 mrad, in view of various constraints. Specifically, the multibunch kink instability and beamstrahlung photons impose a minimum value for the crossing angle, while synchrotron radiation and dispersion in the solenoid field give rise to an upper bound. A crab cavity with about 1 MV maximum voltage at 30 GHz will avoid luminosity loss due to the crossing angle. The relative phase error between the two crab cavities on either side of the collision point should remain within 0.1°. The voltage increases and the phase tolerance decreases with rf wavelength. Schematics of the CLIC IP region are displayed in Figure 3.67.

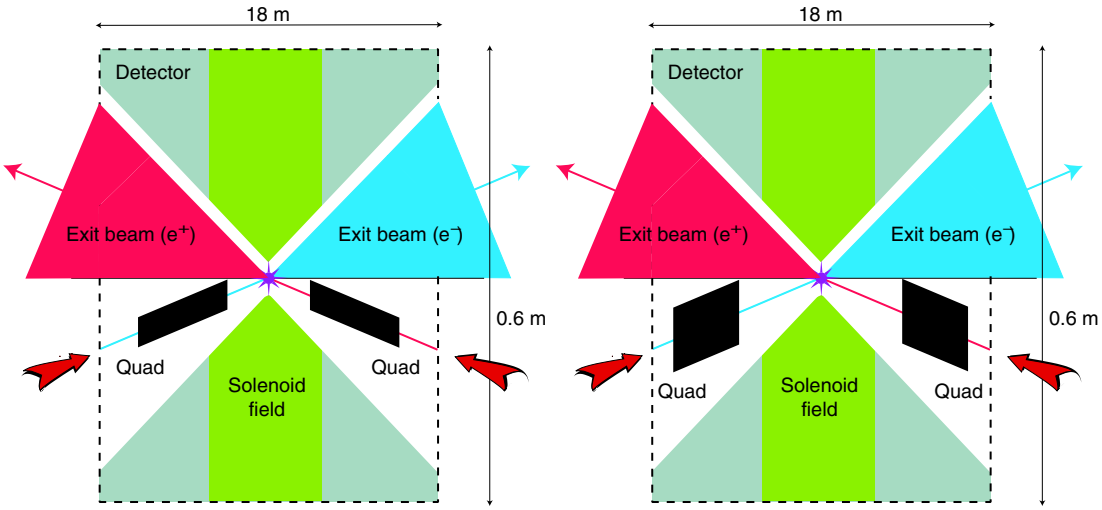

FIGURE 3.67. Top view of the CLIC IP region with the detector, the colliding beams, and the final quadrupoles for the base-line (left) and the compact final-focus optics (right) at 3 TeV. Scales are indicated. The transverse size of the detector is about 17 m.

A related critical issue is the collision of beams with nanometer size. The vertical rms beam size is about 1 nm at 3 TeV and 4 nm at 500 GeV. The final quadrupoles need to be stabilized to a fraction of this value, *i.e.*, stabilization levels of about 0.2 nm at 3 TeV and 0.8 nm at 500 GeV are required for frequencies above several Hz. In order to assess the feasibility, a stability project was launched and preliminary results have been obtained. The acoustic waves generated by beam impact at collimators or beam dump and their potential effects were studied. The integrated motion of the ground above 4 Hz was found to be not larger than a few nm in sites like the LEP or SLAC tunnels. However, the motion of quadrupoles in a realistic accelerator environment, such as the CLIC Test Facility 2 (CTF2), was measured to be about 10 nm. It is therefore planned to explore the improvements attainable by an active stabilization system. The magnet motion measured under different conditions will then serve as an input to simulation studies of the time-dependent luminosity performance. Preliminary results indicate that actively stabilized supports built by industry succeeded to damp the floor vibration in a test-stand installation by a factor of 20. Rms motion of a CLIC prototype quadrupole placed on a stabilized table was measured to be 0.9±0.1 nm vertically above 4 Hz with a nominal flow

of cooling water. Horizontally and longitudinally, without cooling water, the measured numbers are 0.4±0.1 nm and 3.2±0.4 nm.

Tuning and feedback strategies are essential for reaching the design performance. A fast feedback at the collision point, acting over a few pulses, will be supplemented by an ultra-fast intra-train feedback, the potential performance of which has been investigated by simulations. In addition, tight local orbit control in the beam delivery system, and automated optical tuning loops optimizing luminosity-related signals will likely prove indispensable for maintaining the desired spot size. The extraction and disposal of the spent beam as well as diagnostics for the disrupted beam and the beamstrahlung photons are important topics for further studies.

Depolarization during the collision is significant at 3 TeV. An effective decrease of the polarization due to the collisions of about 7% and a total depolarization through the whole complex of 23% are predicted. Though it may be less critical at 500 GeV, a polarimeter on either side of the collision point will be beneficial even for the lower energy.

3.4.2.7 Machine-Detector Interface and Beam-Beam Interaction

The machine-detector interface has been investigated for a center-of-mass energy of E_{cm}=3 TeV. At lower energies it will be simpler.

In the interaction point, the electro-magnetic forces of the two colliding beams focus each other. This enhances the luminosity but also leads to the emission of beamstrahlung. In CLIC with center-of-mass energies of up to 1 TeV the critical energy of this radiation is below the beam energy, but this is not the case at E_{cm}=3 TeV. The resulting luminosity and luminosity spectrum have been simulated using GUINEA-PIG. At 3 TeV, the beamstrahlung has a total power of about P=4.6 MW, but it is emitted into small cones in the forward direction and does not produce direct backgrounds. However, protection of the magnets in the spent beam line is an issue which has not yet been investigated. Secondary particles—especially neutrons—are also a concern.

In addition, the beam-beam interaction will generate background via coherent and incoherent pair creation. In the coherent process, a hard beamstrahlung photon turns into an electron-positron pair in the strong field of the oncoming bunch. GUINEA-PIG simulations show that about 6.8×10^8 pairs are produced per bunch crossing; a number comparable to the number of beam particles. Thus these particles influence the beam-beam interaction significantly. Initially they have small angles but they can be deflected by the beams. The number of particles produced via the incoherent process is much smaller than the number of particles in the bunch (about 4.5×10^5), but they can have significant inherent angles.

A simplified detector geometry has been simulated using GEANT to evaluate the background. It consists of the beam pipe, a vertex detector, a central tracker, and the calorimetry. Around the quadrupoles, which are inside of the detector, tungsten masks are placed to shield the main part of the detector from backscattered particles.

The full crossing angle between the two beams is θ_c=20 mrad. A first design of the final quadrupole has an outer radius of r=20 mm. The exit hole for the spent beam can thus be large enough to extract the bulk of the coherent pairs. Also the effect of the multibunch

kink instability is small for this crossing angle. The blow-up of the spot size due to the coupling of the beam to the detector solenoid field B_z=4 T is still acceptable.

A preliminary design of the mask has been developed (Figure 3.68). Its inner opening angle is chosen such that all particles from coherent pair creation and the bulk of the particles from incoherent pair creation should enter the mask. Assuming a distance of the mask opening to the IP of 1 m, this angle must be larger than 60 mrad for B_z=4 T. To allow for some contingency, a value of θ_i=80 mrad is chosen. The outer angle is then defined by the required thickness of the mask. Studies for TESLA indicated that a mask thickness of 5 to 7.5 cm is sufficient. The outer angle has therefore been set to 120 mrad, which leads to a mask thickness of 8 cm. It should be possible to increase the thickness of the mask by adding material on the inside, an option that was excluded in TESLA because of the space requirement of the cryostat around the quadrupole.

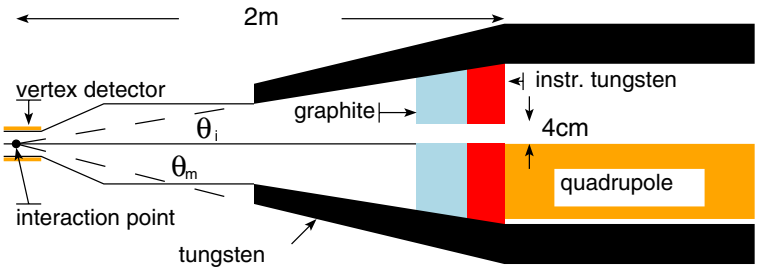

FIGURE 3.68. View from above on the adopted mask design. The sketch is stretched in the vertical direction. Care has to be taken that no particles are backscattered through the hole in the mask.

Inside the mask described, a second mask is placed which consists of tungsten covered on the IP side by a low-Z material. This is necessary to reduce to a negligible level the rate of particles that are scattered back from the quadrupoles into the vertex detector. This mask is instrumented to allow a fast luminosity measurement and the tagging of low angle particles. The lowest angle for this tagging is likely to be θ_0=40 mrad. At smaller angles one expects a large energy flow from the pair background. The inner mask needs one hole for the incoming beam and another one for the outgoing beam. The one for the spent beam has a radius of r=2 cm to keep the number of coherent pair particles lost inside of the detector small. The simulation predicts a total energy deposition in the inner mask of 250 TeV per side and per bunch crossing. The hole for the spent beam is small enough so that the inner mask can still shield the vertex detector from neutrons coming from the tunnel. Simulations have verified that backscattering of charged particles is almost completely suppressed, reducing the hit density in the vertex detector by an order of magnitude. However it has to be ensured that no charged particles are scattered back through this hole, since they could hit the vertex detector.

The vertex detector will be directly hit by a number of particles from the incoherent pair production that have large initial angles and transverse momenta. Assuming that it covers

an angle of $|\cos\theta| \leq 0.98$, the minimum inner radius to ensure less than 1 hit per mm^2 and bunch train is r=30 mm in a magnetic field of B_z=4 T.

The number of hadronic background events per bunch crossing is high, about 2.3 events with a center-of-mass energy above 5 GeV. These events have been simulated in the detector using GUINEA-PIG, PYTHIA and GEANT. Most of the energy goes into very small angles, so it is lost inside of the masks. The hadrons significantly contribute to the total density of charged hits in the vertex detector with a highest density of ρ=0.25 mm^{-2} per bunch train. Also the secondary neutron flux due to the hadronic showers in the detector (including masks and low angle taggers) have been simulated. The neutron flux found at a radius of r=0.3 m is 3×10^9 cm^{-2} per year. It reaches a maximum around the masks and is lower at the IP.

3.4.3 Power-Source Subsystems

3.4.3.1 The RF Power Source—General Principles

CLIC requires short rf pulses of high peak power at 30 GHz (130 ns long, with 230 MW per accelerator structure). Since no conventional rf source at 30 GHz can provide such pulses, the two-beam acceleration technique is used, in which an electron beam (the drive beam) is accelerated using standard, low-frequency rf sources and then decelerated to produce rf power at high frequency.

In linear collider projects based on conventional rf sources (klystrons), pulse compression or delayed distribution techniques are used in order to obtain the needed high peak power and short pulse length. Similar techniques are used in the CLIC two-beam accelerator. In this case, however, the compression and distribution are done with electron beams. The main advantage of electron beam manipulation, with respect to manipulation of rf pulses, consists of the very low losses that can be obtained while transporting the beam pulses over long distances and compressing them to very high ratios. A further advantage is the possibility of pulse compression, achieved by interleaving bunched beams by means of transverse rf deflectors. The pulse length is given by the filling requirement of the accelerator structures and by the number of bunches in the main beam. The 30 GHz frequency is effectively obtained through the short bunch length and a distance between the bunches in the train being a small multiple of the nominal rf period. The net result of the whole process is so-called frequency multiplication (from 0.937 GHz to 30 GHz). In the following we will describe the CLIC rf power source complex used to generate all the rf power needed for one of the two main linacs (electron or positron). Possibilities to combine some elements of both the e^+ and e^- complexes are under study. A schematic layout of one complex is shown in Figure 3.69.

The CLIC rf power source essentially combines and transforms several long, low-frequency rf pulses into many short, high-power pulses at high frequency. During the process, the energy is stored in a relativistic electron beam, which is manipulated in order to obtain the desired time structure and then transported to the place where the energy is needed. The energy is extracted from the electron beam in resonant decelerating structures (the Power Extraction and Transfer Structures—PETS), which are located parallel to the main accelerator. The key points of the system are an efficient acceleration of the drive beam in conventional structures, the introduction of transverse rf deflectors to compress the drive

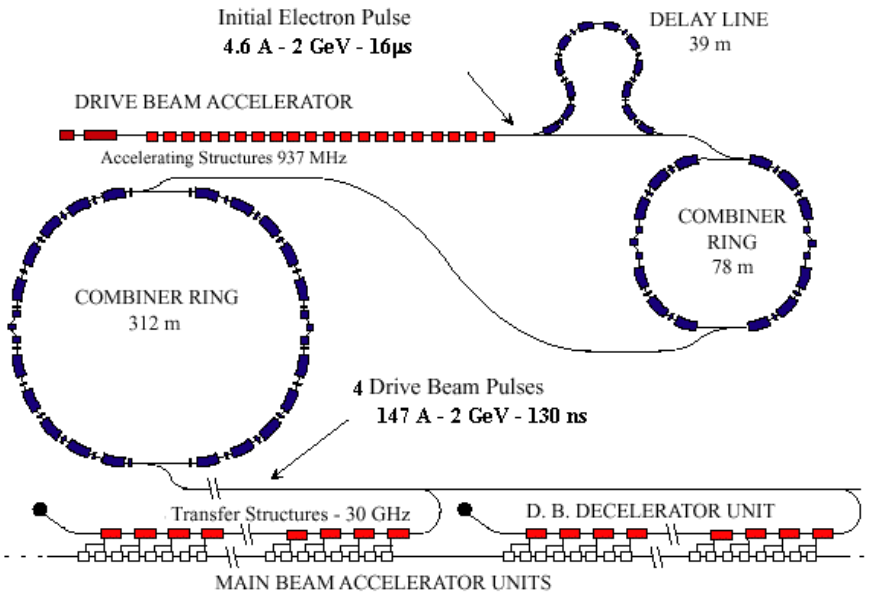

FIGURE 3.69. Schematic layout of the CLIC rf power source. Two such complexes (one for each of the main linacs) will be needed to provide the power for 500 GeV c.m. CLIC operation. Only two of the 4 decelerator/accelerator units composing a linac are shown.

beam, and the use of several drive-beam pulses in a counter-flow distribution system, each one powering a different section of the main linac. The method discussed here seems relatively inexpensive, very flexible and can be applied in various linear colliders over the entire frequency and energy range.

The drive-beam generation complex is located at the center of the linear collider complex, near the final-focus system. For 500 GeV c.m. operations, two times 4 decelerator units, each 625 m long, are required to power the two main linacs which each accelerate the colliding beams up to 250 GeV. In this case, the energy for the rf production is initially stored in a 16.7 μs long electron beam pulse (corresponding to twice the length of one main linac) which is accelerated to about 2 GeV by a normal-conducting, low-frequency (937 MHz) traveling wave linac. The linac is powered by conventional long-pulse klystrons. A high-energy transfer efficiency is paramount in this stage. The drive beam is accelerated in relatively short structures (4.5 m long), so that the rf losses in the copper are minimized. Furthermore, the structures are fully beam-loaded, *i.e.*, the accelerating gradient is nearly zero at the downstream end of each structure and negligible rf power flows out to a load. In this way, about 97% of the rf energy can be transferred to the beam.

The beam pulse is composed of 32×4 subpulses, each one 130 ns long. In each subpulse the electron bunches occupy alternately even and odd buckets of the drive-beam accelerator fundamental frequency (937 MHz). Such a time structure is produced after the thermionic gun in a subharmonic buncher, whose phase is rapidly switched by 180° every 130 ns. This provides us with a means to separate the subpulses after acceleration, while keeping a constant current in the accelerator and avoiding transient beam-loading.

As the long pulse leaves the drive-beam accelerator, it passes through a delay-line combiner where "odd" and "even" subpulses are separated by a transverse rf deflector at the frequency of 468.5 MHz. Each "even" bunch train is delayed with respect to the following "odd" one by 130 ns. The subpulses are recombined two-by-two by interleaving the electron bunches in a second rf deflector at the same frequency. The net effect is to convert the long pulse to a periodic sequence of drive-beam pulses with gaps in between. After recombination, the pulse is composed of 16×4 subpulses (or trains) whose spacing is equal to the train length. The peak current and the bunch frequency (of 937 MHz) are doubled.

The same principle of electron-bunch pulse combination is then used to combine the trains four-by-four in a first combiner ring, with a 78 m long circumference. Two 937 MHz rf deflectors create a time-dependent local deformation of the equilibrium orbit in the ring. This bump is used for injection of a first train in the ring (all its bunches being deflected by the second rf deflector onto the equilibrium orbit). The ring perimeter is equal to the spacing between trains plus $\lambda/4$, where λ is the spacing between bunches, equal to the wavelength of the rf deflectors. Thus, for each revolution period, the rf phase seen by the bunches circulating in the ring increases by 90°, and when the second train is injected, the first one does not see any deflection and its bunches are interleaved with the ones which are injected (at a $\lambda/4$ distance). This is repeated twice, then the four interleaved trains are extracted from the ring by an ejection kicker half a turn later, and the same cycle starts again. After the first combiner ring the whole pulse is composed of 4×4 trains. The trains are combined again, using the same mechanism, in a second combiner ring, with a 312 m long circumference, yielding another factor of 4 in frequency multiplication, and obtaining the final 4 trains required for each main linac. At this point, each final train is 39 m long and consists of 1952 bunches with a charge of 9.8 nC/bunch and an energy of 2 GeV.

Such drive-beam pulses are distributed down the main linac via a common transport line, in a direction opposite to the direction of the main beam. The periodic distance between trains is now 1248 m, corresponding to twice the length of the linac section which they will power, so that they will arrive at the appropriate time to accelerate a high-energy beam traveling in the opposite direction.

Pulsed magnets deflect each beam at the appropriate time into a turn-around. After the turn-around each pulse is decelerated in a 624 m long sequence of low-impedance PETS (which is by definition one drive-beam decelerator unit) down to a minimum energy close to 0.2 GeV. The resulting output power is transferred to the structures which accelerate the high-energy beam in the main linac. As the main beam travels along, a new drive-beam train periodically joins it and runs in parallel but ahead of it to produce the necessary power for a 624 m long linac unit. At the end of a unit the remaining energy in the drive beam is dumped while a new one takes over the job of accelerating the main beam. The main characteristics of the CLIC rf Power Source are given in Table 3.32.

TABLE 3.32
Power source basic parameters.

Parameter	Symbol	Value
Drive-beam pulse		
Energy (initial)	$E_{in,dec}$	2 GeV
Energy (final, minimum)	$E_{fin,dec}$	200 MeV
Average current in a pulse	I_{dec}	147 A
Train duration (FWHH)	τ_{train}	130 ns
Number bunches/train	$N_{b,dec}$	1952
Bunch charge	$Q_{b,dec}$	9.8 nC
Bunch separation	$\Delta_{b,dec}$	0.067 ns
Bunch length, r.m.s.	$\sigma_{z,dec}$	0.4 mm
Normalized emittance, r.m.s. (injection)	$\gamma\epsilon_{dec}$	150 μm·rad
Decelerator unit		
Repetition rate	f_{rep}	200 Hz
Unit length (total)	$L_{unit,tot}$	624 m
Unit length (active)	$L_{unit,act}$	400 m
Number of PETS/unit	$N_{PETS,unit}$	500
Power extracted/metre	P_{out}	458 MW
Main beam energy gain/unit	ΔE_{main}	62.5 GeV

3.4.3.2 Drive Beam Generation Complex

3.4.3.2.1 Overview of the System Each drive beam injector is composed of 5 subsystems:

1. A thermionic gun.
2. A bunching system providing a bunched beam at 10 MeV.
3. An injector linac accelerating the beam up to 50 MeV.
4. A spectrometer line with beam diagnostic and collimation.
5. A matching section to the Drive Beam Accelerator. Figure 3.70 gives a schematic layout of one injector.

The total pulse, at the injector exit, is 16.7 μs and is composed of 32 $\times$ 4 subpulses. The time structure is produced after the thermionic gun in a subharmonic buncher, in such a way that the electron bunches of each subpulse occupy alternatively even and odd buckets (Figure 3.71).

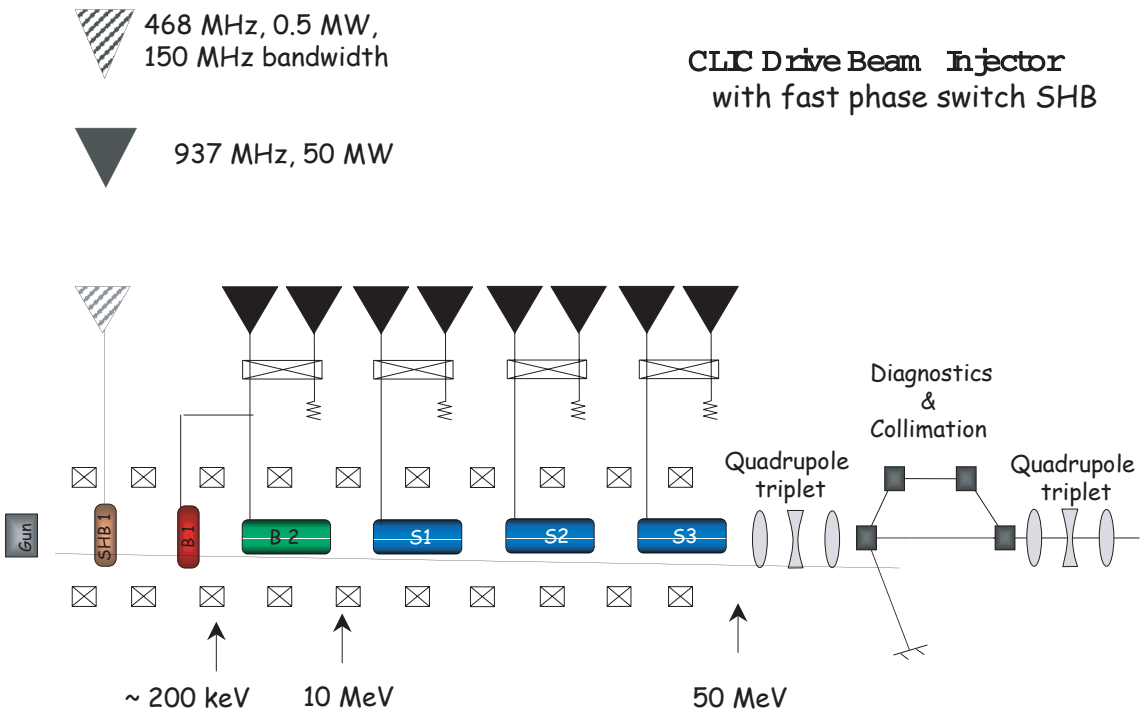

FIGURE 3.70. Layout of the CLIC Drive Beam Injector.

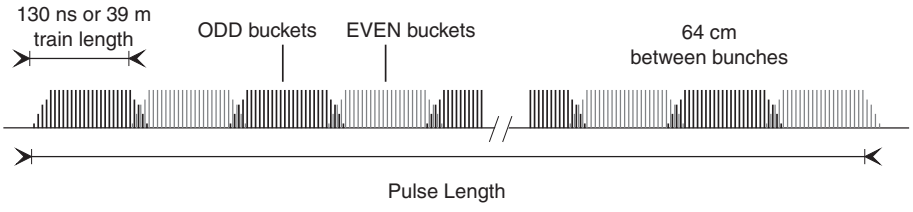

FIGURE 3.71. Combined pulses at the drive-beam injector linac entrance.

3.4.3.2.2 Injector Characteristics The bunching system of the drive-beam injector is made of one subharmonic buncher (468.5 MHz), powered by one klystron of 1 MW, and of one buncher (937 MHz) powered by two 50 MW-klystrons. The rest of the injector consists of three accelerator structures (937 MHz), identical to those of the drive-beam accelerator, each powered by two 50 MW-klystrons.

At the injector exit, the beam reaches the energy of 50 MeV and fulfills the following necessary conditions:

i. The total number of bunches has to be a multiple of 32 (frequency multiplication factor).

ii. The pulse for the PETS requires bunches of lower intensity for the pre-fill of the structures and bunches of constant charge for the power generation. The energy spread at the exit of the injector linac is partly correlated due to the beamloading. The uncorrelated energy spread is 0.75% and the total energy spread is less than 1%. Such value is obtained with a beam collimation at $\pm$ 3 σ_E before the injection in the accelerating linac. The rms value for the single bunch length is 4 mm at the injector exit. Since a large beam size would cause losses in the decelerating structures, it is crucial to obtain a beam at 2 GeV with an emittance as small as possible. Assuming an emittance blow-up of 50% between the injector and the decelerator, a normalized emittance of 100 μm·rad is an upper value at 50 MeV. Table 3.33 summarizes the beam characteristics at the injector exit for 500 GeV. Figure 3.71 shows the composition of the bunch train at the linac entrance.

TABLE 3.33
Beam characteristics at the drive-beam injector exit.

Parameter	Unit	Value
Beam energy	MeV	50
Pulse length (Total train)	μs	16.7
Beam current per pulse	A	5
Charge per pulse	μC	80
Number of bunches per pulse		7808
Bunch length (FWHH)	ps	32
Bunch length (r.m.s.)	mm	4
Normalized emittance (r.m.s.)	mm·rad	$\leq$ 100
Energy spread	%	$\leq$ 1
Repetition frequency	Hz	200

3.4.3.2.3 A Photoinjector Option The possibility to use an rf photoinjector as the drive beam source is under investigation. A CW laser working at 468.5 MHz provides a

continuous train. During 17 μs the necessary power is generated in order to create the charge of 80 μC on the photo-cathode. The laser beam illuminates the photo-cathode of an rf gun powered by a klystron at 937 MHz. It generates an electron beam with a momentum of several MeV at the exit of the photoinjector. The requested sequence of pulses can be directly injected into the injector linac. However several issues remain to be addressed and an R & D program has been set up to try to overcome these issues.

3.4.3.2.4 Accelerator Lattice and Dynamics The drive beam accelerator consists of 108 accelerator structures (each powered by two 50 MW klystrons). The initial beam energy is 50 MeV, the final one 2 GeV, and the average beam current is 4.59 A. Each structure is ~4.5 m long and has a loaded gradient of about 4 MV/m. Simulations were however carried out with a slightly higher beam power corresponding to a final energy of 2.1 GeV and a beam current of 4.88 A, for these values corresponded to the $\pi/2$ phase-advance main-linac structure studied at the time of the tracking in an attempt to resolve the surface-field question. The results obtained in this case should be rather pessimistic.

Simulations for CTF3 showed that the best compromise between wakefield and dispersive effects can be achieved by using a triplet lattice. Two structures are placed between the triplets and the total length per cell is 14 m. The relative strength of outer and inner quadrupoles is chosen to achieve a round beam in the structures (left side of Figure 3.72). The transverse wakefields were derived by scaling the ones calculated for CTF3 with respect to the frequency. To evaluate the beam stability, a beam with an initial offset has been tracked through the perfectly aligned linac using PLACET. The transverse Q-factors in the simulation were 50% larger than calculated to allow for imperfect SiC loads. As can be seen in the right side of Figure 3.72, the initial jitter of the beam is amplified. However this amplification seems acceptable. The bunches coming after the phase switch which generates the odd and even bucket subpulses are more strongly kicked than the other ones. If the transition is done more gradually, as it will be in practice, then the kick will be much smaller.

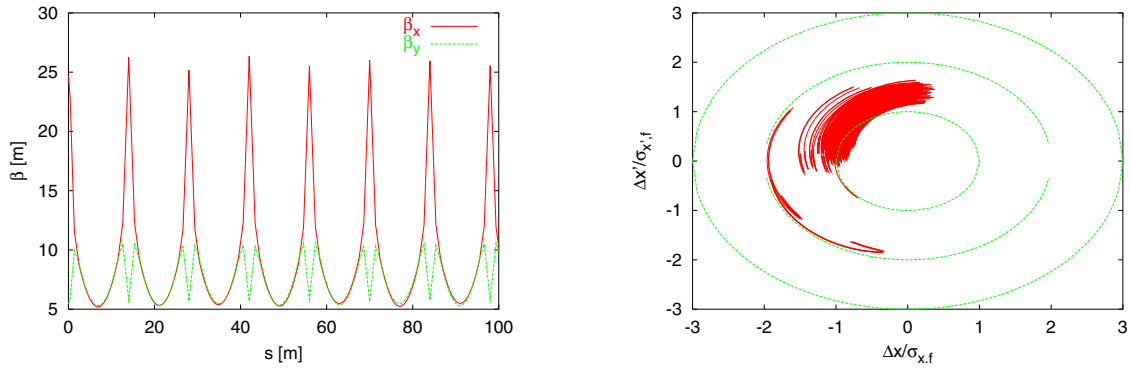

FIGURE 3.72. Left: The beta functions in the drive beam accelerator. Right: The final offset of a beam entering the structure with an offset of one rms bunch size σ. The value is normalized to the final beam size.

3.4.3.3 Accelerator Structures, Design, HOM Damping

The accelerator structures common to the drive-beam accelerator (DBA) and drive-beam injector of CLIC each consist of 42 cells adding to the length of ∼4.5 m indicated previously (mechanically a little more). It will operate in $2\pi/3$ mode, fully beam loaded by a beam current of 4.59 A. It has a moderate accelerating gradient and a nominal unloaded gradient of 7.2 MV/m.

Two types of structures have been studied. The first type considered is the "Tapered Damped Structure" (TDS) originally designed for the CLIC main accelerator and downscaled by a factor of 32. Dipole mode damping in TDS is obtained by coupling SiC loads through 4 waveguides to the accelerating cavities. The cut-off frequency of these waveguides is chosen above the operating frequency, but below the higher order mode frequencies. It thus serves as a high-pass filter between the cavity and the dampers. A TDS scaled to 937 MHz would however be very large (outer diameter 1.4 m). The impractical size of the TDS was one of the reasons to study in detail a second and novel type of structure, called SICA for "Slotted Iris—Constant Aperture." It has 4 radial slots in each iris, which virtually do not perturb the fundamental mode field. Dipole mode currents however are intercepted by the slots. The slots are radially extended into ridged waveguides which contain tapered SiC loads. These are designed as to drastically reduce the Q of the dipole modes (to values typically below 20). As opposed to the TDS, where the higher order modes are separated by a filter from the accelerating mode, mode separation in the SICA uses the geometric differences and special symmetries of the mode patterns. SICA structures were successfully built and tested at 3 GHz and are being implemented as DBA structures for CTF3. At 937 MHz, SICA structures would have an outer diameter of approximately 250 mm. The left side of Figure 3.73 shows an artist's conception of the accelerator structure and its right side shows a photograph of a machined disc for the 3 GHz prototype.

Cell dimensions and some of the fundamental mode characteristics of the beginning, middle and end SICA cells are given in Table 3.34, for both the 3 GHz structure built for CTF3 and the scaled 937 MHz version envisaged for the CLIC drive beam accelerator.

Another feature of the SICA structures is the constant iris aperture which reduces the short range wakes. The detuning is obtained by introducing nose cones with varying depths. These nose cones lead to a larger ratio of surface field to accelerating gradient in the downstream cells (ratio of up to 3.4), but this is acceptable since the overall accelerating gradient is moderate. Issues which were addressed in the design were i) the field enhancement at the slot edges and ii) the presence of low frequency "slot modes" and their potential impact on the performance. The field enhancement is reduced to an acceptable 40% by a modest rounding of the edges (rounding radius of approximately half the slot width). This additional field enhancement will lead to a maximum surface field of 33 MV/m at the slot edges in the last cell. The slot modes, which occur at frequencies of about 2/3 of the operating frequency, have the electric field across the slots and are strongly damped ($Q \leq 6$) if the cut-off frequency of the ridged waveguide is chosen low enough. The kick factor of the slot mode is found to be at an acceptable 5% of that of the lowest dipole mode. The parameters of the CTF3 and CLIC drive beam accelerator structures are summarized in Table 3.34.

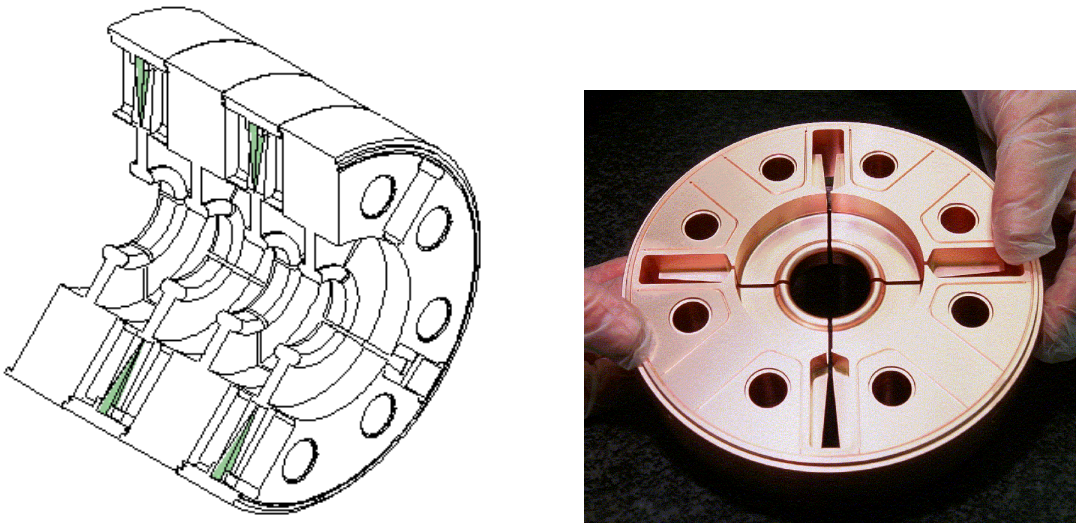

FIGURE 3.73. Left: Conceptual view of the SICA accelerator structure. Right: Machined disc of the 3 GHz version of the SICA structure.

TABLE 3.34: Parameters of the SICA drive-beam accelerator structures.

	3 GHz SICA (CTF3)			937 MHz SICA (CLIC)			Unit
Operating frequency	2998.55			937.05			MHz
Beam current	3.5			4.88			A
	1^{st} cell	center cell	last cell	1^{st} cell	center cell	last cell	
Cavity diameter	82.95	79.00	74.39	265.44	252.80	238.05	mm
Nose cone size	0.00	2.53	4.66	0.00	8.10	14.91	mm
Iris thickness		6.00			19.20		mm
Iris diameter		34.00			108.80		mm
Phase advance/cell		120°			120°		
r'/Q (Linac Ω)	3143	3292	3165	982	1029	989	Ω/m
Group velocity	5.19	3.49	2.36	5.19	3.49	2.36	% c
Q accelerating mode	13860	12771	10950	24794	22845	19588	
Frequency 1^{st} dipole	4147	4197	4097	1296	1314	1279	MHz
Kick factor 1^{st} dipole	555	668	843	16.95	20.22	5.90	V/pC/m^2
Q 1^{st} dipole mode	17.5	6.2	5.8	17.5	6.2	5.7	
Frequency 2^{nd} dipole	4243	4279	4379	1326	1318	1335	MHz
Kick factor 2^{nd} dipole	206	254	197	6.29	8.07	25.00	V/pC/m^2
Q 2^{nd} dipole mode	3.4	17.3	24.4	3.4	3.4	3.4	
Cell length		33.32			106.62		mm
Number of cells/structure		32			42		
Structure length		1.22			4.97		m
Fill time, τ		98			412		ns
Input power		30			88.5		MW
Acceler. voltage unloaded		13.3			32.4		MV
Acceler. voltage loaded		7.9			18		MV
Beam loading, κ		97.4			97.1		%
Efficiency, η		92.5			93.5		%
Number of structures (injector + accelerator)		2 + 16			3 + 108		
Total energy gain		127			2000		MeV

3.4.3.4 Klystrons and Modulators

The drive-beam complex requires high-power klystrons working in the L-band range of frequencies (468 and 937 MHz) for subharmonic bunching, the ×2 delay line combiner, the first ×4 combiner ring and for drive-beam acceleration. Higher frequency klystrons operating at 3750 MHz are also required for rf deflection systems in the second ×4 combiner ring. The klystron-modulators used in the drive-beam systems are shown in Figure 3.74.

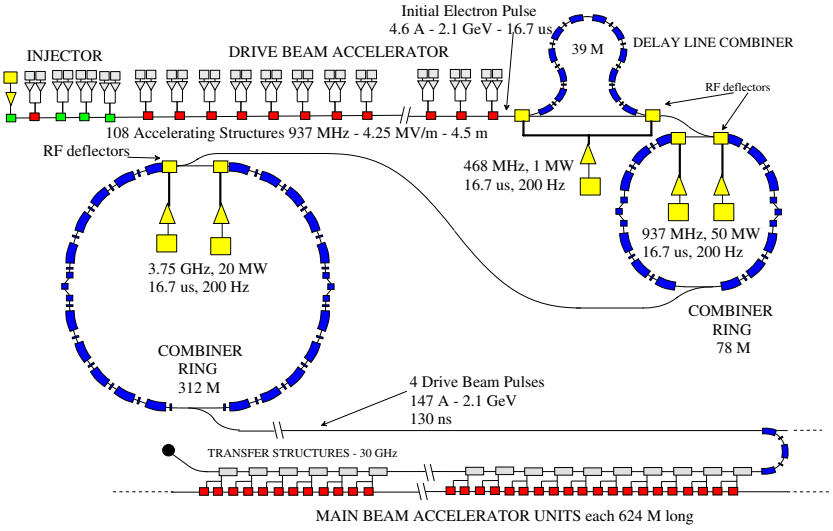

FIGURE 3.74. Drive-beam klystron-modulators for one generation complex.

Most of the very high power klystron-modulators are in the drive-beam accelerators (224 in each accelerator). For this application a multibeam klystron (MBK) having 6 internal beams is being designed. The long-term, targeted peak power for this MBK is 50 MW and 500 kW average for a 3 TeV machine. At the present time, a design study and current experience by manufacturers indicate a possible maximum of 40 MW for a klystron having a good lifetime and reliability. For the 500 GeV mode of operation the CLIC drive-beam can be powered by the layout in Figure 3.75 with each klystron also working at 50 MW in the extreme case, for the repetition rate is twice as high but the pulse length six times shorter than for the 3 TeV mode. In normal operation with two MBK per SICA structure, each klystron must provide a nominal power of ∼44 MW (Table 3.34, input power). However, reliability constraints require that in case of structure failure the gradient of the functioning structures be possibly increased by up to 5%, which means an increase of 10% in power. This implies that the klystrons be able to deliver a power close to the 50 MW considered. It must be noted that if the actual maximum power of the klystrons appears to be lower than 50 MW, then it is always possible to adjust the structure-length and

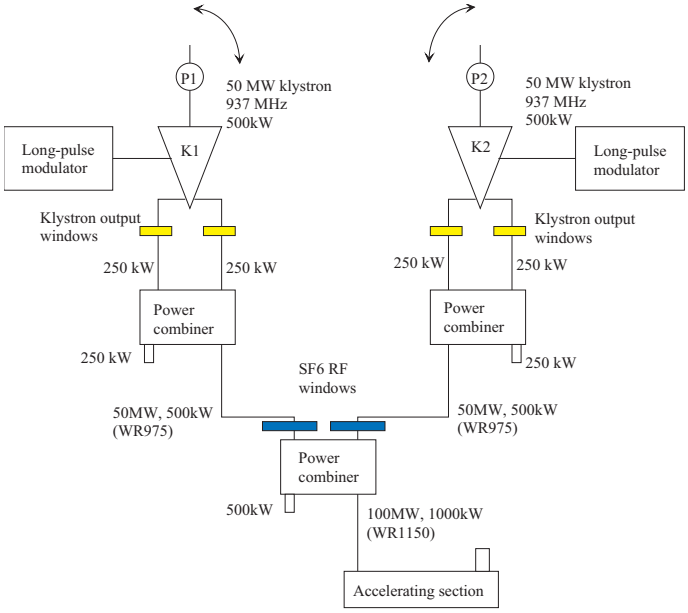

FIGURE 3.75. 50 MW MBK rf module layout.

linac-length in order to accommodate the two MBK per structure layout to this constraint, while keeping the reliability margin. The MBK data for 50 MW peak are given in Table 3.35.

In the drive-beam accelerator each MBK has its own high-power modulator and pairs of these klystron-modulators are connected as modules (Figure 3.75) to provide the rf power for a single structure.

A conventional line-type modulator has been studied that could power a single 50 MW multibeam klystron. This uses a double pulse forming network (PFN) and two thyratron switches that discharge the stored energy into the MBK via a step-up pulse transformer. A similar modulator design could be used for all drive-beam klystrons requiring wide voltage pulses at specific repetition rates. Alternative modulator designs using solid-state switching are to be investigated as a future replacement for the thyratrons. The requirements for very high power conversion efficiency together with high system reliability are important design issues. Table 3.36 gives a summary of the klystron and modulator (MDK) minimum power requirements for the drive-beam in the 500 GeV CLIC scheme, as well as the respective numbers of MDK needed for the accelerators, injectors and rf deflectors.

3.4.3.5 Combiner Rings

The main issue in the pulse compression system (delay line plus combiner rings) is the preservation of the length and longitudinal phase-space distribution of the bunches and the control of bunch-to-bunch phase variations. The rings, the delay line and the transfer lines must therefore be isochronous. The final bunch length must be short (σ_z of 0.4 mm, for a 9.8 nC charge per bunch) in order to maximize the 30 GHz rf power production efficiency in the drive-beam decelerator. High-charge, short bunches can radiate Coherent Synchrotron

TABLE 3.35: Multibeam klystron data

Parameter	Target Design	Present Design	500 GeV Design	Units
RF frequency	937.5	937.5	937.5	MHz
Repetition frequency	100	100	200	Hz
RF pulse width	100	100	16.7	μs
Microperveance	0.5	0.5	0.5	$I/V^{3/2}$
Number of beams	7	6	6	n_b
J_{max}	6	6	6	A/cm^2
Efficiency	65 to 70	65 to 70	65 to 70	%
Gain at saturation	≥ 47	≥ 43	≥ 43	dB
Klystron beam voltage	212	211	189	kV
Klystron beam current	342	293	245	A
Peak rf output power	50	40	50	MW

TABLE 3.36: Drive-beam klystron-modulator requirements.

MDK RF System	Number MDKs	Klystron Type	Repetition Rate [Hz]	Pulse Width [μs]	Frequency [MHz]	Peak Power [MW]	Average Power [kW]
Drive-beam accelerator	432	MBK	200	16.7	937	50	100
Drive-beam injector	16	MBK	200	16.7	937	50	100
Drive-beam injector	2	SBK 150 MHz BW	200	16.7	468	1	3.4
RF deflectors	4	SBK	200	16.7	3750	20	67
RF deflectors	4	MBK	200	16.7	937	50	100
RF deflectors	2	SBK	200	16.7	468	1	3.4

Radiation (CSR), leading to both an energy loss and an intra-bunch energy spread. The energy loss and spread must be kept small, in particular because the bunches belonging to different trains make a different number of turns in the rings (from 1/2 to 7/2) and will develop different energy distributions. This will cause relative phase errors between bunches and some bunch lengthening. These intense and short bunches will also interact with any small discontinuity of the beam chamber. It is therefore highly desirable to manipulate relatively long bunches in the pulse compression system, and to reduce their length just before the injection into the drive-beam decelerator sections.

The upper limit to the bunch length is given by the variation of the rf deflector kick strength along the bunches, due to their phase extension. This variation reduces the clearance from the septum of the circulating bunches for a given kick amplitude and induces a single-bunch emittance growth for the injected ones. These effects are critical in the second combiner ring, where the deflector frequency (3.75 GHz) is the highest. The maximum acceptable bunch length in this location is 2 mm r.m.s. approximately. The correlated energy spread ($\sim 1\%$ r.m.s.) suitable for the final bunch compression is obtained in the drive beam accelerator by the combined effect of the rf curvature and longitudinal wakefields. The need to preserve the correlation all along the compression system means that all the distortions of the longitudinal phase space must be kept small. In particular, attention must be given to the higher orders of the momentum compaction. A numerical analysis has shown that second-order effects would be unacceptable and must be corrected by using sextupoles.

Another concern is the beam loading in the rf deflectors. Again, this is particularly important just before the extraction from the second combiner ring, where the average current in the train and the deflector frequency are the highest. In order to overcome this problem, a traveling-wave iris-loaded structure with a short filling time with respect to the train duration has been chosen. A steady-state condition is then reached with minimum transient effects, although at the expense of a loss in the deflection efficiency. Numerical simulations have shown that a proper choice of the ring tune can minimize the effect.

The extraction system of both rings is also a critical item, the two main issues being the high repetition rate of the extraction kick ($\sim$1 MHz in the first ring and 250 kHz in the second ring, which correspond to 4 and 16 times 2×130 ns, respectively) and the interaction of the system with the high-current beam (particularly in the second ring—147 A). A possible solution is based on the use of pairs of traveling TEM wave transmission-lines.

A preliminary design of the lattices for the delay line and the combiner rings was made in 1999. Since then, the CLIC rf pulse length has been reduced from 143 ns to 130 ns. The drive beam energy and bunch charge have also been modified to 2 GeV and 9.8 nC, respectively. Such parameter changes imply a reduction of the delay introduced in the delay-line as well as a reduction of the circumference and of the magnetic field strength in the combiner rings. The existing lattice design could in principle be modified to fit the new parameters. Another possibility would be to use the design of the isochronous cells retained for CTF3. Such a design is based on the use of three bending magnets per module or cell instead of four. Being more compact, it would be better adapted to smaller rings and transfer lines.

The delay-line geometry was chosen to minimize both CSR emission and overall dimensions and is still based on the same type of isochronous arc design as in the combiner rings. In order to avoid distortions in the longitudinal phase space, all the arcs must be made

isochronous up to the second order by the use of sextupoles placed in the high-dispersion regions where there are no dipoles. The use of different families of sextupoles makes it possible to correct the third order as well.

One 3-bend magnetic chicane is located in the delay line and two in each ring. They are used for fine path-length tuning (0.5 mm tuning range), in order to adjust the relative phase of the bunches and compensate for orbit variations. Each chicane works around an average bending angle of $\theta_0 \sim 150$ mrad. The tuning range is obtained with a bending angle variation of $\Delta\theta$=1.5 mrad; such a small value of $\Delta\theta/\theta_0$ does not perturb the optics. The small finite R_{56} generated by the chicane is compensated in the two adjacent cells, slightly detuned away from their isochronous point.

The ring injection is similar to a conventional fast injection scheme based on a septum and a fast kicker, where the kicker is, however, replaced by an rf deflector. Another deflector is placed upstream of the septum (with a phase advance difference of $-\pi$), and provides the pre-compensation of the kick given by the injection deflector to the circulating bunches. A $\pi/2$ phase advance FODO lattice is used in the injection straight section, with the septum and deflectors close to the focusing quadrupoles, so that the angular kick from the deflector corresponds to a maximum displacement in the septum (left side of Figure 3.76).

All the rf deflectors are short traveling-wave iris-loaded structures, in which the resonant mode is a deflecting hybrid mode with a $2\pi/3$ phase advance per cell and a negative group velocity. The design is basically the same for all the deflectors, with the cell dimensions linearly scaled with frequency. The extraction kickers consist of pairs of TEM traveling-wave transmission-lines, powered in anti-phase, with the wave moving against the beam. The design of the extraction region lattice is based on a triplet placed between the kicker and the extraction septum (right side of Figure 3.76). The phase advance between the kicker and the septum is equal to $\sim \pi/2$. The use of a triplet allows a rather constant β-amplitude along the kicker.

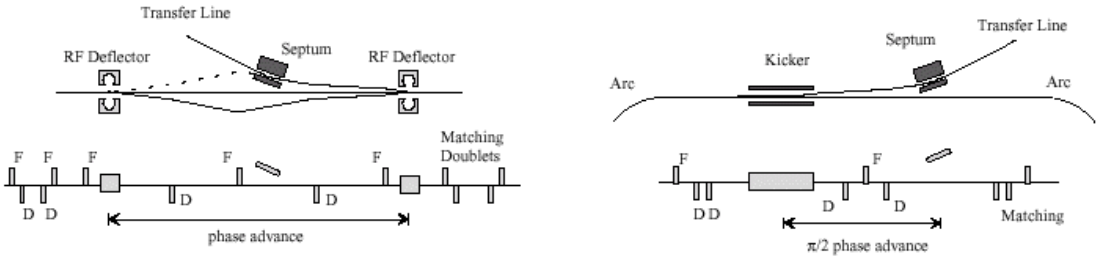

FIGURE 3.76. Schematic layout of the injection insertion with rf deflectors (left) and of the extraction insertion (right). At injection, the circulating bunches will travel on the central or inner orbit, while the injected bunches are kicked by the 2^{nd} deflector onto the equilibrium orbit. The train of combined bunches is ejected before the next pulse reaches the deflecting phase represented by the dotted line trajectory (intercepting the septum).

3.4.3.6 Drive-Beam Decelerator

Each drive beam decelerator has to feed 1000 main linac accelerator structures. It contains 500 Power Extraction and Transfer Structures (PETS). All beam line elements are mounted on girders which have the same length as the ones of the main linac, in order to facilitate the geometrical matching of the two lattices. Each girder supports two quadrupoles and two PETSs. A BPM is located in front of each quadrupole.

If the single bunch effects could be neglected, then the optimum frequency of the PETS would exactly be the same as the one of the main linac accelerator structures. Since one cannot neglect the single bunch effect, the case for optimum efficiency is obtained by using PETS with a frequency slightly different from the main linac frequency. Depending on their longitudinal position, the particles in the bunch are indeed decelerated differently. The maximum of the deceleration energy defines the minimum initial energy of the beam, which is required for the beam to pass through a given number of structures and which is directly related the overall efficiency. For the given bunch length of σ_z=400 μm, the optimum frequency is $f_{PETS} \approx 30.45$ GHz (left side of Figure 3.77). It should be noted that the maximum output power, obtained by adjusting the beam current, is reached for a much smaller detuning. However the maximum deceleration is also decreasing. A bunch charge of N=6.13×10^{10} produces an output power of 512 MW per PETS structure when the losses in the structures are neglected. After subtracting the losses this provides the required power of 231 MW per main linac structure. The initial beam energy has to be E_0=1.994 GeV. The lowest final energy in the beam is then $\check{E}_f$=0.1994 GeV. The final beam energy distribution is shown in the right side Figure 3.77. The energy spread in the beam is very large and the ratio of the lowest to the highest energy is 10. The decelerator lattice must accommodate a very large energy spread. This can be easily achieved by using a FODO lattice. The length of the FODO cells is kept constant along the decelerator and the quadrupole strength is adjusted so that the phase advance per cell is constant for the particle that is decelerated most. Particles that are decelerated less are automatically focused to smaller amplitudes.

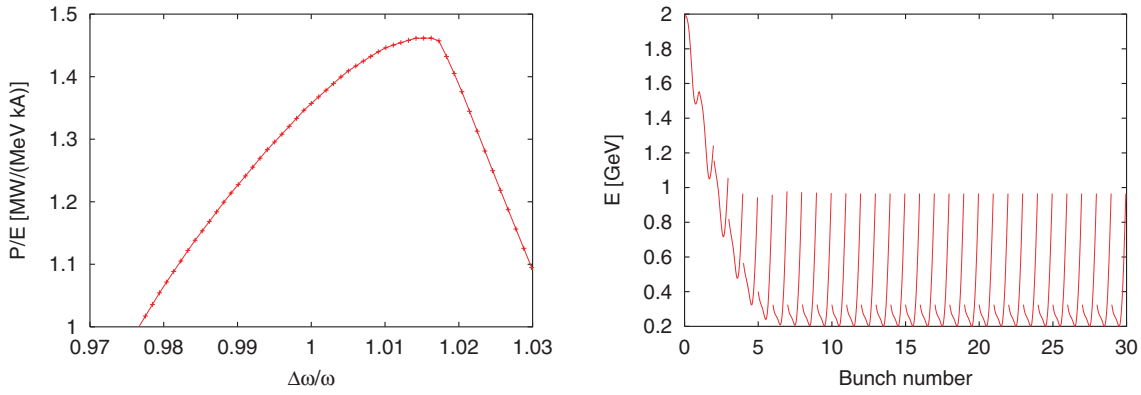

FIGURE 3.77. Left: The ratio between output power and maximum decelerating field as a function of the fundamental frequency of the PETS. Right: The final energy distribution in the various bunches of the drive-beam train.

To evaluate the beam stability in the decelerator, the envelope of a 3-σ beam with an initial offset $\Delta y = \sigma_y$ has been simulated using PLACET. In the program, the longitudinal and transverse wakefields are modelled using a single mode for each. The different group velocities, which are high, are taken into account and the beam is tracked through the structures in several steps using the proper field profiles. The deviation of the particle velocity from the speed of light is also accounted for. The left side of Figure 3.78 shows the result together with the envelope of a nominal 4-σ beam without offset. The wakefield effects are small. The ballistic method is foreseen to correct the initial misalignments of the quadrupoles and of the BPMs. For the simulation, we assumed an initial r.m.s. position error of 100 μm for all the elements. The envelope that embraces the 3σ-envelopes of the 100 cases simulated is shown in the right side of Figure 3.78 together with three particular cases (three different seeds).

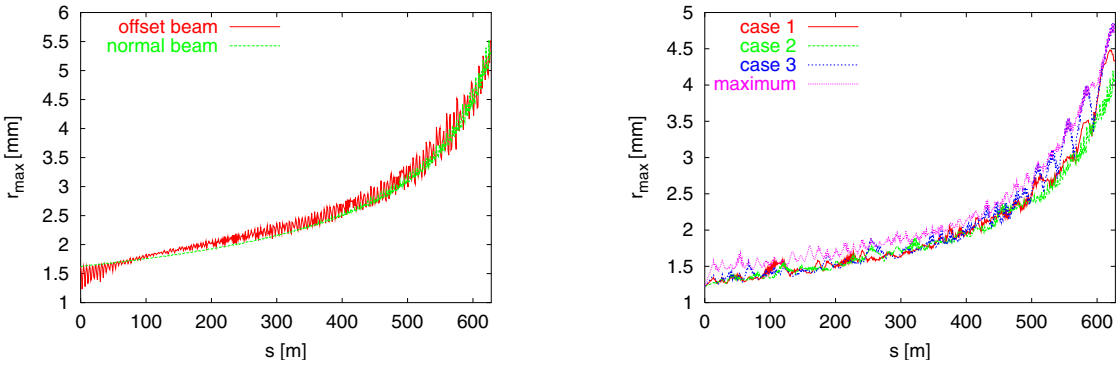

FIGURE 3.78. Left: The 3σ-envelope of a beam with initial offsets of $\Delta x = \sigma_x$ and $\Delta y = \sigma_y$. For comparison the 4σ-envelope of a beam with no offset is also shown. Right: the 3σ-envelopes in a decelerator after beam-based alignment. Three examples are shown together with the envelope that contains all of 100 simulated cases.

3.4.3.7 Power Extraction and Transfer Structures

3.4.3.7.1 Definition and Functions of the PETS The Power Extraction and Transfer Structure (PETS) is a passive microwave device in which the bunches of the drive beam interact with the impedance of the periodically corrugated waveguide and excite preferentially the synchronous TM01 mode at 30 GHz. In the process, the beam kinetic energy is converted into electromagnetic energy at the mode frequency, which travels along the structure with the mode group velocity. The rf power produced is collected at the downstream end of the structure by means of the Power Extractor and conveyed to the main linac structure by means of rectangular waveguides. The circularly symmetric structure (C-PETS) concept with distributed damping was eventually adopted, for it satisfies the requirements and ensures the azimuthal uniformity of the longitudinal electric field. In its configuration, the C-PETS is a circular waveguide with a shallow sinus-type

corrugation with damping slots and rf loads as displayed in Figure 3.79, which shows the C-PETS with beam chamber diameter 25 mm.

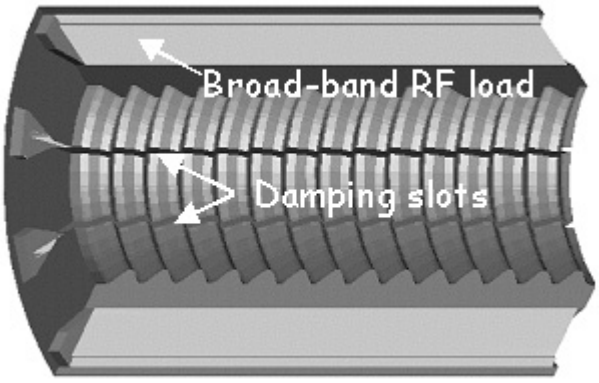

FIGURE 3.79. A quarter geometry of the C-PETS with 12 damping slots and SiC loads.

3.4.3.7.2 Structure Parameters Table 3.37 gives the main geometric and rf parameters of the C-PETS (with a 25 mm beam chamber aperture) which has been chosen as the power extracting structure for the drive-beam accelerator.

3.4.3.7.3 RF Power Extraction The quasi-optical approach was used for the rf power extraction from the regular part of C-PETS. This choice was done for high efficiency, large bandwidth and mode purity. The power extractor consists of (Figure 3.80) the mode launcher, which converts the TM_{01} mode of the circular waveguide (WG) to the TEM mode of the oversized coaxial WG and of the diffractor, which modifies the TEM mode into the TE_{10} modes of the following 8 rectangular WG's, that are then combined into two output WG's. The simulated rf power extraction efficiency is about 99% at 30 GHz, with a mode purity better than -30db, for both the reflected and transmitted ones.

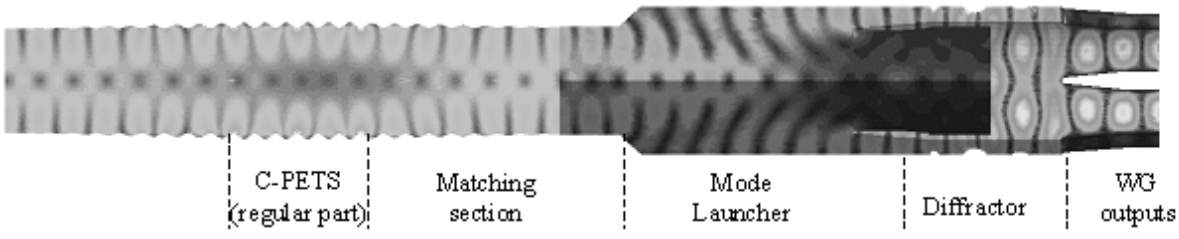

FIGURE 3.80. The electric field pattern of the rf power extractor for the C-PETS.

TABLE 3.37
Parameters of the C-PETS.

Parameter	Value	Units
Beam chamber diameter	25	mm
Synch. mode frequency	29.9855	GHz
Synch. mode v_g/c	0.85	
Synch. mode R'/Q	244	Ω/m
Synch. mode Q-factor	12000	
Number of damping slots (1.0 mm width)	8	
Transverse mode v_g/c	0.793	
First dipole mode kick-factor	0.58	V/pC/m/mm
Transverse mode Q-factor	< 50	
Structure length	0.8	m
Nominal output rf power	512	MW

3.4.3.7.4 Transverse Mode Damping A new concept of distributed damping of the transverse modes in a circularly symmetric structure has been developed. It is best explained in terms of array antennas. The damping is provided by thin longitudinal slots running all along the length of the structure. Every period of the slot-loaded structure acts like a single source in an array antenna, radiating through the slots to the outside. The radial component of the radiation (damping) is a function of the phase advances between two cells. The smaller the phase advance, the stronger the damping. Broadband rf loads terminate the slots. In the design of a 20 mm beam aperture C-PETS, the damping is provided by 12 equally spaced radial slots of 0.5 mm, as shown in Figure 3.79. Each of the 12 loads consists of a long SiC rod with a triangular cross-section, which is matched to the slot. The slot depth and load geometry are chosen to minimize the external Q-factor of the first dipole mode around 30 GHz. To verify the damping ability, a full-scale simulation of C-PETS (100 cells) was done with the special EM computer code GDFIDL. The loaded Q-factor was calculated to be about 35. This value is very close to the one calculated with HFSS during the design stage.

The long-range transverse wakes and transverse impedances are shown in Figure 3.81. The second big spike in the wake distribution for the undamped case (left side of Figure 3.81) results from a partial (about 30%) reflection from the ends of the structure. In the presence of damping the reflection is not seen because of the strong attenuation of the reflected wave. A comparison of the transverse impedances with and without damping (right side of Figure 3.81) shows that low-frequency trapped modes are significantly suppressed with this distributed damping technique. Comparing time domain simulations (see above) with wakefield reconstruction from the frequency domain data (HFSS) for a bunch length of 600 μm established that the influence of the first dipole mode is dominant (more than 90%). Furthermore, the single-mode concept was considered for the beam dynamics simulations both for the short-range and long-range wakefield effects. On the basis of beam dynamic simulations with optimized efficiency and beam stability, a 25 mm

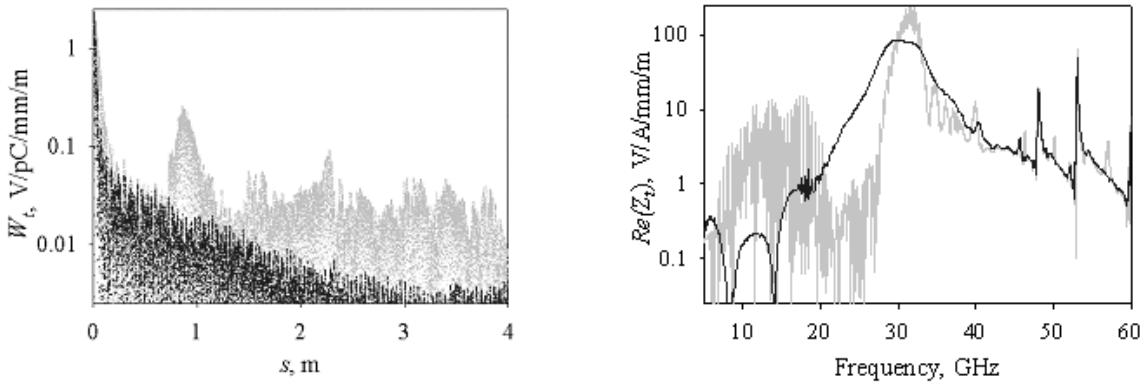

FIGURE 3.81. Left: The long-range wakes in the C-PETS. Right: The transverse impedance in the C-PETS.(grey: without damping, dark: with damping.)

beam aperture C-PETS with 8 damping slots, each 1.0 mm wide, is now proposed (parameters of Table 3.37). The peak electric field on the surface of the structure with the nominal rf power output was calculated to be about 90 MV/m. Due to the damping slots it is further enhanced by 20%—up to 110 MV/m. This field level is within the acceptable range for the 30 GHz structures.

BIBLIOGRAPHY for CHAPTER 3

[1] R. Brinkmann, *et al.* (eds.), TESLA Technical Design Report Part-II, DESY-2001-011, March 2001.

[2] R. Brinkmann, *et al.* (eds.), Conceptual Design of a 500 GeV Linear Collider with Integrated X-ray Laser Facility, Vol. I, DESY-1997-048, May 1997.

[3] N. Toge, ed. [JLC Design Study Group], "JLC design study," KEK-REPORT-97-1 (1997).

[4] T.O. Raubenheimer, ed. [NLC ZDR Design Group], "Zeroth order design report for the Next Linear Collider," SLAC-R-0474 (1996).

[5] C. Adolphsen *et al.* [International Study Group Collaboration], "International study group progress report on linear collider development," SLAC-R-559 (2000).

[6] N. Phinney, ed. [NLC Collaboration], "2001 report on the Next Linear Collider: A report submitted to Snowmass '01," SLAC-R-571 (2001).

[7] The CLIC Study Team, Ed. G.Guignard, A 3 TeV e^+e^- Linear Collider Based on CLIC Technology, Report CERN 2000-008 (July 2000). `http://cern.web.cern.ch/CERN/Divisions/PS/CLIC/General.html`

[8] H.H. Braun, R. Corsini (Ed.), T. D'Amico, J.P. Delahaye, G. Guignard, C.D. Johnson, A. Millich, P. Pearce, L. Rinolfi, A.J. Riche, R.D. Ruth, D. Schulte, L. Thorndahl, M. Valentini, I. Wilson, W. Wuensch, The CLIC RF Power Source - A Novel Scheme of Two-Beam Acceleration for Electron-Positron Linear Colliders, CERN 99-06 (1999).

[9] M. Korotsolev, F. Zimmermann, "CLIC damping ring design study," presented at the 8th European Part. Acc. Conf. (EPAC02), Paris, June 2002.

[10] F. Zimmermann, *et al.*, "Design Status of the CLIC Beam Delivery System," presented at the 8th European Part. Acc. Conf. (EPAC02), Paris, June 2002.

CHAPTER 4

Upgrade Paths to Higher Energies

4.1 TESLA

The TESLA linac design for 500 GeV c.m. energy with an accelerating gradient of 23.8 MV/m is based on the technology developed and proven during the first phase of the R&D program at the TTF. While an upgrade to higher energy could in principle be done by extending the linac length, we do not consider this option here, mainly because of cost reasons. It should also be noted that the detailed planning and the legal procedure for land acquisition and construction permission (in German: *Planfeststellungsverfahren*) for the TESLA site at DESY do not include the possibility of an extension of the length beyond the foreseen 33 km for the baseline 500 GeV design. An energy upgrade for TESLA will thus require to increase the beam energy gain per unit length of the accelerator:

- By further reduction of the inter-cavity spacing the linac fill factor can be increased. The concept presently under development (so-called superstructures) uses pairs of 9-cell cavities with spacing reduced to half rf wavelength. The rf power is transmitted through this interconnection so that only one high power input coupler is needed per cavity pair—thus reducing the number of couplers by a factor of 2. Building the linac with superstructures improves the fill factor—and hence the maximum energy for a fixed accelerating gradient and site length—by about 6%.
- The fundamental limit for the gradient in niobium structures at 2 K is above 50 MV/m, and at the TTF several 9-cell cavities have already reached gradients around 30 MV/m. Electropolishing followed by low-temperature bake-out has yielded systematically high performance single-cell cavities, with gradients up to 42 MV/m. The maximum gradient achieved with an electropolished 9-cell cavity is 35 MV/m.
- The Lorentz force detuning (which increases as the square of the accelerating gradient) can be compensated by active mechanical stabilization using fast piezo tuners; this removes the need to increase the regulation rf power overhead at higher gradients. The method was successfully demonstrated at the TTF at 24 MV/m.

As a reasonable estimate for the maximum gradient in the TESLA linac we assume E_{acc}=35 MV/m at Q_0=5×10^9. Using superstructures, the energy reach of the machine is

TABLE 4.1
TESLA parameters for an upgrade to 800 GeV. It is assumed that the linac is built with 2 9-cell superstructures and the rf power has been doubled (see text).

		TESLA-800
Accelerating gradient	E_{acc} [MV/m]	35
Fill factor		0.79
Repetition rate	f_{rep} [Hz]	4
Beam pulse length	T_P [μs]	860
Number of bunches per pulse	n_b	4886
Bunch spacing	Δt_b [ns]	176
Charge per bunch	N_e [10^{10}]	1.4
Emittance at IP	$\gamma\varepsilon_{x,y}$ [10^{-6} m·rad]	8, 0.015
Beta at IP	$\beta^*_{x,y}$ [mm]	15, 0.4
Beam size at IP	$\sigma^*_{x,y}$ [nm]	391, 2.8
Bunch length at IP	σ_z [mm]	0.3
Beamstrahlung	δ_E [%]	4.3
Luminosity	L [10^{34} cm^{-2}s^{-1}]	5.8
Power per beam	$P_b/2$ [MW]	17
Two-linac primary electric power	P_{AC} [MW]	≈160

then E_{cm}=800 GeV. A parameter set for this energy is shown in Table 4.1. The beam delivery system and the magnets in the main linac are designed to be compatible with operation up to 400 GeV beam energy. Obtaining high luminosity at maximum energy requires upgrading of the cryogenic plants (approximately doubling the 2 K cooling capacity) and of the rf system (doubling the number of rf stations). The higher beam pulse current and the reduced bunch spacing also require an upgrade to the injection system (*e.g.*, increased rf power in the 5 GeV pre-linac and in the damping ring, faster kickers for damping ring injection/extraction).

It should be noted that operation above the 500 GeV reference energy is already possible without any hardware modification. The cooling plant capacity has a 50% overhead in the baseline design, which allows an increase of the gradient by 20–30%[1], depending on the variation of Q_0 versus g. With constant rf power, the beam current decreases as $I_b \propto 1/g$; this effect is counter-balanced by a stronger adiabatic damping of the emittance, so that one might expect a constant luminosity. However, since the cavity filling time increases as $g/I_b \propto g^2$, the beam pulse length and thus the luminosity goes down, putting a reasonable upper limit on the initial energy reach of the machine at about 700 GeV. The luminosity as a function of energy calculated for the 500 GeV baseline design without any hardware modifications is shown in Table 4.2.

[1]Only the rf wall losses scale as g^2/Q_0, the other contributions to the 2 K load (static losses, wakefields, about one half of the total load) remain unchanged.

TABLE 4.2
Luminosity achievable with the TESLA-500 baseline design at higher center-of-mass energies without any upgrade of installed hardware. The numbers quoted take into account the reduction of beam current with increasing energy, the increase in cavity filling time, and a reduction of the repetition rate to 4 Hz at 600 GeV and 3 Hz at 700 GeV.

c.m. Energy [GeV]	Luminosity [10^{34} cm^{-2}s^{-1}]
500	3.4
550	3.06
600	2.16
650	1.89
700	1.17

4.2 JLC-C

As is described in Section 3.2.2 the energy upgrade scenario for the C-band JLC starts from a 400-GeV c.m. collider, consisting of two 200-GeV C-band linacs in the upstream ends of a tunnel that is long enough to accommodate the 1-TeV machine. The upgrade itself consists of filling the remaining downstream parts of the tunnel with X-band linacs to reach 1 TeV c.m.

The advantages of this "C+X" scenario over that of X-band alone are:

(a) It allows an early start of the first stage because of the maturity of C-band rf technology.

(b) The initial buildup of the luminosity after the construction is expected to be faster owing to the looser tolerances.

(c) The actual integrated luminosity over years can be greater in spite of the lower instantaneous luminosity, owing to the more reliable hardware system.

An obvious disadvantage of the C+X scenario is:

(d) Discontinuity of the R&D between the first and second stages.

In this respect, one could start out with low-gradient X-band linacs instead of C-band (an "X+X" scenario). The luminosities of these two scenarios are similar (depending on the initial X-band gradient) and are slightly lower in the X+X scenario. The choice between the C+X scenario and the X+X scenario depends on how one evaluates the advantages of (b) and (c), and the disadvantage of (d).

The beam parameters for the C+X scenario are basically identical to those of the X+X scenario. This fact does not sacrifice the C-band performance as described in Section 3.2.2. One problem in the compatibility of the beam parameters is the bunch length. It has to be about 200 μm in the C-band linac and about 100 μm in the X-band linac for the control of the energy spread and BNS damping. For the 1 TeV operation of the C+X collider we shall choose $\sim$100 μm. In this case we choose the off-crest phase $\sim -10^\circ$ (BNS damping side) in

the C-band section and the resulting energy spread will be eliminated in the X-band section. We believe, though detailed studies are still on the way, that we can choose an appropriate bunch length between 200 μm and 100 μm for operation anywhere between 400 GeV and 1 TeV.

Thus, the constraints coming from the frequency compatibility requirement are:

- The bunch compressor system must be capable of controlling the bunch length over the wide range between ∼200 μm and ∼100 μm. (Although the megatable quotes the C-band main linac injection energy as 8 GeV, the same as for the X-band case, this value can presumably be lowered for the C-band case. Then the second bunch compressor will be easier to design.)

- The accelerator structure must be designed so that the wake function has a node at 1.4 ns.

4.3 JLC-X/NLC

As described in the Overview (Section 3.3), the JLC-X/NLC linear collider has been designed to facilitate the upgrade to energies greater than 1 TeV. The baseline upgrade is accomplished by installing additional rf modules into the second half of the linac tunnel which is empty in the initial Stage I (500 GeV) configuration. The upgrade could either be completed using modules of the baseline rf system, identical to those for 500 GeV, or it could use higher efficiency rf units which will likely be developed over the next few years. To ensure the feasibility of the upgrade, all of the luminosity studies have been performed for the Stage II (1 TeV) configuration and the component tolerances have been specified for the Stage II design. In particular, the beam properties for the Stage II operation are identical to those for Stage I. Thus, no modification of the injector system is required and only the permanent magnet final doublet needs to be replaced in the beam delivery system. The expected cost for the full energy upgrade is roughly 25% of the initial total project cost (TPC).

The Stage II parameters can be found in Table 3.14 of the JLC-X/NLC Overview. As in Stage I, the beams consist of bunch trains with 192 bunches separated by 1.4 ns. The repetition rate would be decreased to 100 Hz in Japan and would remain at 120 Hz in the US. The luminosity would be 2.5×10^{34} cm^{-2}s^{-1} (3.0×10^{34} cm^{-2}s^{-1}) in Japan (US) at the nominal center-of-mass energy of 1 TeV. Although not listed, the collider is also designed to operate with 96 bunches of 1.5×10^{10} particles and a 2.8 ns bunch spacing—this latter option provides higher luminosity but also more beamstrahlung and emittance dilution.

The energy reach of Stage II is roughly 1.3 TeV without modification of the rf system. This is possible because the JLC-X/NLC traveling-wave accelerator structures are tested to a full unloaded gradient of 65 MV/m; this differs from the testing of the standing-wave superconducting structures which are only tested to the maximum *loaded* gradient of 23 to 35 MV/m. The luminosity versus energy for the Stage II JLC-X/NLC is plotted in Figure 4.1. Thus, as discussed in the Overview, the JLC-X/NLC linear collider is designed to fully cover the energy region between 90 GeV and 1.3 TeV.

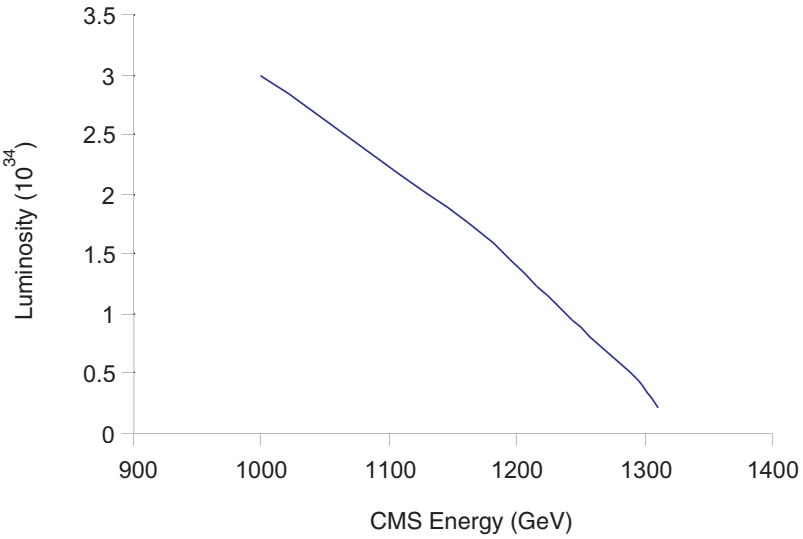

FIGURE 4.1. Energy versus luminosity for the Stage II NLC rf system

To accommodate the physics demands for energy flexibility, the design includes two interaction regions. One is optimized for high energy, 250 GeV to 1.3 TeV, and is configured so that it is ultimately upgradable to multi-TeV. This final focus can actually accommodate beams of up to 2.5 TeV in the length of about 800 m. The other interaction region is designed for precision measurements at lower energy, 90–500 GeV, although it could be upgraded to operate at ∼1 TeV as well.

To capitalize on the multi-TeV potential of the new design, it was also necessary to eliminate other bending between the linac and the high energy IP. In the NLC design, a 20 mrad crossing angle at the IP is used to avoid parasitic interactions of one bunch with the later bunches in the opposing train and to ease the extraction line design. The linacs are not collinear but are oriented with a shallow 20 mrad angle between them to produce the desired crossing angle at the high-energy IR without additional bending. The beams to the second IR are bent by about 25 mrad, which is acceptable for energies up to 1 TeV. The low-energy IR has a larger 30 mrad crossing angle for compatibility with a possible γ/γ option. Finally, in the JLC design, the primary IP has a crossing angle of 7 or 8 mrad and the non-collinear linac layout has not been planned. However, the crossing angle of the second IP is 30 mrad as in the NLC design.

As stated, the luminosity listed for the Stage II design is based on the same injector and beam delivery system as for Stage I. Of course, it will likely prove possible to further increase the luminosity by upgrading the performance of the injector systems to decrease the extracted vertical beam emittance. It is expected that the emittance transport through the linacs will perform better than required as described in Section 3.3.6. In this case, the primary limitations will be stabilization of the pulse-to-pulse jitter due to the high disruption parameter which will start to approach the values in the TESLA design. An estimate of the ultimate luminosity from the collider can be found in Table 3.17 of the JLC-X/NLC Overview.

Finally, ongoing R&D at KEK, SLAC, FNAL, and LLNL is aimed at improving the efficiency of the rf units. The three places where significant improvements might be expected are the modulator, the klystron, and the pulse compression system which have design efficiencies of 80, 55, and 75%, respectively, in the baseline design. Working in collaboration with the IGBT manufacturers, the modulator efficiency might be increased to 85% by improving the rise and falls times of the IGBTs. Similarly, simulations have indicated that ∼65% efficiency for the klystrons may be possible either with improved single beam PPM klystron designs or by developing a sheet beam or multibeam klystron; the sheet beam concept is being pursued at SLAC while the multibeam klystron design is being studied at KEK. Lastly, the biggest improvement might come from improvements to the pulse compression system. The SLED-II baseline system has an efficiency of roughly 75%. An optimized Delay Line Distribution System (DLDS) or Binary Pulse Compression system (BPC) might have efficiencies of ∼90%. Work investigating the viability of a four times single-moded DLDS compression system will begin at SLAC and KEK after the demonstration of the SLED-II compression system. If found viable, then this DLDS system could simply replace the SLED-II without changes to the other rf system components.

Similarly, ongoing R&D at many laboratories, including SLAC, KEK, and CERN, is aimed at higher acceleration gradients. The maximum gradient that can be supported in copper accelerator structures is not clearly known. With the development of a new coupler design, a recent X-band test structure has operated at 90 MV/m with a breakdown rate of less than 1 per 24 h—the maximum allowable rate for JLC-X/NLC operation being 1 per 10 h. Additional design modifications might support still higher gradients. In addition, R&D at CERN and SLAC studying different materials has shown that as much as a 50% increase in the gradient may be possible by using Tungsten, Molybdenum, or Stainless Steel in the accelerator structure irises.

If structures that support ∼100 MV/m can be developed over the next decade, then the upgrade to Stage II could have an energy reach well in excess of 1.5 TeV and approaching 2 TeV. Looking further in the future, as described in the Overview, the JLC-X/NLC facility has been configured to simplify the evolution to a multi-TeV collider with c.m. energies of roughly 3–5 TeV. It is likely that much of the infrastructure could be reused and the injectors and beam delivery systems would need relatively straightforward upgrades. Only the main linac structures and rf sources would need to be replaced. Furthermore, and perhaps more importantly, the knowledge gained from operating a normal conducting linear collider would be indispensable for the design and construction of a multi-TeV linear collider.

4.4 CLIC

The CLIC design aims at reaching multi-TeV c.m. energies as stated in the introduction of the 500 GeV-CLIC description. These high energies can be reached in natural steps of about 140 GeV center-of mass (c.m.) which correspond to a typical gain of 70 GeV per beam in a 625 m long unit with an average accelerating gradient of 150 MV/m. It has to be mentioned that adjusting the rf structure layout in these units allows to vary the energy gain per step and hence tune the final c.m. energy. Studies of low emittance transfer and beam characteristics for a luminosity of the order of 10^{35} $\mathrm{cm}^{-2}\mathrm{s}^{-1}$ indicated that beam

dilution and sensitivity to vibration in the last doublet are limiting the plausible maximum c.m. energy to around 5 TeV. This is true even though the wakefield effects of 30 GHz structures are controlled by a judicious choice of bunch length, charge and focusing strength. The accelerator physics limitation comes mainly from the fact that the vertical geometric beam size at the IP becomes critically small for the requested performance and imposes very tight jitter as well as vibration tolerances in the final focusing system.

The "Two-Beam Acceleration" method of CLIC is such that the design remains essentially independent of the final energy for all the major subsystems, like the main beam injectors, damping rings, the drive-beam generators, the rf power source, the main-linac and drive-beam decelerator units, as well as the beam delivery systems. For the main linacs however, the existence of lattice sectors with different quadrupole length and spacing (see below) makes it necessary to shift the low-energy sectors toward the linac-injection points, which move apart when the tunnel is extended, and to install the new higher-energy sectors in the already existing tunnel segments. Transporting the girders equipped with up to four accelerator structures and the quadrupoles should not be difficult and could possibly be achieved within a few months. The basic differences related to the c.m. energies reside in the number of two-beam units involved in each linac and in the length of the pulse required in each drive-beam accelerator. As an illustration, these two numbers are equal to 4 units and 17 μs, 22 units and 100 μs, and 37 units and 154 μs, at 500 GeV, 3 TeV and 5 TeV c.m. respectively. These numbers correspond to two-linac lengths of 5 km, 28 km and 46.5 km as well as total collider-lengths of about 10 km, 33 km and 51.5 km, assuming that the length of the BDS system remains unchanged at the various energies while the layout and the magnet strengths may have to be adjusted. These total collider-lengths have been submitted to the engineering feasibility-study carried out using a site near CERN with the interaction point on the present CERN site. As already quoted in the 500 GeV c.m. description, a length of up to 40 km total is available in a molasse of SPS/LEP quality which corresponds to the cheapest conditions in the region and would cover an energy slightly above 3.5 TeV c.m. Going beyond this total tunnel length would imply entering into limestone on one side and/or crossing a 2 km wide underground fault on the other side. In spite of the technical difficulty, the second solution looks preferable and the extra cost would approximately correspond to doubling the cost per unit length over the 2 km crossing distance. Crossing this fault would then open the possibility of extending the tunnel to the next major fault which is not recommended to be breached. With this extension, the maximum tunnel length which can be considered is 52 km, which happens to be sufficient for a 5 TeV collider with the parameters indicated.

Given the main goal and the limitations mentioned, the CLIC design has been optimized for a 3 TeV colliding beam energy which should meet the post-LHC physics requirements. The ultimate energy considered as reachable is 5 TeV. All the subsystems listed have been initially designed for a 3 TeV c.m. energy and scaled down whenever necessary in order to satisfy the requirement at 500 GeV. This approach, together with the fact that developments continue, explain why the description of the 500 GeV collider is not entirely consistent. For more complete information, the detailed description of the 3 TeV CLIC design is given in Reference [1]. However, design modifications took place since the publication of Reference [1] and have been included in the 500 GeV CLIC chapter. The present section underlines the differences associated with an upgrade from 0.5 TeV to 3 TeV in this framework.

The injection system of the main beam remains essentially unchanged at 3 TeV. However, while the klystrons of the injector linacs have to provide the same peak power, the average power they deliver is lower at 3 TeV than at 0.5 TeV since the repetition rate is two times smaller. Considering the drive beam generation, the characteristics of each bunch train (modified with respect to [1, 2]) are the same, *i.e.*, an energy of 2 GeV, an average current of 147 A and a length of 130 ns, but the number of bunch trains depends on the c.m. energy of the main beam. This means that the duration of the initial long pulse accelerated by each drive-beam linac operating at 937 MHz differs and corresponds to two times the linac length (given by the number of the rf power source units required), *i.e.*, is proportional to the energy ratio. The direct consequence is to increase the pulse length of the drive-beam accelerator klystrons by a factor of 6. However, since the repetition rate is reduced from 200 to 100 Hz, the average power to be provided by these klystrons only increases by a factor of 3 when going from 0.5 to 3 TeV c.m. and the same klystrons can be used in principle in both cases. It could however be preferable to start with klystrons designed for a shorter pulse length, which are possibly cheaper, and to exchange them later at the end of their lifetime with better performing ones. The modulator design could also be compatible with a later extension of the pulse length in order to save investment costs at the beginning. As discussed previously, the power consumption for accelerating both the drive beams goes up from ∼106 MW at 0.5 TeV to ∼319 MW at 3 TeV. The combiner rings clearly remain identical while the repetition rate of the rf deflectors is halved and their pulse is six times longer (increasing by three the average power delivered by their klystrons). Each decelerator unit then remains the same at any c.m. main-beam energy so that all the technical problems related to the drive-beam control, rf power extraction and transfer to the accelerator structures are identical at 0.5 GeV and 3 TeV for instance.

As explained in the CLIC description, the damping rings (DR) have been designed for the energy of 3 TeV, where the requirements are more stringent, and optimized with respect to IBS and radiation damping. This design doesn't yet quite satisfy the target values for the transverse emittances considered in order to reach the planned luminosity. Even though the difference looks manageable at 0.5 TeV, it becomes more difficult at 3 TeV. Therefore, investigations continue for reaching the nominal DR value of 3 nm for the extracted vertical emittance. The present design, which is a snapshot of where we now stand on the path toward a satisfying solution, gives a value of 7.5 nm for this quantity. This would correspond to an increase of the emittance at the main linac end from 10 to 14.5 nm and induce a luminosity loss of 20%. Prospecting further for an improved design of the damping ring is all the more important as the last solution proposed has still potential difficulties with the dynamical aperture after chromaticity correction and possibly with the tolerance on the impedance in order to control the collective instabilities.

It is assumed that the longitudinal beam characteristics at the exit of the DR are the same at 0.5 and 3 TeV. Under these conditions, the two stages of the bunch compressor remain unchanged when upgrading the energy and the total compression ratio is equal to 37.4. The transfer lines, the booster linac and the turn-around loops remain unchanged for the main-beam injection energy of 9 GeV is the same at any final c.m. energy. The vertical emittance blow-up taking place between the damping ring and the entrance of the main linac is estimated to be 2 nm, which brings the nominal $\gamma\varepsilon_y$ value to 5 nm at the linac-injection.

The essential characteristic of the CLIC two-beam scheme is the modularity of its power source (each module feeding 1000 accelerator structures for a nominal 70 GeV energy gain per beam, which can be adjusted). It is therefore very likely that the energy will not be raised from 500 GeV c.m. to 3 TeV at once, but via intermediate stages which will first depend on the evolution of physics, and then on the needs to learn in practice how to run such a collider under conditions which become progressively more severe. There is *a priori* nothing magic about the choice of 3 TeV c.m. from the physics point of view and this choice was arbitrary in order to be in the multi-TeV range. In the same way, the selection of 500 GeV c.m. for the present technical review is somewhat arbitrary and one might in reality take advantage of the easily upgradable two-beam technique of CLIC, for possibly starting with lower c.m. energies associated with the top-particles or Higgs-particles. In any case, the upgradability of CLIC in relatively small energy steps would allow to provide center-of-mass energies in a large range of values in response to the actual requests coming from particle physics.

At 3 TeV, each linac contains 22 rf power source units, that is 22000 accelerator structures representing an active length of 11 km. With a global cavity-filling factor of ∼78% due to the presence of drifts and focusing quadrupoles, the total linac length is ∼14 km each. To keep the filling factor about constant along the linac, the target values of the FODO focal length and quadrupole spacing are scaled with $E^{1/2}$. For practical reasons however, the beam line consists of 12 sectors (instead of 5 at 500 GeV), each with constant lattice cells and with matching insertions between sectors. The total number of quadrupoles is equal to 1324 per linac and their length ranges from 0.5 at the beginning to 2.0 m in the last sector (where a single quadrupole replaces the four structures of a girder). The rms energy spread along the linac is about 0.55% average for BNS damping and decreases to ∼0.36% at the linac end (1% full width). The static correction of the trajectory is based on pre-alignment with a system of wires, the ballistic alignment method completed by a few-to-few correction, structure re-alignments and on emittance-tuning bumps as described for 500 GeV. The bins for ballistic correction contain 12 quadrupoles each for any final energy, but the number of tuning bumps is increased from 2 to 10 when the c.m. energy goes from 0.5 to 3 TeV. These various corrections aim at maintaining the vertical emittance growth in the linac below 5 nm or 100% relative blow-up. Simulations indicate that repeating the static corrections at times (at a repetition rate which goes from low for the ballistic, *i.e.*, every few weeks, to frequent for the tuning bumps) makes the emittance control feasible, although the wakefields at 30 GHz are high and the alignment tolerances small. Figure 4.2, left, indeed shows that emittance growth in static conditions can be limited to about 25%, thus leaving a margin for time-dependent effects. Dynamic misalignments due to element motions are dealt with in a way which depends on their frequency range. For slow motion (below a few Hz), a certain number of feedbacks (up to 40) are distributed along each linac for recentering the trajectory and an IP feedback corrects for beam separation at collision. For fast motion, it is important to have a site with low noise conditions. In this respect, the site near CERN studied for its engineering feasibility is very quiet, in particular if the whole main tunnel is located inside the molasse, although progress in stabilization techniques would permit to use the extended tunnel mentioned previously. Measurements indicate that fast motion amplitudes of the ground in the molasse remain below 4 nm for frequencies above 4 Hz (about the limit of the feedbacks). In order to cover the gap between this amplitude measured on the floor and the tolerances for the quadrupoles, and to have means

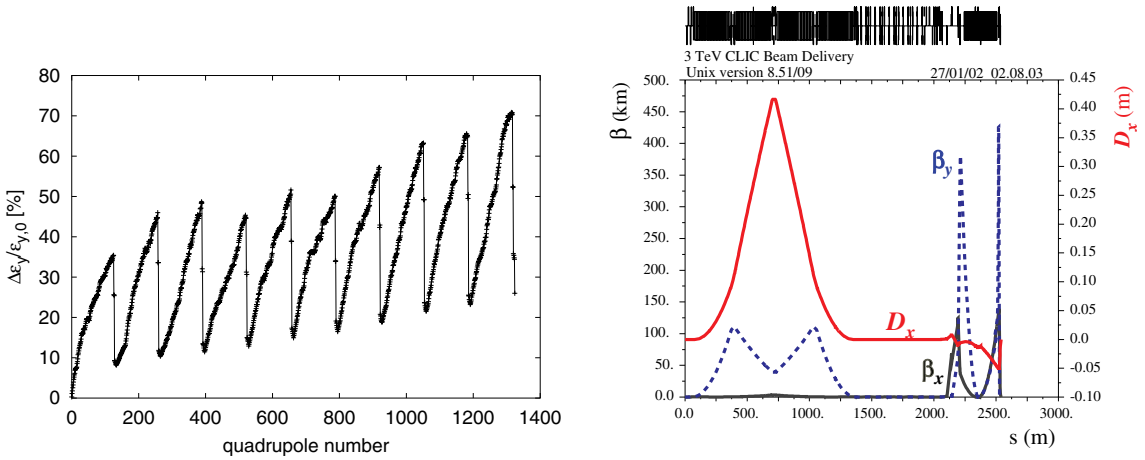

FIGURE 4.2. Left: Emittance evolution in the main linac after static correction which includes ten emittance bumps. Right: Optics of the compact beam delivery system at 3-TeV c.m.

to counteract the motion due to technical activity (like cooling), passive and active stabilization supports are considered and studied. Preliminary tests show that feet stabilized with commercial supports using rubber pads and piezoelectric movers give results which meet the requirements for the linac quadrupoles even in a noisy environment. Further reduction of the vibration amplitudes by a factor of 2–5 is investigated for the last FF doublets which predominantly contribute to the luminosity reduction. This clearly requires active stabilization, optimized by the use of permanent magnets in order to reduce their weight.

The BDS system has to be somewhat adjusted to the collision energy. In particular, the design scaling and the bending angles are different at 3 TeV and 0.5 TeV c.m. The design was initially done at 3 TeV, where it is most critical, and changing the energy by a large factor presently assumes some changes in the magnet positions, and in the bend and quadrupole strengths. However, the total length of the BDS remains constant as well as the total crossing angle of 20 mrad which is set from the beginning between the two main tunnels. Calculations indicate emittance growth close to the acceptable limit in the presence of sextupole aberrations and Oide effects, provided the last focusing quadrupoles are properly stabilized. Collimation efficiency remains to be checked through numerical simulations. The optics, the collimator survival and the control of wakefield effects are still being studied and improved. The final focus system is tuned on β^* values of 6 mm horizontally and 70 μm vertically, which gives a peak luminosity of $8{\times}10^{34}$ cm^{-2}s^{-1} with a good luminosity spectrum. The static luminosity optimization procedure needs further studies together with the time-dependent effects and their control via feedbacks including a luminosity-related feedback. The BDS optics at 3 TeV is given in Figure 4.2, on the right.

The main-beam injection system and the drive-beam generation system are both located in a central area. The central area also includes the underground collision point, the detector cave and the main-beam dumps. Hence most of the electrical power and a large fraction of the cooling power required must be provided there. In this configuration, upgrading the

energy doesn't imply any modifications of the accelerator and ring complex. It is sufficient to make the layout suitable for a later extension of the installed electrical and cooling power in order to cope with the extra power needed for the drive-beam, and to modify the Pulse Forming Network (PFN) of the klystron modulators to cover longer pulse lengths. The distributed power required along the tunnel (mainly for the cooling systems of the rf structures) is low by comparison with the one of the central area and to first order increases linearly with its length (one service shaft per 5 power-source unit, typically). The power in the central area has a constant component (for services, detector, magnets), a component for the main-beam injectors which is constant for a constant repetition rate (but would be halved in the present assumption to reduce f_{rep} by two) and a third component for the drive-beam acceleration which basically is proportional to the ratio of the c.m. energy after and before the upgrade, divided by the reduction factor of f_{rep}.

A study of the CLIC physics prospects and of the experimental conditions is carried out for the nominal c.m. energy of 3 TeV [3]. The definition of the beam parameters and their optimization required by the physics imply close interaction between the collider design and a dedicated physics investigation. This activity aims at optimizing the experimental conditions through studies of the beam delivery and of the interaction region and the related backgrounds. In relation to machine-detector interface, it covers investigations for various beam parameters and collider characteristics of the luminosity spectra, backgrounds (muons, electron pairs, gammas, hadrons, jets, and so on) and design of the masks in front of the last quadrupole doublet. It is providing feedback to the CLIC design study on the machine parameters and has already served as a basis for proposing possible ways (see the main description) to deal with the different regimes of operation of CLIC.

BIBLIOGRAPHY for CHAPTER 4

[1] The CLIC Study Team, Ed. G. Guignard, A 3 TeV e^+e^- Linear Collider Based on CLIC Technology, Report CERN 2000-008 (July 2000).
`http://cern.web.cern.ch/CERN/Divisions/PS/CLIC/General.html`

[2] H.H. Braun, R. Corsini (Ed.), T. D'Amico, J.P. Delahaye, G. Guignard, C.D. Johnson, A. Millich, P. Pearce, L. Rinolfi, A.J. Riche, R.D. Ruth, D. Schulte, L. Thorndahl, M. Valentini, I. Wilson, W. Wuensch, The CLIC RF Power Source—A Novel Scheme of Two-Beam Acceleration for Electron-Positron Linear Colliders, CERN 99-06 (1999).

[3] CLIC - Physics Study group
`http://clicphysics.web.cern.ch/CLICphysics/`

CHAPTER 5

Test Facilities and Other Project R&D Programs

5.1 TESLA

In this section a brief description of the test facilities for the TESLA linear collider, the main achievements to date, and the future R&D program are given. Additional information on the superconducting linac technology can be found in the TESLA machine overview chapter (Chapter 3).

The development program for the TESLA technology is centered at the test facility at DESY (TTF) and has been pursued from the beginning by a broad international collaboration (initiated by the late Bjørn H. Wiik in 1992). To date, the TESLA collaboration has 44 members from 11 countries (Armenia, China, Finland, France, Germany, Italy, Poland, Russia, Switzerland, United Kingdom and USA). The TTF (Figure 5.1) includes infrastructure labs and shops for superconducting cavity treatment, test stands and the accelerator module assembly as well as a test linac for an integrated system test of the TESLA accelerator prototype with beam. Two more test facilities, focused mainly on the generation of high quality electron beams with photocathode rf guns, exist at FNAL (A0 facility) and DESY-Zeuthen (PITZ facility). At A0 the generation of flat (large ratio of horizontal to vertical emittance) electron beams using an innovative beam optics scheme were experimentally demonstrated for the first time in May 2000.

The processing of the cavities fabricated in industry involves chemical etching of the inner surfaces, high temperature treatment at 1400°C, and high pressure rinsing with ultra-pure water. Recently, electropolishing (EP) was shown to be a very successful method to achieve cavities with excellent performance. This method, pioneered at KEK, is developed in collaboration with CERN and KEK. High quality clean rooms provide a dust-free environment during the treatment and assembly procedures. All cavities undergo a quality test (measurement of Q_0 versus gradient) in a vertical bath cryostat at 2 K with continuous wave (CW) rf excitation. Some of the cavities are also tested with pulsed rf after assembly of the main power and higher order mode (HOM) couplers. So far, nearly one hundred 9-cell cavities and a number of shorter structures have been processed and tested at TTF. The evolution of cavity performance on the test stand over a period of six years is shown in

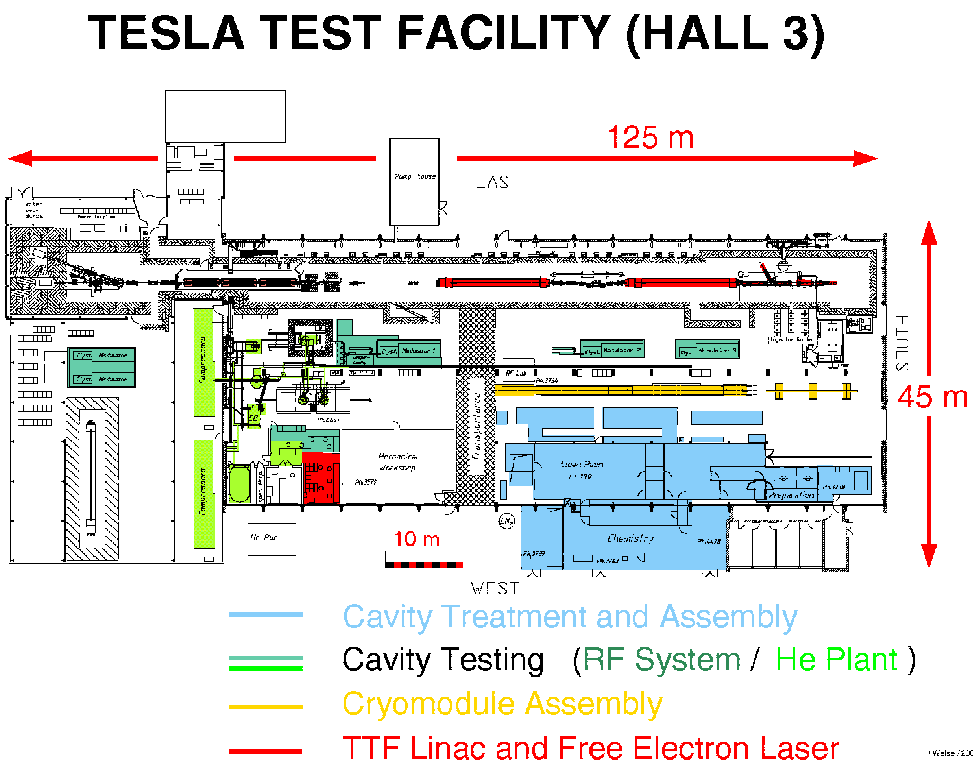

FIGURE 5.1. Layout of the TESLA Test Facility at DESY.

Figure 5.2. The two data sets shown differentiate between the performance obtained when cavities were tested for the first time and the performance after additional processing (best test). In view of future large scale production, it is particularly important that the TESLA 500 GeV design gradient has on average already been surpassed in the first test, *i.e.*, with cavities having gone through the standard treatment only once without having to be returned to the shops for additional processing. This proves that the superconducting cavity technology is mature for mass production of these accelerator structures at the required gradient of 23.8 MV/m with sufficient reliability and reproducibility. The present cavity R&D program is focused on pushing the routinely achievable gradients to higher values in order to secure the energy upgradability of the TESLA linac. The results obtained with the EP treatment for short structures (several single cell resonators reached gradients above 40 MV/m) let this method appear to be the most promising candidate for further improvement of the Niobium surface and thus the maximum accelerating field. In context with the ongoing EP R&D program, but not fundamentally linked to it, it was also found that a bakeout at very moderate temperature (typically 120°C) can be very effective to avoid a drop in the quality factor at high gradients. Application of these methods to 9-cell cavities has just started and already produced the best 9-cell cavity ever tested at TTF (see Figure 5.3). As this report is being written, another six cavities have reached gradients between 31 and 35 MV/m. More experience will be gained in the near future, and eventually an entire accelerator module with electropolished cavities will be constructed and

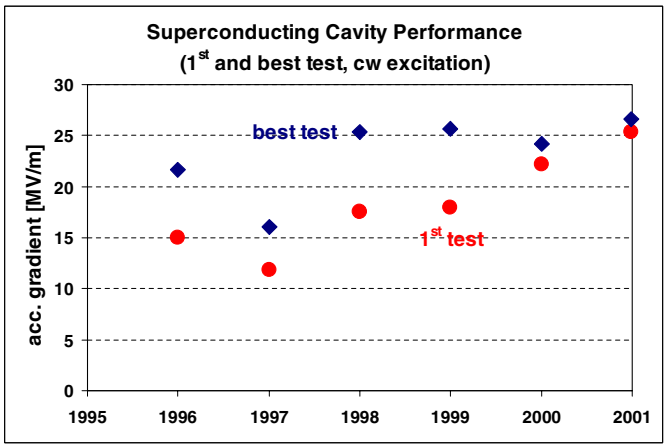

FIGURE 5.2. Evolution of the average gradient obtained with 9-cell cavities in CW-tests in the years 1995 to 2000 (the time on the horizontal axis refers to the preceding 12 month period, over which the test results have been averaged). Both data for first test and best test (after additional treatment) are shown.

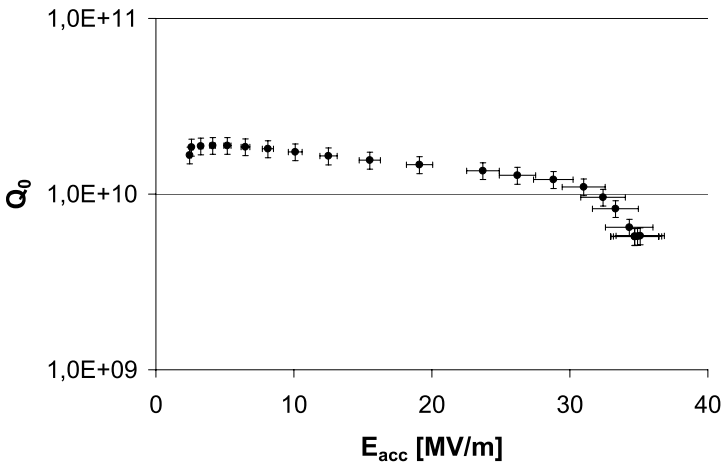

FIGURE 5.3. Performance (quality factor versus gradient) of a 9-cell electro-polished cavity on the CW test stand, March 2002.

tested. This module will also include the piezo-tuner device to compensate for Lorentz-force detuning, which has already been successfully demonstrated in a 9-cell cavity at 23.5 MV/m.

The linear accelerator at TTF serves two purposes: first, it provides an integrated system test of the TESLA linac components with beam and second, it is used as a driver for a SASE FEL in the VUV wavelength regime. This two-fold use of the TTF linac occasionally makes scheduling of beam time more complicated than for a single-purpose facility. However, there are benefits and synergies which outweigh these complications, such as having the same

operations crew for both FEL and linac technology oriented studies, and the need for a highly reliable around-the-clock operation for the FEL users as an efficient motivation and driving force to achieve this reliability in all technical components of the linac.

Operation of the linac began in May 1997 with the first accelerator module. So far, three modules have been tested with beam (at present, modules 2 and 3 are installed and in operation). The photocathode rf gun injector is capable of delivering bunch trains with parameters very close to the TESLA linear collider specifications in terms of beam current and pulse length. It also delivers bunches with sufficiently low emittance for successful operation of the FEL. A full description of the experience gained at the TTF linac in its first phase of operation (TTF-I for short) is beyond the scope of this brief overview. Among the highlights of most recent operation are the achievement of saturation at the FEL, a first successful phase of routine operation for users of the FEL photon beam, and continuous operation with accelerating gradient (21 MV/m), beam current (7–8 mA) and pulse length (0.8 ms) near the TESLA design values. While the linac rf is operated at 5 Hz repetition rate, the beam repetition rate has up-to-date been limited to 1 Hz because of insufficient stability of the photocathode rf gun.

The TTF-I program is being concluded in autumn 2002. The last tests are devoted to one more accelerator module (named module 1*, because it is the original module 1 equipped with new cavities), which is expected to yield an average accelerating gradient of 25 MV/m, and to a beam test with a first version of the so-called superstructure concept. In a superstructure, two cavities are fed with rf power by a single coupler which saves length (the fill factor is increased by 6% in comparison with the present TTF modules) and cost by reducing the number of couplers. First beam tests with two superstructures at a gradient of 15 MV/m have been performed successfully, proving the principle of this concept and confirming very satisfactory damping of higher order modes in the structures. After completion of that experimental program, the linac will be lengthened by three more modules (two of which contain only cavities which have reached 25 MV/m or more on the test stand) in an already completed additional tunnel, and the FEL installations will be modified to prepare for the second phase (TTF-II) of the user facility, commissioning of which will begin in the second half of 2003. An overview of the TTF milestone plan, together with a summary of the milestones reached during the TESLA R&D program, is given in Table 5.1.

TABLE 5.1
Milestones reached during the TESLA R&D program and schedule for the near future.

Date	Milestone
1992	TESLA Collaboration established
1994	5-cell cavities reach 25 MV/m at Cornell
1995	First TESLA 9-cell cavity reaches 25 MV/m
May 1997	Beam accelerated in first TTF module at 16 MV/m
January 1999	FNAL rf gun in operation at TTF
February 1999	Second TTF module at 20 MV/m
September 1999	Third TTF module at 22 MV/m
1999/2000	Average gradient of TESLA cavities exceeds 25 MV/m on test stand
February 2000	First lasing of TTF FEL at 108 nm wavelength
May 2000	Demonstration of flat-beam electron source at FNAL-A0
March 2001	Publication of the TESLA TDR
September 2001	TTF FEL demonstrates power gain of 10^7 in saturation at 80–120 nm wavelength
Autumn 2001	Beginning of experimental user program with FEL photon beam
January 2002	First beam at PITZ rf gun
March 2002	Electro-polished 9-cell cavity reaches 35 MV/m
Spring 2002	Routine operation of TTF linac with high up-time ($\sim$90%) near TESLA design parameters
July–Sept. 2002	Test of superstructure
July–Oct. 2002	High gradient test of 4^{th} module (module 1*)
November 2002	Beginning of extension of TTF linac to five modules (40 cavities) in total
Spring 2003	RF test of new modules 4 and 5
Second half 2003	Commissioning of TTF Phase-II

5.2 JLC-C

The ATF at KEK will also serve as a facility for an injector study of JLC-C because the beam parameters of JLC-C are almost identical to those of JLC-X/NLC. On the other hand, no special test facility for the main linac rf system for JLC-C is being planned. However, an FEL SASE source called SCSS (SPring-8 Compact SASE Source) is under construction at SPring-8 in Japan since 2001. Its rf system is almost identical to that of JLC-C so that it indeed serves as a test facility for the JLC-C. The high power test of the components including the accelerator structure and the pulse compressor will be done by

March 2003. The beam acceleration up to 500 MeV will start in the second half of 2005. 1 GeV will be reached in the second half of 2006. (These dates are subject to change due to the re-organization of SPring-8.) The layout is schematically depicted in Figure 5.4.

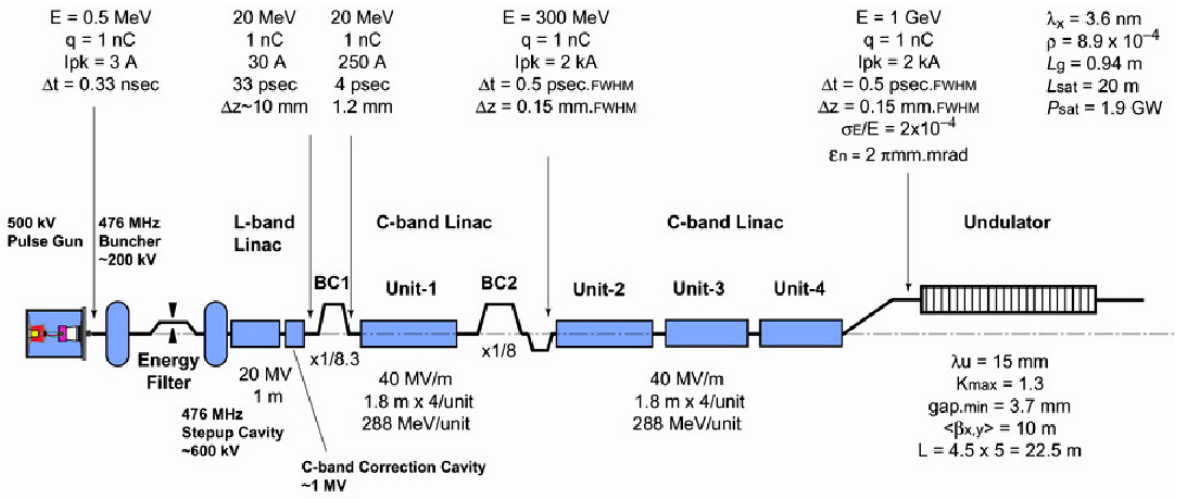

FIGURE 5.4. Layout of the first stage of SCSS.

The acceleration scenario beyond the injector is as follows:

- The electron beam parameters at the end of the first bunch compressor (BC1) are: Energy 20 MeV, bunch charge 1 nC, bunch-to-bunch spacing 2.1 ns, train length 300 ns, bunch length 4 ps (FWHM).
- The first C-band rf unit (8 m) accelerates the beam to 300 MeV.
- The second bunch compressor (BC2) compresses the bunch length to 0.5 ps (FWHM, $\sigma_z \sim 80\mu$m).
- Three C-band units (Units 2, 3, and 4) accelerate the beam to 1 GeV. The unloaded gradient in all the C-band cavities is 40 MV/m.

The first stage of SCSS will verify the performance of the following items for the JLC-C:

- RF system test as a whole, including the beam up to the full accelerating gradient.
- High power properties of the pulse compressor and the choke-mode cavity.
- RF BPM resolution and accuracy.
- Multibunch operation (this is not essential for SASE, but the same beam train length as for JLC-C has been chosen.)

There are still some differences from the JLC-C rf system:

- Solenoid-focusing klystrons are used in the SCSS.
- Multibunch beam dynamics studies are insufficient because the emittance of SCSS is 100 times larger than the vertical emittance of JLC-C and the number of rf units is much smaller. Also there is a minor difference in the bunch-to-bunch spacing (1.4 ns in JLC-C and 2.1 ns in SCSS).

5.3 JLC-X/NLC

The primary rf R&D program is centered around the NLC Test Accelerator with the accelerator structure development and the SLED-II demonstration. However, the JLC-X/NLC incorporates a very broad R&D program on luminosity related issues as well. These include the ATF prototype damping ring at KEK, the ASSET and Collimator Wakefield Test facilities at SLAC, and the Stabilization Demonstrations. In addition, the largest linear collider test facility that has been constructed was the Stanford Linear Collider (SLC). This facility was built with the dual purpose of demonstrating the feasibility of a linear collider while studying the Z^0 boson.

The SLC contained all of the same subsystems that exist in the next-generation linear colliders: a positron source, a polarized electron source, damping rings, bunch compressors, a main linac, a beam collimation system, and final foci with beam extraction lines. In addition, as will be needed in a future collider, the SLC contained extensive emittance diagnostics and many beam feedback loops that automated much of the required beam tuning. A schematic is shown in Figure 5.5.

The SLC was proposed in 1980 and construction started in 1983 with commissioning beginning in 1987. After two difficult years of commissioning, the first Z^0 was seen at the IP in 1989. A steady stream of improvements were made to the collider over the following decade including: over 50 beam size (wire) monitors to diagnose the sources of emittance dilution, beam collimators and muon spoilers to reduce backgrounds in the detector, new damping ring vacuum chambers to improve the extracted beam stability, and constant replacements of hardware that was not sufficiently reliable or stable. In addition, many new techniques were developed including: BNS damping to control the Beam BreakUp instability, new beam steering methods such as Two-Beam Dispersion Free Steering, and beam-beam deflection scans and dither feedbacks to tune the beam delivery system. In the end, the collider was operating near its design luminosity but in a parameter regime very different from that initially conceived; a plot of the beam sizes at the IP is shown in Figure 5.6. The success of the SLC is a true credit to the creativity and dedication of the large number of people who worked on it, as well as the inventiveness and audacity of its progenitors. It is also worth noting that, although the difficulties encountered when commissioning the SLC were much larger than anticipated, the single best measurement of $\sin^2\theta_W$ was still made at this facility.

Many of the detailed experiences from the SLC are either not applicable or have already been incorporated into the next-generation designs. However, it should be noted that the tolerances in the SLC were *looser* than in *any* of the current linear collider proposals

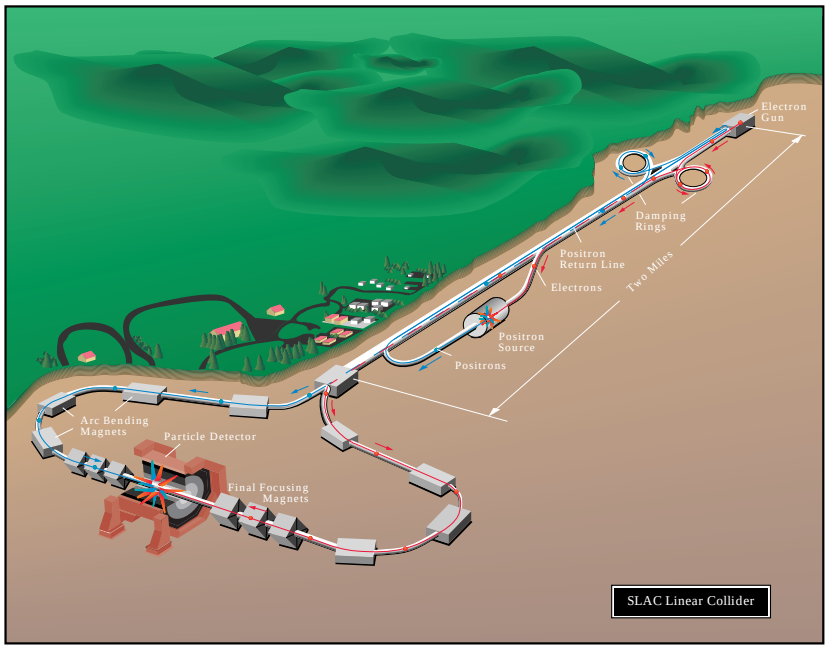

FIGURE 5.5. Schematic of the Stanford Linear Collider.

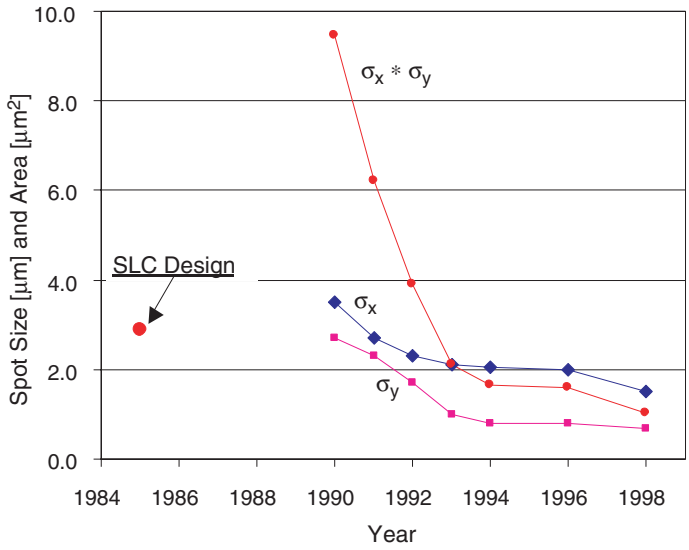

FIGURE 5.6. Spot sizes and cross-sectional area at the SLC IP as a function of time from 1990 through 1998; the design spot sizes were 1.7 μm by 1.7 μm.

and the difficulties of these future colliders should not be minimized. In particular, there are still a number of more global "lessons" that are important to remember. First, a linear collider lacks the inherent stability of the storage ring—every rf pulse differs from the previous, making hardware and beam stability, especially from the sources and the damping rings, essential. Next, reliable hardware is mandatory as demonstrated by the experience with the SLC, and more recently with the Tevatron and HERA. If the hardware interruptions are too frequent, then the collider is not up long enough to make effective progress on the luminosity. It was only after the SLC achieved reasonable reliability that the many beam tuning challenges for a linear collider could be addressed. Third, noninvasive diagnostics are needed often to determine hardware problems as well as beam physics issues. Of course, BPM's are placed throughout in all designs but the 50+ beam size monitors in the SLC allowed rapid localization and diagnosis of subtle hardware problems that would have been hard to trace otherwise. Finally, simulations do not accurately represent the true difficulty of operating the beams and tuning the luminosity. It is important to allow for multiple backup tuning solutions as well as parameter flexibility because the biggest difficulties that will likely be encountered are those that are not yet considered or simulated.

Beyond the SLC, many additional test facilities have been created at KEK and SLAC to specifically validate the X-band linear collider design. These include: the NLC Test Accelerator (NLCTA), which is an rf systems test; the Final Focus Test Beam (FFTB), which studied the issue of focusing the beam to the very small spot sizes needed to attain the desired luminosity; the Accelerator Test Facility, which is a prototype damping ring for a normal-conducting linear collider; the Accelerator Structure SETup (ASSET), which is used to directly measure the long-range transverse wakefields; the Collimator Wakefield Test, which is used to measure the short-range wakefields from beam collimator-like devices; and the Stabilization Demonstrations, which have quantified the expected stability, have stabilized a 100 kg block, and will demonstrate the required stabilization in an IR-like environment.

It should be noted that most of these facilities are dedicated to studying issues related to luminosity—only the NLCTA is devoted to the rf system goals. Although the rf system is the most visible of the technological components required for a linear collider, it is also relatively straightforward to validate. A small systems test of 0.1–1% of the rf system is all that is really needed. In contrast, validating the damping ring concepts, the particle sources, the emittance preservation, or the beam delivery system could be a much more daunting task. Fortunately, the normal-conducting designs allow the linear collider subsystems to be based on other operating accelerators or accelerator subsystems as well as making use of the essential experience from the SLC. In particular, the polarized electron source and the positron production system are modest extensions of the SLC sources. The damping rings are similar to third-generation synchrotron light sources and are required to produce an equilibrium emittance that is only a factor of 2 below what has been achieved at the Advanced Light Source (ALS) in Berkeley or the ATF at KEK. The bunch compressor is based on experience from the SLC bunch compressor and is similar to, although not as difficult, as the bunch compressors for the new SASE-based short wavelength FEL drivers. Much of the emittance preservation techniques and the final focus systems were demonstrated at the SLC and the Final Focus Test Beam (FFTB).

5.3.1 NLC Test Accelerator

The Next Linear Collider Test Accelerator (NLCTA) has been a testing ground for the X-band rf system components and has demonstrated the viability of an early version of the NLC rf system. The facility was proposed in the early 1990s to provide system integration testing of the NLC X-band rf components being developed at SLAC and KEK while these systems were still in an early stage of development. The design philosophy was to make it large enough to yield meaningful operating statistics, and to make it capable of accelerating an NLC-like beam to verify performance, especially in regard to the beam loading compensation. The system was rapidly commissioned and in 1997 accelerated beam to 350 MeV while demonstrating the desired beam loading compensation. The system was upgraded in 1999 to deliver twice the rf power to structures to be able to generate higher acceleration gradients, and the rf control system was upgraded to allow around-the-clock unmanned operation.

The rf system design of the NLCTA is similar to that proposed in the 1996 NLC ZDR. The initial implementation of the NLCTA contained four rf stations (including the injector), each of which consisted of a modulator powering a single 50 MW klystron which drove a SLED-II pulse compression system. The SLED-II pulse compression systems compressed the 1.5 μs klystron pulses by a factor of 6 in time and gained a factor of 4 in peak power. The resulting 200 MW, 240 ns pulses in the NLCTA powered two 1.8 m long X-band accelerator structures (100 ns fill time) to produce $\sim$ 50 MV/m unloaded gradients.

A schematic of the NLC Test Accelerator is shown in Figure 5.7. The fourth rf station shown in the figure was later eliminated from the plan. The first rf station is used to power the injector, which was designed to generate beams with NLC-like currents ($\sim$1 A), but with the bunch spacing equal to the X-band period (88 ps). The beam source is a 150 kV, thermionic DC gun, and the injector is followed by a chicane that allows for collimation of the longitudinal bunch tails generated by the direct DC-to-X-Band bunching. The two accelerator structures used in the injector are half the nominal length to reduce the beam loading and allow for higher currents which compensate the collimation losses in the chicane (typically 1/3). To improve the bunching efficiency, the first structure has a low beta section in its upstream end and is preceded by two pre-bunching cavities, all powered from the SLED-II pulse.

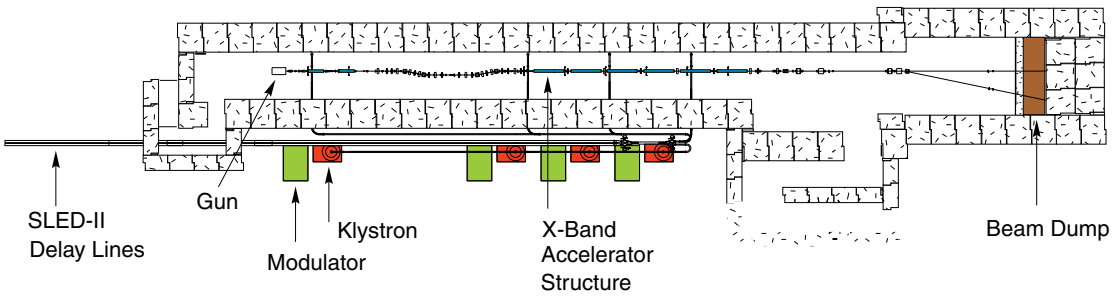

FIGURE 5.7. Schematic of the NLC Test Accelerator.

The injector was commissioned in late 1996 and, by the end of 1997, both linac rf stations were operational and the pairs of 1.8 m structures were typically run at unloaded gradients of 44 MV/m in the first station and 37 MV/m in the second station. At these levels, beam-loading compensation measurements were made that demonstrated 17% compensation to within the 0.3% level required for the NLC. The facility delivered beam with a peak energy of roughly 350 MeV. A photograph of the beam line, with the four 1.8-m accelerator structures after the injector, is shown in Figure 5.8.

FIGURE 5.8. Photograph of the beam line in the NLC Test Accelerator.

Subsequent operation brought the gradients up to the 50 MV/m design value but the maximum gradients were limited by rf breakdown. The standard processing technique is to process to higher than nominal gradient and then reduce the gradient for operation. However, to achieve higher gradients, upgrades to the rf stations were required. During a two to three year period, both of the linac modulators were partially rebuilt, some of the SLED-II components replaced with ones capable of handing higher peak power, and a second 50 MW XL4 klystron was added to each station. Also, an automated rf processing system was developed and the machine protection system improved to allow for around-the-clock, unmanned structure processing.

During this period, the NLCTA program focused on processing one of the Damped-Detuned Structures (DDS) to 73 MV/m with 240 ns pulses. After roughly 1000 hours of processing at 60 Hz, it became clear that stable operation at such a gradient would not be attainable. Also, *in situ* beam-based measurements of the structure phase advance profile revealed large changes, suggesting substantial erosion of copper, in the upstream structure irises. The 1.8-m accelerator structures are nearly constant-gradient structures and thus the iris radii and the rate of rf power flow is large at the upstream end. Subsequent measurements

of the other structures in the NLCTA showed similar patterns of damage occurring at gradients as low as 50 MV/m. This prompted an aggressive program to develop more robust high-gradient structures.

Before operating the relatively long 1.8-m prototype structures, many shorter X-band accelerator structures had been processed to much higher gradients. Single cell standing-wave cavities had operated at 150–200 MV/m and a short 20 cm structure had operated at 120–150 MV/m. In addition to being much shorter than the prototype 1.8-m structures, all of these structures had much lower rates of rf power flowing through the structure. Given this previous experience and the observed pattern of damage in the 1.8-m structures, where only the upstream end seemed to be affected, it was hypothesized that the damage was related to the group velocity of the rf power flowing through the structure. To study this idea, the first test structure was constructed by cutting off the last 1/3 of the DS2 structure, so that the maximum group velocity was 5% instead of 12% of c, and brazing on a new input coupler. This structure rapidly processed ~ 65 MV/m.

Next, a series of test accelerator structures were constructed to explore the dependence of the damage and breakdown on both the structure length and on the group velocity of the rf power through the structure. Both traveling-wave and short standing-wave structures were built and tested. In addition, new processing, cleaning, and handling procedures were implemented. While these tests confirmed the initial hypothesis that there is a strong correlation between the group velocity and the breakdown/damage gradient levels, the test structures were still limited to operating at gradients of ~ 70 MV/m due to the breakdown rate in the input and output couplers.

Most recently, it was found that pulsed heating in the input and output couplers may have been limiting the true performance of these test structures. Sharp edges in the coupler design were observed to have significant damage while the rest of the structures looked fine. Figure 5.9 is a photograph of one of these edges which shows damage that looks like melting of the copper although the expected temperature rise was relatively low.

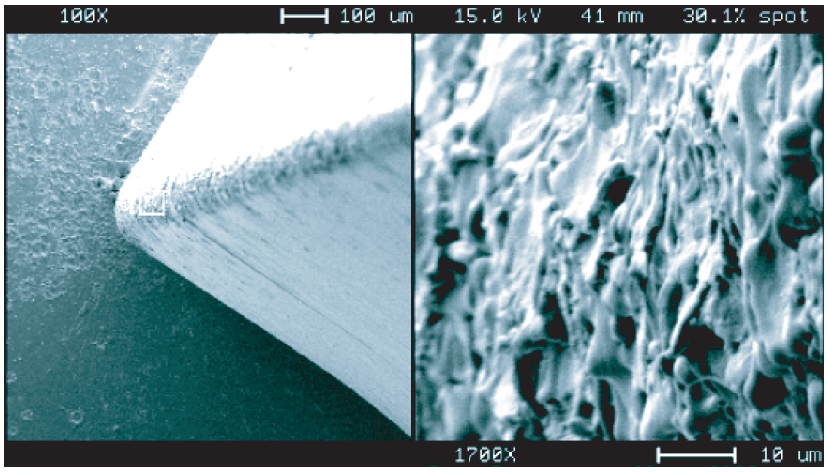

FIGURE 5.9. Scanning electron microscope photograph of damage along the sharp edge of an input coupler under two different magnifications.

The latest test structure was constructed with new input and output couplers. This structure was rapidly processed to 80 MV/m and then operated stably at 73 MV/m with a breakdown rate much less than required for JLC-X/NLC operation. It was subsequently processed up to 92 MV/m and has been operating at 90 MV/m with less than one breakdown event per day, a factor of 2 better than the JLC-X/NLC specification. The gradient performance of a number of the test structures is shown in Figure 5.10. Clearly, the latest structure, with the improved couplers, is performing well above the gradients desired for the JLC-X/NLC. Note, however, that the T-structures do not yet include the damping slots and manifolds.

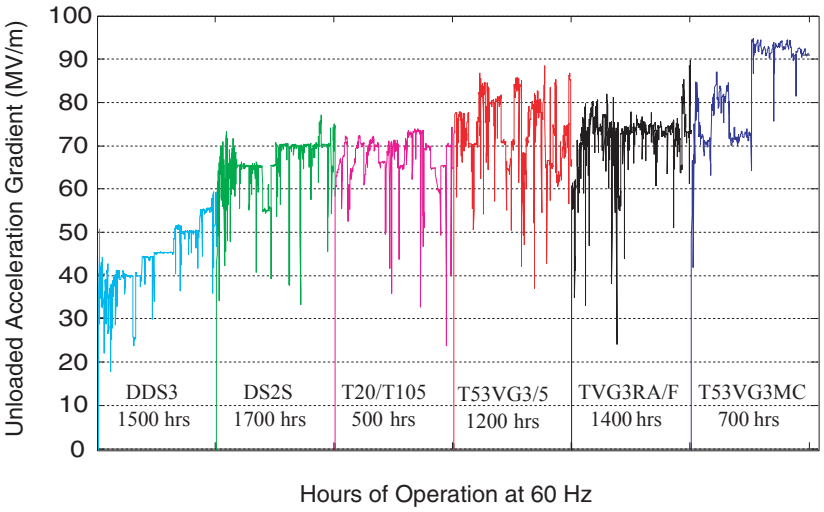

FIGURE 5.10. Gradients achieved in DDS3, a 1.8-m structure, and a number of test structures constructed from 2000 through 2002; note that most of the test structures exceeded the 70 MV/m goal and the most recent test structure, with a new design for the input and output couplers, is operating at 90 MV/m.

The structure testing for the gradient program has been done exclusively at NLCTA using the four accelerator slots in the two linac rf stations. To date, 12 structures have been tested in the two rf stations, which have been run in parallel for about 7000 hours at 60 Hz. As part of this testing, the SLED-II pulse compression systems have operated stably, producing up to 280 MW, 240 ns pulses. Although there have been klystron failures due to cracked windows and vacuum leaks, none have failed for more fundamental reasons (*e.g.*, chronic beam interception) after more than 30,000 hours of operation.

While the NLCTA essentially demonstrated an X-band rf system, construction of the facility began in 1993 when the rf components were still at an early stage of development. For example, the modulators that were built were of a line-type design, like the SLAC Linac modulators, with PFN's, thyratrons and transformers, rather than the current design which is based on solid-state switches. Similarly, the XL4 klystrons that were installed are solenoidal focused and not the periodic permanent magnet (PPM) focused tubes that are envisioned for the NLC. The SLED-II pulse compression system that was built was an improved version of the one initially tested to 200 MW in the SLAC Klystron Test Lab but is a single-moded design with components whose ultimate power handling capability is

probably more limited than that currently needed. Finally, the original accelerator structures were of the DS and DDS design that had been built to test long-range wakefield suppression methods but were limited to operating at ~ 40 MV/m by rf breakdown and damage.

To test the present generation of X-band rf components, the NLC Test Accelerator is being upgraded. A solid-state modulator has been installed and will power four additional XL4 klystrons. These will feed a dual-mode SLED-II pulse compression system to produce roughly 600 MW in 400 ns by the middle of 2003; this is 30% greater than the present JLC-X/NLC specification. Finally, the rf power will be delivered to the NLCTA enclosure and will power 5.4 m of accelerator structure. In parallel, further testing of the PPM klystrons at KEK and SLAC will complete the demonstration of the JLC-X/NLC rf power source. During this period, the original NLCTA rf stations will continue to be used for high gradient testing. Full JLC-X/NLC prototype structures with the short-range and long-range wakefield control (HDDS1/HDDS2) will be tested in the middle of 2003 to verify the gradient performance.

5.3.2 Accelerator Structure SETup

The Accelerator Structure SETup (ASSET) is a facility dedicated to measuring the long-range transverse wakefield from an accelerator structure. The facility was constructed in 1995 and is located in Sector 2 of the SLAC linac. It uses the 1.19 GeV damped electron and positron beams from the SLC damping rings; the positron bunch comes first and excites the cavity, and the electron beam is then used to measure the resulting transverse wakefield. A chicane directs the positron beam to a dump, and the wakefield deflection of the electron beam can be detected using the ~ 30 BPMs along Sector 2 which yield a resolution on the transverse wakefield measurements of roughly 0.1 V/pC/mm, more than sufficient for the JLC-X/NLC beam dynamics. The timing of the two beams can be adjusted so that the wakefield can be measured in the time domain, exactly as the bunch train would sample the wakefield, without resorting to a scan in frequency space that can miss high-Q resonances or the impact of higher frequency bands. A schematic of the facility is shown in Figure 5.11.

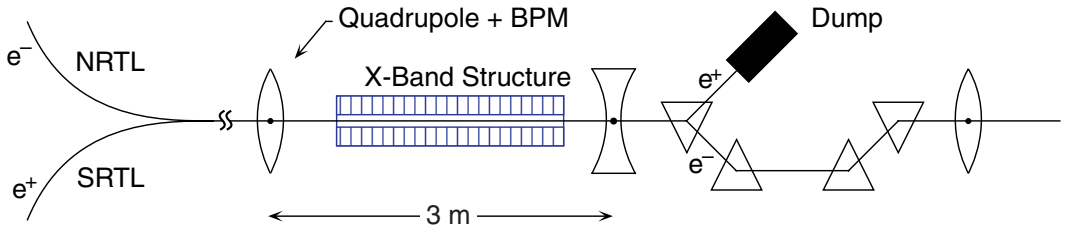

FIGURE 5.11. Schematic of the ASSET test facility.

The facility has been used to measure the wakefields in five JLC-X/NLC X-band accelerator structures as well as a JLC-C choke-mode structure from KEK and an X-band structure from CERN that was designed to study strong damping of the transverse wakefield as

proposed for CLIC. The accuracy of the measurements has been used to benchmark the wakefield calculation codes as illustrated in Figure 3.45 of the JLC-X/NLC Overview. The facility has also been used to verify the dipole-mode Beam Position Monitor (S-BPM) concept which would be used to align the X-band accelerator structures in the JLC-X/NLC linear collider. The resolution of the S-BPM is submicron and the accuracy appears to be similar.

The ASSET facility will continue to be used to measure the long-range wakefields of the JLC-X/NLC prototype structures. The next structure to be tested, the HDDS2, will be ready in mid-2003. This structure design will be tested in both the NLCTA to demonstrate the gradient performance as well as ASSET to verify the wakefields. In parallel, a dual-wire measurement is being developed as an alternate technique of directly measuring the transverse wakefield. This technique should prove to be much simpler and speedier to implement than mounting the structures in the ASSET facility and then measuring the wakefields using a beam. The ASSET facility will be used to benchmark this alternate approach.

5.3.3 Collimator Wakefield Test

To keep the background levels in the detectors manageable, the beam tails will have to be collimated with very high efficiency in all of the linear collider designs. Unfortunately, the transverse wakefields from any components that are placed close to the beam, such as a collimator, may amplify the beam jitter or dilute the beam emittance. There are few quantitative measurements of the collimator wakefields and it is difficult to model or calculate the high-frequency impedance due to a tapered planar collimator.

The collimator wakefield test facility is a dedicated facility that was designed to measure the short-range transverse wakefields induced by collimators or similar components that must be placed close to the beam. It is located in Sector 2 of the SLAC linac, close to the ASSET facility, and uses the damped 1.19 GeV beams from the electron damping ring. The apparatus consists of a large vacuum vessel roughly $1.7 \times 0.6 \times 0.3$ m into which an insert with up to five collimator apertures is placed. The vessel and insert can be moved vertically in 1 μm steps over a distance of ± 1.5 mm. The wakefield measurements are performed by moving the collimator and measuring the resulting deflection of the beam on $\sim$30 downstream BPMs. The resulting resolution of the transverse wakefield is better than 0.1 V/pC/mm. A photograph of the facility and a typical measurement are shown in Figure 5.12.

At this time, two inserts have been measured: a set of copper collimators to measure the geometric wakefields and benchmark the analytic approximations and a set of graphite collimators constructed at DESY. In 2003, it is planned to measure a set of collimators that will study the resistive wakefields and another set to study geometric wakefields in a regime that is closer to that expected in the JLC-X/NLC. Depending on the results, future studies can be scheduled as needed.

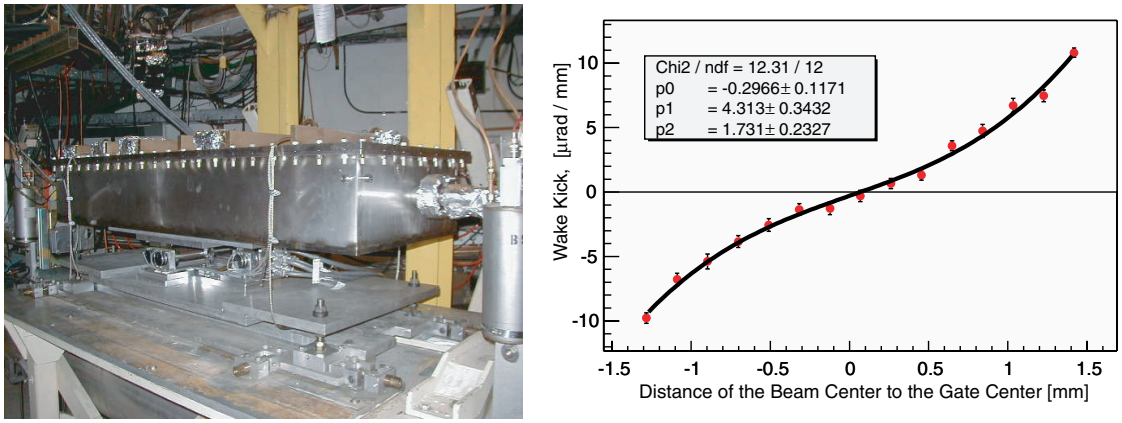

FIGURE 5.12. Photograph of the collimator wakefield test facility and an example of a measurement which also shows the nonlinearity of the wakefield when the beam is close to the collimator edges.

5.3.4 KEK Accelerator Test Facility

Aside from the SLAC/SLC, the ATF is the only linear collider R&D facility devoted to the production of low emittance beams, a critical challenge in LC beam dynamics and technology. The ATF is by far the largest of the linear collider test facilities, and includes a 1.5 GeV S-band injection linac, a ∼130 m circumference damping ring and an extraction line for beam analysis.

The ATF was built to demonstrate the feasibility of producing the low emittance beams required for a linear collider. As such, it has focused primarily on beam dynamics issues rather than technology. Experience from the SLC has shown that while technology is an important cost factor, beam dynamics, especially in the damping ring, can be a critical performance limitation. Technology development at ATF is centered on precision beam instrumentation, stabilization techniques and tuning methods.

The ATF international collaboration was formed in 1992 and initially included all major labs then involved in LC R&D. Construction was completed in 1997 and since then, the ATF has operated 20 weeks per year. Active members in the ATF collaboration include KEK, eight Japanese Universities, SLAC, LBNL, BINP and Tomsk.

The layout of the ATF is shown in Figure 5.13 while the design parameters are summarized in Table 5.2 and compared with what has actually been achieved. The emittances given are based on wire scanner measurements of the extracted beam, with the ring operating at 1.28 GeV in single bunch mode. The quoted errors are estimated from analysis of the fitted wire scanner data, combined with the observed statistical fluctuations of the measurements.

To achieve the low emittance goal, ATF operation has focused on six main areas of investigation: (1) tuning techniques and error correction, (2) single bunch collective effects (*e.g.*, intrabeam scattering), (3) wiggler performance, (4) damping ring acceptance, (5) extracted beam jitter, and (6) multibunch instabilities.

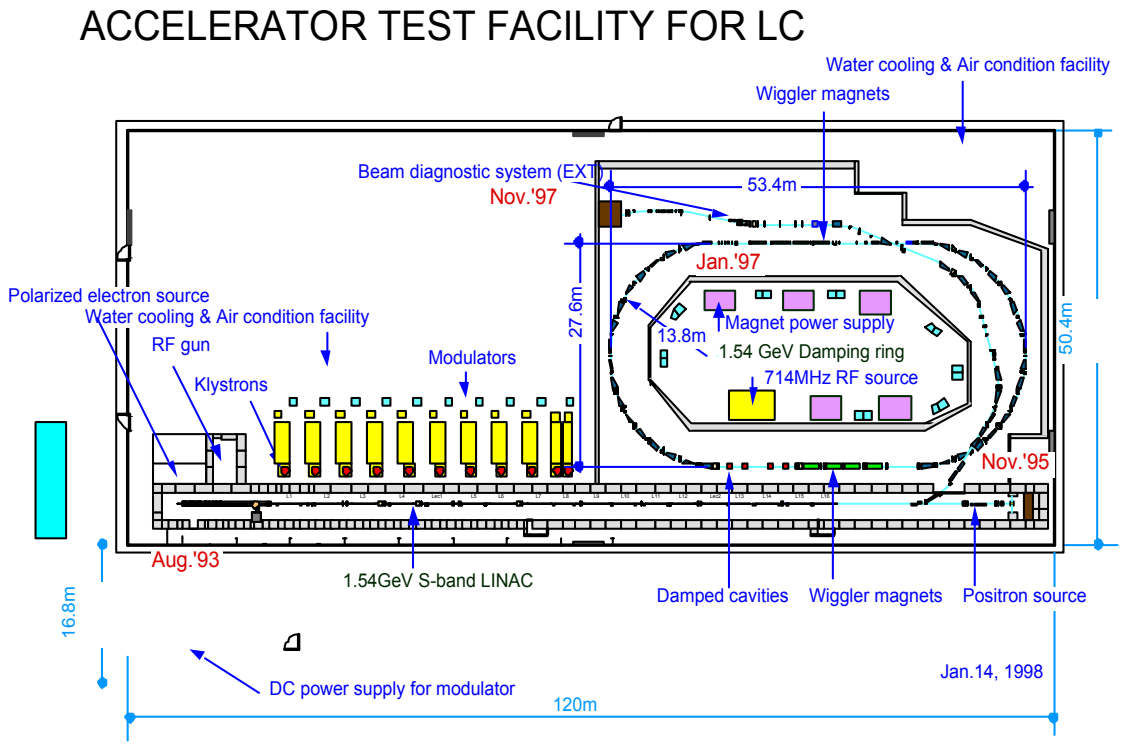

FIGURE 5.13. Layout of ATF.

TABLE 5.2
The design goals of the ATF and the accelerator performance achieved. The numbers in parenthesis indicate the number of particles per bunch for the particular measurement.

Items	Achieved Values	Design
Linac status		
Maximum beam energy [GeV]	1.42	1.54
Maximum gradient with beam [MeV/m]	28.7	30
Single bunch population	1.7×10^{10}	2×10^{10}
20 multibunch population	7.6×10^{10}	20×10^{10}
Energy spread (full width) [%]	<2.0 (90% beam)	<1.0 (90% beam)
Damping ring status		
Maximum beam energy [GeV]	1.28	1.54
Momentum compaction	0.00214	0.00214
Single bunch population	1.2×10^{10}	2×10^{10}
COD (peak to peak) [mm]	x ∼2, y ∼1	1
Bunch length [mm]	∼6	5
Energy spread [%]	0.08	0.08
Horizontal emittance [m·rad]	$(1.33\ \pm0.04)\times10^{-9}$ (2×10^{9})	1.4×10^{-9}
	$(1.94\ \pm0.11)\times10^{-9}$ (8×10^{9})	
Vertical emittance [m·rad]	$(1.1\ \pm0.1)\times10^{-11}$ (2×10^{9})	1.0×10^{-11}
	$(2.2\ \pm0.1)\times10^{-11}$ (8×10^{9})	
Multibunch population	$19\times(0.6\times10^{10})$	$20\times(1\times10^{10})$
Multibunch vertical emittance [m·rad]	$(2\text{–}3)\times10^{-11}$	1.0×10^{-11}

5.3.4.1 Emittance

The primary design goal of the ATF damping ring is to obtain a vertical normalized emittance less than 3×10^{-8} m·rad with a high intensity ($0.7–3.0\times10^{10}$ e^-/bunch) multibunch (10–40 bunches/train) beam. The ATF damping ring currently operates at 1.28 GeV beam energy at a repetition rate of 3.125 Hz with one bunch train of 20 bunches with 2.8 ns bunch spacing and $0.1–1.0\times10^{10}$ particles/bunch. Extremely low emittance studies have been done in single bunch mode, resulting in the smallest single bunch, low current emittance recorded in the world, 2.8×10^{-8} m·rad (normalized).

The tuning procedure to obtain low emittance involves the successive application of steering, dispersion, and coupling corrections. Considerable work has been done to characterize the damping ring optics, resulting in high confidence in the present model. For instance, beam-based magnet field measurements (lattice diagnostics) uncovered quadrupole field-strength errors on the order of 1%. Correcting the optics model to account for these errors produced a model accurate to 0.01%. To correct residual alignment errors, beam-based alignment of focusing and sextupole magnets has begun. In late 2002, using new high-resolution ring BPMs, a quick, accurate beam-based alignment procedure has been developed to provide insight into the nature of the optics corrections that are presently used for emittance optimization. This should make it possible to identify sources of instability and quantify the physical limits on the minimum vertical emittance. This is one of the highest priority beam studies.

The contribution of the wiggler magnets to the damping time was found to be consistent with the design. However, they are not presently used because of a dynamic problem (the first field integral differs considerably from zero).

The transverse acceptance after tuning was found to be 0.38×10^{-6} m·rad, which is considerably smaller than the design specification of 0.90×10^{-6} m·rad (3σ of the assumed injected beam size) and also smaller than the simulation value from SAD of 1.5×10^{-6} m·rad ($\Delta p/p = \pm1.5\%$). However, the measured value is still more than 3σ of the actual injected beam size (rms 0.040×10^{-6} m·rad).

During ATF construction, the floor was carefully engineered with 14 m deep concrete pilings in order to produce a mechanically stable platform for the ring. Nonetheless, early experience with the ring showed a sensitivity of the floor to thermal and seasonal drifts, especially in the circumference. Correction procedures have been developed.

With respect to intrabeam scattering, single bunch studies have shown a dependence of the measured emittance on both the bunch current and the longitudinal emittance, indicating strong intrabeam scattering (IBS). The results indicate a stronger effect than would be suggested by current IBS theory, and further study is needed. With the installation of an rf photocathode gun as described later, it will be possible to continue these IBS studies at higher current, with charge up to 2×10^{10} e^-/bunch.

5.3.4.2 Extraction kicker

To stabilize extraction from the damping ring, the ATF has a double kicker system in the ring and extraction line which compensates for jitter in the kick angle due to the kicker magnet. This scheme has been shown to reduce the extracted beam fractional jitter to

2.8×10^{-4} in single bunch mode. The improvement due to the double kicker cancellation is at least a factor of 3.3. The multibunch performance of this system has not yet been verified, but this will be done when a multibunch BPM currently being developed becomes available.

5.3.4.3 R&D on Diagnostic Devices

Additional studies at ATF have been aimed at developing the technology required to accurately measure very small beams. There are five wire scanners in the extraction line, a laser-wire monitor in the ring, and Optical Transition and Diffraction Radiation (OTR and ODR) monitors under development in the extraction line.

The ATF **laser wire** closely resembles a design which is expected to be widely used in the LC. A laser beam with a very thin waist is generated in an optical cavity formed by nearly concentric mirrors. The laser intensity is amplified by adjusting the cavity length to meet the Fabry-Perot resonance condition. The cavity constructed for the ATF has produced a beam waist of 12 μm (2σ) and an effective power of 100 W, with good long-term stability. The laser wire is installed in the ring at a location with a transverse electron beam size of $\sim$10 μm. It has been used over the last year to make accurate measurements of the vertical emittance of each bunch in the ring.

Optical Transition Radiation profile monitors are also expected to see widespread use in the LC in order to provide one-shot images of low emittance beams with a resolution well below typical beam sizes. The 2-D image produced by OTR is desirable in order to accurately determine x-y and y-z coupling and other phase space distortions. A monitor currently being tested has the resolution required for LC design parameters (2 μm), well below the current state of the art for such monitors (20 μm). To date, beam sizes of 5 μm have been imaged and tests of transition radiation target longevity have been done.

A "proof-of-principle" experiment on the use of **Optical Diffraction Radiation** (ODR) as a single pulse beam profile monitor has been done using the electron beam extracted from the DR. Measurements have been made of the yield and the angular distributions of the optical diffraction radiation from a thin metal target at different wavelengths, impact parameters and beam characteristics.

5.3.4.4 Polarized Positron Production

Studies are underway at ATF to demonstrate a new method of generating highly polarized positrons through Compton scattering of polarized laser light off relativistic electron beams, where the photons produced are subsequently converted into pairs. A preliminary experiment was performed in the ATF extraction line in 2002, and a yield of 1×10^{6} polarized photons/pulse was measured.

5.3.4.5 Multibunch Operation

An early study for multibunch operation demonstrated a new technique for beam loading compensation in the injector linac, where two rf side-bands were applied to compensate for the bunch-by-bunch energy deviation due to beam loading.

In October 2002, the thermionic gun and buncher system were replaced by a Cs2Te cathode rf source in order to increase the injection efficiency into the ring to ∼100% and to improve performance during multibunch operation. This successfully doubled the stored charge in the ring (6×10^9/bunch with 19 bunches), but the charge uniformity and stability is still poor due to the available laser and will be improved soon. The higher charge will allow more precise studies of single bunch intensity dependent phenomena such as intrabeam scattering, fast ion instability and impedance effects.

5.3.4.6 Future plans

The immediate ATF goals are understanding the minimum achievable single bunch emittance and obtaining stable operation with three 20 bunch trains. A program of theoretical and experimental studies has been planned that is focused on understanding the correction and optimization procedures, the stability of the ring component alignment, intrabeam scattering emittance growth and the multibunch beam dynamics mentioned before. Table 5.3 lists ATF historical milestones and plans.

TABLE 5.3
ATF timeline and plans

Date	Milestone
1992	ATF Collaboration established
1993	Injector completed (80 MeV)
1995	Linac completed
1997	Ring and extraction transport completed
1998	Vertical emittance measurement using Touschek effect and high resolution synchrotron light interferometer
2000	Vertical emittance minimization using wire scanners and intrabeam scattering results
2001	Photocathode gun tests showing excellent transmission
2001	Instrumentation achievements: ring laser wire, high precision OTR, multibunch BPMs and X-ray SR beamline
2002	Photocathode gun installation and BPM upgrade for beam-based alignment
2003	Beam-based alignment
2003	Multibunch instability studies
2004	3 pm·rad single vertical emittance (0.75×10^{-8} m·rad normalized)
2004	High intensity multibunch operation (1×10^{10} e^- in each of 20 bunches)

5.3.5 Final Focus Test Beam

The Final Focus Test Beam (FFTB) at SLAC was constructed during the early 1990s by an international collaboration that included most of the laboratories interested in linear colliders at that time. The primary goal of the facility was to focus the low emittance 50 GeV SLAC electron beam down to a spot of 1 μm by 60 nm with beta functions of $\beta_x^\star$=3 mm and $\beta_y^\star$=100μm. This was to demonstrate the optical demagnification that would be required in a future linear collider. A secondary goal of the experiment was to develop and demonstrate some of the high resolution diagnostics, controls, and tuning schemes that would be required in a future collider.

To achieve the small spot sizes, the final focus system is roughly 180 m long with another 180 m of beam line that transports the low emittance beam from the SLAC switchyard to the final focus proper. From the beginning, the FFTB contained 34 quadrupole magnets, 14 dipoles, and 8 sextupoles. The optics was chromatically corrected to third-order by placing the correction sextupoles in pairs, separated by a $-I$ transform, and not interleaving the horizontal and vertical chromaticity corrections. This is quite similar to the correction schemes presently proposed for the future linear colliders.

Each of the quadrupole and sextupole magnets was installed on a remote-controlled magnet mover which had a range of $\pm$1.5 mm horizontal and vertical motion and $\pm$5 mrad rotation about the beam axis, and a step size that was 0.3 μm and 1 μrad, respectively. These magnet movers reduced the need for dipole correctors, and very few correctors were installed. In addition, high resolution BPMs were mounted in the bore of each quadrupole; these BPMs were measured to have pulse-to-pulse resolutions that were 1 μm and drifts of less than 3 μm per week. A set of three 5.7 GHz rf BPMs were also installed at the nearest upstream vertical image of the IP where the nominal beam size was 500 nm; these BPMs were measured to have a resolution of 30 nm. Finally, wire scanners with wire diameters of 3.8 μm were installed and used to measure beam sizes of 0.7$\pm$0.1 μm with aspect ratios of 200:1. All of these diagnostic and control devices demonstrated performance close to what will be needed in a future linear collider. Figure 5.14 shows a schematic of a magnet mover and the reconstructed beam trajectories through the three rf BPMs along with the BPM resolution that can be extracted from the three simultaneous measurements.

The FFTB ran six times between 1993 and 1997 with periods that ranged from a few days to almost two weeks. During the runs, beam-based alignment would be used to align the quadrupoles and sextupoles and verify the quad-to-BPM offsets. The linear optics would then be tuned and finally the nonlinear optical elements would be adjusted to achieve the small spot sizes. The left side of Figure 5.15 shows a histogram of the measured vertical spot size from the December 1997 run. The measured spot size was 70$\pm$7 nm, and was stable over a 48 hour period. The expected spot size at this time was 59$\pm$8 nm, including contributions from both the actual rms size of the beam and the rms beam jitter at the focal point, which was measured to be approximately 35 nm; the expected spot size is shown in Figure 5.15 by the red bar above the histogram. Similar results had been measured during previous runs. The right side of Figure 5.15 shows the signal from the Shintake Laser-Interferometer IP beam size diagnostic during the December 1994 run. The beam size is measured with Shintake monitor by detecting the Compton scattered electrons while scanning the beam across the interference fringes generated by crossing two laser beams at a small angle. This device has a beam size resolution of roughly 40 nm.

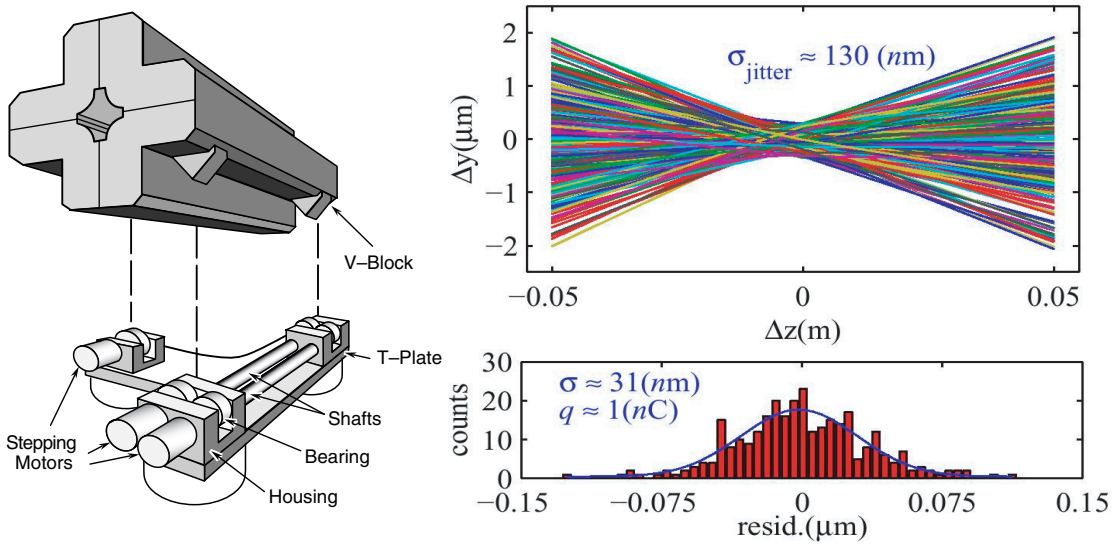

FIGURE 5.14. Examples of diagnostics and controls developed for the FFTB: (left) schematic of a remote magnet mover with 300 nm steps in X and Y and (right) measured beam trajectories through an rf BPM triplet having ∼30 nm resolution showing 130 nm of beam jitter.

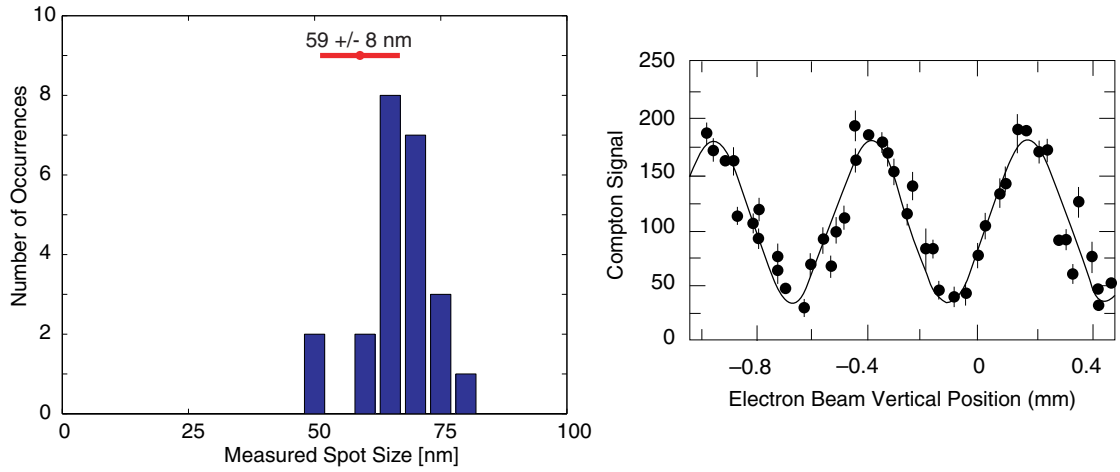

FIGURE 5.15. Histogram of the FFTB vertical spot size measurements (left) with an average of 70±7 nm versus the expected size of 59±8 nm and (right) a plot showing a typical measurement using the Shintake laser interferometer corresponding to a 77 nm beam spot.

Most of the magnets were installed on vibration-damped Anocast stands and there appears to be little amplification of the natural ground motion by the support, mounting, or mover system. In addition, measurements comparing the motion with and without coolant flow show a difference of only 2–3 nanometers. Because they were significantly larger and heavier, the final doublet magnets were mounted on a special table with a separate mover system. Subsequent vibration measurements showed that the table was moving by about 40 nm. This is consistent with independent measurements of the motion of the beam relative to the IP beam size diagnostic.

In summary, the FFTB project demonstrated that the optical demagnification required by the linear collider designs is possible to achieve and maintain. The project also developed and then demonstrated much of the diagnostic and control hardware that will be needed in a future linear collider including the high-resolution beam position monitors, beam size monitors, and magnet movers. Finally, many of the tuning and beam-based alignment techniques that will be needed were demonstrated giving additional confidence in the linear collider designs. At this time, the FFTB enclosure is being utilized for other purposes and there are no plans to revive the beam line as a final focus system.

5.3.6 Stabilization Demonstrations

The stabilization demonstrations involve work on four different fronts. First, extensive vibration and drift measurements have been made around the world to understand the natural levels of motion. In particular, fast ground motion (relevant for collision stability) has been measured at many laboratories as well as the potential NLC sites in California and Illinois and many of the JLC sites in Japan; the spectra from some of these measurements can be seen in Figure 3.52 of the JLC-X/NLC Overview. Most of the sites considered thus far are sufficiently quiet that there is a significant margin for additional cultural noise. In addition, to understand the tolerances on the cultural noise, transmission measurements from either the surface to the tunnel or between two twin tunnels are being carried out or will be made in 2003. Results of these studies will guide the design of passive vibration protection for the vibration producing equipment. Similarly, the slow motion (relevant for emittance preservation) has been studied extensively at FNAL, SLAC and locations in Japan. These sites are expected to have tolerable slow ground motion, as confirmed either by direct measurements or by comparison with geologically similar sites. As part of the investigation of the slow ground motion a new hydrostatic level system has been developed with submicron resolution. Such a system may also be used as part of the alignment system for a future linear collider.

Second, the effect of cultural vibration sources on the stability of the linac quadrupoles has been studied because, although the jitter tolerances are relatively loose at 10 nm, there are thousands of magnets that require this level of stability. The feasibility of such stability has been demonstrated in several earlier independent measurements, such as those at the FFTB; however in the linacs there may be additional sources of noise. Presently, SLAC and FNAL are studying the vibration transmitted to the quadrupoles from rf structures, which may have large vibration due to the flow of cooling water. Preliminary tests, which used a simplified model of the linac rf girder, showed ∼300 nm of motion on the rf structure but little coupling of the structure to the quadrupole and confirmed the feasibility of achieving

the required quadrupole stability. Design of a full linac girder prototype is ongoing and will be done with consideration of the stability requirements.

Next, the final doublet magnets, that focus the beams down to the very small spot sizes at the IP, have tolerances of roughly 1 nm, a factor of 10 tighter than most of the other quadrupoles. Furthermore, the supports for these magnets are complicated because the magnets are, at least partially, located inside the high-energy physics detector. For these reasons, it is thought that some active stabilization system will be required for these magnets. Although commercial systems are available that can achieve the required stability, they are not well adapted to the details of the interaction region where an extended object must be stabilized in a very compact region with strong magnetic fields. To this end, a program at SLAC has used inertial sensors and electrostatic actuators to stabilize a 100 kg block in six degrees-of-freedom and is developing compact, nonmagnetic, high performance sensors; these are shown in Figure 5.16. In 2003, this inertial system will be used to stabilize an extended object that more closely represents a final quadrupole magnet, and then the system will be demonstrated in an environment that approximates the real interaction region. In parallel, an "optical anchor," where optical interferometers are used to rigidly anchor an object to an accurate reference, is being studied at the University of British Columbia. This system has the advantage of having better low frequency (f <1 Hz) performance than the inertial systems but must be based on a very stable reference. It is likely that the final system will involve a combination of inertial stabilization and optical anchors.

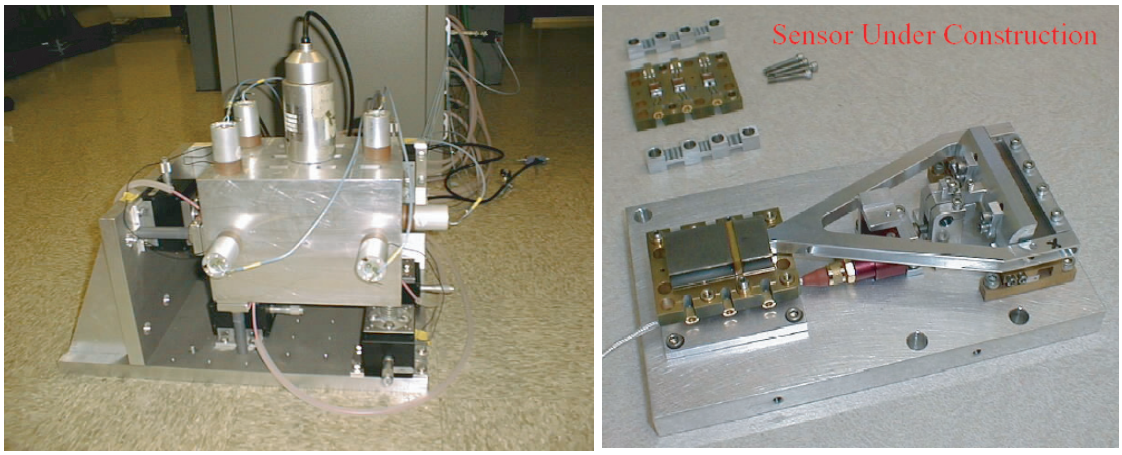

FIGURE 5.16. Photograph (left) of 100 kg block stabilized in six degrees-of-freedom and (right) of the compact nonmagnetic inertial sensor under development.

Finally, a fast intra-train feedback system is being developed to further ensure the stability of the beam at the IP. This feedback system must operate extremely rapidly because the full JLC-X/NLC bunch train is only 270 ns long. Presently, groups from Queen Mary College in London and Oxford University are working on FONT, Feedback On Nanosecond Timescales. This facility uses the NLCTA beam to simulate the beam entering and exiting the IP as illustrated in Figure 5.17. Tests have shown that FONT is able to reduce the

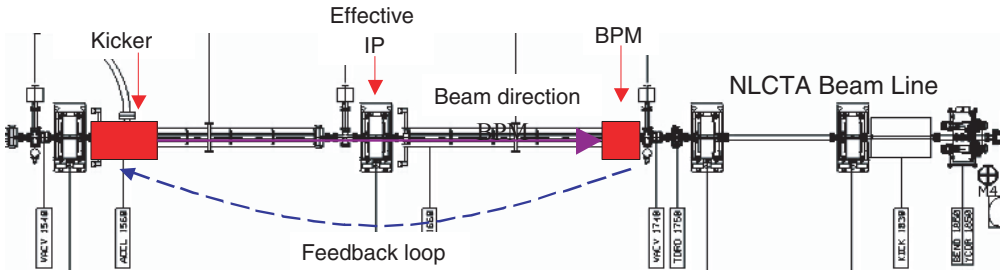

FIGURE 5.17. Schematic of the FONT experiment in the NLC Test Accelerator.

amplitude of an induced oscillation by roughly a factor of 10 with a latency of ∼60 ns. In 2003, new kicker power supplies and improved feedback electronics will be tested with the NLCTA beam to demonstrate improved latency times.

5.4 CLIC

5.4.1 The Test Facility CTF3 Under Construction

5.4.1.1 Introduction

The CLIC design relies on electron acceleration with high gradients of 150 MV/m at 30 GHz with rf pulse length of 130 ns. The rf power requirement is 460 MW per meter of linac length. Therefore a very efficient and reliable source of rf power is required. The scheme is based on a drive beam running parallel to the main beam, whose bunch structure carries a 30 GHz component. The rf power is extracted from the drive beam in Power Extraction and Transfer Structures (PETS) and transferred to the main beam [1].

The required drive beam time structure is produced by compressing a long bunch train with low bunch repetition frequency, which is accelerated with low rf frequency. Subsequent packets of this bunch train are interleaved in isochronous rings, which thereby increase the bunch repetition frequency and the peak current in these packets. Power efficiency being of utmost importance for CLIC, the drive beam with high peak current is accelerated in fully beam-loaded low-frequency cavities, so that the power, except for wall losses, is completely converted to beam energy. New accelerator structures are required with very strong damping of beam induced Higher Order Modes (HOM) to keep the bunch trains stable.

The main goal of CTF3 is to demonstrate the key concepts of the new rf power generation scheme, namely the bunch compression scheme and the fully loaded accelerator operation. The drive beam pulse obtained after compression (140 ns, 35 A) will be sent to special resonant structures to produce 30 GHz rf power with the nominal CLIC parameters, to test accelerating cavities and waveguide components.

The facility [2] will be built in the existing infrastructure of the LPI (LEP-Pre-Injector) complex and will make maximum use of equipment which became available after the end of LEP operation. In particular, the existing rf power plant from LIL at 3 GHz and most of

the magnets will be used. The project is based in the CERN PS Division with collaboration from many other Divisions at CERN, as well as from INFN Frascati, SLAC, IN2P3/LAL at Orsay, Rutherford Appleton Laboratory (RAL) and the University of Uppsala.

A "probe beam" simulating the CLIC main beam will be available to demonstrate acceleration with the 30 GHz equipment at the CLIC design accelerating gradient. An intermediate test station is foreseen immediately after the linac for power-testing CLIC components at longer pulse length than presently available at CTF2 at the earliest possible moment.

The final configuration of CTF3 is shown in Figure 5.18 and the main systems of CTF3 are described here. The schedule planned for CTF3 is indicated in the Figure 5.19.

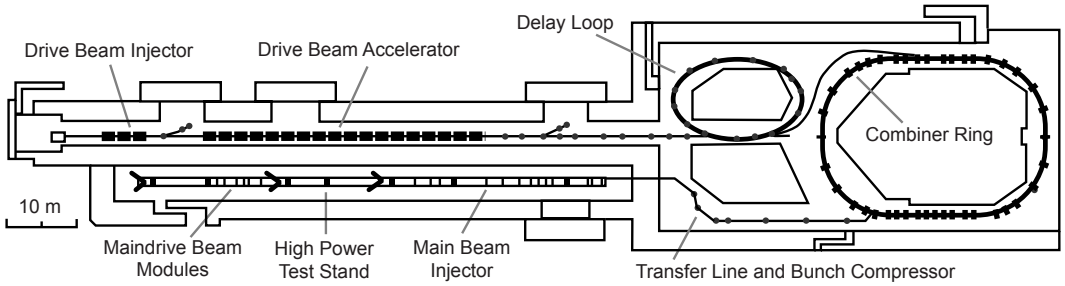

FIGURE 5.18. Layout of the final configuration of CTF3.

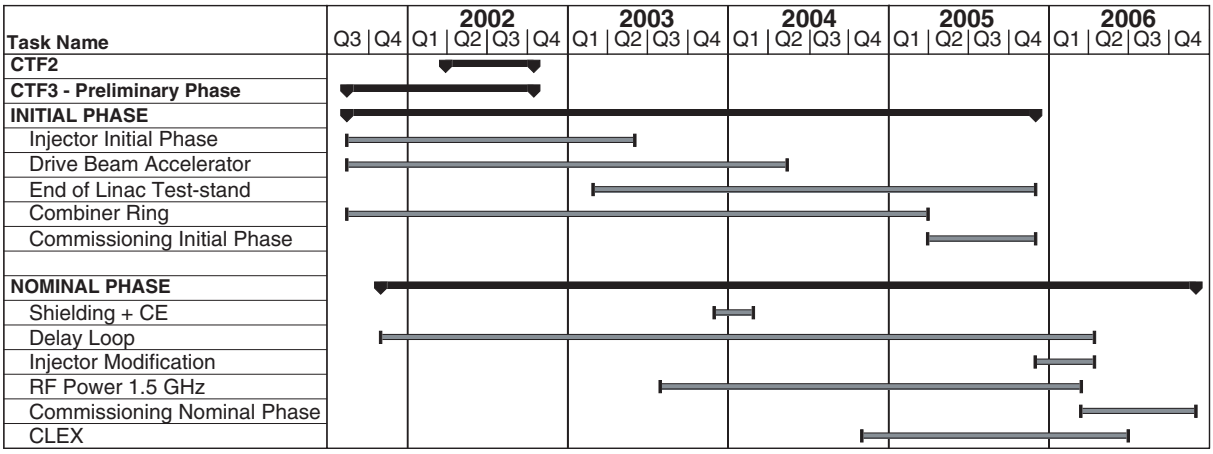

FIGURE 5.19. Chart with CTF3 schedule.

5.4.1.2 Drive Beam Injector

The drive beam injector [3] is built in collaboration with SLAC (providing the gun triode and the beam dynamics design) and LAL/Orsay (providing the gun electronics circuitry and the 3 GHz pre-bunchers).

The 1.6 μs long drive beam pulse is generated by a 140 kV, 9 A thermionic triode gun. The gun is followed by a bunching system composed of a set of 1.5 GHz subharmonic bunchers, a 3 GHz pre-buncher and a 3 GHz tapered-velocity traveling-wave buncher. The phase of the subharmonic bunchers is switched rapidly by 180 every 140 ns. In order to obtain a fast switching time ($\leq$ 4 ns), the 1.5 GHz rf source must have a broad bandwidth (about 10%) and a peak power of 500 kW [4]. The bunches thus obtained are spaced by 20 cm (two 3 GHz buckets) and have a charge of 2.3 nC each, corresponding to an average current of 3.5 A. As a result of the phase switching, the drive beam pulse is composed of 140 ns subpulses, which are phase-coded and can be separated later by transverse deflectors working at 1.5 GHz.

The injector is completed by two 3 GHz traveling-wave structures, bringing the beam energy up to about 20 MeV. Solenoidal focusing with a maximum on-axis field of 0.2 T is used all along. A magnetic chicane with collimators downstream of the injector will eliminate the low energy beam tails produced by the bunching process. The chicane region will also be instrumented to perform beam-size and energy-spectrum measurements. An alternative option to the thermionic injector scheme, based on the use of an rf photoinjector, is also under study as a potential later upgrade [5].

5.4.1.3 Drive Beam Accelerator

The drive beam pulse is brought to its final energy (150 MeV) in the drive beam accelerator, composed of 8 modules of 4.5 m length. Each module consists of two accelerator structures, identical to the ones used in the injector, a beam position monitor, a quadrupole triplet and a pair of steering magnets. Beam simulations have shown that the initial value of the normalized rms emittance (100 μm·rad) is conserved during acceleration despite the high beam current and the long beam pulse, provided that the transverse Higher Order Modes (HOMs) are suppressed. The traveling-wave structures work in the $2\pi/3$ mode, have an active length of 1.13 m with a filling time of 100 ns and operate at a loaded gradient (nominal beam current) of about 8 MV/m, with an rf-to-beam efficiency of 92% approximately. The structure (called SICA, for Slotted Iris Constant Aperture) uses four radial slots in the iris to couple the HOMs to SiC loads (see Figure 5.20). The selection of the modes coupled to the loads is determined by their field distribution, so that all dipole modes are damped. The Q-value of the first dipole is reduced to about 5. The HOM frequency detuning is obtained by nose cones of variable geometry. The aperture can therefore be kept constant at 34 mm, yielding a small amplitude of the short-range wakefield. A SICA test prototype is under construction. The rf power is supplied by eight 30 MW klystrons and compressed by a factor of 2 to give a peak power at each structure input of about 30 MW. The pulse compression system is based on the existing LIPS system; however, a programmed phase ramp is used to get an almost rectangular rf pulse [6] with the required phase stability. New cavities to complement and partly replace the existing storage cavities, the BOC (Barrel Open Cavities) are presently under development.

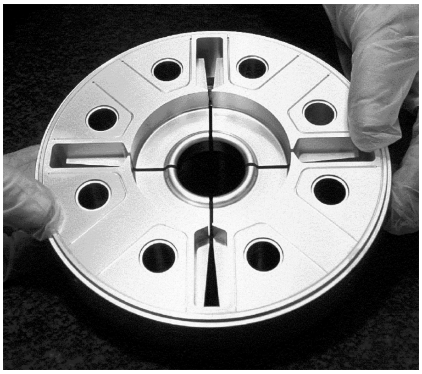

FIGURE 5.20. Prototype cell for the SICA structure.

5.4.1.4 Delay Loop and Combiner Ring

After the linac, a first stage of electron pulse compression and bunch frequency multiplication of the drive beam is obtained using a transverse rf deflector at 1.5 GHz and a 42 m long delay loop. The phase-coded 140 ns long subpulses are first separated and then recombined by the deflector after half of them have been delayed in the loop. The beam is then a sequence of five 140 ns long pulses with twice the initial current, separated by 140 ns "holes" (see Figure 5.21). An 84 m long combiner ring is then used for a further stage of pulse compression and frequency multiplication by a factor of 5, through injection with 3 GHz transverse rf deflectors [2].

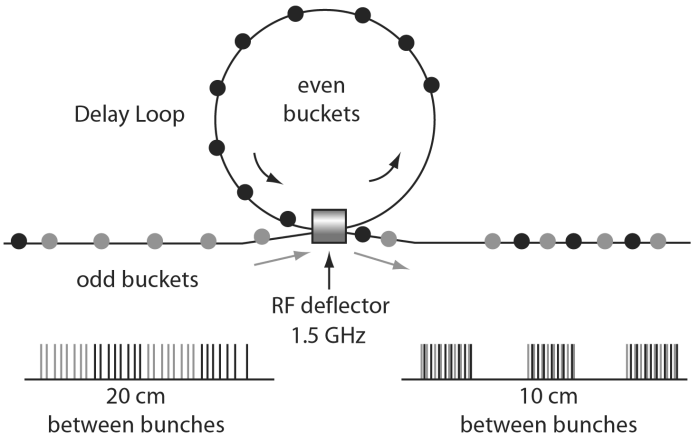

FIGURE 5.21. Schematic description of the pulse compression and frequency multiplication using a delay loop and a transverse rf deflector. Note that the last bunch coming from the left is in an even bucket again for consecutive deflection into the delay loop, therefore shifted in phase. After the delay loop, there are 140 ns between the trains. After the combiner ring, a single 140 ns long drive beam pulse with a current of 35 A is obtained. The final bunch spacing is 2 cm.

The design of the delay loop, the combiner ring and the related beam lines is under the responsibility of INFN/Frascati [7]. Both the delay loop and the ring must be isochronous in order to preserve the short bunch length required. The combiner ring consists of four isochronous arcs, two short straight sections and two long straight sections for injection and extraction. The ring arcs are triple-bend achromats, with negative dispersion in the central dipole. A precise tuning of the momentum compaction value can be obtained by a variation of the magnetic strength of the central quadrupole in each arc. Three sextupole families in the arcs provide a cancellation of the second-order momentum compaction, while controlling both the horizontal and vertical chromaticities. Two wiggler magnets are foreseen in order to adjust the ring circumference precisely to a N+1/5 multiple of the bunch spacing (with a total adjustment range of $\pm$ 1 mm), and are placed in the short straight sections (one similar wiggler is located in the delay loop). Prototypes of these wigglers are under construction. The injection and extraction regions of the ring, with similar requirements, have identical lattices. Injection and extraction septa are placed symmetrically in the center of the long straight sections. The π betatron phase advance between the two ring-injection deflectors is obtained by four quadrupoles arranged symmetrically around the septum. In the extraction region this assures the required $\pi/2$ phase advance between the extraction kicker and the septum.

A potential problem of the combination process with a high bunch charge is the effect of multibunch beam loading on the fundamental mode of the deflecting cavities. Detailed studies of the effect have been made [8], showing that the transverse beam stability can be sufficiently improved by a proper choice of the deflector parameters, of the β-function at injection and of the ring tune. The results are summarized in Figure 5.22 for position errors Δx and angle errors Δx'.

The use of short, high-charge bunches puts severe requirements on the ring impedance and makes coherent synchrotron emission a serious issue. The main effects are beam energy loss and energy spread increase.

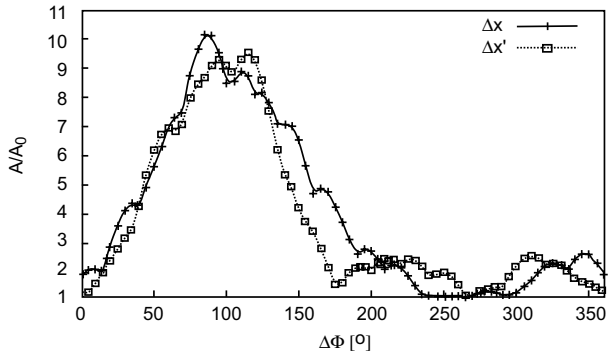

FIGURE 5.22. Amplification of an initial error in position Δx (crosses) and angle Δx'(squares) of the injected beam as a function of the betatron phase advance in the ring, after five turns. The ring tune has been chosen in the low amplification region, close to a phase advance of 260°.

In order to minimize these effects, the rms bunch length can be increased from its value of 1.3 mm in the linac to a maximum of 2.5 mm in the delay loop and ring, by a magnetic chicane placed at the end of the linac. After combination, the individual bunches are then compressed in length to about 0.5 mm rms in a magnetic bunch compressor. The drive beam pulse is then transported to the 30 GHz test area.

5.4.1.5 Main Beam and 30 GHz Test Area

A single 30 GHz decelerating structure, optimized for maximum power production, will be used in a high power test-stand where CLIC prototype accelerator structures and rf components can be tested at nominal power and beyond. Alternatively, the drive beam can be used in a string of decelerating structures to power a representative section of the CLIC main linac and to accelerate a probe beam. The probe beam is generated in a 3 GHz rf photoinjector and pre-accelerated above 100 MeV using 3 GHz accelerator structures recuperated from LIL. It can be accelerated further to about 500 MeV in 30 GHz CLIC accelerator structures powered by the drive beam, operated at a maximum gradient of 150 MV/m. This setup will allow to simulate realistic operating conditions for the main building blocks of the CLIC linac.

5.4.2 Development of the CLIC Accelerator Structures

CLIC presently runs a program of high-power structure tests using CTF2 as a power source. CTF2 [9] provides 30 GHz rf pulses of up to 280 MW with a pulse-length variable from 3 to 15 ns. This pulse length is larger than the fill-time of the structures built so far, but is short compared to the nominal 130 ns pulse-length of CLIC. Since the available power level exceeds by far the power needed for structure testing, a relatively simple pulse-stretching device could be envisaged in order to increase the pulse length in CTF2 up to 30 ns. Such a device has been made operational in CTF2 so that tests with longer pulses could be done before the dismantling of CTF2 planned in the autumn of 2002. Tests with a copper structure with reduced aperture achieved the same average gradient of 105 MV/m with either 15 or 30 ns pulse length.

The test facility CTF3 under construction and described previously will allow to produce 30 GHz rf power pulses of nominal length. Some 30 GHz structure testing with this new source will start in late 2004. Another experiment is in preparation at JINR/Dubna which will test pulsed heating limitations in 30 GHz cavities using a FEL as 30 GHz power source.

The program of structure tests is based on results obtained during the last ten years. The feasibility of reaching a gradient of 150 MV/m using the CLIC technology was demonstrated at SLAC and KEK with a small aperture X-band structure [10]. In CTF2, the constant impedance copper structures tested have reached mean accelerating gradients of 72 MV/m for a surface field of 317 MV/m. At these field levels, considerable surface damage is observed on the first iris, which connects the input coupler cell with the first regular cell and is exposed by far to the highest surface field. No significant damage is seen in the downstream cells. The damage pattern follows the field distribution. Structure rf conditioning to reach the damage level takes $\sim 3 \times 10^5$ rf pulses. An experiment was then performed where an iris made of tungsten replaced the damaged region. Although the structure was powered for 5×10^5 pulses to the same field levels as before, no damage

occurred on the tungsten iris. A short pulse experiment has been performed using a 3 ns long pulse on a structure with standard copper irises applying a 160 MV/m gradient for 5×10^5 pulses. The pulse energy was the same as in the 72 MV/m and 15 ns run, but no damage occurred.

High power structure tests have been carried out during 2002 with reduced E_{surf}/E_{acc} ratio in the cells and in the coupler. Structures have been built with this end in view. The first structure already tested has an a/λ of 1.75, a phase advance $2\pi/3$, E_{surf}/E_{acc}=2.2 and v_g=0.046c. The couplers are of the mode launcher type. The surface field of the coupler nowhere exceeds the field of the regular cells and all the irises are made of tungsten with copper rings clamped in between. Very recent measurements showed that accelerating fields of 125 MV/m in average and of 152 MV/m in the first cell, corresponding to a peak surface field is 340 MV/m, were obtained in this structure, after 1.5 million rf pulses and without damage. They also indicate that the mode-launcher type power coupler overcomes the field limitations encountered with the couplers used so far.

The second structure has the same cell geometry, but is entirely made from OFHC copper and assembled by braze/diffusion bond at 820°C in vacuum. It reached an average accelerating field of 102 MV/m with a peak accelerating field in the first cell of 114 MV/m and a peak surface field of 255 MV/m. This structure showed signs of surface damage on the first regular iris, where the surface E-field is highest. The third structure, with molybdenum irises, was conditioned to an average accelerating gradient of 150 MV/m, with a peak accelerating field in the first cell of 193 MV/m and a peak surface field of 432 MV/m. No damage was observed. Comparing results from these structures will allow distinguishing material from geometry effects. A second set of structures (one tungsten/copper, one copper only) will be built using a phase advance of $\pi/2$ with a/λ=2, E_{surf}/E_{acc}=2 and v_g=0.083c. These structures have a higher v_g than the first ones. High power tests of both sets and structure comparison will allow distinguishing effects due to surface field and to group velocity.

5.4.3 Study of the Magnet Vibration Stabilization

The magnet vibration tolerances for frequencies above approximately 4 Hz are severe in CLIC, of the order of 14 nm (4 nm) horizontally and 1.3 nm (0.2 nm) vertically, in the linacs (and in the final focus respectively). The most challenging requirements are in the vertical plane. Tolerances for uncorrelated rms vibration above 4 Hz are 1.3 nm for all the linac quadrupoles and 0.2 nm for the final doublet. It must be determined early whether these tolerances are feasible. A CLIC study on magnet stability and time-dependent luminosity was proposed in 2000 [11] to address this critical issue and the goal was stated as: "Show that the present design parameters of CLIC are feasible in a real accelerator environment, using and further developing latest cutting-edge stabilization technology and time-dependent simulation programs."

The study started after it was approved and funded in January 2001. Major steps have been taken in order to address the stated challenge:

- Vibration measurements with sub-nm resolution and accuracy were demonstrated in the frequency range of interest (>2 Hz). Four identical vibration sensors were acquired.

- A test-stand for magnet vibration measurements was set up at CERN in the immediate neighborhood of roads, operating accelerators, manual shops, and regular office space.
- Available industrial solutions for vibration damping were reviewed and two state of the art systems were acquired. One system employs an active piezoelectric feedback on ground vibration (STACIS2000 from TMC). The other system (PEPS-VX from TMC) is an air-pressurized solution, offering passive damping, a micrometer alignment slow feedback, and a faster active feedback on table top motion.
- A table with a minimal structural resonance above 230 Hz was acquired to provide a stiff support of prototype magnets.
- A cooling water system (from tap water) was installed to test magnet vibration with cooling water flow.
- Also relying on active collaborations with DESY and SLAC colleagues, advanced simulation tools were set up.

The experimental work on stabilizing existing CLIC prototype magnets has started in April 2002. Results with the STACIS2000 system show that the system damps the floor vibration by about a factor of 20. Using this system, CLIC quadrupoles have been stabilized vertically to an rms motion of (0.9±0.1) nm above 4 Hz (see Figure 5.23), or (1.3±0.2) nm with a nominal flow of cooling water. For the horizontal and longitudinal directions respectively, a CLIC quadrupole was stabilized to (0.4±0.1) nm and (3.2±0.4) nm [12]. It is noted that the measured vibration levels in principle meet the requirements for the CLIC linac quadrupoles. An improvement by about a factor of 5 is required for the two final quadrupoles in the vertical direction.

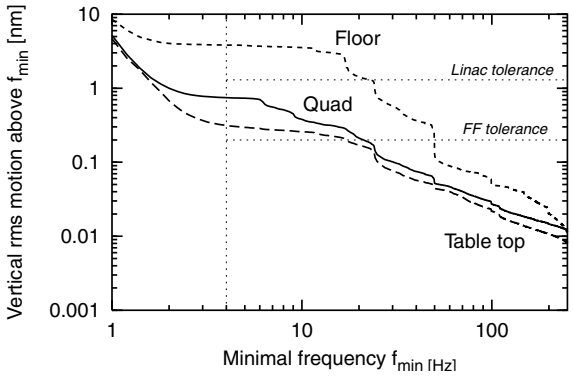

FIGURE 5.23. Vertical rms amplitude of vibration, integrated from above a given frequency f_{min}, versus this frequency. Vibration was simultaneously measured on the floor, on the quadrupole, and on the tabletop.

Future studies will aim at further reducing vibration levels, studying alignment stability, measuring structural resonances in magnets and supports, exploring environmental effects (*e.g.*, more studies on cooling water, magnetic fields, and so on), employing an alternative pneumatic system, and using the measurements for predictions of the CLIC luminosity stability. In addition, work will also aim at establishing a firm basis for a CLIC specific engineering solution that in principle could be based on or could include the tested technology.

BIBLIOGRAPHY for CHAPTER 5

[1] R. Corsini (ed.) and 15 co-authors, "The CLIC RF Power Source - A Novel Scheme of Two-Beam Acceleration for e Linear Colliders," CERN 99-06 (1999).

[2] R. Corsini, A. Ferrari, L. Rinolfi, T. Risselada, P. Royer, F. Tecker, "CTF3 Design Report," Edited by G. Geschonke (CERN) and A. Ghigo (INFN), CERN/PS 2002-008(RF) and LNF-02/008(IR), (2002).

[3] H. Braun and 6 co-authors, "An Injector for the CLIC Test Facility (CTF3)," CERN/PS 2000-052, Proc. of the XX Linac Conference, August 21–25, 2000, Monterey, USA.

[4] G. Phillips, "A 500 kW L-Band Klystron with Broad Bandwidth for Sub-Harmonic Bunching in the CLIC Test Facility," Proc. of the 5th Modulator-Klystron Workshop for Future Linear Colliders, April 26–27, 2001, Geneva, Switzerland.

[5] I.N. Ross, "Feasibility Study for a CERN CLIC Photo-Injector Laser System," CLIC Note 462 (2000).

[6] I. Syratchev, "RF Pulse Compressor Systems for CTF3," Proc. of the 5th Modulator-Klystron Workshop for Future Linear Colliders, April 26–27, 2001, Geneva, Switzerland.

[7] C. Biscari and 12 co-authors, "CTF3 - Design of Driving Beam Combiner Ring," Proc. of the 7th European Particle Accelerator Conference, June 26–30, 2000, Vienna, Austria and CLIC Note 471 (2001).

[8] D. Alesini, R. Corsini, A. Gallo, F. Marcellini, D. Schulte, I. Syratchev, "Studies on the RF Deflectors for CTF3," Proc. of the 7th European Particle Accelerator Conference, June 26–30, 2000, Vienna, Austria and CLIC Note 472 (2001).

[9] H.H.Braun for the CTF Team, "Experimental results and technical research and development at CTF2," Proc. 7th Eur. Part. Accel. Conf. (EPAC2000), Vienna, 2000.

[10] M. Dehler, I. Wilson, W. Wuensch, "A Tapered Damped Accelerating Structure for CLIC," CERN/PS 98-040 (LP), Proc. of the XIX Linac Conference, August 23–28, 1998, Chicago, USA.

[11] R. Assmann: "Proposal for a CLIC Study of Final Focus Stabilization Technology and Time-Dependent Luminosity Performance." Unpublished. Available at `http://www.cern.ch/clic-stability`

[12] R. Assmann et al, "Status of the CLIC Study on Magnet Stabilization and Time-dependent Luminosity Performance," Proc. of EPAC2002 (Paris).

CHAPTER 6

Technology, RF, and Energy Working Group Assessments

6.1 INTRODUCTION

The charge of the Technology, RF Power, and Energy Performance Working Group is recalled here:

> "This group will play a role similar to the first ILC-TRC Linac Technology working group, but will broaden its scope to analyze all those factors which affect the energy performance of all four machines. It will look at sources, injectors, magnets, cryogenics, klystrons, power supplies, modulators, rf pulse compression systems, rf amplitude and phase stability, and any other parts of the designs which determine whether the machines can reliably reach their operating energy, be tunable, and efficient in their use of electric power."

The working group has addressed the charge by subdividing its activities into five subgroups whose responsibilities are briefly described:

1. Injectors and Technology Subgroup

   Members: **H. Weise**, H. Edwards, K. Hübner, P. Logatchov, M. Ross, N. Toge

   All critical technological aspects of the machines not covered in the linac sections (Section 6.3, Section 6.4, and Section 6.5) and not directly related to luminosity performance are discussed here. It includes guns and targets, positron production as well as the hardware of damping rings and beam delivery systems. In addition the main linac beam monitors are examined in this subgroup. For the convenience of the reader, the few luminosity issues connected with the injectors, upstream from the damping rings, are also presented in the corresponding chapter (see also Chapter 7).

2. RF Power Sources Subgroup

   Members: **Y.H. Chin**, H.H. Braun, L. Lilje, P. Logatchov, R. Pasquinelli, T. Shintake

   This subgroup covered the klystrons, modulators, and associated power supplies for the main linacs, and in the case of CLIC, for the drive beam linacs. In addition the main linacs low-level rf systems are discussed in this section.

3. RF Power Distribution Subgroup

   Members: **K. Hübner**, H.H. Braun, Y.H. Chin, L. Lilje, R. Pasquinelli, M. Ross, T. Shintake, P. Wilson

   This subgroup dealt with the transfer of rf power from the klystrons to the main linac accelerator structures. It covered the waveguide architecture and associated rf power components. This obviously included the pulse compression systems for the JLC-C and JLC-X/NLC projects. For CLIC, the drive beam system is considered as a distributed klystron and is globally discussed here. In addition, the reader will find in Section 6.4.5 a compilation of overall linac efficiencies for the four machines.

4. Accelerator Structures Subgroup

   Members: **P. Wilson**, C. Adolphsen, H.H. Braun, H. Edwards, L. Lilje, N. Toge, T. Shintake

   This subgroup looked at all aspects of the main linacs accelerator structures. Accelerating gradient and wakefield suppression (or High Order Mode damping) are obviously the most important parameters, but other aspects are also considered here, like coupler performance, mechanical and vacuum properties, and fabrication techniques. For the superconducting cavities, the cryostat design and cryoplant issues were also discussed by this subgroup.

5. Reliability Subgroup

   Members from Energy Working Group: **R. Pasquinelli**, C. Adolphsen, K. Hübner, M. Ross, T. Shintake, H. Weise

   This subgroup was common to the two original working groups, Technology, RF, and Energy and Luminosity Performance. The members of this subgroup from the Luminosity Working Group are given in Chapter 7.

   Although the reliability of individual components has been discussed to some extent in the previous sections, a more global approach has been taken in the Reliability subgroup. In particular, the implications of component reliability and machine architecture on the overall performance in terms of final machine up-time were discussed here. The Machine Protection System is also discussed by this subgroup.

   Contrary to the other sections, the global reliability findings are presented in Chapter 8 of the report, not in Chapter 6.

The Working Group has not examined those technology aspects that were already demonstrated. This was the case, for instance for the prelinacs of the JLC-X/NLC projects.

A major modification of the JLC-X/NLC main linacs was presented to the Working Group in September 2002, namely the replacement of the DLDS scheme by a SLED-II-based version. This modification was consistent with the original findings of the Working Group. Although many evaluations had already been made, especially by the Power Distribution subgroup, it was decided to evaluate the new scheme and incorporate the results in the final document. The original findings concerning the DLDS-based scheme are left in the Power Distribution section, for completeness.

In order to present the conclusions of each subchapter with a format as uniform as reasonably possible, the Working Group has defined categories of concerns applicable across all the reviewed items. Ranked in decreasing order of criticality, the Working Group distinguishes:

Show stoppers: A situation for which it is not plausible that the problem can be overcome by more R&D. In this case a radical design change is required. It is not surprising that the Working Group has not identified any show stoppers, as many experienced scientists have studied the projects in detail for many years.

Major concerns: A major concern appears when a problem is identified which could turn into a show stopper if the corresponding R&D is not successful AND this R&D is not planned, not funded or not possible at present. Hence, the Working Group strongly recommends to consider this R&D.

Concerns: A concern corresponds to either:

- A problem that has been identified and which could turn into a show stopper if R&D is not successful, BUT this R&D is foreseen (on going or planned, but not necessarily funded). Hence the group supports this R&D as important.
- An inherent negative feature which might have adverse effects on cost, operability, or maintainability.

Plausible solutions: The feasibility of the system has been demonstrated or is plausible by comparison to similar configurations. Further R&D is useful, but not mandatory for demonstrating the feasibility; it could be conducted for furthering engineering study or cost reduction.

In the conclusions of each section a recommended program of R&D is indicated together with the findings of the subgroup. The reader will find a comprehensive review of those R&D items, sorted by machine, detailed and ranked in Chapter 9. The R&D rankings that are quoted in some of the following subchapters are also defined in Chapter 9.

6.2 INJECTORS AND TECHNOLOGY

6.2.1 General Source Intensity Issues

The primary function of the positron and electron injectors is to provide a stored beam for each damping ring that meets the intensity and intensity stability specifications. In order to determine the specifications it is important to:

- Catalog beam loss mechanisms within the injector and then compute the required beam from the primary source
- Catalog the effects associated with beam intensity fluctuations, especially downstream of the electron damping ring

The latter includes the effects that beam intensity fluctuations can have on positron production. This has been done for the JLC-X/NLC injector systems and is reflected in the performance summary tables (see NLC ZDR).

There are three places in the injector system where losses greater than a few percent are expected:

- At the source, where the beam is captured into a longitudinal bucket
- At the end of the first linac section, where a bending system greatly narrows the energy acceptance
- As the beam is captured in the damping ring, if the longitudinal or transverse phase space exceeds the ring acceptance

For example, in the SLC positron source, the yield just after the first capture structure was 4 positrons per incoming electron. This yield decreased to about 2.5 e^+ per e^- after the capture region and energy cuts as was expected. However, the yield then decreased further during the transport and acceleration to the positron damping ring. Typical injection efficiency was about 70%. Overall, the system had a yield of roughly 1 captured positron in the damping ring for every electron incident on the target, which was ∼60% of what was predicted. In contrast, the polarized electron transport was much better. During typical operation roughly 72% of the charge from the gun was bunched and captured in the electron damping ring and during good periods the yield was as high as 84%. Almost all of the losses occurred in the bunchers or just downstream at relatively low beam energy. There were only a few percent losses during injection into the damping ring.

The losses in the SLC were not nearly as severe as they would be in a future linear collider because the beam power in the SLC injector was only ∼1 kW. In the NLC and TESLA injectors, the beam power will be roughly 50 and 200 times higher than in the SLC. However, the location of the losses should be well known. The TESLA positron source design artificially reduces the energy acceptance in the bending section at 115 MeV with moveable collimators. In the simulations, this acceptance is matched to the damping ring (DR) acceptance. Similarly in the NLC design, the energy spectrum is collimated in a

chicane located at 80 or 250 MeV for the e^- and e^+ sources, respectively. Then both the energy spectrum and the transverse phase space are collimated at 1.98 GeV before injection into the damping rings [1].

The greatest concern is in the initial longitudinal phase space capture section, where both the modelling and the hardware systems have a poor performance record in existing machines and test facilities. Losses at the end of the linac, related to a low energy tail produced in the subharmonic bunchers, can be up to 30%. R&D is needed to develop simulation codes that are more useful than those usually used (*e.g.*, PARMELA) and to test them. It should be noted that rf gun performance is usually much better, leading to losses closer to 0%. A new simulation tool (ASTRA) was used and it showed some significant differences from PARMELA, especially with respect to the longitudinal phase space. Successful benchmarking was started and is still continuing at TTF and DESY Zeuthen (PITZ).

If large beam losses are expected, then there must be a system designed to accept them. In the case of TESLA, where the beam power captured in the ring is expected to be 250 kW, commissioning dump systems at low energy as well as at 5 GeV are needed, each at the ends of the corresponding linac sections, and capable of handling up to 25 or 30% of that power. At 5 GeV energy, this dump system is challenging because of space constraints in the tunnel.

In the TESLA design the electron beam at the end of the main linac is used for positron production. For both the electron and positron injector systems, the bunch population jitter should be propagated through the system in the simulations in order to estimate these effects. In particular, the ±5% peak-to-peak jitter of the electron beam should be reviewed with respect to positron production. While transverse wakefields in the TESLA linacs are extremely small, the wakes from the beam delivery collimators are not, and they contribute to the bunch-to-bunch position fluctuations at the IP. The importance of this effect has to be investigated as well.

The important parameters of the electron and positron sources are summarized in Table 6.1 and Table 6.2 respectively.

6.2.2 Electron Source

Linear colliders need polarized e^- sources for their operation but could take advantage of an unpolarized source for commissioning, machine studies and perhaps unpolarized luminosity operation purposes, if needed. The need for a low technical risk, reliable injector system strongly impacts the design effort. The chosen technologies are based on the experience with previously built and operated colliders like, for example, the SLC and fourth generation light sources (LCLS and TESLA-FEL). With respect to the polarized source all LC projects are planning for a dc photocathode gun very similar to the successfully operated SLC polarized source [2]. Therefore the technical risk seems low enough.

6.2.2.1 Luminosity Issues

Electron polarization of 80% is required. Polarization at the damping ring entrance is achieved by producing polarized electrons at the source and transporting them through the

TABLE 6.1
Tables for Electrons

	TESLA	NLC	CLIC
Parameters at damping ring			
Energy E_0 [GeV]	5.0	1.98	2.42
Number of particles/bunch N_p	2×10^{10}	0.8×10^{10}	0.63×10^{10}
Bunch length (FWHM) [mm]	<10	10	3
Energy spread $\Delta E/E_0$ [%]	1	1	2
Normalized RMS emittance $\gamma\varepsilon$ [μm·rad]	40	100	10
Position jitter	0.1σ	1.0σ	
Number of bunches	2820	192	154
Repetition rate [Hz]	5	120	200
Bunch spacing [ns]	337	1.4	0.666
Polarization [%]	80	80	75
Gun			
Peak current [A]	2	1	3
Bunch length [mm]	600	150	100
Number of particles/second [s^{-1}]	2.8×10^{14}	1.8×10^{14}	1.9×10^{14}
Laser pulse length [ns]	2	0.5	
Laser energy/bunch [μJ]	4.6	4.2	
Bunching system			
f_{RF1} [MHz]	108	714	1500
f_{RF2} [MHz]	433		1500
f_{RF3} [MHz]	1300 (normal conducting)		
Pre-linac			
f_{RF} [MHz]	1300 (super-conducting)	2856	1500

TABLE 6.2
Tables for Positrons

	TESLA	NLC	CLIC
Parameters at (pre) damping ring			
Energy E_0 [GeV]	5.0	1.98	2.42
Number of particles/bunch N_p	2×10^{10}	0.9×10^{10}	0.63×10^{10}
Bunch length (FWHM) [mm]	<10	15	7
Energy spread $\Delta E/E_0$ [%]	±0.8	±1.0	±2.0
Normalized edge emittance $\gamma\varepsilon$ [m·rad]	0.014	0.03	0.09
Position jitter	0.1σ	1.0σ	
Number of bunches	2820	190	154
Repetition rate [Hz]	5	120	200
Bunch spacing [ns]	337	1.4	0.666
Reachable polarization [%]	45–50	Not fully studied	Not fully studied
Incident beam			
Method	Undulator	e^- drive linac	
Incident beam energy [GeV]	250–150	6.2	2.0
Target			
Material / thickness [rad. length]	Ti / 0.4	WRe / 4	
Number of targets	1	3	1
Number of particles/second [s^{-1}]	2.8×10^{14}	2.6×10^{14}	1.9×10^{14}
Peak energy deposition [J/g]		<35	<42
Average power deposition [kW]	5		16
Positron yield			
At damping ring	2 - 1	1	0.6

subsequent buncher and linac sections. A rigorous spin tracking study for this case has not yet been performed, mainly due to the fact that no major problems are envisioned. In addition, the emittance was evaluated with the help of space charge tracking codes like PARMELA. TESLA calculates a normalized RMS emittance of 42.5 μm·rad, while JLC-X/NLC assumes 100 μm·rad based on a more conservative approach to error margins.

6.2.2.2 Choice of Technology

For the production of polarized electrons, a polarized high-power laser (typically 5 μJ per pulse, wavelength around 800 nm) illuminates a semiconductor photocathode (GaAs) placed in a high-voltage dc gun (typically 120 to 200 kV at gradients of a few MV/m). The produced polarized electron beam is then bunched by means of one or several subharmonic pre-bunching cavities, accelerated first by solenoid-focused normal-conducting accelerator sections, and finally further accelerated by either normal-conducting (CLIC and JLC/NLC) or superconducting sections (TESLA). The energy needed for the damping ring injection varies between 1.98 and 5 GeV. The main difference between the linear collider approaches is the bunch spacing (nanoseconds for JLC/NLC and CLIC, a few 100 ns for TESLA), and the number of bunches per train (CLIC: 154, JLC/NLC: 192, and TESLA: 2820–4886). Both parameters directly reflect the choice of linac technology. The bunch train length, which must be less than the rf pulse length, is below 1 μs for normal-conducting accelerator sections while for superconducting sections it is 1 ms.

6.2.2.3 Key Issues

The key issues in providing a reliably operating polarized e^- source are: ultra-high vacuum conditions (10^{-11} mbar) in the gun, low dark currents, *i.e.*, modest electric fields at the cathode, operating within the cathode charge limit which defines the maximum current density at the cathode, allowing sufficient cathode recovery time during multibunch operation, and laser technology.

The successful operation of the SLC injector qualifies the choice of technology. But because of the higher bunch train charge requirements, JLC/NLC and CLIC need improvement of the photo-cathodes with respect to the SLC cathodes. Recent results from a gradient-doped cathode are very promising: the cathode operated for roughly 6 months during the 2002 E-158 experiment at SLAC and produced roughly 5 times the charge required for the JLC/NLC design during tests. Additional studies will be aimed at developing a further optimized cathode material.

A laser very similar to the one needed for driving the TESLA polarized gun is currently under construction. This laser is being built for time resolved spectroscopy at the TTF FEL. It delivers 800 μs long trains of 10 μJ pulses at a wavelength around 800 nm in a first step separated by 1 μs [3]. The pulse length can be adjusted between 20 ps and 200 fs. This common effort of different institutes uses a Nd:YLF burst-mode laser, a weak TiSa seed-pulse oscillator and two nonlinear crystals as an optical parametric amplifier. The collaboration aims for a pump-probe facility with sub-picosecond time resolution to be used at the TTF FEL in 2004. Bigger subsystems of this new laser are going to be installed at the rf gun test facility PITZ (DESY Zeuthen) in 2002.

One important parameter in the laser specification is the amplitude or energy jitter which directly converts to an intensity jitter of the source. The intensity jitter transforms into an emittance jitter due to space charge forces and an energy jitter due to beam loading. The TESLA design assumes a bunch-to-bunch population jitter of ±5% peak-to-peak. This requirement is based on the TESLA low emittance transport calculation. The new laser has demonstrated 800 μs long trains with an energy stability at the interaction region on the order of a few percent rms which is consistent with the TESLA specifications. For the NLC the population jitter is specified to be smaller than 1% full-width for the train-to-train jitter and 2% rms for bunch-to-bunch jitter. The CLIC design requires 1% rms bunch-to-bunch population jitter and 0.5% train-to-train jitter. The resulting laser specification has not been met. Further R&D is needed for both designs.

The photoinjector option of the CLIC (3 TeV c.m.) drive beam has to be mentioned [4]. This injector option is discussed for the production of a long bunch train (92 μs) consisting of more than 40,000 bunches with a bunch charge of 17.5 nC in a bunch length of less than 20 ps. The needed charge stability is 0.1% rms which requires detailed investigations as described in [5]. These issues will be addressed during the CTF3 program. Although the envisaged laser chain consists of proven technology, a number of technical challenges exist. According to [4], single cathodes have shown that the high current density (21 mA/cm^2), which is crucial for a CLIC drive-beam photoinjector, is achievable.

6.2.2.4 Acceleration to Damping Ring Energy

The pre-bunching and bunching sections of the polarized electron sources are based on existing technology. In case of TESLA the severe thermal loads of the following normal conducting pre-accelerator cavities caused by the almost 1 ms long rf pulses are taken into account. As a result of three dimensional thermal stress analysis, a moderate accelerating gradient below 15 MV/m was chosen. TESLA uses normal conducting cavities up to an energy of 280 MeV in order to allow for solenoidal focusing. The acceleration up to damping ring energy is based on either the TESLA machine or on well known warm S-Band (JLC-X/NLC) or L-Band technology (CLIC).

6.2.3 Positron Source

Two different schemes for the production of positrons are discussed. The CLIC and the JLC/NLC designs are based on a conventional target system similar to the existing SLC positron source [6]. The TESLA design uses a scheme, originally proposed at Novosibirsk [7], where photons are generated by the high energy electron beam in an undulator placed just after the exit from the main linac. These photons are converted into e^+e^- pairs in a relatively thin target.

6.2.3.1 Conventional Layout

The conventional target system of the JLC-X/NLC design uses an unpolarized electron gun. In order to get a sufficiently constant bunch population, a photocathode-based design is chosen which allows bunch-to-bunch intensity adjustments from the source laser. A bunching system is followed by a 10 GeV or 6 GeV drive linac operating at S-Band

frequency, in the JLC-X and NLC, respectively. With the help of an rf separator, the electrons are directed to three out of four quasi-independent target/capture sections. The energy deposited in each target has to stay below the threshold for material damage. This design addresses the risk of target mechanical failure, but it requires that large-emittance, low-energy positron bunches be steered onto a common trajectory with an rf deflector. It may be difficult to achieve the desired throughput and stability of the system because of possible aperture limits of the combiner itself, or other components associated with the combiner.

For JLC-X/NLC, the positrons produced in the shower from each target are collected using a 5.8 T magnetic flux concentrator, overlaid with a 1.2 T dc solenoid field, captured and accelerated to 250 MeV in a 1.4 GHz L-Band linac, combined into the desired bunch train format, and finally accelerated in a 1.75 GeV L-Band booster linac.

For CLIC, the positrons produced in the shower are collected using a 7 T magnetic flux concentrator, overlaid with a 0.5 T dc solenoid field, captured and accelerated to 200 MeV in a 1.5 GHz L-Band linac, and finally accelerated in a 2.2 GeV L-Band injector linac. The technology is described in [8] based on old parameters.

The large L-Band aperture is needed because of the large positron emittance; longer rf wavelength increases the positron capture efficiency.

6.2.3.1.1 Luminosity Issues Because the acceptance of this positron system is large compared to the SLC's, it is possible to achieve the required "yield" (ratio of main linac positrons to electrons) with a reduced drive beam energy (6 GeV (NLC), 2 GeV (CLIC) compared to the SLC's 30 GeV). Simulation studies of the positron production system indicate that the desired yield will be achieved; the simulation codes have been benchmarked against the SLC positron system (NLC), and this allows some confidence in their predictions.

Yield calculations have been performed with complete target-to-damping-ring tracking calculations. Yield is defined as the number of positrons within the pre-damping ring acceptance per incoming electron and GeV. The damping ring transverse acceptance is 0.03 m·rad (NLC) and 0.09 m·rad (CLIC), with an energy acceptance of 1.0% and 2% respectively. The calculated yield is 0.16/GeV and 0.31/GeV respectively.

The positron distribution at the entrance of the NLC pre-damping ring is assumed to be flat. The edge emittance (defined as the maximum transverse action) is 0.03 m·rad (note that the damping ring is designed for a 1.5 times bigger injected emittance to allow for errors).

6.2.3.1.2 Target Fracture Limit Since the total number of positrons required for the JLC/NLC bunch train is almost two orders of magnitude greater than the number of positrons in the single SLC bunch, the previously mentioned multiplexing of target/capture sections is mandatory. A simulation of pulse heating and thermal shock wave in W-Re targets shows that, with fresh nominal tensile strength material, the fracture limit is 70 J/g. The SLC target is about 60 mm in diameter and was operated for 15,000 hours at 120 Hz and 50 J/g before failure. Mechanical tests of the failed SLC target showed that the material was badly fatigued and radiation damaged. The NLC target is designed to receive

less than 50 J/g, and the operational plan avoids operation of the target to the fatigue limit. The number of operating hours required to reach the fatigue limit depends on the target size. The design CLIC [9] energy deposition (42 J/g) is also within the damage limit, provided the target is large enough and replaced often enough.

6.2.3.2 Undulator Source

The TESLA positron injection system [10] has to provide a total charge of 5×10^{13} e^+ per beam macro pulse. Thus it appears that a conventional source is not realistically feasible. The chosen undulator-based positron source uses the high energy electron beam at the end of the main linac. The TDR specifies an undulator length of approximately 100 m where high energy photons are produced with a beam power of typically 135 kW (The NLC group calculates that the specified undulator must be 135 meters in length to produce the desired photon beam [11]. The photons from the undulator hit a thin (0.4 radiation lengths) rotating Ti-alloy target. An adiabatically varying solenoid field is used to capture the produced positrons with a design efficiency of 16% for an initial field of 6 T. Studies of radiation damage and associated lifetime limitations have not been performed.

6.2.3.2.1 Undulator The use of a permanent magnet planar undulator based on existing technology would allow the production of an unpolarized positron beam. The approximately 100 m (135 m) long undulator can be treated as almost conventional since the FEL undulators in preparation for TTF2 as well as for other FELs have tighter tolerances and similar lengths. At DESY and Argonne in a first step, 30 m of undulator will be built. The operation of a 15 m long planar undulator at the TTF-FEL is well understood. Argonne is operating 22 m of undulator, SPring-8 25 m. The LCLS undulator is designed [12] with 100 m length. All these hybrid undulators are more ambitious than the TESLA unpolarized positron source undulator. Technically more ambitious is the possibility to use a superconducting helical undulator that could make polarized positrons available. The TESLA design describes this as an option for a potential upgrade at a later stage of operation. A proof of principle experiment for the production of polarized positrons using a helical undulator is proposed by SLAC [13].

6.2.3.2.2 Positron Pre-Accelerator TESLA proposes to use a normal-conducting standing-wave linac as positron pre-accelerator (PPA). The choice of standing-wave structures is based on a detailed optimization procedure, which has been described together with the final cavity design [14]. Since the cavities have to be operated with 950 μs long rf pulses, the chosen accelerating gradient is moderate (max. 14.5 MV/m). An alternative traveling-wave design is described in [15]. After approximately 55 m the positron beam energy is slightly below 300 MeV, the total capture efficiency from the target to the PPA exit was simulated to be just above 20%. This corresponds to two positrons per 250 GeV electron. This overall yield is reduced at lower electron energies. Therefore the planar undulator cannot be used below about 150 GeV, because it would have to become significantly longer than 100 m.

According to simulations, the positron distribution at the entrance of the damping ring is not flat but more Gaussian-like. The rms emittance is 0.01 m·rad, the edge emittance (defined as the maximum transverse action) is 0.014 m·rad.

Passage through the undulator, placed between the end of the 250 GeV linac and the beam delivery system, causes the energy spread in the electron beam to increase from 0.5×10^{-3} to 1.5×10^{-3} with an average energy loss of 1.2%. The emittance growth is 0.1% in both planes.

It should be noted that, independently of the ILC-TRC, the NLC group has been studying an undulator-based positron source for use in the NLC but have found significantly different positron yields than those described here or in the TDR. These calculations suggest that a 250 GeV e^- beam with a 135-m undulator, would have a yield of 1.8 e^+ per incoming electron if the capture efficiency could be pushed to 25% and the yield with a 160 GeV e^- beam would be 0.6, roughly half of the yield of 1 quoted previously [16, 17]. A capture system efficiency of 25% is also felt to be quite aggressive and an efficiency of 16%, as quoted in the TDR, is more reasonable however the yields will decrease accordingly. Another issue identified by the NLC group is that the potential for radiation damage in Titanium may be significantly higher than in Tungsten and this requires further study. The ILC-TRC was not able to evaluate these differences.

6.2.3.3 Critical Assessments of the Positron Production

The challenge of the positron production in conventional systems is clearly the peak energy deposition in the target. For the undulator-based design the target does not seem to be a critical issue. In addition such a system eliminates the need for multiple targets, may ease the requirements on the pre-damping ring (JLC/NLC design), and provides a straightforward upgrade path to polarized positrons (although challenging in its technical realization). Of principal concern are the logistical issues associated with providing a high-energy electron beam. Also, the linkage between the electron linac, the positron production, the positron damping ring, and the injection into the positron linac has consequences for the machine timing. The corresponding problems were studied [18]. For full performance, the primary electron energy must be above 150 GeV. If lower energy running at maximum luminosity becomes important, then additional electron beam pulses and by-pass beamlines can be used to drive the positron source independently from the lower-energy beam used for the HEP experiment.

The injector commissioning strategy of TESLA includes a low-intensity auxiliary e^+ source for commissioning and machine study purposes. This auxiliary source should be capable of generating a full bunch train of a few percent of the design bunch intensity. In addition, the electron driver of the auxiliary positron source will be built so that full beam loading of the TESLA positron linac can be reached with electrons. Without these measures the initial positron production must await significant progress in the operation of the electron injector and main linac.

The TESLA undulator-based source seems to be well understood from the theoretical point of view, but there remain questions about the specific yields and radiation damage issues. Unfortunately, because of the needed electron beam energy, experiments are not easy to carry out. With respect to a helical undulator for the production of a polarized positron beam, studies could and should be conducted. All projects would benefit from a well-developed technology in this field.

The installation and commissioning of the conventional positron source are independent of the schedule of the electron systems. Nevertheless, for JLC/NLC/CLIC, some part of the commissioning will be done with electrons.

6.2.4 Damping Ring Technology

Although the damping rings rely on common accelerator technology, they all include a number of challenges. For example, the best synchrotron light source instrumentation available is required and there are extreme beam power issues. The TESLA damping ring energy per bunch train is 45 kJ, while for example in PEP II it is 60 kJ. With 5 Hz repetition rate the TESLA damping ring beam power is 0.225 MW. TESLA uses two long damping rings, storing the bunch trains in a compressed mode, with the bunch spacing reduced by about a factor of 16; even with this compression, a large ring circumference of about 18 km is still required. The layout has two 8 km straight sections placed entirely in the main linac tunnel; additional tunnels are used for the 1 km circumference loops at either end. About 400 m of wiggler sections are needed to achieve sufficient damping. Fast kickers with <20 ns rise and fall time are required for compression and decompression of the bunch train at injection and extraction. JLC-X/NLC and CLIC use main damping rings with approximately 350 m circumference. For the positrons a pre-damping ring with large acceptance and about 200 m circumference is added.

6.2.4.1 Key Components

The key components of the damping rings are dipole, quadrupole and wiggler magnets, rf systems, kicker magnets, and beam diagnostic components. From the technical point of view, other critical issues are the impedance of the vacuum system, the alignment tolerances, and overall stability, *i.e.*, magnet power supply jitter, thermal instabilities, *etc.* The discussion of the damping ring-related luminosity issues can be found in Chapter 7.

JLC-X/NLC and TESLA [19] describe beam transport magnets and give specifications for magnet power supplies. All magnets seem to be feasible. The experience from existing damping rings and storage rings seems to be sufficient.

All proposed wiggler magnets are based on permanent magnet hybrid technology. This technology is in use at many synchrotron light sources around the world. The total wiggler length varies from 46 m (NLC) to 400 m (TESLA). Permanent magnets are vulnerable to radiation damage and have to be protected with an appropriate collimation system.

The rf system design of all proposals is based on existing state-of-the-art superconducting (CESR, KEKB) or normal conducting (PEP-II) installations at the B-factories.

Without beam-based correction algorithms the damping ring alignment tolerances cannot be met. The assumed procedure for all LC designs is to align the components with an achievable position tolerance of typically 0.1 mm and a roll angle of typically 0.2 mrad. Then beam-based correction algorithms have to be applied. This subject is discussed in Chapter 7.

6.2.4.2 Kicker Magnets

Because of their beam pulse structure, JLC-X/NLC and TESLA require very different kicker technologies. For TESLA, the kicker rise and fall times determine the size of the damping ring. Pulse-to-pulse stability requirements are similar (few $\times 10^{-4}$) but may be slightly more challenging to fulfill for TESLA.

The demonstrated performance of the SLC kickers was used as a guideline for JLC-X/NLC kicker system specifications. The SLC e^- kickers had 60 ns rise time with two points of equal kick along the flat top separated by about 60 ns. The kickers had substantial (few percent) pre and post kicks (more than one rise time away from the main pulse). The slow rise and fall was caused by the thyratron rise time, circuit elements in the pulser and the impedance of the magnet. The SLC kickers contributed a significant impedance to the rings. Kicker R&D at SLAC has addressed the latter, and pulser R&D for the NLC modulator has addressed the switch and circuit element problems. A magnet has been built. Its impedance has been measured and it will be installed in SPEAR.

SLC kicker amplitude stability was 0.01%, adequate for NLC but still a source of pulse-to-pulse jitter. In order to reduce the jitter for JLC-X/NLC a kicker compensation "achromatic" pair has been included in the design. The system is under test at KEK/ATF and is expected to reduce the effect of the kicker jitter by a factor of 10.

The TESLA damping ring extraction kicker is a critical element. Since the bunches are extracted one by one from the TESLA damping ring, the kicker must have very fast rise and fall times of 20 ns. At present a study with industry aims for an 8 kV, <20 ns flat top, 3 MHz repetition rate pulser to be suited for one 30–40 cm long, 50 ohm kicker magnet. In parallel, a pulser at 1 MHz, <20 ns rise/fall time has been commissioned. Bursts of 2000 pulses, 1 μs distance, 2 kV, 5 Hz burst repetition rate, were produced. At higher voltages, this switch needs better cooling. Therefore the industrial switch is going to be built with an improved cooling system.

Two prototype TESLA kicker magnets were built, a ferrite as well as a stripline kicker, both to be used for testing in combination with the previously mentioned pulser. The vacuum tube is a ceramic tube, the kicker elements are outside the vacuum. After a series of studies and measurements a 600 nm coating was chosen to control the impedance. The kicker field was weakened by less than 3%. The kickers are almost matched to 50 ohms, but for the stripline one might go to 25 ohms in order to increase current and strength. The ferrite-type gives higher fields but cannot be used for pulses shorter than 20 ns. Pulse-to-pulse stability and kicker tails are critical issues and therefore part of the ongoing development program.

6.2.4.3 Vacuum System

The design of the vacuum system has to take into consideration impedance as well as other instability thresholds. In all cases a low impedance design of the vacuum chamber is required. The threshold for microwave instabilities is in both cases, JLC-X/NLC and TESLA, a factor of 2 above the design bunch intensity. The designed impedance Z/n is 30 mΩ or slightly below. Although simulation tools have become much better over the last years, the exact prediction of the impedance is difficult. Therefore all future changes in the damping ring designs should be accompanied by a careful impedance calculation. The detailed technical layout also has to take into account the excellent vacuum pressure of typically 10^{-10} mbar required to limit possible ion effects. Solutions have been worked out for B-factories and synchrotron light sources.

6.2.5 Diagnostics

In a linear collider, beam instrumentation has a greater role than in any other kind of accelerator. Since few tolerances can be met directly in the fabrication and installation process and maintained without using signals from the beam itself, beam instrumentation has the added function of providing the trim information for all subsystems: rf, focusing, positioning and feedback. The beam instrumentation must therefore be reliable and redundant. Furthermore, since both tolerances and beam dimensions are beyond the state of the art for large installed systems, R&D is urgently needed. Instrumentation has been an important part of the linear collider test facility programs, notably at FFTB, ATF and TTF. This work must continue with high priority.

The purpose of beam instrumentation in the linear collider is to validate the performance of each subsystem and to provide input to feedback and optimization controllers. Challenging instrumentation systems are needed for beam position and bunch volume, including phase space orientation. In addition to this, a new type of phase space monitor is required for the measurement of correlations between longitudinal and transverse phase space.

6.2.5.1 Beam Position Monitors (BPMs)

Both BPM resolution and calibration, or control of offsets, are very important for all projects. It is relatively easy to assess single pass resolution, and typical requirements, such as that for NLC (0.3 μm in the linac), are not far from that demonstrated in large systems, such as synchrotron radiation sources. The single pass resolution for APS, scaled to the NLC vacuum chamber size, is 1 μm. Smaller scale tests, like that done at FFTB with cavity BPMs, are considerably better (0.02 μm).

Long term control of offsets, which depends on the system design, has fallen short of the requirements for the JLC-X/NLC linacs and all planned damping rings. System design includes electronic calibration and beam based alignment. It is not possible, at this time, to properly compare performance goals ($\sim$1μm/24 hours) with existing large-scale experience. Small scale tests have been done, also in FFTB, that indicate the goal will be achievable.

For multibunch trains with close spacing (JLC-X/NLC), the required single pass resolution (1 μm) has yet to be demonstrated. For full 714 MHz, bunch-to-bunch separation, resolution of about 5 μm has been demonstrated at ATF. The high-speed multibunch systems will involve state of the art electronic components, will need R&D and are likely to be expensive.

Additional challenges are present with the beam position monitors installed in the cold TESLA accelerator modules. Different types of pickups and cavities have been discussed or tested in TTF. In TTF2 greater focus on the performance of the cavity BPMs will be possible.

6.2.5.2 Profile Monitors

Beam profile monitors provide data on the beam optical match, coupling and emittance for low emittance transport systems. In order to pinpoint error sources the monitors must be distributed along the bunch compressor, linac and beam delivery systems. Profile monitors

in the beam delivery system have special applications, such as at the interaction point, at related upstream focal points and for secondary beams such as bremsstrahlung. Critical performance characteristics that must be tested include:

- Resolution, especially for very high aspect-ratio beams
- Calibration stability (control of systematic errors)
- Durability in very high power density beams
- Operability (the degree to which the measurement interrupts operation)

There is no experience in large systems using profile monitors to accurately uncouple very flat beams, the closest being the wire scanners in the KEK ATF extraction line where the ratio $\varepsilon_y/\varepsilon_x$ is about 1%.

Profile monitor performance comparisons can be readily made for resolution and durability, as shown in Table 6.3.

TABLE 6.3
Comparisons of profile monitor characteristics.

	Resolution	Beam Density Limit	
Wire scanners (Tungsten)	4 μm	3×10^7 @ 1×1 μm	$\sigma_x \times \sigma_y$
Wire scanners (Carbon)	2 μm	3×10^9 @ 1×1 μm	$\sigma_x \times \sigma_y$
Laser wire	0.3 μm	—	
Laser-based interferometer	0.05 μm	—	
Optical transition radiation	2 μm	$5\times10^8/\mu m^2$	

The typical beam density for NLC is 7.5×10^9 @ 10×1 μm for one bunch and 150×10^9 @ 10×1 μm for the full bunch train. The table does not include beam delivery foci regions. R&D is needed for monitors in these regions.

The laser wire, apparently best suited for linacs, cannot be used to measure vertical sizes of beams having very large aspect ratios because of to the finite waist size or Rayleigh range. The beam at the end of the CLIC linac cannot be monitored using a laser wire for this reason; however locations in the beam delivery system are suitable for laser wire measurements.

Bunch length monitoring has the added challenge that the bunch compressors produce non-Gaussian beam shapes and the detailed shape is important. In addition the bunch length monitors are difficult to calibrate. To meet the challenge of bunch length monitoring, the TTF group has tested a number of techniques based on coherent radiation spectrum and electro-optical sampling. The best calibrated bunch length monitor, based on transverse deflecting structures, has been tested at SLAC and is suitable for all projects. The expected bunch length resolution is 10 μm for low emittance beams. The device is expensive since it requires an rf structure, typically 3 m long, with a high power source. R&D will be done at TTF2 to determine the long term, routine performance of this bunch length monitor.

6.2.5.3 Correlation Monitors

The most common emittance growth mechanism involves an increase in projected phase space through the introduction of a correlation, for example $y - z$. The bunch length monitor described previously can be used to monitor the $y - z$ (or $x - z$) correlation in addition to $E - z$ depending on the nearby optics. The device is an excellent tool for measuring correlations within the beam but it is large and cumbersome to integrate into the lattice and therefore cannot be included in all appropriate places. Another tool for measuring beam correlations is required.

6.2.6 Components of the Beam Delivery System

The Beam Delivery System (BDS) transports the beams from the exit of the linacs to the interaction point, where they are brought into collision, and then safely extracted and dumped in high-power beam dumps. This system must produce the necessary demagnification of the beams, must maintain the beams in collision, and must cleanly extract the strongly disrupted beams after the interaction point, and transport them to high-power dumps. In addition to this the BDS must provide a high level of machine and detector protection, in the event of a linac fault resulting in a beam with either a larger energy error or a large orbit deviation. It also must provide beam halo collimation and sufficient beam diagnostics.

This subsection covers the luminosity diagnostics, but not the overall machine physics aspects of the BDS. Magnets, dump design and collimators are not investigated although some of these components are challenging. The problems are common to all designs and therefore should be handled through close collaborations. Fundamental obstacles are not expected.

Luminosity Diagnostics

The purpose of beam diagnostics in the interaction region area is to monitor the luminosity and provide data on the sources of luminosity limitation. In each design, the luminosity is generated by beam intensity, beam size and by the disruption enhancement. There are a number of phase space dilutions and correlations, as well as stability problems that will cause the pulse-to-pulse and bunch-to-bunch luminosity to fluctuate. It may be possible to experience a drop in luminosity without a direct indication from the upstream beam monitors, if, for example, correlated misalignments are present. The luminosity monitoring system must provide information to help unfold the aberration and pinpoint the cause of the drop.

Luminosity monitors must use the neutral beam emitted from the luminous region (beamstrahlung), the radiative Bhabha signal and secondary processes, such as 2 photon and neutron emission, to perform the task. The first two of these were very useful at SLC, but JLC-X/NLC and TESLA have much more intense beamstrahlung and therefore require a new technology. Furthermore, the details of the beamstrahlung distribution will be used to determine the aspect ratio of the luminous region and the related disruption. For both designs, the beamstrahlung average power is about 300 kW. R&D is needed to make a durable, properly integrated beamstrahlung monitor.

6.2.7 Conclusions

The working group has examined the feasibility of these schemes and subsystems, taking into account the results of the ongoing R&D. This section lists concerns and suggestions for useful R&D.

Concerns and R&D:

- The required laser stability for **JLC-X/NLC**, **CLIC** and the **CLIC** drive beam needs more R&D; the design specifications vary from 2% rms to 0.1% rms. (Ranking 3)
- The target fracture limit for **conventional positron sources** except perhaps for CLIC, which is not far from JLC-X/NLC, must be studied further. (Ranking 3)
- The kickers for the **TESLA** damping rings require ultra-fast high voltage switches. (Ranking 2)
- The **TESLA** beam power at damping ring injection/extraction is high. Injection/extraction has to be stopped immediately in case of a fault. (Ranking 2)
- For all machines, beam position monitor resolution requirements are about 3 times beyond the state of the art, and the (more critical) systematic errors are largely unstudied. Both require R&D. (Ranking 2)
- For all machines, the beam size and luminosity monitors are beyond the state of the art and require R&D. (Ranking 2)
- For the photo-cathode sources, laser improvement for **TESLA** and development for **JLC/NLC** and **CLIC** are strongly recommended. (Ranking 3)
- Studies of the **cathode charge limit** using the E158 beam at SLAC should be continued for **JLC/NLC** and **CLIC**. (Ranking 3)
- The SLAC study of an undulator-based polarized positron source is important and should be carried out, possibly through collaborations. For both JLC/NLC and TESLA the proof of principle, yield, and target issues should be **evaluated**. (Ranking 4)
- The present kicker program for **TESLA** should be strengthened. (Ranking 2)
- For all machines:
  - Existing test facilities should be used to commission new beam diagnostic elements.
  - Challenging issues common to all designs should be addressed through close collaborations.
  - Tracking simulations describing the polarized sources should be checked carefully. There is a history of poor performance at existing injectors. (Ranking 3)
  - Studies of polarized rf photocathode guns should be encouraged. (Ranking 4)
  - A detailed layout up to DR energy should give intensity overhead, location of beam loss, positron beam stability (especially TESLA) and longitudinal emittance. (Ranking 3)

6.3 RF POWER SOURCES

6.3.1 Klystrons

The high power klystrons are among the most challenging components in the rf system for linear colliders, and their development is indeed critical for all the projects at hand. The klystron design parameters, achievements to date, levels of industrialization, and future R&D plans for all five projects are summarized in Table 6.4. The choices of operating frequency and rf pulse performance requirements are naturally linked to those of the corresponding accelerator structures. As a result, there is a clear distinction between the various linear collider projects in their approach to an efficient power source system. All projects, based on normal conducting accelerator technology, adopted pulsed-power systems similar to the original conventional S-band linac technology. They require high-peak power klystrons in the range of 50 to 80 MW with microsecond-long pulses at 100–200 Hz repetition rates. High voltage modulators and klystrons are lumped into single rf units and they are installed together in utility tunnels separate from the main linac tunnel. The klystrons are operated at saturation to improve stability and efficiency. The TESLA rf power source system has to deal with a much longer pulse (millisecond long), since its superconducting cavities are designed to have a half-millisecond filling time. A lower peak power (10 MW) klystron powers 36 cavities with a 1.5 millisecond long pulse at a 5 Hz repetition rate. The low voltage (12 kV) modulators are lumped together in the surface halls spaced 5 km apart along the linac and are connected to their pulse transformers installed close to the klystrons in the tunnel by 12 kV-pulse cables. This configuration eliminates a separate tunnel for the power sources, but in turn requires linac operation to be interrupted for replacement of klystrons. The klystrons are operated at 90% of saturation to provide reserve power for rf feedback.

Among the klystron parameters, the rf efficiency is one of the most important because it determines the quality of a tube. In general, high efficiency is more challenging to klystrons operating at higher frequency, since beams with higher density in a tube behave more nonlinearly because of increased space charge. This makes the design of the klystron (particularly that of the output cavity) much more difficult. Nevertheless, X-band klystrons both at JLC-X and NLC achieved 55% level efficiencies as seen in Table 6.4. The key to this success is the development of the PPM (Periodic Permanent Magnet) focusing system and the incorporation of this technology into the klystron design. Success also comes in large part from the development of new simulation and modelling tools [20]. The PPM focused klystron eliminates the need for power-consuming solenoid magnets, and thus increases the net rf efficiency. Its relatively weak focusing strength demands a lower perveance ($I_0/V^{3/2}$), which in turn makes efficiency even higher. The drawback with a PPM klystron is that it requires a high cathode voltage (480 kV at X-band), raising the burden for the modulators. An alternate approach taken by TESLA is the multibeam klystron (MBK), where seven, low voltage, low microperveance beams are used in parallel in one vacuum vessel [21]. The TH1801 multibeam klystron has achieved an output power of 10 MW at 1.5 ms pulse length with 65% efficiency. It still uses a focusing solenoid, but the solenoid power is only several kW, resulting in only a few percent rf efficiency reduction. The benefit of low perveance can be seen clearly in Table 6.4 where all successful klystrons with efficiencies of 55% or more have a microperveance of 0.5–0.8 mA/kV$^{3/2}$.

TABLE 6.4: Klystron Summary

	TESLA	JLC-C	JLC-X	NLC	CLIC
Klystron type	MBK (7 beams) (Multibeam Klystron)	SBK (Single-Beam Klystron)	SBK MBK in design	SBK Sheet-BK in design	937 MHz MBK for Drive Beams
Focusing system	Solenoid	Solenoid/PPM (Periodic Permanent Magnet)	PPM	PPM	Solenoid
Number of klystrons for two linacs	572	4,276	4,064	4,064	448
Operating frequency [MHz]	1,300	5,712	11,424	11,424	937
Output power [MW]	10	50	75	75	50
Cathode voltage [kV]	110–120	350	480–500	480–500	189
Average rf power [kW]	150 @10 Hz	12.5 @100 Hz	18 @150 Hz	14.4 @120 Hz	100 @200 Hz
Efficiency goal [%]	65	50	55	55	65
Microperveance	0.5 each	1.5	0.8	0.75	0.5 each (6 beams)
Pulse length [μs]	1,500	2.5	1.6	1.6	16.7
Bandwidth [MHz]	n/a	100	100	100	4 (-1dB)
Lifetime goal [h]	60,000 (40,000 h in TDR)	50,000	50,000	>20,000	>25,000
Best performance so far	10 MW, 1.5 ms, 10 Hz @TH1801	53 MW, 2.5 μs, 50 Hz @E3746 No.3	74 MW, 1.4 μs, 25 Hz @PPM-2 65 MW, 1.5 μs, , 53% 50 Hz @PPM-3	72 MW, 3.13 μs, 1 Hz @75XP1 50 MW, 2.4 μs, 120 Hz, 57% @50XP	Design studies
Efficiency achieved so far	65% @TH1801(MBK)	47% @E3746 No.3	56% @PPM-2	56% @75XP1 45% @TH2104(SBK)	Design studies
Lifetime achieved so far [h]	30,000 @TH2104C A year @TH1801 Prototype 2 (4 MW)	2,500 @E3746 No.3	n/a	30,000 @60 Hz@XL-4	Design studies
Power margins	10% for control 6% for waveguide loss	Operated at saturation	Operated at saturation	Operated at saturation	Not studied yet
Vendor's name, if any	Thales, CPI in future	Toshiba	Toshiba	CPI, Toshiba, Marconi	Thales
Level of present industry involvement	High	High	High	Medium (DFM, CPI for 75XP3-2 body)	Design stage
Plan of more industry involvement	CPI VKL 8301 (MBK), UK, Russian, and more	Continue to work with Toshiba	Continue to work with Toshiba	DFM with CPI and other companies	Design stage
Future plan of R&D	Development of horizontal MBK with Thales Study of components to improve lifetime	PPM No.2 More E3746 (solenoid) for SASE FEL (SCSS) Deign of mass production version	PPM-3 in testing Design of PPM-4 (mass production version) More PPMs for J-LUFT project	XP3 in remodelling XP4 in design	Build prototypes

The JLC-C project relies on the more conventional solenoid-focussed klystron, at least in its initial phase.

CLIC is also considering using a multibeam klystron in the drive-beam accelerator [22]. In the present stage of the CLIC project, no prototype klystron and no modulator has been built for their requirements (937 MHz operating frequency, 50 MW output power, 100 μs pulse length, 100 Hz repetition rate, and 65% efficiency, for operation at 3 TeV c.m. energy). Hardware studies will probably begin after the feasibility of the CLIC drive beam scheme has been demonstrated with CTF3. However, Thales has already performed a design study of an MBK tube for this set of parameters. The main result of this study is that a 6 beam MBK with somewhat reduced performance (efficiency of 65% and output power of 40 MW) operating at 215 kV is believed to be feasible.

Although the X-band PPM klystrons produced at JLC-X and NLC have shown more or less satisfactory results in terms of their design output power and pulse length, testing has been generally limited to 25 Hz (PPM-2 of JLC-X) or 1 Hz (XP1 of NLC) repetition rates because of the insufficient cooling systems employed in these prototype designs. However, the latest model for JLC-X, PPM-3, which has a cooling system designed for 100 Hz operation has shown rather promising results in this respect: it so far reached 65 MW at 1.5 μs and 50 Hz with 53% efficiency (PPM-3 is still being tested and performance is not yet limited by the tube characteristics). Its operation is limited to 50 Hz because of the performance of the modulator; the cooling capacity measurements indicate that one can operate it at 100 Hz or even higher repetition rates. The latest version of the 75 MW NLC klystron, the XP3, was designed for 120 Hz, 3.2 μs pulse length operation. However, the two tubes of this design that have been built have had a variety of problems (low gain, oscillations and gun arcing), and are being autopsied to try to understand the causes of their failures. A rebuilt XP3 tube is expected by April 2003, and a more robust design (XP4) should be ready in the summer of 2003. JLC-X and NLC personnel are also designing multibeam or sheet-beam PPM klystrons in order to improve efficiency and lifetime and/or to double the peak power at a much lower voltage.

Both high power PPM klystrons and multibeam klystrons are very new technologies in the industrial world, and the increased complexity of these tubes may cause higher construction costs as well as higher failure rates. Lifetime testing has only recently started for all linear collider projects. Among these tests, the JLC-C E3764 No. 3 klystron achieved more than 2,500 hours of accumulated operation without a major failure [23]. The 50 MW X-band solenoid-focusing XL4 klystrons have been operated cumulatively over 30,000 hours at 60 Hz at the NLCTA. The first TESLA MBK TH1801 has operated for about 5,000 hours with reduced performance (4 MW-output power, 1.5 ms-pulse length, and mostly 1 Hz repetition rate). It was also operated at the full specifications over several weeks. However, these achievements are still far from the desired lifetime goals in the range of several tens of thousands of hours. S-band experience with the SLAC 5045 klystron [24] (65 MW peak power, 27 kW average power, 350 kV beam voltage, and 40,000 hours lifetime) indicates that similar lifetimes may eventually be achievable. The S-band experience at SLAC also shows that the most likely cause of klystron failure is cathode arcing due to barium evaporation and deposition on the anode surface. The cathode lifetime is also related to its operating temperature: every increase of 25°C cuts its lifetime in half. Some industrial companies such as Thales have also investigated the lifetime issue in detail as part of a study of klystron mass-production. According to their study, the cathode emission is the

main factor affecting the lifetime of the TESLA MBKs as opposed to barium (the second TESLA MBK TH1801 failed recently due to gun arcing). They are planning cathode studies aimed at increasing their lifetime beyond 40,000 hours. The problem with verifying lifetime of this length is that several years of operation are required. All available studies should be centralized, compared and analyzed so that more accurate predictions of lifetime can be made from various klystron designs and short-term operational data.

The total number of klystrons required for linear colliders is such that industrial involvement is clearly needed for mass production. However, the specifications of klystrons for linear colliders are much more demanding than those for any klystron now commercially available. Thus the involvement of commercial klystron manufacturers from an early phase of R&D is very important to allow them to become familiar with the idiosyncrasies of high-peak power klystrons. The required level of industrialization of klystron production is high for all LC projects. TESLA, JLC-C and JLC-X have successfully produced klystrons through their various industrial partnerships. At TESLA, industrial involvement is expanding, with several proposals in the works. Both JLC-C and JLC-X have worked intensely with Toshiba and will continue to work with this company to refine their designs and reduce costs. NLC has launched the so-called Design For Manufacturing (DFM) klystron program with industry during the past three years to produce lower-cost 50 MW and 75 MW PPM klystrons. The involvement of multiple manufacturers for each project will help reduce acquisition costs via competitive bids. Soon, CPI will join the companies manufacturing MBKs and PPM klystrons, of which Thales, and Toshiba, respectively, are the dominant producers. The international microwave klystron industry is thus gaining experience that it will need to handle the large klystron orders from any of the linear collider projects.

6.3.2 Modulators

Modulators are also critical components of the rf power system. Like all the rf subsystems, high efficiency, high reliability, and low cost are the goals for successful modulator design. The design parameters, achievements to date, the level of industrialization, and future R&D plans of all 5 projects are summarized in Table 6.5. The design parameters and the stability requirements of the associated DC power supplies are summarized in Table 6.6. Modulators used to be dominant cost drivers in the JLC-X and NLC designs when line-type modulators were initially envisioned. Line-type modulators like those used in the SLAC linac have some major deficiencies. The thyratron switch tube needs frequent tuning and has a short lifetime of around 15,000 hours. The thyratron is a fast ON switch, but is slow to turn OFF. The overall efficiency of this type of modulator is as low as 50–60% because of the large losses in the various components and the relatively slow pulse rise and fall times due to their high ratio step-up transformer. The Pulse-Forming Network (PFN) needs a large number of parallel LC circuits to get good pulse flatness. For a 1.5 ms long pulse for TESLA, the size and cost are quite high.

An approach that mitigates many of these problems, which was adopted at NLC and later at JLC-X, is to use the fast ON-OFF Insulated Gate Bipolar Transistor (IGBT) as the power switch and to incorporate that technology into an induction-linac type modulator design. The IGBT switch is anticipated to have a longer lifetime than the thyratron. The solid-state induction modulator is basically a large stack of small pulse transformers in

TABLE 6.5: Modulator Summary

	TESLA	JLC-C	JLC-X	NLC	CLIC
Modulator type	Bouncer Solid-state switch (IGBT)	Smart modulator Thyratron switch	Linear induction Solid-state switch (IGBT)	3-turn induction Solid-state switch (IGBT)	Line-type with double PFN and two thyratrons
Transformer ratio	1:12	1:16	1:1	1:3	1:10
Output peak voltage [kV]	130	400	500	500	190
Output peak current [A]	150	317	2120	2120	250
Number of klystrons to be fed	1	1	8	8	1
Pulse flat top [μs]	1,500	2.5	1.6	1.6	16.7
Rise and fall time [μs]	200	1–2	0.2	0.2	<4
Pulse flatness during flat top	$< \pm 0.5\%$	$< \pm 0.5\%$	$< \pm 0.3\%$	$< \pm 1\%$	$< \pm 0.1\%$
Pulse to pulse voltage fluctuation	$< \pm 0.5\%$	<1% (p-p)	$< \pm 0.1\%$	$< \pm 0.1\%$	$< \pm 0.1\%$
Efficiency goal [%]	85	>60	>80	>80	95 w/o charging supply auxiliaries and solenoids
Reliability (MTBF) goal [hours]	100,000	n/a	>10,000	>10,000	n/a
Best performance so far	128 kV, 89 A, 1.7 ms, 10 Hz @TTF3, 117 kV, 131 A, 1.7 ms, 10 Hz @TTF1,2	350 kV, 2.5 μs, 60 Hz @Smart No.1	Design studies	500 kV, 650 A, 2.5 μs, @4-Dog	Design studies
Pulse flatness achieved so far	$< \pm 0.5\%$	$< \pm 0.5\%$	Design studies	n/a	Design studies
Pulse to pulse voltage fluctuation achieved so far	$< \pm 0.5\%$	n/a	Design studies	n/a	Design studies
Efficiency achieved so far	>85% @TTF3	>52.4% @Smart No.1	Design studies	>80% @4-Dog	Design studies
Lifetime achieved so far [hours]	35,000 @10 Hz@TTF3	15,000 @Smart No.1	Design studies	n/a	Design studies
Vendor's name, if any	PPT, ABB, FUG, Beerwald	Nihon Koshuha	Mitsubishi	In house production	Design stage
Level of present industry involvement	High	High	High	Medium. Bechtel for engineering design	Design stage
Plan of more industry involvement	Already ongoing with PPT, ABB, FUG and Russian	Continue to work with Nihon Koshuha	Already ongoing with Mitsubishi and Hitachi	n/a	Design stage
Future plan of R&D	Modular layout. Enhance reliability and maintainability. Intelligent diagnostics and interlock to improve lifetime.	Smart modulator No.2. Modular design. Closed type for SASE FEL. Improve reliability and lifetime of thyratron.	4-Pack by mid 2003. 50 kV prototype by mid 2002. High voltage IGBT with faster rise and fall time. Reliability.	8-Pack modulator for 8-Pack Project Phase II by mid FY2003. Cooling. Reliability. Circuit and klystron protection.	Build prototypes.

TABLE 6.6
Power Supply Summary

	TESLA	JLC-C	JLC-X	NLC	CLIC
Charging voltage [kV]	10	47	3.2	4	45
Average power [kW]	150	39	313	500	151
Efficiency [%]	>94 (HVPS)	n/a	96	96	>92
Stability [%]	0.5 (p-p)	±0.13	±0.1	±0.1	±0.1

which the primaries of the cores are driven in parallel by separate sets (called cells) of IGBT switches and capacitors operated at relatively low voltage (2–4 kV), and the high voltage is developed at the secondary in series [25]. The idea is so simple and flexible that the same design can be used for different voltages and pulse lengths with minimum changes, unlike the line-type modulators where the whole system, in particular the PFN, would need a major change. The driver cell (an IGBT switch and two capacitors on a printed circuit board) is designed as a plug-in module that can be easily accessed and replaced in the field for fast maintenance. Additional driver cells are installed as hot spares to enable longer periods of continuous operation without interruption for maintenance. NLC has already built a 4-pack prototype with a 3-turn secondary and has demonstrated an efficiency of about 80% and a pulse shape with fast rise time of about 300 ns (fall time is slower). JLC-X has adopted a similar design, but uses a single-turn straight secondary with a simpler insulation design and lower cost of the secondary conductor, in exchange for more cores. To compensate a 2% voltage droop during the flat top, an appropriate fraction of IGBT drivers is triggered with programmed delays resulting in a pulse flatness of ±0.3%. This level of pulse flatness during the flattop, as well as $< 0.1\%$ pulse-to-pulse voltage fluctuations, are required to keep the rf-to-beam phase error below 1°.

There are many other technical issues to be addressed and investigated such as IGBT protection and reliability in the pulsed-power operation where the IGBT drivers are not well modelled (very high dI/dt, peak current, high voltage lasting for only a few microseconds, *etc.*). The diode testing is underway at SLAC to look for signs of arc damage under controlled faulting. In the first high voltage test, about 20% of IGBT drivers were damaged by a single arc, seemingly because of ringing in the 3-turn secondary when the klystron faulted. Even after installing snubbers to compensate the mismatch, single IGBT driver failure was found to occur. It stopped only after the EUPEC IGBT drivers, found to have an unbalanced induction layout inside, were replaced with more balanced and higher voltage rated Mitsubishi drivers. Since then, the NLC 4-pack modulator is producing 400 kV-1.5 μs long pulses for the 8-pack Phase-I project with no apparent degradation. The production cost per klystron when driving 8 klystrons with a single induction modulator is estimated to be lower than for a 2-pack line-type modulator by a factor of 2–3. The latest cost estimate shows that the modulators are no longer the largest cost driver at NLC and JLC-X compared to other rf components.

The induction technique described previously cannot be applied to a millisecond long pulse for TESLA, since it would require a large amount of magnetic material and/or a large number of secondary turns to avoid saturation. Instead, a classical twelve-to-one turns ratio

transformer is used although the primary is driven using solid-state switches. To avoid having very large storage capacitors to achieve good pulse flatness ($< \pm 0.5\%$) during their long (1.5 ms) HV pulses, a bouncer circuit is used [26]; otherwise the droop of 19% on the main capacitor bank during the pulse would produce an intolerable pulse distortion. This modulator consists of a DC power supply (10 kV), a main capacitor bank, a bouncer circuit, two solid-state switches, one for the main capacitor bank (IGBT or IGCT, Integrated Gate-Commutated Thyristors) and another for the bouncer circuit (SCR), and a pulse transformer. The bouncer circuit is basically a resonant LC circuit producing a single sine wave to compensate for the main capacitor droop. Several bouncer-type modulators were built and are in use at TTF. They have shown more than 85% efficiency at a pulse length of 1.7 ms with 200 μs rise and fall times at 10 Hz. They have also achieved a pulse flatness of $< \pm 0.5\%$ and a pulse-to-pulse voltage fluctuation of $< \pm 0.5\%$. A klystron-modulator unit has an interlock system in the event of a klystron gun spark. To ensure that the energy deposition in the spark remains below 20 J to avoid damage to the klystron gun, the relevant IGBT switch will be immediately opened to disconnect the capacitor bank from the sparking klystron. The energy stored in the transformer leakage inductance and the power cable will be dissipated in two networks of resistors. Five modulator/transformer/klystron systems are operational. One modulator at TTF has been working since 1994 for about 35,000 hours of operation at a 10 Hz repetition rate, and is still in operation. The use of IGBT switches assures high reliability. The location of modulators in the surface halls allows for fast repair in case of problems. The next phase of development will be the design of a modular layout to allow for fast exchange of components and to further enhance reliability and maintainability.

Because of the long pulse length for TESLA, the size of the pulse transformer core is large, since it is proportional to the product of the voltage and the pulse length. The transformers are placed in the tunnel, close to the klystrons. A design already exists for a transformer, which fits the tunnel layout, but the connectors, which should allow quick exchange in the tunnel, remain to be designed. The maximum distance of pulse delivery from the modulator to the transformer in the tunnel is about 2.8 km. The power loss in the HV cable will be 2% on average. There is a concern of pulse shape distortion, in particular at the leading edge of the pulse, if the cable impedance is not matched to the klystron impedance and the skin effect of cable inner conductor is not minimized [27]. The cable must be designed for the appropriate dV/dt conditions, but the voltage is quite low (12 kV), and the insulation should therefore be no problem. If the design and the fabrication are done correctly, then the HV cable is not regarded as a significant concern. The prototype cable was ordered, and the testing will start soon.

At CLIC, a conventional line-type modulator with a double PFN and two thyratron switches has been studied to drive a single 50 MW multibeam klystron [22]. They are also investigating alternative modulator designs using solid-state switches as a future replacement for the thyratrons.

As is the case of klystrons, the involvement of industry at an early stage to build prototypes of critical components or integrated systems is very important to familiarize manufacturers with the new technologies. A series of Modulator Workshops have been held in the US during which industrial designers and manufacturers have been introduced to the requirements of the linear collider projects. TESLA is already working with several companies (PPT, ABB, FUG, and Beerwald) to deliver subunits of the latest bouncer

modulators. PPT could now take over the task to build and deliver a complete modulator. JLC-C and JLC-X have been producing their modulators in industrial partnerships with various companies (Nihon Koshuha, IHI, Mitsubishi, and Hitachi), beginning with the initial design. NLC has contracts with Bechtel-Nevada to provide a detailed mechanical engineering design and sophisticated machining capabilities. Bechtel has also contributed to the fabrication of several prototype solid-state induction modulators in collaboration with LLNL. The industrialization of the linear collider modulators is well under way, worldwide.

6.3.3 Low-Level RF Control

The requirements for the low-level rf (LLRF) control system are defined in terms of phase and amplitude stability of the accelerating field during the flat top portion of the rf pulse. The stability requirements, the status of the design and hardware developments, and future R&D plans for all five projects are summarized in Table 6.7. All projects rely on beam induced signals to adjust the phase of the rf at the structures. Superconducting rf cavities require more complex low-level control than normal conducting systems. Both feed forward and feedback loops are needed and the LLRF system must be carefully specified in order to avoid unnecessary complexity and retain the needed flexibility.

For both TESLA and JLC-X/NLC there must be a system that distributes a reference clock that is accurate enough to allow the acceleration of a pilot beam bunch through the linac. A successful demonstration of a fiber optic based X-band distribution system was done at SLAC. The system uses two way optical transmission on a fiber with an active feedback system for compensation. Both beam pickups (in the JLC-X/NLC) and signals from the accelerator structures themselves (in all machines) are used to control the fine phase adjustment of the structure.

At TESLA, it is desirable to keep the bunch-to-bunch energy spread below 5×10^{-4} in order to assure that the single-bunch chromatic effects do not become a dominant emittance growth factor. This requires tight control of the accelerator field in the vector sum of 36 cavities (one klystron unit) on the order of 0.03% (correlated errors) and 0.5% (uncorrelated) for the amplitude and 0.2° (correlated) and 3° (uncorrelated) for the phase. The major sources of perturbations at TESLA are fluctuations of the bunch current and changes in resonant frequency resulting from the deformations of the cavity walls which can be induced by mechanical vibrations (microphonics) and Lorentz forces (at TTF, the effect of microphonics is small compared with Lorentz detuning). The amplitude and phase errors due to the Lorentz force (and microphonics) are on the order of a few % and 10°–20°, respectively (without piezoelectric tuners). The non-repetitive errors due to bunch charge variation and microphonics are much smaller than those due to the Lorentz force detuning. The feedback scheme works at the design gradient of 23.8 MV/m, but the additional power required for field control at the planned upgrade to 35 MV/m will exceed the klystron power reserve of 10%. However, the repetitive time-varying Lorentz force detuning can be reduced by more than one order of magnitude by using a piezoelectric tuner in an adaptive feedforward way, as successfully demonstrated by a recent experiment at TTF. This scheme will reduce even the 10% power reserve needed at the nominal operating gradient.

TESLA developed a digital LLRF system using an I/Q modulator scheme to control both the in-phase (I) and quadrature (Q) components of the cavity field [28]. The I/Q concept

TABLE 6.7: Low-level RF Control System Summary

	TESLA	JLC-C	JLC-X	NLC	CLIC
RF-to-bunch phase stability	<0.5degree	n/a	1 degree	1 degree	0.25 degree
Pulse-to-pulse phase stability	<0.5degree	n/a	1 degree	1 degree	0.25 degree
RF amplitude stability [%]	<0.03	n/a	<0.1	<0.1	<±0.1
Power routing changing speed [ns]	3–4,000	n/a	10	10	n/a
Main source of errors	Lorentz-force detuning. Microphonics. Bunch current fluctuation.	n/a	Thermal expansion of rf structures and delay lines. Beam-loading. Modulator voltage ripple.	Thermal expansion rf structures and delay lines. Beam-loading. Modulator voltage ripple.	Have to be found with CTF3.
Design type	Digital I/Q modulator	n/a	To be decided.	Digital IF techniques.	n/a
Status of design	Concept proved by TTF1. To be implemented in TTF2.	n/a	Under way.	Under way.	Prototype under construction for CTF3.
Status of hardware and testing	Studies under way.	n/a	Cavity BPM tested at ATF.	Prototypes planned.	Ready by end 2002.
Future plan of R&D	Work on adaptive feed-forward. System identification. High level automatization. Piezoelectric tuning mechanism. Cost reduction. Improve redundancy.	n/a	System test at ATF linac using a beam. Improve redundancy for cost reduction.	High speed DAC/ADC module. A full 8-pack test planned.	n/a n/a

allows for detection and control in all 4 quadrants including zero, and is most suitable for the control of large cavity detuning since it minimizes the coupling between loops. The rf signals from each cavity are converted to an intermediate frequency (IF) of 250 kHz and sampled at a rate of 1MHz to provide digital I/Q information for individual cavity fields. The vector-sum of 36 cavities is calculated using digital signal processing (DSP) and the amplified error signal is combined with the feedforward signal and fed back to the vector modulator that controls the klystron input-power driver. The digital technique allows for calibration and corrections to be made and updated. In this method, all 36 cavities driven by a single klystron are treated like one cavity and the feedback algorithm is applied only to the vector-sum. Therefore, fast control of an individual cavity field is not possible. The major advantage of the digital feedback is the built-in diagnostics, which is essential for the operation of 36 cavities driven by one klystron. The phase calibration of individual cavities and the vector sum are measured relative to the beam by measuring the beam loading induced in the cavities. This can be done at a total charge of 200 nC presently; the goal is to get as low as 8 nC for calibration.

A smaller-scale LLRF system was implemented at TTF with 16 cavities and it was demonstrated via beam measurements (typically 0.15% rms energy fluctuations during the macro-pulse and 0.25% pulse-to-pulse) that the $<2\times10^{-3}$ amplitude stability and <0.5% phase stability required at TTF can be achieved with a (dead reckoned) feedforward table and the feedback system. The residual errors were dominated by repetitive factors that were reduced by the feedforward by about one order of magnitude. These results show promise that the tight requirements on amplitude and phase stability at TESLA can be achieved by the combination of these feedback and adaptive feedforward systems. An improved digital controller for the TTF LLRF is under development. In the new system, a single digital signal processor replaces the six used in the prototype. It will be used to increase the system flexibility and to more effectively apply modern technology.

At JLC-X and NLC, the rf modulation system is used as a fast phase shifter, since the klystron is operated at saturation and the rf output is thus kept at a constant power level. The rf amplitude stability must be provided by control of the modulator pulse amplitude and is expected to be better than 0.1% pulse-to-pulse. The objective of the JLC-X/NLC LLRF system is therefore to compensate the beam-loading effects, the repetitive phase variations during the pulses due to modulator voltage ripple, and the phase drifts caused by thermal expansion of the accelerator structures and the SLED-II power delay lines. The goal of phase control is to achieve a 1° rf-to-bunch setting accuracy and a 1° pulse-to-pulse stability.

At JLC-C an additional antisymmetric phase modulation is needed to produce an AM modulation at the input of the compressor which compensates for its intrinsic distortion.

Unlike TESLA, JLC-X and NLC use a SLED-II pulse compression scheme to drive four pairs of klystrons to individually deliver rf power to four accelerator structure clusters (each consisting of six structures) in the proper sequence, synchronous with the beam. The compression of rf power is achieved for SLED-II by quickly modifying the relative phase of the klystron drive during each pulse. The wide bandwidth of the system (>100 MHz) allows rapid phase changes in about 10 ns. Even with a state-of-the-art stabilized fiber optics rf reference/distribution system, there will still be phase drifts present in the system. In order to optimally phase the rf pulse going to each rf structure cluster in the presence of phase errors and drifts, the absolute phase of the accelerator rf will be determined by

measuring the relative phase with the respect to the beam. The rf-to-beam phase is monitored using rf detectors on the structure outputs. This signal is fed back to the klystron driver so that the phase of the rf pulse going to each rf structure cluster can be adjusted individually. Thus, six structures in one rf cluster are treated like a single structure with respect to the fast phase feedback. The phase differences among the six structures in the same rf cluster are set initially and not adjusted thereafter.

At NLC, programmable high speed digital IF techniques are planned for both arbitrary klystron drive modulation and accurate rf vector detections, rather than the I/Q approach currently used at NLCTA, in order to reduce system cost and improve accuracy [29]. Prototype studies have just begun and have produced some encouraging initial test results. A full 8-pack test installation is planned. At JLC-X, the beam-based phase stabilization system for rf pulse transmission through the SLED-II lines is under development. A cavity beam pickup has been developed and a test result at the ATF linac demonstrated that it can detect the beam phase within 1°. At CLIC, prototypes of LLRF systems are under construction for CTF3. They should be ready by the end of 2002.

6.3.4 Conclusions

6.3.4.1 TESLA

Both Thales MBK klystrons and bouncer modulators met pulse performance requirements (peak power for klystron or peak voltage for modulator, pulse length, efficiency, repetition rate) for TESLA. However, the lifetime of the MBK klystron has not yet been demonstrated.

R&D (Ranking 3):

- The lifetime test of the MBK klystron, particularly because of cathode degradation, should be pursued as planned.
- The improvement of the LLRF system design should be given high priority.

6.3.4.2 JLC-C

The repetition rates of the klystron and the modulator need to be improved to meet design requirements (100 Hz).

The efficiencies of the klystron and the modulator need to be improved to meet design requirements (50% including solenoid-power and 65%, respectively).

R&D (Ranking 2):

- The operation of the klystron and modulator at 100 Hz repetition rates should be demonstrated.
- The LLRF system needs to be designed and demonstrated.

- The lifetime tests of the klystron and the modulator should be pursued as planned.

R&D (Ranking 4):

- The development of the C-band PPM klystron should be supported and continued.
- Some R&D may also be necessary for a new modulator design with a solid-state switch to improve the pulse shape efficiency and to minimize the time for maintenance.

6.3.4.3 JLC-X/NLC

The latest test result of the JLC-X PPM klystron is gratifying and looks promising.

The latest test result of the NLC 4-pack induction modulator prototype is looks encouraging. More klystron arcing tests are needed to verify the protection circuit of the IGBT switches.

R&D (Ranking 2):

- The operation of the JLC-X PPM klystron at 150 Hz (JLC-X) or 120 Hz (NLC) repetition rates needs to be demonstrated.
- The operation of the NLC induction modulator at full specifications needs to be demonstrated.

R&D (Ranking 3):

- NLC should continue its current PPM klystron R&D to achieve pulse performance and repetition rate requirements. Since the lifetime test is yet to be performed, development of this alternative design to the JLC-X PPM klystron should be continued.
- Development of the JLC-X linear induction modulator should be supported and pursued as planned as an alternative design.
- The improvement of the LLRF system design should be given high priority.
- The lifetime tests of the klystrons and the modulators should be pursued as planned.

6.3.4.4 CLIC

Neither drive beam prototype klystron nor modulator has been built so far and both are still in the paper study stage. Hardware studies will probably not begin before the feasibility of the CLIC drive beam scheme has been demonstrated with CTF3. Thales has a design study of a 6 beam MBK with somewhat reduced performance that needs to be demonstrated (937 MHz-operating frequency, 40 MW-output power, 16.7 μs-pulse length (500 GeV c.m.), 100 Hz-repetition rate, and 65% efficiency). It must be noted, however that

more klystrons can be used if the peak power requirements cannot be met. The 90% design efficiency for the modulator will be difficult to achieve with the conventional line-type modulator that is currently under consideration.

R&D (Ranking 2):

- R&D study of an MBK tube including prototyping should be started for the 3 TeV upgrade.

R&D (Ranking 3):

- A more efficient type of modulator should be studied for the 3 TeV upgrade.

6.4 RF POWER DISTRIBUTION

6.4.1 TESLA

For TESLA-500, the rf power is generated by 10 MW klystrons having two output windows, operating at 1.3 GHz, and providing an rf pulse of 1.37 ms at a repetition rate of 5 Hz. The rf waveguide system distributes the rf power to 36 nine-cell superconducting cavities per klystron. Thus, the basic rf unit consists of one klystron feeding 36 standing-wave cavities. Each cavity transfers 231 kW to the beam during the 0.95 ms long beam pulse. Each linac contains 286 of these units.

The rf distribution is a linear system branching off identical amounts of power for each cavity from a single line by means of directional couplers. Further functions of the waveguide system are to protect the klystron from reflected power, to avoid cross-talk between the cavities and to allow proper phasing and impedance matching. The latter function is provided in each branch by a three-stub waveguide transformer, which has each stub equipped with a motor remotely controlled by the low-level rf system.

Since not all cavities will reach the same accelerating gradient, the worst performing cavity in the group of 36 cavities limits the gradient. In principle, this can be mitigated by:

- Grouping cavities after acceptance tests (all cavities are tested in vertical cryostats)
- Detuning particular cavities
- Developing adjustable hybrid couplers plus tuners

The rf distribution is not under vacuum but in air; the cavity vacuum is isolated from the distribution system by the two rf windows in the main coupler.

A detailed description can be found in Chapter 3. Figure 6.1 gives the schematic layout of the system.

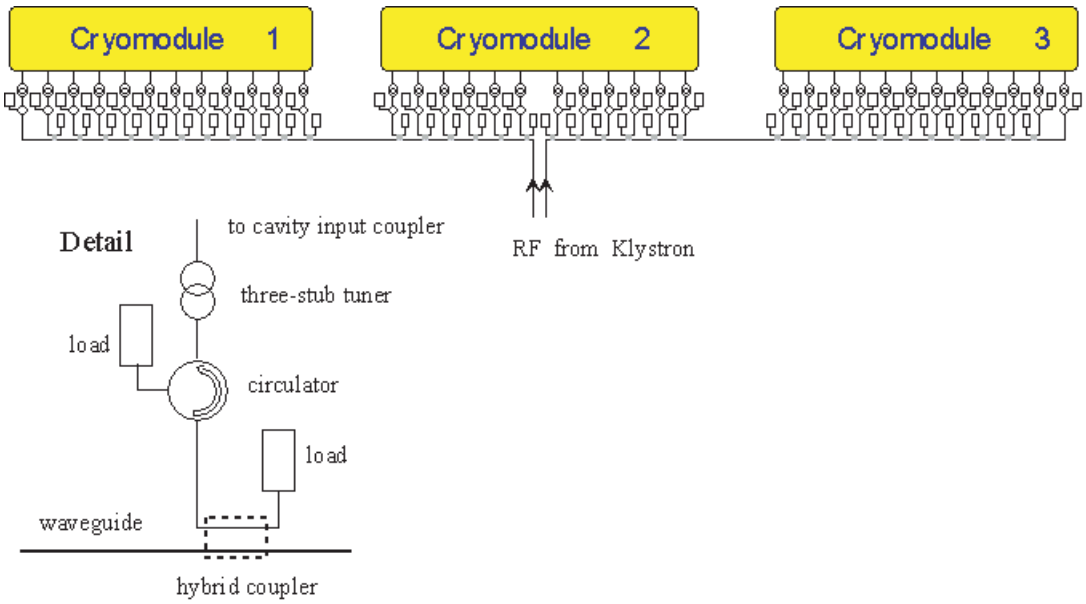

FIGURE 6.1. Schematic layout of the TESLA waveguide distribution system

The advantages of the concept are:

+ Simple, modular, proven technology for hybrid, circulator, tuner and loads
+ Used in TTF, similar to the rf system in the electron ring of HERA (though not pulsed)
+ No need for pulse compression
+ High efficiency (higher than tree-like distribution)
+ The rf power in the components is relatively low
+ No vacuum or overpressure in the distribution system which facilitates change of components
+ Low number of klystrons (572 in total)

Its disadvantage is:

– 36 cavities are off in case of a klystron or modulator fault leading to a drop of 0.87 GeV (0.35%) in beam energy

All the components are already in use in TTF1 at nominal power and comply with the specifications for TESLA 0.5 TeV.

In order to save costs, to improve engineering margins, and to improve performance, alternative and complementary designs for the following components are being developed:

- Three designs for adjustable (±1 dB) hybrid couplers to match the power to different cavity quench thresholds. High-power tests are planned for 2003/2004;
- A magic tee E-H tuner as waveguide type transformer instead of the three-stub plunger for higher power capability independent of the transformation ratio, providing a phase shift range of ±180°. High-power tests are foreseen in November 2002;
- The use of welding techniques instead of flanges for cost reduction and improved reliability. Tests of this technique are foreseen in 2004.

The waveguide system has to operate at a higher peak and average power for TESLA upgraded to 800 GeV, where each branch has to sustain 0.7 MW peak and 8 kW average forward power instead of 0.35 MW and 5 kW respectively. In case the superstructure concept is adopted, these values increase to 1.3 MW peak and 14 kW average.

- Experience exists with waveguides at the required power levels (test at DESY done).
- The hybrid couplers have to be tested at the higher power (tests foreseen in 2004).
- Alternatives exist for the circulator: either the circulator is pressurized with nitrogen or a new circulator is designed. The former has been tested and peak values of 4 MW have been reached albeit with a reduced repetition rate. Further developments of this approach are foreseen. The design of a new circulator is pursued together with three firms. The designs will be completed in 2002 and first tests are foreseen in 2003.
- The loads have been tested up to 10 kW which is sufficient for 800 GeV, but not quite sufficient for use of the superstructure at 800 GeV. However, commercially available loads exist for the latter application.

6.4.2 JLC-C

The power distribution system combines the outputs from a pair of 50 MW klystrons operating at 5.712 GHz in a 3 dB hybrid, increases the peak power to 350 MW by an improved SLED-type rf pulse compressor and splits the power with three magic tees in order to power four TW accelerator sections. Thus, the basic rf unit consists of two klystrons feeding four accelerator sections. Such a unit is also the smallest possible vacuum unit separated by two gate valves from the adjacent accelerator sections.

Each linac consists of 989 of these units. The layout of this rather classical system is shown in Figure 3.22 in Chapter 3.

The most demanding part of the system is the rf pulse compressor which is of a novel design. It consists of a coupled cavity chain acting as a delay line and comprising two storage cavities ($TE_{01,15}$ mode) coupled by a cavity operating with the $TE_{01,05}$ mode in between. The phase advance has been chosen to be $\pi/2$. The coupling irises between the cavities limit the group velocity. However, they cause frequency dispersion in the

propagating wave, which would result in a large distortion of the output waveform if not compensated by AM modulation of the input to the compressor. This amplitude modulation is produced by an anti-symmetric phase modulation of the input to the two klystrons and produces a compressed output pulse with a flat top of about 500 ns.

It has been shown recently that this phase modulation can be used to also take advantage of the rf power produced during the rise time of the modulator. Cold model measurements indicate that this new modulation scheme increases the compression ratio from 3.25 to the desired factor of 3.5. The expected power efficiency is larger than 70%. A further increase of the efficiency is conceivable by using larger storage cavities but no definitive R&D plan exists for this development.

The advantages of the system are:

+ Its simplicity as far as the high-power hardware is concerned
+ Shorter waveguide lengths than other pulse compression systems
+ Since the size of one rf unit is rather small, testing of one full rf unit is relatively easy
+ If one rf unit stops, then the energy drops only by 0.25 GeV (0.1%)

Its disadvantages are:

– The inherent lower rf efficiency of this SLED-type pulse compression
– Large number of klystrons (3956 in total compared to 448 of CLIC or 572 of TESLA)

In order to limit the critical detuning of the cavities forming the pulse compression system due to variations of the operating temperature, cavity models made from copper-plated invar have been developed but they have not yet given fully satisfactory results. New cavities for the high power test are under design.

The standard waveguide components such as bends, couplers and flanges have been developed and will be tested under nominal power in 2003 to 2004.

One rf unit will be tested at full power in 2004 in preparation for the C-band linac foreseen to drive the FEL of the SPring-8 Compact SASE Source (SCSS) by RIKEN. This will demonstrate the feasibility of the rf pulse compressor at high-power; it will also test the stability and reliability of the whole unit under operating conditions, including the robustness of the approach to control phase and amplitude of the klystron outputs.

The planning of SCSS foresees a full test of the first part of the linac consisting of the L-band injector and one C-band unit providing 300 MeV electron beam in 2005. This will be an excellent opportunity to test the C-band system under operational conditions and provide precious information on the possible design improvements to be made for a linear collider.

The original upgrading to higher energies foresaw the development of klystrons with twice the power and an extension of the linac by a factor of $\sqrt{2}$ in order to reach 1 TeV in the center-of-mass. Since this klystron development is not so obvious and the efficiency of an X-band linac is superior, the most probable upgrade path of a 0.5 TeV C-band collider is

the addition of an X-band part. Hence, no specific C-band development for the upgrade is required. Since there will be sufficient time for the development, a Delay Line Distribution System (DLDS) can be envisaged for this upgrade which has a higher efficiency than the compact SLED system.

6.4.3 JLC-X/NLC

6.4.3.1 Baseline Design

The basic rf unit consists of one modulator, four pairs of 75 MW klystrons operating at 11.4 GHz, a SLED-II type dual mode rf pulse compression system, and the waveguide distribution system. Each pair of klystrons delivers an rf pulse of 150 MW and 1.6 μs duration to a SLED-II system, which compresses the pulse by a factor of 4 to the required 0.4 μs using two 29 m long delay lines operating with the TE_{01} and TE_{02} modes. The 450 MW output pulse is fed through a low-loss circular waveguide and four magic tees to a girder containing six accelerator structures. Thus, the basic unit is composed of one modulator and 8 klystrons feeding 24 accelerator sections.

Each linac consists of 254 such rf units. The total length of the beam line pertaining to one rf unit is about 26.0 m of which 21.6 m is active length. The length of the delay lines exceeds the length of the beam line because the present layout is not yet optimized.

Originally, it was proposed by JLC-X and NLC to use the more efficient Delay Line Distribution System (DLDS) as the pulse compression system instead of SLED. It has an expected compression efficiency of about 85%. However, testing of a full system would have required a substantial investment since the basic units are relatively large. Furthermore, it was deemed that the time required to fully develop and test such a system would be unacceptably long. Also the multibranch vacuum system of the DLDS system has an extension which gave rise to concern. In particular, the demonstration of the dual-moded DLDS of NLC would have required eight 75 MW klystrons with a pulse length of 3.2 μs instead of only two 75 MW klystrons with a shorter, and therefore, much easier to obtain pulse length of 1.6 μs, which is sufficient for a demonstration of the preferred dual-moded SLED-II system. In addition, there is already a lot of experience with the SLED-II system though it has always been only single-moded and its dual-mode operation remains to be demonstrated. For these reasons, it has been decided to choose the simpler and probably more robust SLED-II solution.

The advantages of the scheme are:

+ A lot of operational experience exists with SLED-II in NLCTA
+ The power in the compressed rf pulse is only 450 MW over 400 ns (the DLDS system proposed had 510 MW instead)
+ The klystrons have to produce a pulse of only 1.6 μs compared to 3.2 μs in the dual-moded DLDS solution
+ The energy drop due to a trip of an accelerator structure is only 0.27 GeV (0.1%) because only one of the four rf feeds per rf unit is affected

+ The total number of gate valves is reduced to about 500 compared to more than 1600 with DLDS

The disadvantages are:

– The inherent lower efficiency of the SLED-II system (75% instead of 85% for DLDS)

– The eight delay lines of 17 cm diameter have a length (29 m) that exceeds the length of the associated beam line by 3 m (optimization of the layout is under study); these delay lines have to be accommodated, either in the klystron gallery (easier) or in the tunnel (less convenient)

– The dual-moded SLED-II system has never been tested

– 4064 klystrons are required which is a relatively large number (CLIC 448, TESLA 572)

– The vacuum system has an extension of about 300 m in four branches

– The trip of one modulator reduces the energy of the beam by 1.1 GeV (0.43%)

It is planned to test the dual-moded SLED-II in NLCTA with four 50 MW klystrons of the XL4 type providing an rf pulse of the nominal length of 1.6 μs. Thus, it will be possible to produce an output pulse of 600 MW in 400 ns. This is 33% more power than the nominal power and will allow testing of the system with a good engineering margin. These tests should be completed in 2003. They are very welcome as the existing experience is only with a single-moded SLED-II and power levels lower than the nominal one. Test results are available for 270 MW over 240 ns and 480 MW over 150 ns. In addition, there are plans to install 2 PPM 75 MW klystrons later to replace the four XL4 50 MW klystrons.

There is also the interesting option to operate the klystrons with 2.4 μs pulse length which would provide a compression factor of 6 and about 600 MW instead of 450 MW in 400 ns to each string of six accelerator structures at the end of each feeder.

6.4.3.2 Upgrading Options

At present, it is proposed to do the upgrading to 1 TeV center-of-mass by completing the linacs with either the replicas of the rf components used for 0.5 TeV or, more probably, by installing improved versions of these components.

As explained before, the DLDS system remains an interesting upgrading option providing about 10% higher efficiency. Two options are available:

- A single-moded DLDS as it was considered for JLC-X
- A dual-moded DLDS as it was considered for NLC

These two options are described in Section 6.4.3.2.1 and Section 6.4.3.2.2 for completeness and as reference.

6.4.3.2.1 Single-moded DLDS The basic rf unit consists of eight 75 MW klystrons operating at 11.4 GHz, the waveguide distribution system, the Delay Line Distribution System (DLDS), and 24 90-cm traveling-wave accelerator sections. The klystrons provide an rf pulse of 1.6 μs. The function of the waveguide system is to add the eight klystron pulses, to cut the resulting 600 MW pulse into four slices in time and to distribute each 400 ns slice to one of the four rf feeds. The latter consists of a magic tee and two linear systems consisting of a waveguide and two hybrid couplers (4.8 dB and 3 dB respectively) to distribute the power to three cavities per linear branch. Thus, the basic rf unit is composed of eight klystrons feeding 24 accelerator sections. A single mode is used in all the waveguides and the ones transporting power over longer distances are circular and operate with the TE_{01} mode in order to minimize the losses.

The waveguides and the accelerator sections of each DLDS unit form a connected vacuum system. It can be isolated from the other DLDS systems by gate valves on both sides of the string of the six accelerator structures at the end of each feeder. Thus, there is a vacuum valve every 5.6 m in the beam line.

Each additional linac for the upgrading contains 234 of such rf units providing in total an additional energy gain of 250 GeV per linac. The accelerator sections pertaining to two contiguous rf units are interleaved and cover a period of 169 m length per rf unit. The schematic layout of the rf unit is shown in Figure 6.2 and of the interleaved configuration in Figure 6.3.

The advantages of this scheme are:

+ High efficiency (about 85%) with most of the losses in the rectangular waveguide components
+ Component development and system architecture for the single-moded DLDS profits from the component development done for SLED-II and the operational experience with these components
+ Compared to the dual-moded DLDS: it is more compact and has less variety of components; the rf pulse length is only 400 ns in all parts of the delay lines, which provides a better engineering margin
+ Compared to the dual-moded DLDS scheme, no increase in the klystron pulse length (1.6 μs) is required
+ Lower number of klystrons for the upgrade (3741 in total compared to 4064 in the baseline)
+ Uniform distribution of the klystrons with a periodicity of about 25 m in the service tunnel, which is an advantage in the dual deep-tunnel configuration.
+ Extensive use of vacuum valves provides vacuum isolation of the individual DLDS systems, which facilitates repair and maintenance.
+ The energy drop due to a trip of an accelerator structure is only 0.27 GeV (0.1%) because the rf power in each of the four rf feeds per rf unit can be controlled independently by proper phasing of the klystrons.

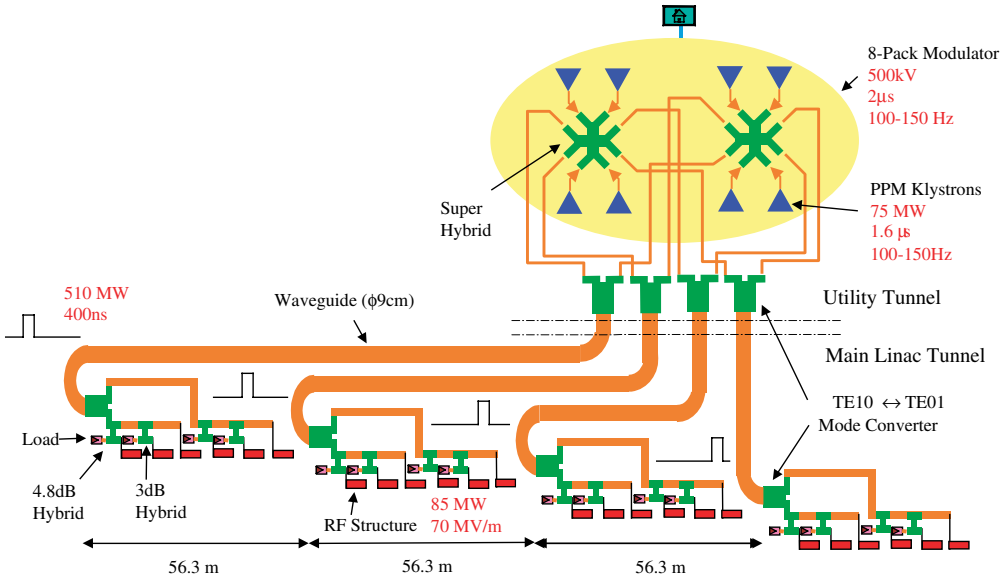

FIGURE 6.2. Schematic layout of a single-moded rf unit.

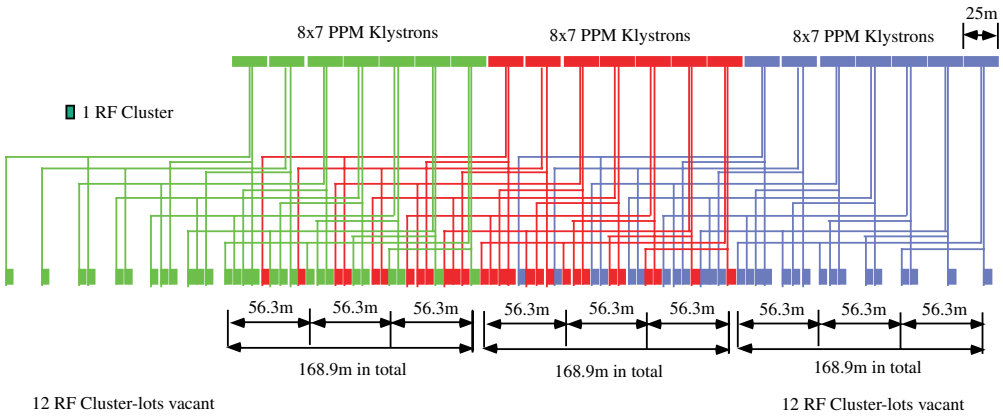

FIGURE 6.3. Interleaved single-moded DLDS scheme.

The disadvantages are:

- Waveguide components (hybrids, *etc.*) have to withstand 600 MW at 400 ns
- Interlock required against error in phase switching which could suddenly dump four times the nominal rf pulse energy into one feeder and the accelerator sections connected to it
- A high number (maximum 15) of waveguides of 3.54 inch diameter has to be accommodated in the tunnel, taking space in the tunnel cross-section
- These waveguides are not easily accessible for leak test and repair
- DLDS has no internal vacuum separation and requires waveguide flanges every 8 m
- Insertion of diagnostic sections entails irregular arrangement of DLDS
- A fully fledged power test requires a considerable amount of equipment, in particular eight klystrons and associated modulators
- Temperature effects affect the rf phasing and have to be compensated (phase measurement required)

6.4.3.2.2 Dual-moded DLDS This design is based on the assumption that 75 MW klystrons providing an rf pulse of 3.2 μs at a repetition rate of 120 Hz become available. The power distribution has the same function as in the single-moded DLDS case except that the input pulse is twice as long and is therefore cut in eight slices in time (10 ns phase switching time) in order to obtain the required 396 ns long 85 MW pulse at the input of the accelerator sections. A further difference is the use of two modes (TE_{01} and TE_{12}) in the long circular delay lines, which are needed in three out of the four main arms of one rf unit. The maximum length of an arm is 400 m. At the end of the dual-moded delay lines, the power in the TE_{01} mode flows into another, shorter TE_{10} delay line which feeds six accelerator sections via a magic tee and a linear distribution system, each feeding three sections. The power in the TE_{12} mode is converted to TE_{01} and extracted to directly feed six accelerator sections in the same configuration as described previously. Thus, each of these arms feeds 12 accelerator sections. The DLDS transmission efficiency expected is about 85%, with most of the losses occurring in the rectangular waveguide components. In total, an rf unit comprises 48 90-cm traveling-wave accelerator sections powered by only eight klystrons.

There are 117 of these rf units foreseen per 250 GeV linac. Nine 8-pack rf units (72 klystrons) are clustered together to form a nonet or a sector. The beam line length of one sector is about 470 m. There are 13 sectors per linac. Vacuum valves in the beamline separate the nonets.

The schematic layout is shown in Figure 6.4 and Figure 6.5.

The advantages of the scheme are:

+ High efficiency (about 85%) with most of the losses in the rectangular waveguide components

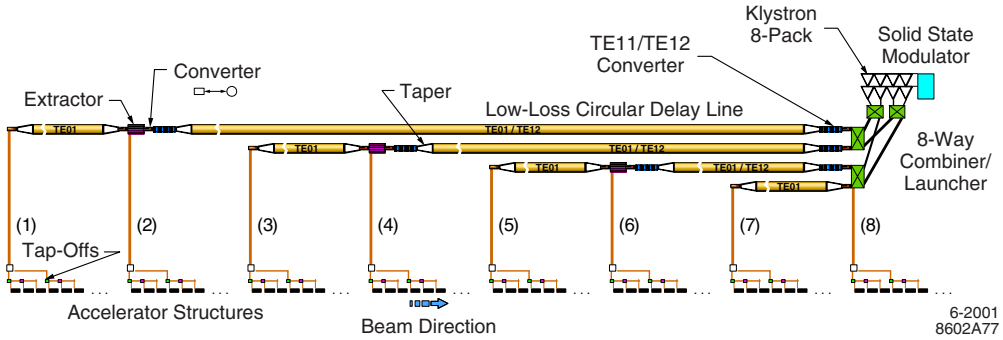

FIGURE 6.4. Schematic layout of a dual-moded rf unit.

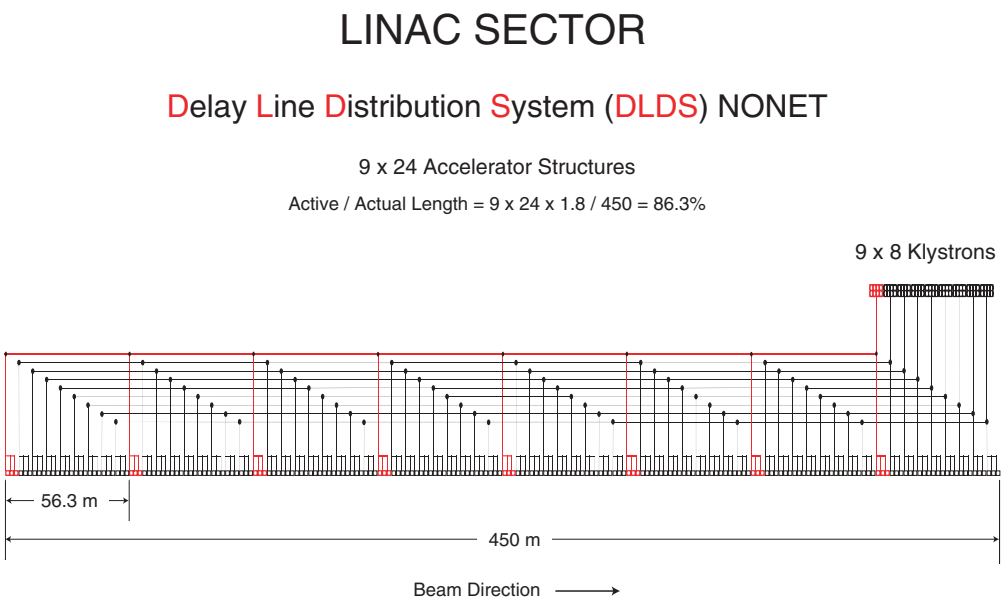

FIGURE 6.5. Interleaved dual-moded DLDS scheme.

+ Dual-mode operation of DLDS reduces the delay line length to about 60% of the single mode design
+ Number of klystrons is reduced by factor of 2 with 8 times pulse slicing, which decreases cost significantly
+ The "8-pack" clustering in nonets is particularly suitable in case the cut-and-fill method is used for the civil engineering of the klystron gallery close to the surface, resulting in a cost reduction
+ The energy drop due to a trip of an accelerator structure is only 0.27 GeV (0.1%) because the rf power in each of the eight rf feeds per rf unit can be controlled independently by proper phasing of the klystrons

In case the accelerator tunnel is deep underground, the dual tunnel layout is mandatory and the klystrons must then be distributed uniformly as done for the single-moded DLDS. However, the dual-mode delay line approach can also be applied in this case.

The disadvantages are:

– Klystron pulse is relatively long (3.2 μs), which seems to be a real challenge at 75 MW
– Testing of the full system needs a large investment since the basic unit is very large
– 48 accelerator sections drop out in case of a major fault in the rf power source (*e.g.*, modulator fault) instead of 24 for SLED-II or the single-moded DLDS version
– There are many different high-power components to design, test, and fabricate
– Components have to withstand 600 MW for 400 ns and some for 800 ns
– Very extended common vacuum system is formed by a nonet; the vacuum separation is only every 470 m on the beam line; about 1 km of 6.75 inch diameter circular waveguide have a common vacuum
– There are many waveguides in the tunnel (maximum number 36 at certain positions) which cover a significant part of the tunnel cross-section. Access to this bundle of waveguides is difficult for leak detection and repair.
– Temperature effects affect the rf phasing and have to be compensated (phase measurement required)
– An interlock is required against error in phase switching which could suddenly dump eight times the nominal rf pulse energy into one feeder and the accelerator sections connected to it

6.4.4 CLIC

CLIC operates with an rf frequency of 29.985 GHz. Since no high-power klystrons are available at this frequency, the two-beam approach has been chosen for the generation of the rf power. In contrast to the other schemes, the whole power generation system is

considered in the following as this particular approach to rf power generation is not treated in Section 6.3.

In order to produce the 130 ns long 230 MW rf pulse for each 0.5 m long accelerator section, a high-intensity electron beam, the drive beam, is decelerated in the Power Extraction and Transfer Structures (PETS) transforming kinetic energy into rf energy. Each PETS feeds two accelerator structures through very short waveguides as the drive beam runs parallel to the main beam with about 0.5 m between them. The drive beam powering one rf unit is a 39 m, 130 ns long bunch train with 2 cm spacing between the bunches. It has an initial energy of 2 GeV and is decelerated down to 0.2 GeV. At this point the beam has degraded and has to be dumped. It traverses a total of 455 PETS with a total active length of 400 m. The overall length of one unit is 624 m. Thus the basic rf unit consists of these 455 PETS and 909 TW accelerator sections. The energy gain of the main beam is 63 GeV per unit.

Note that the 30 GHz wave is induced in the PETS by the 30 GHz harmonic in the beam. This frequency is the second harmonic of 15 GHz, the fundamental frequency of the train determined by the 2 cm bunch spacing. In order to maximize the amplitude of this harmonic, the bunch must be much shorter than the rf wavelength which is 1 cm. For this reason, the rms bunch length is chosen to be 0.4 mm in the drive beam during deceleration. However, the bunch length is 2 mm in the drive-beam (linear) accelerator and combiner rings in order to limit coherent synchrotron radiation and adverse higher-order mode effects. It is shortened after the 180° bends by a bunch compressor just before the first PETS.

For 0.5 TeV in the center-of-mass (CLIC-500), four rf units per main linac are required and therefore a drive beam with four subpulses or bunch trains each 39 m long has to be produced per main linac. Each subpulse is formed by interleaving 32 bunch trains with an initial bunch spacing of 64 cm. These trains are produced by a 2 GeV normal-conducting, low-frequency (937 MHz) TW linac, the drive-beam accelerator, powered by high-efficiency long-pulse klystrons. The accelerator structures in this linac are optimized for maximum transfer of rf energy to the beam and are also fully beam-loaded in order to get highest rf to beam efficiency (97%). They operate at a fairly low loaded gradient (4 MV/m). The gun produces all the required 4×32 required bunch trains in one 17 μs long beam pulse. In each of the four subpulses, the electron bunches occupy either even or odd buckets of the drive-beam accelerator fundamental frequency, the bunches alternating between even and odd every 130 ns. Such time structure is produced after the thermionic gun in a subharmonic buncher, whose phase is rapidly switched by 180° every 130 ns. This coding of odd and even trains provides a means to separate the trains after acceleration in the linac, while keeping a constant current in the accelerator and avoiding transient beam loading.

The interleaving of the 32 trains per subpulse takes place in the following chain consisting of a delay-line combiner and two combiner rings resulting finally in four well separated subpulses with 2 cm bunch spacing. As the long pulse leaves the drive-beam accelerator, it passes through a delay-line combiner where odd and even trains are separated by a transverse rf deflector operating at 468.5 MHz. Each even bunch train is delayed in a loop of appropriate length with respect to the following odd one by 130 ns. The even and odd trains are recombined two-by-two by interleaving the trains in a second rf deflector, which results in 4×16 trains whose spacing is equal to the train length and with a bunch spacing of 32 cm in each train.

In the next stage, the trains are combined four-by-four in a first combiner ring with a 78 m circumference. It is equipped with two 937 MHz rf deflectors creating a time-dependent local deformation of the equilibrium orbit in the ring at the injection septum. After combination, the four interleaved trains having a bunch spacing of 8 cm are extracted by an ejection kicker. The whole pulse is composed of 4×4 trains. The four trains pertaining to one subpulse are combined again, using the same scheme, in a second combiner ring of 312 m circumference, yielding the required final 4 subpulses per pulse. At this point, each 2 GeV subpulse is 39 m long and consists of 1952 bunches spaced at 2 cm.

Each main linac has its own drive beam generation complex.

The advantages of the scheme are:

+ It is the only plausible technology having the potential to reach beyond 1.5 TeV center-of-mass for an e^+e^- collider, which could be already used at lower energy to get valuable experience (the baseline design is for 3 TeV)
+ Only a relatively small number of high-power klystrons is required, in total 448 in the drive-beam accelerators and four for the rf deflectors (same number for 3 TeV)
+ RF power generation is localized, which facilitates operation, repair, and maintenance
+ Upgrading of the rf power source for extension of the linacs to reach higher energies is easy because of the modular concept. It needs only lengthening of the klystron and gun pulse.
+ A single tunnel is sufficient
+ There are no active rf components in the tunnel
+ The concept allows the generation of nearly any rf frequency, the only condition being that the bunch spacing corresponds to a subharmonic of the rf
+ The drive beam generation is grouped together with the electron and positron injectors, resulting in a very compact facility where all the active high-power components, electrical power distribution, and cooling are concentrated. Access for intervention and maintenance is easy since the facility is at the surface housed in tunnels produced by cut-and-fill.

Its disadvantages are:

– One rf unit is very large, which requires a sizable investment for a fully fledged test
– The trip rate of the acceleration sections and of the PETS must be very low given the large number of these components in one rf unit, because a trip of one of these components removes one rf unit, resulting in an inadmissible energy drop of 63 GeV (25%) stopping the whole linac, at least with the present design
– A fault or failure of a critical subsystem in one of the drive-beam generation systems stops the whole main linac, which it is supposed to power
– Machine protection and beam loss control in the drive linac are very challenging

  - Four alcoves (250 m^2) are required in the tunnel per linac for the turnarounds of the subpulses and four smaller ones for the drive beam dumps (80 m^2)

A number of ideas exist about control of the field level in individual PETS and accelerator sections, which would make the requirement on the trip rate less severe, *e.g.*, tests of PETS using controllable recirculation of power have been performed in CTF2 with satisfactory results. This would allow one to control the gradients of each PETS and its associated two accelerator sections. The control of the gradients in the latter is more important as their surface fields are in the 300 MV/m range, whereas the level in the PETS is less than 100 MV/m. Such a system would limit the energy drop to 0.25 GeV (0.1%), which is acceptable for smooth operation.

The CLIC Test Facilities 1 and 2 (CTF1 and CTF2) have demonstrated the principle of the two-beam scheme. The next test facility (CTF3) will address a whole set of more advanced issues.

- Preliminary phase (2002):
  - Achieved:
    * Tests of isochronous ring with low intensity
    * Tests of deflection and funnelling, interleaving of 5 pulses in the isochronous ring
  - Planned:
    * Improved precision of interleaving and more uniform intensity in the train, test of CTF3 deflector
    * Test of photoinjector including the laser and bunch coding techniques in 2003 to decide on the front-end option
- Phase I (2004): Full beam loading in the drive-beam linac, and wakefield control in the accelerator sections of the drive linac. A special PETS for high power generation provides experience in operation and reliability of this device although parameters of the real CLIC PETS are different.
- Phase II (2005/2006): Combining techniques (funnelling with rf deflectors in a isochronous ring at higher beam intensity), experience with design of low-impedance ring and measurements of impedance, study of coherent synchrotron radiation effects

R&D work on the methods to switch off a small number of accelerator structures after a trip is mandatory but not yet planned. Work on the high efficiency modulator/klystron assemblies for the CLIC drive beam accelerator has been started. A study of the high-efficiency 937 MHz multibeam klystrons operating with a pulse length of up to 92 μs with 100 Hz has been completed indicating that a peak power of 40 MW is feasible. Note that the requirement is 50 MW peak power. Either further studies indicate a path to 50 MW or, if 40 MW is indeed confirmed, the accelerator structures of the drive beam accelerator have to be shortened and the number of rf units increased appropriately. Unfortunately, hardware development is delayed for lack of resources.

The upgrading to higher energies requires the production of more subpulses taking into account that the energy increase is quantized in steps of 0.13 TeV in the center-of-mass. Each step means lengthening of each linac by one basic unit (624 m) and of the pulse to be produced by the drive linac. The latter can be done by lengthening the PFN chains in the klystron modulators provided the original rf components were already designed for the pulse length and the average power needed in the final stage.

6.4.5 Power Efficiency

This summary given in Table 6.8, Table 6.9, Table 6.10, and Table 6.11 show the overall efficiency defined as the ratio of beam power to ac modulator input power for the schemes under consideration. The efficiency of the subsystems is also given if available. All the numbers are the nominal numbers, *i.e.*, the goals. The achieved numbers are given if available.

TABLE 6.8
TESLA 0.5 TeV

Efficiency [%]			
Goal	Achieved	Systems	Comments
85	85	Modulator	
65	65	Klystron	
94		Waveguide and circulator	
52		AC to rf	AC to rf at coupler
59		RF to beam	AC power for cryogenics/ AC power for rf=0.26
24		Overall	including power for cryogenic cooling of modules

TABLE 6.9
JLC-C 0.5 TeV

Efficiency [%]		
Goal	Achieved	Systems
67	48	Modulator
50	44	Klystron
80		Pulse compressor
24		AC to rf
26		RF to beam
6–7		Overall

TABLE 6.10
JLC-X/NLC 0.5 TeV

Efficiency [%]			
Goal	Achieved	Systems	Comments
80	50–60	Modulator	
55	60	Klystron	
75		SLED-II compression	klystron output to acc.section input
33		AC to rf	AC to acc.section input
27		RF to beam	input acc.section to beam
9		Overall	

TABLE 6.11
CLIC 0.5 TeV

Efficiency [%]		
Goal	Systems	Comments
90	Modulator	
65	Klystron	
93	Drive beam acceleration	RF input of drive linac to drive beam
82	Deceleration	Drive beam to transfer structures
95	Transfer structure	Power to transfer structures to rf output
95	Power transfer	RF output to input acc.sections
40	AC to rf	AC to acc.section input
23	RF to beam	
9	Overall	

6.4.6 Conclusions

The Working Group has examined the feasibility of each individual scheme and its subsystems taking into account the results of the R&D work done. Concerns and R&D tasks are listed here.

TESLA

Concerns and R&D:

- The proposed system for TESLA-500 is tested but a long-term test at nominal power of a number of modules has not yet been conducted. This should be planned in either TTF1 or TTF2. (Ranking 2)
- R&D is required for the upgrading to 800 GeV. Once the components are developed, they should be thoroughly tested. The proposed solutions look plausible. (Ranking 1)

JLC-C

Concern and R&D:

- Operation at full power of rf pulse compressor and, later, of a full rf unit are needed. The planned high-power tests of pulse compressor and of a full rf unit for SCSS are very welcome as well as the operation of four units for SCSS. (Ranking 1)

JLC-X/NLC

Concerns and R&D:

- Operation of a basic unit needs demonstration; in particular, tests with the nominal power level and pulse length using the new dual-moded SLED-II are required. (Ranking 2)
- The planned test of a subset (four XL4 klystrons and one dual-moded SLED-II) at nominal power in NLCTA, including the testing at higher power levels to establish an engineering margin, is currently supported at SLAC. Eventually, a complete basic unit (modulator, 8 klystrons, four dual-moded SLED-II, and all waveguide components) should be assembled and tested. (Ranking 1)

CLIC

Major concerns and R&D:

- A system is required to allow the switching-off of a small number of accelerator sections in main linac (or a requirement of excessively low trip rate of these sections and PETS). (Ranking 1)

- Machine protection for the drive-beam decelerator (beam loss control, radiation levels) is required. Conceptual studies and R&D to find solutions are strongly recommended. (Ranking 2)

Concerns and R&D:

- Generation of drive beam by fully loaded linac, delay-ring and combiner rings, should be supported at CTF3 (Ranking 1)
- Drive beam stability in intensity and phase should be tested at CTF3. Support should be provided for laser R&D (PILOT). (Ranking 2)
- The large size of one basic rf unit requires a large investment for a complete test

6.5 ACCELERATOR STRUCTURES

6.5.1 Technology for Superconducting Structures: TESLA

6.5.1.1 General Design Goals

The main goals of the TESLA international collaboration during the past decade have been to increase the achievable gradient by a factor of 4 from the 5–8 MV/m available ten years ago, and to decrease the cost per unit length of the superconducting cavities by a similar factor. Improved understanding of gradient limiting mechanisms, combined with new techniques to fabricate, treat and prepare cavities now reliably yields accelerating gradients of more than 25 MV/m. In the most recent batch, more than twenty one-meter long niobium structures yielded an average gradient over 25 MV/m during CW (continuous wave) operation. Eight 9-cell cavities, while operating with the TESLA pulse-length of one millisecond, reached gradients of 30–35 MV/m. In the TTF, the maximum average gradient achieved in a module with stable rf operation was 23 MV/m and, when operating with beam, the maximum average gradient of a module was 21 MV/m.

Having nearly met the gradient goals, the TESLA collaboration proposes to build a 500 GeV c.m. energy linear collider with a 23.8 MV/m linac gradient. An upgrade to 800 GeV c.m. energy requires operation at a gradient of 35 MV/m, which was recently achieved in CW tests of 3 electropolished nine-cell cavities, with a fourth cavity capable of a gradient of 34 MV/m.

6.5.1.2 Choice of Structure Parameters

6.5.1.2.1 Choice of Frequency The losses in a microwave cavity are proportional to the product of conductor area and surface resistance. For a given length of a multicell resonator, the area scales with 1/f while from BCS (Bardeen, Cooper, Schrieffer) theory the superconducting surface resistance scales as f^2. In practice, there is always a residual surface resistance for a non-ideal surface, which is assumed to be independent of frequency. At an operating temperature T=2 K, it is found that the BCS resistance dominates above 3 GHz and hence the losses grow linearly with frequency. For frequencies below 300 MHz,

the residual resistance dominates and the losses scale as 1/f. To minimize the dissipation in the cavity wall one should therefore select f in the range 300 MHz to 3 GHz. Cavities in the 350 to 500 MHz regime are in use in electron-positron storage rings. Their large size is advantageous to suppress wakefield effects and higher-order mode losses. However, for a linac of several 10 km length the niobium and cryostat costs for these bulky cavities would be prohibitive, hence a higher frequency has to be chosen. Considering material costs, f=3 GHz might appear the optimum, but there are compelling arguments for choosing about half this frequency:

- The wakefield losses scale with the second and third power of the frequency ($W_{long} \sim f^2$, $W_{trans} \sim f^3$). Beam emittance growth and beam-induced cryogenic losses are therefore much higher at 3 GHz.
- The f^2 dependence of the BCS resistance sets an upper limit of about 30 MV/m at 3 GHz. Hence, choosing this frequency would definitely preclude a possible upgrade of TESLA to 35–40 MV/m. The choice for 1.3 GHz was motivated by the availability of high power klystrons.
- For cost optimization a cavity length of at least 1 m is desirable. For 3 GHz the number of cells would be larger. Hence the problem of trapped modes and field flatness would be a more serious issue.

Niobium film cavities have also been studied in detail by a CERN group at 1.5 GHz [30], but compared to bulk niobium cavities, they do not reach the same performance.

6.5.1.2.2 Cavity Geometry A multicell resonator is indispensable for maximizing the active acceleration length in a linac of several 100 GeV. With the increasing number of cells per cavity, however, difficulties arise from trapped modes and uneven field distribution in the cells. The design of the cell shape was guided by the following considerations:

- The cell shape is azimuthally symmetric with an ellipsoidal longitudinal profile
- A large iris radius is chosen to reduce wakefield effects

For the TESLA cavities, R_{iris}=35 mm was chosen, leading to a cell-to-cell coupling of 1.87% and a ratio of peak field on the iris to accelerating field of E_{peak}/E_{acc}=2. The contour of a half-cell is composed of a circular arc around the equator region and an elliptical section near the iris.

The half-cells at the end of the 9-cell resonator have a slightly different shape to ensure equal field amplitudes in all 9 cells. In addition, there is a slight asymmetry between the left and right end cell, which prevents trapping of higher-order modes.

6.5.1.2.3 Number of Cells The reference design is a 9-cell structure which was the optimum for cost efficiency and technical feasibility. With more than 9 cells the desired field flatness of more than 98% is difficult to achieve.

The proposed 2 × 9 cell superstructure increases the filling factor by about 6% and reduces the number of power couplers and other rf components by a factor of 2 as well as the number of flange connections. The field flatness can be achieved with a frequency tuner on each of the substructures. HOM damping is achieved with the same principle as in the reference design. This concept was tested with beam in late 2002, in a 2 × 7 prototype superstructure.

6.5.1.2.4 Active Tuning The electromagnetic fields exert a force on the currents induced in a thin surface layer leading to a deformation of the cavity and a frequency shift. In the present TTF cavities this shift amounts to 250 Hz at 25 MV/m during the 1 ms long beam pulse.

For TESLA-800 an active piezoelectric tuner is foreseen to compensate the detuning during each rf pulse. In a test at 24 MV/m the detuning was fully compensated. With the piezoelectric frequency stabilization the cavities can be operated at 35 MV/m with the rf power overhead of 10% while an overhead of 40% would be needed without piezo compensation.

Tests on the pulsed operation of piezo crystals at liquid helium temperatures in a radiation environment are underway. There will be further tests on cavities in 2003. The incorporation of the piezos into the tuning mechanism is underway.

6.5.1.3 HOM Damping

The intense electron bunches excite higher order eigenmodes (HOMs) in the resonator whose energy must be coupled out to avoid multibunch instabilities and beam breakup. This is accomplished by HOM couplers mounted on the beam pipe sections. The HOM couplers are mounted at both ends of the cavity with a nearly perpendicular orientation to ensure damping of dipole modes of either polarization. A 1.3 GHz notch filter is incorporated to prevent energy extraction from the accelerating mode.

A problem arises from trapped modes which are concentrated in the center cells and have a low field amplitude in the end cells. An example is the TE_{121} mode. By an asymmetric shaping of the end half-cells, the field amplitude of the TE_{121} mode is enhanced in one end-cell while preserving the field homogeneity of the fundamental mode. The two polarization states of dipole modes would, in principle, require two orthogonal HOM couplers on each side of the cavity. In a string of cavities, the task of the orthogonal HOM coupler can be taken over by the HOM coupler of the neighboring cavity. The viability of this idea was verified in measurements.

In experimental tests on 9-cell structures, it was verified that all HOMs, which couple strongly to the beam (high R/Q), were damped with the exception of one mode at 2.58 GHz. This effect has by now been well understood and good damping can be restored by a re-orientation of one of the HOM couplers. Very high frequency modes will be absorbed by a high loss material at a temperature level of 70 K inserted into the beam pipe between cryomodules to avoid additional heat load into the helium at 2 K.

6.5.1.4 Fabrication and Assembly

The superconducting resonators are fabricated from 2.8 mm thick niobium sheets by electron-beam (EB) welding of deep-drawn half-cells. The tubes for the beam pipes and the coupler ports are made by back extrusion and are joined to the cavity by EB welds.

6.5.1.4.1 Niobium Specification The most important metallic impurity in niobium is tantalum, with a typical concentration of 500 ppm. The interstitially dissolved gases (mainly oxygen) act as scattering centers for the unpaired electrons and reduce the thermal conductivity at 2 K. The niobium ingot is outgassed by several melting cycles in a high vacuum electron beam furnace. The interstitial oxygen, nitrogen and carbon contamination is reduced to a few ppm. The Nb ingots are forged and rolled into sheets of 2.8 mm thickness. After rolling, the Nb sheets are first degreased and cleaned by chemical etching. The sheets are then annealed for 2 hours at 700–800°C in a vacuum oven at 10^{-6} mbar to achieve full recrystallization and a uniform grain size of about 50 μm.

The niobium sheets for the last two cavity production series were all eddy-current scanned to eliminate material with tantalum or other foreign inclusions before the deep drawing of half cells. More than 95% of the sheets were found free of defects; the remaining ones showed grinding marks, imprints from rolling or large electrical signals due to small iron chips. Most of the rejected sheets were recoverable by applying some chemical etching. The eddy-current check has proven to be an important quality control procedure, not only for the cavity manufacturer but also for the supplier of the niobium sheets.

6.5.1.4.2 Cavity Fabrication Cavity fabrication is a delicate procedure, requiring intermediate cleaning steps and a careful choice of the weld parameters to achieve full penetration of the joints. First, two half cells are connected at the iris; the stiffening rings are welded in next. At this point weld shrinkage may lead to a slight distortion of the cell shape which needs to be corrected. Particularly critical are the equator welds which are made from the outside. A reliable method for obtaining a smooth weld seam at the inner cavity surface is to apply 50% of the power to the first weld pass, and 100% on the second. A slightly defocused electron beam rastered in an elliptic pattern is used.

The electron-beam welding technique of niobium cavities has been perfected in industry to such an extent that the weld seams do not limit cavity performance below 30 MV/m.

Stringent requirements are imposed on the weld preparation to prevent the degraded performance at the equator welds encountered in the first production series of TESLA cavities. After mechanical trimming, the weld regions are cleaned by a light chemical etching followed by ultra-pure water rinsing and clean-room drying. The cleaning process is performed not more than 8 hours in advance of the EB welding.

The challenge for a welded construction is the tight mechanical and electrical tolerances. These can be maintained by a combination of mechanical and radio frequency measurements on half cells and by careful tracking of weld shrinkage (see below). The procedures established during the TTF cavity fabrication are suitable for large series production, requiring quality assurance measurements only on a small sample of cavities. The cavities are equipped with niobium-titanium flanges at the beam pipes and the coupler ports. NbTi can be electron-beam welded to niobium and possesses a surface hardness

equivalent to that of standard UHV flange material (stainless steel 316 LN/DIN 1.4429). Contrary to pure niobium, the alloy NbTi (ratio 45/55 by weight) shows no softening after the heat treatment at 1400°C and only a moderate crystal growth. O-ring type aluminum gaskets provide reliable seals even in superfluid helium, which is only needed for the vertical CW acceptance test.

After implementation of the additional quality control measures (eddy-current scanning, etching and cleaning the weld regions), no foreign material inclusions nor weld contaminations have been found in new cavities tested so far. Three companies have been qualified for the cavity fabrication.

6.5.1.4.3 Fabrication Tolerances The tolerances on cavity fabrication are described in Table 6.12.

TABLE 6.12
Tolerances on cavity fabrication.

Cavity length [mm]	±3
RF frequency [MHz]	±0.1
Field flatness [%]	98

These specifications have been met in the second and third production series of the TTF cavities after the following checks on the fabrication process were introduced:

- Frequency measurement on all half cells
- Contour measurement on selected half cells
- Frequency measurement on selected dumb-bells
- Frequency measurement on all dumb-bells after welding of the stiffening ring

6.5.1.4.4 Alternative Fabrication Methods The standard fabrication by deep-drawing and electron-beam welding is a proven and cost-efficient technology. It has been demonstrated that it is industrially feasible. There exist alternative fabrication techniques: spinning and hydroforming. Both techniques have shown very good performance in one-cell cavities resulting in gradients above 38 MV/m (spun) and 41 MV/m (hydroforming) respectively. The fabrication of multicell cavities is underway. Tests are expected to take place in 2002.

6.5.1.4.5 Post-Fabrication Treatment A layer of 100–200 μm is removed in several steps from the inner cavity surface to obtain good rf performance in the superconducting state. The standard method applied at DESY is called Buffered Chemical Polishing (BCP), and uses an acid mixture of HF (48%), HNO_3 (65%) and H_3PO_4 (85%) in the ratio 1:1:2. The acid is cooled to 5°C and pumped through the cavity in a closed loop. After rinsing

with ultra-pure water and drying in a class 100 clean room, the cavities are annealed at 800°C in an Ultra High Vacuum (UHV) oven to out-gas dissolved hydrogen and relieve mechanical stress in the deep drawn niobium. In a second UHV oven the cavities are heated to 1300–1400°C at which temperature the other dissolved gases diffuse out of the material, and the residual resistivity ratio RRR increases by about a factor of 2 to around 500. To absorb the oxygen diffusing out of the niobium and to prevent oxidation by the residual gas in the oven (pressure $<10^{-7}$ mbar), a thin titanium layer is evaporated on the inner and outer cavity surface (Ti being a stronger getter than Nb). The titanium layer is later removed by 80 μm and 20 μm BCP of the inner and outer cavity surface respectively. This high-temperature treatment with Ti getter is referred to as post-purification. A severe drawback of post-purification is the considerable grain growth of the niobium: post-purified cavities are vulnerable to plastic deformation and have to be handled with great care. After the final heat treatment, the cavities are mechanically tuned to adjust the resonance frequency to the design value and to obtain equal field amplitudes in all 9 cells. This is followed by a light BCP, three steps of high-pressure water rinsing (100 bar), and drying in a class 10 clean room. The final acceptance step is an rf test in a superfluid helium bath cryostat.

6.5.1.4.6 Industrialization The manufacturing process of all TTF cavities has been done in industry. There exists a detailed specification for the niobium material as well as for the cavity fabrication so that very reproducible performance can be achieved. This has been demonstrated in the last two cavity production series.

All the chemical treatment steps can be done in industry. Chemical etching of niobium cavities is a standard procedure which has been used at CEBAF, LEP and also for cavities in synchrotron radiation storage rings.

Studies have been conducted by industrial companies showing the industrial feasibility of the cavity processing and serve as a solid basis for the cost estimate.

6.5.1.5 Structure Environment

6.5.1.5.1 Cryomodule Each 9-cell cavity is equipped with its own titanium helium tank, a tuning system driven by a stepping motor, a coaxial rf power coupler capable of transmitting more than 400 kW, a pickup probe, and two higher-order mode (HOM) couplers. To reduce the cost for cryogenic installations, 12 cavities and a superconducting quadrupole are mounted in a common vacuum vessel and constitute the cryomodule. Within the module the cavities are joined by stainless steel bellows and flanges with metallic gaskets. The cavities are attached to a rigid 300 mm diameter helium supply tube which provides positional accuracy of the cavity axes of better than 0.3 mm. Invar rods ensure that the distance between adjacent cavities remains constant during cooldown. Radiation shields at 5 and 60 K together with 30 layers of superinsulation limit the static heat load at the 2 K level to less than 3 W for the 17 m long module. The design of the cryomodules is advanced and suitable for industrial production.

The cavities are cooled to 2 K to achieve a high quality factor of more than 10^{10} (5×10^{9}) at 23.8 MV/m (35 MV/m). The pressure drop in the Helium supply line for TESLA in the most unfavorable case (3.8 km) is 0.94 mbar causing a temperature difference of

about 0.1 K. For stable cavity operation, it is desirable to have pressure fluctuations of less than 1 mbar.

6.5.1.5.2 Cryoplant Superconducting technology has been used in many circular accelerators such as LEP, TRISTAN, Tevatron and HERA, and many new projects either under construction (LHC, JHF, SNS) or in the planning stage have adopted this technology in their design. That proves that cryotechnology is rather mature and commonly available. The TESLA cryosystem design was based on the experience at CERN for the LHC cryosystem. These studies, including the layout of the TESLA cryoplants, have been carried out in close collaboration with industry. All major components for the TESLA cryogenics have been successfully used for years in similar plants. HERA experience already shows that an availability of the cryosystem of greater than 98% can be achieved.

6.5.1.5.3 Couplers For the coaxial power coupler an elaborate two-window solution was chosen for optimum protection of the cavity against contamination during mounting in the cryomodule and against window fracture during linac operation. The coaxial couplers consist of a "cold section" which is mounted on the cavity in the clean room and closed by a ceramic window, and a "warm section" which contains the transition from the coaxial line to the waveguide. This part is evacuated and sealed against the air-filled waveguide (WR 650) by a second ceramic window.

Couplers have been limiting elements of superconducting cavities in the past. The first series of TESLA high power input couplers have been the limit for one module assembled for the TTF linac. After a few months at lower power levels (corresponding to 15 MV/m) in the machine the power could not be raised without new conditioning. The major change in the new series of couplers tested in the recent module run was to implement a bias voltage between inner and outer conductor to suppress multipacting. This concept has already been used with success for the power couplers for the superconducting cavities in LEP.

The biased couplers have performed up to 2 MW at 1.3 ms in a traveling-wave mode in warm test stands. In the horizontal test stand several cavities have run with these couplers above 30 MV/m without beam. For these couplers no new conditioning was needed after running the linac at lower gradients and the power could be raised within one shift.

6.5.1.6 Gradient Limitations

6.5.1.6.1 Status for TESLA-500 The most recent TTF cavities exceed the 23.8 MV/m operating gradient of TESLA-500. The last production series with the standard BCP achieves an accelerating gradient of 26.1±2.3 MV/m at Q=10^{10}.

After having passed the acceptance test in the vertical bath cryostat, the cavities are welded into their liquid helium container and equipped with the main power coupler. The accelerating fields achieved in the vertical and the horizontal test are well correlated. Only in rare cases was a reduced performance seen, usually caused by field emission. Several cavities improved their performance in the horizontal test because of operation with short (millisecond) pulses instead of the continuous wave (CW) operation in the vertical cryostat. The results show that good performance of the cavities can be preserved if great care is taken to avoid dust contamination during mounting of the helium vessel and power coupler.

In one of the cryomodules installed in the TTF linac, the maximum usable gradients were measured for each of the eight cavities. The average gradient was 22.7 MV/m, indicating that installation of the individual cavities into a module does not degrade their performance. A long-term test at maximum gradient is underway.

The typical processing times for the high power couplers and cavities are a few days. Recently, the use of preconditioned couplers has shown to reduce the conditioning time significantly to about a day. A viable alternative is to coat the couplers with a thin TiN layer, A TiN coated coupler has shown the same time processing as a pre-processed coupler.

6.5.1.6.2 Status of R&D for TESLA-800 For further performance improvement, the most promising method today for surface preparation is electropolishing. The Buffered Chemical Polishing (BCP) used at TTF to remove a 100–200 μm thick damage layer produces a rough niobium surface with strong grain boundary etching. An alternative method is electropolishing (EP) in which the material is removed in an acid mixture under current flow. Sharp edges and burrs are smoothed out and a very glossy surface can be obtained. The electrolyte is a mixture of H_2SO_4 (95%) and HF (46%) in a volume ratio of 9:1. The bath temperature is 30–40°C. The process consists of two alternating steps: oxidation of the niobium surface by the sulphuric acid under current flow (current density about 500 A/m^2), and dissolution of the Nb_2O_5 by the hydrofluoric acid. The material removal is around 40 μm per hour.

Results on single-cell cavities at KEK and from a collaboration of CERN-CEA-DESY demonstrate that electropolishing is the superior surface treatment method. Accelerating gradients of 35–42 MV/m have been achieved in more than a dozen single-cell resonators. This includes electron-beam welded as well as hydroformed and spun cavities. Recently it has been found that an *in-situ* baking of the evacuated cavity at 100–150°C, following EP and clean water rinsing, is an essential prerequisite for reaching the highest gradients without a strong degradation in quality factor. This baking was applied to all single-cell cavities and yielded reproducible results. Several surface analytical studies have been done and the effect is linked to the diffusion of impurities (most notably oxygen). A program of measuring the basic properties of the *in-situ* baked niobium used in the cavities is pursued at the same time.

The transfer of the electropolishing method to multicell cavities has been studied at KEK for some years. Electropolishing has been used by Nomura Plating for KEK's cavities for many years (*e.g.*, Tristan, KEK-B). In a collaboration of KEK and DESY the electropolishing of TESLA nine-cell cavities is being studied. In a first test a 9-cell resonator from the first production series (the niobium material of this production series was not eddy-current scanned) has been electropolished by Nomura Plating, improving its performance from 22–32 MV/m. More recently, three electropolished cavities from the last production series achieved the performance needed for TESLA-800 in a CW measurement: 35 MV/m at a Q_0 larger than 5×10^9. The cavities were tested for several hours at CW. A fourth cavity of this batch achieved 34 MV/m. Another four cavities will be electropolished at KEK and tested at DESY in 2002. To further study the EP technique of multicell cavities, DESY is setting up an electropolishing facility for 9-cell and 2×9 superstructure cavities.

6.5.1.6.3 Dark Current Dark Current measurements at the TTF linac have shown that the threshold gradient is typically 1 MV/m below the maximum gradient as determined in the vertical test. Two accelerator sections with eight cavities each were studied. In both cases one single cavity produced most of the dark current. At high gradient (20.8 MV/m in module 3) a current of up to 100 nA was measured. Detuning of the particular bad cavity reduced the dark current for the remaining seven cavities to approximately 30 nA. Up to the highest possible gradient, the measured dark current showed a pure Fowler-Nordheim behavior. Signals were measured on beam axis using Faraday-cup like devices as well as Compton diodes. This *in-situ* measurement takes into account both the dark current emitted in the individual cavities and the capture probability in the presence of the neighboring cavities. Even though the first dark current measurements at gradients close to the limiting gradient meet TESLA requirements, on-going measurements will give more results for the next accelerator sections. A more quantitative dark current measurement during the vertical cavity tests could improve the understanding of gradient limitations during operation.

6.5.1.6.4 Superstructure A fundamental design goal for a linear collider is to minimize the cost of the accelerator while maximizing the active acceleration length. Hence, it is desirable to use accelerator structures with as many cells as possible, both to reduce the number of couplers and waveguide components and to increase the filling factor. However, the number of cells per cavity (N) is limited by the conditions of field homogeneity and the presence of trapped modes. The sensitivity of the field pattern to small perturbations grows quadratically with the number of cells. The probability of trapping higher-order modes within a structure also increases with N, and such modes with a small field amplitude in the end cells are difficult to extract by the HOM couplers.

The limitations on the number of cells per cavity can be circumvented by joining several multicell cavities to form a so-called superstructure. Short tubes of sufficient diameter (114 mm) enable power flow from one cavity to the next. The chain of cavities is powered by a single input coupler mounted at one end. HOM couplers are located at the interconnections and at the ends. All cavities are equipped with their own tuners. The cell-to-cell coupling is 1.9%, while the coupling between two adjacent cavities in a superstructure is two orders of magnitude smaller at 3×10^{-4}. Because of this comparatively weak inter-cavity coupling the issues of field homogeneity and HOM damping are much less of a problem than in a single long cavity with N=18 cells. The shape of the center cells is identical to those in the 9-cell TTF structures while the end-cells have been redesigned to accommodate the larger aperture of the beam tube. The cavities are tuned to equal field amplitude in all cells and are then welded into their liquid helium tanks and joined to form the superstructure. It has been verified that the pre-tuning of the cavities can be preserved during the assembly steps.

The main concerns for a chain of cavities fed by a single input coupler is the flow of the rf power through the interconnecting beam pipes, and the time needed to reach equal field amplitude in all cells during pulsed-mode operation. The power flow has been extensively studied with two independent codes, HOMDYN and MAFIA. The relative spread in energy gain in a train of 2820 bunches is predicted to be less than 10^{-4}, indicating that the energy flow is sufficient to refill the cells in the time interval between two adjacent bunches.

The 2 × 9 cell superstructure under consideration improves the filling factor by 6% and requires a factor of 2 fewer main power couplers in the machine, which is an important cost factor. The combination of two 9-cell resonators achieves a high filling factor of 85% and is 2.39 m long. This structure can be (electro-)chemically treated and handled with an upgraded version of the facilities at TTF. Keeping the total length of the collider constant, the superstructure allows to reach the 500 GeV c.m. energy with a gradient of 22 MV/m, compared to 23.8 MV/m with individual 9-cell cavities. In the superstructure the main power coupler must transmit 437 kW of traveling wave power at 500 GeV c.m. energy and 705 kW at 800 GeV. The TTF couplers have been tested up to 1500 kW and should be sufficient to feed the superstructure. To provide an additional safety margin for the operation at 35 MV/m (TESLA-800) the diameter of the cold coupler section will be increased from 40 mm to 60 mm. The higher-order modes have been extensively studied for the superstructure. Nearly all modes propagate through the 114 mm diameter beam pipe and are efficiently damped with 4 HOM couplers mounted at the interconnection and at both end tubes. The details of the dipole mode impedances differ somewhat from the 9-cell cavity, but the overall effect on the beam dynamics is similar.

Two 2 × 7 cell niobium prototypes are undergoing a beam test in the TTF linac. In these prototypes the 7-cell cavities are joined by welding. The third generation of TTF input coupler and three HOM couplers are used. The beam test will help verify the energy spread computations and the rf measurements on the copper models. In addition the performance of the HOM couplers, which are exposed to a higher magnetic field due to the enlarged beam tube diameter, can be tested. Preliminary results from rf measurements show that the tuning of the structure and the damping of the HOMs works as expected.

6.5.1.7 Superconducting Cavity Operating Experience

6.5.1.7.1 Background Superconducting cavities behave differently from normal conducting structures in that their maximum operating gradient is set by cavity quench, field emission, or Q degradation- not under normal circumstances by structure breakdown. If quenches have not limited operation at a lower gradient, then field emission and Q degradation (below the allowed Q_0) set the maximum operating gradient of a cavity. This maximum gradient is not a hard limit. It results in high cryogenic load, radiation, and dark current from particular cavities, but does not trip off cavities. If observed to increase during operation, then the gradient of particular cavities can be lowered.

A cavity quench can trip off cavities, but it is a thermal process, not a breakdown or discharge. Therefore it is not the dramatic event that occurs in superconducting magnet systems because the stored energy is very limited. The time constant of development of the quench depends on the power supplied. If a lot of excess power is supplied, then the quench develops rapidly. If one is at the threshold, then the quench develops slowly (100 μs to 1 ms). This slow growth of a normal zone can be detected in a decrease of gradient in a cavity with constant input power. This information can be used to inhibit rf power part way through the pulse (a soft inhibit). Additionally the gradient can be slightly reduced on subsequent pulses until a stable gradient level is reached. A complete shutoff of the rf station is not necessary. However, in some cases hard inhibits may occur. Those can be handled by detuning the frequency of the cavity that trips off. After detuning the rf station can be switched on again.

There is one other situation where a breakdown in a superconducting cavity can behave like breakdown in a copper cavity. This is the situation for High Peak Power Processing (HPPP). HPPP is used to improve cavity performance. As input power as high as possible is applied to the cavity for short pulses (∼1/2 ms), emitter sites can be blown up before the quench has time to develop. The result is a crater on the Nb surface, and, when successful, destruction of the emitter and higher gradient performance. This is not a standard procedure during beam operation.

Performance can also be limited by the input coupler. Input couplers can be limited by multipacting, electron emission, vacuum increase and breakdown at the windows much as in normal conducting cavities. The couplers are rf processed off line prior to installation on the cavities. Then they are processed for a short time on the cavities, both warm and cold.

6.5.1.7.2 Observations and Operating Experience When trying to extrapolate to the operation of 20000 cavities of the collider, there is to date limited experience on what makes cavities trip and just how often. Emphasis has been placed on other more pressing operational issues rather than on the accumulation of statistics of cavity trips under long-term stable conditions. Our basic impression is that cavity operation is very stable by itself when other disturbances are not present. This section outlines some of the experience.

Vertical Dewar Tests After chemical preparation the bare cavities are mounted in a dewar for initial measurements of Q versus E and maximum gradient attainable. These are CW measurements, and though there are a few processing events, this is not a processing activity but rather a measurement of the cavity performance. Because it is CW, the test time can reflect considerable effective pulse operation time for the bare niobium cavity. The time at CW operation is limited by the cryogenic system that supplies the vertical dewar (the system is different from that supplying the modules).

CHECHIA Tests CHECHIA is a horizontal test cryostat. Fully dressed cavities including power input coupler, helium vessel and tuner are tested here. These tests are with pulsed rf like in final operation (without beam). The achievable gradient is again measured, and cryogenic measurements are made to determine the cavity Q. Often the limiting gradient is higher than in the vertical CW test because of the pulse length and duty factor. A relevant observation during these tests is that to carry out the Q measurement the cavity must operate without any trips for a few hours. Measurements are done at a number of gradient values, each taking one hour. If anything happens to stop the measurement (trip), then the measurement must start over. As this is standard procedure on all cavities tested in CHECHIA, we can assume that the trip rate is low relative to one event per hour. The couplers of the last series with bias voltage have been run to gradients of more than 30 MV/m. Testing time in CHECHIA could be extended but would need to go to about a day or two in order to be meaningful for extrapolation to linear collider klystron up time estimates and energy reduction from trips and their recovery.[1]

[1] If the measurement results in 1 trip per cavity in 30 hr, with an arbitrary choice of a 1/2 minute recovery time, then an average of three klystrons would be down per linac. This corresponds to an energy reduction, on average, of one percent (one percent is within the TESLA energy budget).

ACC1 Test 2002 In April-May 2002, one eight-cavity module (ACC1, Mod3) has been run at high gradient and long pulse.[2] The main goals of this run were to exercise the module at near its maximum gradient and to accelerate long bunch trains. The run was carried out under dynamic conditions with beam tuning going on and various levels of operator expertise. Data analysis is still in progress.

Some of the preliminary results are given here. Seven of the eight cavities were operated at gradients between 19 and 22 MV/m. The overall average gradient was between 19.5 and 21 MV/m (as measured with the beam). Typical module on time was ∼90%. Trips have been counted but their source has not been investigated. Over a total of 42 days, 291 trip events were recorded, an average of 8.4 events/day at 5 Hz for the 8-cavity module (when corrected for operating part of the time at 1 Hz). This trip rate includes amongst other things both cavity and coupler trips. Partway through the run time, a soft rf inhibit was implemented so that potential quenches could be detected without tripping the interlock system.

Although this run cannot be extrapolated to determine the collider linac operational reliability, we believe these experiences are positive and point out some of the basic differences between superconducting and normal conducting cavity operation. We also believe that a sophisticated and flexible low-level rf system will be needed to handle a variety of exceptions. We note as well that the cavities in this test have been in operation for over 12000 hr at lower gradients. There was no need for reprocessing them to get back to the maximum value. For this run they were operated very close to their limit, a situation that will not occur for the 500 GeV collider.

For the couplers no reconditioning was needed for the ACC1 run. The couplers of this module are equipped with a bias voltage that can be used to suppress multipacting.

The couplers from the first series without bias voltage on the other accelerating module in the linac limit the cavities to a gradient of 15 MV/m. Reconditioning of these couplers was not performed due to the limited time.

6.5.1.8 Potential for Upgrading to Gradients Above 35 MV/m

Theoretical arguments [31] indicate that the critical magnetic field for rf is the superheating field, which is about 230 mT for niobium at 2 K. Using 4.26 mT/(MV/m) for the TESLA structure, this translates into a limiting gradient of 54 MV/m. The highest value for the rf critical field at 2 K measured to date [31] is 175 mT, corresponding to a gradient of 41 MV/m. However, it can be argued that this lower measured value was due to heating at surface imperfections, and that with further improvements in surface quality critical fields closer to the theoretical limit will be obtained [32]. Improvements in structure design could also, in principle, marginally increase the limiting gradient. Thus it seems reasonable that gradients on the order of 50 MV/m might eventually be achieved with niobium.

There is the possibility of using other Type II superconductors for the cavity surface, such as Nb_3Sn (T_c=18.2 K, B_c=535 mT). This material has already been investigated in the hope that, because of the high value for T_c, high Q's could be obtained at 4.2 K. So far, however, the measured value for the surface conductance at 4.2 K has fallen well below the

[2] This module was built up in 1999. Three more modules have been built and are awaiting the performance test in the Linac at the end of 2002.

theoretical value [32]. Other materials, such as Al Nb_3, Si V_3 and alloys in the Al_x Ge_y Nb_z family, have transition temperatures and critical fields comparable to or greater than that of Nb_3Sn. Although results to date for investigations of alternative materials have not been encouraging, it seems reasonable to support a continuing low level program of research into these materials (perhaps in a university setting) because of the potentially high payoff.

6.5.2 Technology for Normal Conducting Structures

6.5.2.1 Introduction

6.5.2.1.1 Normal Conducting Versus Superconducting The possibility of building a linear collider in the 1 TeV c.m. energy range began to be taken seriously at SLAC in the late 1970s. In order to reach an energy of this magnitude in a reasonable length, it was clear that the accelerating gradient would have to be considerably higher than that of the SLAC linac, which was then about 12 MV/m. There was no thought of using superconducting technology, since at that time the highest gradient (limited by rf breakdown) achieved in any cavity geometry approaching a practical accelerator structure was about half the modest SLAC gradient (which was limited only by klystron power). At the SLAC S-band frequency of 2.856 GHz, accelerating gradients approaching 30 MV/m were, in fact, being attained at linacs elsewhere. Consequently, it was assumed that a future high-gradient linear collider would need to be based on normal-conducting, copper structures.

The largest application of normal-conducting rf accelerator structures then (as now) was the 3-km long SLAC linac itself. Since its initial operation in 1966, the linac has been continuously upgraded for higher energy, higher intensity and lower beam emittance. Many linear accelerators built for physics research or for industrial and medical applications have been based on SLAC linac technology. As the SLC (SLAC Linear Collider) came on line, much experience directly relevant to an S-band linear collider was obtained. However, a 1 TeV linear collider operating at the SLAC gradient would have to have an active length of at least 50–60 km. Thus there was a clear challenge to develop rf technology that would make the machine shorter, and most importantly, affordable. To meet this challenge, it was equally clear from fundamental scaling laws that the operating frequency would have to be higher than S-band.

6.5.2.1.2 Choice of Operating Frequency The choice of an operating frequency has profound consequences for almost every aspect of linear collider design. The broad reasons for the frequency choice for each design are given in the Overview sections. It is useful to expand on this discussion by focusing on the rf technology underlying these frequency choices.

At SLAC during the 1980s, frequencies ranging from S-band to 17 GHz were given serious consideration in various paper designs. In 1986, motivated in part by the nascent work at CERN on a site-filling TeV linear collider, it was decided it was time to cut metal and build both a prototype klystron and pulse compression system. An X-band frequency was chosen as a compromise between the drive for high gradient, the difficulty of building a klystron at a higher frequency, and the cost and availability of rf components (medical radiation therapy accelerators already existed at X-band). The exact frequency of 11.424 GHz was chosen to be a multiple of the SLAC linac frequency. The JLC-X project later adopted the

same frequency, making possible a close collaboration between the two laboratories on almost all aspects of the technology of a high-energy linear collider. The JLC-X/NLC group believes that the choice of an X-band frequency gains the major cost benefits of a high frequency rf system, while still allowing achievable alignment tolerances associated with stronger wakefields. Until recently, the design was based on unloaded/loaded gradients of 70/55 MV/m; with the adoption of the SLED II pulse compression system, the values are now 65/50 MV/m.

The CLIC group at CERN proposes a novel two-beam accelerator aimed at multi-TeV energies. This concept allows for high frequency since it does not rely on conventional rf sources, which become progressively limited in output power with increasing frequency. A frequency of 30 GHz was chosen because it gives a high "transformer ratio" (the gradient is related to the linac/drive beam frequency ratio). Also, this frequency was considered to be close to the limit beyond which standard technology for the fabrication of copper structures can no longer be used. The high frequency for the CLIC design makes it possible to keep the rf energy required per pulse at a reasonable level for a loaded gradient as high as 150 MV/m. However, the small beam aperture of the accelerator structure puts stringent requirements on wakefield control.

The JLC-C design proposes a frequency of 5.7 GHz, with unloaded/loaded gradients of 44/34 MV/m. By choosing a frequency midway between S-band and X-band, the design approach is to achieve a reasonably high gradient while exploiting the advantages of more conventional lower frequency technology. For example, klystrons are easier to build and pulse compression is achieved using a simple high-Q energy storage cavity rather than an expensive system of long delay line pipes.

6.5.2.1.3 Implications of Frequency Choice for Structure Design With the large variation in the proposed operating frequencies, one might wonder if there is indeed an optimal frequency. In examining the design choices for these proposals, one instead sees that with increasing frequency there is a general tradeoff of potential cost savings versus increasing operational difficulty. On the plus side, higher frequency affords shorter structure filling times, shorter bunch trains lengths (typically several times the fill time) and higher structure shunt impedance. With higher impedance, reasonably good rf-to-beam efficiencies are achievable at higher gradients, which makes the linac shorter. With a shorter linac and bunch train length, less rf energy per pulse is required, which decreases the number of power sources. Opposing this trend is the increasing cost of rf energy with frequency (the CLIC approach circumvents this limitation by using low frequency klystrons to accelerate drive beams that are compressed and de-accelerated to produce short, high frequency, high peak power rf pulses). Also, higher peak power and gradients are required which impose operational limitations due to breakdown and breakdown related damage, although in general, higher gradients have been achieved at higher frequency. Finally, the transverse wakefields in the structures increase with frequency, making structure alignment tolerances tighter and the required suppression of the long-range wakefield greater. To offset the stronger wakefield effects, beam currents that yield less than optimal rf-to-beam efficiency are typically chosen. Thus, the choice of operating frequency tends to depend on one's perception of affordability and manageable operating conditions.

6.5.2.1.4 General Structure Requirements Having chosen a frequency, there are four general requirements on the accelerator structure design: it must transfer the rf energy to the beam efficiently to keep the machine cost low; it must be optimized to reduce the short-range wakefields which depend on the average iris radius; it must suppress the long-range transverse wakefield to prevent multibunch beam breakup (the resonant amplification of bunch betatron motion by the bunch-to-bunch transverse wakefield coupling); and it must operate reliably at the design gradient. The design choices and R&D related to meeting these requirements are discussed in the sections that follow. In addition, there are sections that address structure fabrication, operating environment, operating experience, and the potential for increasing gradient.

6.5.2.2 Choice of Structure Parameters

For the JLC-X/NLC, the choice of structure parameters was greatly influenced by the trade-off between increasing rf-to-beam energy transfer efficiency and lowering short-range wakefield related emittance growth. The emittance growth is caused by the head-to-tail transverse wakefield deflections generated when the bunches travel off-axis through the structures. Resonant head-to-tail amplification is suppressed by introducing a correlated energy spread along each bunch (called BNS damping). The size of the remaining non-resonant emittance growth depends on a number of factors including the average iris radius, the bunch charge, and the achievable beam-to-structure alignment (the goal is about 10 μm). The average iris radius and the bunch charge also affect the rf-to-beam efficiency: higher efficiency generally comes at the expense of increased emittance growth. As a result of this basic trade-off and cost driven constraints on structure length and peak power, an average iris radius of 18% of the X-band wavelength was chosen for the linac structure design.

Defining the structure parameters required a number of other design choices. A traveling-wave structure was selected because standing-wave designs are generally more expensive. A disk-loaded waveguide geometry was used since disk-shaped cells are easy to manufacture. The iris surface field along the structure was held roughly constant to avoid having one region of the structure limit the gradient because of rf breakdown. The gradient profile was shaped by varying the rf group velocity along the structure, a common method for achieving a constant gradient. The initial choice for the phase advance per cell was 120°, the same as for the SLAC S-band structure. This value yields a high shunt impedance per unit length. The choice of both the structure filling time and rf pulse length were strongly influenced by the rf attenuation time in the structure (about 100 ns), which varies weakly with group velocity. That is, nearly optimal rf-to-beam efficiencies can be achieved with filling times equal to the attenuation time for low beam loading, and the rf pulse length needs to be significantly greater than the filling time, but not too large or it becomes more economical to increase the machine repetition rate rather than the pulse length.

The choices in these respects constrained the basic structure geometry, and resulted in a 206-cell, 1.8-m long structure with a group velocity varying from about 12% to 3% c. The initial choice of a 70 MV/m unloaded gradient (G_U) is close to optimal in the tradeoff between energy-related costs (*e.g.*, modulators and klystrons), which scale roughly

as G_U, and length-related costs (*e.g.*, structures and beam-line tunnel), which scale roughly as $1/G_U$. However, once high gradient testing of such structures began in earnest, it became clear that they would not reliably operate at this gradient due to breakdown limitations.

This discovery prompted an aggressive program to develop higher gradient structures (see Section 6.5.2.6). The results from this program have led to the adoption of a lower group velocity (5.1% c to 1.6% c) structure design for the JLC-X/NLC main linacs. This structure is shorter (0.9 m versus 1.8 m), has a longer filling time (120 ns versus 104 ns) and has a somewhat lower shunt impedance (81 Mohm/m versus 89 Mohm/m) than the 1.8 m design.

The rf-to-beam efficiency achievable in a structure depends on the choice of beam current and bunch train length in addition to the structure parameters. In the present JLC-X/NLC configuration, a 0.86 A, 269 ns long bunch train is accelerated during each pulse. This requires an rf pulse length of 400 ns including rise time, so the fill-time efficiency (bunch train length divided by rf pulse length) is 67%. The beam current produces 23% beam loading relative to the 65 MV/m unloaded gradient, and results in a steady-state rf-to-beam efficiency of 53%. Thus, the overall efficiency is 36 %, ignoring energy overhead. A higher efficiency could be achieved by increasing the beam loading, but the wakefields would be unacceptably large, the loaded accelerating gradient would be reduced, and the linac would have to be longer.

From the fundamental rf frequency point of view, the JLC-C structures follow the same design criteria. They exhibit comparable parameters: length 1.8 m, phase advance $3\pi/4$ per cell, iris radius ranging from 0.171–0.126 λ, group velocity from 11.4% c to 3.6% c.

The present CLIC parameters are based on the Tapered Damped Structure (TDS) design. The design criteria for the TDS included requirements on short and long range wakefields and optimization of the shunt impedance. The average iris radius to wavelength ratio (a/λ) was chosen to be 0.2. This is a compromise between low short-range wakefields, favoring large a/λ, and the desire for high shunt impedance, favoring small a/λ. A cell design with 0.55 mm thick irises and a $2\pi/3$ phase advance was also chosen to maximize shunt impedance.

However, recent observations of field limitations due to electrical breakdown and related surface damage in 30 GHz prototype structures have shown that the present TDS design will not meet the gradient requirements for CLIC without modifications to its geometry. A weak point of the TDS design is the excessive pulsed surface heating in the vicinity of damping waveguide entrances. A program of structure development and high power testing using different structure geometries and materials is under way, accompanied by theoretical studies of wakefield control. The goal is to produce a new design meeting the gradient, pulse length and wakefield requirements of CLIC. The directions being taken in this process are discussed in Section 6.5.2.3 and Section 6.5.2.6.

6.5.2.3 Wakefield Suppression

Once the basic structure design had been selected, a method for suppressing the long-range transverse wakefield was needed. The long-range wakefields are generated as the beams traverse the accelerator structures, and if not suppressed, would produce an enormous amplification of any betatron motion of the bunch train. Several techniques to reduce these wakefields have been developed and are described here. For the JLC-X/NLC and CLIC, the

techniques were developed for their initial structure designs and are described in this context.

For the JLC-X/NLC, the transverse wakefield must be reduced by about two orders of magnitude during the 1.4 ns between bunches. To achieve this difficult goal, a combination of cell detuning and damping was chosen. For the detuning, each cell of the structure is made to have a slightly different dipole frequency so that the wakefields destructively add by the time the next bunch arrives. The frequency variation is chosen to produce a Gaussian-like distribution in the product of the dipole mode density and the dipole mode coupling strength to the beam. This detuning produces an approximately Gaussian falloff in the net wakefield generated by each bunch, and works well to suppress the wakefield for about 30 ns, after which the amplitude increases due to a partial recoherence of the mode excitations. To offset this rise, weak mode damping was introduced by coupling each cell through longitudinal slots to four TE_{11} circular waveguides (manifolds) that run parallel to the structure. This reduces the dipole mode quality (Q) factors from about 6000 to 1000, limited by the propagation time of the dipole-mode energy through the cells.

Successful implementation of the damping and detuning required major advances on two fronts. One was the accurate modelling of wakefield generation in structures whose geometry varies from cell to cell. This was achieved using an equivalent circuit model where the circuit parameters were obtained via 3-dimensional finite-element calculations of a subset of cells. Another key advance was in the precision machining of the cell shapes to produce the desired acceleration and dipole mode frequencies.

The wakefields of three damped and detuned, 1.8 m structures have been measured to date. Although the wakefields for all three structures were larger than acceptable for the JLC-X/NLC, the suppression was within factors of 2–5 of the two-orders of magnitude reduction required. In two cases, there were known errors during the structure fabrication, which when simulated in the structure model, yielded wakefields in good agreement with the measurements. In the third case, good agreement was achieved after including 12 MHz rms, random cell-to-cell frequency errors in the model, which were larger than the 5 MHz rms errors expected from a limited set of cell measurements made prior to assembly. These comparisons have lent confidence that the wakefields can be accurately modelled. Currently, these techniques are being applied to the high gradient structures being developed, with testing expected in summer 2003.

The C-band group structures include an azimuthal choke joint in each cell for wakefield damping. With this geometry, the acceleration-mode fields are confined within the cell volume while the dipole mode fields extend radially beyond the choke area where they are absorbed in a SiC ring. Although this strong-damping scheme is simpler than that of JLC-X/NLC, the addition of the choke joint reduces the acceleration mode shunt impedance by about 20%.

A full length (1.8 m) "choke-mode" structure was built and its wakefield measured. The results showed that the dipole modes Q's were reduced below 20 as desired. However, a trapped mode in a higher band made the net wakefield higher than acceptable after 1.6 ns. The origin of the trapped mode was subsequently discovered, and corrections will be made in future designs so that it is heavily damped.

For the CLIC TDS design, the long-range wakefield must also be reduced by a factor of about 100 between bunches (0.7 ns). The approach chosen to achieve this uses a

combination of detuning and strong, local damping. The damping is realized by four transverse waveguides coupled to each cell, each terminated by a SiC load, arranged in a "flying chimney" configuration. The acceleration mode is below cutoff in these waveguides, but like the C-band choke joints, they produce a moderate loss (20%) in the acceleration mode shunt impedance.

To test this scheme, a 15 GHz scaled version was built so the larger iris radii would allow wakefield measurements in the ASSET facility at SLAC. A two-orders of magnitude wakefield reduction was observed by 1.4 ns, the equivalent bunch spacing at 15 GHz. However, a low frequency trapped mode in the beam pipe to vacuum vessel interface region produced a wakefield that dominated at longer times. This mode can be easily eliminated in future designs.

As noted previously, the pulse surface heating near the waveguide entrances in the TDS cells is large (250°C at the design gradient of 150 MV/m). Changes to the cell and waveguide geometry are being studied to reduce the pulse heating. Another damping approach being developed uses radially slotted irises to transport the dipole mode energy outside the cell. The geometry reduces pulse heating because of the small slot sizes. To test this concept, a short 3 GHz structure with slotted irises has been fabricated and high-power tested up to a 25 MV/m average accelerating field with 1.5 μs pulses. No degradation in performance was seen due to the slots.

6.5.2.4 Fabrication

6.5.2.4.1 JLC-X/NLC Over the past decade, manufacturing processes for X-band cells and structures have been developed by a SLAC-KEK collaboration, with participation by Lawrence Livermore National Laboratory and the involvement of several precision machining companies. In addition, the JLC group at KEK, in Japan, has made good progress toward developing industrial partnerships for fabricating cells and assembling structures.

The process developed for building the 1.8-m structures begins with the rough machining of high-purity copper disks using conventional lathes and mills. Rough machining leaves more than 40 μm of extra copper on all surfaces except for the coupling slots and manifolds. Follow-up precision turning, performed using single-crystal diamond tools, yields μm level accuracy and 50-nm (rms) surface finish. As the diamond turning is completed, microwave quality-control measurements are made of the acceleration and dipole-mode frequencies of each disk. If a systematic shift of the acceleration frequency is found in a series of consecutive disks, then adjustments are made to the nominal dimensions of the subsequent cells to offset the net phase-advance error. This feedforward correction procedure yields structures with a net phase advance within a few degrees of the design value. The dipole-mode frequencies are checked to eliminate cells with values significantly different (by a few MHz) from those of neighboring cells.

After cleaning and rinsing with ozonized water, the cells are stacked in a special V-block fixture and bonded together by a two-step diffusion bonding process: first at 180°C and then at 890°C. The complete structure is then assembled with flanges, vacuum ports, WR90 waveguides for the acceleration mode, and WR62 waveguides for the dipole modes. It is then brazed in a hydrogen furnace at 1020°C. After a vacuum bake-out, the structure

is installed on a strongback for final mechanical measurement and straightening guided by data from a Coordinate Measuring Machine. This procedure has yielded 1.8-m structures meeting the JLC-X/NLC straightness requirement of 10 μm rms.

A diffusion bonding technique has been adopted for assembling the main body of the JLC/NLC X-band accelerator structures mainly because of its ability to maintain excellent disk-to-disk tolerance during the processing, as well as mechanical sturdiness and good vacuum sealing capability. The initial consideration was that for diffusion bonding to produce acceptable bonding quality, the use of diamond-turned surfaces is of critical importance. However, recent experiences in building accelerator structures for high-power testing indicate that disks that are conventionally machined with poly-crystal cutting tools also exhibit good results in the diffusion bonding processes.

The choice of the cutting tools for the precision machining of X-band accelerator structures (*i.e.*, diamond versus poly-crystal) is another open issue. From the standpoint of controlling the resonant frequencies of individual disks, diamond-turned disks can be fabricated so as to make the post-assembly frequency tuning unnecessary. However, structures made with conventionally machined disks can be also tuned relatively easily via bead-pull measurements. Studies of the relative merits of these two approaches are needed to help the JLC-X/NLC group form the best strategies for mass-producing satisfactory accelerator structures in a cost-effective manner.

The structure manufacturing efforts will grow in the future with the increasing involvement by Fermilab, which joined the NLC collaboration in 1999. Working with off-site fabrication shops, the NLC group there has thus far built three, 20 cm X-band structures. In the next year, they plan to produce at least 5.4 m of low group velocity structures for the 8-Pack rf-system demonstration at the NLCTA. The group's long-term goal is to develop the industrial partnerships needed to manufacture the full complement of X-band structures for NLC.

6.5.2.4.2 CLIC So far nine 30 GHz prototype structures (without HOM damping) have been built and high power tested. These prototypes were of the constant impedance type. Eight of the structures were fabricated from 86 OFHC copper disks using single-point diamond turning and were assembled using a specially developed CLIC brazing and diffusion bonding technique at 820°C. This assembly technique results in fundamental-mode Q values close to the theoretical values (∼99%). In contrast to JLC-X/NLC structure fabrication, all brazing operations are done in vacuum instead of hydrogen. The CLIC team has not had any temperature control problems and wants to avoid diffusing hydrogen into the copper.

The cells for all structures have been machined by European industry. The ± 2 μm machining tolerances imposed by long range wakefield constraints were in all cases met. All but one of these structures were assembled and brazed at CERN (one was assembled and brazed by industry). Seven of the eight structures had single-feed, conventional couplers which produced a very asymmetric field in the first cell of the structure, and created a very high ratio of peak surface field to accelerating field.

A study of the mass-production cost of the precision machining of these copper disks was made by four independent firms in 1993. The four estimates were very close and showed

that the cost was very reasonable. An equivalent study for structure assembly and brazing has not yet been made.

The ninth structure that was built is very different. It was made by clamping tungsten irises and copper disks together, and was mounted and tested in a vacuum can. Its couplers are of the single-feed mode-launcher type and were also clamped onto the structure. These couplers produce a very symmetric field in the first cell of the structure, with peak surface fields less than those in the other cells. The clamping and vacuum-can technique was first used by the CLIC team for the TDS wakefield measurements described earlier.

6.5.2.5 Structure Environment

The accelerator structure dimensions must be kept stable as rf power and beam current are varied. For the normal-conducting designs, it is not necessary to actively tune the structures by mechanical means. However, the average temperature needs to be controlled to about 0.5°C to prevent significant changes in the bunch energy and energy spread. Such tolerances have been easily met in a wide variety of linac systems.

The JLC-X/NLC designers are evaluating a less costly cooling scheme compared to that in the SLAC linac and NLCTA. It would use a relatively low flow of water, about a third of that nominally used, to cool the several kilowatts of power dissipated per meter of structure. In this case, the structure temperature rise during operation is estimated to be about 10°C. It is expected that temperature stability requirements can be met but further engineering is required to determine the minimum cost design.

6.5.2.6 High Gradient Development

6.5.2.6.1 High Gradient Structure Development for JLC-X/NLC High-power testing of NLC and JLC prototype structures began in earnest in 1999 with the improvements to the high power testing capability at the NLC Test Accelerator (NLCTA). The difficultly encountered in processing one of the 1.8-m structures to 70 MV/m with 240 ns pulses led to the discovery that breakdown-related damage was producing a significant alteration in the rf properties of the structure at gradients less than 70 MV/m. The damage was manifested as an increase in the rf phase advance through the structure and was associated with severe pitting of the cell irises. Phase advance measurements of several other 1.8-m structures showed that the damage had begun at unloaded gradients above 45–50 MV/m. A revealing observation was that the damage was much more pronounced in the upstream ends of the structures where the rf group velocity is greatest. Such a dependence on group velocity may be due to the higher rf power required to achieve a given gradient at higher group velocity.

Besides the phase shifts, the breakdown rate in the 1.8 m structures remained high at gradients above 60 MV/m, indicating the damage was likely continuing. Thus, the effective gradient would eventually diminish due to out-of-phase acceleration. The phase change rate was estimated to be about 20° per 1000 hours of operation at a 60–70 MV/m gradient, which would make the structures ineffective in a few months. While ideally no phase change would occur during operation, a shift up to 0.5° per 1000 hours would likely be acceptable. This would result in only a 5% loss of effective gradient in 20 years of operation in a worst case scenario where no effort is made to compensate for the phase change (*e.g.*, increasing the structure operating temperature).

In operational terms, an acceptable breakdown rate depends on (1) the number of structures turned off after a breakdown, (2) the recovery time needed to bring the structures back to full power and (3) the fraction of structures allocated for spares. For the JLC-X/NLC, six structures (one girder's worth) will be turned off after a breakdown in any of the structures, the recovery time will be 10 seconds, which has been tested, and 2% of the structures (19 girders per linac) will be used as "hot-swappable" spares. Given these values, a structure breakdown rate of 1 per 3 hours at the 120 Hz repetition rate would essentially never deplete the structure reserves (this would occur about once per year and would take less than 10 seconds to recover from). At this rate, approximately one structure in each linac would breakdown every 100 pulses, yielding at most a 0.02% change in the beam energy during that pulse. The beam energy would fluctuate by >0.1% only once a year due to multiple structure breakdowns per pulse (the Final Focus bandwidth is ±0.5% in comparison).

To address the structure damage problem, a program was launched in spring 2000 to develop lower group-velocity structures. Much progress has been made since then toward understanding high gradient performance. The advances have resulted from an aggressive experimental program, which has included tests of three pairs of low group velocity traveling-wave structures ('T' series,with different lengths, 20, 53 and 105 cm and group velocities, 5% c and 3% c at the upstream ends), an initial test of a pair of high phase advance traveling-wave structures ('H' series), and operation of three pairs of standing-wave structures. In addition, various improvements were made to the structure cleaning, handling and processing procedures to determine their impact on high-gradient performance. A brief summary of the results from these studies follows.

The rf processing of the T-Series structures started at higher gradients (55–65 MV/m) than that (35–45 MV/m) for the 1.8 m structures. In addition, much less damage was observed in these structures at gradients above 70 MV/m than in the 1.8 m structures at gradients of 50–65 MV/m. After processing to 80–85 MV/m, the breakdown rate at 70 MV/m was dominated by events in the input and output couplers. The breakdown rates in the body of the structures (*i.e.*, excluding the couplers) at 70 MV/m were close to acceptable for the JLC-X/NLC at the design pulse width of 400 ns. For the three 53 cm, 3% c initial group velocity structures that were tested, the breakdown rates were <0.1, 0.2, and 0.3 per hour, respectively, while the goal is <0.1 per hour given the structure length and NLCTA repetition rate of 60 Hz.

An autopsy of the input coupler of one of the structures revealed melting on the edges of the waveguide openings to the cell, and extensive pitting near these edges and on the coupler iris. The waveguide edges see large rf currents that are a strong function of their sharpness, and the associated pulse heating can be significant. By design, the edges in the T-Series structures were sharper (76-μm radius) than those in the 1.8-m structures (500-μm radius). Recent calculations have shown that the pulse heating for the T-Series structures is in the 130–270°C range, well below the copper melting point, but high enough to produce stress-induced cracking, which can enhance heating.

Based on these observations, a 53 cm, 3% c structure was built with couplers designed to have much lower pulse heating. This structure is currently being tested and has performed very well, with no obvious enhancement of the coupler breakdown rates relative to the other cells. For the full structure, a breakdown rate of about 1 per 25 hours has been measured at 73 MV/m with 400 ns pulses, and after further processing to 92 MV/m, a similar rate has

been measured at 90 MV/m. All future structures will be made with couplers similar to those used in this test.

Although the results from the T-Series structures are very encouraging, their average cell iris radii are too small to meet JLC-X/NLC short-range wakefield requirements. To increase the iris size while maintaining a low group velocity, a structure design with thicker irises and a higher phase advance per cell (150° instead of 120°) design has been adopted. Two such structures (H-Series) have been built, one 60 cm long with an initial group velocity of 3% c, and the other 90 cm long with an initial group velocity of 5% c. Both are detuned for wakefield suppression, but do not include manifolds for wakefield damping.

Unfortunately, these structures have the earlier, T-Series type couplers since they were built before the coupler pulse heating problem was discovered. Making the problem worse, the H-Series structures have lower shunt impedance than the T-Series structures, so the pulse heating is relatively high. During their processing at NLCTA, the coupler breakdowns have indeed limited the gradient to values lower than that achieved with the T-Series structures. In addition, at short pulse lengths where the coupler events did not dominate, the processing rate was much slower than that for the T-Series structures. The larger iris thicknesses of the H-Series structures are certainly a contributing factor, but they do not explain the full difference.

The best results to date have been achieved with the 60 cm, 3% c structure, which has been processed to 72 MV/m with 400 ns pulses. At 65 MV/m, the current JLC-X/NLC design gradient, the breakdown rate in the body of this structure meets the goal of <1 per 10 hours while the input coupler breakdown rate is about 25 per hour. The program until summer 2003 is to test several H-Series structures with improved couplers, culminating in one that is fully damped and detuned for wakefield suppression. By the end of 2003, 5.4 m of such structures (with and without damping) will be powered with the 8-Pack rf source to demonstrate full system integration and to improve performance statistics.

Another approach being explored for achieving higher gradients is to use short standing wave structures that require much lower peak power than the traveling wave structures. The standing wave structures tested so far are 20 cm long, contain 15 cells and have a beta coupling of one or two. They are operated in pairs, which allows the power reflected from them during their approximately 100 ns fill/discharge periods to be routed to loads.

Three such pairs have been tested during the past year. However, only one pair performed well at the flattop pulse width of 270 ns and earlier JLC-X/NLC loaded gradient requirement of 55 MV/m (unlike the traveling-wave structures, the standing wave structures do not need to operate above the JLC-X/NLC loaded gradient). After processing, the average breakdown rate for this pair at 55 MV/m was about 0.1 per hour per structure during a several hundred hour period, which is about a factor of 2 higher than desired for these short structures. Also, no discernable shift in frequency (<100 kHz) was measured in either structure after 600 hours of operation. The other pairs showed higher breakdown rates (>1 per hour) at 55 MV/m and one pair showed frequency shifts of several hundred kHz.

From rf and optical measurements made during operation and after removal from NLCTA, it appears that most of the breakdowns occurred in the coupler cells of the standing wave structures. The structure performance roughly correlates with the predicted temperature rises on the input waveguide edges in the coupler cells. That is, for JLC-X/NLC running

conditions, the temperature rise for the best performing pair was 40°C, while that for the other two pairs was 60°C and 150°C. For the next pair of structures to be tested, a coupler with a lower temperature rise (<20°C) will be used, and choke-mode cells will be included to test their high gradient properties in preparation for their use to damp wakefields.

6.5.2.6.2 Basic Studies at NLC on the Physics of RF Breakdown As a complement to the structure testing, the NLC group is committed to a strong program of theoretical studies, computer simulations and experimental measurements directed toward understanding the underlying physics of rf breakdown. A simple theory indicates, for example, that extensive surface damage may occur when an area on the surface is brought to the melting point by electron bombardment before the end of the rf pulse. This points the way toward the use of other materials, such as stainless steel, tungsten or molybdenum as materials for the iris tips in a copper structure (see CLIC results below). Computer simulations, using an advanced 3D particle tracking code, are used to follow the motion of electrons and ions emitted from small areas of plasma formed near field emission sites, and to calculate the power density and resulting temperature rise at areas where the electrons impact on the surface.

A comparison of the results from theory and simulations with experiment is best carried out by high-field tests on simple structures. A well-instrumented test bed has been set up for measurements on short sections of rectangular waveguide with enhanced surface fields, and on short sections of traveling-wave (TW) and standing-wave (SW) structures. So far, waveguide sections having different group velocities and made from different wall materials have been tested. These measurements have provided experimental verification that, compared to copper, significantly higher fields can be sustained on a stainless steel surface without breakdown. A series of tests is now in progress in which a short length of accelerator structure, consisting of two standard structure body cells and two coupling cells, is placed between two low-field mode launcher-type couplers. Because these test sections do not include couplers and are demountable, they can be cycled through the test setup rapidly, compared to the time required to build and test a full structure with couplers. The dependence of processing time, breakdown rate and limiting gradient on a number of structure variables can be studied. Some tests in progress or planned are: the dependence of the preceding breakdown-related parameters on group velocity for TW structures; a comparison of breakdown parameters for TW structures versus SW structures for a given iris aperture; the dependence on iris tip material; the dependence on fabrication variables related to machining and surface preparation; and a measurement of potential surface damage near coupling apertures in structure cells with damping.

6.5.2.6.3 High Gradient Structure Development at CLIC The CLIC group ran a program of 30 GHz high-power structure testing using CTF2 as the power source. CTF2 provided 30 GHz rf pulses of up to 280 MW with a variable pulse length from 3 to 15 ns. This pulse length was larger than the filltime of the structures built so far, but short compared to the nominal 130 ns pulse-length of CLIC. The probe beam of CTF2, with its two magnetic spectrometers, allowed a precise beam-based measurement of the average accelerating gradient in the structures. This was a very useful cross-check of the gradient derived from the 30 GHz power measurements. Since the available power by far exceeded the power needed for structure testing, a simple pulse-stretcher was installed to increase the

pulse length to 30 ns. Unfortunately, CTF2 was closed down and dismantled at the end of 2002 to make way for a new CLIC test facility, CTF3. This new facility will produce 30 GHz rf power pulses of the nominal 130 ns length. High-gradient testing with this new source is expected to start in spring 2004. In another structure-related activity, the CLIC team is collaborating with JINR/Dubna to carry out pulsed-surface-heating tests of copper cavities using their 30 GHz FEL as the power source. These tests will assess the fatigue properties of copper, and other materials may be studied as well.

In 1994, a small aperture (6 mm), low group velocity, 26-cell X-band structure was built with CLIC technology and tested at SLAC. It achieved a peak accelerating gradient of 150 MV/m with a 150 ns pulse (the average gradient was 125 MV/m) without damage, demonstrating the technical feasibility of producing 150 MV/m gradients with copper structures.

The constant impedance copper structures tested before 2002 in CTF2 reached mean accelerating gradients of only 60 MV/m (confirmed by both beam acceleration and rf power measurements). At this field level, considerable surface damage was observed on the first iris which connects the input coupler cell to the first regular cell. No significant damage was seen in the downstream cells. This is easily understandable because the coupler cell has the highest surface field in the structure (the surface field corresponding to a 60 MV/m mean acceleration is 264 MV/m, a ratio of 4.4). The damage pattern resembles the field distribution pattern which suggests a correlation between peak surface field and damage. RF conditioning to the level where damage occurs took typically 3×10^5 rf pulses. In a recent experiment (June 2001), the damaged copper iris was replaced by an iris made of tungsten. In this configuration the structure reached 72 MV/m accelerating field. The corresponding surface field on the tungsten iris is 317 MV/m. Although the structure was powered for 5×10^5 pulses to the same field levels, the tungsten iris was undamaged. When the tungsten iris was replaced by a copper iris and the pulse length was shortened to 3 ns, a record peak accelerating gradient of 160 MV/m was obtained with 5×10^5 pulses. Although the pulse energy was the same as in the 72 MV/m run at 15 ns, no damage occurred.

During 2002, three structures made from either a different material, with a reduced E_{surf}/E_{acc} ratio along the structure were tested at high power in CTF2, or both. The geometry of the structures was deliberately kept simple for these tests with no complicating features such as damping waveguides so that the basic underlying limitations could be clearly observed. The first structure tested had an a/λ of 0.175 with a $2\pi/3$ phase advance, a E_{surf}/E_{acc}=2.2 and v_g=0.046 c. The couplers were of the mode-launcher type. The surface field in the coupler nowhere exceeded the field in the regular cells. All irises were made of tungsten with copper rings clamped between them (see paragraph on structure fabrication). The second structure had the same cell geometry, but was made entirely from OFHC copper and assembled by a braze/diffusion bond at 820°C in vacuum. The third structure had all irises made from molybdenum with copper rings clamped between them.

The first structure, with tungsten irises, was conditioned (15 ns at 5 Hz) to an average accelerating gradient of 125 MV/m, with a peak accelerating field in the first cell of 152 MV/m and a peak surface field of 340 MV/m. When the inside of the structure was examined with an endoscope, there was no observable damage along the body of the structure, and in particular none in the coupler. The second structure, entirely made from copper, reached an average accelerating field of 102 MV/m with a peak accelerating field in the first cell of 114 MV/m and a peak surface field of 255 MV/m. Contrary to the

tungsten-iris structure, the copper structure showed signs of surface damage on the first regular iris, where the surface E-field is highest. The third structure, with molybdenum irises, was conditioned to an average accelerating gradient of 150 MV/m, with a peak accelerating field in the first cell of 193 MV/m and a peak surface field of 432 MV/m. No damage was observed. From these results and past CTF2 results, it is inferred that tungsten and molybdenum can support considerably higher surface fields before breakdown damage occurs, while copper shows surface damage for surface fields exceeding 250 MV/m. This damage inhibits rf conditioning of copper surfaces beyond this level. The same copper structure was tested with a 30 ns pulse length using an rf pulse stretcher in CTF2. The same accelerating gradient was obtained as with 15 ns pulses. This result gives a first indication that the dependence of breakdown level on pulse length is weak if the pulse length is larger than the time needed to develop a full breakdown (typically 10 ns), but small compared to the pulse length for which surface heating becomes important. The achievable rf power level with the CTF2 pulse stretcher was insufficient to drive the tungsten and molybdenum structures to their breakdown points. More tests are needed to evaluate more precisely the dependence of breakdown damage for these materials on pulse length.

A second tungsten-iris structure will be built with a $\pi/2$ phase advance and with an a/λ=0.2, E_{surf}/E_{acc}=2 and v_g=0.083 c. A comparison of the gradients achieved with the two tungsten-iris structures will hopefully enable the effects due to surface field and group velocity to be distinguished.

The lower conductivity of tungsten reduces the Q value relative to copper. For the structure already tested, the Q value is 33% lower. This Q change reduces the rf-to-beam efficiency by approximately 20%. If tungsten is only used in the regions of the cells where the surface electric field is more than 50% of the peak surface field, then the Q would only be reduced by 5%, and the rf-to-beam efficiency by 1%. Studies of the technical feasibility for such a configuration have just started.

A series of tests performed with single cell copper cavities at 21 GHz, 30 GHz, and 39 GHz showed no significant dependence of the breakdown limit on frequency. All these cavities reached peak surface fields around 350 MV/m. Other frequencies could also be created in CTF3 in order to evaluate more precisely the much discussed behavior of rf structures versus frequency. This would be a good opportunity for a global collaboration between laboratories.

6.5.2.6.4 Basic Studies at CLIC on the Physics of RF Breakdown The CLIC team has undertaken a vigorous program of theoretical studies, computer simulations and experimental tests aimed at understanding the underlying physics of rf breakdown. There is evidence to suggest that the melting point of the material used and possibly its vapor pressure may play an important role in determining achievable gradients, and the use of other materials such as tungsten or molybdenum for the iris tips in copper structures is being pioneered.

6.5.2.6.5 High Gradient Structure Development for JLC-C The C-band groups at KEK and RIKEN are planning to conduct their first systematic high-power tests of 1.8 m, choke-mode structures at an unloaded gradient of 42 MV/m during 2003. They are

encouraged by a 1994 high power test of a short, low group velocity (0.8% c), choke-mode, S-band structure, which processed to 50 MV/m.

6.5.2.7 Operational Experience

The bulk of operational experience with X-band structures has come from the NLC Test Accelerator (NLCTA) at SLAC. This facility, which was commissioned in 1996, is a test-bed for X-band accelerator systems. The power sources (XL4 klystrons and SLED-II pulse compressors) have operated reliably, energizing 12 X-band accelerator structures for an integrated total of about 10,000 hours. The NLCTA has accelerated high-quality pulse trains with energy spread within the JLC-X/NLC specification of 0.3%.

The new generation of improved X-band components will be added to the NLCTA over the next two years for a demonstration of the proposed JLC-X/NLC rf system. The components include 11 m of high-gradient accelerator, a multimode SLED II pulse compression system, eight 75-MW klystrons with periodic permanent-magnet focusing, and a solid state, high-voltage pulse modulator.

Operational experience for CLIC structures comes from CTF2. In 1999, a string of five structures was installed in the CTF2 probe beamline and operated for approximately 200 hours at an average gradient of 40 MV/m. The 30 GHz rf power was delivered by 4 power extraction structures installed on the CTF2 drive beam, running parallel to the probe beamline. This CTF2 run gave valuable experience on setup procedures for two beam accelerators. In 2000, CTF2 was converted in a 30 GHz high power test stand allowing testing of only one structure at a time, but at much higher power levels.

6.5.2.8 Potential for Upgrading to Higher Gradients

The scaling of the breakdown-limited gradient with rf frequency has been the subject of both theoretical and experimental investigation for many years. More recently, it has been realized that pulse length plays an important role. Currently, the role that structure geometry (group velocity, standing wave versus traveling wave) and structure material (*e.g.*, tungsten iris tips) plays in determining the breakdown gradient is also being investigated. But it is fair to say that a comprehensive theory of rf breakdown is still some distance in the future, and that we are currently taking a mainly phenomenological approach to the problem (try lots of things and see what works), with some guidance from a few simple theoretical ideas.

From their experiments, Loew and Wang [33] concluded that, at roughly constant pulse length, the breakdown-limited gradient scales approximately as the square root of frequency. Their scaling expression gives a peak surface field of 660 MV/m at 11.4 GHz. A peak surface field of this order at a pulse length of several microseconds was actually reached on the reentrant nose cone of a cavity in the "Windowtron" test stand at SLAC [34]. In addition, we note that the capture threshold for dark current scales linearly with frequency (the threshold is 61 MV/m at 11.4 GHz). These factors encouraged the NLC to continue to focus on the linear collider design effort at X-band, in spite of difficulties associated with a higher frequency, such as tolerances and rf power production.

It was seen in Section 6.5.2.6 that the gradient design goal for the JLC-X/NLC is close to being met. There are prospects for increasing the gradient well beyond the JLC-X/NLC

design goal. In experiments in which breakdown is studied in a short low group velocity section of waveguide made of different materials (see Section 6.5.2.6.2), Tantawi and Dolgashev [35] found that the breakdown field is 20–30% higher for stainless steel compared to copper. This higher gradient could be used either to increase the operational safety margin or to increase the machine energy.

As was also mentioned in Section 6.5.2.6, a gradient of 150 MV/m at a 15 ns pulse length has recently been reached in experiments at CLIC using tungsten irises. It remains to be seen whether this success can be extended to reach the unloaded design gradient of 172 MV/m at 130 ns. In any case, CLIC is not looking beyond the design gradient because pulse surface heating and drive beam energy requirements would pose other serious limitations that seem difficult to overcome in the present CLIC scheme.

The JLC C-band strategy is also not aiming beyond the unloaded design gradient of 42 MV/m. They would add a length of X-band linac to upgrade in energy.

6.5.3 Accelerator Structures: Conclusions

6.5.3.1 Introduction

The choices that were made for operating frequency and technology by all linear collider groups were closely tied to specific performance expectations for the accelerator structures. In particular, all designs assumed that stable operation could be achieved at gradients higher than had been previously demonstrated in comparable structures, and that the long-range wakefields generated in the structures could be suppressed to a level that would keep multiple bunch emittance growth within acceptable limits. Meeting these goals has been the major R&D focus by these groups. The choices made for operating frequency and technology have also had a strong influence on other structure-related issues, such as alignment requirements and ease of fabrication and operation.

An important parameter for any linear collider is the efficiency for the conversion of rf power to beam power. The structure efficiencies (rf input to beam), when accounting for the structure filling time and energy overhead are, for C-band, JLC-X/NLC, and CLIC, 26%, 27%, and 23% respectively. In general, higher efficiencies (and higher beam currents) have been traded off in these designs to reduce wakefield strength, the number of structures, linac length and peak power requirements. On the plus side, the resulting low beam loading (<26%) has the advantage of easing beam current stability requirements. The TESLA structure efficiency is 59%.

6.5.3.2 High Gradient Structure Development

6.5.3.2.1 Concerns for Achieving TESLA Design Gradient The TESLA group has made significant progress during the past decade in improving the surface processing of niobium, allowing them to achieve gradients exceeding 25 MV/m. Thus far, they have produced about 40 nine-cell cavities that have operated at CW with acceptable power losses at gradients between their 500 GeV c.m. design goal of 23.8 MV/m and 35 MV/m. In addition, an eight-cavity cryomodule has accelerated beam at 22.7 MV/m. This is the highest acceleration achieved so far by a TESLA module. Several more cryomodules are in

the queue and they are expected to exceed this gradient. Although the fault rates and recovery times during such operation are just beginning to be better quantified, down-time statistics recorded at 19–22 MV/m suggest that the cavities could run with acceptable down-times in TESLA, at least at these lower gradients. While these results are encouraging, the cavities will likely have to be capable of operating at 35 MV/m initially if the upgrade goal to 800 GeV c.m. is to be considered seriously. The use of an electropolishing technique for etching the cavity surfaces has yielded about 15 single-cell cavities that meet the upgrade requirements. Recently, three nine-cell cavities have also met these criteria during CW operation. During the next year, one of the TESLA group's goals is to build an eight-cavity cryomodule that will accelerate beam at 35 MV/m.

In addition, the long-term behavior of the high power couplers needs to be evaluated further.

R&D (Ranking 2):

- Long term testing of several cryomodules at design gradient (23.8 MV/m) with acceptable quench behavior and coupler performance.

R&D (Ranking 3):

- Evaluate dark current effects at TTF2.

6.5.3.2.2 Gradient Concerns for Normal Conducting Designs The normal-conducting designs have also aimed for high gradients, encouraged by early tests that showed that gradients greater than 100 MV/m are possible. However, these tests were done with standing-wave or low group velocity structures because of the limited peak power available at that time. The higher group velocity structures that were later chosen by the linear collider groups for lower cost (fewer feeds) and lower wakefields have not performed as well. The approach to high gradients has been essentially empirical, as there is little fundamental understanding of rf breakdown and damage mechanisms.

6.5.3.2.3 Concerns for Achieving JLC-C Gradient The unloaded gradient goal of the C-band group at KEK and RIKEN is 42 MV/m. They are planning to conduct their first high power test of their 3.6% c initial group velocity structure in 2003.

R&D (Ranking 1):

- Test structure design at high gradient during 2003.

6.5.3.2.4 Concerns for Achieving JLC-X/NLC Gradient For the JLC-X/NLC, achieving the unloaded gradient goal (originally 70 MV/m with 400 ns pulses) has also been difficult. The initial structure design, in which the group velocity tapered from 12% c to 3% c, incurred significant breakdown related damage near its upstream end at gradients of 45–50 MV/m. A series of six, 5% c and 3% c initial velocity structures that have since been

tested have proven much more robust. Except in the input and output coupler cells, acceptable breakdown rates have been achieved. The high coupler breakdown rates are thought to be related to pulse heating or single-surface multipactoring at the waveguide openings. Recently, a 3% c initial group velocity structure with lower peak magnetic fields in the coupler cells was tested. It achieved acceptable breakdown rates with 400 ns pulses at 73 MV/m, well above the current design gradient of 65 MV/m. However, all of these low group velocity structures have smaller than acceptable iris sizes for the JLC-X/NLC and do not include long-range wakefield suppression. To increase the iris radius while maintaining the low group velocity, a high phase advance (150°) design has been adopted. Testing of a series of such structures has begun. Structures including full wakefield suppression will be tested by summer 2003; this testing is expected to yield an "JLC-X/NLC-ready" design.

R&D (Ranking 1):

- Validate performance of high phase advance, low group velocity structures.
- Choose coupler design and incorporate manifold damping to produce an JLC-X/NLC-ready structure in summer 2003.

R&D (Ranking 4):

- Continue development of standing-wave structure.

6.5.3.2.5 Concerns for Achieving CLIC Gradient The CLIC goal of an unloaded gradient of 172 MV/m in 30 GHz structures is probably the most challenging. Thus far, a gradient of 193 MV/m has been achieved at the upstream end of a short, 5% c group velocity, constant impedance structure made with molybdenum irises. However, due to the power source, the rf pulse length was limited to 15 ns, which is considerably shorter than the 130 ns required. High power testing at 30 ns pulse length has shown similar results. Further high power testing at 30 GHz will be on hold until spring 2004 when a new long pulse power source (CTF3, pulse length variable from 40–500 ns) will start operation.

R&D (Ranking 1):

- Test structures at design gradient and 130 ns pulse length in 2004.
- High power tests of structures with proper wakefield damping.

R&D (Ranking 2):

- Additional tests with tungsten and other iris materials.

6.5.3.3 Basic Studies on the Physics of Surfaces and Breakdown

A program of basic physics studies on gradient limitations is being carried out for both the normal conducting and superconducting projects, in parallel with the effort to develop operationally reliable accelerator structures. For TESLA, these studies include improved understanding of rf surfaces and preparation methods of the surfaces. Another program explores the use of other Type-II superconducting materials. For JLC-X/NLC and CLIC, there is a program of theoretical studies, simulations, and small-scale experiments on breakdown. CLIC is doing pioneering studies on the effect of different iris materials on high gradient performance using a "clamp-together" type structure for fast turnaround. At SLAC, short waveguide sections are being used to explore the effects of different materials. A program using demountable structures with a few cells to explore the effect of different materials, surface preparation procedures and structure geometries is just beginning. At CTF3, one could also test the behavior of structures at different frequencies.

R&D (Ranking 4):

- All projects: strengthen the theoretical studies, simulations and experimental programs aimed at increasing the fundamental understanding of the physics of breakdown in order to achieve higher gradient operation.

6.5.3.4 Wakefield/HOM Suppression

The development of long-range wakefield suppression techniques by all linear collider groups has made considerable progress.

6.5.3.4.1 Concerns for HOM Damping in TESLA For TESLA, the main task is to insure that the dipole modes that couple strongly to the beam are sufficiently damped via HOM couplers at the ends of their cavities. Beam-based measurements of mode properties have shown that this is indeed the case for the strongest bands. However, a trapped mode was found in another band. The HOM couplers have been modified to produce heavier damping of this mode, and will be used in all future cavities. This program is expected to result in satisfactory wakefield suppression.

R&D (Ranking 2):

- Conduct beam test of cavities with modified HOM coupler design starting in 2003.

6.5.3.4.2 Concerns for Wakefield Suppression in Normal-Conducting Machines For the normal-conducting machines, wakefield control has been more of a challenge because of the relatively strong wakefields. These fields need to be reduced by about two-orders of magnitude by the time of the next bunch. The approach has been to use a combination of dipole mode damping and detuning. Different methods have been developed for coupling out the dipole energy for the damping: the C-band group uses so-called choke-mode cells, JLC-X/NLC use distributed coupling to manifolds that run parallel to the structure, and

CLIC uses radial waveguides in each cell. All groups have built test structures whose measured wakefields have come close to meeting design requirements. The reasons for the shortcomings have been identified (*e.g.*, fabrication errors) and are considered correctable.

6.5.3.4.3 Concerns Related to Pulsed Heating A concern related to high power operation is the pulse heating that occurs near the openings of the cells that couple out the dipole energy. The latest design of the CLIC waveguide damped structure has a maximum pulsed temperature rise of 130°C, which is possibly too high. An experimental pulsed surface heating program is underway to determine the acceptable limits for temperature rise. The JLC-X/NLC groups have recently modified the slot shapes in their damped cell design to reduce pulse heating to less than 30°C. Several cells with this new shape will be tested at high gradient by the end of 2002, and complete structures will be tested in spring 2003. The C-band choke mode structure has relatively low pulse heating.

R&D (Ranking 1):

- JLC-X/NLC and CLIC: Incorporate wakefield damping into structure designs without affecting high gradient operation.

6.5.3.5 Tolerances

6.5.3.5.1 Concerns Related to TESLA Structure Alignment Given the low operating frequency of TESLA, wakefield related alignment tolerances for TESLA are relatively loose compared to those for the normal-conducting designs. However, this advantage is partially offset by the difficulty of achieving precise alignment in the cryomodules.

R&D (Ranking 2):

- Demonstrate that multicavity alignment meets requirements.

6.5.3.5.2 Concerns Related to Alignment of Normal-Conducting Structures The smaller size and simpler cooling schemes for normal-conducting structures make them nominally easier to align than the TESLA cryomodules, but the mechanical tolerances are tighter.

R&D (Ranking 3):

- JLC-X/NLC and JLC-C: Demonstrate that the structure alignment meets requirements.

6.5.3.6 Operation and System Tests

R&D (Ranking 2):

- For all designs a test is needed of an rf module, fitted with structures meeting all gradient, wakefield suppression or HOM damping requirements, in an operational setting with beam.

R&D (Ranking 3):

- All designs: Long-term testing of rf modules.

Recommendation: For TESLA, high priority should be given to make TTF2 available for systems tests and high gradient studies in 2003.

6.5.3.7 Structure R&D for Energy Upgrade

TESLA: For the energy upgrade, it is planned to increase the gradient to 35 MV/m. First, it is necessary to show that the gradient is achieved in the standard nine-cells. In a second step the gradient needs to be demonstrated in the 2×9 cell superstructures, if the superstructure is proven to provide sufficient HOM damping. The preliminary results from TTF show that the damping is indeed achieved. As the rf power needed to drive the superstructure is higher than for the standard 9-cells, it needs to be demonstrated that the rf couplers are capable of transmitting the power to the cavity.

R&D (Ranking 1 Upgrade):

- Build an eight cavity cryomodule at 35 MV/m during 2003. Test as soon as possible.
- Evaluate dark current levels and tunnel radiation at 35 MV/m with TTF2.

R&D (Ranking 3 Upgrade):

- Demonstrate superstructures gradient performance, power coupler performance and HOM damping.

JLC-X/NLC: The nominal path for upgrading the JLC-X/NLC energy to 1 TeV is to double the length of the linacs. However, since the SLED-II pulse compression system is capable of providing more peak power by increasing the compression ratio, the possibility also exists for increasing the energy by increasing the gradient. The on-going R&D program of structure development and basic studies of the physics of rf breakdown is directed towards achieving structures which can operate reliably at gradients up to at least 100 MV/m.

R&D (Ranking 4 Upgrade):

- Continue improving structure high gradient performance.

BIBLIOGRAPHY for CHAPTER 6

[1] P. Tenenbaum, P. Emma, L. Keller, Y. Nosochkov, T. O. Raubenheimer and M. Woodley, *Overview of collimation in the Next Linear Collider*, SLAC-PUB-8934. Contributed to IEEE Particle Accelerator Conference (PAC 2001), Chicago, Illinois, 18–22 June 2001.
http://www.slac.stanford.edu/spires/find/hep/www?r=slac-pub-8934

[2] R. Alley *et al.*, *The Stanford Linear Accelerator Polarised Electron Source*, Nucl. Instr. and Meth. **A365**, p.1 (1995), SLAC-PUB-6489 (1994)
http://accelconf.web.cern.ch/AccelConf/p95/ARTICLES/MPE/MPE08.PDF

[3] *Development of a pump-probe facility with sub-picosecond time resolution combining a high-power optical laser and a soft X-ray free electron laser*
http://www-hasylab.desy.de/facility/fel/vuv/projects/pump.htm

[4] E. Bente *et al.*, *The Photoinjector Option for CLIC: Past Experiments and Future Developments*, CLIC note 487, CERN/PS 2001-033 (PP)
http://cern.web.cern.ch/CERN/Divisions/PS/CLIC/Publications/2001.html

[5] I. N. Ross, *Feasibility Study for the CERN CLIC Photo-Injector Laser System*, CLIC Note 462, Central Laser Facility, Rutherford Appleton Laboratory
http://cern.web.cern.ch/CERN/Divisions/PS/CLIC/Publications/2000.html

[6] P. Krejcik, *et al.*, *Recent Improvements in the SLC Positron System Performance*, Proc. 3^{rd} EPAC, Berlin, 1992 (also SLAC-PUB-5786, March 1992)
http://www.slac.stanford.edu/pubs/slacpubs/5750/slac-pub-5786.pdf

[7] V.E. Balakin and A.A. Mikhailichenko, *The Conversion System for Obtaining High Polarized Electrons and Positrons*, Preprint INP 79-85, 1979, and K. Flöttmann, *Investigations Toward the Development of Polarized and Unpolarized High Intensity Positron Sources for Linear Colliders*, DESY-93-161,1993
http://tesla.desy.de/new_pages/TDR_CD/PartII/chapter04/references/Flo93.pdf

[8] L. Rinolfi, *A CLIC Injector complex for the main beams*, CLIC 354.

[9] T. Kamitani, L. Rinolfi, *Positron production at CLIC*, CLIC 465
http://ps-div.web.cern.ch/ps-div/CLIC/Publications/2000.html

[10] *TESLA Technical Design Report*, Part II, chapter 4.3
http://tesla.desy.de/new_pages/TDR_CD/PartII/chapter04/chapter04.pdf

[11] Sheppard, J., Energy Loss and Energy Spread Growth in a Planar Undulator, LCC-086 (2002).

[12] *Linac Coherent Light Source (LCLS) Conceptual Design Report*, Chapter 8, SLAC–R–593, April 2002, UC-414
http://www-ssrl.slac.stanford.edu/lcls/cdr/LCLS_CDR-ch08.pdf

[13] *A Possible Test in the FFTB of Undulator Based Positron Sources*
http://www-project.slac.stanford.edu/lc/local/MAC/MAY2002/MAC_Sheppard.pdf

[14] Ed. K. Floettmann, DESY, Ed. V.V. Paramonov, INR, *Conceptual Design of a Positron Pre-Accelerator for the TESLA Linear Collider*, DESY TESLA-99-14, p.30
http://tesla.desy.de/new_pages/TESLA_Reports/1999/pdf_files/tesla1999-14.pdf

[15] K. Floettmann *et al.*, *Travelling-Wave Positron Injector for TESLA*, DESY TESLA-99-03
http://tesla.desy.de/new_pages/TESLA_Reports/1999/pdf_files/tesla1999-03.pdf

[16] Sheppard, J., Planar Undulator Considerations, LCC-085 (2002).

[17] Sheppard, J., Positron Yield as a Function of Drive Beam Energy for a K=1, Planar Undulator-Based Source, LCC-092 (2002).

[18] W. Kriens, *Basic Timing Requirements for TESLA*, DESY TESLA-01-10
http://tesla.desy.de/new_pages/TESLA_Reports/2001/pdf_files/tesla2001-10-2.pdf

[19] C. Sanelli *et al.*, *Technical Layout of the TESLA Damping Ring*, LNF-01/003 (IR), 2001
http://wwwsis.lnf.infn.it/pub/LNF-01-003(NT).pdf

[20] Y. H. Chin, "Modeling and Design of Klystron," in Proc. of Linac98 (Chicago, IL, USA, 23–28 Aug 1998), p.367.

[21] S. Choroba, "Klystrons for TESLA," presented at LC2002, SLAC, 2002
http://www-conf.slac.stanford.edu/lc02/wg2/WG2_Chroba_Stefan.pdf

[22] A. Buenas and P. Pearce, "A Klystron-Modulator RF Power System for the CLIC Drive-Beam Accelerators," CERN Report, CLIC Note 435, 2000.

[23] H. Matsumoto, T. Shintake, et. al., "Operation of the C-Band 50MW Klystron with Smart Modulator," in Proc. of APAC98 (KEK, Tsukuba, Japan, 23–27 March 1998), p.157.

[24] S. L. Gold, "5045 Klystrons & Thyratron Reliability " presented at LC2002, SLAC, 2002
http://www-conf.slac.stanford.edu/lc02/wg2/WG2_Gold_3602.pdf

[25] R. L. Cassel, J. E. Delamare, M. N. Nguyen, G. C. Pappas, E. Cook, J. Sullivan and C. Brooksby, "The Prototype Solid State Induction Modulator for SLAC NLC," in Proc. of PAC01 (Chicago, IL, USA, 13–22 June 2001), p.3774.

[26] H. Pfeffer, L. Bartelson, K. Bourkland, C. Jensen, Q. Kerns, P. Prieto, G. Saewert, and D. Wolff, "A Long Pulse Modulator for Reduced Size and Cost," Fermilab Report, FERMILAB-Conf-94/182, 1994.

[27] H.-J. Eckoldt, "Pulse Cable for TESLA Modulators," DESY Report, TESLA 2000-35, 2000.

[28] S. N. Simrock, I. Altmann, K. Rehlich and T. Schilcher, "Design of the Digital RF Control System for the TESLA Test Facility," in Proc. of EPAC96 (Sitges, Barcelona, Spain, June 10–13, 1996), p.349.

[29] S. Holmes, C. Ziomek, C. Adolphsen, et. al., "Low-Level RF Signal Processing for the Next Linear Collider Test Accelerator," in Proc. of PAC97 (Vancouver, B.C. Canada, 12–16 May 1997), p.3027.

[30] V. P. Arbet-Engels, C. Benvenuti, S. Calatroni, P. Darriulat, M. A. Peck, A. M. Valente, C. A. Van't Hof. "Superconducting niobium cavities, a case for the film technology," *Nuclear Instr. and Methods, Phys Res, A*: 463 (2001), No. 1–2, pp. 1–8.

[31] Padamsee, Knobloch and Hays, *Rf Superconductivity for Accelerators* (John Wiley, New York, 1998), p. 101–102.

[32] Hassan Padamsee, personal communication.

[33] Gregory A. Loew and J.W. Wang, "RF Breakdown Studies in Room Temperature Electron Linac Structures," SLAC-PUB-4647 (May 1988).

[34] L. Laurent, personal communication.

[35] S. Tantawi, personal communication.

CHAPTER 7

Luminosity Performance Working Group Assessments

7.1 INTRODUCTION

7.1.1 Charge and Guidelines

Following the charge from ICFA which commissioned the second ILC-TRC report, the Steering Committee created two working groups to provide technical assessments of the current linear collider designs. This chapter provides the report of the second of these groups, the Luminosity Performance Group.

The charge to the Luminosity Performance Group is the following:

> "This group will play a role similar to the former Beam Dynamics group, but will broaden its scope to analyze all those factors which affect the ultimate luminosity performance (both peak and integrated) of all four machines, including but not limited to, emittance dilution, beam jitter, tunability, and reliability. It will look at all phenomena which can reduce the luminosity at each machine subsystem, so as to predict the final emittances and luminosity reachable at the interaction point. Wherever possible, the members of this group (including a few detector representatives) should set common standards and use common computer codes to predict emittances, jitters, *etc.* Calculations should take into account mechanical and electrical tolerances, ground motions at various sites, *etc.* The standards and assumptions should be clearly spelled out."

A group of 13 technically knowledgeable experts on linear colliders was formed to address this charge. The generic linear collider complex was divided into 4 subsystems. Four subgroups were formed, and each was charged with addressing the luminosity performance issues for its subsystem. A fifth subgroup was formed to address the impact of machine reliability on the integrated luminosity performance of the collider. The following general guidelines were established for the review of each subsystem:

- Establish the key performance parameters which relate directly to the luminosity (peak and integrated) of the collider, or which relate to the performance of a downstream system. (The design values of these performance parameters are provided in the megatables.)
- Establish a common set of technical issues that are to be considered in evaluating the ability of a specific design to achieve the required performance.
- Establish a common method (a set of assumptions, analysis tools, codes, *etc.*) to be used to address each of the technical issues.
- For each of the four linear collider technical approaches, assess the ability of the proposed approach to realize the performance parameters. Identify the most difficult technical issues and indicate the scope of future R&D, if any, required to establish with confidence that the performance goal can be reached.

7.1.2 Subgroup Organization and Membership

The following is a tabulation of the subsystems, the members of the associated subgroups, and a description of the topics included in the analysis of each subsystem. Except where noted, each subsystem of TESLA, JLC-X/NLC, and CLIC was analyzed. No luminosity issues have been separately examined for JLC-C, since the designs of the damping rings and of the beam delivery system are identical to those of JLC-X, and no design was made available to the committee for the JLC-C main linac optics. For the same reason, compatibility issues arising in the upgrade of JLC-C through the addition of an X-band extension were also not considered by the group.

1. Sources (Section 6.2)

   Members: **W. Decking**, DESY (Subgroup leader); J. Gareyte, CERN; K. Kubo, KEK; P. Tenenbaum, SLAC

   This group considered luminosity-related issues originating in the electron and positron sources. Because these issues are so intimately related to source technology, it was decided to merge this subgroup with the Injector technology subgroup of the Energy and Technology Performance Group (Chapter 6). The luminosity issues treated by this subgroup include electron source average current and polarization, and positron source yield and total emittance. Their conclusions are reported in Section 6.2.

2. Damping Rings (Section 7.2)

   Members: **J. Rogers**, Cornell (Subgroup leader); R. Assmann, CERN; W. Decking, DESY; J. Gareyte, CERN; K. Kubo, KEK; A. Wolski, LBNL

   This group considered luminosity-related issues for the TESLA and JLC-X/NLC damping rings. The CLIC damping ring was not considered because a lattice

meeting all the requirements was not available to the group in time for the necessary evaluations to be made.

The luminosity parameters which were considered included extracted beam emittance and jitter, particle loss, and electron polarization. The beam dynamics issues which were studied included dynamic aperture in the presence of wiggler nonlinearities, emittance correction algorithms, beam jitter generated by ground motion and the extraction kickers, classical, ion-driven and electron-driven instabilities, intrabeam scattering, and depolarization effects.

3. Low Emittance Transport (Section 7.3)

Members: **D. Schulte**, CERN (Subgroup co-leader);
P. Tenenbaum, SLAC (Subgroup co-leader); R. Assmann, CERN;
W. Decking, DESY; J. Gareyte, CERN; W. Kozanecki, CEA/Saclay;
K. Kubo, KEK; N. Phinney, SLAC; J. Rogers, Cornell; A. Seryi, SLAC;
N. Walker, DESY; A. Wolski, LBNL

This group considered luminosity issues in all the beamlines between the exit of the main damping rings and the interaction point. This includes the bunch compressor, the main linac, and the beam delivery system.

The luminosity parameters which were considered were emittance growth and beam jitter generated in the beamlines. The beam dynamics issues studied included single bunch and multibunch wakefields due to rf structures and collimators, chromatic emittance growth, beam jitter due to natural and cultural noise sources, synchrotron radiation, and beam-beam effects. Simulations were performed to study static-error tuning algorithms for each machine, using several different programs. The effect of dynamic misalignments on luminosity performance, including the effects of feedback systems, was evaluated.

4. Machine-Detector Interface (Section 7.4)

Members: **W. Kozanecki**, CEA/Saclay (Subgroup leader); N. Phinney, SLAC;
J. Rogers, Cornell; D. Schulte, CERN; A. Seryi, SLAC; R. Settles, MPI;
N. Walker, DESY

This group studied the issues related to the machine-detector interface. The systems that were examined include the interaction region, the spent-beam extraction lines, the background-suppression systems (post-linac collimation and synchrotron-radiation masking), and the beam-energy and beam-polarization diagnostics. The essential design choices (many of which are fundamentally linked to the crossing-angle issue) were examined from the viewpoints of beam-beam and single-beam backgrounds; detector coverage; stabilization, magnet technology and integration of final-doublet quadrupoles; technical feasibility and operability of the extraction line; and performance of the proposed collimation schemes in the presence of beam halo.

5. Reliability and Operability (Chapter 8)

Members from the Luminosity Performance Group:
N. Phinney, SLAC (Subgroup leader); R. Assmann, CERN;
W. Kozanecki, CEA/Saclay; D. Schulte, CERN; N. Walker, DESY

This group studied the impact of the design integrated luminosity performance on the required reliability of components and subsystems, and on the overall operability of the linear collider complex.

Because this topic is so intimately coupled to technology, this subgroup joined together with a similar subgroup from the Energy and Technology Performance Group. In addition to a consideration of the direct impact of component failure and replacement time on machine uptime, the group also considered requirements on the machine protection systems, and attempted to evaluate the tuning time required to re-establish the luminosity after a failure. The analysis and conclusions of this joint group are presented in Chapter 8.

7.1.3 Subgroup Report Structure

The reports of the subgroups presented in the three subsequent sections of this chapter have been organized in a parallel fashion. Each section begins with an overview, which sets the stage for the rest of the section. The major issues affecting the luminosity at the reference energy (500 GeV c.m.) are then presented. This constitutes the bulk of the work. Luminosity issues at the upgrade energy are briefly considered in a dedicated subsection. Each section includes a ranked list of recommended R&D items, and closes with an assessment of the feasibility of the system, together with a prioritized list of concerns. Note that in Section 7.2 and Section 7.3, when the Damping Ring or LET working group concludes that the "feasibility" of a certain result is established, it means that the working group believes that this result, for example, luminosity performance, can realistically be approached or reached, but not necessarily without a considerable amount of work and time for machine tuning. This is in contrast to the criterion for "feasibility" of system designs in Chapter 6 where it is expected that specifications, for example, to reach a certain rf power or beam energy, must be met at the outset.

The R&D items are ranked according to the following criteria:

Ranking 1: R&D needed for feasibility demonstration of the machine

Ranking 2: R&D needed to finalize design choices and ensure reliability of the machine

Ranking 3: R&D needed before starting production of systems and components

Ranking 4: R&D desirable for technical or cost optimization

The R&D items associated with all three subsystems are collected in Chapter 9 in a comprehensive list, ranked and sorted by machine.

7.2 DAMPING RINGS

7.2.1 Introduction

7.2.1.1 System Description

In this section we consider luminosity-related issues for the TESLA and JLC-X/NLC damping rings, from the injection kickers to the extraction kickers. Finally, as noted in Section 3.3, the beamline optics for the JLC-X and NLC designs differ slightly due to different optimizations. In this section, we only analyzed the NLC optics; however, the JLC-X optics is similar, and thus the designs are frequently referred to as the JLC-X/NLC design. A full solution for the CLIC damping ring lattice that satisfies the necessary requirements, including dynamic aperture, was not available to the committee at the time of the report and was therefore not evaluated in detail. TESLA uses one damping ring for electrons and one for positrons. To accommodate the large number of bunches, the TESLA damping rings each have a 17 km circumference and share the tunnel with the TESLA linac, leading to an unconventional "dog-bone" design. JLC-X/NLC and CLIC damp the positrons in a pre-damping ring (PPDR) with a large acceptance before transfer to a positron main damping ring (MDR). In these designs a single damping ring is used for electrons. The JLC-X/NLC and CLIC main damping ring designs are similar to the ATF damping ring, with which there is a great deal of operational experience.

7.2.1.2 Luminosity Issues

We consider the extracted beam parameters which are relevant for emittance preservation in the subsequent parts of the machine and the luminosity. These are: the extracted vertical, horizontal, and longitudinal emittances; variation (train-to-train and along the train) of extracted $\langle x \rangle$, $\langle x' \rangle$, $\langle y \rangle$, $\langle y' \rangle$, $\langle \Delta t \rangle$, and $\langle \Delta p/p \rangle$; extracted electron polarization; and particle loss.

Critical issues for emittance preservation and luminosity are:

- Correction of vertical emittance in the misaligned damping rings.
- Control of impedance to avoid the longitudinal microwave instability.
- Ion-related tune shift and instability in the electron damping rings.
- Electron-cloud-related tune shift and head-tail and coupled bunch instabilities in the positron damping rings.
- Dynamic aperture in the presence of wiggler nonlinearities.

7.2.2 Experience at Operating Machines

7.2.2.1 Introduction

The linear collider damping ring designs should be evaluated in the context of operational experience with similar machines: the SLC damping rings, third generation light sources,

and the ATF damping ring. The linear collider damping ring designs, the ATF damping ring, and the third generation light sources have the common goal of maintaining a very low vertical emittance and low beam jitter. The ATF damping ring is the only ring which has achieved a vertical emittance close to that required for the planned linear collider damping rings. Third generation light sources, which need to maintain a long Touschek lifetime, do not attempt to achieve a vertical emittance as low as needed for the planned damping rings. The ATF was able to reach its target emittance (roughly a factor of 2 larger than the design emittance of the planned damping rings) even in the presence of substantial ambient temperature fluctuations, which would be much smaller in the case of the underground enclosures planned for the linear collider designs. The ATF uses combined function magnets, which complicate tuning and beam-based alignment (because the quadrupole magnets cannot be varied independently of the dipoles). The ATF serves as a good testbed for tuning and alignment techniques, especially for the JLC-X/NLC MDR and CLIC MDR, which also use combined-function magnets. The ATF is sensitive to intrabeam scattering due to its low emittance and low (1.3 GeV) energy, and has been used extensively to investigate intrabeam scattering. All of the planned damping rings use wigglers to provide most of the damping. The ATF usually operates with its damping wigglers off, so experiments in other machines may be necessary to gain experience with wiggler-related effects.

The SLC experience emphasized the importance of low particle losses and the suppression of collective instabilities. Based on the SLC experience, particle losses and extracted beam stability are likely to be more important for integrated luminosity than extracted emittance. Excessive loss leads to radiation damage and downtime for the replacement or repair of damaged components. Beam instability and jitter can lead to severe instantaneous luminosity reduction, and can cause fluctuating backgrounds which make the machine inoperable. In contrast, because of the expected emittance growth in the linac, the dependence of the luminosity on the extracted emittance is weak (less than linear).

7.2.2.2 Experience at the SLC Damping Rings

7.2.2.2.1 Particle Loss The linear collider damping rings differ from the third generation light sources in that there is a very large average beam power entering the rings. In the SLC, the average beam power was approximately 2 kW in the e^- ring and 1.2 kW in the e^+ ring. The capture efficiency was 90 to 95% for e^- and 70 to 80% for e^+ (due to the larger incoming emittance for e^+), so there were losses of 100 to 200 W at 1.19 GeV in both rings. This particle loss caused the failure of kicker magnets, resulted in the replacement of all of the permanent magnet sextupoles, damaged coils in the dipole and quadrupole magnets, and damaged sputter ion pump cables. Some of these component failures could have been avoided with a different, radiation-resistant design. However, the average beam power entering the linear collider damping rings is one to two orders of magnitude larger than that entering the SLC damping rings. The capture efficiency for all damping ring designs must be close to 100%.

7.2.2.2.2 Beam Stability and Jitter The SLC damping rings suffered from several operationally significant collective instabilities. A longitudinal coupled bunch π-mode instability was cured with a passive cavity. Subsequently, a longitudinal microwave

instability was diagnosed, which had a relaxation-oscillator behavior, and created a sawtooth in the bunch length and phase [1]. The phase jitter caused the occasional loss of beam on collimators in the linac, or in the IR, tripping off the detector.

For a month following a vacuum accident in the e^- ring, the vertical emittance was degraded by a factor of 4–20. Ions were trapped in the beam immediately after injection when the beam was large. As the beam shrank a coherent ion instability occurred.

Fast temperature changes due to the beam being turned on and off, and slow ones due to access to the machine and to seasonal variation, caused significant changes of the extracted orbit and the ring circumference, respectively.

7.2.2.2.3 Damping Times The measured transverse damping times were somewhat longer than the calculated values and varied with time. These damping times remain unexplained.

7.2.2.3 Experience at Third Generation Light Sources

7.2.2.3.1 Vertical Emittance The vertical geometric emittances specified for the linear colliders are smaller than the emittances that have been achieved in the third generation light sources. The TESLA damping ring specifies an equilibrium vertical emittance below 1.4 pm·rad (0.014 μm·rad normalized), while the JLC-X/NLC damping ring vertical emittance must be below 3.4 pm·rad (0.013 μm·rad normalized). The lowest vertical emittances that have been claimed to date in the ATF and third generation light sources are in the range 10–15 pm·rad [2, 3]. The corresponding beam sizes are on the order of 10 μm. Some direct measurements have been made of emittances in this range, but the data often depend on studies of Touschek lifetime. The equilibrium emittance ratio ϵ_y/ϵ_x must be less than 0.18% in the TESLA damping rings and less than 0.59% in the JLC-X/NLC main damping rings. The NSLS X-ray ring, SPring-8, and Swiss Light Source (SLS) have reported emittance ratios of 0.1% or less, and several other storage rings have reported ratios of 0.5% or less.

7.2.2.3.2 Beam Jitter Transverse beam jitter is due to correlated motion of the quadrupole magnets (from certain types of ground motion) or uncorrelated motion (due to other types of ground motion, or vibration from local sources). The measured quadrupole magnet vibration in the APS (after the addition of viscoelastic pads and welding of cooling water headers to the tunnel ceiling) was 90 nm rms in a 4 to 50 Hz band [4]. Roughly half of the vibration was due to the flow of cooling water.

The beam in a linear collider damping ring can be stabilized by a local orbit feedback at the extraction point. The SLS reports that a global orbit feedback operating at correction rates of up to 1 Hz stabilizes the beam position and angle at the insertion devices to $\sim$0.6 μm rms and $\sim$0.3 μrad rms [5]. This level of stabilization is better than what is needed for the extraction point of the TESLA or JLC-X/NLC damping rings.

7.2.2.4 Experience at the ATF Damping Ring

7.2.2.4.1 Emittance Correction Algorithm The tuning method to minimize the vertical emittance of the ATF damping ring is a series of three corrections based on orbit measurements: (i) COD (closed orbit distortion) correction; (ii) vertical COD and dispersion correction; and (iii) Coupling correction. These corrections minimize, respectively, the following quantities:

$$\sum_{\mathrm{BPM}} x_{\mathrm{meas}}^2 \quad \text{and} \quad \sum_{\mathrm{BPM}} y_{\mathrm{meas}}^2 \tag{i}$$

$$\sum_{\mathrm{BPM}} y_{\mathrm{meas}}^2 + r^2 \sum_{\mathrm{BPM}} \eta_{y,\mathrm{meas}}^2 \tag{ii}$$

$$C_{xy} \equiv \sum_{\mathrm{steer}} [\sum_{\mathrm{BPM}} (\Delta y)^2 \; / \sum_{\mathrm{BPM}} (\Delta x)^2] \tag{iii}$$

Here x_{meas}, y_{meas} and $\eta_{y,\mathrm{meas}}$ are the horizontal position, vertical position and vertical dispersion at each BPM. The factor r is the relative weight of the dispersion and COD, and it was chosen to be 0.05 based on the results of a simulation study. The horizontal and vertical position responses to each horizontal steering magnet are Δx and Δy. Usually two horizontal steering magnets, separated in betatron phase by $\approx 3\pi/2$ horizontally and $\pi/2$ vertically, are chosen for this correction. In the COD correction and the vertical COD + dispersion correction, steering magnets (48 horizontal and 51 vertical) are used. For the coupling correction, trim coils of all 68 sextupole magnets, wired to produce skew quadrupole fields, are used.

7.2.2.4.2 Simulations To study this tuning method, simulations were performed with realistic magnet misalignments and random BPM errors [6]. The measured transverse offsets of all the magnets were used, with random offsets added to account for survey errors. Random rotation errors were also included. Each BPM was assumed to have random offset and rotation errors. These assumed errors are listed in Table 7.1.

TABLE 7.1
Assumed errors in simulation

Magnet offset	measured + random 30 μm
Magnet rotation	random 0.3 mrad
BPM offset	random 0.3 mm
BPM rotation	random 20 mrad

The simulation suggests that the target vertical emittance of 1.1×10^{-11} m·rad, which corresponds to a normalized emittance of 2.8×10^{-8} m·rad, is likely to be achieved. The average simulated emittance and the fraction of seeds which gave an emittance less than 1.1×10^{-11} m·rad are listed in Table 7.2. Note that this should be regarded as the emittance in the zero intensity limit. Further simulation showed that the expected emittance strongly

TABLE 7.2
Simulated vertical emittance after corrections

Correction	Average vertical emittance [$\times 10^{-11}$ m·rad]	Fraction of seeds yielding emittance [$<1.1\times 10^{-11}$ m·rad]
COD	2.3	20%
+ Dispersion	1.7	51%
+ Coupling	0.58	91%

depends on the BPM offset error. If the BPM offset error is assumed to be 0.1 mm rather than 0.3 mm, then the average simulated vertical emittance after corrections is reduced to 0.27×10^{-11} m·rad.

7.2.2.4.3 Experiments In the experiments the typical measured rms COD, rms vertical dispersion and C_{xy} are consistent with the simulated COD (including the effects of BPM offset and rotation error), vertical dispersion and C_{xy} after corrections. The consistency suggests that the error assumptions of the simulation are valid.

The beam size in the damping ring (DR) is measured using two kinds of monitors. One is a two-slit optical interferometer which measures the interference pattern created by the synchrotron radiation (SR monitor). The other is a laser-wire monitor using a thin horizontal "wire" of light created in an optical cavity. As the laser wire is scanned vertically the photons Compton-scattered by the beam are detected.

In the extraction line, the beam size is measured using tungsten wire scanners. There are five wire scanners in the dispersion-free region of the beam line. The emittance is determined using the measured beam sizes and beam optics between the wire scanners.

Figure 7.1 shows the emittance as a function of the bunch intensity. The left figure shows the horizontal emittance measured in the extraction line. The right figure summarizes measurements of the vertical emittance using the laser wire monitor and the wire scanners on different days with different conditions, but all after low emittance tuning. The curves in these figures are from calculations, including intrabeam scattering, using the SAD program [7] assuming emittance ratios (ratio of vertical to horizontal emittance) of 0.002, 0.004, and 0.008.

The measured horizontal emittance agrees well with the calculation. There was a large variation in the measured vertical emittance on different days, suggesting different conditions in the damping ring or in the extraction line. The diagnostics used for the vertical emittance measurements were at their resolution limit, and work on these measurements is continuing. It was concluded that the vertical emittance, extrapolated to zero current, was smaller than 1.1×10^{-11} m·rad, corresponding to a normalized emittance of 2.8×10^{-8} m·rad at 1.3 GeV.

7.2.2.4.4 Intrabeam Scattering Due to the high electron density and relatively low beam energy (1.3 GeV), strong intrabeam scattering (IBS) was observed in the ATF DR. Intrabeam scattering is expected to have a much smaller effect at the TESLA and

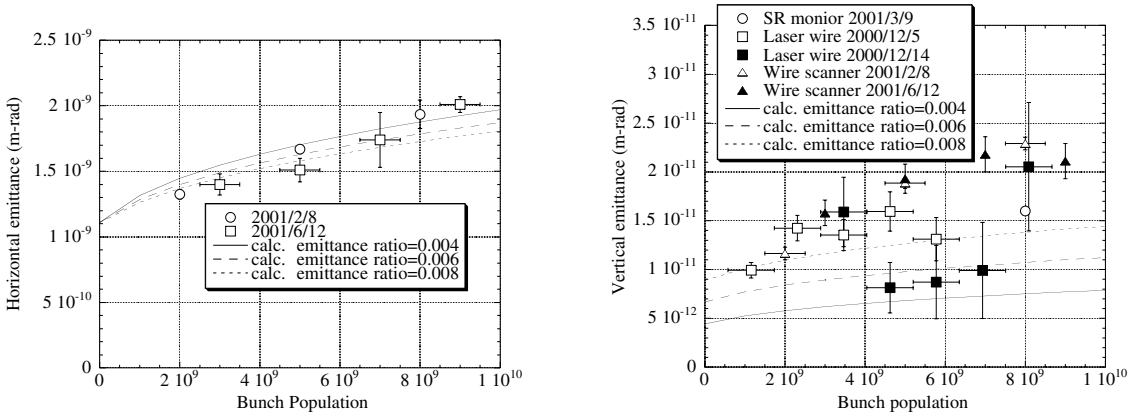

FIGURE 7.1. Left: Horizontal emittance measured in the extraction line versus bunch intensity. Right: Vertical emittance measured in the damping ring and in the extraction line versus bunch intensity. The curves are from calculations assuming emittance ratios of 0.004, 0.006, and 0.008.

JLC-X/NLC damping rings. The increase of the horizontal emittance with intensity is shown in Figure 7.1. The effect is more clearly observed in the energy spread. In order to evaluate the energy spread of the extracted beam, the horizontal beam size was measured using a screen monitor at a high dispersion region in the extraction line.

The left side of figure of Figure 7.2 shows the energy spread measured in the extraction line as a function of the bunch intensity. The intensity dependence of the horizontal emittance and the energy spread agree with the intrabeam scattering calculation, assuming a zero current emittance ratio between 0.004 and 0.008.

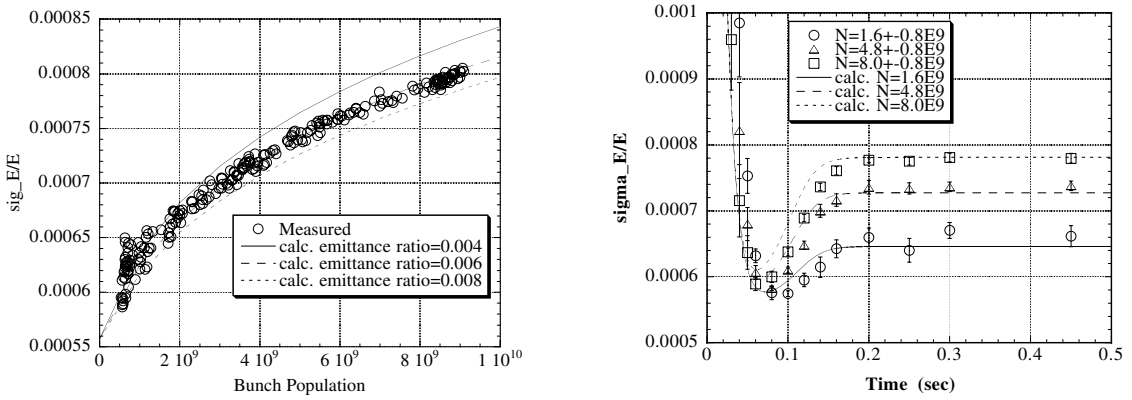

FIGURE 7.2. Left: Energy spread measured in the extraction line versus bunch intensity. The curves are from calculations assuming emittance ratios of 0.004, 0.006, and 0.008. Right: Energy spread versus store time for three different bunch intensities. The curves are from calculations assuming an emittance ratio of 0.006.

The right side of Figure 7.2 shows the energy spread as a function of store time in the damping ring at different intensities. The horizontal emittance was also measured in the extraction line as a function of the store time. The results show that the beam energy spread and the horizontal emittance exhibit a minimum at a store time of 70 ms, before reaching stable equilibrium values. This behavior is explained by the fact that the vertical damping time (calculated to be 27 ms) is longer than the longitudinal (20 ms) and horizontal (17 ms) damping times. At first, while the vertical emittance is still large, the longitudinal and horizontal emittances are damped. Later, the vertical emittance becomes smaller, so intrabeam scattering increases the longitudinal and horizontal emittances. The curves are from simulations based on SAD, assuming an emittance ratio of 0.006.

The calculation of intrabeam scattering has uncertainties, particularly in the value of the Coulomb log factor [7]. For the design of future damping rings it is necessary to understand the reliability of the calculation. The measured data are consistent with the SAD calculation assuming an emittance ratio of 0.006. However, the accuracy of the theory cannot be evaluated because of the uncertainties in the measurement of the vertical emittance. A report comparing different theoretical models with data from the ATF shows consistency between the experiments and theory, if a zero current emittance ratio between 0.004 and 0.008 is assumed, and the Coulomb logarithm is allowed to vary [8]. Better measurements of the vertical emittance are needed to fully validate the theory.

7.2.3 Extracted Emittances

7.2.3.1 Introduction

The extracted emittances from the damping rings have a direct influence on the emittance at the interaction point and the luminosity of the collider. The emittances of the beams extracted from the damping rings depend on the equilibrium emittances, the damping rates and store times. The equilibrium emittances are dependent on the tuning and alignment of the lattice, collective effects such as intrabeam scattering, and impedance-driven emittance growth. The vertical divergence of the radiation introduces a fundamental lower limit on the vertical geometrical emittance of 0.11 pm·rad and 0.24 pm·rad, for the TESLA DR and JLC-X/NLC MDR, respectively. Mismatch of the linear or nonlinear injection phase space can increase the effective injected beam size, and this can increase the extracted emittance.

The principal alignment issues are those which increase the vertical emittance, either through the generation of vertical dispersion or from betatron coupling. Coupling correction systems are specified and designed to minimize the vertical emittance generated by these effects. We first consider the alignment tolerances in the JLC-X/NLC and TESLA damping rings, and describe the respective coupling correction schemes, before evaluating the effectiveness of these schemes. We then discuss various collective effects, and complete the discussion by considering emittance dilution from the extraction systems. Our calculations include: a correction model; misalignment and ATL ground motion models; a lattice with sextupoles and wigglers; rf parameters; intrabeam scattering; an extraction kicker model; impedance, electron cloud, and ion effects.

7.2.3.2 Alignment Tolerances

The low target values for the emittance in the damping rings are demanding, and will require the effective use of a combination of techniques for correcting both the dispersion and coupling. Vertical emittance generation and correction have been studied in the TESLA and JLC-X/NLC damping rings using analytical estimates and simulations. The simulation codes, MAD and MERLIN, have each been applied to both rings. Only a restricted subset of the errors and limitations that are to be expected in practice have so far been considered in any detail. These are:

- Quadrupole vertical alignment errors
- Quadrupole rotations about the beam axis
- Sextupole vertical alignment errors
- Limited BPM resolution
- BPM vertical alignment errors

The BPM resolution limits the precision with which the dispersion may be measured. Since dispersion correction to better than 1 mm is generally required, if the energy variation is limited to the order of 0.1% the BPM resolution must be 1 μm or better.

Demonstration of effective emittance correction in simulations at the present level is a necessary but not sufficient condition for the ability of the designs to achieve the specifications. The simulations may also give some indication of the likely difficulty of achieving the specified emittances given a more complete set of machine errors, although this involves some subjective judgment.

Other considerations that will likely be important, and should be included in further simulations, are:

- Dipole vertical alignment[1] and rotation errors
- Horizontal orbit and dispersion errors
- Optics errors arising from focusing variations
- BPM rotations
- Effects of nonlinear wiggler fields
- Limitations from malfunctioning BPMs and correctors
- Tuning of the skew quadrupoles used to implement beam coupling in the TESLA damping ring

[1] This is potentially more important for combined-function dipoles as in the JLC-X/NLC main damping rings

Both TESLA and JLC-X/NLC tuning algorithms depend on application of response matrices, which need to be accurately determined and, in the simulations, are calculated for the ideal machine. The effectiveness of the correction can be sensitive to the response matrices. Verification of storage ring optics by analysis of the measured response matrices has been applied at a number of machines and has proven a valuable technique.

7.2.3.2.1 Sensitivity Indicators and Estimates To understand the performance requirements on the damping rings, it is useful to estimate the sensitivity of the ring to random misalignments. In a storage ring, the equilibrium vertical emittance is determined by the residual vertical dispersion and betatron coupling in the bending magnets (including the wigglers) where the beam emits synchrotron radiation. Usually the betatron coupling and vertical dispersion are generated by errors distributed around the ring. There are three main driving terms: closed orbit offsets, quadrupole rotations, and vertical sextupole misalignments. It is straightforward to estimate the contributions to the vertical equilibrium emittance from random quadrupole rotations and sextupole misalignments. The effect of the closed orbit offsets is more difficult to calculate because it depends on detailed correlations from point to point; however, the sensitivity also tends to be much weaker than for either of the other effects.

Table 7.3 compares the energy, circumference, and typical operating emittances of the Advanced Light Source (ALS), the Advanced Photon Source (APS), the ATF at KEK, and the Swiss Light Source (SLS), with the NLC and TESLA damping rings. Although the synchrotron radiation facilities have operated with small $\varepsilon_y/\varepsilon_x$ emittance ratios, only the ATF approaches the emittance values that are required in the linear collider damping rings.

TABLE 7.3
Comparison of calculated sensitivities in operating rings with the NLC and TESLA damping rings. Y_{align}: sextupole vertical misalignment; Roll align: quadrupole roll alignment; Y_{jitter}: quadrupole vertical jitter; $\Delta k/k$: fractional quadrupole strength error. [9]

Parameter	ALS	APS	ATF	SLS	NLC MDR	TESLA DR
Energy [GeV]	1.9	7	1.3	2.4	2	5
Circumference [m]	200	1000	140	288	300	17,000
$\gamma\varepsilon_x$ [μm·rad]	24	34	2.8	23	2.2	8
$\gamma\varepsilon_y$ [nm·rad]	500	140	28	70	13	14
Y_{align} [μm]	135	74	87	71	31	11
Roll align [μrad]	860	240	1475	374	322	38
Y_{jitter} [nm]	850	280	320	230	75	76
$\Delta k/k$ [0.01%]	1.5	1.4	2.1	1.5	1.8	1.1

Table 7.3 presents, in its lower half, two sets of numbers that describe the sensitivities of the rings to random errors due to vertical misalignments of the sextupoles or rolls of the quadrupoles. These numbers assume purely uncorrelated errors and are equal to the values that would generate the equilibrium vertical emittance. Following these are the values of

the random vertical quadrupole motion that would cause beam motion equal to the beam size and quadrupole strength fluctuations that would lead to an x or y tune shift of 0.001.

It should be noted that none of these values are alignment tolerances. The real misalignments of the components will not be purely random and the actual tolerances must include the effectiveness of the emittance correction procedures, which are discussed in the following section. However, the values in Table 7.3 are useful to compare the *relative* difficulty of operating the rings to the linear collider damping rings. One can see that the vertical alignment sensitivities are typically ∼100 μm in the operating facilities while they are about 40 and 15 μm in the NLC and TESLA rings, respectively. The operating rings typically have a roll sensitivity that is a few hundred μrad, which is similar to the NLC ring, but the TESLA ring is roughly an order-of-magnitude tighter. The jitter sensitivities, in the operating rings, are a few hundred nanometers while those in the NLC and TESLA damping rings are a factor of 3 tighter. Finally, the sensitivities to the quadrupole strength errors are typically 0.01% and are not significantly tighter in the damping rings.

The alignment and jitter sensitivities indicate that the operation and emittance tuning of the linear collider damping rings should not be vastly different than in the operating synchrotron radiation facilities and, in this sense, the damping ring operation should be possible. However, while not vastly different, the damping rings will require more effort to control and stabilize the beam than has been typically achieved. Since the radiation facilities already devote significant effort to achieving excellent beam stability, the required improvement over those results could be significant. Although vertical emittance is an important parameter for a light source (a lower emittance gives a higher brightness photon beam) the radiation facilities generally do not attempt the lowest possible emittances in standard operation, since this has a detrimental effect on the beam lifetime. Thus, although some light sources have achieved vertical emittances close to those required in the damping rings, there is limited experience in tuning operating storage rings for such conditions.

7.2.3.3 Vertical Emittance Correction

The ATF has achieved a vertical dispersion of 3 mm rms, using BPMs with an intrinsic resolution of 20 to 40 μm, and averaging. Assuming that the TESLA and JLC-X/NLC damping ring BPMs achieve an intrinsic resolution of 1 μm, dispersion correction to levels well below 1 mm rms in TESLA and JLC-X/NLC should be straightforward. Achieving the unprecedented vertical emittance in the TESLA or JLC-X/NLC damping rings will be challenging, but there are no indications that the damping ring emittance goals are unrealistic.

7.2.3.3.1 Evaluation of TESLA DR Emittance Correction Algorithm The TESLA correction system uses a BPM and steering magnet located at every quadrupole. Initial correction uses a combined orbit and dispersion response matrix to set the steering magnet strengths. This generally brings the vertical emittance to less than a few times the target, with further dispersion correction usually being effective in reaching the target.

The correction algorithm acts only in the vertical plane and is appropriate for an uncoupled machine. When the coupling bump is turned off, a global correction is achieved for 85% of random seeds. With the coupling bump, the success rate is 70%. The TESLA damping ring correction algorithm should be improved to accommodate the coupling bump.

7.2.3.3.2 Evaluation of JLC-X/NLC MDR Emittance Correction Algorithm The JLC-X/NLC MDR correction system consists of BPMs placed at each quadrupole, with the quadrupoles and sextupoles positioned on movers. An orbit correction is first performed using the response matrix between the BPMs and the quadrupole movers, and a dispersion correction is then applied in an analogous fashion, using a response matrix between the vertical dispersion at the BPMs and the sextupole movers.

In practice, this simple correction strategy is effective since it minimizes local errors. For a given set of misalignments, the correction system is capable of meeting the specification for the vertical emittance in about 90% of cases.

7.2.3.3.3 Summary Table 7.4 summarizes the evaluation of the vertical emittance correction. We find that:

- In a simulation model including the most important misalignments and limited BPM resolution, the emittance (disregarding collective effects) is corrected to below the design level for most, but not all, random seeds. The margin is adequate for both TESLA and JLC-X/NLC. Experiments in the ATF give confidence that the simulation models work well, and additional correction strategies will tend to widen the margin.
- When the coupling bump is turned on in the TESLA damping ring, the vertical-only correction is not as effective. It is expected that when horizontal correction is added, the correction algorithm will be effective for TESLA with the coupling bump.

TABLE 7.4
Summary of vertical emittance correction evaluation. All simulated misalignments and rolls have a Gaussian distribution truncated at 3σ.

	TESLA DR	NLC MDR
Quadrupole vertical misalignment [μm rms]	100	100
Quadrupole roll [μrad rms]	100	100
Sextupole vertical misalignment [μm rms]	100	100
BPM resolution [μm]	1	0.5
BPM vertical misalignment[a] [μm rms]	10	5
Energy variation [%] for dispersion measurement	$\pm$0.2	$\pm$0.1
Fraction of random seeds for which the vertical emittance is corrected to less than the design value [%]	85 (no coupling bump) 70 (with coupling bump)	90

[a] Relative to the design orbit.

7.2.3.4 Fast and Slow Ground Motion

The amplitude of fast magnet motion following from the standard ground motion models [10] is too small to have an effect on emittance. Slow magnet motion may be described by the ATL model, which gives temporal and spatial correlations in reasonable agreement with observations. We have used a 2-dimensional implementation of the model in MERLIN to estimate the timescale over which orbit and dispersion correction need to be applied.

7.2.3.4.1 Evaluation Figure 7.3 and Figure 7.4 show the normalized vertical emittance in the TESLA damping rings and the JLC-X/NLC main damping rings resulting from diffusive (ATL) ground motion, for noisy (A=10^{-17} m^2/m/s) and intermediate (A=5×10^{-19} m^2/m/s) sites. Starting from lattices with the only misalignments being 100 μrad rms rotations of the quadrupoles about the beam axes, 50 hours of ATL motion were applied, and the orbit and dispersion were corrected by using the procedure described above. The BPMs were fixed to girders, and thus moved with the ground motion, but not with the correction of the quadrupole positions using the magnet movers. ATL motion was then applied at hourly intervals up to 24 hours, either with no correction or with orbit correction only. No vertical dispersion correction was applied. Averages over 20 seeds are shown. An hourly orbit correction to 5 μm rms is sufficient to maintain the vertical emittance well within tolerances for the TESLA DR and JLC-X/NLC MDR for both noisy and intermediate sites over a 24 hour period. Because the model includes only the most important effects, we expect that the correction will be somewhat less effective in the actual damping rings.

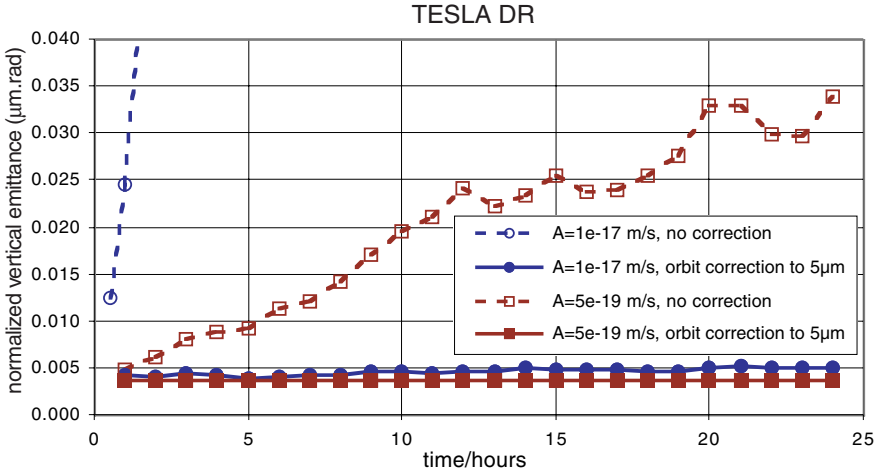

FIGURE 7.3. Vertical emittance in the TESLA damping rings resulting from diffusive (ATL) ground motion.

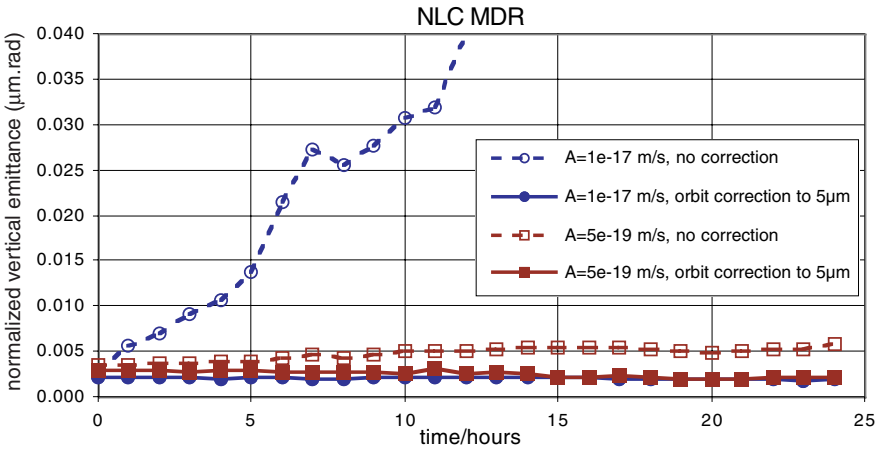

FIGURE 7.4. Vertical emittance in the NLC main damping rings resulting from diffusive (ATL) ground motion.

7.2.3.4.2 Summary

- The effect of ground motion on the emittance can be continuously corrected in the TESLA damping rings and the JLC-X/NLC main damping rings using only hourly orbit corrections. As Figure 7.3 and Figure 7.4 show, dispersion correction, which is incompatible with luminosity production, is needed less than once per day.

7.2.3.5 Classical Collective Instabilities

The high bunch density, together with the small value of the momentum compaction factor, make the damping rings prone to single bunch effects like the longitudinal microwave instability. The instability can only be avoided by making the beam enclosure sufficiently smooth. A very comprehensive calculation of the residual high frequency broad-band coupling impedance of the NLC damping rings has been done. Summing the calculated wakefields of the major components of the vacuum chamber gives a value of Z/n=25 mΩ, mostly resistive [11]. TESLA calculates Z/n=25 mΩ for the resistive part (mainly from kickers) and 28 mΩ for the inductive part (mainly from bellows and BPMs). Using the Keil-Schnell-Boussard criterion for a rough estimate one finds a microwave instability impedance threshold of 70 mΩ for the NLC MDR and 59 mΩ for the TESLA electron DR at the design bunch intensities. Thus the impedance threshold is two to three times higher than the estimated impedance for both machines. Bunch lengthening is only about 5%. This looks comfortable, but experience has shown that impedances measured with beam in real machines are usually larger than anticipated. For instance measurements of bunch lengthening in the KEK ATF indicate a value of Z/n three times larger than calculated. Measurements of bunch lengthening in KEKB give values of Z/n (76 mΩ in the HER and 72 mΩ in the LER) which are five times larger than the design values. We conclude that the vacuum chamber of the damping rings must be designed with extreme care in order to minimize its impedance.

Coupled bunch instabilities are also important in damping rings, owing to the large number of bunches stored. At low frequencies the resistive wall instability dominates and must be suppressed by feedback (up to about 10 MHz). Considerable experience has been gained in recent years on damping of higher rf cavity modes and on high frequency feedback. Residual effects can be suppressed by a bunch-by-bunch feedback as foreseen for JLC-X/NLC and TESLA.

7.2.3.5.1 Summary

- Experience with other modern machines indicates that extreme care will be needed to attain the low impedances required to avoid the single bunch longitudinal microwave instability in the TESLA damping rings and the JLC-X/NLC main damping rings.
- Coupled bunch instabilities can be suppressed using standard bunch by bunch feedback techniques.

7.2.3.6 Space Charge

Space charge should have negligible effects in damping rings except for TESLA where the space-charge induced tune spread would reach 0.26 in the vertical plane. Such a value is known to produce emittance increase through resonance crossing, though the effects in this case have not been quantified. A sixfold increase in the vertical emittance would reduce the tune spread to 0.1, a value thought to be tolerable, but with a sizeable luminosity penalty. Since most of the tune spread arises in the long straight sections, it is proposed to increase the beam dimensions there by fully coupling the transverse oscillations. This reduces the vertical tune spread to 0.06, which is expected to be tolerable. A difference in the vertical and horizontal tunes of 0.02 arising within the coupling bump region gives rise to a 10% vertical emittance increase outside the coupling bump. Much smaller tune differences can readily be achieved.[2] A variation of beam intensity or size of 10 to 20% is also of no practical importance for the bump closure.

7.2.3.6.1 Summary

- The coupling bump appears to be a satisfactory solution to the space charge tune spread in the TESLA damping rings.

7.2.3.7 Ion Effects in the Electron Damping Rings

The ion effects have been estimated based on a design vacuum pressure of 10^{-9} Torr for both the JLC-X/NLC and TESLA damping rings.

[2] Phase measurements with a random error of less than 0.2°, which produces a tune change of 0.0006, are routinely made in CESR.

7.2.3.7.1 Ion Trapping Without an ion-clearing gap, all ions are trapped in the TESLA e^- DR. A gap of roughly 600 ns in the TESLA bunch train is needed to clear CO^+ and lighter ions. Such a gap would create, through beam loading, a phase variation across the train of 1.2°. This small phase variation would not have significant consequences. The injection/extraction gaps in the JLC-X/NLC e^- MDR are sufficient for ion clearing.

7.2.3.7.2 Tune Shift In the JLC-X/NLC e^- MDR, CO^+ and heavier ions accumulate during the passage of the bunch train. In the straight sections of the TESLA e^- DR, all ions accumulate, producing an unacceptable tune shift of 0.28 at the end of the bunch train. It may be necessary to design the TESLA e^- DR for a vacuum of 10^{-10} Torr, especially in the straight sections.

7.2.3.7.3 Fast Ion Instability At the design vacuum pressure of 10^{-9} Torr, the calculated growth time of the fast ion instability is of the order of 100 μs in the TESLA e^- DR and the JLC-X/NLC e^- MDR. Although the very complex dynamics of this two-stream instability makes it difficult to predict the behavior of the beam from such a simple calculation, this is cause for concern. More precise evaluations using computer simulations are needed before the present designs can be validated.

7.2.3.7.4 Summary

- The TESLA damping ring requires an ion-clearing gap of 600 ns.
- The TESLA damping ring should be designed for an average pressure of the order of 10^{-10} Torr to avoid an unacceptably large tune spread.
- The fast ion instability may have a growth rate too fast to control with feedback in both the TESLA damping rings and the JLC-X/NLC damping rings. There are very large uncertainties in the estimate of the growth rate. If simulations or experiments show that the growth time is less than a few hundreds of μs, then a redesign of the vacuum system for substantially lower pressure may be required.

7.2.3.8 Electron Effects in the Positron Damping Rings

Electrons present in the vacuum chamber are accelerated toward the walls by the passage of the positron bunches. Upon impact secondary electrons are emitted, thus increasing the electron density. If the secondary electron yield (SEY) is sufficiently large, then the total number of electrons increases until global neutralization is reached. The initial electrons can be produced in large numbers by synchrotron radiation photons impinging on the vacuum chamber walls. In the JLC-X/NLC damping rings this source is largely suppressed since most of the photons escape into the antechamber. However, the small fraction which remains may constitute a sufficient seed. In any case there are always the electrons produced by beam ionization of the residual gas. All calculations and simulations suggest that neutralization is reached well before the end of the bunch train, even when starting from ionization electrons. Figure 7.5 shows the average electron density in the TESLA DR and JLC-X/NLC MDR chambers as a function of the SEY of the chamber material,

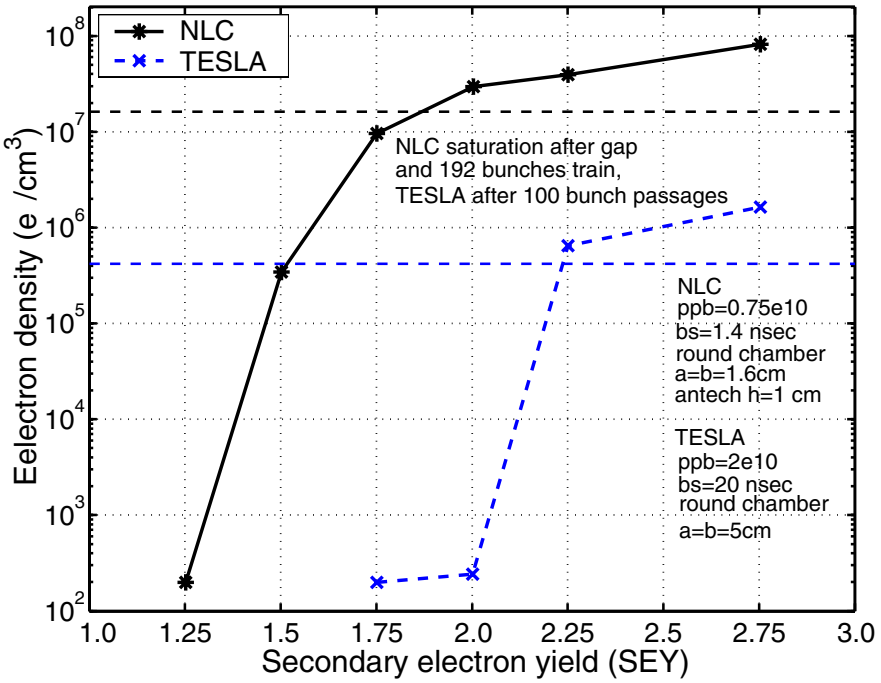

FIGURE 7.5. Average electron density versus secondary electron yield for the TESLA DR and the NLC MDR. The simulation uses only the round chamber geometry of the TESLA DR field-free straight sections, and only the chamber geometry (which includes an antechamber) of the field-free regions in the NLC MDR. The neutralization densities for NLC and TESLA are represented by the upper and lower horizontal dotted lines, respectively.

predicted by simulation. The simulation uses the round chamber geometry of the TESLA DR straight sections, and the chamber geometry (which includes an antechamber) of the field-free regions in the NLC MDR. Above a critical value for the SEY, the neutralization density is reached for both rings. The peak SEY at normal incidence is typically 1.0 to 1.5 for TiN coated copper, 1.4 to 1.7 for copper, and 2.2 for aluminum, depending on the preparation of the surface and scrubbing by the beam. Stainless steel, which has an SEY similar to copper, is likely to be unacceptable as a chamber material due to its high resistivity, which exacerbates the resistive wall instability.

When the neutralization density is reached, fast coupled bunch instabilities with growth times as small as 15 to 30 μsec as well as single bunch instabilities are predicted. At this time the simulation results should be regarded as estimates, which must be refined, taking advantage of the constant progress of the knowledge in this field, both from experience and theory. Analytical estimates can be made of the incoherent tune shift, head-tail instability threshold, and coupled bunch instability growth time, by assuming global neutralization and a uniform electron density across the chamber [12]. These estimates are given in Table 7.5, and should be regarded as order-of-magnitude estimates only. The assumption of uniform electron density across the chamber is optimistic, because some simulation results indicate an enhancement of the electron density within the positron bunch of one to two orders of magnitude. We note that the fastest transverse feedback systems built to date

TABLE 7.5
Analytical estimates of electron cloud effects in the damping rings.

	TESLA DR	JLC-X/NLC MDR	JLC-X/NLC PDR
Incoherent tune shift	0.06	0.019	0.003
Head-tail threshold charge/nominal charge	2.6	0.8	10
Coupled bunch growth time [μs]	170	20	370

have a damping time for coupled bunch instabilities of a few hundreds of μs. Experience with e^+e^- colliders suggests that the maximum tolerable incoherent tune shift is of the order of 0.1. If the neutralization electron density is reached, then the estimated incoherent tune shift and coupled-bunch growth time in the TESLA damping ring are barely tolerable, and the JLC-X/NLC MDR is likely to suffer from both head-tail and coupled bunch instabilities. It is imperative for the success of these machines to suppress the electron cloud to well below the neutralization density. Possible cures are coating the chamber walls to reduce the secondary emission and superimposition of a magnetic field in otherwise field free regions. Gaps in the trains may also help suppress the electron cloud, but may be impractical due to the loss of luminosity and the increase of beam loading effects.

7.2.3.8.1 Summary

- Without intervention to reduce the electron cloud density well below the neutralization density, the damping rings are likely to suffer from an unacceptable incoherent tune shift, head-tail instability, or coupled bunch instability. The TESLA damping rings may be particularly susceptible to a large incoherent tune shift. The JLC-X/NLC main damping rings may be particularly susceptible to head-tail and coupled bunch instabilities.

7.2.3.9 Intrabeam Scattering

Intrabeam scattering limits the six-dimensional phase space density and therefore can be important in damping rings. Several computer programs exist to accurately calculate the effect of IBS. They are being checked by comparison with measurements done in the KEK ATF, described in Section 7.2.2.4. Calculated extracted emittances in the presence of IBS are listed in Table 7.6. We have used the Piwinski formalism. IBS has very little influence on the TESLA damping ring due to its relatively large energy. It has a small but significant influence on the horizontal and vertical emittances of the JLC-X/NLC main damping ring. There is significant theoretical uncertainty in the calculation of IBS growth rates, as described in Section 7.2.2.4. If it is found that IBS prevents the design emittances from being reached, then a lattice redesign or energy increase may be necessary. Such a change, if needed, is expected to be successful. IBS is a major problem for the design of the CLIC main damping ring, which must deliver extremely small emittances, and is an important driver in the optimization of the lattice.

TABLE 7.6
Intrabeam scattering calculation results.

	TESLA DR		JLC-X/NLC MDR	
	e^+	e^-	e^+	e^-
Equil. $\gamma\epsilon_x$ / $\gamma\epsilon_y$ (no IBS) [μm·rad]	8.0 / 0.014	8.0 / 0.014	2.2 / 0.013	2.2 / 0.013
Calculated extr. $\gamma\epsilon_x$ / $\gamma\epsilon_y$ (with IBS)[a] [μm·rad]	8.1 / 0.014	8.1 / 0.014	2.5 / 0.018	2.5 / 0.017
Specified extr. $\gamma\epsilon_x$ / $\gamma\epsilon_y$ [μm·rad]	8.0 / 0.020	8.0 / 0.020	3.0 / 0.020	3.0 / 0.020

[a] The values for TESLA assume that there is no coupling bump.

7.2.3.10 Extraction Kickers

An extraction kicker that does not turn off fully when the next stored bunch passes will deflect the stored bunch, ultimately increasing its emittance through filamentation. Preliminary simulations indicate that the residual kick must be held within the limits shown in Table 7.7 to avoid appreciable emittance growth through filamentation.

TABLE 7.7
Acceptable residual extraction kicker deflection.

	TESLA DR	JLC-X/NLC MDR
Nominal deflection [mrad]	0.6	2.5
Maximum acceptable residual deflection [μrad]	2–3	20–30
Maximum acceptable residual deflection/nominal deflection [%]	0.3–0.5	0.8–1.2

7.2.4 Extracted Beam Jitter

7.2.4.1 Introduction

Jitter in the quantities $\langle x\rangle$, $\langle x'\rangle$, $\langle y\rangle$, $\langle y'\rangle$, $\langle \Delta t\rangle$, and $\langle \Delta p/p\rangle$ in the extracted beam can cause emittance growth downstream through wakefield and filamentation effects. We evaluate jitter from several significant sources. Our calculations include: a ground motion model; an extraction kicker model; and an rf system model.

7.2.4.2 Vertical Beam Jitter from Ground Motion and Vibration

Vertical motion of the quadrupole magnets will result in vertical orbit jitter and a jitter of the first moments $\langle y\rangle$ and $\langle y'\rangle$ of the extracted beam. Some types of ground motion result in a correlated motion of the quadrupole magnets. Other types of ground motion,

and vibration from local noise sources (*e.g.*, the flow of cooling water), result in uncorrelated motion. In this section we calculate the orbit jitter due to correlated and uncorrelated motion.

7.2.4.2.1 Correlated Motion We use the "quiet" (A), "intermediate" (B), and "noisy" (C) ground motion models of [10] (see also Section 7.3.4.1) with parameters of [13] to calculate the orbit jitter due to ground motion. These models contain both diffusive (ATL) motion and a set of elastic ground wave peaks. It is found that the ATL part of the ground motion spectrum has a negligible effect. Table 7.8 summarizes the predicted jitter of a bunch train from elastic ground waves in models A, B, and C. The jitter is negligible in models A and B, and still within tolerable limits in model C. In all cases the jitter within a single bunch train is negligible.

TABLE 7.8
Predicted beam jitter from correlated ground motion.

	$\langle y \rangle_{rms} / \sigma_y$	
Model	TESLA DR	JLC-X/NLC MDR
A	0.0012	0.00054
B	0.016	0.0071
C	0.217	0.099

7.2.4.2.2 Uncorrelated Motion For both the TESLA DR and the JLC-X/NLC MDR, an uncorrelated vertical motion of the quadrupole magnets of approximately 80 nm rms would result in an orbit jitter equal to the vertical beam size. The measured quadrupole magnet vibration in the APS was reduced, with great effort, to 90 nm rms in a 4 to 50 Hz band [4], indicating that with considerable care it should be possible to keep the vibration in this range.

This degree of uncorrelated vibration is considerably larger than that due to ground motion, even with model C. It may be difficult to reach the pure ground motion level in damping rings, due to the high density of local noise sources, and the low resonant frequency of heavy magnet support systems. It should be noted, however, that local orbit feedback at the extraction point, such as has been demonstrated at the SLS ($\sim$0.6 μm rms in position and $\sim$0.3 μrad rms in angle [5]; see Section 7.2.2.3), should be capable of stabilizing the extracted beam position and angle jitter at the 0.1 σ level.

7.2.4.3 Horizontal Beam Jitter from Extraction Kicker Errors

Bunch-to-bunch variation in the kick delivered by the extraction kicker leads to jitter in the horizontal motion of the extracted beam. A roll of the extraction kicker about the beam axis leads to a vertical kick to the extracted beam. This vertical kick is systematic and can be corrected by steering in the extraction line. Variations in the vertical kick due to jitter in

the kick strength are negligibly small. These parameters and errors are summarized in Table 7.9.

TABLE 7.9
Nominal parameters and jitter in the damping ring extraction kickers.

	TESLA DR	JLC-X/NLC MDR
Horizontal deflection θ_x [mrad]	0.6	2.5
Specified bunch-to-bunch variation $\Delta\theta_x$ [μrad]	$\pm$0.42 ($\pm$0.07%)	$\pm$1.25 ($\pm$0.05%)
Specified roll angle [μrad]	<35	<35 [a]
Vertical deflection θ_y [nrad]	<21	<88
Normalized horizontal kick stability $\Delta\theta_x/\sigma_{x'}$	$\pm$ 0.11	$\pm$ 0.052
Normalized systematic vertical deflection $\theta_y/\sigma_{y'}$	< 0.11	< 0.063

[a] Assumed value for JLC-X/NLC MDR.

JLC-X/NLC plan to use a system in which two kickers are driven by a common source. The second kicker, a half-integer number of betatron wavelengths down the extraction line from the first kicker, cancels the jitter caused by the first kicker. The degree of cancellation that is possible is unknown. A single-bunch experiment [14] with a double-kicker system at the ATF showed a reduction of the net jitter by a factor of 3.3. The values in Table 7.9 do not include any horizontal jitter cancellation or effect of a second kicker on vertical deflection. Pulse-to-pulse variation in existing kicker systems is of the order of 0.1% [15].

7.2.4.3.1 Summary

- A single well-designed extraction kicker may just suffice for the TESLA and JLC-X/NLC damping rings, but it is more likely that a double-kicker system (as planned for JLC-X/NLC) may be needed.

7.2.4.4 Circumference Variations

The circumference of a ring may vary due to ground motion, earth tides, temperature variations, and magnet vibration. Only the diffusive (ATL) component of ground motion, earth tides, and temperature variations have significant effects on circumference, and each of these acts on long time scales of the order of a day or longer. These circumference changes will result in a variation of the beam energy. We consider changes on the time scale of one day, assuming that energy correction can be done daily. We assume a "noisy" (A=10^{-17} m^2/m/s) ground motion model and a tidal strain of 4×10^{-8} [16]. Table 7.10 summarizes the estimates of circumference and energy variation. Because of its large circumference, the TESLA damping ring is influenced by tides more than by ATL; the reverse is true for the JLC-X/NLC main damping ring. In all cases the energy variation is

TABLE 7.10
Estimates of circumference and energy variation due to ATL ground motion and earth tides.

	TESLA DR	JLC-X/NLC MDR
Circumference C [m]	17,000	231
Circumference variation ΔC_{rms} (ATL) [μm]	170	20
Circumference variation ΔC (tidal) [μm]	680	9.2
Energy variation $\Delta E_{rms}/E$ (ATL)	8.4×10^{-5}	2.9×10^{-4}
Energy variation $\Delta E/E$ (tidal)	3.3×10^{-4}	1.4×10^{-4}

less than the energy spread of the beam. The effect of temperature is more difficult to estimate. Experience with other machines suggests that the small temperature variations expected for the damping rings will not have a significant effect on beam energy (see Section 7.2.2.2).

7.2.4.5 Longitudinal Phase Transients from Beam Loading

Random variations in bunch charge, gaps in the fill pattern, and transients in the beam current due to injection and extraction can cause variations in beam loading, which, in turn, affect the energy and rf phase of the extracted bunches. These beam loading variations were simulated using a macroparticle model for the bunches. Table 7.11 shows the parameters included in the simulations. The bunch population variation is an uncorrelated Gaussian random variable.

TABLE 7.11
RF system and lattice parameters for longitudinal jitter simulations.

	TESLA e^+ DR	TESLA e^- DR	JLC-X/NLC MDR
Harmonic number h	28200	28200	714
Number of bunches	2820	2820	3 trains of 192
Slip factor η	0.12×10^{-3}	0.12×10^{-3}	0.295×10^{-3}
Energy loss per turn U_0 [MeV]	21	12	0.792
RF voltage [MV]	54	36	1.07
Number of cavities	12	8	3
R/Q per cavity [Ω]	45	45	118
Q_L	1.1×10^6	1.1×10^6	2273
Bunch population variation $\Delta N/N$	0.05 (peak-peak)	0.05 (peak-peak)	0.02 (rms)

For each of the rings the energy jitter at extraction is negligible compared with the energy spread of the beam. For the TESLA rings the size of the gap due to extraction is one missing bunch (assuming no ion clearing gap) and the phase jitter at extraction is dominated by beam loading due to the random bunch population variation. The phase jitter in the TESLA e^+ DR (0.035° rms at 500 MHz) and e^- DR (0.029° rms) is roughly

0.05 mm or 1% of the bunch length. In Section 7.2.3.7, it was noted that an ion clearing gap of up to 600 ns will be needed for the TESLA e^- DR. This introduces, through beam loading, an additional systematic phase variation with a full width of 1.2°, which is roughly 2.0 mm, or 33% of the rms bunch length. For the JLC-X/NLC MDR the phase variation is dominated by the gap between trains. This phase slewing is systematic from train to train, with a full width of 5.4° at 714 MHz, which is 6.3 mm or 1.7 times the rms bunch length.

7.2.5 Particle Loss

7.2.5.1 Introduction

Particle loss in the damping rings must be minimal to reduce radiation damage, to prevent lost particles from intercepting beam diagnostics, and to avoid loss of bunch charge (and luminosity). We consider particle loss due to injection into the nonlinear lattice, and Touschek scattering. Our calculations include: a lattice with sextupoles and wiggler nonlinearities; physical apertures; and rf parameters.

7.2.5.2 Injection Efficiency

The injection efficiency of a damping ring depends on the 6-dimensional phase space distribution of the injected beam, including jitter, and is limited by the physical and dynamic apertures in the ring. Collective effects that can influence the dynamics should also be taken into account.

In damping rings, the wigglers give much larger energy losses than is common in conventional storage rings, and systematic nonlinearities in the wiggler fields can destabilize the dynamics to a significant extent. To estimate the severity of the effect, a description of the calculated field as a kick map may be constructed. A symplectic integrator using the kick map is then used in a tracking code to determine the dynamic aperture. This procedure, applied to the JLC-X/NLC main damping ring wiggler, is described in [17]. An attempt was made to apply the same procedure to the TESLA damping ring wiggler, but a good match of the kick map to the calculated field was not obtained. A linear hard-edged dipole model was used for the JLC-X/NLC positron pre-damping ring wiggler.

Preliminary results including sextupole magnets and nonlinear wiggler fields derived from field maps indicate that the dynamic aperture is limited by the wiggler nonlinearities in the TESLA damping rings and the JLC-X/NLC main damping rings[3]. The simulations indicate some particle loss at injection in the TESLA positron damping ring, for which the injected emittance is large. Optimization of the wiggler and/or lattice to improve dynamic aperture is needed. The dynamic aperture is more than adequate in the TESLA electron damping ring and the JLC-X/NLC main damping rings because of the much smaller injected emittance. Simulations of the JLC-X/NLC positron pre-damping ring with a linear hard-edged dipole wiggler model indicate adequate dynamic aperture. The simulations do not include systematic and random multipole errors or random wiggler errors, which may further reduce the dynamic aperture.

[3]When the tracking simulations use a linear hard-edged dipole wiggler model, the calculated dynamic aperture is much larger than when the nonlinear wiggler kick map is used.

Necessary work is in progress to: improve the calculation of wiggler fields, including end fields; to develop a more robust field fitting procedure; and to develop a dynamic model that will avoid many of the approximations required for the kick map approach. Future R&D should include wiggler prototyping and benchmarking the tracking calculations against experience in operating machines.

7.2.5.2.1 Summary

- Simulations of injection efficiency including sextupole magnets and nonlinear wiggler fields derived from field maps show that the dynamic aperture is limited by the wiggler nonlinearities in the TESLA damping ring and the JLC-X/NLC main damping rings. The simulations do not include systematic and random multipole errors or random wiggler errors, which may further reduce the dynamic aperture.
- The simulations indicate some particle loss at injection for the TESLA positron damping ring, because the injected emittance is large and the dynamic aperture is similar to the size of the injected beam. This indicates that an optimization of the wiggler and/or lattice to improve dynamic aperture is needed. The dynamic aperture is more than adequate in the JLC-X/NLC main damping rings because of the much smaller injected emittance.

7.2.5.3 Touschek Lifetime

The Touschek lifetime in low-energy, low emittance damping rings is short. For both the TESLA damping ring and the JLC-X/NLC main damping rings the Touschek lifetime is several orders of magnitude larger than the store time (see Table 7.12), so Touschek loss will not significantly decrease the bunch population. The short Touschek lifetime in the JLC-X/NLC MDR prohibits commissioning and tuning of the damping ring with long stores at nominal parameters. This is not expected to be a severe shortcoming.

The values of the Touschek lifetime listed in Table 7.12 assume a constant energy aperture of 1.0% for both TESLA and JLC-X/NLC. Careful studies of momentum aperture need to be made to better quantify the injection efficiency and the Touschek lifetime.

TABLE 7.12
Touschek lifetime at equilibrium emittance for a momentum aperture of 1.0%.

	TESLA DR	JLC-X/NLC MDR
Touschek lifetime [s]	1300	56
Store time [s]	0.2	0.025

7.2.5.4 Space Charge

The effect of space charge on particle loss has not been analyzed. We note, however, that the space charge tune shift is large only when the beams are small and most particles are

well within the dynamic aperture. For this reason space charge is not likely to be a significant source of particle loss. Nonetheless, we recommend that particle tracking simulations including space charge should be run to rule out the possibility that space charge tune shifts could result in particle loss.

7.2.6 Extracted Polarization

7.2.6.1 Introduction

All linear collider projects foresee producing an electron beam with 80% polarization at the source. This polarization should be preserved during the subsequent transport to the IP. A first estimate of the depolarization time was obtained from first order perturbation theory, as implemented in the code SLIM [18, 19]. The calculations include: a linear lattice with a hard-edged dipole linear wiggler model, and orbit errors. The treatment of spin motion is valid under the assumptions that for the low energies considered (1.98 GeV for JLC-X/NLC, 5 GeV for TESLA) the spin precession is dominated by the effect of vertical closed orbit distortions leading to the coupling of spin to the horizontal dispersion [19]. This assumption may not be valid for large transverse particle amplitudes. Further work should thus include spin-tracking studies.

7.2.6.2 SLIM calculations

The calculations were performed for the JLC-X/NLC main damping ring and the TESLA positron ring with a vertical orbit error of 1 mm rms simulated through randomly distributed vertical kicks.

Figure 7.6 shows the depolarization time as a function of the energy for the JLC-X/NLC damping ring.

Figure 7.7 shows the depolarization time for the TESLA damping ring with the vertical bends and the coupling bump in the straight sections.

7.2.6.3 Summary

First order perturbation analysis shows that both damping rings have a safety margin of several orders of magnitude for the depolarization time. Even directly on a resonance, the depolarization time is on the order of 100 times the storage time for the TESLA damping ring. The NLC damping ring shows only the first order synchrotron resonances. This huge margin suggests that depolarization is not an issue in the damping rings. Spin tracking should be used to understand the behavior of particles with large betatron amplitudes at injection.

7.2.7 Upgrade to Higher Energy

7.2.7.0.1 TESLA Upgrade For an upgrade of TESLA from 500 GeV to 800 GeV c.m. energy (see Table 4.1), the bunch spacing within a train is halved from 20 ns to 11.5 ns, the bunch population is reduced from 2.0×10^{10} to 1.4×10^{10} and the extracted transverse

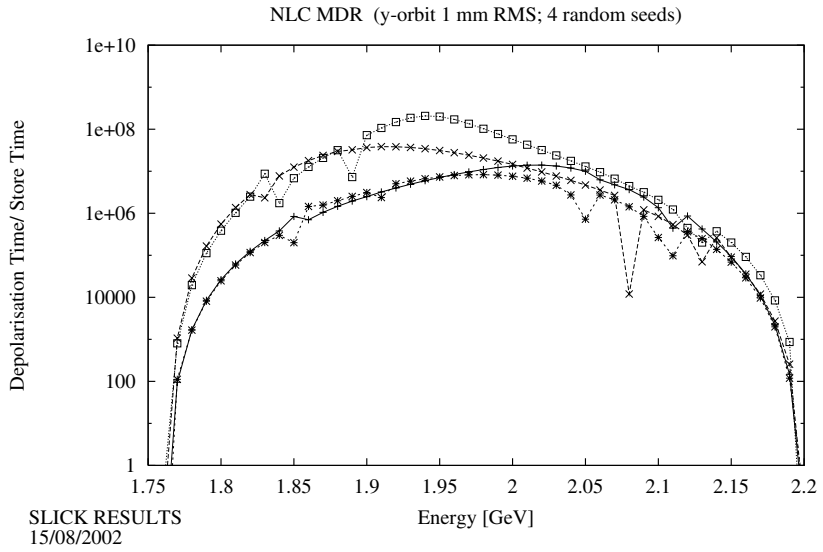

FIGURE 7.6. Depolarization time of the NLC main damping ring (normalized to standard store time 0.025 sec) versus energy.

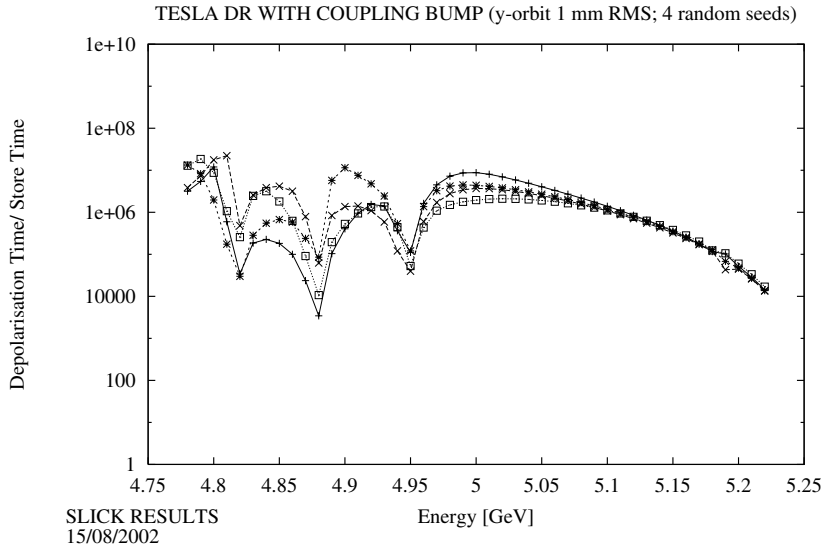

FIGURE 7.7. Depolarization time of the TESLA damping ring with vertical bends and coupling bump (normalized to standard store time 0.2 sec) versus energy.

emittances are reduced from $\gamma\epsilon_x$ / $\gamma\epsilon_y$=8.0 / 0.020 μm·rad to 6.0 / 0.010 μm·rad. This requires the development of injection and extraction kickers which are twice as fast as those for 500 GeV, and requires better correction of dispersion and coupling. As for the 500 GeV case, these kickers are technologically challenging, and simulations of the correction algorithms are needed to verify that the required emittance can be maintained. The electron cloud instability and ion effects are expected to be more severe, although we have not evaluated these at 800 GeV. An alternative energy upgrade, albeit with lower luminosity, is possible (see Table 4.2). This upgrade does not require improved damping ring performance.

7.2.7.0.2 JLC-X/NLC Upgrade An upgrade of JLC-X/NLC from 500 GeV to 1 TeV has no consequences for the damping ring complex.

7.2.7.0.3 CLIC Upgrade An upgrade of CLIC from 500 GeV to 3 TeV requires a reduction of the extracted beam emittances from $\gamma\epsilon_x$ / $\gamma\epsilon_y$=1.6 / 0.005 μm·rad to 0.45 / 0.003 μm·rad. As in the 500 GeV case, simulations of dispersion and coupling correction and IBS and other collective effects are needed to evaluate the damping ring design for 3 TeV.

7.2.8 Conclusions

Overall, the TESLA and JLC-X/NLC damping ring designs are well advanced. The required performance is not far from the performance achieved by the ATF. (We note that the JLC design for 150 Hz must be completed).

This committee examined many potential problems. Many of these were found to have satisfactory solutions or negligible impact: correction of the emittance increase due to ground motion; coupled bunch instabilities due to wakefields; space charge; intrabeam scattering; beam jitter due to ground motion and vibration, and beam loading; circumference variations; Touschek lifetime; and polarization preservation. However, we have identified several other issues that are critical for successfully producing the design luminosities. These issues are listed in Section 7.2.8.1 in order of greatest to least concern.

7.2.8.1 Concerns (TESLA and JLC-X/NLC)

- Without intervention to reduce the electron cloud density well below the neutralization density the e^+ damping rings are likely to suffer from an unacceptable incoherent tune shift, head-tail instability, and/or coupled bunch instability. The TESLA damping rings may be particularly susceptible to a large incoherent tune shift. The JLC-X/NLC main damping rings may be particularly susceptible to head-tail and coupled bunch instabilities. We note that PEP-II and KEKB have used multiple techniques to suppress the electron cloud, but do not operate with their design bunch pattern due, at least in part, to the electron cloud instability. This issue poses a serious technical risk. A solution to this problem must be aggressively pursued (TESLA, JLC-X/NLC).
- The fast ion instability may have a growth rate too fast to be controlled with feedback in both the TESLA damping rings and the JLC-X/NLC damping rings. There are

very large uncertainties in the estimate of the growth rate. If simulations or experiments show that the growth time is less than a few hundreds of μs, then a redesign of the vacuum system for substantially lower pressure (as low as 10^{-10} Torr) may be required (TESLA, JLC-X/NLC).

- Simulations indicate some particle loss for the TESLA e^+ damping ring, because the injected emittance is large and the dynamic aperture is similar to the size of the injected beam. The limited dynamic aperture, caused by nonlinearities from the wiggler field, may result in unacceptable radiation in the tunnel. This issue requires an aggressive effort to optimize the TESLA DR wiggler and/or lattice design. Such an effort is expected to produce a satisfactory solution (TESLA).
- The broadband impedance budgeted for the TESLA damping rings and JLC-X/NLC main damping rings is roughly one third of the measured value in recently constructed machines in which pains were taken to minimize the impedance. While the estimated impedance threshold for the longitudinal microwave instability is a factor of 2–3 larger than the design impedance for the TESLA DR and JLC-X/NLC MDR, it is expected to be difficult to achieve that margin. This issue places stringent demands on the calculations for, and design and implementation of, the vacuum chamber (TESLA, JLC-X/NLC).
- In a simulation model including several significant classes of misalignments and design BPM resolution, the emittance (disregarding collective effects) is corrected to below the design level for most, but not all, random seeds in both the TESLA DR and the JLC-X/NLC MDR. The dependence of luminosity on DR equilibrium emittance is soft, and the experience at the ATF shows that such simulations can successfully predict the effectiveness of the correction algorithm. However, not all effects have been included in the simulation, and the margin is not large. Additional correction strategies should be considered to widen this margin. This issue also places stringent demands on BPM resolution and stability (TESLA, JLC-X/NLC).
- To avoid an unacceptably large tune spread due to ions, the TESLA e^- damping ring should be designed for an average pressure of the order of 10^{-10} Torr and must use an ion-clearing gap. (TESLA).
- While calculations indicate that the dynamic aperture for the JLC-X/NLC e^- and e^+ MDR and the TESLA e^- DR is adequate, it decreases rapidly for off-momentum particles. Efforts should be made to increase the dynamic aperture for off-momentum particles (TESLA, JLC-X/NLC).
- We have not calculated the effect of collective instabilities on the closure of the coupling bump in the TESLA damping rings. Such a calculation should be made to determine whether a problem exists (TESLA).

7.2.8.2 Comments on CLIC

We note that most of these issues are critical for the CLIC damping rings as well. Initial design studies suggest that emittance growth from intrabeam scattering and electron cloud instabilities will present serious challenges for CLIC. IBS is an important driver in the optimization of the CLIC main damping ring lattice.

7.2.9 Items for Further R&D

We present here the suggested R&D items for the Damping Ring designs. The items have been ranked in their importance according to the ranking scheme described in Section 7.1.3. No specific R&D items appear for CLIC, for the reason noted in Section 7.2.1.1.

7.2.9.1 Ranking 2

Items Common to All Machines:

- Further simulation studies are needed to understand the magnitude of the electron cloud effects and to explore possible means of suppression of these effects. Experiments in existing rings are needed to test the electron cloud simulations. Possible cures for the electron cloud (including chamber coatings, superimposed magnetic fields, and gaps in the bunch pattern) need to be experimentally investigated.
- Further simulations of the fast ion instability are necessary. Experiments in the ATF and other suitable rings are needed to test the predictions of the simulations.
- Extraction kicker stability, required at the level of $< 10^{-3}$, is an important issue. Further studies including experiments with the ATF double kicker system are needed.
- Additional simulations of emittance correction are needed, including the effects listed in Section 7.2.3.2. Additional experiments in the ATF and other operating rings are needed to test emittance correction algorithms.

Items Specific to TESLA:

- Inclusion of systematic and random multipole errors and random wiggler errors are needed in the particle loss simulations. Further dynamic aperture optimization is needed.
- The energy and luminosity upgrade to 800 GeV will put tighter requirements on alignment and on suppression of electron and ion instabilities. Further studies of these effects are required.

7.2.9.2 Ranking 3

Items Common to All Machines:

- Detailed reviews of the impedance budgets are needed.
- Development of BPMs with $\leq$0.5 to 1 μm resolution and excellent stability ($\sim$10 μm over 1 day) is necessary. The development of fast, high resolution beam size diagnostics must be continued.

Items Specific to TESLA:

- A calculation of the effect of collective instabilities on the closure of the coupling bump in the damping rings should be made to determine whether a problem exists.

Items Specific to JLC-X/NLC:

- Inclusion of systematic and random multipole errors and random wiggler errors are needed in the particle loss simulations. Further dynamic aperture optimization is needed.
- Further experiments at the ATF and other low-emittance rings are necessary to determine the validity of the theoretical models of IBS.

7.2.9.3 Ranking 4

Items Common to All Machines:

- Additional experiments in the ATF and other operating rings are needed to verify that beam-based alignment can be used to align BPMs with respect to their associated quadrupole and sextupole magnets within a few μm and to study drifts and systematic errors in the BPMs.

Items Specific to TESLA:

- A correction algorithm including both vertical and horizontal planes is needed.

7.3 LOW EMITTANCE TRANSPORT (LET)

7.3.1 Introduction

The Low-Emittance Transport (LET) region of a linear collider includes all of the beamlines between the exit of the main damping ring and the interaction point. Generically, the LET includes the bunch compressor, main linac, and beam delivery sections of the linear collider.

The principal luminosity requirements of the LET are: preservation of the small emittances generated by the main damping rings, in order to achieve a small beam spot at the interaction point; and minimization of relative beam motion at the IP, to permit the beams to collide. Generically, the obstacles to achieving the requirements are as follows:

- The normalized emittances of the linear colliders are all significantly smaller than those achieved at even the brightest of the synchrotron light sources; hence, the tolerances on traditional sources of emittance dilution (synchrotron radiation, magnet misalignment, *etc.*) are correspondingly tighter than in any existing facility.

- The small betatron functions and strong focusing required to achieve the desired spot size impose stringent optical requirements on the beam delivery (magnet strength tolerances, matching of sextupole strengths for aberration cancellation, *etc.*)
- The RMS vertical beam size at the IP is in all cases measured in nanometers, and the beams must collide with an offset significantly less than the beam size in order to achieve acceptable luminosity. Extremely small motions of the LET magnets can drive the beams out of collision.

The bunch compressor and beam delivery regions of the various LET designs must satisfy fairly similar requirements, and are to some extent interchangeable. The differences in the designs, their parameters, and their overall performance are driven primarily by the different choices in main linac accelerating technology, and the ways in which the main linac technology interacts with the beam dynamics:

- The superconducting, low-frequency (1.3 GHz) TESLA cavities generate much weaker short-range wakefields than the higher-frequency JLC-X/NLC (11.424 GHz) or CLIC (30 GHz) accelerator structures; this in turn implies that the transverse alignment tolerances for the latter designs will be tighter than for TESLA.
- The JLC-X/NLC and CLIC designs have compensated their relatively strong wakefields through use of stronger focusing in the main linac, a correlated energy spread for the suppression of the most severe wakefield-driven instability (see Section 7.3.2.1), improved diagnostics (primarily higher-resolution BPMs, BPMs integrated into rf accelerator structures, and additional profile monitors), and improved correction systems (remote-controlled translation stages for quadrupoles and rf structure girders). These features permit the "warm," high-frequency LET designs to meet their tighter alignment tolerances and achieve luminosity performance comparable to TESLA's, at the expense of introducing more stringent requirements on the instrumentation and correction devices.
- TESLA accelerates a long (950 μsec) train of bunches in a single rf pulse, which in principle permits significant optimization of certain parameters within a train (for example, the relative offset and angle of the beams at the collision point). The JLC-X/NLC and CLIC designs use shorter trains (100 to 300 nanoseconds), which limit the effectiveness of any intra-train feedback or optimization.
- The high-frequency LET designs accelerate a large number of bunch trains per second (100 to 200 for JLC-X/NLC and CLIC, compared to 5 for TESLA), which allows them to implement highly effective train-by-train feedback systems, including feedbacks which maintain the collision of the very small spots at the IP. The effectiveness of these train-by-train feedbacks compensates for the relatively limited effectiveness of intra-train feedbacks for the "warm" designs.

In addition, the LETs all operate in a regime in which the intense interaction of the colliding beams must be taken into account. TESLA's IP parameters result in a larger enhancement of the luminosity from the beam-beam pinch effect than the parameters chosen for JLC-X/NLC or CLIC (the enhancement factor is 2.1 for TESLA, 1.5 for

JLC-X/NLC, and 1.4 for CLIC); but as a consequence, TESLA is more sensitive to beam-beam offsets at the IP and to correlated distortions of the bunch shape.

In this section we enumerate the beam dynamics effects in the LET which can lead to degraded luminosity, and summarize their expected impact on each of the linear collider designs. For this purpose the effects have been divided into four categories: effects present in a beamline with no misalignments or other errors of any kind (Section 7.3.2); effects which are static or quasi-static (Section 7.3.3); dynamic misalignments from ground motion or cultural noise sources (Section 7.3.4); and other dynamic effects in the accelerator (Section 7.3.5). Although there are several areas of concern which have been identified by this review, and a number of research and development topics which must be addressed, it is the consensus of the reviewers that, from the point of view of luminosity performance, the feasibility (as defined in Section 7.1.3) of each LET design has been established.

A Note on LET Subdivisions As mentioned previously, the LET is typically divided into three regions. The bunch compressor, as the name suggests, contains elements for reducing the length of the bunch extracted from the damping ring to something acceptable to the main linac and IP; it also contains a spin manipulation beamline, which allows the beam polarization vector at the IP to be adjusted to match the experimental requirements. The bunch compressor is followed by the main linac, which accelerates the beam to the desired energy. The main linac is followed by the beam delivery system, which consists of a post-linac collimation system for removal of particles which would generate unacceptable detector backgrounds, followed by a final focus system, which performs the chromatically corrected demagnification of the beam to a small enough RMS transverse size to generate luminosity. JLC-X/NLC and CLIC each include a two-stage bunch compressor system, with a low-frequency "pre-linac" sandwiched between the two bunch compressor stages. JLC-X/NLC also includes a coasting transport line between the last accelerating element of the main linac and the start of the post-linac collimation system. TESLA's bunch compressor region includes a set of horizontal and vertical doglegs immediately upstream of its spin manipulation system.

In addition, each linear collider design includes a collimation system immediately downstream of the main damping ring for removal of particles with large betatron amplitudes; these so-called "pre-collimation" systems have not yet been designed, and thus are not reviewed here. Also, the CLIC bunch compressor design did not become available until fairly late in the review process; as a result, its design and properties are generally not considered here. It is not expected that these omissions will have any significant impact on the conclusions of this review. Finally, as noted in Section 3.3, the beamline optics for the JLC-X and NLC designs differ slightly due to different optimizations. In this section, we only analyzed the NLC optics; however, the JLC-X optics is similar, and thus the designs are frequently referred to as the JLC-X/NLC design.

7.3.2 Performance Limitations Present by Design in Error-Free Machine

Even in the absence of misalignments or other errors, each LET design will experience a number of effects which limit the final performance of the system. Inherent design limitations are often the most difficult to address *post facto*, hence it is essential that they be understood and limited well in advance.

At present, the majority of all present-by-design limitations are well under control in all three LET designs. Outstanding issues include the wakefield effects due to collimators in the vertical plane, and electron or ion effects on multibunch emittance. In addition, the luminosity bandwidth of the CLIC beam delivery system is somewhat smaller than desired, although this is considered a problem in optimization rather than a fundamental limitation.

7.3.2.1 Single Bunch Beam Breakup (BBU)

A beam which undergoes a betatron oscillation in a linear accelerator can experience a resonant type of head-tail instability known as beam breakup (BBU). BBU can be suppressed by limiting the bunch charge, or through introduction of a longitudinally correlated energy spread; the latter process is usually referred to as "BNS Damping," after its inventors [20]. Figure 7.8 shows: (a) the "BNS" energy spread introduced to eliminate single-bunch BBU, and (b) the total RMS energy spread in the main linac of each design, including the incoming energy spread. Table 7.13 shows the single-bunch emittance growth in the linac for a $1\sigma_y$ initial oscillation under 3 conditions: without the initial energy spread and without the "BNS" energy spread; without initial energy spread but with "BNS" energy spread; with both initial and "BNS" energy spread. Table 7.13 shows that the present TESLA parameters are far from the BBU regime, but that JLC-X/NLC and CLIC require "BNS" damping. Nonetheless, it is clear that single-bunch BBU in the main linac is not a serious limitation for any of the designs.

TABLE 7.13
Emittance growth due to a $1\sigma_y$ initial oscillation in the main linac. Cases without and with correlated energy spread, but without initial energy spread, are shown; also shown is the case with both initial and correlated energy spread.

	TESLA			NLC			CLIC		
Initial energy spread	No	No	Yes	No	No	Yes	No	No	Yes
BNS energy spread	No	Yes	Yes	No	Yes	Yes	No	Yes	Yes
$\gamma\epsilon_y$ initial [nm·rad]	20	20	20	20	20	20	5	5	5
$\Delta\gamma\epsilon_y$ [nm·rad]	0.162	0.107	4.3	235	3.04	7.7	28.8	0.26	2.1
$\Delta\gamma\epsilon_y/\gamma\epsilon_y$ [%]	0.81	0.54	22	1180	15.2	39	574	5.2	42

Although the bunch compressors and pre-linacs of the LET designs also contain accelerator structures, the parameters of these systems are such that beam breakup is not a concern for any of them. This is amply demonstrated in Section 7.3.2.3, in which a 1 σ initial betatron

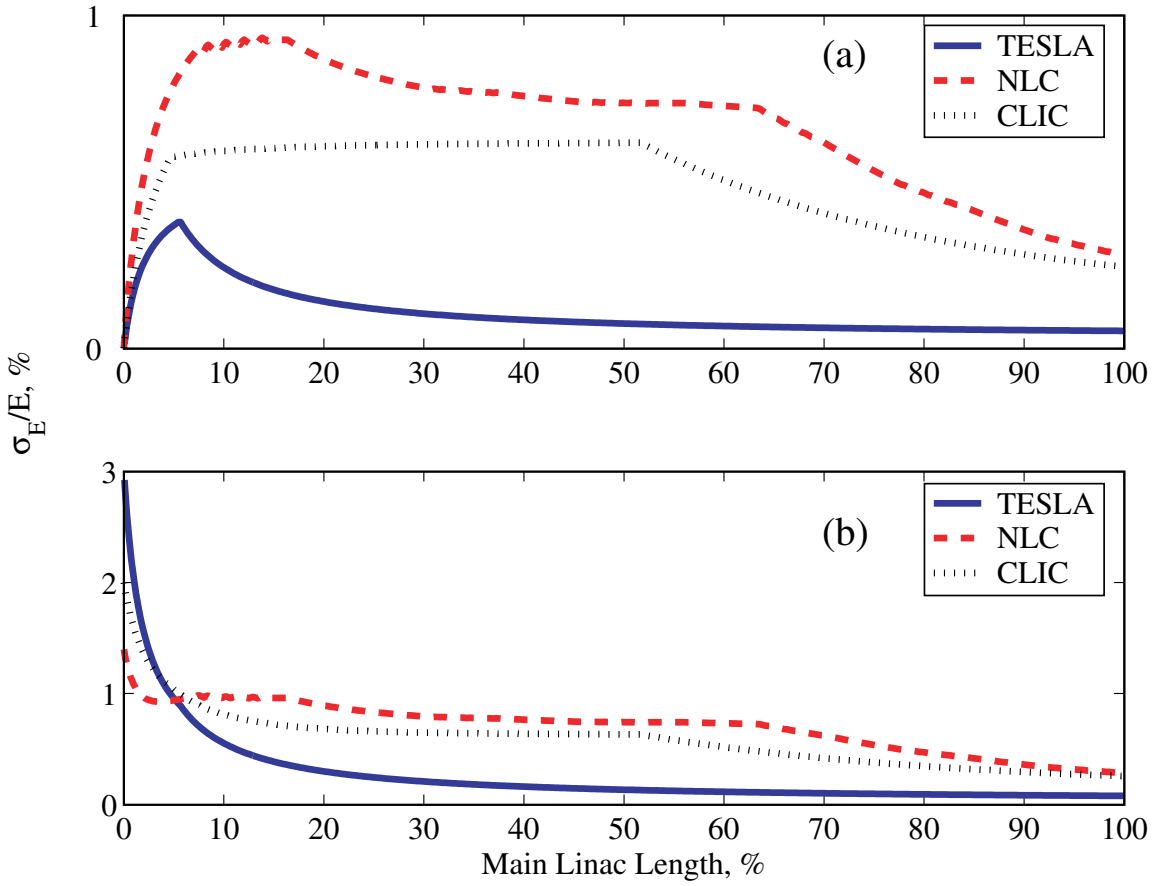

FIGURE 7.8. Energy spread in the main linac of each linear collider design: (a) correlated ("BNS") energy spread for BBU control; (b) total energy spread, including incoming energy spread and BBU-control energy spread.

oscillation leads to relatively little BBU-induced emittance growth upstream of the main linac in all cases.

7.3.2.2 Multibunch Beam Breakup

Multibunch beam breakup is a phenomenon similar to the short-range instability of the same name; in this case, the transverse wakefields from leading bunches in a train can resonantly deflect the trailing bunches in the same train.

The main approach to managing multibunch BBU is reduction of the long-range wakefield. The techniques used by each project for this purpose are discussed in Section 6.5.1.3 and Section 6.5.2.3. Using the design long-range wakefields, all projects have evaluated the vertical emittance growth due to a 1 σ_y initial offset for all bunches. Table 7.14 summarizes the simulation results for multibunch beam breakup and the design multibunch wakefields. Note that single-bunch wakefields and BNS damping are present in the multibunch simulations. Injected energy spread is not. The multibunch emittance growth is negligible

in the case of TESLA, which is a consequence of the weak long-range wakefields in the low frequency, superconducting cavities. The emittance growth is larger for the normal-conducting machines, and is larger than the emittance growth from single-bunch BBU shown in Table 7.13. The multibunch emittance growth remains within the realm of acceptability, however, especially when the effect of the uncorrelated energy spread at main linac injection is included [21]. The uncorrelated energy spread will lead to a faster de-coherence of the oscillation and the multibunch growth will be suppressed to below the values in Table 7.14.

TABLE 7.14
Growth in normalized vertical emittance due to a 1 σ_y offset of all bunches at the start of the linac. The simulation included single bunch wakefields and BNS damping, but no initial uncorrelated energy spread. NLC result from T. Raubenheimer, private communication. TESLA result based on DESY TESLA-00-28, 2000. CLIC result from D. Schulte, private communication.

	$\Delta\gamma\epsilon_y$ [nm·rad]	
Machine design	Single-Bunch	Total (SB+MB)
JLC-X/NLC	3.0	6.8
TESLA	0.11	0.11
CLIC	0.3	1.6

The simulation of long-range BBU is straightforward and high confidence can be placed on the simulation results, provided that two prerequisites are satisfied in the real-world implementation of the LET. The first prerequisite is that the design process for the structures be mature: the process used to calculate the long-range wake given the structure geometry parameters as input must be accurate. The second is that the construction process for the structures be mature: the geometry parameters that yield the desired long range wakefield must be achieved in the actual structure. The former pre-requisite has been achieved, and excellent agreement is found between calculated and measured higher-order modes. In the implementation phase, all designs have encountered abnormalities which have driven the measured wakefield away from the design wakefield, but these abnormalities are in general understood, and it can be reasonably expected in all designs that the accelerator structures will meet the design requirements for HOM's. The simulations described previously have shown that, for structures which possess the design wakefield, multibunch BBU will not be a problem for any LET. Although the pre-linacs and bunch compressors have not been explicitly evaluated here, no source of multibunch BBU is expected in these areas.

7.3.2.3 Optical Sources of Emittance Growth

Optical sources of emittance growth in a perfect beamline include uncorrected chromaticity, uncorrected high-order dispersion functions, and aberrations related to the presence of high-order multipole magnets (sextupoles and higher). Typically these sources contribute to beams which pass on-axis through perfect accelerators, and in general some of the sources

contribute even more strongly to beams which undergo betatron oscillations through the accelerator.

The optical emittance growth for on-axis beams is summarized in Table 7.15; all growths are acceptably small. Table 7.16 shows the simulated emittance growth for beams with 1σ initial offsets in either horizontal or vertical. In Table 7.15 and Table 7.16, the values reported are *e*ffective emittances, in which the beam sizes and angular divergences have been corrected to suppress the contribution of non-linear tails; also, the contribution of the design value of $\eta^*_{x'}$ to the angular divergence has been removed in the case of the JLC-X/NLC and CLIC final focus systems.

For a filamenting oscillation, the expected fractional emittance growth for a 1 σ oscillation is $\sqrt{2}-1$, or 41%; this value is shown in the "Ideal" row of Table 7.16. Most of the emittance growths in Table 7.16 are somewhat larger, typically 50% and in some cases 90%, which indicates that there are other nonlinear effects which are important. No significant dependence on the phase of the initial oscillation was seen. In all three cases, the expected jitter on the beam at the entrance to the LET is on the order of 0.1σ; since the emittance effect scales quadratically with the jitter amplitude, this source of emittance growth is expected to be acceptable in all cases.

The TESLA design anticipates the use of vertical dipole magnets to permit the main linac to follow the curvature of the earth; this causes a periodic vertical dispersion which, in principle, can cause some emittance dilution through unclosed high-order dispersion functions. Because the vertical dispersion function is small—typical values of η_y would be 150 μm—and the residual dispersion from misalignment and steering is expected to be several times as large (see Section 7.3.3), we do not expect this source to contribute to the TESLA emittance budget.

7.3.2.4 Bandwidth

The bandwidth of a beamline refers to its general capacity for transporting beams with off-nominal centroid energies without introducing unacceptable emittance dilution. Bandwidth is a key consideration for any beamline which can be expected to experience significant jitter in the energy of the incoming beam, or any beamline which relies upon delicate cancellations of optical aberrations: specifically, the spin manipulation beamlines of TESLA and the NLC, the 180° arc at the 8 GeV point in the NLC, and the beam delivery systems of each LET fall into this category.

In the case of the spin manipulation beamlines the incoming energy centroid jitter is simply the jitter in damping ring extraction energy, which is expected to be negligible compared to the RMS energy spread of the beam in all cases (see Section 7.2.4.4). Previous studies of the NLC spin manipulation system have shown that the emittance dilution due to chromatic effects is minuscule [22]; the TESLA system is nearly identical to the NLC design, and the TESLA damping ring energy spread is comparable to the NLC damping ring energy spread, so the TESLA system should be similarly well-behaved.

The beam dynamics of the NLC's 180° arc was the subject of a detailed study [23]; the study indicated that the vertical emittance growth reached 3 nm·rad for 2% energy error, and was dominated by high-order chromaticity and dispersion. The design specification for

TABLE 7.15: Emittance growth in Linear Collider LETs for on-axis beams. Initial emittances are damping ring extraction for TESLA and NLC, main linac injection for CLIC.

	TESLA		NLC		CLIC	
	$\Delta\gamma\epsilon_x$ [μm·rad]	$\Delta\gamma\epsilon_y$ [nm·rad]	$\Delta\gamma\epsilon_x$ [μm·rad]	$\Delta\gamma\epsilon_y$ [nm·rad]	$\Delta\gamma\epsilon_x$ [μm·rad]	$\Delta\gamma\epsilon_y$ [nm·rad]
Initial values	8	20	3	20	1.8	5.0
Budget	2	10	0.6	20	0.2	5
On-axis	0.12	1.5	0.06	0.8	0.02	0.44

TABLE 7.16: Emittance growth in Linear Collider LETs from 1 σ oscillations in horizontal or vertical planes. These values are growth in addition to the on-axis growth, and include short-range wakefields. Initial emittances are damping ring extraction for TESLA and NLC, main linac injection for CLIC. "Ideal" refers to the expected effect for a fully filamented oscillation, $\Delta\gamma\epsilon = (\sqrt{2}-1)\gamma\epsilon$. Note that emittance growths due to initial oscillation scale *quadratically* with the amplitude of the oscillation.

	TESLA				NLC				CLIC			
	1 σ_x		1 σ_y		1 σ_x		1 σ_y		1 σ_x		1 σ_y	
Location	x/σ_x	$\Delta\gamma\epsilon_x$ [μm·rad]	y/σ_y	$\Delta\gamma\epsilon_y$ [nm·rad]	x/σ_x	$\Delta\gamma\epsilon_x$, [μm·rad]	y/σ_y	$\Delta\gamma\epsilon_y$ [nm·rad]	x/σ_x	$\Delta\gamma\epsilon_x$ [μm·rad]	y/σ_y	$\Delta\gamma\epsilon_y$ [nm·rad]
Start	1	0	1	0	1	0	1	0	1	0	1	0
End BC	0.67	2.9	0.65	7.2	0.99	0.8	0.79	5.2	N/A	N/A	N/A	N/A
End ML	0.28	4.5	0.19	13.1	0.39	1.8	0.29	12	0.44	0.70	0.45	1.8
IP	0.26	4.6	0.20	15.7	0.31	1.8	0.33	12	0.21	0.70	0.45	2.0
Ideal	0	3.3	0	8.3	0	1.2	0	8.3	0	0.75	0	2.1

the pre-linac calls for an energy jitter of 1% full width [24]; for such an energy jitter the emittance growth in the arc should be negligible.

In the case of the beam delivery system, the only appropriate metric for bandwidth is the luminosity performance. This is because both the size of the two beams and their relative offsets are crucial in determining the delivered luminosity, and because the beam-beam effect can amplify or mitigate the impact of offsets, skewness, or kurtosis in the colliding beams. For present purposes, the chosen metric is the luminosity obtained when a beam of varying centroid energy is transported through the beam delivery system to collide with a beam of nominal (250 GeV) centroid energy. The energy variation is accomplished by systematically varying the on-crest energy gain of all linac structures. The resulting luminosity bandwidth of TESLA, NLC, and CLIC is shown in Figure 7.9. Note that the principal source of luminosity dilution in all 3 cases is the beam delivery system and not the main linacs. Figure 7.9 implies that, from the point of view of luminosity, NLC will likely be more tolerant of klystron phase and amplitude jitter or loss of rf power units than TESLA or CLIC will be.

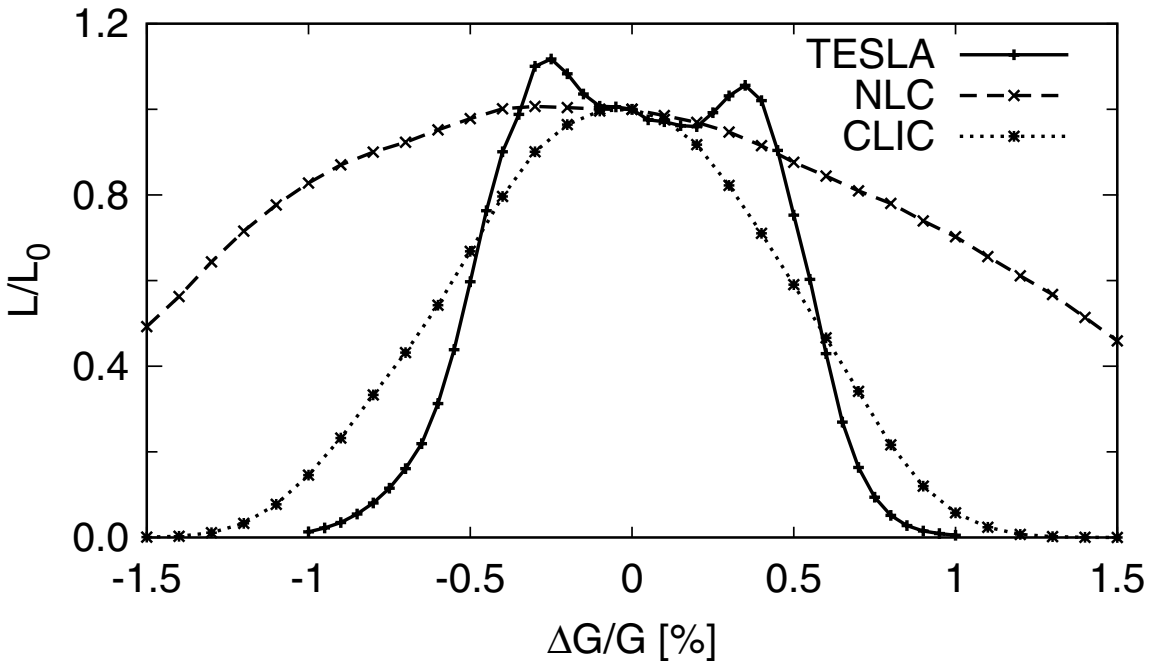

FIGURE 7.9. Relative luminosity as a function of beam energy. In this case, the energy of one beam at the IP is held constant, while the IP energy of the other beam is varied by uniformly scaling the accelerating gradient of its linac.

7.3.2.5 Synchrotron Radiation

Despite the implications of the name "LINEAR collider," the LETs contain bending in their spin manipulation, bunch compression, and beam delivery areas; the JLC-X/NLC also

contains several diagnostic chicanes in the main linac and horizontal extraction and injection lines to transport the beam to and from the main linac bypass line. These bend magnets can all introduce emittance growth through incoherent emission of synchrotron radiation photons in bend magnets. The bend magnets are all in the horizontal plane, and thus the emittance growth is confined to this plane. The expected emittance growths in the cases of TESLA, JLC-X/NLC, and CLIC, are 0.037 μm·rad, 0.216 μm·rad, and 0.005 μm·rad, respectively. In addition, the vertical bends used to transport the TESLA beam from the damping ring elevation to the main linac elevation contribute 0.245 nm·rad vertical emittance growth. Although the TESLA main linac is curved to follow the curvature of the Earth, the radius of curvature is large and the resulting emittance growth is orders of magnitude smaller than the design emittance.

In the case of high-energy linear colliders, an additional source of emittance dilution arises from the stochastic energy loss in the final bends and final doublet; these synchrotron emissions cause a breakdown in the chromatic correction of the final focus and can lead to vertical beam size growth [25]. For beams with the nominal IP parameters listed in Table 2.6, this effect results in vertical RMS beam size increase of 1.2% for TESLA, 1.8% for JLC-X/NLC, and 2.2% for CLIC. Particles far from the beam core, which do not contribute much luminosity, will be more strongly influenced by this effect than the luminosity-producing particles in the core, and therefore the RMS beam size increase overestimates the luminosity effect; a luminosity-weighted beam size calculation shows a spot size increase of 0.8% for TESLA, 1.3% for JLC-X/NLC, and 1.4% for CLIC.

In addition to the incoherent synchrotron radiation effects described, linear collider bunch compressors are potentially subject to emittance dilution from coherent synchrotron radiation (CSR). The horizontal emittance growth from CSR is 0.08 μm·rad for both the TESLA and JLC-X/NLC bunch compressors. Emittance growth from CSR is a strong function of bunch length; thus, this effect will be important to evaluate in the case of the CLIC bunch compressor system.

7.3.2.6 Collimator Wakefields

The collimator jaws in the post-linac collimation region and the final focus of the LETs introduce single-bunch transverse wakefields. The principal effect of these wakefields is to amplify any incoming jitter; the kick given by a collimator is proportional to the beam transverse position in the collimator, hence the collimators add an angle jitter which is proportional to position jitter. From this it follows that the collimators at the betatron phase of the final doublet are the most critical, since these collimators add to the position jitter of the beam at the IP. In addition, any collimator at a location of nonzero dispersion will couple the incoming energy jitter into betatron motion. Finally, the collimator wakefields will also introduce some single-bunch emittance dilution, since the tail of each bunch will be deflected but the head will not be. This emittance dilution has a longitudinal correlation—a "banana"—which can be quite damaging to the luminosity performance (see Section 7.3.2.9).

In order to afford some protection against collimator damage from individual errant pulses or bunch trains, each LET post-linac collimation system uses a set of thin collimators ("spoilers"), which enlarge the beam angular divergence through multiple Coulomb scattering; these are followed at some distance by thick collimators ("absorbers"), which

stop the beam halo and, if necessary, the core of an errant beam. The geometric wakefield was calculated using the expressions in [26], while the resistive wakefield was calculated using the expressions in [27]; the overall procedure describing the algorithm used here is summarized in [28]. Table 7.17 shows the jitter amplification figure of merit for each subcomponent of the post-linac collimation systems of each LET design, based on the collimation system descriptions [29]. For betatron collimators the figure of merit ($\mathcal{A}_{x,y}$) represents sigmas of outgoing angle jitter for 1 σ of incoming position jitter; in the case of the energy collimators the parameter $\mathcal{A}_\delta$ has units of sigmas of angle jitter per percent energy centroid jitter. Table 7.17 shows the collimator-wakefield contribution to beam jitter at the IP, which is the most relevant to luminosity performance. There is also a collimator wakefield contribution to beam jitter at the final doublet magnets, but the luminosity impact of this jitter is small and is not tabulated here.

TABLE 7.17
Jitter-amplification figures of merit for collimators in the final doublet betatron phase. "N/A" indicates that the collimator classes in question (FF spoilers, *etc.*) are not present in the design and thus contribute no wakefields.

	TESLA			NLC			CLIC		
Parameter	$\mathcal{A}_x$	$\mathcal{A}_y$	$\mathcal{A}_\delta$	$\mathcal{A}_x$	$\mathcal{A}_y$	$\mathcal{A}_\delta$	$\mathcal{A}_x$	$\mathcal{A}_y$	$\mathcal{A}_\delta$
δ spoilers	0.035	0.054	0.27	0.0010	0.045	0.053	0.0017	0.16	0.049
δ absorbers	0.0063	0.034	0.058	0.0053	0.016	0.019	0.0035	0.37	0.10
β spoilers	0.066	0.55	0	0.081	0.59	0	0.099	1.67	0
β absorbers	0.032	0.51	0	0.0032	0.014	0	0.12	0.33	0
FF spoilers	0.080	0.73	0.019	N/A	N/A	N/A	0.034	0.32	0.13
FF absorbers	0.024	0.38	0.029	0.062	0.53	0.0019	N/A	N/A	N/A
Total	0.24	2.26	0.34	0.15	1.20	0.074	0.26	2.84	0.027

The values in Table 7.17 indicate that, in the horizontal plane, 24%, 15%, and 26% of the doublet-phase jitter will be coupled into the IP phase; since this jitter adds in quadrature with the collimator-free jitter, the resulting growth in the absolute jitter amplitude will be at the few percent level in all cases, which should be acceptable. Similarly, an energy jitter of 1% will contribute 0.34 σ_x^*, 0.074 σ_x^*, and 0.026 σ_x^* at the IP for the three designs; assuming that the energy jitter is comparable to σ_E/E in each case, this should also be negligible.

The situation is somewhat less favorable in the vertical plane. In this case, the IP jitter for each LET design will be dominated by FD-phase jitter which is coupled to the IP phase by the collimator wakefields. This is probably unacceptable for any LET design. Several strategies for mitigation of jitter amplification due to collimator wakefields are presented in [28], including: relaxing the collimation depth requirements by increasing the aperture of the vertex detector; reducing the taper angle of the collimators, although this may prove difficult from an engineering point of view; and elimination of collimators that have little influence on the collimation efficiency, including potentially eliminating some of the spoilers in the betatron collimation section if possible. It is also worthwhile to note that in the case of CLIC, the spoilers have been assumed to be copper-coated beryllium, 0.5 radiation lengths thick; this requires that each spoiler include a 71 cm long region with a 215 μm half-gap, which causes a huge resistive wakefield. Use of copper or titanium would nearly eliminate this part of the wakefield, which is the dominant contribution to the CLIC spoiler

wakes. Finally, the collimator apertures can be relaxed without any change to the vertex detector if non-linear focusing is used to "fold" the final-doublet phase of the beam halo into a smaller area [30]. The NLC LET design includes octupoles for this purpose, but the study of collimator wakefields assumed that the octupoles are switched off and that the collimators must be set tightly in order to obtain a conservative performance estimate. It is expected that the octupole solution can be adapted to any of the LETs.

The emittance dilution from wakefields near the center of a collimator can be estimated as follows [31]:

$$\frac{\Delta\epsilon}{\epsilon} = (0.4n\mathcal{A})^2$$

where n is the number of sigmas of beam jitter. The values in Table 7.17 indicate that beam jitter at the level of 10 σ_x or 1 σ_y will lead to significant emittance dilution from this source.

It is important to remember that the theory used to perform the calculations is rather complicated and makes a number of simplifications relative to a realistic, engineered system of collimators with adjustable gaps. In all cases, the LETs were designed using a simpler theory applicable only to round collimators, which indicated that the small gaps needed for background control would be acceptable from a wakefield point of view; the results are new, and are a product of the ILC-TRC process. Also, the experimental measurements of collimator wakefields have in some cases yielded deflections which are smaller than those predicted by the theory, and no measurements have yet been performed in the regime which is relevant for the LET designs. This constitutes an excellent candidate for further R&D, especially given the existence of a dedicated collimator wakefield test facility [32].

7.3.2.7 Damping Ring Extraction Phase Variation

In Section 7.2.4.4, it was determined that the centroid energy jitter at damping ring extraction would be extremely small for both TESLA and NLC. For TESLA, the phase jitter at extraction (see Section 7.2.4.5) is 2 mm full width, which corresponds to 33% of the rms bunch length of 6 mm. For NLC, the phase jitter would be 6.3 mm full width. NLC's extraction phase variation is longer than the RMS bunch length of 3.6 mm given in Table 2.3; it is therefore important to ensure that the extraction phase variation does not cause unacceptable changes in the longitudinal phase space of the beam at the IP.

Figure 7.10 shows the longitudinal phase-space parameters—$\Delta E/\sigma_E$, $\Delta\sigma_E/\sigma_E$, $\Delta z/\sigma_z$, $\Delta\sigma_z/\sigma_z$—as a function of extraction phase for NLC. The variations in centroid energy and energy spread are both small compared to the nominal energy spread; similarly, the variations in arrival phase and bunch length are both small compared to the nominal bunch length. Thus, all of the parameters are tolerably insensitive to the injection phase. With its smaller phase jitter, TESLA's longitudinal phase space properties are also acceptable.

7.3.2.8 Multibunch Collective Effects—Ions and Electrons

Linear collider LET designs are unique amongst single-pass accelerators in that their combination of small emittances and long bunch trains imply a potential sensitivity to electron-cloud and ion effects. Preliminary estimates indicate that neither of these effects will have significant impact in the bunch compressor or main linac of any LET, but more study is required of how these phenomena influence the beam in the beam delivery system.

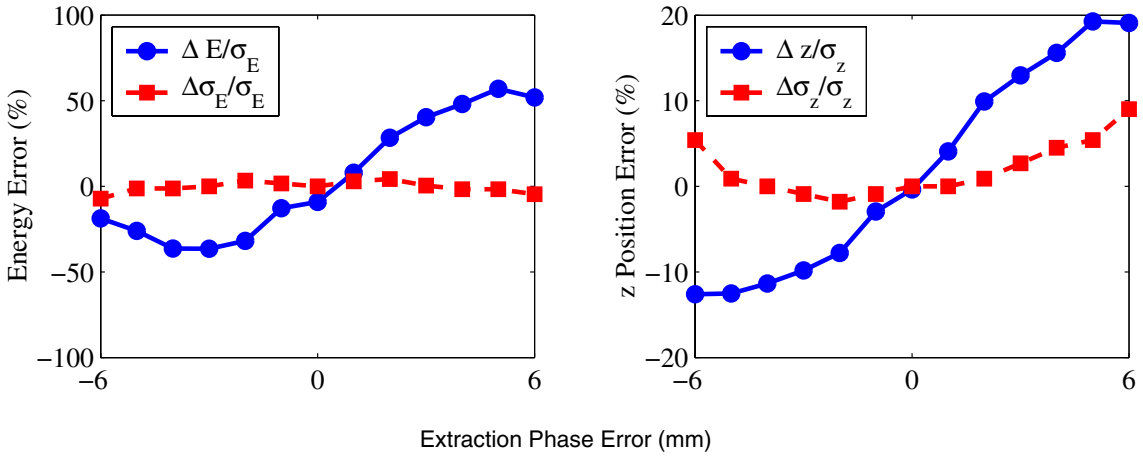

FIGURE 7.10. Variation in NLC IP parameters as the phase of LET injection is varied from −6 mm to 6 mm: (left) centroid energy and energy spread, normalized to design RMS energy spread; (right) centroid longitudinal position and bunch length, normalized to design RMS bunch length. Note that vertical axis is in percent in both cases.

7.3.2.9 Beam-Beam Effects

At the interaction point, the beam has to be focused to very small transverse dimensions so that high luminosity can be achieved. As a result, each bunch gives rise to a very strong electromagnetic field which focuses the oncoming beam. The strength of this focusing is described by the disruption parameter $D = \sigma_z/f$, which is the ratio of the bunch length to the focal length. In the horizontal plane of all designs one has $D_x \ll 1$; in this case one beam focuses the other like a thin lens. In the vertical plane all designs have $D_y \gg 1$; the beams act as thick lenses. The beam fields strongly modify the particle trajectories during the collision, which results in an increase of the luminosity by a factor of 1.5–2, see Table 2.6, but also to the emission of beamstrahlung which degrades the luminosity spectrum; for a more detailed discussion, see Section 7.4.2.1. At E_{cm}=500 GeV all designs have chosen beam parameters that lead to a dilution of the luminosity spectrum that is comparable to initial state radiation. A better spectrum can be achieved in all of them at the cost of a reduced luminosity.

If the beams do not collide exactly head-on but with small offsets, which are induced by dynamic effects, then the luminosity is reduced. The dependence of the luminosity on the offset is strongly modified by the beam-beam effect compared to the expectation for rigid beams which do not focus one another. Figure 7.11 shows the dependence of the luminosity on the vertical offset for all designs. It is evident that a small offset leads to a larger relative luminosity loss in TESLA than in JLC-X/NLC or CLIC, while at larger offsets the loss in CLIC is larger than in TESLA; the effect is due to the larger vertical disruption D_y in TESLA.

In addition, each bunch can include a longitudinally correlated emittance dilution—a correlation of transverse and longitudinal positions of particles within the bunch—which is induced by wakefields and dispersive effects. It has been shown that this correlation must be

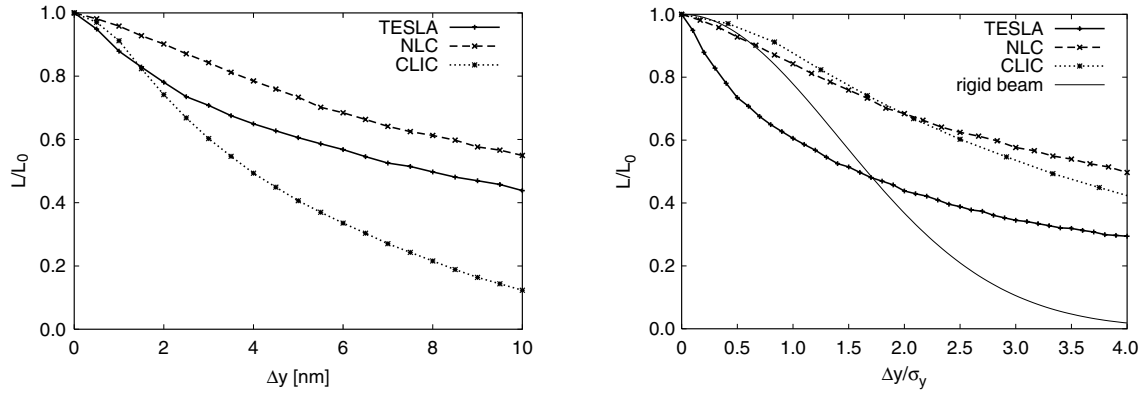

FIGURE 7.11. Luminosity as a function of the vertical offsets of the two beams in absence of correlated emittance growth. Left: offset in absolute values. Right: offset in units of beam size σ_y; an approximation for the luminosity of rigid beams which do not focus one another is shown for comparison.

taken into account in the presence of strong beam-beam interaction (the so-called banana effect); this is again particularly important in the case of TESLA because of the large D_y. It has been shown for TESLA that already a very small growth of the emittance may lead to a large loss in luminosity [33], even if the mean angle and position are corrected to zero.

For this review, simulations of the luminosity in presence of static emittance growth have been performed for all designs [34]. A simplified model for the initial static misalignments was used to achieve the budgeted vertical emittance growth. The beam offsets and angles were not set to zero but rather optimized to obtain maximum luminosity, assuming that no dynamic effects are present. In Figure 7.12, the luminosity in TESLA is shown as a function of the emittance growth in the linac. Three cases are compared: correction of the mean offset and angle to zero; optimizing the mean offset to maximize luminosity while zeroing the mean angle; optimizing the mean offset and mean angle to maximize luminosity. The differences are very significant: in the case of angle and offset optimization, the luminosity impact of a correlated emittance dilution is almost identical to that of an uncorrelated emittance dilution, which is also shown in Figure 7.12 for reference. For the other machines the differences still exist but are less important. With full optimization all designs came close to their target luminosity. If one compares the luminosity found to the target value $\mathcal{L}_0$ before subtracting the allowance for tuning, then one finds $\mathcal{L}/\mathcal{L}_0 = 0.96$, $\mathcal{L}/\mathcal{L}_0 = 1.05$, and $\mathcal{L}/\mathcal{L}_0 = 1.13$, for TESLA, JLC-X/NLC, and CLIC. So the effect of the correlation is not severe in case it is static.

The correlation can however be important in the case for which one cannot optimize the luminosity but is limited to the use of BPM based corrections; this is the case for many feedbacks in the presence of dynamic errors. While TESLA will be more sensitive to the correlated emittance growth than the other machines, it has the advantage of the very long bunch train. This makes it possible to perform a more complete optimization of the collision parameters: the vertical crossing angle and offset can be adjusted bunch to bunch within a train, until maximum luminosity is achieved. This reduces the sensitivity to the banana effect. The dynamic issues will be discussed in more detail in Section 7.3.4.

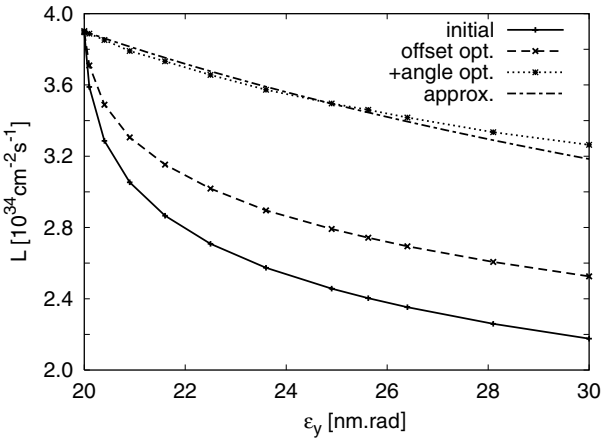

FIGURE 7.12. The luminosity in TESLA as a function of the vertical emittance growth using different levels of optimizations: zeroing the offset and vertical crossing angles of the beams (crosses), varying the offset to maximize luminosity (x's), and varying both the offset and the vertical crossing angle to maximize luminosity (stars). For comparison the approximate scaling with $\mathcal{L} \propto 1/\sqrt{\epsilon_y}$ is also shown; this is the luminosity scaling for an uncorrelated emittance growth.

7.3.2.10 Multibunch Beam-Beam Effects

In the normal conducting designs, the multibunch kink instability is a potential source of luminosity loss. If bunches collide with a small vertical offset at the interaction point, then they receive a strong vertical deflection. After the collision these bunches will have parasitic crossings with the next ones of the incoming beams and, because of their now large vertical offset, will kick them vertically. In the likely case that all bunches in each train have the same offset Δy_0 with respect to the oncoming train, this effect will increase the effective offset at the interaction point Δy. In the limit of an infinitely long train and for small offsets one can express Δy as a function of the crossing angle θ_c in a similar fashion as in [35]:

$$\Delta y = \frac{\Delta y_0}{1 - n_c \frac{4Nr_e}{\gamma\theta_c^2}\frac{\partial y'}{\partial \Delta y}}, \qquad n_c \frac{4Nr_e}{\gamma\theta_c^2}\frac{\partial y'}{\partial \Delta y} < 1$$

Here, n_c is the number of parasitic crossings before the beams are separated, r_e is the classical electron radius and $\partial y'/\partial \Delta y$ is given by the beam-beam deflection at the collision point and is derived from simulation. For NLC and CLIC one has $n_c = 14$ and $n_c = 15$ and finds $\Delta y = 1.16\Delta y_0$ and $\Delta y = 1.14\Delta y_0$, respectively. Consequently, the luminosity loss due to beam jitter is increased by at most 30% compared to the single bunch case. In JLC-X (n_c=9) the crossing angle is smaller than in NLC (7 mrad compared to 20 mrad) so this formula cannot be applied. In this case, the offset continues to increase from bunch to bunch, and numerical evaluation is necessary. In Figure 7.13 the tolerable offset is shown as a function of the acceptable luminosity loss. In case of NLC and CLIC the multibunch effect is small, as expected, while it tightens the JLC-X tolerances by a significant factor. In JLC-X, to achieve $\Delta y = 1.2\Delta y_0$, which would be roughly comparable to the effect in the NLC, either the crossing angle has to be increased or it would be necessary to have a

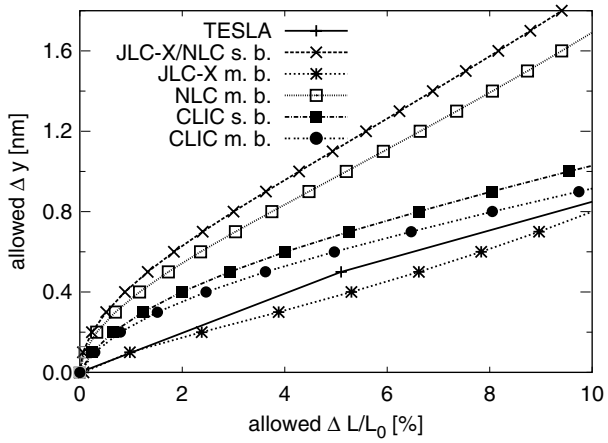

FIGURE 7.13. The allowed offset as a function of the allowed luminosity loss. In the case of NLC and CLIC the multibunch case (m.b.) does not require much better stability than the single bunch case (s.b.). In the case of JLC-X the tolerance is tightened significantly by the multibunch kink instability. In TESLA no multibunch effects exist.

conductive shield between the incoming and the outgoing beamline starting at about 60 cm from the IP, leading to n_c=2. The resulting wakefield effects and the impact that the shield has on the background conditions in the detector need careful study. In the case of TESLA, the very large bunch spacing implies that even if a crossing angle were adopted there would be no parasitic crossing, hence no luminosity loss from the multibunch kink instability.

7.3.2.11 Bunch-Charge and Train-Charge Variation

The luminosity impact of bunch-by-bunch and train-by-train variation in charge extracted from the damping ring has not been reviewed. The impact of variation in charge is expected to be small for all LET designs.

7.3.2.12 Emittance Growth in Error-Free LET—Summary

It is now possible to summarize the sources of emittance growth which are anticipated in the error-free LET:

- Initial emittances (see Table 2.3)
- On-axis optical growth, from Table 7.15
- Single-bunch jitter, from Table 7.16, and assuming that the initial beam jitter is 0.1 σ in each plane and betatron phase
- Multibunch wakefield effects, from Table 7.14, and assuming the same 0.1 σ jitter
- Incoherent and coherent synchrotron radiation, including the final doublet, from Section 7.3.2.5

- Assuming that the initial jitter is 0.1 σ, and that the jitter has filamented as shown in Table 7.16, the effect of collimator wakefields can be neglected for the error-free LET, although these wakefields are likely to become more important when beam jitter induced by quadrupole vibration is included
- The beam-beam offset at the IP due to incoming jitter will be under 0.1 σ in all cases, and the luminosity loss indicated by Figure 7.11 can be neglected
- The luminosity loss from the "banana" and from the beam delivery system bandwidth are neglected

Table 7.18 summarizes the resulting growth in emittance, and compares the result to the IP emittances from Table 2.6. In most cases the emittance growth which is inherent to the designs is small compared to the growth budget, which implies that there is considerable "margin" available to errors and tuning limitations. The exception is the horizontal plane emittance growth in NLC, which exceeds 50% of the growth budget.

TABLE 7.18
Emittance growth for each LET design due to effects present in an error-free LET lattice. "N/A" indicates a value that was not yet available at the time of writing. Initial emittances for TESLA and JLC-X/NLC are damping ring extraction values, while for CLIC, main linac injection values are used.

Item	TESLA		JLC-X/NLC		CLIC	
	$\gamma\epsilon_x$ [μm·rad]	$\gamma\epsilon_y$ [nm·rad]	$\gamma\epsilon_x$ [μm·rad]	$\gamma\epsilon_y$ [nm·rad]	$\gamma\epsilon_x$ [μm·rad]	$\gamma\epsilon_y$ [nm·rad]
Initial	8.0	20	3.0	20	1.8	5
On-axis optical	0.12	1.5	0.06	0.8	0.02	0.44
Jitter	0.05	0.16	0.02	0.12	0.007	0.02
MB BBU	0	0	0.006	0.04	0.005	0.013
Incoherent SR	0.037	0.57	0.22	0.52	0.005	0.14
Coherent SR	0.080	0	0.08	0	N/A	0
Total	8.29	22.2	3.39	21.5	1.84	5.61
Nominal at IP	10	30	3.6	40	2	10

7.3.3 Quasi-Static Errors

The luminosity performance of a linear collider is influenced by a large class of errors that are approximately constant in time. This class of quasi-static errors is typically related to manufacturing or installation tolerances of the beamline elements. With few exceptions, quasi-static errors are amenable to tuning via the use of beam-derived signals (BPM or beam size measurements, luminosity, *etc.*). Thus, in most cases the problem of quasi-static errors reduces to ensuring that the specifications on the diagnostics and control points of the LET are adequate, and that the algorithms that fall between the diagnostics and the control points are properly designed and capable of functioning in the real-world accelerator environment.

The most pressing issues in the LET's quasi-static regime are the alignment of the beamline elements, especially those in the main linacs, and the tuning of the beam delivery system. This is where the vast majority of the effort has been invested in LET studies in the last several years. Ironically, it is just this aspect of the LET that has proven impossible to review adequately due to the sheer volume of the task. Fortunately, all other quasi-static error issues in the LETs appear to be in good condition, and even the tuning and alignment issues are close enough to convergence to give confidence that in the near future a review of the latter will be completed and that it will, indeed, find that the LET can be tuned to yield the desired luminosity performance.

A Note on Emittance Budgets All three of the LET designs considered has a "budget" of the amount of emittance dilution that can be accepted, and a tentative distribution of the amount of dilution from each source (quadrupole misalignments, rf misalignments, *etc.*). These budgets are briefly described in Chapter 3. Although we conclude that the total budgeted emittance dilution is reasonable in each case, we were not able to validate the expected distributions; in particular, emittance dilutions from the misalignments of the main linacs tended to be larger than what is anticipated in the designs. A completely validated emittance budget, backed by an expected distribution of sources which is supported by analytic and/or simulation studies, is an important R&D project which must be pursued.

7.3.3.1 Beamline Magnets: Field Quality, Strength Errors, and Stray Fields

Comprehensive studies on the effect of magnet field quality and absolute setting accuracy have not been performed for any of the candidate LET beamlines. Nonetheless, there is good reason to believe that the tolerances on these parameters will be extremely loose for nearly all magnets in all the LET designs.

A small number of magnets will have relatively tight tolerances on their strength and/or field quality: the final doublet quadrupoles and a few other quads at the high-beta points in the beam delivery areas, the quadrupoles in the spin manipulation beamlines, and the quadrupoles in the high-beta points of the NLC's pre-linac energy collimation may fall into this category. These devices constitute a small fraction of all the magnets in the LET, and thus can be constructed and tested to tighter tolerances than the "rank and file" magnets. If necessary, tuning multipole magnets can be used to compensate multipole errors in some of the magnets. Finally, beam-derived signals can be used to tune the strengths of the magnets in many cases.

The effects of stray fields, from the magnetic field of the Earth to "cultural stray fields" introduced by the accelerator and its support systems, have not been considered in any systematic fashion. Their impact on the accelerator in general and in particular on the tuning algorithms should be studied carefully.

7.3.3.2 RF System Errors

Fixed errors in the phase or amplitude of the accelerating field can arise from calibration errors in the rf sources, or from installation or construction errors in the accelerator structures. The luminosity performance is most dependent upon the accurate control of the

bunch compressor rf systems. The sensitivity of several parameters to the bunch compressor rf phase and amplitude jitter is studied in Section 7.3.5.3; the sensitivity to static errors is comparable to the sensitivity to jitter. In the likely event that these tolerances cannot be met *ab initio*, it will be necessary to tune the bunch compressor rf systems with beam-derived signals (see Section 7.3.3.4).

The principal luminosity impact of small errors in the other rf systems is an energy mismatch between the beam and the final focus; in Section 7.3.2.4 it was shown that the bandwidth over which the final focus will deliver luminosity was about 1% at best for all three designs. All three LET designs can accommodate errors in the IP beam energy by adjusting the linac energy gain or by adjusting the strengths of magnets in the beam delivery system. A secondary impact of small rf errors is that the beam energy is not known precisely at all points in the LET, and hence the knowledge of the optics is limited. Limited knowledge of the optics can influence the effectiveness of beam-based tuning, as discussed in Section 7.3.3.4.

7.3.3.3 Misalignment of Elements at Time of Installation, and Beam-Based Alignment

The alignment tolerances of elements in the LET which are required for luminosity performance are extremely tight. Table 7.19 shows RMS vertical misalignments of the main linac components which would result in a 1 nm vertical emittance growth, and the expected *ab initio* accuracy of equipment installation. Inspection of Table 7.19 shows that none of the LET designs will meet the required performance if the beam is simply steered to minimize the RMS BPM readings, and therefore a more aggressive beam-based alignment procedure is required. In addition, both JLC-X/NLC and CLIC have tight beam-to-rf-structure tolerances that can only be met by using certain beam signals to align the rf elements; TESLA currently foresees no need for such a correction.

Each of the LET designs has received significant attention in the area of main linac alignment and tuning; tuning and alignment of the bunch compressors and beam delivery systems is much less mature. The key features of each design as regards beam-based alignment are summarized here.

TESLA: The TESLA main linac quadrupole magnets are superconducting; each quad is installed at the longitudinal center of a cryomodule which also contains a beam position monitor near the quad position, a vertical steering dipole, a horizontal steering dipole (in the case of horizontally focusing quads) and 12 accelerating cavities. Not all cryomodules contain quads: in the first half of the linac, 50% of all cryomodules are so equipped, while in the second half only 33% of all cryomodules contain quads.

During cryomodule assembly, the contents of each module are aligned with respect to its external fiducials to the tolerances shown in Table 7.19. The assembled module is then installed in the tunnel and aligned to a precision of 0.2 mm with respect to the survey line. The survey line itself is constructed with an absolute accuracy of approximately 20 μm over several hundred meters.

The procedure for beam-based alignment of the linac calls for minimization of the BPM RMS values, followed by dispersion-free steering [36] (DFS) to minimize the

TABLE 7.19
Upper table: RMS misalignments required to achieve a 1 nm growth in vertical emittance in the main linac of each LET. Emittance growth estimates assume that the beam is steered to zero BPM readings (TESLA), or that the beam is steered via quad movers and that rf girders are then aligned to the beam trajectory (JLC-X/NLC and CLIC). Lower table: Expected *ab initio* component installation accuracy.

	TESLA	JLC-X/NLC	CLIC
Luminosity tolerances			
BPM offsets [μm]	11	1.3	0.9
RF structure-to-girder offsets [μm]	300	200	115
RF structure-to-beam offsets [μm]	300	5.0	4.0
RF structure tilts [μrad]	240	135	225
Installation accuracy			
Quadrupoles [μm]	300	50	50
with respect to	Cryomodule	Survey line	Stretched wire
Structure offsets [μm]	300	25	20
with respect to	Cryomodule	Girder	Girder
Structure tilts [μrad]	300	33	20
with respect to	Cryomodule	Girder	Girder
BPMs [μm]	200	100	10
with respect to	Cryomodule	Quadrupole	Stretched wire
Module/girder offsets [μm]	200	50	7
with respect to	Survey line	Survey line	Stretched wire
Module/girder tilts [μrad]	20	15	7
with respect to	Survey line	Survey line	Stretched wire
BPM resolution [μm]	10	0.3	0.1
Structure BPM resolution [μm]	N/A	5	10

emittance. Depending on how well the DFS converges, local orbit oscillations designed to globally cancel either dispersion or wakefield emittance growth can be applied.

JLC-X/NLC: The JLC-X/NLC quadrupoles are at room-temperature: the baseline design calls for maximal use of hybrid iron-dominated/permanent magnets, with iron-dominated electromagnets in a small number of locations where the hybrids are not acceptable. Quadrupoles are installed on dedicated supports (*i.e.*, they do not share a girder with any rf devices), and each quad is mounted on a remote-controlled magnet mover based on the FFTB design [37]. Each quad also has a BPM attached to it, so that the magnet mover moves both the quad and the BPM. Six rf structures, each 0.9 m long, are installed on a single 6 m girder. Each rf girder has a mover which allows horizontal, vertical, pitch, and yaw motions.

Quadrupole-BPM packages and rf girders are assembled and aligned to the tolerances specified in Table 7.19. The girder is then installed in the tunnel and aligned to the survey line with accuracy of 50 μm and 15 μrad in the vertical.

The beam-based alignment procedure calls for the initial use of quadrupole variation to measure the approximate BPM-to-quad offset. The beam is then steered to minimize the RMS of the BPM readings via the quadrupole movers. It is foreseen that some form of DFS may be required for the NLC main linac quads, as well as orbit bumps for minimization of dispersion. The alignment of the rf girders relies upon measurement of the beam-to-structure offsets via measurement of the phase and amplitude of higher order modes in the structures [38]. This technique permits the offset of the beam with respect to the structure to be measured with an approximate accuracy of 5 μm. The girder is then moved to reduce the average offset and the average slope of the structure readouts to zero. Because the betatron phase advance per structure is not large, this allows the wakefield deflections of the 6 structures on a girder to be nearly cancelled.

CLIC: The CLIC main linac quadrupoles are electromagnets with dedicated supports. Each quad is mounted on a magnet mover, and also contains dipole steering magnets. There is a beam position monitor immediately upstream of each quad; the BPMs do not move with the quadrupoles. Four rf structures, each 0.5 m long, are mounted on a common girder 2.23 m long. Adjacent girders are mounted to common articulation points which can be remotely actuated to adjust the positions and angles of the girders. Note, however, that the girders cannot be moved independently of one another: moving a single articulation point changes the position of the two girders mounted to that articulation point. Like the JLC-X/NLC structures, the CLIC structures are instrumented to permit measurement of high-order mode amplitude and phase (and thus beam-to-structure offset), with an assumed resolution of 10 μm.

The rf girders are assembled and pre-aligned to the tolerances specified in Table 7.19. RF girders, quadrupoles, and BPMs are installed in the tunnel and final alignment is accomplished with a combination of laser and wire-alignment systems.

Main linac alignment proceeds in several stages. Initially the beam is steered to minimize the RMS of the BPM readings. The quads and BPMs are then ballistically aligned [39], and the rf structures are aligned by moving the rf girders so that the average offset and slope of the readings in the structure's beam position readouts is

minimized. Finally, the emittance growth due to any residual wakefield effects is minimized by measuring the emittance as a function of the vertical position of a selected set of rf structures, and seeking the minimum.

7.3.3.4 Integrated Simulations of Linear Colliders

As stated in Section 7.3.3.3, significant effort has been invested in the simulation of beam-based alignment of the main linacs. Here, all projects foresee to use either dispersion free steering or ballistic alignment (which in the normal conducting machines includes alignment of the rf structures to the beam by use of the internal BPMs) followed by an optimization of the emittance by the use of emittance tuning bumps. In dispersion free steering (DFS), segments with a large number of quadrupoles (about 40 to 50) are corrected by minimizing the difference between the trajectories of two beams with different energies and simultaneously minimizing the absolute offsets of the beams in the quadrupoles. In the ballistic method a ballistic beam is used to align a number of consecutive BPMs (typically 12 to 16) and when the quadrupoles are switched on again, they are aligned in a second step to restore the ballistic trajectory.

Cross-checks of the simulations performed for the different projects are necessary to establish the validity of the results. The two main programs used in this review to simulate the correction in the main linac are LIAR [40] and PLACET [41]. The comparison of the results was difficult because LIAR used dispersion free steering while PLACET used ballistic alignment. In the framework of this review it was possible to include dispersion free steering in PLACET. While some effort was made to ensure comparability, details of the methods simulated still differ.

LIAR has been used to simulate the effect of dispersion free steering in NLC and TESLA; the resulting emittance growth (before application of the emittance tuning bumps) in the main linac was found to be 20% for NLC [42] and 143% for TESLA [43]. In comparison, one of the models of dispersion free steering implemented in PLACET yielded emittance growths of 13% for NLC and 110% for TESLA. While the agreement is not completely satisfactory, we feel confident that the remaining differences can be resolved. They are likely due to the mentioned details of the methods simulated. These comparisons were made to verify that the implementation of similar correction algorithms yields similar results in the different programs. The very implementation chosen for this comparison is not necessarily the best choice for all of the machines.

Earlier studies of TESLA's beam-based alignment algorithm indicated that the emittance growth at the end of the linac would be at the level of 22%, that the primary source of emittance dilution was wakefields from misaligned rf cavities, and that nearly all of the emittance growth could be cured through use of dispersion-free orbit bumps in the linac [44]. Those studies neglected the effects of pitched rf cavities, which are an additional source of dispersion; including the cavity pitch angles results in a substantially larger dispersive emittance growth at the end of beam-based alignment. An example of a simple modification of the algorithm that can lead to significantly smaller emittance growth is the following. These studies require that the position and angle of the beam be fitted at the entrance to each correction bin using BPMs; the limited precision of this operation degrades the quality of the DFS fit, which contributes significant additional emittance growth [45]. This part of the growth can be avoided, if either the fit is not performed (which requires a

stable incoming beam) or if the BPM resolution is improved by a factor of 2 (which one may be able to achieve by averaging over multiple bunches).

No direct comparison could be made to cross-check the simulations of the ballistic alignment. Since both methods, dispersion free steering and ballistic alignment, correct the dispersion quite well, one would expect that the remaining emittance growth is dominated by the wakefields. In this case it should be the same for both methods. Indeed, simulations for CLIC using PLACET showed that they yield very similar results with both methods, after application of the emittance tuning bumps. Also in the case of TESLA, simulations of ballistic alignment have been performed; they resulted in a growth of about 50% before application of the tuning bumps [45]. This is similar to the value obtained by dispersion free steering, assuming a stable beam. These results give some confidence in the implementation of the methods.

Further study is needed to understand the remaining differences between the programs. The actual implementation of dispersion free steering in the SLC proved to be difficult, likely because of the presence of systematic errors [46]. Therefore an in-depth discussion of all relevant error sources and their inclusion in the simulations has to take place; the impact of dynamic errors on the beam-based correction is of special concern. This will require significant further effort.

7.3.3.5 Multibunch Emittance Growth Due to Structure Offsets and Other Imperfections

Long-range wakefield deflections within a bunch train can be caused not only by coherent betatron oscillations (BBU as discussed in Section 7.3.2.2), but also by offsets of the rf structures or an imperfect trajectory. The multibunch emittance growth has been calculated with realistic offset errors and the design long-range wakefields, as summarized in Table 7.20. The growth is small for all proposals.

TABLE 7.20
Multibunch growth in normalized vertical emittance due to trajectory offsets in the rf structures with realistic machine imperfections. The NLC result [47] assumes 30 μm rms structure-to-structure offsets on a girder as the dominant error source. The TESLA result [48] assumes 500 μm rms structure-to-structure offsets. The CLIC result is from [49].

Machine Design	$\Delta\gamma\epsilon_y$ [nm·rad]
JLC-X/NLC	1
TESLA	0.6
CLIC	0.1

In the case of structures which rely, wholly or in part, upon detuning for wakefield control, there are additional tolerances on the pitch angle of the structure with respect to the beam trajectory, on the straightness of the structure, and on achieving the correct higher order mode frequencies. These tolerances are particularly relevant for TESLA and JLC-X/NLC; the CLIC structures rely much more heavily on damping of higher order modes, and less heavily on detuning, which makes them less sensitive to errors in these parameters.

In a pitched structure the modes in the front and back of the structure are excited with the wrong phase relation for cancellation via detuning or "beating" of the modes. This contribution was quantified for the JLC-X/NLC case with the old 1.8 m long structure, where vertical emittance growth of 1.6 nm·rad is predicted due to the long-range wakefields which result from 50 μrad random structure tilt errors. This is a purely multibunch effect, and it is in addition to the single-bunch emittance growth from structure tilt errors discussed in Section 7.3.3.3. The contributions should be properly evaluated for all LET designs based on their present structure configurations.

Structures that rely upon detuning must also achieve tolerances on structure straightness, since cell-to-cell deformations of the structure, like structure pitch angles, can cause a breakdown in the "beating" of modes which reduces the overall wakefield. This error can be more significant than the structure-to-structure alignment tolerance: for example, the JLC-X/NLC structure-to-structure alignment tolerance for 2 nm·rad worth of multibunch vertical emittance growth is 42 μm, while the cell-to-cell tolerance for the same quantity of emittance growth is only 20 μm [47]; again, this emittance growth is in addition to the single-bunch growth reported in Section 7.3.3.3. Since several JLC-X/NLC prototype structures achieved cell-to-cell construction tolerances which were approximately 2 μm, we conclude that this source of emittance growth can be essentially eliminated.

A third issue for structures which rely upon detuning is that structure fabrication errors can lead to an unacceptable wakefield, depending on the distribution of the errors. In the case of JLC-X/NLC, it has been shown that a 3 MHz RMS error in frequency can cause an emittance growth of more than 50 nm·rad if (a) the error is not correlated from cell to cell in a given structure, and (b) the errors are repeated exactly from structure to structure. Other error modes, such as errors which are random cell-to-cell and also structure-to-structure, are far less critical. Gradual changes in the structure wakefield due to aging, sagging, or damage during fabrication or installation must also be considered. Similarly, the TESLA wakefield assumes 1 MHz RMS dipole mode variation randomly distributed over the ensemble of cavities, and assumes that the limited precision of cavity fabrication is sufficient to guarantee this variation. If the cavity fabrication process does not yield the desired distribution of higher order mode frequencies, then the resulting wakefield could be more severe than is presently anticipated.

The multibunch effects of structure misalignments and fabrication errors are nearly static. Consequently, it is possible to carefully measure the bunch-by-bunch offsets within a bunch train at a few locations and correct these offsets via feedback. The feedbacks in question are both "slow" (in the sense that they apply nearly the same correction to each bunch train) and "fast" (in the sense of using high bandwidth deflectors to shape the bunch trains). All designs can profit from intra-train feedbacks, and improvements in multibunch emittance dilution of up to a factor of 10 [50] or even more [48] are predicted.

In summary, multibunch emittance growth due to structure offsets is for all designs small compared to single bunch effects. This statement is true if the design long-range wakefields are achieved (see comments on multibunch BBU in Section 7.3.2.2). We note that the quoted results have been obtained without emittance bumps for TESLA and the NLC. The effect from emittance bumps should be included in the multibunch simulation. As multibunch effects depend strongly on the structure deformation, further beam dynamics studies should be performed once structure designs are finalized and more operating experience is available for prototype structures.

7.3.4 Dynamic Misalignments

The small vertical emittance and nanometer-size beam at the interaction point (IP) necessarily lead to tight stability tolerances on the components of the LET. The previous section discussed beam-based alignment methods to achieve these tight tolerances starting from more realistic installation errors. This section discusses how well those tolerances can be maintained over time in the presence of ground motion and vibration. Element motion can degrade the luminosity through two mechanisms: separation of the beams at the IP and emittance growth, both caused by trajectory changes.

Beam separation occurs on a faster time scale than emittance growth, so fast that it would be impossible to maintain luminosity for more than a few seconds without beam-based feedback. All linear colliders will rely on the beam-beam deflection signal to maintain collisions with a feedback similar to that pioneered at the SLC. For JLC-X/NLC and CLIC, the primary IP feedback system operates at the machine repetition rate (*i.e.*, train to train), analogous to the SLC system. Both machines plan additional mechanical stabilization of the final doublets (FD). TESLA plans to use fast kickers within the long ($\sim$1 ms) bunch train to correct the offset based on the signal from the first few percent of the bunches. Because of the large capture range of this feedback, further stabilization of the FD is not currently foreseen.

The second loss mechanism, emittance growth, is driven by the slower drift of the orbit in the upstream sections of the LET, resulting in spurious dispersion, coupling, *etc.* Feedback is necessary to maintain the "gold orbit" established by the initial tuning. This feedback operates train to train and hence, the warm machines have an advantage because of their higher repetition frequency. For both the IP offset and beam size stabilization, TESLA has the tightest tolerances due to the large vertical disruption parameter (see Section 7.3.2.9). For a 10% luminosity loss, TESLA must achieve a beam-beam offset less than 0.8 nm ($0.16\sigma_y$), compared with 2 nm for JLC-X/NLC ($0.67\sigma_y$) and 1.2 nm for CLIC ($0.8\sigma_y$). TESLA is also very sensitive to longitudinal correlations within the bunch ("banana effect"), which coupled with the low repetition rate of the feedback, makes it difficult to maintain the orbits to the required tolerance.

Long term stability on time scales of hours to months can have a significant impact on integrated luminosity performance as it determines the frequency of invasive tuning. This has been studied extensively for both the linac and beam delivery system using a slow diffusive ground motion model. The studies concluded that the luminosity would be stable for extended periods providing the gold orbit was maintained by feedback or corrections, and the BPM offsets are stable.

Although a large number of studies have been done over the years, and as part of this review, the results presented have all come from simulations. The ground motion models are based on data derived from measurements at various sites but a complete representation of an actual site is very difficult. For example, although many noise sources were identified, the SLC beam jitter was never fully understood. These simulations are indicative of the expected performance but they have not been benchmarked against real machines.

7.3.4.1 Ground Motion Models

It is important to model element motion in both the spatial and the frequency domain to properly understand its impact. The frequency spectrum is important when considering the feedback performance, and spatial information is important for correlation effects. For example, even large amplitude motion which is spatially correlated does not affect collider performance. Sources of motion include natural ground motion, human-produced "cultural noise" and noise sources on the support girders themselves (*e.g.*, cooling water flow). In addition, the girders may amplify existing noise sources.

Ground motion amplitudes vary significantly from site to site, and depend on many conditions. Fast vibration can range from sub-nanometer to hundreds of nanometers. The coherence of the motion depends on geology (*i.e.*, sound phase velocity) and on the spatial distribution of the noise sources. Slow motion depends mostly on natural (human independent) phenomena and parameters, such as rigidity and homogeneity of the rock, underground water flows, rain, depth, and atmospheric pressure variation.

Several comprehensive studies of ground motion have been made and more are in progress. Different types of motion (slow diffusive ATL motion, systematic motion, elastic waves, vibration, *etc.*) have been identified and characterized and their properties studied. These studies, both experimental and theoretical, have been used to create quantitative models of ground motion which include both natural and man-made sources that are typically present in the tunnels of large accelerators. To span the intrinsic variability of the phenomena and of site conditions, three models of ground motion were considered.

Three noise models (**A**—"Low," **B**—"Intermediate," and **C**—"High") were used to cover a wide range of conditions. These models are based on measurements on the tunnel floor of LEP and at representative sites in California for **A**, at the SLAC tunnel and the Aurora mine near Fermilab for **B**, and on the tunnel floor of HERA for **C**. (Section 7.3.4.6 contains more discussion on expected noise for the different LC projects.) For this study, the ground motion models were considered project independent. Additional contributions coming from noise generated on the girder or amplified by imperfect girders are project specific and are evaluated separately for each machine. Another potentially important source of noise is the experimental detector which affects the stability of the final doublet (FD). This FD noise is assumed to be project independent (although different technical solutions are envisioned for CLIC, JLC-X/NLC and TESLA as discussed later).

The spatial and temporal properties of ground motion may be described by a 2-D power spectrum. The traditional 1-D power spectra for absolute motion and for relative motion between two separated points can be obtained from the 2-D spectrum, and an example is shown in Figure 7.14 for the three models studied. The models include a contribution from diffusive ("ATL") motion that dominates at low frequencies and vanishes for high frequencies, and a contribution from isotropically distributed plane waves propagating in the ground which represent fast motion including cultural noise. Details of the models and relevant parameters can be found in [52]. To simulate the effects of ground motion on collider performance, the models were implemented in the codes Matlab-LIAR and PLACET.

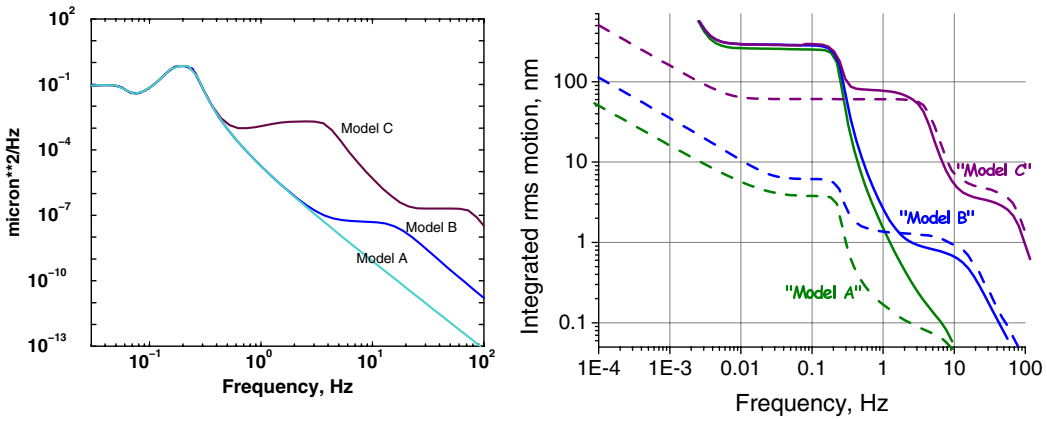

FIGURE 7.14. Ground motion model spectra. The absolute spectra (left), the integrated absolute spectra (right, solid lines) and the integrated relative (for ΔL=50 m) spectra (right, dashed lines).

7.3.4.2 Detector Noise and Active Stabilization

Any additional vibration introduced by the experimental detector is a specific concern since the final doublets (FD) may be partially supported by the detector, and they have the tightest jitter tolerances. Unlike ground motion, which has been studied extensively, little data is available on the motion of elements inside the detector. Some measurements were made at SLD in 1995 [51] and in 2000, and the 1995 measurements are shown in Figure 7.15. The data indicate about 30 nanometers of final doublet relative motion due to detector vibration from measurements made under less than optimal conditions. At HERA differential motion across the IR hall was measured to vary from 100 nm to 200 nm depending on conditions, but this hall is situated in a very noisy location [53]. These measurements are not really indicative of what can be achieved as neither detector was designed to minimize vibration. Data taken in the detector hall of OPAL at LEP showed integrated ground motion of only 0.7–1.2 nm rms above 5 Hz. This would be relevant if the FDs were cantilevered from the tunnel rather than partially supported by the detector (as for SLD). The optimal support system for the FDs is still under study. At the stability level required for the warm machines (nanometers above 5–10 Hz), mechanical resonances of the magnet itself or other effects which can move the magnetic center are concerns and require further study.

Given the uncertainties in detector noise, we have assumed a project independent model for detector vibration, based loosely on the SLD measurements, and shown in Fig. 7.15 (left). In a properly designed site, one could expect a lower value to be achieved. This amplitude of FD motion would require active stabilization for the warm machines. JLC-X/NLC and CLIC propose to use a combination of laser interferometers and/or mechanical motion detectors as sensors driving piezoelectric or electrostatic mechanical actuators or dipole correctors to adjust the position of the FD magnetic center. This approach can optimally

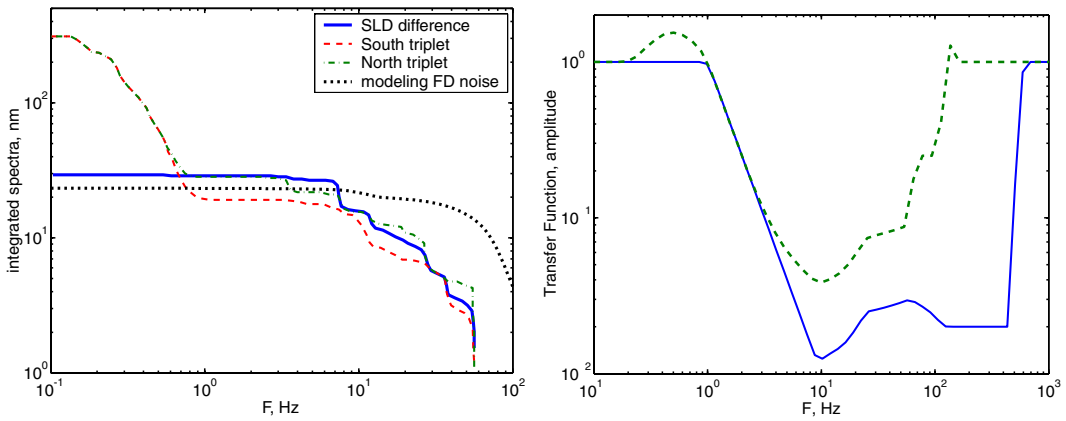

FIGURE 7.15. Results of 1995 vibration measurements on the SLC detector [51] (left plot). The integrated spectra show that the difference of the motion (solid line) of the South triplet (dashed curve) and the North triplet (dash-dot curve) is about 30 nm, as measured by two STS-2 seismometers installed on the triplets. The black dotted line shows an approximation for the FD noise used in the integrated simulations, which extends to higher frequencies to represent more accurately the expected spectrum after low frequency detector modes have been suppressed. The right plot shows the modelling transfer functions used in simulations to represent FD stabilization (dashed: already achieved; solid: expected performance with new sensors).

be applied to magnets which are stiff and light in weight, such as permanent magnets, but compact superconducting magnets may also be a possibility. In recent studies, a CLIC electromagnet has been stabilized to 0.9 nm above 4 Hz, a factor of 10 reduction with respect to the supporting ground [54]. Continuing such studies and demonstrating the performance of a full system is an important R&D item.

For TESLA, with an intratrain feedback capture range of about 100 nm, there would be no need for additional FD stabilization even under SLD conditions. However, differential motion at the level measured at HERA could pose a problem for TESLA and would be prohibitive for a warm machine.

7.3.4.3 Simulation Results

To study the effects of ground motion and its interaction with feedback systems, new integrated simulations of fast (train-to-train) luminosity stability were performed as part of this review. The simulations included the three ground motion models and detector noise model just described, a realistic model of train-by-train and an idealized model of intratrain IP collision feedback, and an idealized model of active stabilization of the final doublets. The train-by-train feedback, based on the NLC design [55, 56, 57], was reoptimized for each vibration assumption. The intratrain feedback was simulated in a "simple" version where the average position and angle offset was simply zeroed, and latency was ignored. For TESLA, a "full optimization" version was also studied which varied the offsets during the train passage to find maximum luminosity. This is useful because the banana effect can

cause the optimal offsets to change on a train-to-train basis. The doublet stabilization was modelled by the idealized transfer function shown in Figure 7.15 (solid) and for some cases with a more realistic curve (dashed). The former represents expected performance with new sensors being developed, the latter what has been already achieved.

As a starting point, the machines were misaligned and then a simple one-to-one trajectory correction was applied to mimic a "tuned" collider. In addition to quad and structure offsets, structure tilts must be included, as their effect is significant and had been omitted from some previous studies. The rms magnitudes of the misalignments were chosen to produce nominal luminosity on average and to reproduce approximately the expected amount of yz and $y'z$ correlation along the bunch to realistically account for the banana effect (see [58] and [57]). In all cases, the time-dependent luminosity was calculated for 256 trains at the machine repetition rate, corresponding to an elapsed time of 51 s for TESLA, 2.1 s for JLC-X/NLC and 1.3 s for CLIC. For TESLA, this time is long enough to see a slow degradation in luminosity from emittance growth due to orbit errors in the BDS, and consequently requires the inclusion of an upstream orbit feedback, not needed on a 1–2 s time scale. The simulations were done with Mat-LIAR and PLACET, with good agreement between the codes for the cases cross checked. Both used GUINEA PIG for a full simulation of beam-beam effects. The Mat-LIAR simulations alone required over half a year of CPU time. For these studies, only one bunch was tracked, and bunch-to-bunch effects were ignored. Figure 7.16 is an example of results showing luminosity as a function of train number for each project.

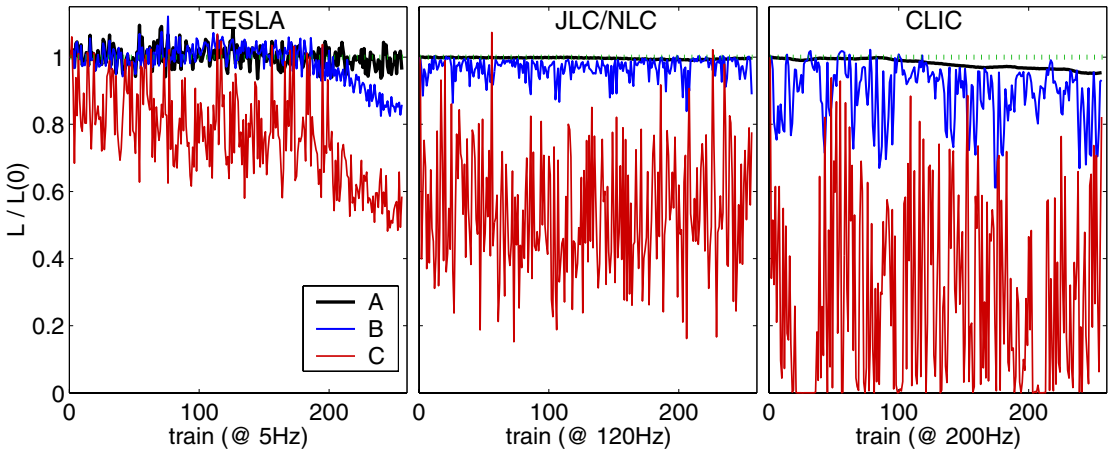

FIGURE 7.16. Example of simulations of TESLA, JLC-X/NLC and CLIC for three models of ground motion with simple intratrain IP feedback for TESLA and train-to-train feedback for the others. The final doublet follows the ground with no additional vibration due to the detector.

The simulation results are summarized in Figure 7.17 showing the percentage of luminosity obtained for each LC under GM models **A** through **C**, with and without additional final doublet vibration induced by the detector, and with different combinations of IP feedbacks and FD stabilization. Each point represents three different seeds for the machine and for

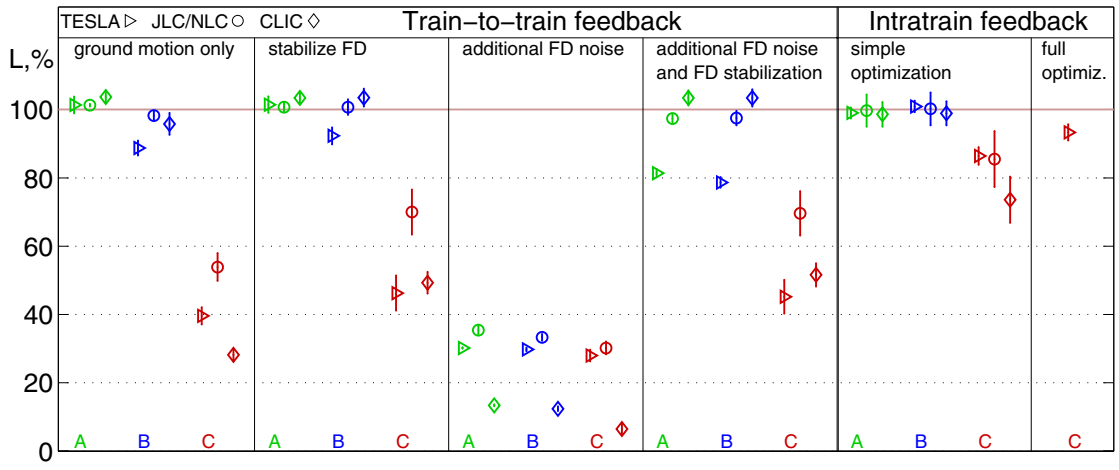

FIGURE 7.17. Percentage of luminosity obtained for each LC with ground motion models **A**, **B**, **C**, with and without additional vibration of FD, and with different combinations of IP feedbacks and FD stabilization. With the intratrain feedback, neither FD noise nor stabilization was included. The results are averaged over 256 trains (50 for TESLA). The error represents the statistical variation in mean luminosity.

the ground motion. The results are averaged over 256 trains (50 for TESLA). From these studies, one can draw the following conclusions:

- For ground motion models **A** and **B** with no additional detector noise, all designs maintained nominal luminosity with the specified beam-based IP feedback alone (simple intratrain for TESLA, train-by-train for the others).
- If a pessimistic estimate of detector noise is included, then the luminosity for JLC-X/NLC drops to ∼35% and for CLIC to ∼12%, independent of ground motion model. Doublet stabilization effectively recovers full luminosity, but only for models **A** and **B**. For TESLA, the intratrain feedback is expected to compensate for detector noise.
- For ground motion **C**, there was a significant deterioration of the luminosity. Even without detector noise, the luminosity dropped to below 30% for CLIC and below 60% for JLC-X/NLC. Doublet stabilization only improved this to 50–70%, independent of whether detector noise was included. For TESLA, the luminosity was 85% assuming a simple intratrain angle and offset feedback. This could be raised to 95% with the intratrain luminosity maximization.

For completeness, TESLA was also simulated using only a 5 Hz train-to-train feedback, without the planned intratrain system. For the worst case of model **C** with additional detector noise and no stabilization, the luminosity dropped to about 30%.

In addition to ignoring multibunch effects, a number of other potentially important issues were either not included or considered in too idealized a fashion. Realistic effects of the intratrain position and angle kickers were not included, but are being studied [59]. The

results for the intratrain IP feedback would indicate that it can be quite effective for all designs, but this is misleading as the feedback latency was not included in the simulations and is significant for the warm machines. For more pessimistic assumptions on FD stabilization, (Figure 7.15 right plot, dashed line) less FD vibration can be accommodated without degrading the luminosity, although for the case of NLC, model **B**, SLD noise and poorer stabilization, the luminosity loss was only 25% . Another concern is jitter amplification, due either to wakefields in the post-linac collimation system (see Section 7.3.2.6), or to multibunch beam-beam effects with a crossing angle (see Section 7.3.2.10). The interplay of different feedback systems with different time scales has not been considered in sufficient detail. Hardware imperfections have also been omitted such as beam losses affecting position monitors or finite resolution of the fast luminosity monitors. These studies also did not evaluate the effect of stabilizing other quads in the linac or beam delivery system, which could improve performance.

7.3.4.4 Impact of Jitter on Slow Tuning

The stability results quoted in the previous section assume that a machine has been tuned to peak luminosity at time zero. This is a valid approach to investigate the stability of the luminosity, but the effectiveness of the initial tuning itself (outlined in Section 7.3.3.4) will also be influenced by the dynamic errors. If train-to-train luminosity variation is significant, then the tuning will need to average many trains, increasing the "tuning" time. However, the tuning will only converge if it can be completed before any uncompensated slow drifts can accumulate. Results from the previous section's stability studies suggest typical RMS train-to-train luminosity variation should be <10% for models **A** and **B**, and as large as 25–30% for model **C**. For TESLA with simple intratrain feedback, this can be reduced to ∼15%, and to ∼8% with the full feedback. Figure 7.18 shows simulations of TESLA with ground motion **C** and the full feedback, where the optimal vertical offset and angle found by feedback can vary between trains by 36% of the nominal beam size.

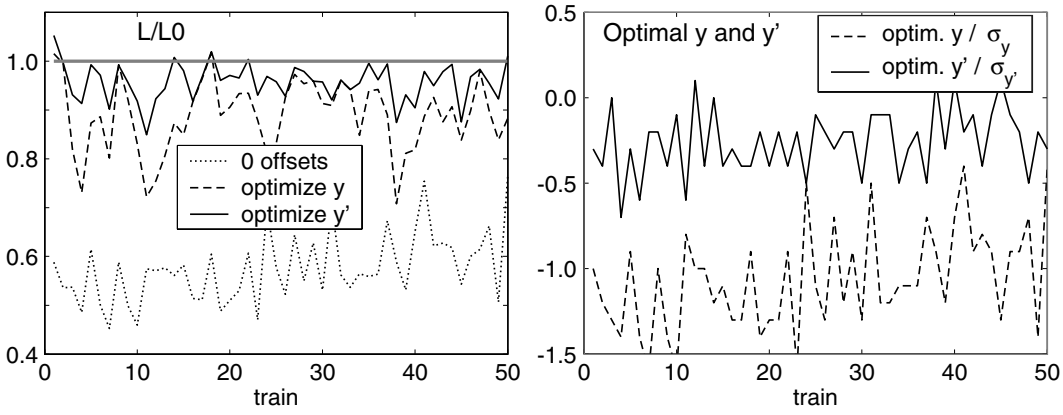

FIGURE 7.18. TESLA simulations with ground motion **C** and intratrain IP feedback with full optimization. Left: Normalized luminosity. Right: Optimal y/σ_y and $y'/\sigma_{y'}$ with respect to zero offsets. Only one seed is plotted.

Luminosity variability is not the only issue of importance for tuning. Train-to-train position or energy jitter throughout the LET can cause train-to-train changes in the beam size and shape, as well as backgrounds. These all impact the accuracy of the beam size and position diagnostics required to tune up the machine. Experience at the SLC would indicate that an untuned machine can be more unstable than a tuned machine, making it difficult for the procedures to converge.

Additional technical sources of noise, not included in these simulations, can potentially increase the train-to-train jitter. Extreme care should be taken not to allow machine components to introduce noise above the bandwidths of the various feedbacks (for TESLA this includes high-frequency noise within the bunch train). Obvious candidates for potential "white noise" sources are damping ring extraction kickers, rf systems, and any other pulsed systems. TESLA is especially sensitive here, due to the tight beam-beam tolerances set by the high disruption parameter. At some point, the jitter will become a significant hindrance to the tuning. An averaging over several trains, to reduce the impact of luminosity fluctuations on slow tuning, will be more efficient in warm machines due to their higher repetition rate. In TESLA the intra-train feedback and the possibility of performing some tuning scans within a single bunch train may improve the situation; the extent to which this compensates the lower repetition rate, and the implications for hardware performance, remain to be studied in detail.

The impact of ground motion and technical noise on the tuning is extremely important for all machines. Until these effects are evaluated, it is difficult to quantify with confidence the achievable luminosity.

7.3.4.5 Effects on Longer Time Scales

The previous discussion covered motion on the very fast time scale. On a very long time scale, ground motion (for example, diffusive motion, ground settling, seasonal or diurnal drifts, *etc.*) will gradually degrade the linac alignment, and decrease the luminosity. Many of these effects are modelled by the ATL law or, for systematic motion, with the ATTL law, but typically under the assumption of uniform geology. Care must be taken to ensure that natural geologic discontinuities and non-uniformities do not break the expected correlations of the motion.

Projects foresee different strategies for dealing with these effects. TESLA assumes that the trajectory will be sufficiently stable to be corrected by dipoles located at the quadrupoles. Component realignment would be limited to the yearly shutdowns. JLC-X/NLC and CLIC plan to use active mover systems to quasi-continuously align the components onto the beamline. If the BPM electronics are stable, then invasive beam-based alignment (discussed in Section 7.3.3.3) should not be needed during the course of a run.

For the ground motion models considered, the impact on integrated luminosity should be minimal. In the intermediate time scale, accumulated misalignments will first appear as aberrations in the beam delivery system, which should be curable by BDS orbit correction and slower tuning knobs. The interplay of the BDS orbit correction and IP feedback needs to be studied, especially for TESLA, given its low repetition rate and tight sensitivity to beam-beam offsets. There are also still outstanding questions about the details of the orbit correction implementation that require further study.

7.3.4.6 Assessment of Site and LC Technological Noises

To assess the expected vibration levels at various proposed sites, it is important to consider not only external site and geology dependent noise, but also internally generated noise from collider components. The internal sources depend on the technology chosen but may be almost site independent. The following is a discussion of issues affecting stability conditions for various tunnel and collider configurations, attempting to classify them in comparison with models **A**, **B**, **C**.

If a linear collider is built in a deep tunnel in competent rock, then the noise from external sources when measured on-the-floor will be close to ground motion model **A**. This model was based on data from the LEP tunnel at CERN (about 100 m depth) and similar behavior can be expected in a deep tunnel in Illinois, California or Japan (given appropriate geology). Measurements suggest that surface activity does not greatly influence the noise level in the tunnel.

If a linear collider is built in a shallow tunnel, but on a layer of competent rock, then the noise from external sources is expected to be between ground motion model **A** and model **B**, assuming that the site is sufficiently remote and nearby surface activity is limited. (An issue for further R&D is to clarify requirements on noise sources). An example might be a cut-and-cover tunnel on one of the California sites.

If a linear collider is built in a shallow tunnel in a sedimentary layer with considerable on-surface urbanization and activity, then the noise from external sources when measured on-the-floor may reach or exceed ground motion model **C**. An example would be an LC constructed in the vicinity of DESY in a HERA-like tunnel, for the portion lying under an urbanized area. The more rural part of the tunnel where the IR would be located should be quieter. Further R&D is required to estimate noise levels (issues such as resonances of the top sedimentary layers need to be understood) and measurements are planned. The same estimates would apply to shallow tunnels at KEK or near Fermilab. In general, a shallow tunnel in unfavorable geology and/or in an urbanized area represents the greatest uncertainty and risk in estimating noise levels, and requires extremely careful study.

Technology-generated internal noise will be different for warm and cold machines. One category is the noise generated by machinery (such as cryo systems, water pumps, *etc.*) and power supplies located in parallel utility tunnels or on the surface and transmitted to the collider components through the ground. Such noise sources are of concern (an item for further R&D), and no detailed evaluation is available for either technology. However, such noise sources can likely be suppressed by proper design and vibration isolation (to avoid transmission to the ground), as successfully done in industry and in other projects such as LIGO. Noise sources (*e.g.*, power supplies, electronics with fans, *etc.*) located in the tunnel present another challenge which must be evaluated and their effects minimized (R&D item).

Another category of project-specific internal noise is vibration generated by components located on the support girders. For warm machines, the main issues are vibration generated by cooling water and mechanical coupling from pulsed rf sources to the structures. The linac quadrupoles typically have separate supports and are coupled to the structures only via the ground, and possibly via the beampipe bellows if the BPMs are fixed to the quadrupoles (as for NLC). NLC studies have shown that, while vibration of rf structures due to cooling water can be several hundred nanometers (which is tolerable for them), the coupling to nearby quadrupoles is only about a percent [60], *i.e.*, several nanometers.

Vibration due to cooling water in the quadrupoles was measured to be only on the nanometer scale [61]. Taken together, these considerations suggest that in favorable tunnel and geology, the vibration of linac quadrupoles for warm machines can be as small as the level of the ground motion model **B**, and pessimistically, within a factor of 2–3. Further R&D is needed to demonstrate that the stability of the quadrupoles is sufficient in the full scale final design of the warm machines.

To reach multi-TeV energies, it may be necessary to reduce component motion to somewhat below the level of model **B**. If passive stabilization is not sufficient, then active methods may be used. Recent stabilization studies at SLAC and CERN [62] indicate nanometer stability may be feasible. In CLIC studies, vertical vibration in a water-cooled stabilized linac quad was found to be 0.9 nm without and 1.3 nm with nominal water flow above 4 Hz [63]. Further R&D is needed both to demonstrate a full scale system and to study compatibility with operation of the collider.

For TESLA, possible sources of internal vibration are the rf pulse in the cavities (due to Lorentz forces, piezo-tuners, and microphonics, the first of which is known to cause longitudinal contraction of the cavities by several microns [64, 65]), as well as coupling from the cryogenic systems (pumps, *etc.*). The superconducting TESLA linac quadrupoles are in the same cryomodule as the cavities and supported via a common "girder" (the 300 mm gas return pipe). An important design issue is to ensure that the quadrupoles are sufficiently decoupled from vibration sources in the cryostat. In the latest generation of cryomodule, the quadrupole is mounted directly under a support structure at the center of the module. This location was chosen to maintain static alignment tolerances during pumping and cooldown in spite of the large asymmetrical forces [66], and it may also help reduce vibrations. Both the quadrupoles and the cavities are mounted between bellows to decouple motion through the vacuum chamber, but neither the vibration modes of the quadrupole nor the coupling to the cavities have been quantitatively analyzed.

The first cryomodules installed at TTF in 1995 were equipped with a large number of vibration sensors [67], but no reliable measurements of quadrupole vibration are available and serious investigations have started only recently. Both experimental studies and numerical analysis need to be urgently pursued in order to ensure that the quadrupole vibration amplitudes are not significantly larger than anticipated.

This discussions has focused primarily on the main linacs, where there are hundreds of sensitive components. The beam delivery system has elements with tighter tolerances, but they are sufficiently few that they do not pose a major risk even if individual stabilization were required.

7.3.5 Other Time-Dependent Sources of Error

Although vibration and ground motion are the most important sources of time-varying performance in the LET, they are not by any means the only ones. The remaining time-dependent sources of error are summarized here.

7.3.5.1 Magnet Strength Jitter and Drift

The limitations on magnet strength variation are primarily set by the collision-steering requirements of the linear collider, rather than the emittance control requirements. The RMS beam-to-quad offsets in the quadrupoles after all steering and alignment is complete will typically be tens of micrometers for JLC-X/NLC and CLIC, and hundreds of micrometers for TESLA. These values are large compared to the tolerances established in Section 7.3.3.3 because DF steering tends to result in large but correlated beam-to-quad offsets that cancel one another out over one or two betatron wavelengths. In order to limit the amount of unwanted beam steering occurring in an inter-train period, the fast variation in quad strength must be on the order of 100×10^{-6} for JLC-X/NLC or CLIC, and 250×10^{-6} for TESLA. In the case of TESLA, the tolerance depends upon the IP collision feedback to remove the cumulative effect of the LET quads upon the beam-beam offset; JLC-X/NLC and CLIC tolerances do not rely upon such a feedback. None of the tolerances listed above particularly challenge the state of the art for magnet power supplies. The fast strength variation in permanent magnet quads has not been quantified at this level, but is expected to be acceptable.

Since the TESLA dipole correctors will be used to move the effective quad centers by a similar distance (hundreds of micrometers RMS), their fractional tolerance is comparable to the quad tolerance. Similarly, the horizontal bending magnets can steer the beam at the IP and will demand very tight control of their strength. In many cases, this tolerance can be relaxed by powering bend magnets in series from one $\eta = 0$ point to the next. This tolerance has not recently been evaluated for any of the designs. Another tolerance of some concern is the strength of the vertical bend magnets used to transport the TESLA beam from the damping ring (at tunnel ceiling elevation) to the main linac (at tunnel floor elevation).

Magnets in the beam delivery area also have a strength tolerance based on IP spot size dilution. This topic has been studied in great detail [68, 69]; in general, stability at the 100×10^{-6} level is acceptable for most beam delivery quads, 10–50×10^{-6} is required for several others, and the final doublet magnets have relatively severe tolerances, often as tight as 1×10^{-6}. These tolerances are relevant for a time period between optimizations of the waist position (typically performed by maximizing luminosity), which can be up to a few hours. These tolerances might be of some concern in the case of a crossing angle: inhomogeneous heating of the doublet magnets by time-varying beam tails in the neighboring extraction line may cause unacceptable variation in the strength and/or center position of the final lenses, especially in the case where the latter are permanent magnets. The strength tolerance on strings of bend magnets in the final focus may also be unusually tight, since these magnets can move the beam horizontally in the strong sextupoles of the final focus, which would cause a shift in the longitudinal position of the focal point.

7.3.5.2 Relative Arrival Time

If the beams do not collide at the correct longitudinal position, then the luminosity will be reduced due to the hourglass effect. Estimates based on linear optics give a tolerance of approximately 0.2 β_y^* for the permissible error in the z position of the collision [70]. Although in principle such a path length difference could be caused by a betatron oscillation, the amplitude of the oscillation would have to be of the order of centimeters to

make up a path length change at the level of 100 μm; we therefore discount such a possibility. Other potential sources of IP arrival time variation are tidal effects and timing system jitter. For all these reasons, it is probably essential to have an arrival-time monitor near the IP. In addition, TESLA will probably require some form of chicane for path-length control, since the phase relationship between the electrons and positrons is locked by their positron production and damping ring designs.

7.3.5.3 RF Amplitude and Phase

The relevance of main linac rf amplitude and phase jitter to luminosity performance has not been studied in great detail, primarily because the simple studies which have been performed have shown that, so long as the beam energy at the IP remains within the system bandwidth, these jitters have no impact on luminosity. In general, the tolerances implied by the IP energy stability needs of the experimenters are far tighter than any luminosity tolerance.

This is not true for the bunch compressor rf systems, which manipulate the longitudinal phase space. Table 7.21 shows the tolerances on bunch compressor amplitude and phase which lead to: (a) change in longitudinal IP position of 0.2 β_y^*; (b) change in bunch length of 5%; (c) change in centroid energy of 0.2%; (d) change in RMS energy spread by 25%. If one accepts that the four tabulated sensitivities are equal in their importance to luminosity performance, then the tolerances on bunch length and longitudinal position of the collision point will set the tolerances on the bunch compressor rf systems.

The studies described have all been performed on perfect lattices. Preliminary studies with tuned lattices indicate that no additional difficulties will arise in this case, although this cannot be entirely ruled out without further studies.

The amplitude and phase stability tolerances for the bunch compressor rf systems shown in Table 7.21 are somewhat tighter than the requirements on the main linac systems. These tolerances should nonetheless be achievable with a careful design, which should be possible given the relatively small number of bunch compressor systems.

JLC-X/NLC and CLIC have an additional rf-related tolerance: specifically, the amplitude and phase tolerance for the crab cavities near the IP. The phase difference between the two cavities, $\phi_{e^+} - \phi_{e^-}$, must be stable to approximately 0.025° in the case of NLC (assuming a crab cavity which operates at S-band); this is also discussed in Section 7.4.3.2. The relative phase tolerance for the CLIC crab cavity is comparable, assuming a similar frequency. This tolerance corresponds to a 2% luminosity loss due to horizontal beam offsets at the IP. The other crab cavity tolerances, such as voltage and absolute phase, are much looser and not expected to pose a problem [71].

7.3.5.4 Linac Energy Management

The energy profile along a linac is not constant. The accelerating voltage seen by the beam is a function of the klystron output voltage, the transmission into the structure, the phase between the beam and the rf, and the setting for the rf phase (as a function of BNS damping and bunch charge). All these might change with time, resulting in a varying acceleration from structure to structure. In addition, some accelerator sections can be

TABLE 7.21: Performance sensitivity of bunch compressor rf parameters.

	TESLA		NLC					
			L-Band		S-Band		BC2 X-Band	
Parameter	ϕ [°]	Ampl. [%]	ϕ [°]	Ampl. [%]	ϕ [°]	Ampl. [%]	ϕ [°]	Ampl. [%]
$\Delta z = 0.2\beta_y^*$	0.1	0.5	0.2	2.3	5.5	0.3	0.4	3.0
$\Delta\sigma_z/\sigma_z = 5\%$	4.6	1.4	0.6	2.6	2.4	0.3	7.0	1.4
$\Delta E/E = 0.2\%$	1.7	6.4	0.5	4.2	5.4	0.8	0.8	7.5
$\Delta\sigma_E/\sigma_E = 25\%$	2.0	3.0	1.2	6.0	3.6	0.6	2.0	2.7

switched off completely, due to klystron problems, *etc.* As a consequence, the energy at a given linac point is usually different from its design value. The mismatch between beam energy and linac magnet strength will induce optical errors and can severely deteriorate the emittance optimization in the linac. This was strongly experienced at the SLC, where a change in klystron complement could severely reduce the achievable luminosity. In practice, this means that the quadrupoles must either be rescaled when the klystron complement changes, or else that the lattice must be designed so that the emittance dilution which occurs when the complement changes is tolerably small.

The optical mismatch induced by energy errors is usually not severe, causing a multiplicative emittance growth. This was studied for the NLC, showing that a maximum emittance increase of 5 nm·rad can be expected [72]. Expected effects should be quantified for all proposals, though no major problem is expected.

The robustness of the linac emittance optimization algorithms against energy errors is expected to be more critical. This is most obvious for emittance bumps, which depend on phase advances and beta functions at the locations of errors (anywhere) and the location of correction (bump). Any changes in the Twiss functions can deteriorate the efficiency of correction. This was studied for the corrected NLC linac, but without emittance bumps [72]. A peak emittance growth of 16 nm·rad is predicted, with a typical value of 4 nm·rad. It was observed in the simulation that seeds which experienced a large emittance growth also experienced a large increase in the RMS orbit as reported by the beam position monitor system, which suggests that the emittance degradation was caused by a betatron oscillation that was permitted to propagate freely down the length of the linac. If this is the case, then the inclusion of train-by-train steering feedbacks in the simulation would likely reduce the resulting emittance degradation.

Expected energy errors due to regular imperfections and klystron failures should be included into the simulations of all projects. The change in emittance should be calculated, in order to establish sufficient robustness of correction algorithms against energy errors. If a lattice re-scaling is required, then scaling algorithms should be included into the machine designs and their performance should be quantified. This seems especially important for NLC where permanent linac magnets are used with mechanical strength tuning. The problem of klystron failures does not apply for the CLIC drive beam concept, where luminosity can in any event only be delivered with all drive beams operational.

7.3.5.5 Beam Position Monitor Offset Stability

As discussed in Section 7.3.4, slow ground motion will gradually drive a linear collider out of alignment, and re-steering will be required to recover full luminosity. Re-steering to a particular set of BPM readings ("gold orbit") will succeed only if the BPM offsets do not vary dramatically once the "gold orbit" has been empirically determined. If the offsets do vary, then a more laborious and invasive tuning procedure is required to generate a new "gold orbit." If this procedure needs to be repeated too frequently, then luminosity will never be delivered.

The linac beam-to-quad sensitivities in Table 7.19 also constitute permissible BPM offset changes in the linac after the invasive alignment procedure is complete. The stability requirement for TESLA is therefore approximately 11 μm RMS, which is comparable to the

estimated stability of the LEP BPM system [73]. The NLC requirement is 1.3 μm RMS; in addition, because the NLC design anticipates that the BPMs will be rigidly mounted to quads which are on movers, the NLC quadrupole centers must be stable to this level as well. Stability of BPM electrical offsets at this level has been demonstrated over a 1 week timescale [74], but the larger picture—stability of BPMs and, in the case of NLC, quad centers over months—has not been demonstrated at this level. The CLIC requirement of 0.9 μm is in a similar situation.

These numbers correspond to the required stability of the main linac BPMs. At this time, no similar specifications are available for the BPMs in the beam delivery regions, which may have even tighter requirements. It is also important to note that poor BPM stability can be partially compensated by more aggressive use of global tuning knobs throughout the LET. This option has not been adequately studied at this time.

7.3.5.6 Time-Dependent Stray Fields

At this time, none of the LET designs has a specification of any sort on time-dependent stray fields in the accelerator housing. The consensus of the reviewers is that this phenomenon will not be a significant problem for any of the designs.

7.3.6 Luminosity Issues Related to Energy Upgrades

The most obvious luminosity impact of an energy upgrade in a linear collider is that the normalized emittance dilution in the bend magnets of the beam delivery system scales with the sixth power of the beam energy. In the case of TESLA, horizontal emittance growth increases to 0.01 μm·rad at 800 GeV c.m., while in the case of NLC it reaches to 0.04 μm·rad at 1 TeV c.m. The CLIC beam delivery system for 500 GeV c.m. becomes intractable at an energy of approximately 1.25 TeV c.m.; the system has been designed to permit operation at 3 to 5 TeV c.m. after reduction of the bending angles in both the collimation and final focus regions, and realignment of the other magnets to the new line formed by the bends—no change in the system length is required. The NLC system is similarly designed to operate at energies above 1 TeV c.m. with a geometry change. In both the NLC and CLIC cases the geometry change can be accommodated in a tunnel of reasonable cross-section. The chromatic breakdown due to synchrotron emissions in the 500 GeV c.m. final doublet would increase to unacceptable levels in all three designs; thus, in each design a longer final doublet is envisioned for energies significantly above 500 GeV c.m., except in CLIC, where the doublet length is already sufficient for 3 TeV c.m. Since a longer final doublet introduces more chromaticity, this modification implies somewhat tighter tolerances on the final focus, and can lead to a reduction in bandwidth. Finally, in all cases the vertical beam size is reduced at higher energy, due to adiabatic damping of the emittances and also, in some cases, due to reduced normalized emittances and/or β^* values; this will make the collision stabilization problem more difficult.

In addition to these general issues, each energy upgrade plan has unique features which will impact the luminosity performance. These are summarized here.

TESLA: The TESLA energy upgrade parameters call for:

- A reduction in linac repetition rate from 5 Hz to 4 Hz, which will reduce the effectiveness of train-by-train feedbacks
- An increase in the number of bunches to 4886 per train, and reduction of inter-bunch spacing to 176 ns, which may have some impact on the intra-train feedback; in principle, reduction of the inter-bunch spacing could also increase the severity of long range wakefields, but in practice this does not appear to be the case for the TESLA design wake
- Reduction in single-bunch charge to 1.4×10^{10}, which will reduce the influence of single-bunch transverse wakefields, although this is already not much of a problem for TESLA
- Reduction in damping-ring normalized emittances from 8 μm·rad $\times$ 20 nm·rad to 6 μm·rad $\times$ 10 nm·rad, and in IP normalized emittances from 10 μm·rad $\times$ 30 nm·rad to 8 μm·rad $\times$ 15 nm·rad; preserving the smaller emittances may imply improved performance from the beam instrumentation

NLC: The NLC energy upgrade parameters call for:

- Installation of an additional 6.5 km of accelerator structures and FODO lattice in the section of the tunnel presently occupied by the bypass line, which may lead to additional wakefield emittance growth.
- Increase in β_x^* from 8 mm to 13 mm, which will modestly loosen the beam delivery system tolerances.

CLIC: It should be noted here that the CLIC design and research effort has been targeted at the requirements of the 3 TeV c.m. configuration; the resulting parameters were then scaled appropriately to the 500 GeV c.m. energy of the reference design. By comparison to the latter set, the CLIC energy upgrade calls for:

- Addition of over 11 km of 30 GHz linac per side, which may lead to significant additional wakefield emittance growth; it is anticipated that several additional emittance bumps are required per main linac to manage this source of luminosity degradation
- Reduction in $\gamma\epsilon_x$ at damping ring extraction from 1.6 μm·rad to 0.45 μm·rad, and a reduction in the same parameter at the IP from 2.0 μm·rad to 0.68 μm·rad; this may make the emittance preservation problem more severe, and will further constrain synchrotron radiation emittance growth in all parts of the LET
- Reduction in linac repetition rate from 200 Hz to 100 Hz, which will make train-by-train feedbacks less effective
- Reduction in β_x^* from 10 mm to 6 mm, which will make the final focus more difficult to tune and stabilize, and will lead to increased synchrotron radiation emittance growth in the final doublet; increase in β_y^* from 50 μm to 70 μm, which will ease all of the same issues.

The CLIC upgrade from 500 GeV c.m. to 3 TeV c.m. is foreseen to proceed in stages, so that no single step of the upgrade process becomes intractable. One can nonetheless anticipate that the performance requirements of CLIC beamline devices at the final stage may be substantially stricter than those at the initial stage.

Finally, another option for high-energy operation for all LET designs is to operate the 500 GeV c.m. configurations with reduced current. This permits operation at a higher gradient, hence higher energy, but with a reduced luminosity due to the reduced beam current. The detailed luminosity implications of this option have not been evaluated.

7.3.7 Conclusions

The working group on the Low Emittance Transport (damping ring exit to IP) has studied the designs for the TESLA, JLC-X/NLC, and CLIC LET regions. The studies have included luminosity issues in an error-free LET, as well as luminosity degradation that arises from static and dynamic misalignments and errors, and has also briefly considered the issues relevant to higher-energy operation of each system.

The consensus of the working group is that **from the point of view of luminosity performance, the feasibility (as defined in Section 7.1.3) of each LET design has been established.** Our additional major conclusions are as follows:

- The basic, error-free designs of each LET are in a mature state. Decks exist for all important beamlines, and the fundamental design issues for a linear collider LET have been properly addressed. These issues include but are not limited to: synchrotron radiation, transverse wakefields from accelerator structures, optical aberrations in the final focus and elsewhere, and severity of the beam-beam interaction.
- The simulation codes used to assess the performance of the LET have been checked and carefully cross-compared for the case of the error-free designs, and in general agreement between the codes is good; this leads to confidence in the results of tuning or dynamic simulations performed using the same codes. Similarly, multiple codes were used in the study of dynamic misalignments, and their results were generally in good agreement.
- Simulations of main linac alignment and tuning were performed on multiple simulation codes. The results agree at the level of approximately a factor of 2 in the worst case; it is believed that the discrepancies are due to differences in the details or assumptions of the algorithms, and will be resolved presently. The linac simulations show performance that is consistent with achieving the luminosity goals of the different designs, although much remains to be done.
- A significant gap in current understanding of LET performance is the absence of detailed, integrated simulations of both initial tuning and ongoing operation of each design.
- A site with ground motion comparable to models **A** or **B** would be an acceptable situation for all LET designs. A site with motion comparable to model **C** would permit TESLA to deliver 90% of its "vibration-free" luminosity, and would limit

JLC-X/NLC and CLIC to 70% to 80% of "vibration-free" luminosity, if aggressive measures were taken to combat the loss due to element motion. There is significant concern that the good operating conditions present in simulation, and required if the aggressive measures are to succeed, can be achieved in real life.

- All LET designs, regardless of ground motion conditions, will require some form of IP collision feedback based upon the beam-beam interaction; either intra-train or train-by-train operation can be considered. This implies that one or several BPMs which are critical to the operation of the LET have to be placed in the pathological near-detector environment, in which radiation levels and BPM backgrounds will be high.

- In the presence of significant detector noise which is coupled to the final doublet magnets, active stabilization of the final doublets is essential for JLC-X/NLC and for CLIC. For TESLA it is expected that an intra-train collision feedback could be used rather than magnet stabilization, although use of the latter technology as well is not ruled out.

- In order to ensure compliance with system vibration tolerances, it is important to accurately determine the degree and character of noise sources in the tunnel, and in particular those on the beamline itself. None of the designs have a girder prototype which has been fully characterized in terms of vibration.

- Train-to-train luminosity fluctuations due to element motion may be on the order of 10%. Such large variations will impact the convergence speed of tuning which is based on maximization of the luminosity signal, and in severe cases may prevent convergence altogether. In general, the performance of the slow or near-static tuning algorithms in the presence of ground motion, luminosity variations, and other dynamic effects is an area which requires considerable further study.

7.3.8 Concerns

In addition to these conclusions, the working group notes a number of particular concerns related to luminosity performance of the LET designs. From highest to lowest priority, these concerns are:

- All of the LET designs rely on beam instrumentation performance that meets or exceeds the state of the art. Some key examples from the various designs include: stable, high precision BPMs; BPMs incorporated into accelerator structures; BPMs in the IR for train-by-train or intra-train collision feedback; laser wires with high resolution and signal/noise ratio; fast and precise luminosity monitors; and diagnostics for the longitudinal phase plane.

- The simulations of static tuning are not yet complete: the main linac simulations need to completely converge, and similar exercises must be carried out for bunch compressor and beam delivery regions. The impact of dynamic effects during the process of static tuning must be evaluated.

- A more complete evaluation of in-tunnel noise sources, both "cultural" and "technical," is required. Recent experiments at Fermilab have demonstrated the difficulty in assessing the impact of these sources [75].
- The present designs include an uncomfortably large jitter amplification due to collimator wakefields in the vertical plane. Recent measurements of collimator wakes indicate that the theory may overestimate the effect by as much as a factor of 2, which indicates that the desired accuracy of theoretical predictions (approximately 10%) is not yet achieved.
- The final doublet technology selected for JLC-X/NLC or CLIC must meet stringent requirements on stability in position and focusing gradient. At this time, it is not possible to make a convincing argument that an engineering solution for this problem is in hand. Note that, in the case of TESLA, it is expected that the desired gradient stability will be provided by the large inductance of the proposed superconducting magnet design, and the position stability is addressed through use of an intra-train collision feedback.
- More studies on the beam-beam "banana" instability are required to ensure that the intra-train collision feedback and luminosity optimization proposed for TESLA will function properly in practice. This is also a concern for the JLC-X/NLC and CLIC intra-train feedbacks, but the issue is less severe in these cases because train-by-train feedback and final doublet active stabilization are expected to provide most of the collision stabilization needed for luminosity.
- In the case of JLC-X, because of the small crossing angle (7 mrad) and short inter-bunch interval (1.4 ns), the parasitic collisions make the luminosity very sensitive to relatively small beam offsets at the IP. This sensitivity can be mitigated through the use of an electromagnetic shield between the incoming and outgoing beams, but this shield must intrude quite far into the IR to reduce the luminosity loss to a level comparable to what is foreseen for NLC or CLIC. The issues of acceptable luminosity loss, required shielding, and the machine-detector interface implications of the shielding must be carefully considered for JLC-X with a 7 mrad crossing angle.
- Although the "as-designed" long-range wakefields are quite acceptable from the point of view of achieving luminosity with long bunch trains, any error in the construction of the structures that changes the wakefields can exert tremendous leverage on the luminosity performance. It is important to ensure that the structures can be manufactured with wakefields which are acceptably close to the "as-designed" ideal, and that the error models used to simulate manufacturing defects reflect reality.
- The CLIC bunch compressor design is not quite complete, and a full estimate of the emittance growth induced by coherent synchrotron radiation has not yet been performed.

7.3.9 Phenomena That Were Not Reviewed

There were several areas in which a potential luminosity issue was identified, but insufficient information existed to quantify the performance risk. These areas are:

- Ion and electron cloud effects in the single-pass LET
- Dark current as a source of long-range wakefields, or a source of background for the instrumentation
- Beam halo, which can drive similar effects to the dark current, and which was poorly modelled and understood in the SLC
- Stray fields, in particular their impact on the tuning procedures
- Variation in the charge extracted from the damping rings

7.3.10 Items for Further R&D

We present here the suggested R&D items for the LET designs. The items have been ranked in their importance according to the ranking scheme described in Section 7.1.3.

7.3.10.1 Ranking 1

No Ranking 1 items were found in this review. It is the consensus of the reviewers that, from the point of view of luminosity performance, the feasibility (as defined in Section 7.1.3) of each LET design has been established.

7.3.10.2 Ranking 2

- Complete the static tuning studies described in Section 7.3.7 and Section 7.3.8.
- Develop the most critical beam instrumentation, including the intra-train luminosity monitor required by TESLA, the train-by-train luminosity monitor required by JLC-X/NLC and CLIC, and ensure that an acceptable laser-wire profile monitor can be provided where needed in each design.
- Perform the calculation of coherent synchrotron radiation in the CLIC bunch compressor.
- Develop a sufficiently detailed prototype of the main linac module (girder or cryomodule with quadrupole) to provide information about on-girder sources of vibration.

7.3.10.3 Ranking 3

- Estimate the technical noise level which will be present at the beamline due to klystrons, pumps, and other sources which are necessarily close to the accelerator.
- For JLC-X/NLC, demonstrate the magnetic center stability (at the 1 to 10 μm level) required in LET quadrupoles over the relevant time scale of minutes to days.

- Perform collimator wakefield measurements which are relevant to the LET designs, and investigate other solutions to the beam halo problem which would permit relaxation of the collimation aperture in the event that the wakes turn out to be as large as presently anticipated.
- Develop the BPMs required for emittance preservation and operation of the beam-beam collision feedback.
- Compute the detailed tolerances for fast vibration, magnet strength stability, rf stability, *etc.*, and verify that static tuning will converge in the presence of these dynamic errors.
- Estimate the robustness of tuning algorithms in the presence of malfunctioning BPMs, correctors, and element translation stages.
- Characterize the likely cultural noise at any prospective LC site.
- Design the "pre-LET" collimation systems which are intended for use between the damping ring extraction and the LET.
- Estimate electron/ion effects in the LET.
- Demonstrate the mechanical alignment techniques which will be used prior to commissioning.
- Complete calculations of the multibunch wakefield effects in the pre-linac and bunch compressor regions.

7.3.10.4 Ranking 4

- Study the implications of reducing the value of D_y for TESLA, in the event that such a reduction is desired in order to ease the tolerances on the "banana" instability.
- Perform further simulations and studies of the formation of beam halo in the LET.
- Perform further studies on the impact of dark current on the LET.
- Demonstrate the feasibility of an intra-train feedback which operates within the short time required for JLC-X/NLC and CLIC.

7.4 MACHINE-DETECTOR INTERFACE

The present section is organized as follows.

The main issues affecting the baseline designs are outlined in Section 7.4.1 and discussed in detail in Section 7.4.2 to Section 7.4.7. The luminosity performance of the collider, as well as some of the essential design choices, are deeply related to the impact of the beam-beam interaction on the center-of-mass (c.m.) energy spectrum, on the phase space of the outgoing beam, and on the collision backgrounds (Section 7.4.2). All of these affect the IR layout and the spent-beam extraction scheme (Section 7.4.3), as well as some of the

final-doublet specifications (Section 7.4.4). The interrelated subjects of beam halo, collimation and machine protection are considered in Section 7.4.5, followed by a comparative overview of accelerator-induced backgrounds (Section 7.4.6). The location of the beam energy and polarization measurements (Section 7.4.7) is intimately linked to the crossing-angle issue. Energy tunability and upgradability are briefly discussed in Section 7.4.8, and the main conclusions are regrouped in Section 7.4.9.

Where appropriate, recommendations for further R&D are regrouped at the end of each section, ranked according to the definitions of Section 7.1.3; within each ranking category, the items are listed in order of decreasing importance.

7.4.1 Overview

Many of the critical issues in the Beam Delivery system: optical design, beam dynamics, tuning algorithms, beam-line diagnostics, and halo collimation, are largely generic across Linear Collider designs. Except for collimation, all of them are discussed elsewhere in this report. The discriminating issues affecting the design and performance of the Interaction Region (IR) and Machine-Detector Interface (MDI) are fundamentally related to the choice of linac rf technology through the time structure of the colliding beams.

First, the short interbunch separation (0.7–2.8 ns) in the warm-machine designs requires the beams to collide with a crossing angle (7–20 mrad) to avoid multiple collisions: their horizontal separation at parasitic crossings must be sufficient to suppress the multibunch kink instability. In contrast, the ability of superconducting-rf systems to sustain a long train of widely spaced bunches allows the beams to collide head-on. This has several consequences.

- The non-zero crossing angle of the warm designs complicates their IR layout. The main issues here include the need for crab crossing (Section 7.4.3.2) and for separate incoming and outgoing transport lines, as well as tougher technological requirements on the final-doublet (FD) quadrupoles (Section 7.4.4).
- The head-on geometry of the TESLA design constrains the layout of the spent-beam extraction line (Section 7.4.3.3), with implications in the areas of FD aperture, masking, accelerator backgrounds, machine protection, and hardware reliability. It also limits the availability, and perhaps the performance, of beam-energy and -polarization diagnostics (Section 7.4.7).

Second, warm and superconducting rf systems are naturally optimized for bunch trains of very different length and repetition rate, resulting in contrasting sensitivities to, and cures for, collision jitter and vibration throughout the machine (Section 7.4.4).

- The high repetition rate ($\sim 10^2$ Hz) of the warm machines makes it possible for train-to-train collision-feedback systems to compensate for magnet vibrations (and other rapidly varying sources of luminosity loss in the BDS) up to about 10 Hz. Higher-frequency vibrations must be damped by proper design of supports, and/or actively compensated. Depending on the actual ground-motion and magnet-motion spectrum, satisfactory performance of these feedback and stabilization techniques may prove essential in achieving the luminosity goals.

- In TESLA, the large number of bunches per train, combined with the wide bunch spacing, allows for an intra-train collision feedback that devotes the first few percent of every train to restoring collisions between two trains initially separated by potentially large transverse offsets . This technique significantly relaxes the tolerances on ground motion and other sources of vibration throughout the machine.

Finally, the time structure of the beam impacts the design of the machine-protection and collimation systems (Section 7.4.5), as well as the sensitivity of some particle detectors to beam-induced backgrounds (Section 7.4.6).

- In the case of an errant beam pulse, the post-linac collimation section must gracefully handle an entire bunch train in JLC, NLC or CLIC. But it is only required to withstand at most two bunches in TESLA[4] where the long spacing between bunches allows an emergency-extraction kicker to direct the remainder of the beam onto the main dump before it can damage the beam line. This feature reduces by a factor of 40 (compared to NLC) the amount of beam that may be accidentally lost in the TESLA BDS in case of a major hardware fault in the linac, albeit by shifting part of the emphasis onto the reliability of the machine-protection system. In all machines however, the critical issue in collimator design remains single-bunch damage.
- The sensitivity of individual experimental subdetectors to machine-induced backgrounds may favor one or the other time structure, depending on their time resolution and integration window. However, the predicted background levels appear sufficiently moderate that differences between machines can be mitigated by adjustments in detector design: this issue is not considered critical, at the present level of understanding, for any of the linear-collider concepts.

7.4.2 Beam-Beam Effects, Luminosity Spectrum, and Collision Backgrounds

In all designs, the luminosity goals lead to IP beam sizes small enough for each bunch to generate an intense electromagnetic field which focuses the opposite bunch, leading to an increase in total[5] instantaneous luminosity, but also to a significant broadening of the angular spread of the outgoing beam (200–400 μrad) and to the emission of beamstrahlung (Figure 7.19). Each primary-beam particle radiates, on the average, one to two photons with a typical energy of several GeV. This process dilutes the luminosity spectrum toward lower e^+e^- c.m. energies (Figure 7.20), and is an abundant source of backgrounds ($e^\pm$ pairs, minijets, and backscattered secondaries).

Analytical treatment of the beam-beam interaction is not possible, so one has to resort to simulations. Two widely used packages are CAIN [76] and GUINEA-PIG [77]. Their predictions of the beamstrahlung flux and of the total energy carried by the pairs were compared for TESLA parameters, showing very good agreement [78]. GUINEA-PIG estimates of the luminosity enhancement expected at SLC for different beam parameters also agreed well with actual measurements [79]. One can therefore consider these simulations as quite reliable.

[4] At least for fast energy errors. Other fault scenarios are discussed in Section 7.4.5.2.
[5] That is, integrated over the entire energy spectrum

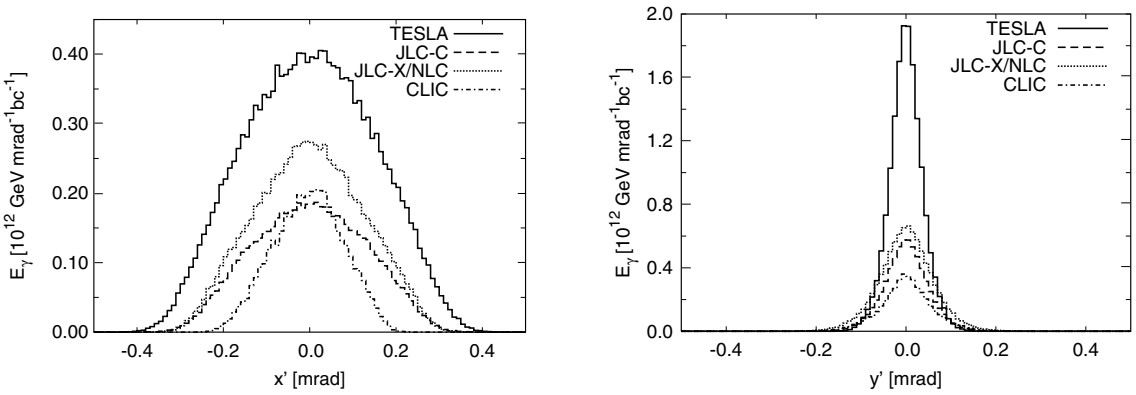

FIGURE 7.19. Angular distribution of beamstrahlung photons in the horizontal (left) and vertical (right) planes, for TESLA (top curve), JLC-C and JLC-X/NLC (middle curves) and CLIC (bottom curve). The flux predictions assume perfectly centered collisions of ideal gaussian beams, and correspond to the parameters listed in Table 7.22.

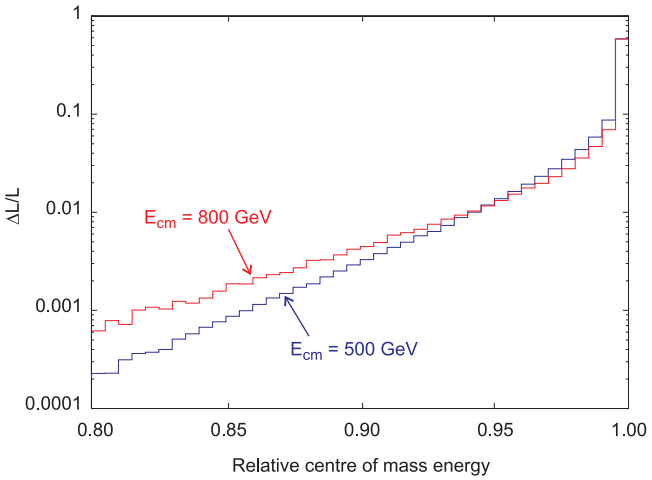

FIGURE 7.20. Luminosity spectra for 500 GeV and 800 GeV c.m. energy (TESLA parameters).

7.4.2.1 Luminosity Spectrum

The predicted c.m. energy distributions are fairly similar in all designs. At $\sqrt{s}$=500 GeV, the average energy loss per beam particle δ_B ranges from 3–5%, with about 65% of the total luminosity at c.m. energies above 99% of the nominal value, and 85–90% of the luminosity within 5% of the nominal c.m. energy (Table 7.22). The degradation of the spectrum by beamstrahlung is found to be comparable to that due to initial-state radiation. In all machine designs it is possible (if so required by the experimental program) to sharpen the energy spectrum at some cost in luminosity.

TABLE 7.22: Linear colliders: beam delivery system and interaction point parameters

	TESLA		**JLC-C**		**JLC-X/NLC**[a]		**CLIC**	
	500 GeV	800 GeV	500 GeV	1000 GeV	500 GeV	1000 GeV	500 GeV	3000 GeV
Beam delivery system length[b] [km]	3.2		3.8		3.8		5.2	
Collimation system length[b] [km]	1.4		1.4		1.4		4.1	
Final Focus system length[b] [km]	1.2		1.6		1.6		1.1	
$\gamma\varepsilon_x^*$ / $\gamma\varepsilon_y^*$ [m-rad $\times 10^{-6}$]	10 / 0.03	8 / 0.015	3.6 / 0.04		3.6 / 0.04		2.0 / 0.01	0.68 / 0.01
$\beta_x^\star$ / β_y^* [mm]	15 / 0.40	15 / 0.40	8 / 0.20	13 / 0.11	8 / 0.11	13 / 0.11	10 / 0.05	16 / 0.07
$\sigma_x^\star$ / σ_y^* [nm] before pinch[c]	554 / 5.0	392 / 2.8	243 / 4.0	219 / 2.1	243 / 3.0	219 / 2.1	202 / 1.2	60 / 0.7
$\sigma_z^\star$ [μm]	300		200	110	110		35	
$\sigma_{\Delta E/E}^\star$[d] [%]	0.14 / 0.04		0.25		0.25		0.25	0.35
Distance between IP and last quad	3.0		4	3.5	3.5		4.3	
Crossing Angle at IP [mrad]	0		7		7 (20)		20	
Disruptions D_x / D_y	0.23 / 25.3	0.20 / 28.0	0.29 / 17.5	0.10 / 10.3	0.16 / 13.1	0.10 / 10.3	0.04 / 6.4	0.07 / 6.3
Υ_0	0.05	0.09	0.07	0.28	0.13	0.28	0.25	5.0
δ_B [%]	3.2	4.3	3.4	7.5	4.6	7.5	4.4	21.1
n_γ [number of γs per e]	1.56	1.51	1.36	1.30	1.26	1.30	0.75	1.53
$N_{\text{pairs}}(p_T^{\text{min}} = 20$ MeV/c, $\Theta_{\text{min}} = 0.2)$	39.4	37.3	10.7	15.0	11.9	15.0	7.2	43
$N_{\text{hadron events}}$/crossing	0.248	0.399	0.075	0.270	0.103	0.270	0.066	2.26
$N_{\text{jets}} \times 10^{-2}$ [$p_T^{\text{min}} = 3.2$ GeV/c]	0.74	1.90	0.23	2.27	0.36	2.72	0.29	150.5
Geometric Luminosity[e] [10^{33} cm^{-2}s^{-1}]	16.4	28.1	8.76	18.5	17.7 (14.2)	18.5 (22.2)	16.0	47.0
H_D	2.11	1.90	1.61	1.42	1.49	1.42	1.42	1.70
Luminosity dilution for tuning [%]	0		5		5		10	0
Peak Luminosity[e] [10^{33} cm^{-2}s^{-1}]	34.5	53.4	13.6	24.9	25.1 (20.1)	25.0 (30.0)	21.0	80.0
$L_{99\%}$ [%]	66	62	67	58	64	58	71	41
$L_{95\%}$ [%]	91	86	90	86	85	77	87	53
$L_{90\%}$ [%]	98	95	97	87	94	87	93	62

[a]Numbers in ( ) correspond to US site with 120 Hz repetition rate.

[b]System length includes both incoming beamlines.

[c]For all designs except CLIC, the IP spot sizes are calculated as usual from the emittances and beta functions. With the design emittances in CLIC, nonlinear aberrations in the final focus system increase the final spot size by 20 to 40%.

[d]Energy spread is for electrons / positrons if different.

[e]For the sake of uniformity, the geometric luminosity is simply defined as $N^2/4\pi\,\sigma_x^*\sigma_y^*$ times the number of crossings per second, and in all cases assumes head-on collisions, no hour-glass effect and no pinch. The peak luminosity is calculated using the Guinea Pig program and incorporates all the effects, including the pinch enhancement, hour-glass, and crossing angle where applicable, plus any additional IP dilutions that may be expected.

7.4.2.2 Beam-Beam Backgrounds

7.4.2.2.1 Bremsstrahlung and Pair Production Bremsstrahlung photons are emitted at small angles (Figure 7.19) with respect to the incoming-beam direction, and can easily be extracted from the detector. But their interaction with beam particles or photons from the opposite bunch constitutes one of the main background sources, through the abundant production of low-energy e^+e^- pairs. The dominant processes are $\gamma\gamma \to e^+e^-$, $e\gamma \to ee^+e^-$ and $ee \to eee^+e^-$. The previously mentioned simulation packages calculate the pair-production rate using the beamstrahlung photons and replacing the primary electrons and positrons with equivalent virtual-photon spectra. The resulting final-state particles are then tracked through the electromagnetic field of the bunches as it evolves during the collision. The energy and transverse-momentum distributions computed in this approximation for the $ee \to eee^+e^-$ process have been compared [80] to a more complete Monte Carlo written by Vermaseren [81]. The two calculations show reasonable agreement, but at large transverse momenta, differences of up to a factor of 2 were found.

Because of their low momenta, the pair-produced electrons and positrons are strongly deflected by the field of the beams, resulting in a strong correlation between their polar angle θ and the maximum transverse momentum p_t (Figure 7.21). The sharp θ-dependent cutoff reflects the fall-off of the electromagnetic field of the bunch at large radial distances. The detector solenoid maps the p_t cut-off into two "stay-clear cones," the apex of which lies at the IP and which contain most of the pair-produced background flux. Only a small—albeit somewhat uncertain—fraction of the pairs is produced with large enough initial angle and/or transverse momentum to escape the cones. While $e^\pm$ pair-production constitutes a potentially serious background source for the vertex detector, appropriate combinations of solenoid field strength, extraction-line aperture, mask angular coverage and vertex-detector radius have been shown to result in tolerable occupancy levels (Section 7.4.6).

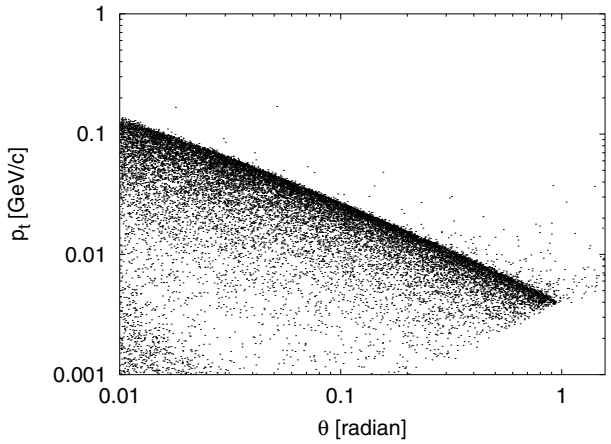

FIGURE 7.21. Polar-angle and transverse-momentum distribution, after the collision, of $e^\pm$ from incoherent pair production. This particular simulation uses CLIC parameters, but such behavior is generic across projects.

The pairs created at the IP are channelled by the solenoidal field to the pair luminosity monitor, the extraction-line chamber, or the first extraction-line quadrupole. The total energy carried by the pairs is quite large. A substantial fraction of these particles will be lost in the spent-beam channel before it leaves the detector (see Figure 7.22 and Section 7.4.3.3), resulting in:

- A significant backscattered neutron flux (Table 7.23)
- Secondary photons from which the detector must be shielded
- Charged electromagnetic-shower debris which are scattered back toward the IP. These soft $e^{\pm}$ follow the field lines of the solenoid which channels them back toward the vertex detector, potentially increasing the background by an order of magnitude.

TABLE 7.23
Neutron hit density in the proposed vertex trackers, in units of 10^9 n/(cm$^2\times$yr) at 500 GeV c.m. energy. The numbers reflect the different masking and extraction-line geometries as optimized by the individual machine and detector study groups. LD and SD refer to the two NLC detector models mentioned in Section 7.4.3.1. Neutron-flux predictions are not yet available for CLIC.

	TESLA [82]	NLC (LD) [83]	NLC (SD) [83]	JLC-X [84]
Pair-induced	1.0	1.8	0.5	0.03–0.13
Backscattered from dump(s)	negligible	0.1	0.1	0.03–0.05

Backgrounds from backscattered debris have been largely mastered in all machine designs. Masking schemes (Figure 7.23 through Figure 7.25) have been devised to shield the detector from backscattered electromagnetic debris and to deplete the neutron flux. The corresponding backgrounds in the tracking detectors have been reduced to acceptable levels. The pair-induced neutron flux, however, remains of concern for some vertex-detector technologies (Section 7.4.6).

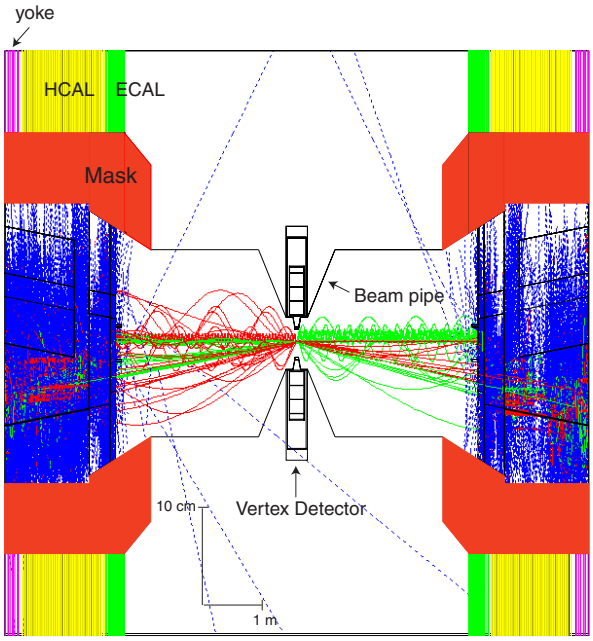

FIGURE 7.22. Simulated beam-beam backgrounds at the IP, showing the trajectories of $e^{\pm}$ pairs and electromagnetic shower debris (x-z view). The dashed blue lines represent photons, red solid lines electrons, and green lines positrons. The incoming e^{-} beam comes in from the left. High-energy $e^{\pm}$ debris roughly follow the initial beam direction into the extraction line, while lower-energy products spiral along the solenoid field lines and hit the front face of the luminosity monitor. Note that pair-induced low-energy e^{-} traveling to the left (the right) are defocused (focused) by the incoming e^{-} (e^{+}) beam (and similarly for positrons). This particular simulation reflects the NLC IR layout and beam parameters, but similar features are found in all projects.

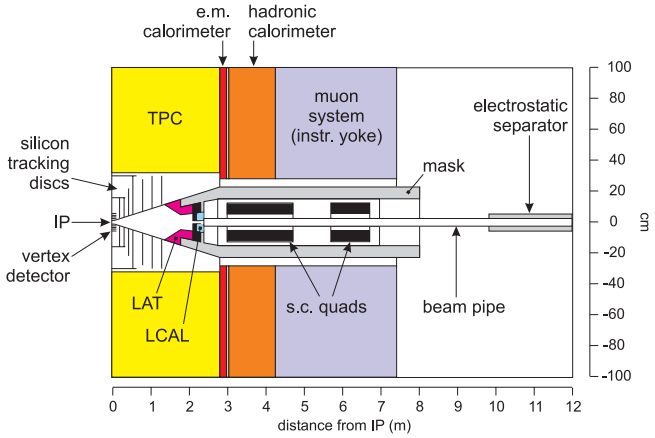

FIGURE 7.23. IP masking and spent-beam extraction in the TESLA design (y-z view).

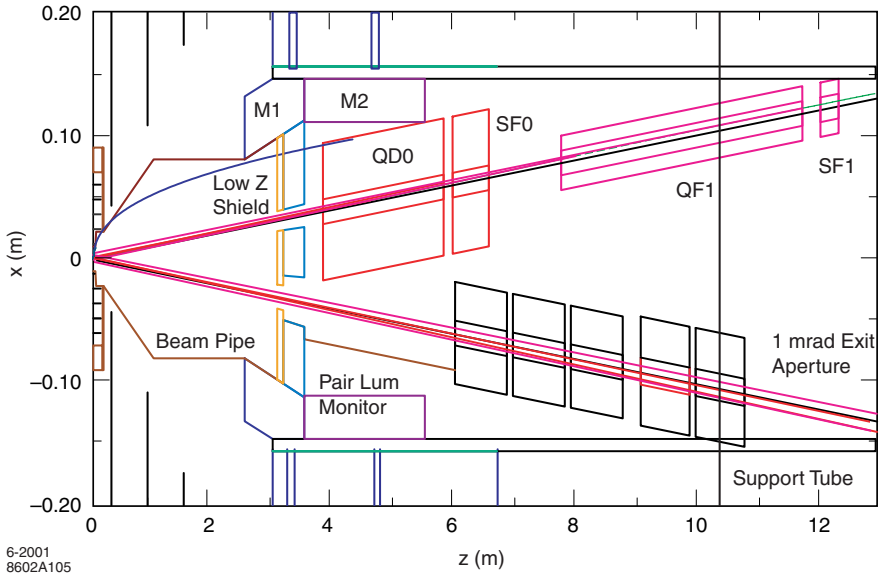

FIGURE 7.24. NLC IR layout (LD detector model, x-z view). M1 and M2 are detector masks, QD0 and QF1 are the final doublet, and SF0 and SF1 are chromaticity-correcting sextupoles.

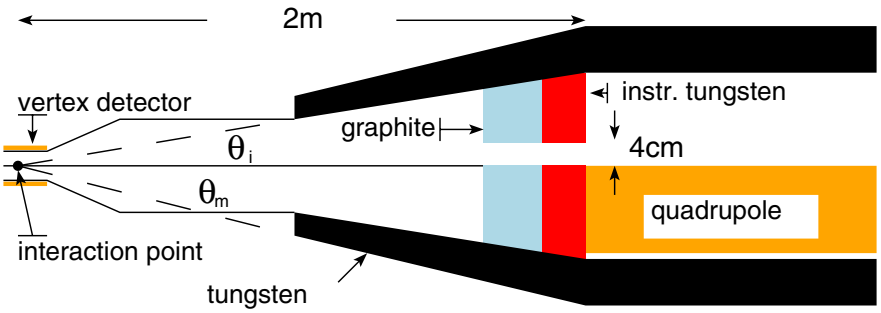

FIGURE 7.25. View from above of the CLIC mask design. The sketch is stretched in the vertical direction. Care has to be taken that no particles are backscattered through the hole in the mask.

7.4.2.2.2 Hadronic Backgrounds The total hadronic cross section in two-photon collisions is poorly known at high energies. The expected number of events with a two-photon c.m. energy above 5 GeV is given in Table 7.22. This comparison is based on the parameterization of Reference [85]; other parameterizations [86] agree to better than a factor of 2 at E_{cm}=500 GeV.

A fraction of the hadronic events are relatively hard and contain so-called minijets. They are due to direct production of quark pairs ($\gamma\gamma \to q\bar{q}$), direct-photon scattering off a parton in a resolved photon ("once-resolved" process: $\gamma q \to gq$, $\gamma g \to q\bar{q}$), or parton-parton scattering if both photons are resolved (eight different "twice-resolved" subprocesses in all)[6]. Table 7.22 lists the predicted number of minijet pairs per bunch crossing with a transverse momentum above 3.2 GeV/c using the parameterization of Reference [87] implemented in GUINEA-PIG; comparable results are obtained if one uses Reference [88] instead. Their potential impact on detector performance is briefly touched upon in Section 7.4.6.

7.4.3 Interaction-Region and Extraction-Line Layout

7.4.3.1 IR Layout

The main characteristics of the proposed IR layouts are as follows:

- TESLA: The beams collide head-on and are separated electrostatically after they exit the detector (Figure 7.23). The final-focus quadrupole doublets are superconducting. The TESLA detector design has a 4 T solenoid field.
- JLC: The beams collide with a crossing angle of 7 mrad. The final-focus quadrupole is a conventional iron magnet surrounded by a superconducting solenoid compensator, where the beams exit through the coil pocket of the quadrupole. The JLC-X detector design has a 3 T solenoid field. No detailed detector or IR design exist for the JLC-C option.
- NLC: The beams collide with a 20 mrad crossing angle and exit past the outer radius of the final quadrupoles (Figure 7.24) into an extraction line. The final-focus quadrupole doublets use permanent magnets (PM), or possibly a compact superconducting design. NLC is considering two detector options: "Large" (LD) and "Silicon" (SD), which use, respectively, a 3 T and a 5 T solenoid field.
- CLIC: The beams collide at a 20 mrad crossing angle (Figure 7.26). The baseline final-doublet system uses PM quadrupoles; a compact superconducting quadrupole is under study. The CLIC detector design has a 4 T solenoid field.

All designs incorporate conical masks to shield the detector from the secondary particle debris produced when the pairs interact. The outer parts of the mask, which must lie outside the pair stay-clear, are instrumented as a Si/W calorimeter and serve as a low-angle tagger (LAT). The inner part, which shadows the face of the quadrupole, is subjected to a high flux of particles from pair creation (several TeV per crossing). Backscattering of

[6]Measuring the total cross-section of the latter two will be an interesting experiment at a future linear collider.

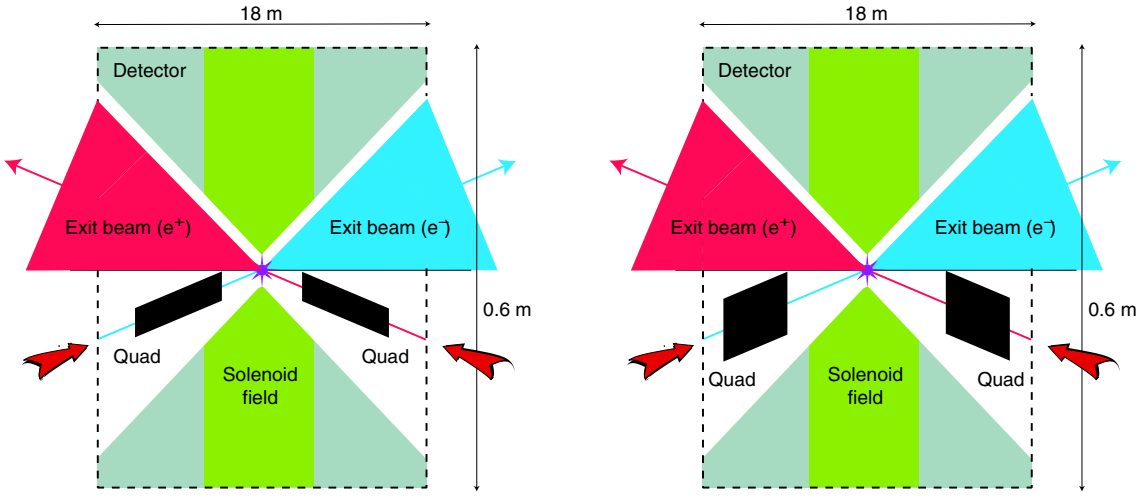

FIGURE 7.26. Top view of the CLIC IP region with the detector, the colliding beams, and the final quadrupoles for the base-line (left) and the compact final-focus optics (right) at 3 TeV. Scales are indicated. The transverse size of the detector is about 17 m.

low-energy secondaries is prevented by a covering layer of low-Z material. This section of the mask is instrumented as a luminosity monitor that measures the number of beam-beam induced $e^{\pm}$ pairs [89].

7.4.3.1.1 Evaluation The interaction region design must provide for: support (and possibly active stabilization) of the final focus quadrupoles; masks for synchrotron radiation, and for photons and neutrons produced by pairs; beam position monitors and feedback kickers; and luminosity and (possibly) beam-size monitors. Almost all of these elements are tightly packed up against (or penetrate) the detector and the solenoid yoke.

The TESLA, JLC-X, and NLC interaction region designs are reasonably mature and contain all of the elements needed in a geometry that is consistent with the detector, solenoid, and return yoke. The CLIC IR design is not as completely developed and cannot be evaluated, but it should be similar to that of NLC.

For the head-on collisions at TESLA, the beam pipe must have a large aperture to accommodate the disrupted beam. Only superconducting (SC) magnets can provide the necessary combination of gradient and aperture. For designs with a crossing angle, the final doublet must be compact to allow the extracted beam to pass outside the quadrupole (NLC, CLIC), or must have some provision for the spent beam to be extracted through a field-free region of the magnet (JLC-X). Since the incoming beam pipe is small, PM quadrupoles can be used. These are rigid and free from external water or power connections, which can be an advantage in suppressing vibration; but they are tunable over a narrow range only.

A comparison of the angular acceptance of the present detector models is presented in Table 7.24. The low-angle coverage, which is important in some SUSY searches, is similar in TESLA (where the mask dimensions are determined by the size of the SC quadrupoles and their cryostat) and in NLC (here the magnet envelope is specified to be within the cone of

TABLE 7.24
Detector polar-angle coverage. All numbers are in mrad and refer to the 500 GeV designs except for CLIC. In the crossing-angle designs, the pair monitor must allow for the passage of both the incoming-beam and the spent-beam pipes, which causes a ∼10% gap in azimuthal coverage for θ <30 mrad.

	TESLA	NLC (LD)	JLC-X	CLIC (3 TeV)
Main detector	>83	>52	>200	>120
LAT (instrumented mask)	27–83	32–52	150–200	40–80
Luminosity (pair) monitor	5.5–28	6.4–32	50–150	10–40

the pair stay-clear to maximize the detector acceptance). In JLC-X the mask dimensions are determined by the large size of the iron quadrupoles and their compensating solenoid. In CLIC at 3 TeV, the acceptance is limited by the pair stay-clear; no optimization has been done yet for the 500 GeV CLIC design.

An important difference between the designs is in the support system for the final doublets, where differential motion of the doublets can cause the beams to miss each other at the IP. TESLA plans to compensate for such motion with intra-train feedback and thus uses conventional separate supports. JLC-X proposes a single carbon-fiber reinforced tube which extends through the detector and supports both doublets. In NLC, each doublet would be mounted inside a cantilevered support tube; a number of different configurations are under study, combined with a feedback system to provide active stabilization of the relative magnet positions using inertial sensors and/or an optical-anchor interferometer [90].

7.4.3.2 Impact of Crossing Angle on Nominal Luminosity

7.4.3.2.1 Horizontal Beam-Beam Overlap In the normal-conducting designs, the crossing angle is large enough to degrade the nominal luminosity by a factor[7] of 4–6, unless compensated by a crab-crossing system as planned for NLC, CLIC and probably JLC. The transverse alignment tolerances of the crab cavities are quite loose. However, there are tight roll tolerances (∼0.4 mrad for a 2% luminosity loss), which means that the cavity must be mounted on a mover system and adjusted.[8] The structures themselves are not an issue; an actual S-band version will be installed at the TTF and used to measure bunch length. The tolerance (see also Section 7.3.5.3) on the relative phase stability of the two cavities (0.025° of S-band) is challenging: some R&D is still needed here, but the engineering appears feasible (the cavities can be driven from a single klystron and one can use the reflected power signal to adjust the relative phases).

7.4.3.2.2 Solenoid-Steering Effects The transverse component of the detector solenoid field present in any crossing-angle configuration shifts the positions and angles of the beams at the IP, as well as the outgoing-beam trajectory, by energy-dependent amounts. While small variations in nominal beam energy may be accommodated by steering correctors and/or quadrupole trim windings, covering a wide c.m. energy range

[7] Including the loss of pinch enhancement ($H_D \to 1$).
[8] The roll control also allows efficient removal of any residual $y - z$ wakefield correlations at the IP.

may require realigning several components in the extraction line, an operational overhead. This has been studied for a 6 T detector at NLC and the shift was less than 1 mm between 90 GeV and 1 TeV. With a 1 cm aperture extraction line, this may be acceptable; alternatively, the aperture could be increased or the magnets could be equipped with movers as elsewhere throughout the complex.

7.4.3.2.3 Dispersion and Emittance Dilution

With a non-zero crossing angle, synchrotron radiation emission and dispersion due to the solenoid and fringe fields can cause vertical beam size growth at the IP. The increase in vertical beam size was found to be negligible [91] for three different solenoid designs considered for the NLC. Simulations for CLIC at 3 TeV, which used a simplified model of the solenoidal field, indicated an acceptable spot size growth [92]. Because the vertical beam size growth is a rapidly increasing function of the transverse component of the solenoid fringe field, it is prudent to make detailed calculations using realistic solenoid field maps as these become available for each machine.

7.4.3.3 Spent-Beam Extraction

The spent-beam extraction line must satisfy a number of difficult constraints. The main dump must gracefully handle both the nominal, highly disrupted charged beam, and a low-emittance outgoing beam for the case when no collision has occurred. At $\sqrt{s}$=500 GeV, 180–360 kW of beam power (assuming nominal conditions and a static, perfect machine) are radiated as photons, which must be absorbed in a straight-ahead dump. Spent-beam losses must be kept at a moderate level, to limit heat deposition and component activation, and to avoid production of excessive backgrounds in the physics detector (and in the post-IP beam instrumentation). The geometry is further complicated by the presence of the incoming beam, whether in a separate beam line or not. The dumps are typically located a substantial distance from the IP to allow the low-emittance beam to expand in size before striking the dump window, and to reduce the neutron backshine. Since the beam power to be absorbed is large for both the neutral and charged beams, it is desirable to minimize the number of expensive, water-cooled dumps.

The main characteristics of the proposed extraction lines are as follows.

- TESLA uses two separate dumps for the beamstrahlung and for the charged spent beam, housed in the same shielded dump hall located 240 m from the IP. The outgoing charged beam is vertically deflected immediately downstream of the IR doublet using a combination of an electrostatic separator and of a superimposed magnetic field (the two fields cancel for the incoming, oppositely charged beam). A thin-bladed septum magnet then separates the spent beam from the incoming beam into two distinct vacuum chambers before the first parasitic crossing (about 50 m from the IP). A large-aperture lattice transports the spent beam to the dump with minimal particle losses. The beamstrahlung dump, located directly above the main charged-particle dump, requires a small aperture to allow passage of the incoming charged beam (Figure 7.27). The current design has an aperture of 20 mm diameter, allowing some 40 kW of beamstrahlung power through to a second dump located after the first dipole bend. Secondaries from the charged-beam dump cannot reach the

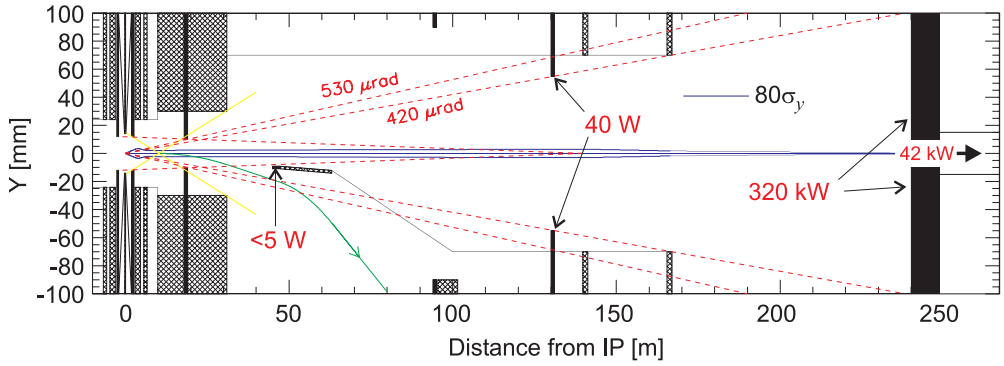

FIGURE 7.27. Vertical layout of the TESLA final-transformer region, as presented in Section II-7.6.2 of Reference [93]. The beamstrahlung power levels are for the 500 GeV machine under ideal conditions.

vertex detector on a straight-line trajectory, but the smaller number from the beamstrahlung dumps can.

- NLC uses a single dump located 150 m from the IP for both the neutral and charged particle beams. The 20 mrad crossing angle allows the outgoing beam to exit in a separate beam pipe, with flexibility in the choice of optics. The first quadrupole is 6 m from the IP. A chicane separates the neutral and charged beams to allow energy and polarization diagnostics at an image point of the IP. The dump is on-axis to accommodate the neutral beam, and a 1 mrad beamstrahlung stay-clear is enforced. Back-scattered secondaries from the dump can reach the vertex detector on a straight-line trajectory, but the distance and apertures limit the solid angle to an acceptable level.

- JLC-X plans to use two separate dumps. A beamstrahlung dump is located 300 m from the IP, while the charged beam is bent toward a separate dump.

- CLIC plans an extraction line similar to that of NLC, but no detailed layout is available yet.

7.4.3.3.1 Evaluation In TESLA, where the outgoing neutral beam and the incoming charged beam share the same vacuum pipe between the IP and the dump, a narrow compromise has to be found between conflicting requirements. The incoming-beam aperture needs to be restricted by masks that protect the detector from synchrotron radiation (SR). The outgoing beam requires a large stay-clear for outgoing SR-photons and beamstrahlung-photons to limit backscattered backgrounds and to avoid excessive heat deposition in the superconducting final doublets. In addition, the low-energy particles in the outgoing beam are overfocused by the strong final doublets, leading to large quadrupole apertures and precluding most extraction-line diagnostics.

The tightest apertures for the outgoing photons are a 10 mm radius SR mask located 18 m from the IP, the extraction-septum blade at 45 m (in the vertical only), and a 55 mm-radius collimator at 130 m that protects the intermediate doublet. The resulting stay-clear angle

of 420 μrad (neglecting the septum blade, discussed further below) seems marginal for the neutral beam, as it is barely larger than the expected angular spread of the beamstrahlung fan (Figure 7.19) assuming nominal conditions, centered collisions and zero beam-beam deflections.

An area of particular concern is that of the extraction septum. Such magnets are delicate to build and subject to failure, especially in as hostile an environment as that of a 11 MW disrupted beam passing a few mm away from a thin blade. In addition, the edge of this septum, located at $\theta_y \sim -200$ μrad (Figure 7.27), further restricts the vertical photon stay-clear.[9] It is highly likely that pulse-to-pulse jitter, ground motion, or diagnostic beam-beam scans will repeatedly induce vertical beam separations that translate into deflections of 100–300 μrad. While beam separation by a few σ suppresses luminosity, beamstrahlung emission persists, potentially sweeping the full photon fan along the septum magnet for at least a fraction of a bunch train.[10] More importantly, time-dependent errors in the linac and the BDS may result in rapidly varying bunch-shape distortions that significantly enhance beamstrahlung production. Recent simulations of such effects [95] suggest that the total radiated beamstrahlung power may exceed 500 kW (compared to 360 kW under ideal conditions), and that photon losses at the septum could average 2–3 kW during routine operation, with rapid fluctuations up to about three times the average value. The resulting neutron flux reaching the detector may be significant because of the proximity to the IP. None of these effects have been taken into account in the present extraction-line and IR designs. Assuming that the septum can be built to safely handle the average loss rate, protecting that area against excessive power deposition will further complicate the machine-protection system. More generally, the tightness of this (and other) extraction-line aperture(s) will no doubt impact the operational flexibility, and therefore the running efficiency, of the TESLA BDS as currently designed.

Another critical component is the electrostatic separator. It is based on a design used at LEP which reached the 50 kV/cm field needed at $\sqrt{s}$=500 GeV, but which exhibited frequent arcing (1 trip/hour) when illuminated by synchrotron radiation. Given the more hostile radiation environment of the TESLA extraction line, this problem must be solved in order not to become a serious reliability issue.

The use of a single dump for both neutral-particle and charged-particle beams also constrains the design of the NLC extraction line. Because the dump has a direct line-of-sight to the IP, it should be located as far downstream as possible to limit the backscattered neutron flux. However, the 1 mrad beamstrahlung stay-clear sets an upper limit on the distance from the IP if the dump window is to have a reasonable size. Since the beamlines are separate, the outgoing aperture does not affect incoming-beam collimation. The outgoing beam size is similar to that for TESLA and the factor of 3 larger beamstrahlung stay-clear appears sufficiently generous to accommodate all possible circumstances (vertically offset beams, large deflections, beam shape fluctuations).

[9] The outer edge of the septum blade is radially constrained by the charged spent-beam stayclear. In the TDR design, the blade is 2 mm thick and its inner edge lies at y=-9 mm; it is protected by a "septum-shadow mask," about 1 mm thick and 1 m long. The nominal charged-beam losses in that area amount to ~1 kW [94]. A more recent study envisages to thicken the magnet blade to 5 mm, leading to an even tighter photon stay-clear.

[10] Until either the beam-beam feedback recenters collisions, or an MPS interlock fires the emergency-extraction kicker.

The optics of the TESLA and the NLC extraction lines have been carefully optimized to minimize charged-beam losses. Both designs achieve a wide momentum bandpass and deliberately concentrate the losses (which mostly occur in the low-energy tail of the spent beam) at one or two locations sufficiently distant from the detector. The losses depend on the disrupted particle distributions at the IP, which are affected by the interplay of various incoming-beam errors with the beam-beam interaction. For instance, while horizontal separation of the beams by a few σ at the collision point has little impact on extraction-line radiation levels, vertical separation enhances disruption (as well as beamstrahlung production) and significantly increases spent-beam losses (Table 7.25). The predicted losses appear manageable at this stage of the design. It should be pointed out, however, that only primary particles were considered in these simulations, and that the predicted beam losses may increase once ground motion and machine imperfections are taken into account. The NLC momentum bandpass appears sufficiently wide (∼70%), and the total power deposition low enough (about 700 W for the worst-case $20\sigma_y$ separation) to provide ample margin, at least at $\sqrt{s}$=500 GeV. This needs to be further reviewed in the TESLA case: the extraction-line optics are constrained by the incoming beam, the total power scraped from the charged beam is an order of magnitude larger than in NLC, and the range of beam-beam offsets considered in Reference [94] is somewhat restricted.

TABLE 7.25
Predicted charged-beam losses in the TESLA and NLC extraction lines at $\sqrt{s}$=500 GeV. All numbers are in % of the incoming-beam population unless specified otherwise. The maximum loss occurs for a vertical separation of 2 σ_y in TESLA and 20 σ_y in NLC.

Vertical IP separation (# σ)	0	2	10	20
TESLA [94] (Peak losses)	0.12	0.15 (0.12 at mirror-quad collimator, 90 m from the IP)	0.10	not evaluated
NLC [96] (Peak losses)	<0.002	∼0.002	0.012	0.030 (140 W/m, 100 m from the IP)

The neutron flux backscattered from the beam dump(s) into the vertex detector has been computed for each of the IR layouts (Table 7.23). Most designs successfully reduced this flux to an order of magnitude below that of the pair-induced neutron flux, whether or not there is a direct line of sight from the main dump to the detector. This conclusion is sensitive to the details of the extraction-line geometry and to the vertex-detector radius. In NLC for instance, the hit rate from backscattered dump neutrons would increase by a factor of 40 if the inner radius of the vertex detector were halved [83]. However, the minimum

achievable detector radius is effectively limited by synchrotron radiation and beam-beam pairs, as well as by these neutrons. The NLC VTX radius is currently set at 1.2 cm as compared to 1.5 cm for TESLA.

7.4.3.3.2 Open Issues and Items for Further R&D

- TESLA: the trade-offs between head-on and crossing-angle collisions, and in particular the implications of the present extraction-line design, should be thoroughly revisited (Ranking: 2). This internal review should include (but not necessarily be limited to):
  - A more realistic estimate of beamstrahlung and spent-beam losses in simulated imperfect machines with dynamical errors
  - A systematic study of the impact of a partially shared beam line on SR masking. Recent simulation results (discussed in Section 7.4.5.1) suggest that in order to effectively collimate the incoming SR fan, the aperture of the mask located 18 m from the IP needs to be such that it intercepts a sizeable outgoing SR flux, potentially resulting in a dangerous background of backscattered, penetrating SR photons
  - A reassessment of the required stay-clear for the outgoing charged and neutral beams. Are the magnitude and the longitudinal distribution of both average and occasional losses tolerable from the viewpoints of thermal effects (SC quadrupoles, septum magnet), neutron background, and performance of crucial instrumentation (BPMs, possibly also beam-energy monitors)? Are the required stay-clear apertures compatible with effective masking of incoming SR?
  - A failure analysis that examines the potential operational impact of large orbit excursions, frozen feedbacks, and septum-blade protection interlocks

  In addition, the following engineering R&D is necessary for the successful operation of the head-on scheme as currently proposed (Ranking: 3):
  - Demonstrate separators with high enough reliability in the predicted radiation environment, and with high enough gradient to operate at $\sqrt{s}$=500 GeV
  - Design an extraction-line septum that can safely withstand realistic beamstrahlung and spent-beam losses
- All projects: because the fringe field of the detector solenoid has a radial component, μm-level vibration of the solenoid field with respect to the beam will induce nm-level jitter of vertical beam position at the IP. The detector and magnet design must ensure correspondingly adequate mechanical stability of the solenoid windings and return yoke (Ranking: 3).
- CLIC: no extraction-line design is available as of this writing (Ranking: 3).

7.4.4 Assessment of Final-Doublet Issues

7.4.4.1 Stabilization

The beams must collide head-on to avoid significant luminosity degradation. This requires limiting the relative transverse beam-centroid jitter at the IP to about one nm.

For TESLA at the DESY site, vibration of the linac and beam-delivery quadrupoles is expected to be sufficiently large that the beams would separate by many σ from one train to the next, independently of doublet motion. The large number of bunches per train (2820), combined with the wide bunch spacing (337 ns), allows for an intra-train collision feedback based on beam-beam deflection and luminosity signals, that devotes the first few % of every train to restoring collisions. This straightforward technique significantly relaxes the tolerances on ground motion and other sources of vibration at the IP (Section 7.3.4.3). The TESLA TDR [93] relies on this feedback alone to guarantee collision stability.

Because of their much shorter bunch trains (100–300 ns), the warm-rf machines cannot rely on intra-train feedback alone. They must be located on a site where ground-motion amplitudes are small enough that vibration of the linac quadrupoles is not an issue. The faster repetition rate ($F_{\rm rep}$=100–200 Hz) allows pulse-to-pulse trajectory and collision feedbacks to compensate for "slow" motion, *i.e.*, at frequencies up to approximately 10 Hz.[11] The remaining concern is fast motion of the final doublets. Ground-motion amplitudes at sites such as the LEP or SLAC tunnels can be low enough without further stabilization. Unfortunately, cultural noise generated by the accelerator or detector will almost certainly produce vibrations in excess of the tolerance (Section 7.3.4.6), and additional stabilization will be needed.

It is critical that the LC detectors at a warm-rf machine be designed to minimize vibrations since the FDs will be partly mounted on the detector. Several active measures are being developed for CLIC and JLC-X/NLC to provide the necessary relative stability between the FDs. These include mechanical stabilization of magnet position via feedback and correction of the magnetic-center position with dipole coils via feedforward. Both methods would rely on inertial measurements of the FD motion by seismometers ("inertial anchor"), and/or on optical interferometric measurements of their position with respect to each other or to stable ground (or a stabilized mirror) under the detector ("optical anchor"). Bench tests of both the inertial sensor and the optical anchor have already demonstrated a sensitivity close to what will eventually be required [90]. CERN and SLAC are presently developing a nonmagnetic inertial sensor and a prototype overall integrated system. Subnanometer position stabilization has been routinely achieved in industry. At the IP of a linear collider, however, it is a major challenge, because of the cramped space available, the presence of the detector solenoid field, the magnetic forces induced by the solenoid on the FDs and the interaction with other feedback systems.

The intra-train deflection-feedback technique is actually also applicable to warm machines, but the much shorter duration of the train implies exacting processing speeds and limits its effectiveness to compensating for residual small offsets not corrected by the techniques outlined previously. Development of such a fast system at SLAC and elsewhere [97, 98] shows promise as an additional safety factor for collision stability.

The impact of the stabilization systems on the hermeticity and the coverage of the detector will require careful consideration. The optical anchor would require optical paths from each FD to stable locations outside the detector, enclosed in an evacuated or sealed pipe to prevent refractive-index fluctuations. While not totally negligible, the radius of such pipes

[11] Beam-beam feedback cannot suppress noise sources at frequencies higher than about one tenth of the signal sampling rate. For instance, random amplitude jitter from upstream sources or magnetic-center vibration of the final doublet could not be effectively compensated for if occurring above about 300 kHz in TESLA (bunch-to-bunch) or 10 Hz in JLC-X/NLC (train-to-train).

would be sufficiently small (<5 cm) that the impact on detector coverage would be moderate. The compactness of the inertial sensors currently under consideration suggests that by themselves, they would not require significant space beyond the blind spot arising from pair stay-clear and masking. The choice of FD support technology, however, may have a larger impact. Two approaches are under study: spring-mounted soft supports with active vibration damping, or rigid supports possibly associated with a larger array of vibration sensors to detect internal vibration modes of the FDs. The choice of support scheme is partially linked to the choice of FD technology (PM or superconducting) and to the stabilization method(s) adopted (mechanical feedback or feedforward-stabilization of magnetic centers). A detailed evaluation will only be possible once designs are more advanced.

7.4.4.1.1 Items for Further R&D

- It is essential for any warm-rf linear collider project to demonstrate FD stabilization in an environment that adequately reproduces the system constraints of an actual detector and IR (Ranking: 3).
- The current TESLA design relies entirely on the intratrain IP feedback to guarantee collision stability. Although a similar technique has been used routinely at SLC, PEP-II and KEKB, its success is crucially dependent on the performance of the corresponding instrumentation (BPMs, pair luminosity monitor) in a high-disruption, high-radiation environment. It may be prudent to incorporate some form of FD stabilization in the baseline design to anticipate unexpectedly large vibration problems (Ranking: 3).
- The detector implications of the proposed support and stabilization scheme(s) should continue to be investigated as part of these studies (Ranking: 4).

7.4.4.2 Magnet Technologies

7.4.4.2.1 Requirements The final-focus quadrupole doublet faces a number of challenging requirements. The doublet must be placed a few meters from the IP, develop a high gradient, accommodate the spent-beam channel, and be mechanically and electromagnetically stabilized. It must be able to operate, with long-term field stability, within a harsh radiation environment.

In addition, it is advantageous if the magnetic field of the doublet is adjustable to accommodate energy-tuning of the collider. This would also permit beam-based alignment.

7.4.4.2.2 Technology Choices and Assessments Table 7.26 presents the details of the baseline design choices for the final focus doublet for each linear collider project.

- TESLA's choice of superconducting technology [99] takes advantage of the lack of a crossing angle: the large mechanical envelope of the doublet and the fringe field present no problem for the extraction line. The aperture must be large enough to accommodate the spent beam and its beamstrahlung. This leads to a high-field

TABLE 7.26
Summary of baseline FD magnet parameters. In the last column, the length refers to the magnet adjacent to the IP.

Project (beam energy)	Technology	Field Gradient [T/m]	Radial Aperture [mm]	Pole Tip Field [T]	Width [mm]	Length [m]
TESLA (250 GeV)	Iron-free superconducting, Nb_3Sn at 1.8 K	250	28	7	355	1.7
NLC (250 GeV)	$SmCo^5$ permanent magnet	144	10	1.44	56	2.0
JLC-X (250 GeV)	Resistive iron electromagnet, with SC shield	188	6.9	1.3	20	2.4
CLIC (1.5 TeV)	Sm^2Co^{17} permanent magnet	388	3.8	1.5	43	3.5

magnet, not unlike an LHC quadrupole, but with the significant complication of the presence of the 4 T detector solenoid field, which requires the use of Nb_3Sn as the superconductor. The required critical-current performance of the cable is demanding but has been reached in R&D samples. The resulting large Lorentz forces on the coils present mechanical design challenges, particularly since the conductor is relatively brittle. The amplitude of magnetic-center vibrations produced by vibrational coupling from the cryosystem (or by cooling fluids) should be estimated to check that they remain within the correction capability of the feedback system. The field strength is fully adjustable over a large dynamic range.

- With a 20 mrad crossing angle, NLC has chosen a PM solution ($SmCo^5$) as its baseline; a compact superconducting magnet for NLC is also under study at BNL. The compact size eases the mechanical stabilization issues and allows a simple design for the extracted-beam channel. Although there is no magnetic shield in the baseline design, depolarization of the PM material in the solenoid field has been studied and found not to be a concern [100]. Because of the dependence of the remanence on temperature, there are tight overall temperature stability requirements (driven by overall field strength changes) and very tight thermal gradient requirements (driven by shifts of the magnetic center). Such thermal gradients might be generated by, for example, asymmetric energy deposition in the FD pole tips. The overall temperature or thermal gradient variations will very likely be slow, and their effects should be compensated by the inter-train feedback system. It may be possible to adjust the field strength over a limited range [101].

- JLC's baseline solution [102] is a small-aperture resistive-iron electromagnet, protected from the solenoid field by a superconducting shield. The problem of the large size of the device is solved by using the coil pocket for the spent-beam channel. Significant issues in this design are possible mechanical vibrations due to cooling water, and perturbations to the spent-beam transport due to fields in the coil pocket. The field strength is adjustable. However the highly saturated pole tip will limit the dynamic range over which adequate field quality can be maintained.

- Like NLC, CLIC uses a compact REC PM design, which can be mechanically stabilized and accommodates a separate spent-beam channel. Sm^2Co^{17} is chosen for its radiation hardness. The 3 TeV design [103] uses a short doublet which does not overlap with the solenoid field but requires in addition a very strong PM sextupole. It also has tight overall temperature stability requirements and very tight thermal gradient requirements. The 500 GeV design needs a field gradient roughly six times smaller, and an inner radius of 6.6 mm. The field-strength adjustability has not been studied.

7.4.4.2.3 Items for Further R&D

- The availability of compact SC final-doublet quadrupoles, with adequate vibration characteristics, would greatly improve the operational flexibility of crossing-angle machines. R&D on this topic should be vigorously pursued (Ranking: 3).
- Adjustability, over a wide range, of the strength of PM FD quadrupoles is highly desirable. R&D on this topic is ongoing, and is strongly encouraged (Ranking: 3).
- For the PM designs, one of the issues is the tight temperature stability and thermal gradient requirements (Ranking: 3). Estimates should be made to ensure that the thermal time constants are sufficiently long for feedback to be useful, and to determine whether there is a risk to develop thermal excursions large enough for them to exceed the range of the feedback systems. If a problem is found, then the use of a temperature-compensated material can be considered.
- For the resistive design, the dynamic range should be evaluated, and the effect of vibrations induced by water cooling on the motion of the magnetic center should be investigated (Ranking: 3).

7.4.5 Beam Halo, Collimation, and Machine Protection

Control of detector backgrounds originating from the accelerator itself is an important concern for luminosity performance. The peak luminosity—often taken as the figure of merit for performance—is useless if the detector is simultaneously blinded by unacceptable background.

Incoming-beam backgrounds can be loosely categorized into two related topics: the beam halo, which can extend many standard deviations beyond the beam core; and the generation of muons from halo particles that are intercepted by physical apertures. All machine designs realized early the need to remove the halo to a certain depth. This "collimation depth" is generally set by the synchrotron-radiation fan generated by the halo particles in the last few magnets close to the IP: by definition, all particles within the collimation depth generate photons that should pass cleanly through the IR.

Halo particles outside of the required collimation depth are removed by physically intercepting them with mechanical "collimators," which are formed by a thick absorber of many radiation lengths (X_0), placed in the optical shadow of a thin (0.25–1 X_0) spoiler. The spoiler is necessary to protect the absorber from a direct hit by the beam, the multiple

Coulomb scattering in the thin spoiler being sufficient to reduce the peak energy density on the face of the absorber to below damage threshold. By definition, the spoilers are the smallest apertures in the machine (relative to the beam size) and therefore likely to be the first aperture hit by a wayward beam. For this reason, machine protection is a significant design constraint for a collimation system. In the following sections only the thin "spoilers" are referred to, as their apertures generally define the collimation depth. It is generally implicit that a spoiler shadows an associated thick absorber, as described previously.

In principle, the loss of particles from the halo should be at controlled points along the lattice (*i.e.*, at the absorbers and spoilers). These locations then become sources of muons. How many of these muons eventually reach the detector depends on many factors: distance from source to the IP, beam-line layout, tunnel geometry and the use of "muon spoilers" or "tunnel fillers."

7.4.5.1 Halo and Collimation Efficiency

The current collimation systems for TESLA, JLC-X/NLC, and CLIC have been outlined in the machine overviews. They share the following common features:

- A pre-linac (low-energy) collimation system to remove beam tails (halo) generated primarily in the damping ring
- A post-linac momentum collimator system
- A post-linac multistage betatron collimation system

These systems exist (at least conceptually) in all the designs, but the level of detailed design work differs across projects. An actual design for the pre-linac low-energy collimation system does not exist, although space has been allowed for it in all machines. In the remainder of this section we will attempt to highlight the differences between the current approaches to post-linac high-energy collimation (Table 7.27), which poses the more difficult problem. It should be noted that, with the exception of the TESLA emergency-extraction scheme, none of the collimation schemes currently being discussed are specific to the machine design, and all are to a certain extent interchangeable (although implementation details would differ).

It is not possible to stop all the halo particles: edge scattering, non-linear fields at high particle amplitudes, *etc.* tend to repopulate the phase space outside the collimation depth. The effectiveness of the collimation system can be defined in terms of either:

- The fraction of initial halo particles that survive (or are rescattered out of) the primary collimation system, and hit secondary collimators or other aperture limitations closer to the IP. This "primary-collimation efficiency" is relevant when estimating muon backgrounds.
- The number of halo particles that lie outside the collimation depth when they reach the final doublet. This parameter is relevant when estimating synchrotron-radiation backgrounds (as well as the rate of lost-particle hits close to the detector, if any).

TABLE 7.27
Main parameters of the post-linac primary collimation system ($\sqrt{s}$=500 GeV); the full list is available in Reference [104]. $\sigma_{x,y}$ are the horizontal and vertical beam sizes at the spoiler (including the dispersive contribution); $\sigma^{\beta}_{x,y}$ refer to the betatron contributions alone. The quoted muon rates include those produced in the collimation section as well as further downstream in the BDS. In some cases, the spoiler settings must be tighter than the effective collimation depth (at the final doublet) because of dispersive or higher-order effects.

		TESLA	JLC-X/NLC	CLIC
Nominal collimation depth	# $\sigma^{\beta}_{x,y}$ at spoiler	12, 74	11, 31	9, 65
Momentum collimator	x gap [mm]	±1.50	±3.20	±1.60
	$\sigma_{x,y}$ [μm]	154, 4.5	534, 29	814, 38
Betatron collimator				
Final-doublet phase	x, y gaps [mm]	±1.50, ±0.50	±0.30, ±0.20	±0.34, ±0.20
	$\sigma_{x,y}$ [μm]	129, 7	28, 6.5	38, 3
IP phase	x, y gaps [mm]	±1.50, ±0.50	±0.30, ±0.25	±0.30, ±0.20
	$\sigma_{x,y}$ [μm]	128, 7	16, 0.8	22, 3
Primary-collimation efficiency		0.01	$<1\times10^{-5}$	$<3\times10^{-4}$
Muons reaching IR (single beam)	for 10^{-3} halo	10–100 (per 150 bunches)	1–10 (per train)	50–500 (per train)
Effective collimation depth	# $\sigma^{\beta}_{x,y}$ at FD	13, 80	15, 31	11, 100

All machines currently have a dedicated primary collimation system located upstream of the final focus system (FFS). Additional secondary or "clean-up" collimators are located in the FFS. The maximum number of halo particles that may be intercepted in this secondary system is limited by the IP muon flux the detector can tolerate. The primary system—which intercepts most of the halo--should have high enough an "efficiency" to reduce the losses in the secondary system to acceptable levels. At the same time, the combination of primary and secondary collimation must bring the halo population outside the collimation depth in the final doublets within tolerance. It is typically required that no SR photon (whether produced by the beam core or by the halo) be allowed to hit any detector or machine component between the entrance to the final doublet on the incoming beam side to the exit of the other doublet on the outgoing side. In addition, no charged halo particles are allowed to hit the beam pipe in the same region.

Whether or not the quoted efficiencies are sufficient depends not only on the tolerance of the detector to the different backgrounds, but also on the population (density) of the actual halo entering the BDS. Analytical estimates of the halo population have been made for all the machine designs [105, 106, 107], and all quote conservative estimates on the order of 10^4 particles per bunch outside the collimation depth, corresponding to a fraction of about 10^{-6} of the total bunch charge. Sources of halo considered were the damping ring, residual gas scattering, wakefields and linac dark current. There is general consensus that the damping rings are a significant source of halo, and that a pre-linac collimation system with an efficiency of better than 10^{-3} is required (the previously quoted halo estimates assume the existence of such a system).

The NLC design[12] uses five betatron spoilers in the primary system placed alternately at the IP phase and at the final-doublet phase, the latter being the most critical. A separate momentum spoiler is located downstream of the betatron spoilers at a high dispersion point

[12]The version discussed here [104] differs from that described in Reference [108] only by the location and/or aperture of some of the spoilers and SR masks.

(∼200 mm). Three additional "clean-up" spoilers are located in the FFS. The primary system allows for a collimated halo population of up to $\sim 10^9$ particles per bunch train (10^{-3} of the full beam current) and achieves a collimation efficiency significantly better than 10^{-5}, resulting in less than 10^4 particles per train being lost in the secondary system (Figure 7.28, left). Simulations of muon production and tracking indicate that a loss rate of 10^9 particles in the primary collimation system produces a few muons in the detector (assuming two magnetized "tunnel-fillers" between the collimation system and the IR). A loss of 10^6 particles in the secondary system produces one muon in the detector, which, given the high efficiency of the primary system, translates into less than 0.01 muon per bunch train. The tolerable loss rate in the primary system, which is three orders of magnitude larger than the analytical estimates of the halo population, allows for a considerable safety margin: this conservative approach is inspired by the SLC experience, where the measured detector backgrounds vastly exceeded predicted levels. In addition, the NLC has implemented a novel non-linear optical scheme[13], in which octupole doublets placed in the FFS "fold" the halo particles into the required collimation depth. These doublets, which work most efficiently only in a final focus system with local chromaticity correction, loosen the required physical apertures of the collimators by a factor of 2–4 compared to those quoted in Table 7.27, reducing the amount of halo that needs to be intercepted.[14]

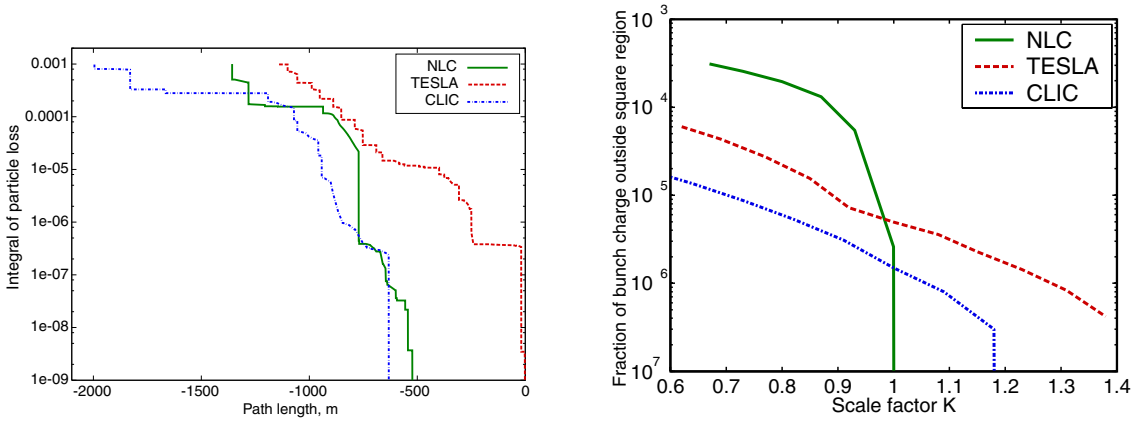

FIGURE 7.28. Collimation-system performance [104] assuming an incident fractional halo of 10^{-3}. Left: fractional loss of charged-halo particles, integrating back, starting at the IP, and normalized to the nominal bunch charge. The horizontal scale shows the distance from the IP. The upstream edge of the secondary-collimation system is located at −543 and −583 m in NLC and TESLA respectively. In CLIC, the last betatron absorber is located at −632 m. Right: number of charged-halo particles per bunch, normalized to the nominal bunch charge, in a rectangular $x-y$ window at the entrance to the final doublet, as a function of the collimation depth. The scale factor K defines the window dimension: for K=1, the window size corresponds to the effective collimation depth listed, for each machine, in Table 7.27.

[13]This concept has also been proposed independently by the TESLA group but is not included in their present design [93].

[14]The collimation-efficiency figures quoted here do not assume the use of tail-folding octupoles.

The TESLA system is somewhat different: five pairs of x-y spoilers are separated by a phase advance of about $\pi/4$, forming an octagon in phase space (the first and last spoilers are degenerate in phase). The first spoiler has a non-zero horizontal dispersion (100 mm) and acts as the primary momentum collimator. There are four additional "clean-up" collimators in the FFS itself. Recent simulation results have shown that with the primary collimation as currently designed, the loss rate in the secondary system amounts to about 1% of the initial halo population. Because the TESLA bunch spacing is longer than the entire bunch train for the warm machines, TESLA generally quotes background rates per bunch crossing. However the subdetector most sensitive to muon background (the TPC) integrates over 150 bunches, so that for the same assumed incident halo fraction of 10^{-3}, the effective halo population becomes similar to that of NLC. TESLA has proposed not to use the tunnel-filler approach to suppress the muons from the primary collimation system, opting instead for smaller magnetized toroids. These have a length of 10 m, diameters between 0.5 m and 1.0 m, and a field of 10–14 kG. Simulations have shown that twenty such toroids distributed in the lattice between the collimators and the IR can reduce the muon rate by three orders of magnitude, allowing a particle loss of $\sim 10^8$ in the primary system for one muon in the detector. Again assuming a collimated halo of 10^{-3}, this translates into up to 30 muons in the detector for 150 bunches. Muons from the secondary system close to the IR must also be considered. Typically 10^6 particles lost in this region generate one muon. With the previously quoted primary-collimation efficiency, the remaining halo in the secondary system amounts to 3×10^7 particles/150 bunches, resulting in $\sim$30 additional muons reaching the detector.

For the purposes of this review, the CLIC-500 collimation system is taken to be a scaled version of the 3 TeV variant. The 3 TeV requirement is primarily reflected in the system length (over 2 km per side, compared to less than 1 km for the NLC and TESLA systems); shorter layouts are currently being investigated. The system consists of an energy-collimation section followed by a betatron-collimation section. The design of the momentum-spoiler optics is primarily driven by spoiler-survival considerations, and is characterized by a single dispersive peak (D_x $\sim$500 mm) with a large vertical β-function ($\sim$100 km) which increases the design beam size at the spoiler to a safe value ($\sqrt{\sigma_x \sigma_y}$ $\sim$180 μm). The downstream betatron system consists of four spoilers at alternating IP and final-doublet phases with much smaller beta functions. Muon studies have been performed for the 3 TeV center of mass case: using three tunnel fillers, the loss rate per muon reaching the IP typically amounts to 3×10^5 particles [109]. At 500 GeV c.m. energy, the tolerable rate should be an order of magnitude higher; a reference fractional halo of 10^{-3} would then result in $\sim$250 muons per bunch train in the detector.

Computations of the collimation efficiency at the final doublet, and of the resulting halo-induced SR backgrounds, are still in progress for the various designs. Recent calculations [104] that include charged-particle tracking (both of halo primaries and of shower secondaries) as well as SR photon production in non-linear magnetic elements, are illustrated in Figure 7.28 (right).

- The design of the NLC collimation system is well advanced. The edge of the collimation depth is sharply defined; but for no halo photons to hit the beam pipe near the IP, rather tight collimator settings ($\pm$0.2 mm) are needed (in the absence of tail-folding octupoles only).

- In TESLA, the boundary of the collimated halo is barely visible, in spite of several tight collimator settings, in particular in the secondary-collimation system. A large number of halo particles ($\sim 10^5$ per bunch) enter the final doublet outside the collimation depth.[15] The simulations also indicate that with the collimator configuration simulated here (which corresponds to that of Reference [93]), some SR photons from the halo ($\sim 2\times 10^4$ γ's per bunch) do hit the detector mask located 3 m from the IP; their total energy (150 GeV per bunch) is however small compared to that of beam-beam induced pairs. More importantly perhaps, the same study also shows a sizeable outgoing photon halo ($\sim 1.2\times 10^5$ GeV/bunch, corresponding to about 1.2×10^7 photons) hitting the downstream SR mask 18 m from the IP: the total energy of the halo photons intercepted by this mask is comparable to that of outgoing SR photons from the beam core hitting the same mask. Finally, about 10^{10} photons/bunch radiated by the core of the incoming beam hit the SR mask upstream of the IP. All of these background sources are cause for serious concern, because the simulations at this stage completely neglect back-scattering and edge-scattering of SR photons off masks and other aperture limitations. It should be noted that the relative intensity of the background sources is extremely sensitive to the interrelated aperture settings necessary to simultaneously accommodate an incoming and an outgoing beam. While it is plausible that the effectiveness of the collimation system may be further improved, these results underscore the urgent need for more detailed studies.

- Detailed simulations of the 500 GeV CLIC system are only beginning, and the collimator configuration is still very much in flux.

7.4.5.2 Machine-Protection Issues

Hardware survival is an integral part of the design of the collimation system. Although the thin spoilers are designed to protect the downstream absorbers from a direct hit from the beam, the extremely high bunch charge densities require protection of the spoilers themselves.

TESLA has the advantage of a long bunch train and large bunch spacing. In the event of a failure, the bunch train can be "kicked out" of the machine and sent to the main dump. This fast-extraction system is located upstream of the momentum spoiler. BPMs strategically placed a few meters upstream identify off-axis or off-energy bunch trains and fire a bank of 40 fast kickers which extract the remainder of the bunch train to the main dump via a dedicated beamline.[16] The system is designed to allow at most two bunches through before firing, at least for the most frequent failure type (a fast energy or betatron error that occurs on the time scale of the interbunch separation). Faults such as power supply failures or shorting magnet coils anywhere along the machine, are expected to develop on a sufficiently slow time scale for BPMs to detect dangerous orbit drifts, or for

[15] The apparent contradiction with Figure II.7.5.3 of Reference [93], in which no particles are found outside the collimation depth, remains to be resolved.

[16] In addition to firing the kickers, a signal is sent to the damping-ring extraction system which aborts the pulse: given the linac length, this corresponds to about 340 bunches which need to be handled by the fast extraction system.

beam-inhibit watchdogs to abort the next pulse whenever a hardware fault is detected in the 200 ms between bunch trains.

The nominal beam size at the downstream momentum spoiler is sufficiently large (even for the worst-case e^+ beam) that it should survive a direct hit from one bunch (possibly two). In the current TESLA design, a further protection for the momentum spoiler is provided by the magnetic energy spoiler (MES), a non-linear optics module which increases the vertical beam size in the event of an energy error, allowing the mechanical spoiler to survive 4–6 bunches. Since the non-linear system also reduces the momentum bandpass (Section 7.3.2.4), its use is still under review. The rationale behind the additional protection of the momentum spoiler reflects the philosophy that fast energy errors are expected to be significantly more frequent than pure orbit errors (with an amplitude large enough to strike the spoilers). The TESLA system reduces the spoiler protection issue to that of single-bunch damage, but at the same time shifts the emphasis onto the reliability of critical MPS components (fast kickers, BPMs, hardware watchdogs, etc).

A TESLA-style fast extraction system is not possible for NLC or CLIC because of the much shorter bunch spacing and bunch train. Here the spoilers must deal with the entire bunch train ($\sim 10^{12}$ particles, compared to $\sim 10^{10}$ for a single TESLA bunch). Both NLC and CLIC have adopted the philosophy of passively protecting the momentum spoilers by placing them at locations of larger horizontal dispersion and vertical β-function. Table 7.28 lists the nominal beam parameters relevant to spoiler survival. The critical figure of merit is the peak particle density, which is proportional to the total number N_p of particles striking the spoiler, and inversely proportional to the area of the beam spot ($\sigma_x \sigma_y$).

TABLE 7.28
Spoiler-survival parameters for the momentum and betatron spoilers ($\sqrt{s}$=500 GeV). For TESLA, N_p is twice the single-bunch population, while for CLIC and NLC it refers to that of the entire bunch train. σ_x and σ_y are the horizontal and vertical beam size at the spoiler (including the dispersive contribution).

		N_p [$\times 10^{10}$]	$\sqrt{\sigma_x \sigma_y}$ [μm]	$N_p/(\sigma_x \sigma_y)$ [μm^{-2}]
Momentum	TESLA	4	26	5.8×10^7
	NLC	144	124	9.4×10^7
	CLIC	62	176	2.0×10^7
Betatron (FD / IP phase)	TESLA	4	30 / 31	$4.6 \times 10^7 / 4.2 \times 10^7$
	NLC	144	13.4 / 3.5	$8.0 \times 10^9 / 1.2 \times 10^{11}$
	CLIC	62	10.9/8.3	$5.2/9.0 \times 10^9$

Estimates based on instantaneous temperature rise and ultimate tensile strength suggest[17] that $N_p/(\sigma_x \sigma_y)$ should remain below 2–3$\times 10^7$ for Cu, and below 1–3$\times 10^8$ for Ti. Table 7.28 indicates that the Ti TESLA spoilers lie comfortably below damage threshold. The CLIC momentum spoiler is below the Cu threshold, while the NLC one is not. For the betatron spoilers, both CLIC and NLC significantly exceed the quoted limit. The NLC design

[17] These threshold values are based on the initial energy loss, and are therefore valid for thin spoilers only. For "thick" spoilers, the thresholds are further reduced by the shower development.

philosophy assumes that a direct hit will locally damage the spoiler, and proposes either "consumable" (or "reparable") spoilers [110], which can be rotated to offer a new undamaged (or reconditioned) spoiler edge to the beam. The current NLC prototype design for the consumable spoiler has the capacity to withstand approximately 1000 damaging pulses before being replaced. The advantage here is the short length and relatively small β-functions of the collimation system, leading to looser tolerances and better wakefield performance; this is offset to some degree by the complexity of the spoiler design itself.

CLIC studies of various linac failure modes suggest that a beam with a betatron amplitude large enough to strike a spoiler, will have its emittance diluted by the strong linac wakefields by as much as two orders of magnitude [111]. But failures causing a significant energy deviation are not necessarily accompanied by a large beam-size increase at the momentum collimator, and some energy errors are small enough for the beam to hit the betatron collimators located further downstream [112]. CLIC is therefore also considering the use of consumable spoilers.

7.4.5.3 Other Considerations

Wakefields: The control of transverse wakefield kicks from the relatively narrow spoiler and absorber gaps must also be considered. All machines propose to use spoilers with long tapers to reduce the effect of the geometric-wakefield kick. The current design of the consumable spoiler for NLC uses tapers constructed from beryllium, which will have a 1 μm copper coating to reduce the resistive-wake effect [110]. The NLC group, in collaboration with other laboratories, has also carried out wakefield tests, using the SLAC linac beam on several different spoiler geometries and materials to cross-check theoretical calculations. The potential impact of collimator wakefields on luminosity has been discussed in Section 7.3.2.6.

Mechanical Design: The gaps of both spoilers and absorbers need to be remotely adjustable so that they can be (i) fully opened during commissioning, and (ii) adjusted during background tuning. The NLC has the most advanced design for the consumable collimator, where a prototype has been successfully constructed and tested: with a few minor engineering modifications it is thought that the design will achieve the required tolerances [110]. R&D is still on-going on the copper coating for the beryllium taper. At other machines, the static-jaw type of collimator is more in keeping with existing designs, although tolerances are tighter. It should be noted that R&D into novel materials and designs for collimators is on-going (for example at LHC), the results of which are also likely to be of benefit to the LC designs. There is clearly room for more work on these topics.

7.4.5.4 Summary and Items for Further R&D

7.4.5.4.1 Collimation-System Concepts Collimation-system concepts appear feasible, be it in terms of optical layout, primary-collimation efficiency, spoiler and absorber design, or machine protection. But the designs are not mature yet: in some areas, substantial uncertainties persist, or realistic performance margins remain to be incorporated.

- The tight aperture settings needed to achieve satisfactory collimation efficiency, coupled with significant beam jitter, can lead to a substantial luminosity degradation by wakefields. (See Section 7.3.2.6). Tail-folding octupoles appear very promising to significantly relax the collimation requirements, but this technique is not yet integrated in all BDS designs. If collimator wakefields are eventually measured to be as large as predicted by current models, then the experimental validation of the tail-folding technique becomes an important R&D topic (Ranking: 3).

- The level of halo SR intercepted in the IR area is of some significant concern in the TESLA case, and its implications for detector backgrounds must be thoroughly investigated. A careful review of the SR flux produced by the core of the beam is also clearly required for all projects. This flux is one to two orders of magnitude larger in TESLA than in NLC (because of stronger bends and quadrupoles). Even though in both cases beam-core photons appear adequately intercepted by the SR masks located 10–20 m from the IP, more sophisticated computations of potential SR backgrounds, that include tip-scattering and back-scattering from all aperture limitations, are highly necessary (Ranking: 3).

- The available halo-related background simulations suggest that the collimation systems as designed would yield, at $\sqrt{s}$=500 GeV, 1–10 muons per effective bunch train into the NLC detector, and approximately ten (fifty) times more at TESLA (CLIC), pessimistically assuming a collimated halo of 10^{-3} of the bunch charge. While considered tolerable (Section 7.4.6.1), the predicted muon rates are sensitive to both the tunnel and the machine geometry: the numbers quoted previously should only be considered as order-of-magnitude estimates (Ranking: 3).

- Background simulations: a great deal of work has been done to understand the halo and its impact on the detector performance. However, given the statistics of the problem (a few particles in 10^{10} can cause an enormous increase in detector backgrounds), there is clearly scope for further studies. Simulation tools are currently being developed to enable better tracking of both primary and secondary particles, while the models of the machines and their environment (*e.g.*, tunnel layout) become increasingly detailed. Studies of "tuned" machines which include errors are also required, to better understand the interaction between luminosity and background tuning (Ranking: 3).

7.4.5.4.2 Machine Protection As some details of the designs continue to evolve, a thorough and recurring review of potential failure modes is mandatory (Ranking: 3). In TESLA for instance, recent simulations show large halo-induced losses [104] early in the collimator section, confirming a risk of beam-induced damage in this area: an additional protection collimator may be required at a high-dispersion point further upstream. Another example concerns the warm machines. It is assumed that the single-bunch damage threshold is independent of whether or not there are following bunches. There could be cases, however, where material survives a single bunch because the beam is blown up, but the total heat deposited by the train causes a problem.

7.4.6 Detector Backgrounds

Several detector designs are being pursued [113]. Proceeding radially outward from the IP, a generic layout contains a silicon vertex detector, main tracker, electromagnetic calorimeter, hadronic calorimeter, solenoid coil, iron yoke and muon system. In general the physics requirements lead to detectors somewhat larger than at LEP/SLC and with much stronger magnetic field ($\geq$3 T) in order to handle the higher energies and more intense backgrounds. This activity is now generating extensive R&D on subdetector technology [114].

While the designs are primarily driven by physics performance, there remains leeway in the choice of subdetector technologies, and it is equally important to ensure robustness against accelerator-induced backgrounds. Their potential impact falls in two categories:

- Degraded performance (tracking efficiency, pattern recognition, energy resolution, background rejection). Tolerance criteria are briefly discussed in Section 7.4.6.1. The expected background rates have been evaluated in a fair amount of detail [83, 115, 116, 117, 118, 119] as part of the IR-design optimization process, and are reviewed in Section 7.4.6.2 to Section 7.4.6.4.
- Radiation damage. This is an issue mainly for CCD-based vertex detectors (Section 7.4.6.4).

7.4.6.1 Detector Tolerance to Backgrounds

The detector tolerance can be quantified by comparing the "pain threshold" (defined as the background level where the performance of a subdetector starts being compromised) to the background level predicted in that same subdetector under nominal operating conditions.

It is typically assumed that a 1% occupancy limit in a tracker is conservative. However this can translate into rather different tolerance levels, depending on the chosen detector technology. The TESLA TPC, for instance, integrates over about 150 bunches, but its exquisite three-dimensional granularity makes it highly background-tolerant: a 1% limit translates into 2550 muons per 50 μs [120]. More generally, the time structure of the beams and the sensitivity window of each subdetector must be taken into account when computing the effective occupancy. Overall, the estimated occupancies in tracking detectors appear moderate even when integrated over the full bunch train of the warm machines.

Tolerable background levels in calorimeters are harder to quantify in a general way, as their impact depends not only on the fraction of cells above threshold, but also on the actual amount of energy deposited and on the physics channel under study. TESLA states [120] that all its subdetectors have higher safety margins than the TPC, and that the whole detector is robust against background underestimations. One could envisage [120] a criterion similar to that of the tracking systems, requiring for instance that less than 1% of the calorimeter cells contain an energy deposition comparable to that of a minimum ionizing particle. Given the high granularity (10^4–10^5 cells) and the integration time (100–200 ns) of the calorimeters currently under study, this translates into a tolerable muon rate of a few per train in the warm machines, equivalent to about 600 muons per 50 μs in TESLA. The same criterion leads to tolerable total energy depositions (excluding the low-angle calorimeters) of the order of a few hundred GeV (per train in warm machines, per

pulse in TESLA). But these are only rough estimates, that need to be validated by physics-performance studies.

7.4.6.2 Beam-Beam Backgrounds

7.4.6.2.1 Pairs The dominant background source is that of incoherently produced $e^{\pm}$ pairs which stem from the conversion of beamstrahlung photons in the strong electromagnetic field of the colliding bunches (Section 7.4.2.2). The overall pair-production rate (Table 7.29), as well as the number of $e^{\pm}$ reaching a "generic" vertex detector (Figure 7.29), are largest in TESLA because of the larger bunch population and larger number of beamstrahlung photons per electron.

TABLE 7.29
Number and energy of pairs produced at $\sqrt{s}$=500 GeV, computed with GUINEA-PIG.

	TESLA	JLC-C	JLC-X/NLC	CLIC
Number of pair particles/crossing	152,000	44,000	52,000	32,000
Number of pair particles/sec	2.1×10^9	0.84×10^9	1.2×10^9	0.99×10^9
E_{tot}/crossing [TeV]	354	117	185	153
$< E(e^{\pm}) >$ [GeV]	2.3	2.7	3.6	4.8
Number of pair particles/crossing ($p_t > 20$ MeV/c, $\theta > 200$ mrad)	39	11	12	7.2

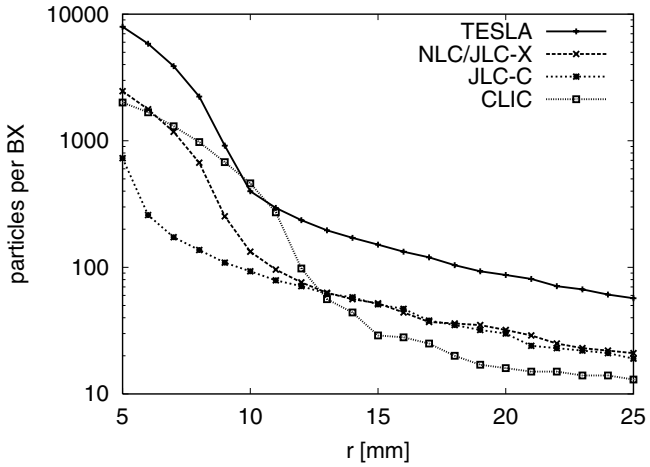

FIGURE 7.29. Number of particles per bunch crossing that hit the innermost layer of the vertex detector. The same solenoidal field B_z=4 T and angular coverage $|\cos\theta| \leq 0.98$ has been assumed for all machines. The radial edge of the stay-clear cone is apparent.

GEANT-level simulations of the optimized IR configurations[18], including beamstrahlung photon and pair production, as well as scattering and transport of secondaries in the presence of masks and detector elements, yield the background estimates listed in Table 7.30 to Table 7.31. The occupancy is far below critical levels in the vertex detectors.[19] The TPC occupancy remains well below the 1% tolerance. The calorimeter occupancy appears of no concern in the TESLA case because of the long bunch spacing. The short trains of the warm machines, however, result in cumulative background energy depositions which may be an issue for some physics topics. The time resolution of the calorimeters will strongly influence the background rejection capability and is an important design consideration.

7.4.6.2.2 Hadronic Events The rate of two-photon hadronic events (Section 7.4.2.2) predicted by GUINEA-PIG for the various machines is listed in Table 7.32 for several sensitivity windows. The resulting charged-hit density in the vertex detectors lies two to three orders of magnitude below that induced by the pairs. Assuming a mean charged-hadron multiplicity of 10–20 particles per event above p_T threshold, a few ten charged tracks would cross the volume of a TPC during the integration time of that detector. While these could in principle fake interesting physics events because they all originate from the nominal IP, the time resolution of the TPC should allow disentangling them from interesting processes, at least in the TESLA case. The energy deposited in the calorimeters is comparable to, or slightly larger than, that from the $e^{\pm}$ pairs.

7.4.6.3 Single-Beam Backgrounds

7.4.6.3.1 Muons The estimated muon flux at the detector has been reported in Table 7.27. At $\sqrt{s}$=500 GeV and assuming the use of some kind of "muon spoilers," the predicted rates remain, in all designs, one to two orders of magnitude below the critical level in the tracking systems (provided the detector granularity is large enough). The rates remain acceptable for the calorimeters, albeit by a narrower margin. As discussed in Section 7.4.5.1, these safety factors remain subject to sizeable uncertainties: population of the incoming halo, tunnel and beam-line geometry, longitudinal distribution of secondary-particle losses, collimation and muon-spoiler efficiencies, *etc.* But the assumptions used in designing the collimation system appear sufficiently conservative to provide a satisfactory margin on muon backgrounds.

7.4.6.3.2 Synchrotron Radiation Synchrotron radiation is produced by the incoming beams in the fields of the last bending magnets and final quadrupoles (as well as by the outgoing beam in the TESLA FD). The collimation systems have been designed so that all SR photons should pass cleanly through IR without striking any part of the detector [121]. Recent comparisons [104] of SR backgrounds in TESLA and NLC demonstrate that

[18] The CLIC simulation reported here actually uses the 3 TeV detector model, but with a reduced vertex-detector inner radius.

[19] provided the readout of the TESLA CCD can be shortened appropriately, as assumed in Table 7.30. Since the CCD readout is slow, it typically integrates over a whole train for the warm-machine designs. Applying a similarly "conventional" CCD technology to TESLA would result in occupancies of 100 mm^{-2} and 8.7 mm^{-2} in layers 1 and 2 respectively. Thus the CCDs must be read out much faster so as to only integrate over about 150 bunches. For this eventuality a "column-parallel" readout is being designed for the CCDs. Other vertex-detector technologies are also being considered [113].

TABLE 7.30: Pair-induced occupancies in the TESLA subdetectors, including secondaries ($e^{\pm}$, γ) [83, 116], at $\sqrt{s}$=500 GeV. The vertex detector is primarily sensitive to charged hits. The sensitivity window is the subdetector integration time. R_V is the radius of the vertex-detector layer. The solenoid field strength is 4 T.

Subdetector	Hits or energy per Crossing	Sensitivity Window	Effective # Bunches	Effective Occupancy	Comment
VXD (layer 1)	3.6 10^{-2} mm^{-2} (340 hits total)	50 μs	148	5.3 mm^{-2}	R_V=1.5 cm
VXD (layer 2)	3.1 10^{-3} mm^{-2} (126 hits total)	250 μs	742	2.3 mm^{-2}	R_V=2.6 cm
TPC	1336 γ, 5 trks	55 μs	160	Few per mil	
ECAL (Barrel + Endcap)	1176 $e^{\pm}$, γ ($E_{th} > 10$ keV) 192 γ, 1.92 GeV ($E_{th} > 3$ MeV)	150 ns	1	1.92 GeV ($E_{th} > 3$ MeV)	

Subdetector	Hits or Energy per Crossing	Sensitivity Window	Effective # Bunches	Effective Occupancy	Comment
VXD (layer 1)	3.8 10^{-2} mm^{-2}	train	192	7.3 mm^{-2}	R_V=1.2 cm
VXD (layer 2)	3.1 10^{-3} mm^{-2}	train	192	0.6 mm^{-2}	R_V=2.4 cm
TPC	1377 γ	train	192	Few per mil	
ECAL (Barrel + Endcap)	1741 γ, 2.53 GeV ($E_{th} > 10$ keV)	train	192	486 GeV ($E_{th} > 10$ keV)	

TABLE 7.31: Pair-induced occupancies in the CLIC subdetectors, including secondaries ($e^{\pm}$, γ) at $\sqrt{s}$=500 GeV. Only charged hits are counted in the vertex detector. The sensitivity window of all subdetectors is assumed longer than the duration of the bunch train. R_V is the radius of the vertex-detector layer. The solenoid field strength is 4 T.

Subdetector	Hits or Energy per Crossing	Sensitivity Window	Effective # Bunches	Effective Occupancy	Comment
VXD (layer 1)	1.0 10^{-2} mm^{-2}	train	154	1.6 mm^{-2}	R_V=1.5 cm
VXD (layer 2)	1.3 10^{-3} mm^{-2}	train	154	0.2 mm^{-2}	R_V=2.5 cm
Central tracker	1400 γ ($E_{th} > 10$ eV)	train	154		
ECAL	5 GeV	train	154	720 GeV	
(Barrel + Endcap)	($E_{th} > 10$ keV)			($E_{th} > 10$ keV)	

TABLE 7.32: Beam-beam induced hadronic backgrounds at $\sqrt{s}$=500 GeV.

	TESLA	JLC-C	JLC-X/NLC	CLIC
Hadronic events/crossing	0.25	0.076	0.10	0.067
$E_{\gamma\gamma-c.m.s.} \geq 5$ GeV				
Hadronic events/100 ns	0.25	5.4	7.4	10
Hadronic events/(148 b or train)	37	15	20	10
	(/148 b)	(/train)	(/train)	(/train)
Number of minijet pairs/crossing [$\times 10^{-2}$]	0.74	0.24	0.36	0.29
p_T^{min}=3.2 GeV/c				
Number of minijet pairs/100 ns	0.01	0.17	0.26	0.44
Number of minijet pairs/(148 b or train)	1.1	0.45	0.69	0.45
	(/148 b)	(/train)	(/train)	(/train)

reasonable solutions are close. But they suffer from some of the same uncertainties as the muon flux predictions, do not yet take into account backscattered photons and scattering off mask tips (which in existing machines often dominate the flux eventually reaching the detector), and are potentially very sensitive to details of the magnet and mask apertures near the IP. Much more detailed simulations are clearly required to produce a comprehensive and robust picture of SR backgrounds, both from the halo and from the core of the beam.

7.4.6.3.3 Beam-Gas Backgrounds The beam-gas rate in TESLA was estimated [116] at 3×10^{-3} electrons/crossing leaving the beam pipe near the IP, for an (easily achievable) residual pressure of 5×10^{-9} mbar. This scales to 0.5 background events per 50 μs in the TESLA TPC. Preliminary estimates for the NLC suggest a somewhat larger rate for the same residual pressure, but even then the predicted absolute background level does not pose a significant problem.

7.4.6.4 Neutrons

Neutrons are produced through photo-nuclear reactions by bremsstrahlung photons from electromagnetic showers. Therefore any $e^{\pm}$ (from pairs, radiative Bhabhas, or spent-beam losses) or beamstrahlung photon hitting a mask or beam-line element is a potential source of neutrons. The dominant sources are neutron production by beamstrahlung-induced pairs (Section 7.4.2.2) and backscattering from the main dumps (Section 7.4.3.3). The main concern here is radiation damage to the vertex detector. The total flux predicted at 500 GeV c.m. energy is of the order of 1–2×10^{9} n/(cm$^2\times$yr) (Table 7.23), which is comparable to the neutron tolerance of present CCD's (1 to 10×10^{9} neutron hits/cm^2) [83, 116, 122]. This may therefore require periodic replacement of at least the innermost layer if this technology is eventually selected. Other vertex-detector technologies are more radiation-tolerant.

7.4.6.5 Items for Further R&D

7.4.6.5.1 Fluctuations The background rates quoted in this report assume ideal, static machines and perfectly centered collisions. Because of ground motion and other dynamical effects, both the position and the shape of the colliding beams will fluctuate from train to train, and even from bunch to bunch. Although strongly suppressed by feedback systems, the residual fluctuations will result in rapid variations in the instantaneous luminosity (Section 7.3.4.3), in the flux and the angular distribution of beamstrahlung photons (Section 7.4.3.3), and therefore in the intensity of beam-beam backgrounds. Because the rate of pairs is proportional to the product of the luminosity by the beamstrahlung flux, and because dynamic beam errors tend to lower the former and enhance the latter, the resulting background fluctuations will be smaller than those of the total photon flux; but they might result in a significant increase (50% or more) of the average level of beam-beam–related backgrounds. This effect has been neglected so far in detector studies and warrants further investigation (Ranking: 4).

7.4.6.5.2 Physics Studies Detailed studies of the impact of machine backgrounds on physics analysis are only beginning and more work is required for all designs. In warm machines for instance, the time resolution of the calorimeters will strongly influence the background rejection capability and is an important design consideration.

7.4.7 Beam Polarization and Energy Measurement

7.4.7.1 Polarimetry

The physics requirement for most studies is a measurement of the e^- polarization to 0.5% or better. For precision measurements at the Z-pole, the goal is 0.1%. SLD reached 0.5%, which was achieved using a Compton polarimeter downstream of the IP to measure the polarization continuously on every pulse, with about one third of the time spent on diagnostic scans to optimize performance and reduce systematics. An absolute accuracy of 0.25% might be achievable with a redesigned polarimeter, but 0.1% is very challenging.

All LC designs include a Mott polarimeter to monitor polarization at the e^- source, and a Compton polarimeter before and/or after the IP.[20] At 0.5–1 TeV c.m. energy, the theoretical beam-beam-induced depolarization of on-energy particles is small (<1%). The absolute uncertainty on the predicted, luminosity-weighted depolarization is likely to be a small fraction of the depolarization itself, but the latter will vary with beam-beam conditions (it can be as large as 10% for the low-energy tail of the luminosity spectrum). Ideally, the polarization should be measured both upstream and downstream of the IP to fully characterize this effect. Whether systematic uncertainties will limit the achievable precision if only an upstream measurement is available, remains an open question. A 0.5% accuracy might eventually be achievable under these conditions; but reaching the ultimate accuracy needed at the Z-pole will no doubt require either a polarimeter both upstream and downstream of the IP, or e^+ polarization.

The TESLA design has a Compton polarimeter 600 m upstream of the IP (the zero-crossing angle makes it difficult to locate diagnostics in the extraction line). This system has been described in detail in Reference [123]. With an appropriate pulsed laser, they estimate a 0.1% statistical measurement in one second and an overall precision of 0.5% as achieved at SLD. The impact of Compton-scattered e^- on detector backgrounds appears minor.[21]

The NLC, JLC X-band and C-band, and CLIC designs all have a crossing angle with a chicane in the extraction line to separate the spent charged-particle beam from the photons and allow energy-spectrum and polarization diagnostics. The NLC optics provides an image point of the IP mid-chicane where these diagnostics would be located, and beam losses are calculated to be acceptably low (at least at 0.5 TeV), but no detailed designs have

[20] Two other methods for measuring the polarization are the "Blondel" scheme, which requires the e^+ beam to be polarized, and the W-pair method, which improves with e^+ polarization. Both of these accurately measure the luminosity-weighted polarization, but they require e^+ polarization or energy above W-pair threshold, and they require time to integrate an adequate sample.

[21] The rate of scattered electrons has been estimated at about 10^4/bunch, with an almost flat energy distribution between 50 and 250 GeV. Tracking studies suggest that about 80% get lost downstream of the first CCS dipole; the corresponding muon rate is negligible (assuming the use of muon toroids). Another 13% hit a collimator 570 m upstream of the IP. A few tens of electrons per bunch may reach the final doublet outside the collimation depth; their impact on detector background remains to be investigated.

been done. A polarimeter upstream of the NLC IP has been discussed but has not yet been explicitly included.

7.4.7.2 Energy Spectrometer

A precise measurement of the beam energy is required for various physics studies. Typical precision goals are ∼40 MeV for the Top mass, ∼50 MeV for Higgs production threshold, 2–5 MeV for Giga-Z and <5 MeV for WW threshold. In addition to the physics analysis, the SLC used the pulse-by-pulse measurement of the beam energy correlated with other machine parameters as a very powerful diagnostic of accelerator performance. The SLC spectrometer measured the distance between synchrotron light fans from two bending magnets in the extraction lines. In principle, this can provide the desired precision, but would be difficult in a higher-energy collider because of the low-energy tail of the luminosity spectrum. Such a device upstream would cause unacceptable emittance degradation. The LEP spectrometer used a dipole magnet between two BPM triplets but high precision requires tight control of the magnetic field and of the BPM stability. It was only able to achieve ∼50 MeV and it will be difficult to push this technology to the desired level. Some other techniques have been proposed, such as Moller scattering off a gas jet, but none of these have been studied in detail.

All of the LC designs presume some energy spectrometer measurement but have not specified the hardware in detail. NLC also has a wire scanner at the extraction line image point to measure the energy spectrum of the spent beam. There are locations in the TESLA extraction line where the vertical beam profile is dispersion-dominated and where it might be possible to place a profile monitor, but no actual design exists yet. So far, none of the diagnostics discussed achieve the precision desired by the particle physicists (in any of the machine designs).

7.4.7.3 Items for Further R&D

- All projects: none of the polarization or energy diagnostics discussed so far achieve the precision desired by the particle physicists (Ranking: 3).
- TESLA: the radiation levels in the extraction line as currently designed appear incompatible with the eventual installation of beam energy and/or polarization diagnostics downstream of the IP. Even though the ECFA study concluded that a downstream polarimeter is not required, it may be prudent for the extraction-line layout to preserve this capability, should it ultimately be required by the particle physics program. This would require reducing the currently predicted radiation levels by at least an order of magnitude (Ranking: 4).

7.4.8 Energy Tunability and Upgradability

This chapter has so far dealt exclusively with the reference designs operating at $\sqrt{s}$=500 GeV. The present section is devoted to the critical issues associated with operation either at lower energies (Section 7.4.8.1), or at the maximum c.m. energy considered, in this

report, by each of the machine design teams (Section 7.4.8.2): 800 GeV for TESLA, 1 TeV for NLC and JLC, and 3 TeV for CLIC.

7.4.8.1 Energy Tunability

While it has been argued that physics output is maximized by always running at the highest possible c.m. energy, most scenarios for a linear collider have included high-luminosity running at several different energies. These might include a resonance scan with a range of a few GeV, the top threshold, the Higgs threshold, or the Z pole.

In all machines, large energy changes will occur only rarely, if only because they would involve extensive setup and retuning of the linac and beam-delivery systems. In addition, for the crossing-angle designs, a small repositioning of some extraction-line elements may be required (see Section 7.4.3.2). If PM final doublets are used, then they would restrict the energy range accessible without a complex and time-consuming exchange of these delicate components buried in the detector [101, 124].

The maximum luminosity achievable at low energy will, in all cases, be limited by the BDS optical bandpass. Operational efficiency may also be hampered by the fact that at low energy, the collimation in the BDS must become tighter (in terms of beam size) because the unnormalized emittance (and therefore the beam size in the final doublet) increases. In addition, for TESLA the positron production scheme (necessitated by the large beam power) causes the e^+ yield to drop rapidly as the e^- energy decreases, further limiting the luminosity achievable at low $\sqrt{s}$.

A separate issue is the need for frequent low-luminosity running at the Z pole for detector-calibration purposes. This has been advocated [125] as an important ingredient to extend the discovery reach beyond the maximum machine c.m. energy, via precision electroweak measurements. The minimum luminosity needed would be about 10^{31} cm^{-2}s^{-1}: it is unlikely that this requirement could be met without exchanging PM final-doublets optimized for higher energies. However, considerations of overall running efficiency are likely to make other detector-calibration methods more attractive. At LEP-2, one of the four detectors requested Z-pole running about every six weeks; the inherent stability of the storage ring made this operationally straightforward, and the amount of retuning required was minimal. The setup and tuning overhead of any linear collider is likely to be much more substantial—even for "low" luminosity.

7.4.8.2 Energy-Upgrade Issues

7.4.8.2.1 Beam-Beam Effects The beam-beam issues associated with the energy upgrade are qualitatively different for TESLA, NLC and JLC on the one hand, and for CLIC on the other. The ambitious luminosity goal of the 3 TeV project, driven by the rapid fall in cross-section at high energy, forces a significant reduction in the transverse size of the beams at the IP, resulting in a violent increase in the strength of the beam-beam interaction.

- Luminosity spectrum: at higher beam energies a more severe energy dilution is typically accepted in exchange for higher total luminosity. For TESLA or JLC-X/NLC, the average fractional energy loss increases by a factor ranging from

1.3–2.5, resulting in a luminosity spectrum fairly similar to that of the reference designs (Figure 7.20). The CLIC parameters at E_{cm}=3 rm TeV are optimized for maximum absolute luminosity in the peak; the average energy loss increases from 4% to 21%.

- Photon, pair and hadron production (Table 7.22): the number of beamstrahlung γ's per electron, the number of $e^{\pm}$ pairs, and the number of hadronic events typically increases by factors of 1.5–3 for TESLA and JLC-X/NLC. For CLIC, the pair rate goes up by more than a factor of 10, and the hadronic event rates by two orders of magnitude.

7.4.8.2.2 Accelerator-Induced Backgrounds

- Beam-beam backgrounds: the above increase in production rates is compounded, for all machines, by the higher energy and multiplicity of the shower secondaries, as well as by the doubling of the bunch-crossing frequency in the TESLA case. Comparative NLC studies at 0.5 and 1 TeV [115] suggest that background levels will remain manageable at high energy in all of TESLA, NLC and JLC, but a thorough evaluation has not been attempted by the committee. At 3 TeV c.m. energy, beam-beam backgrounds increase by large factors, and include the appearance of coherently produced pairs. They have been studied in some detail [126, 127]: the regime is very different (the first layer of the vertex tracker, for instance, is now assumed to lie at a radius of 30 mm instead of 15), and the combined IR and detector optimization is more difficult than at 500 GeV. Similar comments apply to the design of the collimation scheme and the minimization of SR backgrounds.

- Muons become both more abundant and more energetic at high energies, making them harder to deflect and almost impossible to range out. The predicted relative increase in muon flux at the IP, from 500 GeV to the highest machine energy, varies (at constant fractional halo) by one to two orders of magnitude depending on the c.m. energy range, the tunnel layout and the shielding scheme. While detailed estimates are not yet fully consistent across machine designs, enough conservatism has been built into the collimation and muon-shielding schemes that a satisfactory solution is likely to be found even at the highest c.m. energy.

- SR background studies are still at an early stage even for the baseline energy. No fundamental problem is expected here, even though the large increase in critical energy may open new issues.

7.4.8.2.3 IP Stabilization

- In all designs, the nominal vertical spot size decreases[22] by about a factor of 2. For the warm-rf machines, this leads to correspondingly tighter stability and feedback requirements at the IP. TESLA is barely affected because of its intratrain feedback capability.

[22] both because of deliberate reductions in invariant emittance and/or IP β-function, and because of stronger adiabatic damping of the emittance.

- In TESLA, the 800 GeV parameter set (Table 2.1) calls for the (approximate) doubling of the number of bunches per train.[23]
  - This may have implications for the intratrain feedback. If the kickers can be built such that they turn on once per pulse and stay on for the entire duration of the train (with the kick strength modulated under feedback control), then the system response time (processor speed, signal propagation delays) need not be different from that of the baseline version. However the noise bandwidth would be doubled, which might cause a problem.
  - Because of the head-on configuration, the first parasitic crossing now occurs inboard of the extraction-line septum. The vertical separation at that location is sufficient for the long-range beam-beam deflection not to induce significant high-frequency noise on the vertical position at the IP, provided the bunch-to-bunch charge jitter remains below 5%.

7.4.8.2.4 Spent-Beam Extraction In all projects, achieving a satisfactory extraction-line design becomes more difficult at high energy, primarily because of the larger energy spread of the spent beam and of the significantly larger loss rate of both charged and neutral outgoing-beam components.

- NLC: While negligible at 500 GeV for the ideal case (nominal parameters, perfectly centered collisions), the extraction-line loss rate reaches 1.6 kW under equivalent conditions at $\sqrt{s}$=1 TeV. This is considered too high by the NLC design team for clean enough polarization diagnostics, except for dedicated, non-colliding pulses. A chicane spectrometer might still be able to operate satisfactorily.
- TESLA:
  - Loss-rate predictions at $\sqrt{s}$=800 GeV are not available in the literature, but they are expected to be considerably larger than those reported in Section 7.4.3.3 for the reference design[24]. Issues fundamentally associated with the head-on configuration, such as beamstrahlung losses on the septum blade or large loss fluctuations at tight aperture limitations, are likely to be exacerbated by the energy upgrade;
  - Either the gradient or the length (or both) of the electrostatic separators need to be increased.

7.4.8.2.5 Collimation and Machine Protection The combined effect of invariant-emittance reduction and of the higher beam energy increases the energy density at the spoilers by factors of 1.5, 2.0, and 10 in TESLA, JLC-X/NLC and CLIC, respectively. This brings the TESLA spoilers close to the limit for Ti (see Table 7.28 in Section 7.4.5.2), and makes the specifications of the CLIC spoilers at 3 TeV similar to those of the JLC-X/NLC betatron spoilers at 500 GeV.

[23] Strictly speaking, this is a luminosity-upgrade issue, independent of the actual c.m. energy.

[24] The predicted loss rate in TESLA at $\sqrt{s}$=500 GeV is a few times larger than that in NLC at 1 TeV, both under ideal conditions.

7.4.8.2.6 Summary of Items for Further R&D

- TESLA:
  - Reduce the predicted extraction-line losses at 800 GeV from their present unacceptably high levels (Ranking: 3).
  - Design a collimator and SR-masking configuration compatible with tolerable muon-backgrounds and SR-backgrounds at 800 GeV (Ranking: 3).
  - If the head-on scheme is maintained, then demonstrate electrostatic separator performance (80 kV/cm) and a viable extraction-septum design in the presence of realistic radiation and power losses (Ranking: 3).
- JLC-X/NLC:
  - Reduce the predicted extraction-line losses at 1 TeV from their present unacceptably high levels (Ranking: 3).
  - Demonstrate that muon-backgrounds and SR-backgrounds are tolerable at 1000 GeV (Ranking: 3).
- CLIC:
  - The lack of an extraction-line design is a serious energy-upgrade issue (Ranking: 2).

7.4.9 Conclusions

7.4.9.1 Feasibility and Risk Assessment

Overall, the feasibility of the proposed designs at the baseline c.m. energy of 500 GeV is on solid ground. The beam-beam simulations that drive the IR geometry and the background suppression are well understood (including the production, transport and masking of secondaries). The layout of the TESLA and NLC IRs, as well as the conceptual (and in some cases, the engineering) design of their crucial components are quite mature. The collimation and machine-protection concepts have been at least partially validated in simulation and/or in actual prototypes (although realistic performance margins remain to be incorporated in many areas). Extensive background-remediation studies result in predicted levels that should be easily manageable in TESLA (thanks to the large bunch spacing); for some of the subdetetctors at warm machines, the background levels per train deserve attention (but the question is only one of ultimate performance in specific physics channels, not of overall detector capability).

Concerns remain about some of the extraction-line designs and about final-doublet stabilization; these are detailed here in order of decreasing importance.

7.4.9.2 Major Concerns

- **TESLA IR and extraction-line layout.** Both crossing-angle and head-on collisions are feasible in superconducting-rf machines. The latter scheme has been

adopted in the TESLA TDR because of some inherent advantages: simpler IR geometry, looser envelope requirements for the FD quadrupoles, no need for crab-crossing cavities. However, this choice leads to unavoidable compromises in the shared section of the beam line, resulting in:

- Very tight apertures and marginal stay-clear for the outgoing charged and photon beams
- Potentially degraded SR masking
- Overall extraction-line radiation levels significantly larger than in JLC-X/NLC, probably limiting the performance of beam orbit, energy, and polarization diagnostics

In addition, the design of several crucial extraction-line components, as well as their protection in an overconstrained high-radiation environment, constitute a serious engineering challenge.

The combination of these issues raise strong doubts about the operability, reliability, and running efficiency of the extraction line as currently designed. Adopting a crossing-angle geometry would avoid the previously listed difficulties and improve flexibility. There might be implications for the fast-extraction scheme, which would need to be reevaluated. The design of the FD quadrupoles and their support would still be easier than for warm machines because vibration tolerances are looser.

The Working Group recommends that the present extraction-line design be subject to an in-depth internal review along the lines suggested in Section 7.4.3.3, and that until then the possibility of eventually adopting a crossing-angle layout be retained.

7.4.9.3 Concerns

- JLC-X/NLC:
  - Relative transverse stability of the two beams at the IP at high frequencies (>10 Hz) is of paramount importance to the performance of warm-rf linear colliders. Extensive laboratory tests of FD stabilization schemes have been successfully carried out, with more planned at CERN, SLAC and elsewhere. These test-bench demonstrations are being backed up by detailed simulations of feedback performance in the presence of ground-motion and other dynamical errors. It remains essential, however, to demonstrate FD stabilization in an environment that adequately reproduces the *system* constraints of an actual detector and IR.
- CLIC:
  - IP stability. The concerns here are similar to those for JLC-X/NLC, compounded by a significantly tighter vertical vibration tolerance at the highest c.m. energy.
  - Extraction-line design. While the NLC extraction-line concept could plausibly be adapted for CLIC at the baseline energy, the very wide momentum bandpass and high energy densities at $\sqrt{s}$=3 TeV pose a serious design challenge, which remains to be addressed.

- TESLA:
  - IP stability. The TESLA TDR design relies entirely on the intratrain IP feedback to guarantee collision stability. Although a similar technique has been used routinely at SLC, PEP-II and KEKB, its success is crucially dependent on the performance of the corresponding instrumentation (BPMs, pair luminosity monitor) in a high-disruption, high-radiation environment. It may be prudent to incorporate some form of FD stabilization in the baseline design to anticipate unexpectedly large vibration problems.

BIBLIOGRAPHY for CHAPTER 7

[1] P. Krejcik *et al.*, "High Intensity Bunch Length Instabilities in the SLC Damping Rings" in *Proc. 1993 Particle Accelerator Conference*, Washington, D.C. (1993) 3240.

[2] Tanaka *et al.*, NIM A **486** Issue 3, pp521–538

[3] R. Nagaoka, "Work Carried Out at the ESRF to Characterize and Correct the Coupling," in *Proc. Seventh European Particle Accelerator Conference*, Vienna (2000) 131.

[4] S.H. Kim *et al.*, "Investigation of Open-Loop Beam Motion at Low Frequencies at the APS," in *Proc. 1997 Particle Accelerator Conference*, Vancouver (1997) 745.

[5] M. Böge, "First Operation of the Swiss Light Source," in *Proc. Eighth European Particle Accelerator Conference*, Paris (2002) 39.

[6] K. Kubo, *et al.*, "Beam Tuning for Low Emittance in KEK-ATF Damping Ring," in *Proc. Seventh European Particle Accelerator Conference*, Vienna (2000) 483.

[7] K. Kubo and K. Oide, Phys. Rev. ST Accel. Beams **4**, 124401 (2001).

[8] K.L. Bane, *et al.*, in *Proc. 2001 Particle Accelerator Conference*, Chicago (2001) 2955.

[9] T.O. Raubenheimer, A. Wolski, "Comparison of alignment tolerances in linear collider damping rings with those in operating rings," LCC-0112 (2003).

[10] A. Seryi and O. Napoly, Phys. Rev. E **53**, 5323 (1996).

[11] A. Wolski and S. de Santis, "Estimates of Collective Effects in the NLC Main Damping Rings," LCC-0080.

[12] A. Wolski, "Electron Cloud in Linear Collider Damping Rings," Proc. Mini-Workshop on Electron Cloud Simulations for Proton and Positron Beams (ECLOUD'02), CERN (2002). Published in CERN Yellow Report CERN-2002-001.

[13] A. Seryi,
`http://www.slac.stanford.edu/~seryi/gm/model/`

[14] T. Imai, *et al.*, "Highly stable beam extraction by double kicker system," KEK preprint 2002-16, (KEK).

[15] T. Imai, *et al.*, "Double Kicker System in ATF," in *Proc. XX International Linac Conference*, Monterey, CA (2000) 77.

[16] L. Arnaudon *et al.*, "Effects of Tidal Forces on the Beam Energy in LEP," in *Proc. 1993 Particle Accelerator Conference*, Washington, D.C. (1993) 44.

[17] A. Wolski and Y. Wu, "Effects of Damping Wigglers on Beam Dynamics in the NLC Damping Rings," in *Proc. 2001 Particle Accelerator Conference*, Chicago (2001) 3798.

[18] A.W. Chao, NIM 180 (1981) 29.

[19] D.P. Barber, G. Ripken, Handbook of Accelerator Physics and Engineering, A.W. Chao, M. Tigner (editors), World Scientific, 1999, pg. 156–164

[20] Balakin, V. E. and Novokhatsky, A. V. and Smirnov, V. P., *VLEPP: Transverse Beam Dynamics*, in BATAVIA 1983, Proceedings, High Energy Accelerators, 1983, pp. 119–120.

[21] Schulte, D., Tenenbaum, P., Walker, N., Wolski, A., and Woodley, M., *Tests of 3 Linear Collider Beam Dynamics Simulation Programs*, SLAC, LCC-Note, LCC-0091, 2002
`http://www-project.slac.stanford.edu/lc/ilc/TechNotes/LCCNotes/lcc_notes_index.htm`

[22] Emma, P., *Zeroth Order Design Report for the Next Linear Collider*, Stanford University, Chapter 5, pp. 268–271, 1996.

[23] Nosochkov, Y., Raimondi, P., and Raubenheimer, T.O., *Design of Alternative Optics for NLC Prelinac Collimation Section*, SLAC, LCC-Note LCC-0057, 2001
`http://www-project.slac.stanford.edu/lc/ilc/TechNotes/LCCNotes/lcc_notes_index.htm`

[24] Anderson, S. and Shepard, J., *NLC Pre-Linac, 2001 Configuration, Version 2*, April 2001
`http://www-project.slac.stanford.edu/lc/local/Reviews/Apr2001`

[25] Oide, K., *Synchrotron Radiation Limit of the Focusing of Electron Beams*, Phys. Rev. Lett., **61**, pp. 1713–1715, 1988.

[26] Stupakov, G., *High-Frequency Impedance of Small-Angle Collimators*, Presented at IEEE Particle Accelerator Conference (PAC2001), Chicago, Illinois, 18–22 June 2001.

[27] Piwinski, A., *Wake fields and ohmic losses in flat vacuum chambers*, DESY-HERA-92-04.

[28] Tenenbaum, P., *Collimator Wakefield Calculations for ILC-TRC Report*, SLAC, LCC-Note LCC-0101, 2002.

[29] Drozhdin, A. *et al.*, *Comparison of the TESLA, NLC, and CLIC Beam Collimation Systems Performance. Fourth Edition.*, 2002
`http://www-ap.fnal.gov/~drozhdin/prdriver/pap_TESLA_NLC_comparis4_no_distributions_aug30.ps`

[30] Brinkmann, R., Raimondi, P., and Seryi, A. *Halo reduction by means of nonlinear optical elements in the NLC final focus system*, Presented at IEEE Particle Accelerator Conference (PAC 2001), Chicago, Illinois, 18–22 Jun 2001

[31] NLC Post-Linac Collimation Task Force, *New Post-Linac Collimation System for the Next Linear Collider*, SLAC, LCC-Note LCC-0052, 2001
`http://www-project.slac.stanford.edu/lc/ilc/TechNotes/lcc_notes_index.htm`

[32] Tenenbaum, P. *et al.*, *An apparatus for the direct measurement of collimator transverse wakefields*, Contributed to IEEE Particle Accelerator Conference (PAC 99), New York, NY, 29 Mar-2 Apr 1999.

[33] Brinkmann, R., Napoly, O., and Schulte, D., *Beam-Beam Instability Driven by Wakefields*, CERN, CLIC-Note 505, 2001.

[34] Schulte, D., *Luminosity in Future Linear Colliders in the Presence of Static Wakefield Effects in the Main Linac*, CLIC-Note 544 (2002).

[35] Yokoya, K. and Chen, P., *Multiple Bunch Crossing Instability*, SLAC-PUB-4653.

[36] Raubenheimer, T. and Ruth, R. D., *A Dispersion free trajectory correction technique for linear colliders*, Nucl. Instrum. Meth., **A302**, pp. 191–208, 1991.

[37] Bowden, G., Holik, P., Wagner, S.R., Heimlinger, G., and Settles, R., *Precision magnet movers for the final focus test beam*, Nucl. Instrum. Meth., **A368**, pp. 579–592, 1996.

[38] Adolphsen, C. *et al.*, *Wakefield and beam centering measurements of a damped and detuned X-band accelerator structure*, Presented at IEEE Particle Accelerator Conference (PAC 99), New York, NY, 29 Mar-2 Apr 1999.

[39] Raubenheimer, T.O. and Schulte, D., *The ballistic alignment method*, CERN/PS-99-024(LP), 1999.

[40] R. Assmann *et al.*, *The Computer Program LIAR for the Simulation and Modeling of High Performance Linacs*, Proceedings of the 1997 Particle Accelerator Conference, 1997.

[41] d'Amico, E.T., Guignard, G., Leros, N., Schulte, D., *Simulation Package Based on PLACET*, Proceedings of the 2001 Particle Accelerator Conference, 2001.

[42] Tenenbaum, P., 2001
`http://www-project.slac.stanford.edu/lc/local/MAC/OCT2001/PTmacoct2001[1].pdf`

[43] Tenenbaum, P. and Brinkmann, R. and Tsakanov, V., *Beam-based alignment of the TESLA main linac*, Presented at 8th European Particle Accelerator Conference (EPAC 2002), Paris, France, 3–7 Jun 2002.

[44] Brinkmann, R. and Tsakanov, V., *Emittance preservation in TESLA* Prepared for APS / DPF / DPB Summer Study on the Future of Particle Physics (Snowmass 2001), Snowmass, Colorado, 30 Jun-21 Jul 2001.

[45] Shulte, D. and Walker, N., *TESLA beam-based alignment studies*, in preparation, 2002.

[46] T. Raubenheimer, "Comments on Linear Collider Beam-Based Alignment," August, 2002.

[47] Jones, R.M. *et al.*, *Manifold damping of wakefields in high phase advance linacs for the NLC*, 2002.

[48] Baboi, N. and Brinkmann, R., *Higher Order Mode Effects and Multibunch Orbit Stability in the TESLA Main Linac*, DESY-TESLA-00-28, 2000.

[49] D. Schulte, *Emittance Grwoth in the Main Linac of CLIC at 500 GeV*, CLIC-Note 545 (2002).

[50] Tenenbaum, P., *Spectral Content of the NLC Bunch Train due to Long Range Wakefields*, SLAC, LCC-Note LCC-0015, 1999
`http://www-project.slac.stanford.edu/lc/ilc/TechNotes/LCCNotes/lcc_notes_index.htm`

[51] G. Bowden, personal communication, 2002. In these studies, the SLD door was closed, SLD water was ON, magnetic field was OFF. The data shown in the plot were taken on November 3, 1995 at 2:30am.

[52] Seryi, A., *Ground Motion Models for ILC-TRC Studies*, in preparation, 2002.

[53] Montag, C., *Ground motion in the HERA interaction region*, Published in Stanford 2000, Ground motion in future accelerators, pp. 139–146, 2000.

[54] Assmann, R., Coosemans, W., Guignard, G., Leros, N., Redaelli, S., Schulte, D., Wilson, I., and Zimmermann, F., *Status of the CLIC Study on Magnet Stabilization and Time-Dependent Luminosity*, To be published in *Proceedings, EPAC2002*, 2002.

[55] Hendrickson, L., 2002
`http://www.slac.stanford.edu/~ljh/nlcfbck/fbck.htm` and
`http://www.slac.stanford.edu/~ljh/fdesign.htm`

[56] Hendrickson L., Algorithms and simulation results for NLC IP and linac feedback systems, Nanobeam 2002, Lausanne, September 2002
`http://icfa-nanobeam.web.cern.ch/`

[57] Hendrickson L., et al., Implementation of Dynamic Misalignments and Luminosity Stabilization by Beam-Beam Feedbacks in Simulations of Linear Colliders, submitted to PAC2003.

[58] Seryi, A., et al., Effects of Dynamic Misalignments and Feedback Performance on Luminosity Stability in Linear Colliders, submitted to PAC2003.

[59] White, G., *Simulations of TESLA intratrain fast feedback*, 2002
`http://www-project.slac.stanford.edu/lc/local/AccelPhysics/GroundMotion/mtgs/july102002/`

[60] Le Pimpec, F. et al., Vibrational Stability of NLC Linac Accelerating Structure, EPAC2002, 2000. See also in the Proceedings of LINAC2002 and ICFA Nanobeam 2002 Workshop.

[61] Fenn, R., Slaton, T., and Woods, M., *Quadrupole Vibration Measurements for QM1B and QC3 in the Final Focus Test Beam at SLAC*, SLAC, LCC-Note LCC-0036, 2000.

[62] Assmann, R, and Frisch, J., *Nanobeam 2002*, 2002. Reports about stabilization studies in CLIC and NLC
`http://icfa-nanobeam.web.cern.ch/`

[63] R.W. Assmann, et al., Status of the CLIC Study on Magnet Stabilization and Time-Dependent Luminosity, EPAC2002 ,2002.

[64] Liepe, M., *PAC 2001*, 2001. Dynamic Lorentz Force Compensation with a Fast Piezoelectric Tuner.

[65] Liepe, M., *Active Control of Lorentz-Detuning and Microphonics*, April, 2001.

[66] Pagani, C., *Advances in Cryomodule Design and New Approches*, Proceedings of 9th Workshop on RF Superconductivity, Santa Fe, 1999.

[67] Weise, H., *The TESLA Test Facility (TTF Linac—A Status Report)*, Proceedings of PAC 95, 1995.

[68] The Next Linear Collider Design Group, T.O. Raubenheimer, editor, *Zeroth Order Design Report for the Next Linear Collider*, Stanford University, **2**, Chapter 11, p. 713, 1996.

[69] The TESLA Collaboration, R. Brinkmann, editor, *TESLA Technical Design Report*, DESY, **II**, Chapter 7, p. 193, 2001.

[70] The Next Linear Collider Design Group, T.O. Raubenheimer, editor, *Zeroth Order Design Report for the Next Linear Collider*, Stanford University, **2**, Chapter 11, p. 770, 1996.

[71] The Next Linear Collider Design Group, T.O. Raubenheimer, editor, *Zeroth Order Design Report for the Next Linear Collider*, Stanford University, **2**, Chapter 11, p. 769, 1996.

[72] Woodley, M., Tenenbaum, P., Hendrickson, L. and Seryi, A., *Optics simulations for the NLC main linac*, Contributed to IEEE Particle Accelerator Conference (PAC 2001), Chicago, Illinois, 18–22 Jun 2001.

[73] R. Assmann, personal communication, 2002.

[74] Smith, S.R., Tenenbaum, P., and Williams, S.H., *Performance of the beam position monitor system of the final focus test beam*, Nucl. Instrum. Meth., **A431**, pp. 9–26, 1999.

[75] Shiltsev, V., personal communication, 2002.

[76] K. Yokoya, *et. al.*, see
http://www-acc-theory.kek.jp/members/cain/

[77] D. Schulte, CERN-PS/99-014-LP (1999).

[78] The original comparison, made in O. Napoly, I. Reyzl and N. Tesch, DESY-TESLA-99-20A (1999), does show good agreement on the beamstrahlung flux, but suggests that pair-related computations are not fully consistent. This was eventually traced by D. Schulte and the above authors to (i) a cut, in one of the programs, on the pair energy (which eliminated 20% of the particles), and (ii) the fact that GUINEA-PIG outputs the energy and the number of pairs from both beams, while other programs return the background for one beam only. Once these points are taken into account, the agreement is satisfactory.

[79] T. Barklow, *et. al.*, SLAC-PUB-8043 (1999).

[80] D. Schulte, TESLA-97-08 (1996).

[81] S. P. Baranov, O. Duenger, H. Shooshtari and J. A. Vermaseren, in *Hamburg 1991, Proceedings, Physics at HERA, vol. 3* 1478–1482 (see HIGH-ENERGY PHYSICS INDEX 30 (1992) No. 12988).

[82] G. Wagner, "Neutron Background at TESLA," presentation at the 9^{th} International Workshop on Linear Colliders (LC02), Menlo Park, USA (2002).

[83] T. Markiewicz, "NLC IR Overview," presentation at the 9^{th} International Workshop on Linear Colliders (LC02), Menlo Park, USA (2002)
http://www-conf.slac.stanford.edu/lc02/wg4/
WG5_Markiewicz_NLCIROverview(rotated).pdf

[84] ACFA Linear Collider Working Group, "Particle Physics Experiments at JLC," KEK Report 2001-11 (2001).

[85] G. A. Schuler and T. Sjöstrand, CERN-TH/96-119 (1996).

[86] P. Chen and M. E. Peskin, SLAC-PUB-5873 (1992).

[87] M. Drees and K. Grassie. Z. Phys. C, **28** (1985) 451–462.

[88] M. Glück, E. Reya and A. Vogt, Phys. Rev. D **46** (1992) 1973.

[89] O. Napoly and D. Schulte, "Luminosity Monitor Options For Tesla," CERN-OPEN-2000-135, contributed to 19th International Linear Accelerator Conference (Linac 98), Chicago, Illinois, 23–28 Aug 1998.

[90] A. Seryi, "FD Stabilization in NLC,"
http://www-conf.slac.stanford.edu/lc02/wg4/wg4_seryi_0207_2[1].pdf;
J. Frisch, "IP Stabilization for the NLC,"
http://www-conf.slac.stanford.edu/lc02/wg4/WG3-4_Frisch.pdf,
presentations at the 9^{th} International Workshop on Linear Colliders (LC02), Menlo Park, USA (2002).

[91] P. Tenenbaum, J. Irwin, and T.O. Raubenheimer, to be submitted to PRSTAB.

[92] D. Schulte and F. Zimmermann, "The Crossing Angle in CLIC," Proc. 2001 Particle Accelerator Conference (PAC'2001), Chicago, Illinois, USA (2001).

[93] TESLA Technical Design Report, DESY 2001-011, ECFA 2001-209, March 2001.

[94] E. Merker *et. al.*, "The TESLA High-Power Extraction Line," TESLA-01-19 (2001).

[95] A. Seryi, "Beamstrahlung Photon Load on the TESLA Extraction Septum Blade," LCC-Note-0104, SLAC, 2002.

[96] Y. Nosochkov and K. A. Thompson, " Beam Losses in the NLC Extraction Line for High Luminosity Beam Parameters," LCC - 0049 11//00 (2000). Although the parameters in that study are slightly different from those in the present report (Table 7.22), cases 500-H and 1000-H are actually a little more demanding than the current parameters because the vertical spot size is 10% smaller while the number of bunches is 1% lower.

[97] G. White, "IP Feedback Simulation," talk at the ECFA/DESY Workshop, Cracow, Sept.2001:
`http://fatcat.ifj.edu.pl/ecfadesy-krakow` ;
`http://www-project.slac.stanford.edu/lc02/`, presentation at the 9^{th} International Workshop on Linear Colliders (LC02), Menlo Park, USA (2002).

[98] S. R. Smith, "Design of an NLC Intrapulse Feedback System', Linear Collider Note LCC-056 03/01 (2001).

[99] A. Devred et at, "Conceptual Design for the Final Focus Quadrupole Magnets for TESLA," TESLA-2001-17 (2001).

[100] A. Ringwall, "Detector Solenoid Field Effects', in
`http://www-sldnt.slac.stanford.edu/nlc/Meetings/beamdelivery/2000-03-13-Ringwall,Nosochkov,Seryi/index.htm`

[101] T. Raubenheimer & P. Tenenbaum, private communication. An adjustable PM final-doublet concept has been studied (with an earlier version of the FFS optics) using counter-rotating longitudinal slices. In order to obtain 50% strength variation and limit the aberrations, it was necessary to subdivide the quadrupole longitudinally in many 2 cm slices. A potentially more attractive alternative consisted of just two counter-rotating magnets, one inside the other. This was aperture-limited at the downstream end, but could work for roughly half the magnet.

[102] KEK Report 92-16, "JLC-I," (Dec 1992), pp 214–215.

[103] M. Alsksa, S. Russenschuck, "Study of Some Options for the CLIC Final Focusing Quadrupole," CLIC Note 596 (2002).

[104] A. Drozhdin, *et. al.*, "Comparison of the TESLA, NLC and CLIC Collimation-System Performance," in preparation.

[105] P. Tenenbaum, T.O. Raubenheimer, and M. Woodley, "Sources of Beam Halo in the Next Linear Collider Main Linac," PAC-2001-FPAH071, SLAC-PUB-8935 (July 2001) (http://www.slac.stanford.edu/pubs/slacpubs/8000/slac-pub-8935.html)

[106] R. Brinkman, N. J. Walker, and G.A. Blair, "The TESLA Post-linac Collimation System," TESLA 2001-12.

[107] "A 3 TeV e^+e^- Linear Collider based on CLIC Technology," CERN 2000-008 (2000) http://cern.web.cern.ch/CERN/Divisions/PS/CLIC/General.html

[108] P. Raimondi, "NLC Beam Delivery System Developments," http://www-project.slac.stanford.edu/lc/local/MAC/MAY2001/Talks/Mac_May%20Panta.pdf
J. Frisch, *et. al.*, "Collimator Design and R&D," http://www-project.slac.stanford.edu/lc/local/MAC/MAY2001/Talks/Frisch%20MAC%20May.pdf
P. Raimondi, A. Seryi, and P. Tenenbaum, "Tunability Of The NLC Final Focus System," PAC 2001;
"2001 Report on the Next Linear Collider," Report Submitted to Snowmass '01, FERMILAB-Conf-01/075-E, LBNL-PUB-47935, SLAC-R-571, UCRL-ID-144077;
P. Raimondi, "NLC Beam Delivery System & Collimation," http://www-conf.slac.stanford.edu/lc02/wg3/WG3_Raimondi_P.pdf

[109] G.A. Blair, H. Burkhardt, H.J. Schreiber, "Background Simulation for the CLIC Beam Delivery System with Geant," CERN-SL-2002-029 (AP), CLIC Note 519 (2002).

[110] E. Doyle, J. Frisch and K. Skarpaas VIII, "Advanced Collimator Engineering for the NLC," PAC 2001.

[111] R. Assmann, *et. al.*, CERN-SL-2000-058-AP, Proc. EPAC 2000, Vienna (2000).

[112] D. Schulte and F. Zimmerman, "Failure Modes in CLIC," CERN-SL-2001-034(AP).

[113] World Studies on Physics and Detectors for a Linear Collider http://hepwww.physics.yale.edu/lc/

[114] J. Brau, C. Damerell, G. Fisk, Y. Fujii, R. Heuer, H. Park, K. Riles, R. Settles and H. Yamamoto, "Linear Collider Detector R&D," http://blueox.uoregon.edu/~jimbrau/LC/LCrandd.ps

[115] T. Markiewicz, "NLC IR Layout and Background Estimates," Snowmass 2001 http://www-sldnt.slac.stanford.edu/nlc/Meetings/2001-06-30_Snowmass/T1_Talks/2001-07-05%20Snowmass%20-%20NLC%20Backgrounds.ppt

[116] See *e.g.*, Ch. II-7.4.3 and IV-7.1 of Ref. [93]. Table IV-7.1.6 provides a concise overview of the various background sources and of their relative importance.

[117] T. Tauchi, "JLC IR Overview," presentation at the 9^{th} International Workshop on Linear Colliders (LC02), Menlo Park, USA (2002). http://www-conf.slac.stanford.edu/lc02/wg4/WG4_Tauchi.pdf

[118] D. Schulte, "Update of the Status of Machine Detector Interface Studies for CLIC," CERN-PS 2001-074(AE).

[119] F. Zimmermann, "Machine Backgrounds in CLIC," presentation at the 9^{th} International Workshop on Linear Colliders (LC02), Menlo Park, USA (2002). http://www-conf.slac.stanford.edu/lc02/wg4/WG4_Zimmermann_0205_b.pdf

[120] See for instance
http://www-dapnia.cea.fr/ecfadesy-stmalo/Sessions/
MachineDetectorInterface/R_Settles.pdf
There is, however, a varying degree of conservatism in the quoted "pain thresholds." JLC sets significantly tighter limits than TESLA on tolerable vertex-detector occupancy and muon flux per train [117]. The BABAR detector, in contrast, was designed with 10% as the occupancy limit in the drift chamber [128].

[121] In NLC, SR photons are required not to strike masks or detector elements between 13 m upstream of the IP and 6 m downstream. The TESLA requirements are detailed in Ref. [129].

[122] K. Stefanov *et al.*, "Studies of CCDs for Vertex Detector Applications," presentation at LCWS2000 at FNAL.

[123] V. Gharibyan, N. Meyners, K. Schuler, "The TESLA Compton Polarimeter," LC-DET-2001-047 (Feb. 2001).

[124] A hybrid FD for NLC was discussed in Ref. [130]. The defocusing magnet next to the IP was a PM magnet fixed in strength. The energy variability was attained with an SC quadrupole just upstream, and a normal electro-magnet upstream of this which acted as the QF. This system seemed to perform quite well over roughly a factor of 3–4 in energy; beyond this, the PM would have to be modified.

[125] R. Settles, Proceedings of LC93 at SLAC.

[126] D. Schulte, "Backgrounds at Future Linear Colliders," CLIC Note 424, CERN/PS 99-069. Also in Proc. of the Workshop on the Development of Future Linear Electron-Positron Colliders for Particle Physics Studies and for Research Using Free Electon Lasers, Lund, Sweden, 23–26 Sep 1999.

[127] D. Schulte, "Machine-Detector Interface at CLIC," Proc. 5th International Linear ColliderWorkshop (LCWS 2000), Fermilab, Batavia, Illinois, 24—28 Oct 2000.

[128] BABAR Technical Design Report, SLAC-R-95-457 (1995).

[129] O. Napoly, "Collimation Depth Requirements for the TESLA IR," DESY TESLA-01-18, 2001.

[130] Zeroth Order Design Report for the Next Linear Collider, Stanford University, 1996.

CHAPTER 8

Reliability, Availability, and Operability

8.1 CHARGE AND ORGANIZATION

When ICFA commissioned the second ILC-TRC report, two working groups were formed, the first on Technology, RF Power and Energy Performance and the second on Luminosity Performance. Part of the charge to the Technology group was to "determine whether the machines can reliably reach their operating energy, [and] be tunable." The Luminosity group was charged to "analyze all those factors which affect the ultimate performance (both peak and integrated), including ... tunability, and reliability." Because the issues of technology and luminosity reliability are so intimately coupled, a third joint Working group was formed with members from each of the primary working groups.

Working Group Members

Members from Technology Performance:
R. Pasquinelli, FNAL (Subgroup leader); C. Adolphsen, SLAC;
Y.H. Chin, KEK; H. Edwards, FNAL; K. Hübner, CERN; M. Ross, SLAC;
T. Shintake, KEK/Riken; N. Toge, KEK; H. Weise, DESY

Members from Luminosity Performance: **N. Phinney**, SLAC (Subgroup leader); R. Assmann, CERN; W. Kozanecki, CEA/Saclay;
D. Schulte, CERN; P. Tenenbaum, SLAC; N. Walker, DESY

The original goal of the Reliability, Availability and Operability Working Group was to estimate the expected machine availability for each project based on projected reliability of components and subsystems and overall operability considerations. Unfortunately, there was not sufficient data available for any of the projects to make plausible availability estimates. Instead this chapter merely documents the existing partial information on component failure and replacement times. It discusses the impact of such failures on machine uptime, the requirements on machine protection systems, and an evaluation of the tuning time required to reestablish luminosity after an interruption.

8.2 INTRODUCTION

To deliver high integrated luminosity over several years of operation, a linear collider must not only achieve the desired energy and peak luminosity, but also have a very high hardware availability and operating efficiency. The goal would be to have a hardware availability of 85% and deliver on average 75% of nominal luminosity, which is an extremely challenging task. All of the collider designs are very large, complex machines which are pushing the state of the art, with many thousands of components. Unlike a storage ring where the injector chain is only required for filling, the entire linear collider injector systems must operate on every pulse. High luminosity is only achieved when the collider produces and preserves beams of very small emittance. This requires precise alignment of magnets and structures using beam-based techniques, and a variety of sophisticated tuning procedures, which increase the time to recover full luminosity after an interruption. The relevant recovery time for an accelerator is not mean time to repair the component but mean time to reestablish luminosity, *i.e.*, Mean Time Beam Off (MTBO).

While studies analyzing mean time between failures (MTBF) and mean time to repair (MTTR) have been employed routinely in industry for many years, reliability has only relatively recently been given a top priority for accelerators. Most earlier high energy physics machines were innovative technological feats where the emphasis was on achieving breakthroughs in energy and luminosity, usually under tight cost constraints. They were designed and built by teams of skilled physicists, engineers, and craftsmen, who considered the accelerator itself as part of the experimental effort. Given the overhead of fills and ramping for storage rings, the luminosity uptimes achieved were in the range of 50%. This philosophy has evolved with the advent of accelerator user facilities such as the synchrotron light sources, and with the new generation of high energy physics "factories." The large energy-frontier machines such as the Tevatron at FNAL, HERA at DESY, LEP at CERN, and SLC at SLAC have achieved hardware availabilities in the range of 70–90%. In contrast, the B-factories at SLAC and KEK have closer to 95% availability. Synchrotron light or spallation sources have invested significant effort into reliability and now reach 98–99.5% [1]. Operational statistics from a variety of accelerator facilities are presented in the next section.

While the high reliability data is encouraging, great caution is advised in extrapolating the performance of synchrotron light sources (injected beam power <10 W) and cryogenic machines such as LEP and CEBAF to estimates of LC reliability. The design of modern proton linacs, such as the Spallation Neutron Source (SNS) at Oak Ridge, is overwhelmingly constrained by restrictions on beam losses (< 1W/m) that cause residual component activation. The primary reason for this is to facilitate safe hands-on maintenance of the accelerator components. Although protons cause about 100 times more activation per watt than electrons, linear collider designs call for up to 10 times more beam power than the 1 MW SNS (TESLA 11.3 MW/beam, NLC 6.9 MW/beam), so the fractional loss limits are quite severe. For example, the beam power in the TESLA injector complex where there is a large undamped beam is 226 KW, and in JLC-X/NLC only a factor of 4 smaller. A concentrated loss at the level of 100 W (only 0.05% for TESLA, 0.2% for JLC-X/NLC) will cause activation, and great care must be taken to localize these losses in suitably shielded areas. Experience at SLC (30 KW/beam) showed that, in addition to activation, radiation related component failure was a leading cause of problems.

Historically for each new accelerator project, a few of the major components such as magnets or rf power systems were carefully scrutinized with respect to reliability, but the same rigor was not applied to all systems. Significant resources are required for such in-depth analysis and testing, as well as for the added engineering or redundant solutions which would provide high reliability. A recent study for the European Spallation Source (ESS) estimated that a linac designed for extremely high reliability would cost 50% more than a conventional linac [2]. This is not directly applicable to a linear collider as the goals and criteria are different but it is clear that the desire to contain costs always interferes with the desire for high reliability. In a rigorous life cycle cost analysis, it is critical to balance the value of lost physics output against initial project costs.

Poor reliability can impact the peak luminosity achievable as well as integrated performance, as demonstrated by experience with the SLC and more recently with recommissioning the upgraded Tevatron and HERA. If the hardware interruptions are too frequent, then the machine is not up long enough to effectively make progress on the luminosity issues. It was only after the SLC achieved reasonable reliability that the many beam tuning challenges for a linear collider could be addressed. The more complex next generation of colliders must be designed for high availability so that the inevitable challenges can be addressed effectively. More discussion of many of these issues can be found in the NLC Zeroth-order Design Report (ZDR), Chapter 17 [3].

This chapter will attempt to contrast and compare the proposed collider designs and assess the associated reliability issues. It is not possible at this stage to estimate the availability each project may achieve as none of them have completed sufficiently detailed engineering studies. Even for the critical main linac rf components, no project has yet accumulated enough hours of operation at nominal parameters to reliably estimate MTBFs or fault rates for individual components, due to a lack of either final components or test facilities. In addition, the projects are at very different stages in the design process, making comparison difficult. The JLC-X/NLC has the most complete and detailed design for the entire accelerator complex, while TESLA has much more advanced manufacturing studies for the main linac rf, and CLIC is still at an R&D rather than engineering stage. Given the present lack of information, we will simply summarize the issues, list the reliability assumptions, and compare them with what has been achieved with existing technology. Where no information is available for a particular project, that project will simply not be mentioned. We will try to highlight areas where significant work on reliability issues has been performed, and identify areas of concern or where additional R&D is warranted.

Due to the inherently large power densities in the beams of a linear collider, there is a serious risk of damage to beamline components by an errant beam. An extensive machine protection system (MPS) is necessary, monitoring a large number of accelerator systems and beam parameters. The system must inhibit beam in case of a fault and automatically execute a recovery sequence, starting from a benign pilot beam and proceeding to full operating current and rate. Both NLC and TESLA have developed conceptual designs for these systems but much more work is required. The systems will be extremely complex and they must be both robust and redundant. Tuning and recovery procedures are of critical importance for these colliders and they will be discussed in a separate section. Finally, the impact of the machine configurations on commissioning and maintenance will be mentioned.

8.3 COMPILATION OF RELIABILITY DATA

8.3.1 Large Accelerators

To better understand the existing operations of current facilities, the committee has collected significant operational statistics from many of the world's large accelerator complexes. These data describe what has been achieved. They will be compared with the requirements of the linear colliders and thus indicate which components and subsystems require particular effort in order to reach a desired performance.

To predict the integrated luminosity, or integrated beam time delivered by an accelerator, there are three important quantities, HA, BE, and NL.

HA is the fraction of time the machine hardware is available to produce beam. Hardware downtime includes both unscheduled repairs (something critical breaks), scheduled repairs (either at regular intervals or when enough problems have accumulated), and all associated cooldown, warmup and recovery times. For an accelerator, one must consider not only how long it takes to repair a failed component but the total time the beam is off because of the fault, including time lost due to access and the time taken to retune the beam.

BE is the effective fraction of beam time actually delivering luminosity. Beam inefficiencies include Machine Development (time spent studying and improving the accelerator), the impact of tuning procedures, injection and the luminosity decay during a store (for storage rings), Machine Protection trips and recovery (for linacs), and last but not least, the simple fact that accelerators do not manage to deliver the same luminosity every pulse or every store.

NL is the nominal luminosity during a particular run. It may be more or less than design, but usually increases steadily as the accelerator becomes better understood. For a storage ring it is the typical luminosity at the beginning of a store. For a linear collider, it would be the luminosity when the beams are colliding well.

Table 8.1 illustrates the first two measures of performance for modern accelerator complexes, the hardware availability (HA) and/or the overall beam availability (BA), which is the product of HA and BE (BA=HA×BE). It should be noted that different facilities have slightly different methods of accounting for some inefficiencies. Typical synchrotron light source performance metrics use the full calendar duration of the run as scheduled hours so maintenance shutdowns and the associated recovery reduce availability. This is an appropriate way to treat such downtime as modern accelerators do not require routine maintenance and such interventions are only 'scheduled' when there is broken hardware that needs repair. However, for largely historical reasons, many of the numbers in the table include such repair downtime in BE. It should also be noted that the synchrotron radiation facilities are often more tolerant of variations in beam quality, which partially explains their higher achieved BA.

The analysis of recent PEP-II performance shows the relative magnitudes of these quantities [4]. PEP-II was intended to be a "B Factory," and accordingly, some special care

TABLE 8.1: Availability Performance of Various Accelerator Complexes. HA is Hardware Availability; BA is overall Beam Availability, or the product of HA and the Beam Efficiency BE. FNAL data from 2001–2002, SLC data from 1992–1996, PEP/SPEAR data from 2001, HERA data from 2000, LEP data from 1999–2000, KEK data from 2000–2001, APS data from 1999–2002, and CEBAF data from 1999 and 2001.

	FNAL		SLAC					DESY		
System	Tev		SLC [a]	PEP inj	PEP-II	PEP-II	SPEAR	HERA	TTF	TTF
	HA	BA	HA	BA [b]	HA	BA	BA	HA	HA	BA
Cryogenic plant [%]	98.8		na	na	na		na	98.6	97.5	
PS and magnets [%]	92.6		–	98.0	98.0		97.8	94.8	100.	
RF [%]	95.2		–	99.1	99.1		98.3	96.5	98.0	
Utilities [%]	98.3		–	98.0	98.0		99.3	99.5	99.0	
Vacuum [%]	98.1		–	99.7	99.7		98.7	99.1	99.8	
Controls [%]	99.1		–	97.8				99.7	98.8	
Other [%]	98.5							94.1	96.0	
Percent uptime [%]	82.0	50.0	81.1	92.8	94.8	71.5	94.2	83.4	89.5	75.0

	CERN			KEK	ANL	LBNL	TJNAF
System	LPI	SPS	LEP	KEKB inj	APS	ALS	CEBAF
	BA	BA	HA	BA	BA	BA	HA
Cryogenic plant [%]	na		97.8	na	na		98.8
PS and magnets [%]	99.7		99.7	99.5	98.8		94.2
RF [%]	98.7		98.5	98.6	99.0		95.7
Utilities [%]	99.7				99.8		97.3
Vacuum [%]			99.5		99.3		99.1
Controls [%]	99.7		99.7	99.0	99.5		99.5
Other [%]	99.6		93.3	97.5	98.4		81.9
Percent uptime [%]	97.4	55.0	89.2	94.0	95.0	96.0	70.0

[a] SLC numbers not broken down into systems
[b] BE weighted by the need for beam by PEP-II

was taken during the design and construction process to make it reliable. Even though the operation of the storage ring complex is subject to quite different constraints compared to those expected at a linear collider, it is useful to describe its performance record. PEP-II hardware is available 94% of the time (*i.e.*, not broken)and the linac, injector, transfer lines and damping rings are available when PEP-II needs them 92% of the time. Short shutdowns taken for maintenance (incipient failure or component repair) take another 12% and are typically classified as "scheduled" maintenance. Together this gives an overall HA of 76%. When PEP-II is running, the efficiency of delivering luminosity or BE is about 63%. This includes luminosity decay during a coast (12%), injection time (15%) machine development (6%), as well as the difference between achieved and nominal luminosity. The integrated luminosity over a run can be calculated by multiplying these quantities by the NL. For example, in the five months from Feb through June 2002, the peak luminosity was about 4.5×10^{33} $\mathrm{cm}^{-2}\mathrm{s}^{-1}$ and PEP-II actually integrated 28.0 fb^{-1} over 150 days. This calculation gives $[0.76\times0.63\times4.5\times150$ days$\times0.0864] = 27.9$ fb^{-1}. Together the overall PEP-II efficiency HA×BE is $[0.76\times0.63]\simeq 50\%$. For a linear collider where one can neglect the luminosity decay and the injection time, then HA×BE would become $\simeq 65\%$. A similar additional inefficiency beyond HA has been seen at both SLC and TTF, and is reflected in the TTF numbers in Table 8.1.

8.3.2 Extrapolation

Table 8.1 provides the basis for a rough extrapolation of BE and HA to a machine the size of the linear collider. The linear collider is about ten times the size of PEP-II, in terms of its footprint, number of components and total power usage. A very crude extrapolation, without consideration of hardware accessibility (worse for the LC than for PEP-II) and hardware redundancy (presumably better for the LC), gives an expected HA of 40%. As is known from the SLC, HERA and Tevatron commissioning, the BE drops faster than the HA, so the expected BA would be much worse, perhaps below 10%. The extrapolation can be validated in part by looking at routine HERA and Tevatron operation, where the BA, scaled by the actual luminosity compared to the peak, is perhaps 30–40%.

Therefore, if the typical reliability of existing HEP accelerators is simply scaled to the size of a 500 GeV linear collider, then the resulting uptime will be unacceptably low. This means that a new approach is required, and following previous practices will not be adequate. Reliability must be addressed up front by failure analysis, and appropriate remedies must be implemented. Adequate engineering margins for components are also essential. The key issue is the allocation, during development and construction, of sufficient engineering and financial resources to produce a reliable system.

8.4 RF COMPONENTS

Because of the large number of components and relatively short MTBF, the reliability and redundancy of the linac rf systems are key issues in operational performance. In particular, the klystrons (and some modulator components) must be replaced frequently and are considered a consumable expense. In addition, the modulators, klystrons, distribution system, and structures or cavities will experience brief faults or breakdown events where the

hardware can be reset and continue operation after an appropriate timeout. All linear collider designs plan to include spare rf units which can be switched in when a unit faults or needs repair. Critical issues are the frequency and impact of faults, the adequacy of the spares overhead, and the accessibility and duration of repairs.

8.4.1 Main Linac RF Systems

Both TESLA and NLC have constructed test facilities for testing and prototyping the main linac rf components. TTF has over 13,000 hr operating experience with 2 cryomodules (16 cavities), a 1-cavity injector module, 2 klystrons and 2 modulators. Much of this time has been spent running beam for the FEL, which is good for operational discipline but was at relatively low gradients (14 MV/m) and 1 Hz repetition rate. Cavity testing has used another klystron and modulator with over 20,000 hr of operation. NLCTA has 3 modulators and 5 klystrons which initially powered 9 m of accelerator structures, but have recently been used for high gradient testing of up to 4 test structures at the same time. Since 1997, it has accumulated perhaps 20,000 hr of operation, testing a variety of structures at gradients from 35 to 90 MV/m, most of the time without beam. Although most components are not yet of the final design, this experience has been invaluable for both projects and provides an excellent indicator of where critical problems may arise and where specific attention is merited. Because of the prototype nature of the systems and studies, none of the projects has accumulated adequate running time with the final designs, making it difficult to estimate the MTBF for the rf components.

At SLAC and other installations with substantial quantities of klystrons, mature klystron designs have achieved in excess of 40,000 hr lifetime. Nonetheless, state of the art techniques in klystron construction are planned for all projects so there is no directly applicable experience base. The TTF 5 MW klystrons and the SLAC XL4 solenoid focused X-band klystrons have been used reliably for 5 years, but both projects plan to use more efficient klystrons for the collider. The first prototype TESLA multibeam klystron (MBK) achieved the requirements for LC operation, and has operated for about a year (5000 filament hours) at 3–4 MW. The first series production MBK accumulated only 2000–3000 hr in TTF before it was removed for repair. The KEK and SLAC X-band PPM klystrons are only now approaching nominal performance. Conventional modulator designs using thyratrons have frequent failures with an MTBF of 15,000 hr [5]. Modern solid-state designs are expected to have a much longer lifetime and some configurations can easily incorporate features to make them essentially fail-safe. Again there has not been sufficient operation time to date for reliable extrapolation.

In the JLC-X/NLC main linac, the rf unit is an 8-pack consisting of a single modulator powering eight klystrons, which in turn feed four girders of accelerator structures via SLED-II pulse compression systems. Modulator or klystron failures remove the entire 8-pack from service, as do most faults. Both modulators and klystrons are located in an accessible support housing so repairs can occur without interrupting operation. There are 13 spare 8-packs out of 245 (5%) per main linac. Of these, 3% are allocated for 8-pack failures and 2% for feedback and structure trips. The modulators are solid-state IGBT designs with extra boards included which provide excess capacity (4 spares out of 152 or 2.6%). Failed IGBT drivers are bypassed and the overall input voltage is adjusted automatically to compensate. The IGBT switch is believed to have a lifetime of 100,000 hr

but, since repairs can be deferred until the next maintenance period, even a short modulator MTBF should not affect availability. Since the design is modular, the time to replace an IGBT board is short. There are also common mode failures which would remove the entire modulator from service. Assuming an 8 hour MTTR for the entire modulator, the MTBF required for these is only 1200 hr.

A variety of scenarios were studied to verify that 3% overhead was adequate with a conservative assumption of 20,000 hr klystron MTBF [6]. These were also used to estimate the number of crews required for klystron replacement. The scenarios included both start-up and nominal operation, with a variety of worst case assumptions, for a range of crew arrival times. The start-up cases assume that a subset of the klystrons (10% or 20%) will have infant mortality and only a 1000 hr life. Worst case scenarios included the situation where all failures occur on one linac, and the situation where four days a year the failure rate is three times the average. (This last scenario corresponds to an increased rate of failure after a downtime or power outage, as seen at the SLAC linac. It is also appropriate for a Poisson distribution of very low probability events.) Klystron replacement time was estimated at 8 hr with a delay of from 12 to 24 hr before the crew began repairs. Even with these pessimistic assumptions, the overhead available was adequate for all nominal operation scenarios and was exceeded only in the most extreme start-up cases, indicating that the planning is fairly robust. A summary of minimum acceptable MTBFs is given in Table 8.2.

TABLE 8.2
Required MTB Failures for NLC modulators and klystrons with 3% spares allocated.

	Recovery Time [h]	Number of units per linac	Required MTB Failures [h]	Achieved MTBF [h]	(basis)
Modulator	8	254	1200	n/a	
Klystron	8	2032	9200	>40000	SLAC S-band

When SLED-II or a structure breaks down, the power to the associated girder is inhibited, but the other three girders powered by that rf unit continue to operate. After the fault, the girder is ramped back up to full power over a period of 10 s. Modulator and klystron faults (likely arcs) differ in that they will shut off power to all four associated girders. The recovery time in these cases will be about 10 s as well. Table 8.3 lists reliability requirement estimates where, for the given recovery time, the Mean Time Between Faults (MTBF^{ault}) is computed such that the indicated overhead would be depleted only once a year on average due to that type of fault (in such cases, one would have to wait some fraction of the recovery time to be able to resume operation at full energy). Although the actual recovery times will depend on the type of fault, the values here set the scale for the minimum allowed MTBF^{ault}s. The 8 hr MTBF^{ault} listed here was achieved with a test structure operating at 90 MV/m, well above the design gradient of 65 MV/m. This structure did not incorporate the iris size and damping required for the final design, but indicates what should be achievable (see Section 6.5.2).

For TESLA, the rf unit is a modulator powering a single klystron, which in turn feeds three modules of twelve cavities each. A modulator or klystron failure removes a 36-cavity unit from service, as does any klystron, modulator or cavity fault. There are

TABLE 8.3
Required MTB Faults for NLC main linac rf components with 2% overhead allocated.

	Recovery Time [s]	Number of units per linac	Required MTB Faults [h]	Achieved MTBF [h]	(basis)
Modulator	10	254	4	n/a	
Klystron	10	2032	30	n/a	
SLED-II	10	1016	0.6	n/a	
Structure	10	6096	4	8	NLCTA

286 modulator/klystrons and 10296 cavities per linac. The modulators are located in the cryohalls and are accessible for repair. The klystrons, transformers and the high power cables from the modulator are located in the accelerator tunnel and can be replaced or repaired only on maintenance days. The klystron and transformer will be designed for quick connect and disconnect. The actual change out time should be a few hours.

The TESLA modulator uses solid-state (IGBT or IGCT) switches and a bouncer circuit that minimizes the stored energy required. The present design has only 15 switch units per modulator (as opposed to JLC-X/NLC with ∼160) so reliability of the switch components is less of an issue, and methods for providing redundancy are under study. Three prototype modulators have been built, the last two with the planned IGBT design. These two have about 13,000 hr each of TTF linac operation at 1 Hz. The other modulator of an earlier design has been used primarily for cavity, coupler and waveguide testing, with almost 20,000 hr of operation at an average of 3.6 Hz. The TESLA modulator is specified at a MTBF of 2×10^9 pulses (100,000 hr). Repairs are estimated to take a few hours.

In TESLA, cavity faults can be due to breakdown in the couplers or a quench in the cavity itself [7], either of which requires all 36 cavities in the rf unit to be turned off. Coupler breakdown may under some conditions require disconnection of the coupler/cavity and proper termination of both the rf distribution and cavity systems. Since a quench is a thermal process, it is possible to detect most events as they develop and take action to reduce the klystron rf power either within the pulse or before the next pulse. During the high gradient test at TTF in early 2002, recorded trips averaged 11 events per day, for a MTBF^{ault} >17 hr per cavity operating at gradients between 19 and 22 MV/m. This number includes both cavity and coupler trips, and other events such as frequent gun rf trips. In addition, the conditions of the TTF run were far from optimum, with cavities operating very close to their limit and with unstable beam loading conditions.

At 500 GeV TESLA cavities should be some MV/m away from their quench level (assuming higher gradient cavities installed). Unlike normal structures which can breakdown below their operating gradient, superconducting cavity quenches disappear when they are operated a few % below their limit. The LLRF will also incorporate a soft inhibit based on measured beam intensity and individual cavity gradients. Extrapolating this limited TTF experience to 20,000 cavities, 1 trip/cavity in 30 hr would be an acceptable rate (*i.e.*, would deplete the spares once per year on average) only if there was 2% overhead available for faults and the recovery time was less than 3 s. This 2% overhead would need to be in addition to the overhead required to cover klystron failures. No data is available on fault rates for klystrons or modulators during this run, but these rates were low.

RF power input couplers have historically been a severe problem both at CEBAF and at LEP. Considerable R&D has gone into coupler design, including computational tools for analysis of multipacting, implementation of a dc bias between the antenna and the outer coax, and minimization of the warm rf surface along with increased vacuum pumping. The couplers have two ceramic windows between the cavity and external wave guide. This is to greatly reduce the probability of a vacuum failure. A coupler problem that would make a cavity-coupler system inoperable, such as coupler breakdown, would require disconnecting the rf waveguide feed to that cavity and detuning the cavity. One effect that takes time (∼year) to develop is the desorption of gases from the warm rf window area and re-condensation in the cold window area, which then can cause electron emission or coupler events. In the recent run at TTF, coupler events were not a problem (few if any events were recorded) but the coupler operated somewhat below nominal power. Continued long term operational tests of modules at TTF-II will provide extended experience and failure statistics.

RF overhead is required to cover all units with failed klystrons, transformers or low-level rf until the next access for repairs. It must also cover failed modulators until the repair is complete and brief klystron, modulator or cavity faults. In the TDR, the design was to have 2% overhead or 5 stations per linac out of 286. Some of this overhead has since been taken up with fine tuning of the accelerator design by BNS damping and other phase offsets, leaving only 1.3 GeV or less than 2 klystrons per linac. This certainly appears too small even with a 40,000 hr klystron MTBF, so some modification of the parameters will be required. At 500 GeV c.m., use of piezo tuners for Lorentz force compensation would easily allow increasing the gradient to 23.8 MV/m to restore overhead, assuming higher gradient cavities have been installed. Another option is to lower the bunch current and accept a slight reduction in luminosity.

In the JLC-C main linac design, an rf unit consists of a pair of klystrons powered by a single modulator, which in turn feeds four 1.8-m accelerator structures. There are 5% spare units out of 848 per main linac. The modulators use an updated PFN design and a thyratron as switching device, with an estimated lifetime of 10,000–15,000 hr. A klystron lifetime of 50,000 hr is assumed. Most failures remove both klystrons from service, and both modulators and klystrons are located in an accessible support housing.

For CLIC, the klystrons and modulators in the drive beam accelerators are L-band. Each klystron has its own modulator, and pairs of these units power a single accelerator structure. A failure of either klystron/modulator of the pair removes the unit from service. The two accelerators are located in a cut-and-fill tunnel near the surface, with two galleries on either side of this tunnel housing the klystrons while the modulators are on the surface. In this arrangement the elements of the power sources are in accessible areas. There are 112 pairs of klystron-modulator units per drive linac which provides a margin of about 10% since the nominal klystron power is 50 MW but only 44 MW are needed. There are additional units for the rf deflectors of the combiner rings (2×2 of 50 MW at 937 MHz and 2×2 of 20 MW at 3.75 GHz) and for the deflectors of the delay loops (2×1 of 1 MW at 468 MHz). Spare units must also be provided for these parts. The modulators use a PFN design, which is expected to have about the same lifetime as achieved for the other schemes but no prototype has been constructed. A klystron lifetime of 30,000 hr was specified in the klystron design study.

A fault in any main linac structure or in any Power Extraction Transfer Structure (PETS) of one 625 m long section of the drive-beam decelerator presently takes that whole section of linac and decelerator off-line, *i.e.*, approximately 450 transfer structures and two times as many CLIC Accelerating Structures (CAS). Some solution must be developed for isolating only a few structures in the case of a trip. First ideas have been tested at CTF2 and gave promising results, but have not been pursued for lack of resources. The solution would be implemented on the PETS where it would suppress the power in the pair of accelerator structures fed by one PETS as well as in the PETS itself, regardless of whether the fault occurred in the main linac or decelerator structures. Faults in the main linac structures are much more probable than in the drive-beam decelerator because the peak surface field in the PETS is only around 100 MV/m whereas it is 300 MV/m in the CAS.

8.4.2 Other RF Systems

For NLC, the pre-linacs, damping rings, and bunch compressor rf systems all have klystrons and modulators located in an accessible support housing to allow for non-invasive repair [8]. In the injector linacs, the klystrons are powered in pairs (2-packs) by one modulator. In the 6 GeV pre-linacs and e^- drive linac, there are 2 spare 2-packs out of 18 or 19 total (12%). In the booster linacs, there is 1 spare 2-pack out of 6 (20%). The S-band klystrons are assumed to have a lifetime of 40,000 hr, a conservative estimate given SLAC klystron lifetimes. The same lifetime is assumed for the L-band klystrons. Some thought has gone into redundancy for the specialized rf systems but not all details are complete. For the second bunch compressors, the X-band rf has 4 klystrons of which only 3 are required. There is no explicit redundancy yet included for the first bunch compressors and injector capture sections.

The NLC main and pre-damping rings have no spare cavities as they would add unwanted impedance. The ZDR called for three 350 KW tubes per main ring and 2 tubes for the pre-damping ring, but present plans are to use a single 1 MW tube per ring. The klystrons are similar to those used for PEP-II or KEKB with an estimated lifetime of 30,000 hr. This is a reasonable number for well engineered devices (LEP had a klystron MTBF >25,000 hr). The actual average lifetime of the PEP-II klystrons has been ∼6000 hr, dominated by a number of early tube failures. Later tubes have reached the target 25,000–30,000 hr [9]. At KEKB, the 1.0 MW klystrons have an 18,000 hr lifetime and the 1.2 MW Toshiba tubes about 47,000 hr (excluding initial failures in <1000 hr) [10]. It would be possible to configure the system with extra klystrons as hot spares, but this is not presently included.

For the TESLA damping rings, all klystrons and modulators are located in a hall, accessible for repair. There are a total of 4 klystrons and one spare for the e^+ ring, and 2 with 1 spare for the e^- ring. A MTBF of 40,000 hr is assumed. For the injector linacs and bunch compressors, the klystrons are located in the tunnel and the modulators in a nearby cryohall, as for the main linacs. Each 5 GeV linac has 9 klystrons each of which feeds 2 cryomodules operating at a gradient of 20 MV/m. Failure of up to 2 klystrons could be compensated by raising the gradient of the remaining modules to 25.7 MV/m. The compressors have 4 rf stations each of which feeds 3 cryomodules; only three rf stations are required for operation (1 spare). Both the electron and positron pre-accelerators use warm rf. For the positrons, nine 10 MW standard MBK klystrons (40,000 hr MTBF) are required to deliver 250 MeV. The klystrons together with the modulators will be located in a

shielded area, and will be accessible during operation. The electron source has a total of 4 standard MBKs, three of which drive the first normal conducting cavities, while the fourth drives 2 cryomodules. All klystrons and modulators are accessible in a separate hall, along with spares.

In the CLIC scheme, the primary electron linac and the pre-injector linacs have 28 L-band klystrons operating with 80 MW peak power; the injector linac has 24 L-band klystrons at 40 MW; the booster linac after the damping rings has 52 S-band klystrons at 40 MW. These klystrons and their associated modulators are expected to have lifetimes equivalent to the mature SLAC components. The rf systems for the pre-damping and damping rings are not yet designed.

8.4.3 Low Level RF

All of the proposed linear colliders will require extensive, complicated Low Level Radio Frequency (LLRF) systems. For years, LLRF systems have been implemented with analog hardware, as digital techniques did not have the computing speed to handle the required frequencies and bandwidths. With the advent of cellular wireless telephony, significant improvements have been made in the digital rf technology sector. As such, many existing accelerators have adopted digital techniques for the implementation of new LLRF systems.

In a pulsed cold linac, the LLRF system is much more complex than in a normal conducting linac where neither fast intra-pulse feedback or intra-pulse exception handling is possible. Older CW superconducting rf systems, such as those at LEP and CEBAF, have relied on simpler analog implementations. At TTF, the LLRF is done digitally [11]. A further complication with the TESLA design is that many cavities are driven by one klystron and there is substantial Lorentz force detuning.

The tight tolerances due to the very high Q of the superconducting cavities and to variations in beam loading make it necessary to use high speed, 100 KHz bandwidth, feedback as well as feedforward to stabilize the accelerating field. Modern electronic ADCs and DACs are quite capable of the speeds required ($\sim$100 MHz), but the high speed signal processing has yet to be done cleanly. Laboratories that adopted the new digital techniques have consistently greatly underestimated the level of professional manpower it takes to get a system up and running. The field has become so specialized that individuals with the combined rf and computer knowledge are in short supply.

There is very little high intensity operational experience with large-scale digital LLRF systems and gaining this experience should be an urgent priority for TTF. A digital rf system was installed at the PEP-II B factory and one is under construction for the SNS. Even though PEP-II is an e^+/e^- storage ring complex, many of the challenges are similar to those faced in the TESLA design, including the needed high level integration into the control system and the diagnostics that allow precise system optimization at the highest intensities. Experience with the PEP-II system has been very sobering and has shown how important it is to have a well-designed and well-supported system.

In the normal conducting linac the LLRF must program the phase transitions to control the pulse compression. Since the rf pulse is too short to allow beam intensity variations to be compensated by feedback, a feedforward scheme based on a beam intensity estimate from the damping ring will be used. This scheme was tested and used at the SLC. In all

proposed linear colliders, the LLRF is a key component of the machine protection system. The system must be designed with an appropriate level of redundancy and without possible simple single-point failures in order to avoid beam damage in the linac cavities.

8.4.4 High Power Microwave Components

All of the collider designs will deal with high microwave power, tens to hundreds of megawatts. Since the required power levels have not yet been fully demonstrated, the reliable operation of high power components is a concern. Another issue is the segmentation of the power distribution systems. All designs have relatively large regions connected by a common vacuum or cryogenic system, with the result that a failure of a single component can potentially have a major impact and require a lengthy recovery after repair.

The TESLA design has the lowest power requirements, with only 10 MW peak power from the klystrons to 36 cavities and no pulse compression required. For 500 GeV operation, many components are being tested at TTF. The higher gradient 35 MV/m cavities required for energy upgradability will require higher drive power and further R&D on components. Even for these, the power required is modest and problems are not expected. The JLC-X/NLC designs have 510 MW peak power delivered to each 6 structure unit. The CLIC design has 460 MW peak power delivered to the structures, the highest rf power per structure. Due to the distributed two beam nature of the CLIC design, the rf power has only a very short distance to travel between the primary and secondary beams. The critical components are the power extractor and structure coupler.

8.4.5 Cables

The TESLA design has long cables between the modulator and the klystron, up to 2.5 km in length. For reliability, these should be continuous cables for the full length. Repair or replacement of cables in the tunnel may be difficult and spare cables are planned. It is believed that several manufacturers can produce the needed cables, but a field test of powering a klystron with such a long pulsed cable is essential. A test cable (few km) will be delivered and tested at TTF beginning in 2003. In the other LC designs, the klystron is in close proximity to the modulator and long power cables are not an issue.

8.4.6 Evaluation—RF Components

As stated earlier, critical reliability issues for the rf systems are the frequency and impact of faults, the adequacy of the spares overhead, and the accessibility and duration of repairs. It is difficult to estimate the MTBF for any of the components as none of the projects has accumulated adequate running time with the final designs. JLC-X/NLC have taken a conservative approach to the design of the rf system, allocating a large 5% spares overhead for the main linac and providing redundancy elsewhere. All klystrons and modulators are accessible for repair during normal operation. For TESLA, the klystrons are located in the linac tunnel and require access for repair. The original 2% spares allocation has been reduced due to accelerator design modifications, but at 500 GeV this reserve can be recovered by a slight gradient increase. For CLIC, a structure fault would presently take a

whole 625 m section of linac off-line and a solution for isolating smaller segments must be found. The warm rf machines require very high peak rf power which has not yet been demonstrated. This is a high priority technology R&D issue. Issues related to LLRF have been covered in Section 6.3.

R&D issues:

- A comprehensive assessment of the MTBF and MTBO for rf components is required, and an adequate fraction of hot spares must be included in the final design.
- CLIC needs to develop a mechanism to turn off only a few structures in the event of a fault.

8.5 OTHER COMPONENTS

This section discusses a number of areas of concern either because they are potential single point failures or because of the large number of components.

8.5.1 Sources

The electron and positron sources for a linear collider are complex systems which in some cases require regular maintenance and for which a high availability is difficult to guarantee because of the large number of different components. All of the designs plan some level of redundancy for the sources. For the positron target and collection systems, redundancy is more crucial as these systems will have such high radiation levels after use that a prolonged cooldown will be required before repairs. Even with multiple targets, a detailed analysis and optimization of maintenance scenarios may indicate that quick disconnects or robotics are desirable.

The NLC plans to have two identical polarized electron sources including the photocathode gun and laser, either of which can provide the required beam. Similarly, the electron source for the positron drive beam will contain two redundant guns. NLC had originally foreseen two redundant positron target and collection systems, separated by adequate shielding to allow work in one area with beam in the other. Recent evidence for a lower target damage threshold indicates that multiple targets will be required for normal operation. The NLC baseline now contains four targets, of which any three are required for operation and one can be under repair. An undulator-based source is also under study where the layout would include two target assemblies for redundancy. JLC has proposed having two electron sources, either both polarized or possibly with one of them a simpler unpolarized source for commissioning. The positron production system is similar to that of NLC.

TESLA plans for two independent sources, one of which would be an unpolarized rf gun for commissioning and initial operation, and the other a polarized source. The rf gun could be changed later to a polarized source to improve the system availability. For the undulator-based positron target, the radiation levels with a thin target will be much lower than for a conventional target. A standby target system with appropriate handling will be available locally so that it can be moved in place if required. Also planned is an electron

source to be used for positron commissioning. Both electrons and low intensity positrons should be available.

8.5.2 Magnets and Power Supplies

The reliability of magnets and their power supplies is a potential concern for a linear collider because of the large number of devices, even if individual MTBFs are long. For example, the NLC design includes about 4600 dipole, quadrupole and sextupole magnets, essentially all of which are required to operate the machine. A failure of any component takes the collider down. There are also nearly 10,000 correctors, BPMs and movers but, in contrast, the collider can continue to operate with a handful of these out of service, as long as the failure is passive (*i.e.*, not runaway). These components need not have a significant impact on reliability as long as they have moderate MTBFs and as long as the control system provides the capability for rapid diagnosis and response to failures.

For the essential magnets, failures of a magnet itself can be minimized by careful engineering. At NLC, much effort was devoted to Failure Modes and Effects Analysis (FMEA) and an improved prototype quadrupole has been built. The major remaining risk is failure of the power supplies or of the controls and interlocks. To minimize the total number of power supplies, NLC has adopted adjustable permanent magnets wherever possible. Where electromagnets are required, reliability can be enhanced by providing redundancy and by stringing magnets to reduce the number of power supplies.

Permanent magnets offer several advantages for reliability. They require no cooling water or high power electrical cable and connections, all vulnerable to failures. They do require a movable adjustment mechanism but in general, the collider can continue to operate if some magnets are no longer adjustable. Of course, they introduce new potential failure modes such as degradation of the PM material. Given the radiation environment, the lifetime and reliability of both the adjustment mechanism and PM material must be verified. Permanent magnets have been successfully used in wigglers and undulators for light sources. The Recycler storage ring still being commissioned at Fermilab is also composed mostly of permanent magnet dipoles and quadrupoles.

In the present NLC layout, one third of the dipoles and two thirds of the quadrupoles are specified to be permanent magnets. These are used in the injectors, bunch compressors, and main linac beam and bypass lines. They are not used in the damping rings because of the radiation load and they are not used in the beam delivery for energy flexibility. Their use in the main linac beamline is still under discussion due to the desire for energy flexibility and the tight beam-based alignment tolerances. Most of the dipoles, sextupoles and damping ring quadrupoles would be powered in strings, reducing the number of supplies needed from 1000 to perhaps 200.

In the linacs, each quadrupole requires an adjustable strength which scales with the beam energy. To enhance reliability, several linac quads can be strung together on a common supply with individual trim supplies to provide the fine adjustment. This has the advantage that it is possible to match around a failed trim supply, whereas it is difficult if not impossible to match around a quad that is off. Where individual supplies are used, full redundancy will be provided with a spare supply for each quadrupole, or in some cases,

by including a hot spare for a group of several supplies. The first choice automatically recovers from a failure, the latter requires manual intervention.

TESLA considers mainly three types of supplies in order to provide reliable operation and cover the majority of requirements [12]. Low current supplies for steering dipoles and quadrupoles (50 or 100 A, less than 1 kW) are to be built in a modular fashion (up to six power units per supply) so that if one or two units fail the others can take over immediately. These supplies are located in the tunnel and failed units can be replaced on maintenance days. They cause downtime only when the supply can no longer deliver the required current (*e.g.*, when more than two modules out of six fail), or in the event of a failure of the regulation board, which will not be redundant. MTBF of a supply is estimated to be 200,000 hr. There are 1900 of these supplies in the main linacs and 1260 in the damping rings. On the average it is expected that six main linac supplies will fail over a 4 week period and require retuning of adjacent quads or correctors.

In case of a quad or power supply failure, it is assumed that the optics can be rematched by an automated procedure with some slight degradation to the luminosity. The question of how many failures can be tolerated with what penalty in luminosity needs to be simulated. The quads in the upstream end of the linac where the energy spread is large will be particularly sensitive and may warrant redundant supplies. Failure of a corrector magnet or BPM causes a degradation of the orbit in that region, which can usually be compensated by a tuning knob. As with the linac quads, there may be a gradual degradation of the luminosity, which should be simulated to quantify the sensitivity. A few components are more critical, such as the BDS sextupoles, and they probably require some provision for redundancy. The BPMs associated with the fast IP feedback, as well as some others, will also be essential for operation and require some provision for redundancy.

The medium sized power supplies (up to 600 A, 200 V, 120 kW) will be switch mode supplies, which may be pulse-width modulated. MTBF is estimated at 40,000 hr but the supplies will be arranged in groups of a few with spares that will be remotely switchable in case of the failure of one supply. Mean time to determine the fault, switch and put the spare into operation is estimated at 3–5 minutes. The supplies for the beam delivery and extraction lines are located in the tunnels, but switchable spares will be located in service halls with cables running the length of the BDS. Supplies and spares for the damping rings are located in accessible halls and can be changed out during operation. There are about 120 of these supplies for the beam delivery and extraction lines.

There are a few ($\sim$20) big supplies exceeding 120 kW. These will use SCR technology and will be located in accessible halls. MTBF is estimated at 40,000 hr. Some may have spares that can be switched in with high current switches; others will probably require one-to-one replacement. These supplies are used mainly in the extraction line or damping rings.

8.5.3 Cryogenic Systems

Only the TESLA project will have an extensive cryogenic system. Operational statistics from the large cryogenic installations at CERN, DESY, FNAL and KEK demonstrate that such systems can be very reliable. Availability was generally lower during the first year after installation while crews were being trained and design errors corrected [1]. Subsequently, reliability of over 99% was achieved with >100,000 hr of operation. At TTF,

the cryogenic system reliability is 97.5%, the poorest performing subsystem. To achieve a reliability over 99%, redundancy of critical or fragile subcomponents is essential. The proposed TESLA cryogenic facility should be able to achieve the necessary reliability with appropriate engineering.

The TESLA linac is divided into 2.5 km-long cryogenic units. This segmentation choice is influenced by the cryoplant layout with sparse access points, cost considerations and cryostat design constraints. If a part of the linac must be warmed up, for example to fix an internal problem or change a cryomodule, then the whole 2.5 km unit will be warmed up (and a 0.5 km section of insulating vacuum vented). Manual valves on each module can isolate individual beam tube vacuum sections. It is expected that the process, including warmup, repair and cooldown, may take about a month. This may be an availability risk that deserves further study. HERA has 1.6 km vacuum segmentation that has not caused problems. Any risk analysis must also address just what sort of failure would require immediate repair as opposed to a temporary fix and repair in long maintenance periods. Failures that might require immediate repair include: failure of both rf windows in an rf coupler, helium vessel to beam vacuum rupture, large local heat leak. It is important to note that unlike circular machines with magnets, linacs can operate with unpowered modules. In addition, in the cryogenic linac, there are no flange interfaces between the beam tube and helium. Any beam tube to insulating vacuum leaks are at a very low differential pressure.

8.5.4 Vacuum

The vacuum systems of a linear collider pose a potential reliability risk because of their total volume and complexity. There are a large number of pumps for the normal conducting linacs, most of which must be operational; their power supplies and controls may be situated in the tunnel for cost savings. The systems also require a large number of valves to provide segmentation. In TESLA, the consequences of loss of cavity vacuum can be very severe, because of the sensitivity of the cavities to contamination. TESLA has three vacuum systems: the cavity beamline system, the input coupler system, and the cryostat insulating vacuum. The TESLA cavity system has few lumped pumps because of the cryogenic pumping (a total of 200 ion pumps for the linac cavities and one ion pump per module (total 858) for the input coupler vacuum). For the TESLA insulating vacuum there are in total 120 installed turbo pumps. Additional movable pump stations can be added every 50 m for initial pump down or in case of a helium leak to the insulating vacuum.

The number of primary beam line valves in JLC-X/NLC is about 1900 in total for both linacs. The SLED-II system can be easily isolated into 28 m long accelerator vacuum sections. TESLA has a relatively small number of vacuum sectors (16 total). In TESLA there are two manual valves per module in order to allow installation of the modules using a double-lock system so that the cavities remain under vacuum. The manual valves are only operated when the system is warm and the insulation vacuum opened. The TESLA superconducting cavities place constraints on the design of auxiliary components nearby, such as gate valves, BPMs and bellows, so as to minimize particulate matter generation. TTF experience, where all auxiliary components were made and prepared to exacting vacuum dust specifications, shows some degradation in cavities closest to the warm sections. It is not clear if this is due to assembly, inadequate magnetic field shielding or particulate matter from the warm sections.

The danger of a serious disruption of accelerator operation in TESLA by accidental venting of the cavity vacuum is being carefully considered [13]. Following an accidental vent within the cold section of TESLA, such as that caused by errant beam burning a hole in the niobium cavity wall, by input coupler double window failure, or other failure or error, some cavities may become contaminated by the inflow of helium or air. In the case of a helium leak, even though the differential pressure between the helium and vacuum is small, helium will enter some cavities and form liquid. Furthermore, during the warmup that follows, warm gas may carry dust to adjoining modules. In order to minimize this, TESLA is considering automating some of the module manual valves. The present TESLA design includes only one beam line valve per 2.5 km but it would be possible to segment to as short as 150 m sections by automating some of the manual module valves. Even though beam induced holes seem unlikely with the 70 mm diameter cavity aperture and an appropriate machine protection system, both a failure analysis and actual tests seem warranted.

On the other hand, NLC structures have come close to the design performance with little serious concern for dust contamination. The processing of NLC structures is hastened by an *in-situ* 220°C bake. Vent tests have been done with the NLC structures at NLCTA. The recovery is relatively quick, with a three day *in-situ* bake to speed up the processing. Tests of the vacuum performance of the SLED-II components have not been done.

The vacuum specification for the TESLA damping ring straight sections has been tightened to 0.1 nT to prevent collective instabilities (the previous spec was 1.0 nano-torr). This would require an *in-situ* bake, even though there is no synchrotron radiation in the straight sections. The TESLA design calls for 5000 pumps for the damping rings. The NLC damping rings probably also require *in-situ* bake, but the vacuum limit is 10 times higher. Other areas have less stringent requirements and do not pose a concern.

8.5.5 Controls

The control system for a linear collider poses a significant reliability risk itself, unless a serious effort is devoted to careful engineering. There will be a very large number of components distributed over a length of more than 30 km. The distances alone significantly increase the mean time for even the most minor repair, and require that components be remotely diagnosable to a very high degree, well beyond standard practice. This is true whether the remote distance is tens of km at the site or thousands of km in a Global Accelerator Network. This requirement combined with currently available technology lends itself to a model where device control is done by smart network appliances connected by Ethernet. Unfortunately, this model is unlikely to produce the required system availability given the large number of components and typical MTBFs.

Beyond the sheer number of devices, the LC tuning, feedback and machine protection requirements are extremely challenging. These are described in later sections. To reliably deliver high luminosity, the collider depends on extensive feedback and automated tuning procedures, operating continuously. The high beam density implies that an errant beam can easily damage beamline components, necessitating a complex machine protection system involving a large number of components for safe operation. Both the automation and the machine protection require fast communication paths linking distant parts of the machine. Together these requirements make the system intolerant of controller failures and demanding of very high reliability.

NLC has enumerated and evaluated the controls subsystems that form critical single point failures which would jeopardize accelerator component safety. For example, a large error in the overall linac phase probably causes beam loss, which could damage the structures. The timing system, damping ring subsystems (kicker and rf), software systems and machine protection system are all areas of concern. While the cost of redundant networked systems is not large, a careful evaluation is not trivial and must be considered in the design of the machine protection system.

None of the projects have really begun to address these issues in sufficient depth. A few years back, NLC developed a conceptual design for a highly reliable, redundant communication network that minimized exposure to fragile components in the field. At the very least, this design would need to be updated in light of advancing technology. Given the central role of the control system and the complexity and sophistication of the algorithms envisaged, a major effort will be required in this area. It is an important topic for future R&D and eminently suited to international collaboration as most demands are common across designs.

8.5.6 Evaluation—Other Components

All projects envisage some level of redundancy for the sources. NLC has taken a very conservative approach with fully operational spare systems, as has JLC. TESLA has a combination of redundant systems and relatively easy-to-replace hot spares. Redundancy is also foreseen for magnet power supplies, particularly where they are inaccessible as for TESLA. Here the key issue is the allocation, during development and construction, of sufficient engineering and financial resources to produce a reliable system. The vacuum system size and segmentation is an issue for all designs but is also amenable to engineering solutions. TESLA requires a large cryogenic plant which should not itself be a reliability concern. However, the segmentation is such that a very large 2.5 km length of the accelerator must be warmed up together, making repairs very lengthy. A flexible, sophisticated control system is essential for any linear collider, and providing adequate reliability with such a large, complex system will be extremely challenging.

In summary, while there are many areas requiring attention to ensure reliability, there are no fundamental technical reasons why the systems cannot be made reliable. The only clear difference between the projects is the more limited accessibility for TESLA in a single tunnel, which makes the requirements more stringent.

R&D issues:

- A detailed evaluation of critical subsystem reliability is needed to demonstrate that adequate redundancy and MTBFs have been achieved.
- A model for communications and controls with adequate reliability must be developed.
- The TESLA cryogenic and vacuum system segmentation should be reevaluated.

8.6 ENGINEERING MARGINS

The reliability of accelerator components is improved when they are operated well below their maximum rated parameters, *i.e.*, sufficient engineering margins have been allocated for their environment and their support utilities. Perhaps the best example is the question of semiconductor electronics installed in the beam line enclosure near the accelerator, where the air temperature might be well over 40°C, the radiation dose rate might be over 10 rad/hour and the electricity supplied might contain high voltage spikes. Components other than electronics also have engineering margins against which their environment can be rated, but since both the TESLA and NLC designs include tunnel electronics, a specific comparison is appropriate in this case.

For both NLC and TESLA, a substantial lifetime derating factor is required unless controls are used to mitigate the harsh environment. Structure cooling water, nominally at a temperature of 45°C, heats the NLC tunnel. Radiation in the NLC linac tunnel, generated by beam-gas scattering, may amount to 2 W/m. Extrapolating from present NLCTA performance at 70 MV/m and 400 ns, the radiation dose generated by dark current will be similar, but with a softer energy spectrum [14]. The TESLA tunnel is heated by the klystron water which has a nominal return temperature of 80°C. The return water pipes will be insulated, so it is expected that tunnel temperature will remain below 30°C and not change dramatically during short maintenance periods. This moderate and relatively constant temperature has little impact on the cold linac but is probably very important for stable operation of the damping rings. Electronics and power supplies in the TESLA tunnel will be housed in environmental enclosures which must be carefully engineered. Prototypes have been built and will be tested in TTF. Input air and water cooling to the electronics and power supplies will be at 30°C or less.

Radiation in the TESLA tunnel will be from linac dark current, and from the damping ring and other secondary beam transport systems (such as the e^+ target to ring line). Dark current will cause an average load on the cryogenic system via ionization loss to the cavity and helium (cold mass) so the cryogenic capacity effectively sets an acceptable limit for these losses. The goal is 0.1 W/m radiation loss, which is ∼15% of the static and dynamic rf load at 2 K. As the cryogenic load is accumulated over 2.5 km intervals, local spots can have higher loss levels and many sections will have less. Losses from damping rings and transport lines will also contribute, even though specific hot areas will be appropriately shielded. Electronic equipment located in NLC and TESLA klystron enclosures and tunnels may be subject to supply voltage spikes due to the nearby pulse cables and klystrons. Proper attention must be given to electromagnetic and rf noise.

8.6.1 Radiation Damage

The lifetime performance derating associated with radiation dose depends on the type of radiation and the nature of the semiconductor components. For a variety of semiconductors, damage is predicted for gamma doses between 10^3 rad (10 Gy) and 10^7 rad and for neutron integrated fluences (1 MeV equivalent neutron damage per cm^3) between 10^{12} and 10^{16}. For the NLC design, the dose rates have been modelled for small, shielded, 0.6-m deep tunnel wall electronics housing enclosures, which would need to be water-cooled. The modelling indicates that dose rates from radiation sources other than dark current are

low enough (0.5 rad/hr and 3×10^7 n/cm^2/hr of 1 MeV neutrons) to allow the use of non-radiation hard electronics in the enclosures.

Modelling of radiation in the TESLA tunnel is based on 0.1 W/m deposited in the cold mass. For this loss, the radiation dose rate is 1–3×10^{-2} Gy/hr (1–3 rad/hr) in the tunnel at the electronics location. This dose rate decreases by about two orders of magnitude with the planned 50 cm of concrete shielding. For 100,000 hr operation (20 years at 5000 hr), the dose would amount to 10–30 Gy (1–3×10^3 rad). Neutron fluence is estimated to be 10^7/hr with no shielding and a factor of 10 less with 25 cm of shielding (resulting in 10^{11} in 20 years). It is likely that the radiation distribution along the TESLA tunnel will not be uniform (probably more intense downstream from the quadrupoles) and that the more sensitive electronics can be put in lower radiation areas. Dark current levels follow the Fowler-Nordheim law; a change of a few MV/m gradient can change the dark current generation by an order of magnitude. Thus some management of individual cavity gradients may be advantageous in minimizing dose.

8.6.2 Evaluation—Engineering Margins

Experience at SLC showed that the most serious cause of component failure was exposure to radiation. Most radiation exposure was due to steady, relatively low losses, in congested parts of the machine, not in the bulk of the linac. In TESLA, where all machines coexist in a single tunnel, great care must be taken to shield the linac cryostats from radiation generated by other subsystems. In both designs, further study is needed to evaluate the exposure to radiation of the tunnel electronics.

Tunnel air temperature and humidity are the next most important concern. TESLA, with only one tunnel, has a much greater density of delicate equipment which must be housed in environmentally controlled and shielded containers. JLC-X/NLC can separately control the environment of the support tunnel in order to keep it closer to a nominally benign condition, but may require water-cooled tunnel enclosures.

8.7 MACHINE PROTECTION SYSTEM (MPS)

The Machine Protection System (MPS) is responsible for protecting machine components from beam related damage [15]. It automatically controls changes in beam power, both by halting operation when a fault is detected and by restoring operation when the fault is cleared. The minimum response time, the interval between the occurrence of a fault and the termination of the beam sequence, is one full interpulse period for the short train machines (JLC-X/NLC and CLIC) and about 1/10 of the train length ($\sim$100 μs or 300 bunches) for TESLA. Since it is not possible to stop a given beam bunch once extracted from the damping ring and since a single beam bunch is capable of causing substantial damage, a permit signal indicating the readiness of the downstream systems is required before extraction from the ring is allowed. The permit signal is derived from beam data taken on the previous pulse and from a system that monitors the performance of all devices whose state can change substantially between pulses and which are strong enough to steer the beam into a vulnerable machine component. Before operation can be resumed, the MPS

provides for the production of a sequence of pilot and low power pulses that prove the fitness of the downstream systems for high power operation.

8.7.1 Component Vulnerability

Beam initiated damage can result either from low losses lasting many pulses or from high power losses of a single (or a few) bunches or bunch trains. The two effects are known as average power damage and single pulse damage, respectively. The MPS is intended to protect the rf structures, collimators, special instruments and simple vacuum chambers. It is not known for any of the designs if MPS will be responsible for limiting the dose to beamline and support equipment such as permanent magnets and electronics. By their nature linear collider beams have a much greater potential for single pulse damage than beams of present day machines. Tests done at SLAC [16] have shown that a single pulse with charge density of more than 1 pC/μm^2 will perforate a 1.4 mm thick copper iris on which it is normally incident. Calculations done by the CLIC group support these measurements [17]. It is expected that Nb damage will be similar. Simulations done for the NLC structure indicate that, in many failure scenarios, an oscillation large enough to drive the beam into the structure irises does not necessarily enlarge the beam size sufficiently to prevent damage.

Protection of collimators is a special case handled elsewhere in this report (Section 7.4.5). Special instruments may have an associated collimation system specifically for their protection. For the most part, simple vacuum chambers will be hit by grazing incidence, $\sim$1 mrad impact angle beam pulses. Estimates done at SLAC show that an aluminum vacuum chamber will not be perforated by a full NLC train at 1 mrad or lower grazing incidence.

The TESLA beam aperture in the linac is large (70 mm diameter versus 10 mm for NLC), thus it is considerably less likely that the beam can be steered into the cavity walls. Even so there are doubtless failure modes that would destroy some cavities and contaminate others. Full failure mode analysis has yet to be carried out to determine just what the possible fatal scenarios might be. While it might appear that linac quad and steering failures cannot steer the beam sufficiently to reach the aperture, this must be verified by detailed calculations. The pre-linac collimation system is key to assuring that misaligned beam is never injected. For CLIC, simulations with alignment errors indicate that no significant beam loss occurs if a complete drive beam sector fails to deliver rf power, unless the lost sector is one of the first two. In this case, there is severe beam loss due to over-focusing [18].

8.7.2 Permit System

In all designs, the MPS is segmented into three zones: the bunch compressor system, the main linac and the beam delivery, separated by the pre- and post-linac collimation sections which are capable of dissipating the full power. The collimation is not perfect, however, and failures of the bunch compressor system, for example, must be considered a threat to the main linac components.

For both the long bunch train machine, TESLA, and the short bunch train machines, data from position monitors and loss monitors are used to allow operation to continue. In the case of NLC, for example, a beam trajectory outside predetermined limits detected on pulse

n-1 would stop operation before the extraction of pulse n from the damping ring. The beam from pulse n would remain in the ring or would be locally aborted. In the case of TESLA, an aberrant trajectory of the first few bunches in the train would be used to stop extraction of the rest of the train from the damping ring. The minimum response time could be as long as 300 bunches, due to beam and signal propagation delays. In neither design is linac damage completely prevented in all scenarios by the above system.

There are a number of fast devices whose field can change substantially in a time less than the minimum response time and which are strong enough to deflect the beam outside acceptable trajectory limits. The list of fast devices is not complete for any of the designs. For the NLC, for example, the fast device list for the main linac includes focusing magnets and diagnostic section dipoles. It is probable that the magnetic field in these devices can change significantly during the interpulse interval. The list of fast devices also includes elements that can cause simple common-mode failures such as programming controls for linac phasing. Consideration of damping ring beam intensity transients is still to be done.

8.7.3 Power Restoring Sequence

Following a fault, or any interruption lasting a long time compared to the inter-pulse interval of the warm structure machines, operation must re-commence with a completely benign pilot pulse. This is because of the slow devices whose field is only indirectly monitored via beam data. Once the complete fast device list is formulated and evaluated, it may be decided to include all accelerator components in the fast device list. The pilot pulse must be only a single bunch (or a few for TESLA) and must have a charge density less than 1 pC/μm^2. For JLC-X/NLC, this means a reduction of between 10^{-4} and 10^{-5} with respect to the nominal charge density, to be accomplished either by an emittance spoiler, reduced intensity or by a combination of the two.

All critical feedback loops and basic beam position monitors must function on the pilot pulse. This is important especially for TESLA where beam loading signals from the cavities themselves will be used to fine adjust the cavity phases relative to the beam and verify that the beam loading compensation is ready for the rest of the sequence. JLC-X/NLC will have cavity phase monitors that will pick up the phase of the beam to check the sector phasing, and these should have little problem detecting the signal from a very small intensity pilot beam. Once the parameters of the pilot bunch's path through the machine have been checked and found within tolerance, the power ramp sequence can begin. For JLC-X/NLC the sequence begins with pilot bunch operation at the full repetition rate, followed by the removal of the emittance spoiler and restoration of nominal bunch charge and finally by ramping up the number of bunches to nominal.

8.7.4 Average Power

For uncooled components, a beam loss of a few watts/m can be a concern. For a cryogenic system, a few tenths of watts/m loss is a cause for concern. The lost fraction of the beam is 10^{-7} and 10^{-8} in each case, respectively. Average power beam loss is detected using conventional loss monitors. Because small average power losses depend on the extrema of

the beam distribution, the power restoration sequence processor will estimate average power losses expected at each transition before allowing it.

8.7.5 Other Concerns

Aside from direct damage from impact, the presence of the beam can cause unexpected behavior in other ways, primarily from the electromagnetic fields it leaves in its wake. Two good examples of this are the field left in a tuned, unpowered superconducting cavity and the field in a backphased, powered structure (warm or cold). The LLRF controllers must be programmed to deal with such events appropriately to avoid damage.

8.7.6 CLIC Drive Beam MPS

The power in each CLIC drive beam is 63 MW, about eight times the primary beam power of JLC-X/NLC and five times that of TESLA [19]. In addition to the power handling steps described above, there is serious concern for the mechanical deformation that may be caused by a relatively small, 0.1% steady beam loss. The drive beam power extraction structure efficiency will degrade when there are beam losses in the area and it is possible that will feedback on the beam and create additional beam losses. In order to mitigate this problem, the CLIC drive beam power ramp sequence will include intermediate steps where the peak power is nominal but the average power is greatly reduced. Further study is needed to devise protection sensors and explore the beam power managing sequence.

8.7.7 Evaluation—Machine Protection System

The small, very intense, beams in a linear collider require a new approach to machine protection untested at any existing or soon to be completed machine. Furthermore, the pulsed time structure of the beam, as opposed to the CW nature of the Tevatron or LHC is an additional difficulty. There is a proposed protection system scheme that is feasible for both TESLA and JLC-X/NLC that relies heavily on the use of a pilot bunch and a fast permit system. The scheme needs further design and evaluation.

Since a single, nominal intensity bunch will damage almost any accelerator hardware it happens to strike, there is little fundamental difference in the TESLA and JLC-X/NLC MPS exposure or design strategy. The long inter-bunch interval in TESLA allows the beam to be switched off somewhat more quickly than in JLC-X/NLC. Steady, low intensity losses are also important but these can be handled with a conventional MPS strategy.

R&D issues:

- A detailed Machine Protection System design that meets requirements must be developed, including a careful study of failure modes.
- CLIC needs a detailed design of an adequate MPS system for the drive beam.

8.8 RECOVERY AND TUNING IMPACT

When considering reliability in terms of integrated luminosity delivered, it is necessary to estimate the effect of invasive and non-invasive tuning, where invasive refers to interrupting luminosity. Optimization of performance then becomes a balance between peak luminosity and time lost to tuning. In much of the collider, the component alignment tolerances are extremely tight and cannot be achieved by traditional survey techniques. All of the designs foresee extensive use of beam-based alignment. In addition, the tight tolerances make the machines very sensitive to slow drifts due to temperature and ground motion effects. As a result, beam-based feedback systems are mandatory, and both invasive and non-invasive retuning will be required at intervals. A quantitative estimate of the impact requires detailed simulations of the tuning algorithms and feedback in the presence of errors and time-dependent effects, such as ground motion. The tools to perform fully integrated simulations of a linear collider are only now becoming robust and complex enough to address these questions, and hence any estimates are only a first approximation.

As a framework for assessing the operational impact of tuning procedures, five scenarios were considered:

- Tuning during normal luminosity operation
- Beam-trip recovery (seconds to minutes)
- Recovery after a repair not requiring access to the accelerator housing (hours)
- Recovery after a repair requiring access (shifts)
- Recommissioning after a long shutdown (weeks to months)

The shorter the duration of the outage, the less tuning should be needed to recover adequate luminosity. It is however important to remember that the impact of trips (such as rf unit faults) can be significant because of their high frequency, even though the integrated loss per trip may be small.

In making estimates of tuning durations, it is assumed that feedback systems stabilize the beam position and energy at key locations throughout the complex, that machine protection trips and recovery sequences are completely automated and generally require no operator intervention, and that tuning procedures are essentially completely automated. The most invasive procedures required after a long downtime may require operator monitoring, but must be automated to minimize execution time. Those which occur during routine operation should be completely hands off, including optimization procedures both for the linac emittance and for the beam size at the IP. Needless to say, these conditions will not be met for initial commissioning. The level of automation described goes far beyond what has been achieved at existing accelerators, but it is essential. If one simply extrapolated the time required for more manual tuning procedures to the scale of a linear collider, then the beam availability would be unacceptably low. It should also be emphasized that the time estimates give the minimum time required when everything executes perfectly. Experience with existing machines would indicate that typical times for recovery or tuning are considerably longer than the minimal estimate, even when procedures are automated. We first briefly review the various algorithms.

8.8.1 Tuning Procedures

The tuning procedure for each part of the collider starts with beam-based alignment of structures, quadrupoles, and any higher order multipole magnets [20]. This is a multistep procedure where the first step is to find the relative offsets between the quads and the nearby BPMs by means of quad shunting or ballistic techniques. These offsets define a reference trajectory. The beam is steered through the center of the quads using either dipole correctors or movers. Dispersion-free steering can then be used to find a reference orbit with even lower emittance growth. Closed bumps are applied to cancel residual dispersion or wakefield distortion. Finally, damping ring or IP tuning knobs are optimized. Efficient operation of the collider will require many more feedback and tuning procedures than described here but we have tried to focus on those with the largest perceived impact on efficiency.

Beam-Based Alignment (BBA): Quad shunting (or ballistic alignment) is a slow, time-consuming, invasive procedure which is predicted to take a few shifts for each main linac, even assuming completely automated procedures and data taking at multiple locations in parallel. It would be done throughout the complex as part of initial commissioning and redone locally after a hardware change. It is hoped that the entire procedure would not need to be repeated, possibly ever and certainly not more often than after a yearly shutdown.

Trajectory Correction: TESLA has steering dipoles at each quadrupole which are used to simultaneously center the beam in the quadrupoles, minimize the average offset in the cavities and compensate for cavity tilts. JLC-X/NLC and CLIC have movers on the individual quadrupoles and structure girders. The correction algorithm moves the components onto a smooth trajectory for sequential sections of the main linacs, as well as for the rings, pre-linacs, and beam delivery. For initial commissioning and after a long shutdown when large moves are anticipated, the procedure would be invasive and likely take one or more shifts for the whole complex.

Dispersion-Free Steering (DFS): DFS is essentially a back-up BBA technique for residual errors left after initial correction. The incoming energy is varied for sequential sections of the linacs and both the on-energy and off-energy orbits simultaneously minimized. To achieve adequate resolution, the energy change must be large and therefore the procedure is invasive. DFS is also sensitive to various systematic errors and hence is not suitable as the only method of BBA [21]. NLC has estimated it would take 0.5–2.0 hr per main linac, depending on the number of iterations required. Like quad shunting, it is assumed to be needed rarely, but since it is relatively fast, it can be applied as a tuneup method during a run. Some method of dispersion correction will also be needed in the damping rings.

Emittance Bumps: Closed-orbit bumps will be used to compensate for dispersion or wakefield distortions, and are most effective when orthogonal control is possible. (JLC-X/NLC and CLIC have the ability to move structure girders which allows clean wakefield control.) Optimization of the bumps is a procedure which would occur as needed non-invasively during normal operation, although initial tuning after a long outage might be done before delivering luminosity, if the beam quality warranted.

Orbit Correction and Feedback: The beam-based alignment procedures and bumps establish a "golden orbit" which must be maintained to a given precision. Without trajectory control, the orbit would quickly deteriorate due to time-dependent environmental effects resulting in an unacceptable loss of luminosity. All designs foresee pulse-to-pulse trajectory feedback and periodic orbit correction. JLC-X/NLC and CLIC plan to use the orbit correction procedure quasi-continuously during normal operation. They estimate that each main linac could be completely corrected every half hour, in parallel with correcting other parts of the complex as needed. TESLA would use an automated procedure to adjust the corrector dipoles, but simulations are not complete enough to specify how frequently this is needed.

Trajectory feedback would be used to stabilize the beam downstream during the corrections as well as to minimize orbit drifts between correction passes. At SLC, feedback was developed to perform the final optimizations of the beam size at the IP. Emittance bump feedback was also attempted but was never fully successful. It is expected that feedback systems similar to those developed for the SLC will be used extensively for optimization as well as energy and orbit stability. Eventually, non-invasive procedures may not adequately restore the luminosity, and invasive DFS or even beam-based alignment will be needed to compensate for drifts in the diagnostics. Simulations of slow diffusive ground motion have shown that dispersion correction might be stable for months in the linacs, but could be required every few days in the damping rings.

Energy Tuning: To achieve the required beam energy at the IP, the amplitude and phase of thousands of linac rf cavities/structures must be adjusted correctly. For TESLA, the Low Level rf (LLRF) controls of each station adjust the phase and amplitude using only a few pulses. Because of potential energy mismatch problems, the procedure can only be applied step-wise down the linac but should still only take minutes. The JLC-X/NLC LLRF system will measure the phase of the beam induced rf and power source rf at the output of one of the structures on each girder. To cleanly separate these signals, the rf for each girder may have to be shut off for one pulse. The measured phase difference will then be used to adjust the source drive phase to achieve the desired beam-to-rf phase for that girder. Fine energy adjustment and stabilization will be achieved by a feedback system which uses a spectrometer to measure the beam energy and adjusts a set of klystrons. NLC has included provision in their klystron complement for such a feedback, while TESLA has not and will need to add overhead for energy stabilization.

8.8.2 Evaluation of Tuning and Recovery Scenarios

Even without any beam interruption, the various tuning procedures will invariably decrease the delivered luminosity. Orbit correction in the damping rings and linacs will cause some emittance degradation during the procedure, if executed non-invasively, and will require lost beam time, if invasive. Optimization of tuning bumps also impacts the luminosity while the best setting is being determined. While a detailed quantitative estimate cannot yet be made, the NLC luminosity projections include a 5% derating to cover the effects of this

tuning and CLIC includes 10%, but even this is probably an underestimate. Other projects can expect a similar reduction from their ideal luminosity.

An essential requirement for minimizing the impact of tuning is that each system be designed with sufficient overhead that it can accept incoming beams with somewhat worse than nominal parameters. As an example, the NLC damping rings have sufficient damping to reach the specified equilibrium emittance even if the injected beam is 50% larger than nominal. Likewise both electron and positron sources are designed to produce 50% more current than required. Overheads are particularly critical in the injector complexes in order to allow these systems to be tuned while delivering acceptable beam. Ideally, the collimation and masking should also be designed to reduce backgrounds to an acceptable level even when the emittance or tails are not yet fully minimized. Before finalizing any of the designs, all systems should be reviewed to assure that appropriate overheads have been included.

Generally after any beam interruption, the shorter the outage, the shorter the recovery time. For a brief beam trip, the automated recovery procedures as outlined in Section 8.7 should quickly reestablish colliding beams with relatively little loss in luminosity. Frequent trips will still have a cumulative impact even if beam recovers in a few seconds. After a short beam-off for a repair which does not require access to the accelerator housing, recovery will only require resteering back to the gold orbits with some final IP tuning. This should be less than 0.5 hr, some of which might be compatible with starting to deliver luminosity. If the beam-off time is long enough, then time may be required for thermal stabilization; an example would be the damping rings, where the absence of beam (and therefore synchrotron radiation) would allow the ring to cool. A rule of thumb for such interventions would be that the recovery time is roughly equal to the beam-off time.

When access is required to the accelerator housing, there are significant implications for the TESLA one-tunnel approach. For JLC-X/NLC and CLIC, where the various subsystems are in separate housings, unaffected systems could remain up, perhaps even with beam upstream of the housing accessed. These systems would remain in stable operation and be available to deliver beam as soon as required with no additional tuning. For TESLA, access to the main linac tunnel immediately requires that the damping ring and positron source be shutdown. After the access, a large part of the machine has to be restarted from a "cold state." This will almost certainly extend the recovery time by a duration which still needs to be evaluated. A prolonged access also implies recovery time for thermal stabilization. The linac tunnels are expected to run with an equilibrium temperature of 30–35°C. For an access of 1–2 shifts, in principle only trajectory smoothing and bump optimization would be required. Since these procedures are nominally compatible with delivering luminosity, the invasive recovery time could be on the scale of hours, depending on the areas affected.

During an extended shutdown of a few months, one would expect extensive maintenance, installation of new hardware and other upgrades. Recovery typically involves relatively major recommissioning of the machine. Components will likely have moved enough that the full beam-based alignment procedures would have to be performed, as well as linac phasing. In general, a subset of the initial commissioning procedures would be required. Recommissioning could ideally take a minimum of several shifts, but more likely several days to weeks, allowing for the inevitable problems.

A special note here should be made of the impact of the proposed undulator-based positron source for TESLA. Clearly if there is no electron beam, then there can be no positron

beam. For all scenarios outlined previously (and including the initial commissioning), recovery of the positron beam implies recovery of the electron system, and these scenarios need more detailed study.

8.8.3 Commissioning

Any collider design where the injectors and damping rings are in separate housings from the main linac has a significant advantage in staging the commissioning of the machine, as these sections can be fully studied long before the main linac installation is complete. All of the JLC-C, JLC-X, NLC, and CLIC designs have this configuration. CLIC plans to share some components between the positron and electron injectors, necessarily coupling their commissioning. Some site layouts considered for the NLC have the injectors in a central location, which requires long transport lines to bring the beams to the low energy end of the linacs. These lines would be in the same tunnel as the main linac, and in this case, only the beamlines up through the damping rings can be commissioned independently of the main linacs. To set the scale, the NLC schedule includes about 3 years of commissioning for the injector and damping ring systems.

In the TESLA design, the injector linacs, damping rings, bunch compressors, and positron source are all located in the main linac tunnel, making beam tests of those areas incompatible with linac installation. An added complication is that the positron source requires a high energy electron beam and so cannot be tested until commissioning of the electron systems are fairly well advanced. A low current conventional positron source is foreseen to allow some commissioning of the positron systems before the full power source is available. Commissioning with a high power electron beam would also be possible with this source, but would require magnet polarity switching. Overall, the constraints imposed by the single tunnel for all subsystems and linkage between positron and electron beams is likely to have the most detrimental impact during the final installation and commissioning phases, when frequent access for repairs or upgrades can be expected, most of which will interrupt all operation. A working group on TESLA commissioning strategy has been set up to address these issues [22].

8.8.4 Maintenance Model

TESLA plans to have routine tunnel access for maintenance about every 3–4 weeks in order to replace failed klystrons. The actual frequency will be determined by the klystron lifetime achieved and the number of spares available for overhead. As noted in Section 3.1.1, the gradient must be increased to 23.8 MV/m to provide 2% spares, but this increase may not be sufficient to cover both faults and failures with an access interval of 3–4 weeks. To achieve the desired goal, TESLA will need to select a set of operating parameters which provides an adequate overhead, even if it requires slightly lower energy or luminosity.

Before access, a 3 hr cooldown period for radiation is anticipated before tunnel air can be exchanged with outside air. The klystron and transformer will be designed for quick connect and disconnect. Klystron replacement has a target time of 3 hr per tube, a very aggressive goal compared with present experience (8–12 hr replacement time at SLAC). It is assumed that there are sufficient crews to replace all of the expected average of

5–6 klystrons in parallel. Allowing a few hours for luminosity recovery, each such access can be estimated to take a bare minimum of 2 shifts, more likely considerably longer. If the target availability for the collider is 85%, then these activities can potentially already absorb a sizeable fraction of the downtime budget, even under optimistic assumptions.

All of the other designs include utility housings for the modulators, klystrons and power supplies which are fully accessible for maintenance during collider operation. This is partly because the X-band and C-band machines have a factor of 6 (JLC-X/NLC) or seven (JLC-C) more klystrons than TESLA, although CLIC has fewer, about 75% as many. More importantly, the designers of these projects believe that it is essential to be able to maintain, repair and possibly even upgrade key rf components without interfering with beam operation, granting that this activity entails some risk. The experience at most accelerators has been that interruptions are very costly and should be minimized to reliably deliver luminosity. In this context, the additional cost of the support housings would seem to be a worthwhile investment in order to ensure good system availability and maximize integrated luminosity. Other tunnel configurations could certainly be considered for a superconducting machine.

8.8.5 Evaluation

Clearly there is not enough detailed information available at this time to extrapolate from the tuning and recovery durations and estimate the percentage of time during which each project might actually deliver luminosity. NLC has the most complete plan for tuning procedures, with extensive diagnostics and controls included in the design. Detailed simulations of these procedures have allowed estimates of durations and frequencies for retuning. TESLA is in the process of revising the tuning scenario which may result in design changes. Information was not available to evaluate the other projects.

The most significant differences between the projects of importance for tuning, recovery, commissioning or maintenance are the choice of a single tunnel configuration, and the strong coupling of the positron production to the electron operation, for TESLA. The present TESLA design calls for access to the tunnel every 3–4 weeks to replace failed klystrons. There are a large number of other components located in the tunnel, which are inaccessible during normal operation. Because the injectors and damping rings share the linac tunnel, access necessarily affects most systems, prolonging the recovery time. This appears to pose a significant risk to reliably delivering a high integrated luminosity. The shared tunnel also constrains the initial commissioning of the machine. The single tunnel configuration was chosen for cost savings and to meet the demands of the DESY site. It is in no way fundamental to superconducting technology, and could certainly be reconsidered.

R&D issues:

- The performance of tuning procedures should be simulated in the presence of a wide variety of errors, both in the beam and in the components.
- A comprehensive reevaluation of design parameter overheads throughout the complex is required.

- A comprehensive evaluation of the frequency and impact of tunnel access is needed, including the impact of all repairs.
- TESLA needs a detailed analysis of the risk of a single tunnel on operability.
- TESLA needs to evaluate the operational impact of coupled electron/ positron production.
- TESLA needs a detailed analysis of the operational impact of structure faults.
- JLC-X/NLC need to evaluate the impact on operations of the interleaved positron target system.
- JLC-X/NLC and CLIC need to evaluate the systems aspects of a large interrelated alignment system.
- CLIC needs to evaluate the impact on reliability, stability and operations of drive beam faults coupling to the entire linac.

8.9 SUMMARY

Reliability considerations must be a high priority in the final design of a linear collider. While the linear collider is probably not more complex than the full chain of machines required to run the large colliders at CERN or FNAL, these facilities have the advantage that the injector subsystems have typically operated for other uses and had years of debugging to weed out poorly performing systems. The linear collider will need to understand and debug all of these systems almost simultaneously. The storage rings also have a major advantage in that the injectors are not required between fills and so can often be repaired or studied without impact. In a linear collider, all systems from injectors to beam dumps must be fully operational on every pulse. While overhead can be built into systems which deliver the energy, redundancy against single-point failures is crucial for luminosity. As the size of a linear collider and the number of its components increases, the short-term role of feedback and feedforward loops becomes essential for operability, and their failure is totally unforgiving. These conditions set the stage for the design and operation of all the machines studied in this report.

While there appears to be no technical obstacle to achieving the desired reliability in principle, none of the designs have yet developed complete plans. Considerable resources will need to be given to reliability issues in developing the final design. A list of concerns and needed R&D follows. Most of the issues are common to all designs, with a few project-specific topics at the end. The significance of the rankings can be found in Chapter 9.

Reliability Concerns and R&D

Items common to all designs:

- If the typical reliability of existing HEP accelerators is scaled to the size of a 500 GeV c.m. linear collider, then the resulting uptime will be unacceptably low. This means that a new approach is required, and following previous practices will not be adequate. Reliability must be addressed up front by failure analysis, and appropriate remedies. Adequate engineering margins for components are also essential. The key issue is the allocation, during development and construction, of sufficient engineering and financial resources to produce a reliable system. Areas of concern either because they are potential single point failures or because of the large number of components include:
  - Sources and Bunch compressors
  - Electronics located in the tunnel, and other inaccessible components
  - Magnets and power supplies, especially where inaccessible
  - Diagnostics, movers and rf tuners, LLRF, kickers
  - Crab cavities (machines with crossing angles)

  R&D (Ranking 2): A detailed evaluation of critical subsystem reliability is needed to demonstrate that adequate redundancy and MTBFs have been achieved.

- All designs require extensive beam-based tuning procedures to ensure that the magnet and structure alignment tolerances are met. Tuning can have a major impact on achievable luminosity if the required precision is not achieved.

  R&D (Ranking 2): The performance of tuning procedures should be simulated in the presence of a wide variety of errors, both in the beam and in the components.

- The low emittance beams can potentially damage any component they strike, making an extensive Machine Protection System essential. The projects have preliminary concepts of these systems but none have developed an MPS design in sufficient detail. This is an important R&D topic. A related issue, where more attention is needed, is proper protection of components against radiation generated by such high power beams.

  R&D (Ranking 3): A detailed Machine Protection System design that meets requirements must be developed, including a careful study of failure modes.

- Critical reliability issues for the rf systems are the frequency and impact of faults, the adequacy of the spares overhead, and the accessibility and duration of repairs. Here JLC-X/NLC and JLC-C have tried to take a conservative approach and have carefully analyzed the overhead requirements. This is primarily a cost issue for all machines.

  R&D (Ranking 3): A comprehensive assessment of the MTBF and MTBO for rf components is required, and an adequate fraction of hot spares must be included in the final design.

- A critical operability issue for all parts of a linear collider is providing adequate overhead in machine parameters. Each system should allow for some deviation from nominal input parameters.

  R&D (Ranking 3): A comprehensive reevaluation of design parameter overheads throughout the complex is required.

- All machines should evaluate the frequency of access to the tunnel based on expected MTBFs for all components located in the tunnels. It is also critical to evaluate the recovery time, considering regulation of air temperature after access for damping rings, final focus, sources, and main linacs.

  R&D (Ranking 3): A comprehensive evaluation of the frequency and impact of tunnel access is needed, including the impact of all repairs.

- A linear collider requires extensive feedback systems, machine protection, precision diagnostics, and automated tuning procedures. Failures of these systems cannot generally be tolerated. Providing adequate reliability with such a large, complex system of devices and controls will be extremely challenging. This is a common issue which has not yet received the necessary attention.

  R&D (Ranking 3): A model for communications and controls with adequate reliability must be developed.

TESLA:

- The TESLA single tunnel configuration appears to pose a significant reliability risk because of the frequency of required linac access and the impact of access on other systems, particularly the damping rings. This tunnel layout choice is possible because of the smaller number of klystrons but is not inherent to superconducting technology. The final design must balance initial cost against the life-cycle cost of delivered luminosity.

  R&D (Ranking 2): TESLA needs a detailed analysis of the risk of a single tunnel on operability.

- The proposed undulator-based positron source for TESLA requires an electron beam before there can be a positron beam. This affects recovery scenarios as well as commissioning.

  R&D (Ranking 3): TESLA needs to evaluate the operational impact of coupled electron/positron production.

- The 2.5 km segmentation of the TESLA cryogenic system is a concern because of the time required for warm up and cool down. The vacuum system size and segmentation is also an issue.

  R&D (Ranking 3): The TESLA cryogenic and vacuum system segmentation should be reevaluated.

- Recovery scenarios from structure faults need better definition.

  R&D (Ranking 3): TESLA needs a detailed analysis of the operational impact of structure faults.

JLC-X/NLC and JLC-C:

- The interleaved target system for positron production is complex and requires a thorough evaluation of its operational impact.

  R&D (Ranking 3): JLC-X/NLC need to evaluate the impact on operations of the interleaved positron target system.

- For the linacs of the warm rf machines, the tuning procedures require structure alignment as well as quadrupole centering. The systems aspects of this large interrelated system need to be studied in depth.

  R&D (Ranking 3): JLC-X/NLC need to evaluate the systems aspects of a large interrelated alignment system.

CLIC:

- In the present CLIC design, an entire drive beam section must be turned off on any fault. This makes operation impractical unless the fault rate is extremely small.

  R&D (Ranking 1): CLIC needs to develop a mechanism to turn off only a few structures in the event of a fault.

- The extremely high power in the CLIC drive beam requires an extensive and complex Machine Protection System, above and beyond what would be required for the production beams.

  R&D (Ranking 2): CLIC needs a detailed design of an adequate MPS system for the drive beam.

- For the linacs of the warm rf machines, the tuning procedures require structure alignment as well as quadrupole centering. The systems aspects on this large interrelated system need to be studied in depth.

  R&D (Ranking 3): CLIC needs to evaluate the systems aspects of a large interrelated alignment system.

- A variety of common mode problems can arise due to the fact that faults in the CLIC drive beam complex affect the whole acceleration chain of the main linac.

  R&D (Ranking 3): CLIC needs to evaluate the impact on reliability, stability and operations of drive beam faults coupling to the entire linac.

BIBLIOGRAPHY for CHAPTER 8

[1] L. Hardy, "Accelerator Reliability-Availability," Proc. of EPAC02 (Paris, France, June 3–7 2002).

[2] R. Ferdinand, *et al.*, "The European Spallation Source (ESS): Reliability aspects and related budget considerations," presented at Accelerator Reliability Workshop (ESRF, France, February 4–6 2002).

[3] Zeroth-order Design Report for the Next Linear Collider, SLAC Report 474, May 1996.

[4] J. Seeman, SLAC, Private communication.

[5] S. L. Gold, "5045 Klystrons & Thyratron Reliability" presented at LC2002, SLAC, 2002
`http://www-conf.slac.stanford.edu/lc02/wg2/WG2_Gold_3602.pdf`

[6] J. Cornuelle, SLAC, personal communication.

[7] H. Weise, "Operational Experience with the Test Facilities for TESLA," Proc. of LINAC02 (Korea, August 2002).

[8] 2001 Report on the Next Linear Collider, SLAC-R-571, June 2001.

[9] J. Cornuelle, SLAC, personal communication.

[10] S. Isagawa, KEK, personal communication.

[11] S. Michizono, M. Liepe and S. Simrock, "Design of low level rf control for the TESLA superstructure," DESY-M-01-06V, Proc. of PAC 2001, Chicago, Illinois, 18–22 Jun 2001.

[12] J. Eckoldt, "Magnet Power Supplies for TESLA, TESLA Report 2000-37.

[13] M. Seidel, D. Trines, and K. Zapfe, "Failure Analysis of the Beam Vacuum in the Superconducting Cavities of the TESLA Main Linear Accelerator," TESLA Report 2002-006, February 2002.

[14] S. Roesler, J. C. Liu and S. H. Rokni, "Radiation damage to electronics in the beam tunnel of the next linear collider," SLAC-PUB-8490, Proc. of SATIF-5, Paris, France, 17–21 Jul 2000.

[15] C. Adolphsen. *et al.*, "The Next Linear Collider Machine Protection System," SLAC-PUB-8130, Proc. of PAC99, New York, NY, 29 Mar-2 Apr 1999.

[16] M. C. Ross, *et al.*, "Single pulse damage in copper" SLAC-PUB-8605, Proc. of LINAC00 (Monterey, California, 21–25 Aug 2000).

[17] S. Fartoukh, *et al.*, "Heat Deposition by Transient Beam Passage in Spoilers," CERN-SL-2001-012 AP, Paper submitted to Physical Review ST-AB.

[18] D. Schulte and F. Zimmermann, "Failure Modes of CLIC," Proc. of PAC01 (2001) 4068; also CLIC note 492.

[19] C. Johnson and P. K. Klöppel, "Examination of the CLIC drive beam pipe design for thermal distortion caused by distributed beam loss," CLIC-Note-328, Pres. at: American Health Physics Society Topical Meeting on the Health Physics of Radiation Generating Machines, San Jose, CA, 5–8 Jan 1997.

[20] P. Tenenbaum, "Beam-based Alignment of the NLC Main Linac, Part II: Dispersion-free Steering and Dispersion Bumps," LCC-0071, September 2001.

[21] T. Raubenheimer, "Comments on Linear Collider Beam-Based Alignment," August, 2002.

[22] P. Castro, "First Thoughts on Commissioning of the TESLA Collider," TESLA Report 2002-009, September 2002.

CHAPTER 9

Summary of R&D Work that Remains to Be Done for Individual Machines or Collectively for All Machines

9.0 INTRODUCTION

In this chapter, the recommended R&D items that have already been indicated in Chapter 6, Chapter 7, and Chapter 8 are collected together.

To assess more precisely the importance and urgency of the proposed R&D objectives, the Working Groups established a discrete ranking list, against which they can be evaluated. Ordered by decreasing criticality, we distinguish the following:

Ranking 1: R&D needed for feasibility demonstration of the machine

The objective of these R&D items is to show that the key machine parameters are not unrealistic. In particular, a proof of existence of the basic critical constituents of the machines should be available upon completion of the Ranking 1 R&D items.

Ranking 2: R&D needed to finalize design choices and ensure reliability of the machine

These R&D items should validate the design of the machine, in a broad sense. They address the anticipated difficulties in areas such as the architecture of the subsystems, beam physics and instabilities, and tolerances. A very important objective is also to examine the reliability and operability of the machine, given the very large number of components and their complexity.

Ranking 3: R&D needed before starting production of systems and components

These R&D items describe detailed studies needed to specify machine components before construction and to verify their adequacy with respect to beam parameters and operating procedures.

Ranking 4: R&D desirable for technical or cost optimization

> In parallel to the main stream of R&D needed to build a linear collider, there should be other studies aimed at exploring alternative solutions or improving our understanding of the problems encountered. The results of the Ranking 4 R&D items are likely to be exploited for improved technical performance, energy upgrades, or cost reduction.

These rankings were applied to both the 500 GeV c.m. projects and to the corresponding upgrades. They were meant to set a scale for the evaluation of the proposed R&D, but, strictly speaking, not for the relevant concerns. However, in many cases, there is a one-to-one correspondence between concerns expressed in Chapter 6, Chapter 7, and Chapter 8, and R&D items. In fact, these rankings themselves were often perceived by the Working Groups as applicable to allaying the associated concerns.

A discrete ranking, with its benefits in terms of simplicity and clarity, unavoidably raises the difficulty of borderline cases, which can only be mitigated by adding more detailed qualifying statements in the R&D descriptions. In the same spirit, counting the number of items in each ranking for each project would give a wrong indication of the criticality of the project. The difficulty or time scale to attain a given R&D objective were not discussed as such by the Working Groups.

Many R&D items are common to all projects; they are grouped together in the following lists. Within each category, the R&D items have been grouped into those identified by the Energy, Luminosity, and Reliability Working groups. Some items pertinent to more than one Working Group are stated only once to avoid redundancy. In the case of JLC-C, only the linac R&D issues are listed separately from the JLC-X/NLC. No luminosity items have been separately identified for JLC-C, since the designs of the damping rings and of the beam delivery system are identical to those of JLC-X, and no design was made available to the Committee for the JLC-C main linac optics. For the same reason, compatibility issues arising in the upgrade of JLC-C through the addition of an X-band extension were also not considered by the group. Also, no specific luminosity-related issues were identified for the CLIC damping ring because a full solution for the CLIC damping ring lattice was not available to the committee at the time of the report. It should be pointed out, however, that the extracted vertical emittance required for the CLIC damping ring is by far the smallest among all the projects, thereby setting the scale for the design challenge.

9.1 RANKING 1

TESLA Upgrade to 800 GeV c.m.

Energy

> The Energy Working Group considers that a feasibility demonstration of the machine requires the proof of existence of the basic building blocks of the linacs. In the case of TESLA at 500 GeV, such demonstration requires in particular that s.c. cavities installed in a cryomodule be running at the design gradient of 23.8 MV/m. This has

been practically demonstrated at TTF1 with cavities treated by chemical processing[1]. The other critical elements of a linac unit (multibeam klystron, modulator and power distribution) already exist.

- The feasibility demonstration of the TESLA energy upgrade to about 800 GeV requires that a cryomodule be assembled and tested at the design gradient of 35 MV/m. The test should prove that quench rates and breakdowns, including couplers, are commensurate with the operational expectations. It should also show that dark currents at the design gradient are manageable, which means that several cavities should be assembled together in the cryomodule. Tests with electropolished cavities assembled in a cryomodule are foreseen in 2003.

JLC-C

Energy

- The proposed choke-mode structures have not been tested at high power yet. High power testing of structures and pulse compressors at the design parameters are needed for JLC-C. Tests are foreseen at KEK and at the SPring-8 facility in the next years.

JLC-X/NLC

Energy

- For JLC-X/NLC, the validation of the presently achieved performance (gradient and trip rates) of low group velocity structures—but with an acceptable average iris radius, dipole mode detuning and manifolds for damping—constitutes the most critical Ranking 1 R&D issue. Tests of structures with these features are foreseen in 2003.
- The other critical element of the rf system is the dual-moded SLED-II pulse compression system. Tests of its rf power and energy handling capability at JLC-X/NLC design levels are planned in 2003. As far as the 75 MW X-band PPM klystron is concerned, the Working Group considers the JLC-X PPM-2 klystron a proof of existence (although tested only at half the repetition rate). A similar comment can be made regarding the solid-state modulator tested at SLAC.

[1] Knowing that electropolished cavities sustain significantly higher gradients than chemically polished cavities, there is little doubt that cryomodules running at about 24 MV/m can be built.

CLIC

Energy

- The presently tested CLIC structures have only been exposed to very short pulses (30 ns maximum) and were not equipped with wakefield damping. The first Ranking 1 R&D issue is to test the complete CLIC structures at the design gradient and with the design pulse length (130 ns). Tests with design pulse length and with undamped structures are foreseen when CTF3 is available (April 2004).
- The validation of the drive beam generation with a fully loaded linac is foreseen in CTF3. Beam dynamics issues and achieving the overall efficiency look challenging.

Reliability

- In the present CLIC design, an entire drive beam section must be turned off on any fault (in particular on any cavity fault). CLIC needs to develop a mechanism to turn off only a few structures in the event of a fault. At the time of writing this report, there is no specific R&D program aimed at that objective but possible schemes are being studied.

9.2 RANKING 2

TESLA

Energy

- To finalize the design choices and evaluate reliability issues it is important to fully test the basic building block of the linac. For TESLA, this means several cryomodules installed in their future machine environment, with all auxiliaries running, like pumps, controls, *etc.* The test should as much as possible simulate realistic machine operating conditions, with the proposed klystron, power distribution system and with beam. The cavities must be equipped with their final HOM couplers, and their relative alignment must be shown to be within requirements. The cryomodules must be run at or above their nominal field for long enough periods to realistically evaluate their quench and breakdown rates. This Ranking 2 R&D requirement also applies to the upgrade. Here, the objectives and time scale are obviously much more difficult.
- The development of a damping ring kicker with very fast rise and fall times is needed.

Luminosity

Damping Rings

- For the TESLA damping ring particle loss simulations, systematic and random multipole errors, and random wiggler errors must be included. Further dynamic aperture optimization of the rings is also needed.

- The energy and luminosity upgrade to 800 GeV will put tighter requirements on damping ring alignment tolerances, and on suppression of electron and ion instabilities in the rings. Further studies of these effects are required.

Machine-Detector Interface

- In the present TESLA design, the beams collide head-on in one of the IRs. The trade-offs between head-on and crossing-angle collisions must be reviewed, especially the implications of the present extraction-line design. Pending the outcome of this review, the possibility of eventually adopting a crossing-angle layout should be retained.

Reliability

- The TESLA single tunnel configuration appears to pose a significant reliability and operability risk because of the possible frequency of required linac accesses and the impact of these accesses on other systems, particularly the damping rings. TESLA needs a detailed analysis of the impact on operability resulting from a single tunnel.

JLC-C

Energy

- The klystrons and modulators should be tested successfully at the nominal 100 Hz repetition rate.
- This should lead to the full test of the linac subunit, with beam. This will include klystrons, modulator, pulse compression system, LLRF control and several structures in their future environment.

JLC-X/NLC

Energy

- There must be a full test of the JLC-X PPM klystron at the specified repetition rate of 120 or 150 Hz.
- These klystrons should be tested with the NLC modulator (at full specs and including arcing tests) and form part of a linac subunit test. The latter should also comprise the dual-moded SLED-II complete system, several damped and detuned structures, installed in the accelerator environment (with temperature control, for instance), and LLRF and controls systems. The test should be made with beam. The present plan is to perform this sort of test with a full girder of structures (some of them being detuned and damped) in 2004.

CLIC

Energy

- Present tests have demonstrated the advantages of tungsten and molybdenum irises in reaching the highest gradients in accelerator structures. These tests should be pursued, possibly also with other materials, for application to CLIC and possibly other machines.
- The very high power of the drive beam and its stability are serious concerns for CLIC. The drive beam stability should be validated, and the drive beam Machine Protection System, which is likely to be a complex system, should be designed to protect the decelerator structures.
- The test of a relevant linac subunit with beam is required. This is one of the purposes of CTF3, which should start operation in 2004.
- The validation of the proposed multibeam klystron performance is needed to finalize the design choices for the CLIC drive beam generation. This applies particularly to the 3 TeV energy upgrade (long pulse).

Luminosity

Low Emittance Transport

- Calculations of the effects of coherent synchrotron radiation on the CLIC bunch compressors must be performed.

Machine-Detector Interface

- An extraction line design for 3 TeV c.m. must be developed.

Items Common to All Machines

Luminosity

Damping Rings

- For all the damping ring designs, further simulation studies are needed to understand the magnitude of the electron cloud effects and to explore possible means of suppressing these effects. Experiments in existing rings are needed to test the electron cloud simulations. Possible cures for the electron cloud (including chamber coatings, superimposed magnetic fields, and gaps in the bunch pattern) need to be experimentally investigated.
- Further simulations of the fast ion instability are also necessary. Experiments in the ATF and other suitable rings are needed to test the predictions of these simulations.
- Damping ring extraction kicker stability, required at the level of $<10^{-3}$, is an important issue. Continued studies including experiments with the ATF double kicker system are needed.

- Finally, additional simulations of emittance correction in the damping rings are needed, including the effects listed in Section 7.2.3.2. Additional experiments in the ATF and other operating rings are needed to test the emittance correction algorithms.

Low Emittance Transport

- For all low emittance transport designs, the static tuning studies, including dynamic effects during correction, must be completed.
- The most critical beam instrumentation, including the intra-train luminosity monitor, must be developed, and an acceptable laser-wire profile monitor must be provided where needed in each design. A vigorous R&D program is mandatory for beam instrumentation in general; it would be appropriate for a collaborative effort between laboratories.
- A sufficiently detailed prototype of the main linac module (girder or cryomodule with quadrupole) must be developed to provide information about on-girder sources of vibration.

Reliability

- A detailed evaluation of critical subsystem reliability is needed to demonstrate that adequate redundancy is provided and that the assumed failure rate of individual components has been achieved.
- The performance of beam based tuning procedures to align magnets and structures must be demonstrated by complete simulations, in the presence of a wide variety of errors, both in the beam and in the components.

9.3 RANKING 3

TESLA

Energy

- Improvement of the low level rf system design is needed. This system is quite complicated and critical, with many functions (field control, feedback, piezo feedforward, interlocks, fault management) and requires very specialized expertise.
- There must be a long-term testing of rf cryomodules to precisely evaluate potential weaknesses before large scale series production begins.
- Long-term testing of the multibeam klystrons is required to quantify their life-time and MTBF.
- The dark currents at the nominal operating field should be precisely evaluated.
- For the TESLA upgrade to 800 GeV c.m., besides the obvious gradient increase to 35 MV/m (Ranking 1), the capability of rf components (circulators, phase shifters, *etc.*) to handle a higher rf power must be demonstrated.

- In addition the proposed superstructures should be tested at their nominal gradient, with final HOM dampers and with higher power rf couplers.

Luminosity

Damping Rings

- A calculation of the effect of collective instabilities on the closure of the coupling bump in the damping rings should be made to determine whether a problem exists.

Machine-Detector Interface

- If the head-on scheme is maintained, then electrostatic separator performance (gradient 50 kV/cm) and a viable extraction septum design must be demonstrated in the presence of realistic radiation/power losses at 500 GeV c.m.
- The impact of shower debris produced in the secondary-collimation system on halo-induced synchrotron-radiation backgrounds, as well as the background impact of charged secondaries produced by halo particles hitting the FD, must be studied.
- The interplay of incoming-beam SR masking versus outgoing-SR stay-clear must be studied.
- The possibility of incorporating some form of FD stabilization in the baseline design should be investigated, to anticipate unexpectedly large vibration problems.
- The predicted extraction line losses at 800 GeV c.m. must be reduced from their currently unacceptably high levels.
- A collimator and masking configuration must be designed to be compatible with tolerable muon-backgrounds and SR-backgrounds at 800 GeV c.m.
- If the head-on scheme is maintained, then electrostatic separator performance (gradient 80 kV/cm) and a viable extraction septum design must be demonstrated in the presence of realistic radiation/power losses, at 800 GeV c.m.

Reliability

- The proposed undulator-based positron source for TESLA requires an electron beam before there can be a positron beam. This affects recovery scenarios as well as commissioning. TESLA needs to evaluate the operational impact of coupled electron/positron production.
- The 2.5 km segmentation of the TESLA cryogenic system is a concern because of the time required for warm up and cool down. The vacuum system size and segmentation is also an issue. The TESLA cryogenic and vacuum systems segmentation should be re-evaluated.
- TESLA needs a detailed analysis of the operational impact of structure faults.

JLC-C

Energy

- The low level rf system of JLC-C is unique because of the amplitude modulation needed to compensate the dispersion in the pulse compressor. This system is critical, as for the other machines, and requires an improved detailed design.
- Long-term testing of klystrons and modulators is needed to evaluate the life time of these components. Long-term testing of the linac modules is also needed to diagnose possible faults, before a large scale series production can start.

JLC-X/NLC

Energy

- The Low level rf system for JLC-X/NLC needs further improvements, notably to handle recovery scenarios in case of cavity trips or rf faults. Again, this is a complex and critical system, demanding very specialized expertise.
- Long-term testing of rf modules is required, before mass production.
- The continuation of the R&D to develop the NLC PPM klystron is recommended. This is to provide a second design and very likely to improve the overall reliability of klystrons.
- The development of the JLC-X linear induction modulator should continue, again to explore slightly different technical implementations and to improve overall performance and reliability.
- The test recommended in Section 9.2 should be extended to a full test, with beam, of a complete linac unit, with 24 structures and 8 klystrons.
- The studies of the cathode charge limit, using the E158 beam at SLAC, should be continued.
- Studies of conventional positron target performance are also needed. This item and the preceding one apply as well to CLIC.

Luminosity

Damping Rings

- For the JLC-X/NLC damping rings, particle loss simulations, systematic and random multipole errors, and random wiggler errors, must be included. Further dynamic aperture optimization of the rings is also needed.
- Further experiments at the ATF and other low-emittance damping rings are necessary to determine the validity of the theoretical models of IBS.

Low Emittance Transport

- In the low emittance transport, the magnetic center stability (at the 1–10 μm level) required in the quadrupoles must be demonstrated, over the relevant time scales of minutes to days.

Machine-Detector Interface

- Stabilization of the final-quadrupole doublet must be demonstrated in an environment that adequately reproduces the system constraints of an actual detector and IR.
- The predicted extraction line losses at 1 TeV must be reduced from their currently unacceptably high levels.
- It must be demonstrated that muon and synchrotron-radiation induced backgrounds are tolerable at 1 TeV.

Reliability

- For JLC-X/NLC, there is a need to evaluate the impact on operations of the interleaved positron target system.
- For the linacs of the warm rf machines, the tuning procedures require structure alignment as well as quadrupole centering. For JLC-X/NLC, there is a need to evaluate the systems aspects of a large interrelated alignment system. This item also applies to CLIC.

CLIC

Energy

Because the CLIC project is less advanced than the others, the Ranking 3 and Ranking 4 R&D items were not really discussed in detail and the list here is not believed to be complete.

- However, the control of the accelerating field in CLIC, and the necessary Low Level rf system, are unique to this kind of machine. A detailed design of the LLRF system in CLIC is certainly needed. It must be able to correct for beam loading, to handle rf and beam faults and be intimately connected with the drive beam protection system.
- A more efficient type of modulator should be studied, especially for the upgrade to 3 TeV.

Luminosity

Machine-Detector Interface

- For the 500 GeV c.m. design, an extraction line design for the spent beam must be developed.
- Stabilization of the final-quadrupole doublet must be demonstrated in an environment that adequately reproduces the *system* constraints of an actual detector and IR. The performance specifications are about two times tighter than those of JLC-X/NLC.
- It must be demonstrated that muon- and synchrotron-radiation induced backgrounds are tolerable at 500 GeV.

- At 3 TeV c.m. energy, beam-beam backgrounds increase by large factors, including the appearance of coherently produced pairs. The interaction region and detector optimization is more difficult than for 500–1000 GeV operation, so continuation of these studies is important. Similar comments apply to the design of the collimation scheme and the minimization of synchrotron-radiation backgrounds.

Reliability

- A variety of common mode problems can arise due to the fact that faults in the CLIC drive beam complex affect the whole acceleration chain of the main linac. CLIC needs to evaluate the impact of drive beam faults on reliability, stability and operations of the linac.

Items Common to All Machines

Energy

- Improvement (for TESLA), or development (JLC-X/NLC, CLIC) of the source laser are needed, to improve its stability. This is particularly critical for the CLIC drive beam and should be addressed in the CTF3 program.
- A detailed layout up to the damping rings must be used to precisely evaluate the intensity overhead, the location of beam losses, the longitudinal emittance, and the positron beam stability.
- The demonstration of beam-based structure alignment is needed to finalize the tolerance specifications and make sure that they are matched to the system analysis and procedures.
- Tracking simulations of polarized sources should be carried out.

Luminosity

Damping Rings

- For all the damping ring designs, detailed reviews of the impedance budgets are needed.
- Development of BPMs with < 0.5–1 micron resolution and excellent stability (approximately 10 microns over 1 day) is necessary. The development of fast, high resolution beam size diagnostics for the damping rings must be continued.

Low Emittance Transport

- In the low emittance transport systems, the technical noise level present in the beamline, due to klystrons, pumps, and other sources which are necessarily close to the accelerator, must be estimated.
- Collimator wakefield measurements must be performed. In the event that the wakes turn out to be as large as presently anticipated, other solutions must be investigated for the beam halo problem, which would permit relaxation of the collimation aperture, and the experimental validation of the tail-folding scheme will be necessary.

- The BPMs required for emittance preservation in the low emittance transport, and for operation of the beam-beam collision feedback, must be developed.
- The detailed tolerances for fast vibration, magnet strength stability, rf stability, *etc.*, must be computed, and it must be verified that static tuning of the low emittance transport will converge in the presence of these dynamic errors.
- The robustness of emittance tuning algorithms in the presence of malfunctioning BPMs, correctors, and element translation stages must be estimated.
- The likely cultural noise at prospective LC sites must be characterized.
- The pre-collimation systems which are intended for use between the damping ring extraction and the low emittance transport must be designed.
- Electron and ion effects in the low emittance transport should be estimated.
- The demonstration of mechanical alignment techniques to be used in the low emittance transport prior to commissioning, which are already well advanced in some studies, must be continued.
- Calculations of the multibunch wakefield effects in the pre-linac and bunch compressor regions must be completed.

Machine-Detector Interface

- A detailed model of synchrotron radiation backgrounds (core + halo) in the interaction region (inboard of the final bends), that includes backscattering and tip scattering off masks and IR vacuum pipe surfaces, must be developed.
- For an IP with crossing angle, vigorous development of compact SC quadrupoles with adequate vibration characteristics must be pursued, the capability of IP feedback to cope with field fluctuations due to thermal effects in PM quads must be evaluated, and R&D on adjustable PM quads must be pursued.
- The mechanical stability of the solenoid coil and/or iron yoke, which is required to have vibration levels in the micron range, must be evaluated.
- Background-simulation tools for better tracking of both primary and secondary particles must be improved, and the models of the machines (including a study of "tuned" imperfect machines) and their environment (*e.g.*, tunnel layout, muon spoilers) must be refined.
- Beam polarization and energy diagnostics with sufficient precision to meet particle physics requirements must be developed.

Reliability

- A detailed Machine Protection System design that meets requirements must be developed, including a careful study of failure modes.
- A comprehensive assessment of the MTBF and MTBO for rf components is required, and an adequate fraction of hot spares must be included in the final design.
- A comprehensive reevaluation of design parameter overheads throughout the complex is required.

- A comprehensive evaluation of the frequency and impact of tunnel access is needed.
- A model for communications and controls with adequate reliability must be developed.

9.4 RANKING 4

TESLA

Energy

- The understanding of the gradient limits with electropolished cavities is of great importance for TESLA, especially for the 800 GeV upgrade. Studies must continue in this direction, in a collaborative effort with other institutions and universities.
- Several alternative and/or complementary solutions are proposed for the TESLA rf distribution system. They should be tested and evaluated in the long term.

Luminosity

Damping Rings

- A correction algorithm for the TESLA damping rings, including both vertical and horizontal planes, is needed.

Low Emittance Transport

- The implications of reducing the value of D_y for TESLA should be studied, in the event that such a reduction is desired in order to ease the tolerances on the "banana" instability.

Machine-Detector Interface

- If placing beam polarization and energy diagnostics in the spent-beam extraction line eventually proves necessary, then the radiation levels in the present extraction line must be reduced by at least an order of magnitude.

JLC-C

Energy

- The proposed C-band klystrons are solenoid-focused. The development of a C-band PPM klystron and the development of a new modulator are recommended.

JLC-X/NLC

Energy

- Physics studies dedicated to the fundamental understanding of high gradient limits in accelerator structures are highly recommended. This obviously represents a joint effort between laboratories. The various experimental results already obtained under different conditions must be expanded and confronted with the simulations or theoretical expectations, to the extent that they exist.
- Further studies of standing-wave structures are recommended.
- For the energy upgrade, the studies of higher gradient structures could be particularly beneficial. These studies would benefit from a better understanding of the fundamental mechanisms of rf breakdown recommended above for all room-temperature structures.
- The initially proposed DLDS systems are to be reconsidered for the energy upgrade, as they offer a higher efficiency. Further studies on DLDS systems are recommended.

Luminosity

Low Emittance Transport

- The feasibility of an intra-train feedback which operates within the short time required should be demonstrated.(This also applies to CLIC).

CLIC

There are no Ranking 4 items for CLIC.

Items Common to All Machines

Energy

- All designs would benefit from a better understanding of the undulator-based positron production scheme. The SLAC study of an undulator-based polarized positron source should be carried out, possibly in collaboration with other laboratories.
- The studies of polarized rf photocathode guns should be encouraged.
- The ATF study of a Compton-based polarized positron source should be supported.

Luminosity

Damping Rings

- Additional experiments in the ATF and other operating rings are needed to verify that beam-based alignment can be used to align BPMs with respect to their associated quadrupole and sextupole magnets within a few microns, and to study drifts and systematic errors in the BPMs.

Low Emittance Transport

- Further simulations and studies of the formation of beam halo, and the impact of dark current, in the low emittance transport should be performed.

Machine-Detector Interface

- The detector implications of the proposed final doublet support and stabilization schemes should be investigated.
- The impact of dynamic errors on beam-beam backgrounds should be studied.